Sand injectites in the northern North Sea Basin

A thesis submitted to the University of Manchester for the degree of Doctor of Philosophy in the Faculty of Science and Engineering

2021

Sebastian Nnorom

Faculty of Science and Engineering
School of Natural Sciences
Department of Earth & Environmental Sciences

Table of Contents

CHAPTER 7   Quantitative analysis and characterization of the interaction between sandstone intrusions and polygonal fault systems in the Eocene – mid Miocene (Hordaland Group) succession of the northern North Sea Basin

FINAL WORD COUNT: 93,884

List of Figures

Chapter 1

Chapter 2

Chapter 3

Chapter 4

Chapter 5

Chapter 6

Chapter 7

Chapter 8

List of Tables

Chapter 5

Chapter 7

Chapter 8

Thesis Abstract

Subsurface sediment remobilization and injection processes are important component of processes which occur in sedimentary basins worldwide. These processes are largely associated with deep-water clastic systems and have significant impact on the morphology and distribution of deep-water sand reservoirs which in turn have important implications for hydrocarbon exploration and production, and for carbon sequestration in deep-water clastic reservoirs. This research uses an integration of high-resolution 3D seismic data and well data from the Norwegian sector of the northern North Sea Basin to investigate the occurrence of large-scale sandstone intrusions or sand injectites in the Paleogene succession, to unravel their origin and mechanisms responsible for their development, distribution and associated complex geometries.

The observations and interpretation from this study are documented in five result chapters (Chp. 3 – 7) which begins with a short overview of the hydrocarbon reserves/resource distribution of sand injectite fields in the UK and Norwegian sectors of the North Sea with the view to show that sand injectites form attractive exploration targets based on experience from North Sea oil/gas fields. This is followed by Chapter 4, which investigates the occurrence of discordant high amplitude anomalies within the Paleogene interval, which based on well calibration are interpreted as the seismic expression for large-scale sandstone intrusions within multiple stratigraphic intervals. Then, Chapter 5 documents for the 'first time' the occurrence of a Middle – Late Oligocene sand-rich deep-water depositional system modified by subsurface sediment remobilization and injection processes in the eastern part of the study area. The study highlights and describes the seismic expression of sand intrusion complexes developed in association with the depositional system and the implication of such intrusion complexes in deep-water settings. The succeeding Chapter 6 revisits aspects of the model and interpretation for the Late Cenozoic geological evolution of the northern North Sea presented by Løseth et al. (2013) with special emphasis on their proposed source for Oligocene sandstone and the processes responsible for the mounded shape of the Top Hordaland Group Unconformity. The findings based on available data demonstrate that their model for a strictly injected Oligocene sand is inconsistent with our observation. Lastly, Chapter 7 explores the various kind of interaction which exist between sandstone intrusions and polygonal fault systems present within their low-permeable host mudstone succession and how their co-existence may have aided sand injection or controlled the simple to complex geometries of the intrusions.

Understanding the processes responsible for sand remobilization and injection is crucial to understanding the dynamics of a sedimentary basin's evolution. The findings and interpretation presented here contribute to a clearer understanding of some of the factors and processes which favor the development of sand intrusions in the northern North Sea Basin. It also demonstrates the impact of post-depositional processes on deep-water systems because they can impact the distribution and geometries of reservoir units as well as the efficiency of fluid flow and migration through sedimentary successions over long periods.

Declaration

I declare no portion of the work referred to in the thesis has been submitted in support of an application for another degree or qualification of this or any other university or other institute of learning.

Sebastian Nnorom

Copyright statement

I.   The author of this thesis (including any appendices and/or schedules to this thesis) owns certain copyright or related rights in it (the "Copyright") and he has given The University of Manchester certain rights to use such Copyright, including for administrative purposes.

II.   Copies of this thesis, either in full or in extracts and whether in hard or electronic copy, may be made only in accordance with the Copyright, Designs and Patents Act 1988 (as amended) and regulations issued under it or, where appropriate, in accordance with licensing agreements which the University has from time to time. This page must form part of any such copies made.

III.   The ownership of certain Copyright, patents, designs, trademarks, and other intellectual property (the "Intellectual Property") and any reproductions of copyright works in the thesis, for example graphs and tables ("Reproductions"), which may be described in this thesis, may not be owned by the author and may be owned by third parties. Such Intellectual Property and Reproductions cannot and must not be made available for use without the prior written permission of the owner(s) of the relevant Intellectual Property and/or Reproductions.

IV.   Further information on the conditions under which disclosure, publication and commercialisation of this thesis, the Copyright and any Intellectual Property and/or Reproductions described in it may take place is available in the University IP Policy (see http://documents.manchester.ac.uk/DocuInfo.aspx?DocID=24420), in any relevant Thesis restriction declarations deposited in the University Library, The University Library's regulations (see http://www.library.manchester.ac.uk/about/regulations/) and in The University's policy on Presentation of Theses.

Author

I hold a Bachelor of Science degree in Geophysics from the Federal University of Petroleum Resources Effurun, FUPRE, Nigeria (2012) and a Master of Science degree in Petroleum Geoscience for Exploration from the University of Manchester (2015). Upon completion of my MSc. degree, I worked as a Geophysics Teaching Assistant at FUPRE between 2016 − 2017 before commencing my PhD programme in late 2017. My PhD research have equipped me with the knowledge and understanding on sand injectites, and the dynamic processes involved in sand remobilization and injection leading to the formation of large-scale intrusion complexes.

Acknowledgements

Above all I give thanks to Almighty God for his undying love, guidance, protection, and favours through this defining phase of my life and career. I thank Him for seeing me through to the end of it all. My special thanks go to my supervisor Prof. Mads Huuse for his guidance, constructive criticism, and ideas he shared towards a successful completion of my research. The University of Manchester (UoM) is thanked for access to much needed facilities and a conducive environment for studies and research. I also want to thank Dr Kofi Owosu for his help in resolving all technical issues throughout the programme and ensuring the smooth running of all software and hardware in the Basins Lab.

I greatly appreciate CGG for giving access to the high-quality 3D seismic data used for this research. TGS is also appreciated for granting access to the well data used through the Facies Map Browser (FMB). Schlumberger is thanked for granting university license for the use of their Petrel^{TM} software for seismic analysis and interpretation.

My special gratitude goes to my sponsors the Petroleum Technology Development Fund (PTDF) for providing full funding for my PhD programme. Your contribution towards my career and future is greatly appreciated.

Special thanks to my colleagues: Chris Lloyd, Dr Tim, Dr Wumi, Dr Jefferson, Mohammed and others for their company and ideas shared during discussions and outings. Our bonding as a family and care for each other's welfare will forever be remembered.

Finally, I greatly appreciate my parents and siblings for their love, prayers, and encouragement throughout my programme. Your love and support meant a lot.

Thesis synopsis

The outline of this thesis is divided into three sections which are further sub-divided into eight linked chapters which cover all aspects of the topic of study. The different sections and chapters are outlined below:

Section 1 (Chapters 1 – 2): Chapter 1 gives the background and rationale for the current study, location of study, aims and specific objectives, available data and adopted methodology used to achieve the set objectives and deliverables. Chapter 2 presents the geological setting of the study area including a detailed review of previous published literature on the occurrence of sediment remobilization and fluid flow features with a larger focus on sand injectites or sandstone intrusions.

Section 2 (Chapters 3 – 7): Chapter 3 – 7 contains results for the entire study presented in the University of Manchester's alternative format, which will be submitted to peer-review journals for publication. Chapter 3 presents a short review of reserve and resource distribution of sand injectite fields in the UK/Norwegian sectors of the North Sea Basin giving details about their date of discovery, production start date, documented recoverable reserves/resource estimates, injectite reservoir interval & age, reservoir type (based on the style & scale of injection), depositional setting, hydrocarbon type, reservoir properties (porosity & permeability), etc. Chapter 4 documents the three-dimensional geometry, distribution, quantitative geometrical characteristics, and development of clastic intrusions in the Paleogene succession in the study area. All aspects of the remobilization and injection process were also considered from their parent source sands, timing of injection, and their potential priming and trigger mechanisms. Chapter 5 documents the deposition and post-depositional remobilization (i.e., modification) of a Middle – Late Oligocene deep-water sandy depositional system and the controls on its development. In Chapter 6, aspects of the previous model for the development of Oligocene sand intrusions and the modification of the Top Hordaland Group Unconformity documented by Løseth et al. (2013) is revisited based on new insights and observations from a recent high quality broadband 3D seismic data. Finally, Chapter 7 investigates the interaction between sandstone intrusions and polygonal fault systems (PFS) and how the resultant complex geometries of the sand intrusions may be dependent on their co-existence with PFS in the Oligocene succession of the study area.

Section 3 (Chapter 8): This forms the synthesis chapter which summarizes and integrates the principal findings in Section 2. This also addressed some of the research questions raised in section 1.1, and it goes further to highlight the implications of this study to hydrocarbon exploration and production of deep-water sandstone reservoirs and gives recommendations for future work and analysis.

Section 1:

Introduction, Geological setting

&

Review of published literature

Chapter 1

CHAPTER 1   Introduction

1.1 Background and rationale of study

Subsurface fluid flow and sediment remobilization processes and their products (such as sand injectites, silica diagenetic boundaries, polygonal fault systems, and mud volcanoes) are presently recognized as important component of sedimentary basins worldwide (Huuse et al., 2010). This soft sediment deformation processes comprises of all process involved in the remobilization of pre-existing clastic sediments in the subsurface (Van Rensbergen et al., 2003), and the products of these processes have been categorized into two forms based on their modes of occurrence (Huuse et al., 2010): (a) Organized forms e.g., sand remobilization, injection & extrusion; mud volcanoes and fluid-flow products (BSR, fluid pipes, etc.), and (b) Disorganized forms e.g., mass transport deposits. The processes involved in sediment remobilization, injection and fluid flow are complex and are believed to be controlled by various inter-related factors such as fluid properties (such as pressure, volume, and composition), parent and host strata characteristics (grain size and distribution, depositional architecture, thickness, porosity, and permeability) and burial depth (Hurst et al., 2011).

Current advances in subsurface imaging using 3D seismic data, its integration with well data, geochemical, cores and outcrop data has brought about an increase in the studies and understanding of subsurface sediment remobilization and fluid flow processes and products in sedimentary basins (Gay et al., 2006; Cartwright et al., 2007; Huuse et al., 2010). These remobilization events are often facilitated by overpressure conditions in the subsurface, as well as significant sediment and fluid movements, facilitated by either internally and/or externally driven mechanisms (Jolly & Lonergan, 2002; Cartwright, 2007; Huuse et al., 2010; Hurst et al., 2011; Andresen, 2012). The resultant clastic (sand and mud) intrusions in the subsurface, however, has a strong and significant control on post-depositional fluid flow processes in the sedimentary sequence they inhabit over a long duration of time (million years) following the injection event (Milkov, 2000; Cartwright et al., 2007; Hurst & Cartwright, 2007; Huuse et al., 2010). A good and in-depth understanding of sediment remobilization and fluid flow phenomenon is a relevant key to a safe and efficient hydrocarbon exploration, as well as the understanding of the dynamics of sedimentary basin evolution (Harrison & Summa, 1991; Huuse et al., 2010).

Sediment remobilization and fluid flow products have been documented in several hydrocarbon basins (both mature and frontier basins: North Sea, Fareo-Shetland Basin, San Joaquin Basin, Niger Delta, Gulf of Mexico, Colorado Plateau, Offshore Angola, offshore mid-Norway) in the world (Heggland, 1998; Hurst et al., 2005; Gay et al., 2006; Hurst & Cartwright, 2007; Huuse et al., 2010: their Fig 1 & Table 1). Due to the global distribution of sediment remobilization and fluid flow phenomena, several authors have highlighted their occurrences, as well as published regional and/or global distribution maps of these features (see Fig. 9).

Some well cited published literatures on sediment remobilization and fluid flow phenomena include and are not limited to:

- **Sandstone intrusions and associated processes:** Lonergan et al., 2000; Jolly & Lonergan, 2002; Hurst et al., 2003; Duranti & Hurst, 2004; Huuse & Mickelson, 2004; Huuse et al., 2005; Hurst et al., 2005; Duranti, 2007; Braccini et al, 2008; Cartwright et al., 2008; Hurst & Cartwright, 2007; Huuse et al., 2007; Huuse et al., 2009, AAPG; Cartwright, 2010; Huuse et al., 2010; Szarawarska et al., 2010; Hurst et al., 2011; and several others.

- **Mud volcano systems:** Graue, 2000; Milkov, 2000; Hovland et al., 2002; Stewart & Davies, 2006; Davies et al., 2008; Mazzini, 2009; Calves et al., 2010; Gamberi, 2010; Roberts et al., 2010; etc.

- **Gas hydrates and Polygonal Fault systems:** Dewhurst et al., 1999; Cartwright et al., 2007; Goultry, 2008; Cartwright, 2011; Wrona et al., 2017 etc.

One major known occurrence of sandstone intrusion is in the North Sea Basin within the Cenozoic succession of the central and northern North Sea, where the occurrence of sand injectites has been known for more than two decades, and as a whole is referred to as a Large Sandstone Intrusion Province (LSIP), with other adjourning basins such as the San Joaquin Basin, Outer Moray Firth, Barents Sea, Norwegian- Danish Basin and Fareo-Shetland Basin containing kilometre-scale sandstone injectites known to intrude into fine-grained mudstone succession (Huuse & Mickelson, 2004; Cartwright et al., 2010; Huuse et al., 2012). Previous studies of clastic intrusions have demonstrated that their development have major implications for exploration and production of deep-water systems (e.g., Lonergan et al., 2000; Hurst & Cartwright, 2007, Jackson et al., 2011). For example, several studies have shown that the remobilization and injection of clastic sediments can impact reservoir architecture and connectivity, volumetrics, and pore-scale reservoir properties which in turn affects the distribution and geometries of porous and permeable lithologies (Jenssen at al., 1993; Lonergan et al., 2000; Duranti et al., 2002; Molyneux et al., 2002; Huuse & Mickelson, 2004; De Boer et al., 2007; Jackson, 2007; Szarawarska et al., 2010). It is, therefore, important that clastic intrusions and their associated petrophysical properties are accounted for in subsurface 3D reservoir modelling (Purvis et al., 2002; Briedis et al., 2007; Jackson et al., 2011). Evidence from North Sea hydrocarbon fields (e.g., Alba, Balder, Gryphon and Volund) demonstrate that clastic intrusions may represent standalone exploration targets (see Huuse et al., 2004; Hurst et al., 2005; Braccini et al, 2008) and could also pose significant drilling geo-hazards (Huuse et al., 2007). Furthermore, from an applied perspective the development of clastic intrusions may provide insights into the timing and periods of overpressure development and basin-scale fluid flow (see Cartwright, 2010) since their formation requires the presence of significant overpressure within an effectively sealed parent sand body, with substantial volume of fluid (internally or externally derived) to transport the sand in a fluidized flow. Therefore,

constraining their timing of formation within a sedimentary basin may be important during basin analysis (Jackson & Sømme, 2011).

Although North Sea sand injectites have been studied extensively using 3D seismic data, several aspects (e.g., parent source sands, timing of injection, depth of emplacement or burial prior to injection, priming and trigger mechanism) of their formation and distribution are still poorly understood and are still a subject of debate. For example, the series of processes (e.g., overpressure development, liquefaction, fluidization, and hydrofracturing of sealing strata) which facilitates the formation of sand injectites are well known, but the exact details of what triggers sand fluidization and the combination of factors responsible for achieving their characteristic simple to complex geometries remains speculative (Davies et al., 2006; Hurst et al., 2011). This poor understanding and clarity informed the listed questions which this research aims to address for the northern North Sea case study. Some of these questions are addressed by some chapters and are also revisited in chapter 8, while some are recommended as questions to be considered in future research because they require an integration of additional data (e.g., cores data & cuttings samples) which were not available for this study.

a) Why is the study of sand injectites important, and are they attractive exploration targets?

b) Why are sand injectites abundant in the northern North Sea Basin, and what favours their formation in the Paleogene succession of the northern North Sea?

c) What properties (i.e., mineralogical, chemical & physical) of their host mudstones favour the scale of sand remobilization and injection features present in the northern North Sea Basin?

d) What factors control the location/distribution, extent and the resultant simple to complex geometries (i.e., injectite architecture) associated with the large-scale intrusion complexes studied here?

e) Where are the parent source sands for the intrusions, and how are depositional sands differentiated from injected sands?

f) What processes may have facilitated and triggered sand remobilization and injection in the northern North Sea Basin?

g) Were the intrusions formed by single or multiple episodic emplacement events?

h) Are the existing models suggested by previous authors sufficient to account for the magnitude of the large-scale intrusion complexes formed in the study area?

i) Finally, what are their implications for hydrocarbon exploration and production in the study area?

To address some of the above, it is therefore necessary to document their occurrence, geometries, dimensions, and distribution in the study area, since they constitute an important part of the basin stratigraphy, using a more recent and improved image of the subsurface from the northern North Sea Basin.
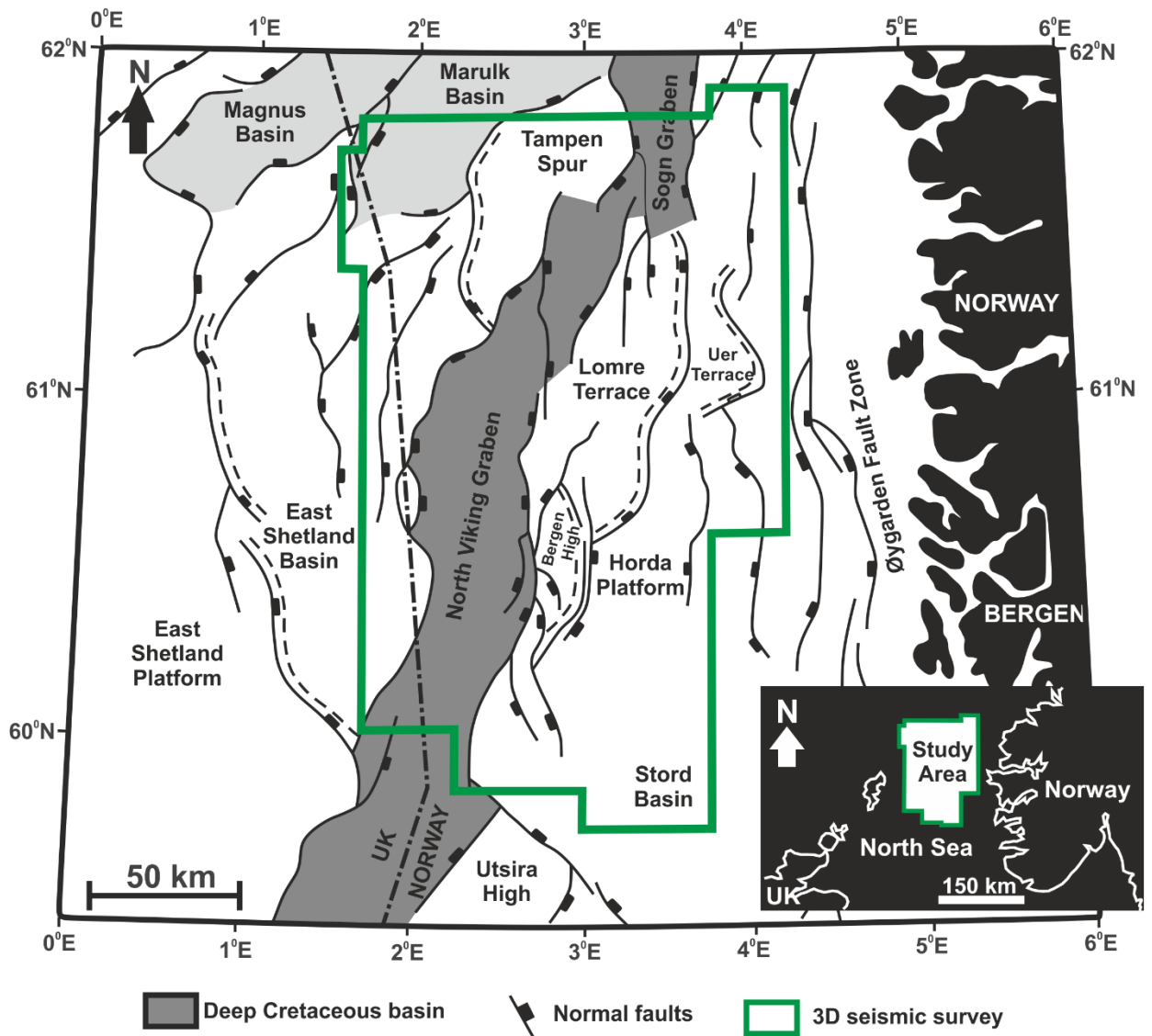
Fig. 1.1: Map showing the location of study in the northern North Sea Basin. The extent of the 3D seismic survey used is shown by the green outline (modified after Nottvedt et al., 1995).

1.2 Location of study

The study area is located in the Norwegian sector of the northern North Sea Basin which is a host to many giant oil and gas discoveries (such as Brage, Gullfaks, Oseberg, Statfjord, Snorre, Troll, Visund field, etc.), located between latitude $59 - 62^0$N and longitude $1 - 4^0$E, and cover mature exploration areas which include (see Fig. 1.1): the whole of the Northern Viking Graben (NVG), Tampen Spur (TP), Horda Platform (HP) and part of the Sogn Graben (SG), including the Måløy Terrace (MT), Uer Terrace (UT) and Lomre Terrace (LT). The study area is bounded to the north by the Marulk Basin, to the south by the Central & South Viking Graben (SVG), to the west by the East Shetland Platform (ESP) and to the east by the Norwegian mainland separated by the Øygarden Fault Zone (Fig. 1.1). Its present-day geometry is dominated by N-S striking and west dipping normal faults and half graben (Fig. 1.1) formed by the Permo-Triassic and Jurassic rifting episodes (Badley et al., 1988; Ziegler, 1990; Faerseth, 1996; Dmitrieva et al., 2012, 2018).

1.3 Research aims and objectives

This research involves the case study of large-scale sandstone intrusions or sand injectites complexes in the Paleogene succession of the northern North Sea characterized by multiple sand remobilization and injection events. The principal aims of this research are to:

- Unravel the origin and processes of sandstone intrusion/injection in the northern North Sea.
- Identify possible mechanisms and controls on their development and associated complex geometries.
- Improve on existing conceptual models for their development based on the availability of improved subsurface data and access to more data.
- Understand the implications of sandstone intrusion complexes for hydrocarbon exploration and production.

The above is achieved with the objectives subdivide into five (5) research themes:

- **Attractive exploration targets:** Document reserve distribution and reservoir properties of hydrocarbon fields associated with sand injectite reservoirs in the UK and Norwegian sectors of the North Sea Basin. Also consider their implications for hydrocarbon exploration and production
- **3D seismic characterization:** Identify, describe, characterize, and document the presence of sand intrusions within the Paleogene interval. Map their distribution (both laterally and vertically) and document their geometries and dimensions (e.g., dip and height of intrusions).

- **Origin and mechanisms:** Investigate their origin (driving and triggers mechanisms) and timing of emplacement to ascertain if they were formed by single or multiple/episodic emplacement events.
- **Depositional versus remobilized and injected sands:** Differentiate depositional sands from injected sands by identifying their possible parent (source) sand bodies within the study area.
- **Interaction of fluid flow features:** To describe and analyse the interaction between sandstone intrusions and polygonal faults both of which co-exist within the Paleogene succession of the northern North Sea. To also consider the possible influence of polygonal faults on the resultant complex geometries of some of the intrusions.

Deliverables:

- Review of regional framework and geology of the study area including review of previous documentation of sand injectites in the North Sea Basin
- Mapped key horizons (e.g., TWT/depth structure maps, volume attributes, attribute render on mapped horizons, etc.) and stratigraphic sequences
- Inventory of scale, geometries, dimensions, and spatial distribution of the sandstone intrusions within the Paleogene succession
- Quantitative characterization of sand injectites and polygonal faults within the Hordaland Group interval
- Generalized conceptual model for sand remobilization and injection in the northern North Sea Basin

1.4 Data and Methods

1.4.1 Data

1.4.1.1 Data type and source

The data used for this study comprises of a high-resolution broadband 3D seismic survey of the northern North Sea provided by CGG (Fig. 1.2). The survey covers the Norwegian sector of the northern North Sea (Quadrant: 29 – 36), part of the Norway southern North Sea (Quadrant: 25 & 26), a bit of Mid-Norway (Quadrant: 6203 & 6204) and part of the UK sector of the northern North Sea (Quadrant: 003 & 211). It covers a vast area of c. 36,400 km^2, straddles the boundary between the UK sector and Norwegian sector of the northern North Sea, covering several discoveries of known commercial quantity (such as the Troll, Snorre, Visund, Gullfaks, etc.) and till date comprises the largest, and most complete of all available 3D seismic data for the northern North Sea Basin. The available datasets are further described in the subsequent sections.

1.4.1.2 3D Seismic Data Description

The 3D seismic data utilized in this study comprises of a pre-stack time-migrated (in time domain: CGG18M01_NVG_EFT) and pre-stack depth-migrated (in depth domain: NVG_Z_8km_8bit_37500cm) high resolution seismic data. The time-migrated data is described below while the depth-migrated data is described in subsequent chapters (see Chapter 6 & 7). The time-migrated data is zero-phase processed seismic data which extends down to a depth of 5000 msTWT and displayed with SEG normal standard polarity, which implies that an increase in acoustic impedance with depth is represented by a positive reflection event (peak or red) and vice versa. The survey consists of 4303 inlines and 7421 crosslines; an inline range of 1691 – 10295 and crossline range of 14636 – 36898; a sub-sampled line spacing of 37.5 m; and 1251 samples per trace at a vertical sampling interval of 4 ms (TWT). Water depth ranges between 100 – 400 m with the interval of interest (Paleogene succession) lying between 500 – 2200 msTWT. The frequency within the interval of interest ranges from 25 – 55 Hz based on the dominant frequency volume attribute applied to the seismic cube, while the dominant frequency is around 50 Hz. Based on available check shot data from wells, the average interval seismic velocity within the interval of interest is 2000 ± 200 m/s. This therefore gives a vertical resolution (λ/4) and horizontal resolution (λ/2) of c. 10 m and ca. 20 m respectively, using wavelength calculated from the dominant frequency and interval velocity of 2000 m/s. The average interval velocity (estimated from some available wells) used in converting vertical measurements in milliseconds two-way travel time (msTWT) to depth (m) at different intervals anywhere depth is quoted in this study is shown in Table 1.1 below.

Table 1.1: Table showing the frequency, interval velocity and other parameters for the observed seismic units.

Seismic Units	Age	Frequency (Hz)	Avg. Int. Velocity (m/s)	Vertical Resolution (λ/4)	Horizontal Resolution (λ/2)
KSU-1	Cretaceous	25	2835	28	57
CSU-1	Palaeocene – Early Eocene	30	2317	19	39
CSU-2	Eocene	40	2108	13	26
CSU-3	Lower Oligocene	40	1742	11	22
CSU-4	Intra-Oligocene wedge	45	2084	12	23
CSU-5	Lower Miocene	50	2135	11	21
CSU-6	Upper Miocene	55	2127	10	19
CSU-7	Pliocene	50	2113	11	21
CSU-8/9	Pleistocene - Holocene	55	2000	9	18

1.4.1.3 Well Data

The northern North Sea is penetrated by several exploration wells, most of which targeted deep Jurassic reservoirs. For this study, several wells were available from the TGS Facies Map Browser (TGS-FMB) but a few (about 100 wells) were selected (Fig. 1.2, Appendix A.2). The selected wells contain complete standard suite of well logs (e.g., gamma ray, sonic velocity, neutron, bulk density, and resistivity logs, etc. see Appendix A.2), lithostratigraphic/formation top data, check shot data and deviation surveys. The selected wells enabled a good correlation across the basin and a proper constrain of horizon interpretation and lithology delineation. Formation top data from the TGS-FMB were compared to those available on the Norwegian Petroleum Directorate (NPD) website to ensure accuracy, with reference made to published literature if required. Completion logs and well reports available on NPD and TGS-FMB were also used where necessary. For some of the wells, detailed chronostratigraphic data were also available from the TGS-FMB.

1.4.2 Methods

1.4.2.1 Seismic-to-well tie

For an accurate tie between the seismic (time domain) and well data (depth domain), synthetic seismograms were generated for some key wells (e.g., see Appendix A.1; Fig. 4.4b & 5.4). This allowed age constraints to be placed on observed reflection events and the assessment of lithology and significance of observed amplitude anomalies within the intervals of interest. As such, this provided an accurate tie between formation tops in wells and reflections on the seismic data and helped in the development of the seismic stratigraphic framework in the study area. For this purpose, a statistically extracted wavelet which extracts the required wavelet parameters from the seismic data trace was applied to some of the key wells selected based on the availability of check-shot data. The synthetic seismogram was then calculated by convolution of the extracted wavelet with the acoustic impedance (reflectivity) log derived from bulk density and sonic logs (e.g., see Fig. 4.4b & 5.4).
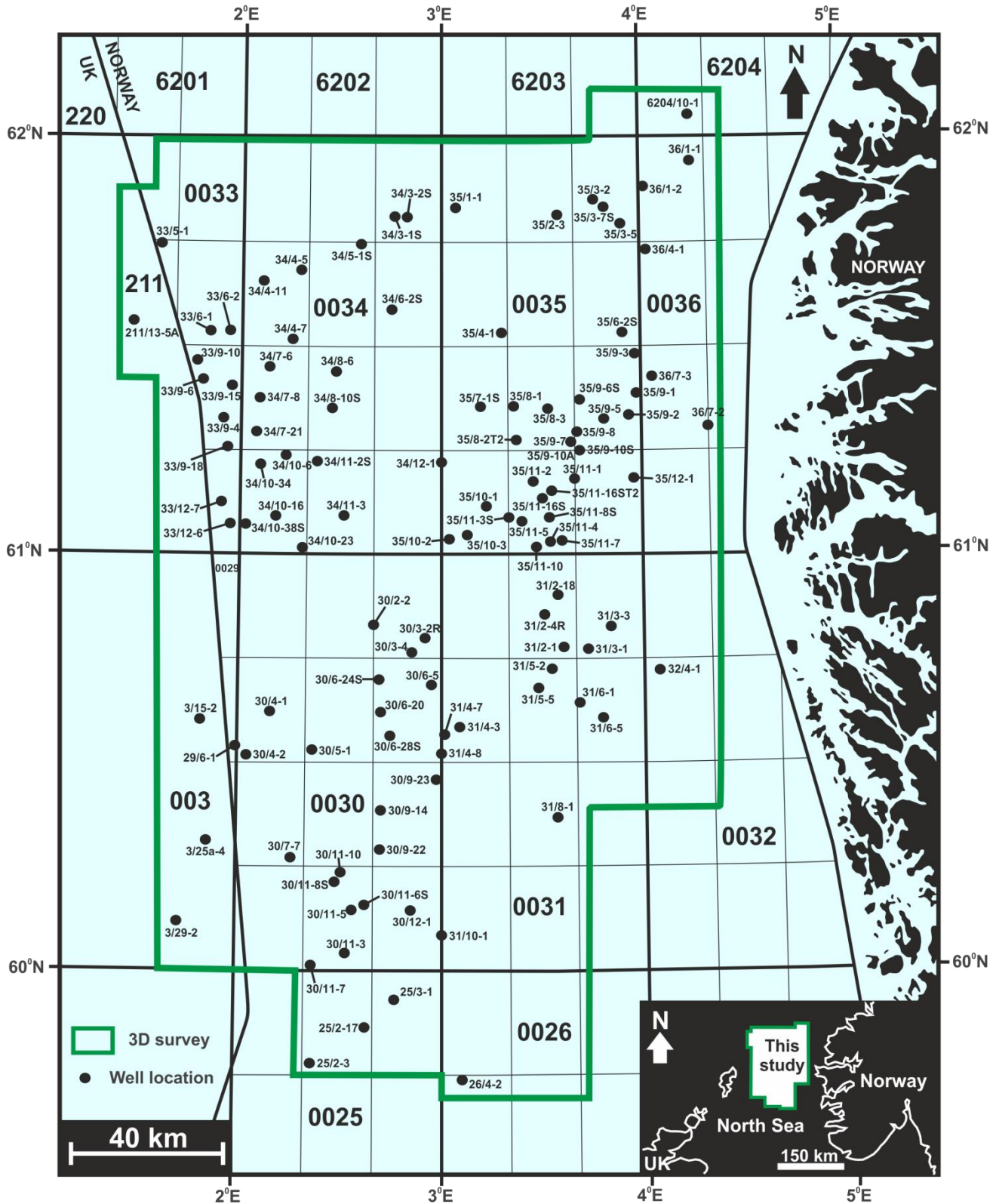
Fig. 1.2: Base map showing the surface location of some selected wells (courtesy TGS Facies Map Browser) and outline of the 3D seismic survey (courtesy of CGG) used for the entire study. A comprehensive list of all the wells is documented in Appendix A.2.

1.4.2.2 Seismic Interpretation and Analysis

Seismic interpretation and analysis were carried out with the aid of the Schlumberger Petrel software using conventional seismic interpretation technique based on Mitchum et al., (1977). From the calculated synthetic seismograms and available formation tops, twelve (12) mappable horizons (including the opal-A/CT diagenetic boundary) were identified, which lie between the Base Cretaceous Unconformity (BCU) and the seafloor and defines the boundary between nine (9) Cenozoic stratigraphic sequences (CSU-1 to CSU-9: see Fig. 2.3 & 4.4a; Table 4.1 & 4.2) based on the northern North Sea stratigraphic framework of Jordt et al. (2000). However, four main stratigraphic boundaries have been mapped (see Fig. 4.5) corresponding to the Base Tertiary (BT)/Top Shetland Group (TSG), Top Balder (TB)/Top Rogaland Group (TRG), mid-Miocene Unconformity (MMU)/Top Hordaland Group (THG) and the Seafloor/Top Nordland Group (TNG). The interval of interest, which is characterized by different soft sediment remobilization and injection features, lies between the Top Hordaland Group and the Top Shetland Group.

TWT structure maps of the mapped horizons were produced and used to generate isochron (time-thickness) maps between the horizons (see Fig. 4.6), while seismic attributes (e.g., RMS amplitude, chaos, and variance; see Brown, 1996, 2001) were generated for the mapped horizons and time-shifted horizons (i.e., horizon slices) to image features of interest. For example, some of the seismic attributes have enabled the identification of a few depositional elements (e.g., channels and fans). However, their identification in most cases have been made difficult due to their complex stacking pattern and associated large-scale post depositional remobilization and injection. Other classical interpretation approach such as time slicing and surface flattening was applied where necessary (Andresen et al., 2019). For the time domain seismic data, direct depth conversion of TWT depths and TWT thickness have been carried out using the average interval velocities (see Table 1.1) obtained from the sonic log data for some of the key wells.

This study focuses on the occurrence of sand injectites in the northern North Sea (NNS) which are manifested as discordant or concordant amplitude anomalies within hundreds of meters of mudstone host interval. Some of these discordant amplitude anomalies were mapped by manual interpretation to show their 3D geometry (e.g., see Fig. 5.13, 6.4a, 6.11, 7.11 & 7.20c). However, due to their usual complex geometries, some could not be mapped, but their spatial and lateral distributions within the Cenozoic units have been outlined to show their occurrence. They have also been grouped into geometrical types following Huuse et al. (2007) and Cartwright et al. (2008) classifications which is based on their seismic expression and relationship to their inferred parent sand body and host strata.

Chapter 2

CHAPTER 2   Geological setting and general review of the occurrence of sediment remobilization and fluid flow features

2.1 Geological setting and Structural framework

The North Sea Basin, of Cenozoic age, is a largely unfaulted epi-continental basin formed as a thermal sag basin above failed Mesozoic rift structures associated with two main stages of rifting (lithospheric extension) events in the Permo – Triassic and in the Late Jurassic to Early Cretaceous (Table 2.1) (Badley et al., 1988; Ziegler, 1990; Jordt et al., 2000; Huuse et al., 2007), with each rifting episode followed by periods of post-rift thermal relaxation (i.e., thermal cooling) and subsidence (Gabrielsen 1986, Badley et al., 1988; Gabrielsen et al., 1986, 1990; Roberts et al., 1990; Ziegler, 1990,1992; Milton, 1993; Faerseth 1996; Faerseth et al., 1997; Christiansson et al., 2000). The North Sea is approximately 150 – 200 km wide and it is a wide zone of extended crust which separates the East Shetland Platform (to the west) from the Horda Platform (to the east) (Fig. 2.1). The Permo – Triassic and Late Jurassic – Early Cretaceous rifting episodes led to the formation of N-S striking, west dipping normal faults which are cross-cut by other large NE-SW and NW-SE trending normal faults with variable dip direction (Fig. 2.1) (Faerseth et al., 1995, 1997), majority of which became inactive after rifting ceased in the Late Jurassic – Early Cretaceous (Dmitrieva et al., 2012, 2018). The main rift structures within the North Sea Basin lies in the central and northern North Sea (i.e., Central Trough, the Outer Moray Firth, Southern Viking Graben and the North Viking Graben), which are characterized by large rotated fault blocks with sedimentary basins within N-S trending asymmetric half grabens associated with crustal extension and thinning (Fjeldskaar et al., 2004; Huuse & Mickelson, 2004). The North Sea is located to the south of the north-west European Atlantic margin which underwent continental break-up at the transition between the Paleocene and Eocene and experienced several episodes of thermal subsidence and inversion in the Cenozoic (Ziegler, 1990; Faleide et al., 2002; Huuse et al., 2007).

The study area is in the northern North Sea which is bounded by the Marulk Basin to the north, the Central & South Viking Graben to the south, the Norwegian mainland to the east, and the East Shetland Platform to the west (Fig. 2.1). This part of the North Sea Basin had a complex structural development, and its evolution and subsidence history are marked by four major well documented tectonic phases which include (Table 2.1; Dmitrieva et al., 2012): (a) the Caledonian orogeny (Late Ordovician or Early Silurian); (b) Permian to Triassic rifting and graben formation; (c) Mesozoic (Late Jurassic – Early Cretaceous) rifting and graben formation; and (d) Late Cretaceous to Recent thermal subsidence and inversion. The rift axis of the first rifting phase (Permo-Triassic) is believed to lie beneath the areas marginal to the Viking Graben (e.g., Horda Platform and the Magnus Basin – Unst Basin region) while the Late Jurassic – Early Cretaceous rift was centred mainly along the of the present-day Viking Graben and Sogn Graben (Badley et al., 1988; Christiansson et al., 2000). The Late Jurassic – Early Cretaceous rift episode was marked by rapid normal fault driven subsidence, reactivation of some older Permo-Triassic rift-related structures, and the formation of N-S trending graben and half-graben within the northern North Sea (Ziegler, 1982; Badley et al., 1988; Gabrielsen et al., 1990; Faerseth et al., 1997). The northern North Sea is characterized by predominant N, NE & NW trending large normal faults, with the eastern margin associated with Øygarden Fault Complex

of Permo-Triassic origin which is referred to as the most extensive (> 300 km) north-striking structural element offshore west Norway by Faerseth et al., (1995) and forms the boundary between the northern North Sea and Norwegian mainland. However, normal faults of Jurassic origin form the boundary between the northern North Sea and the East Shetland Platform to the west of the basin (Fig. 2.1).

In the earliest Cenozoic to Recent age, the northern North Sea experienced several episodes of uplift (Table 2.1) linked to igneous activity and the opening of the North Atlantic (Jordt et al., 2000; Dmitrieva et al., 2012). Studies have shown that most of this uplift occurred along the margins of the basin at three different periods: Late Cretaceous – Early Paleocene, Late Eocene – Early Oligocene and Late Pliocene – Pleistocene time (Jordt et al., 2000). This uplift along the basin margins resulted to large volume of coarse clastic sediments being delivered into the basin, leading to the development of depocentres during the Late Paleocene, Early Eocene, Early Oligocene, and Early Miocene time (Fig. 2.2a to 2.2c) along boundary faults (Mesozoic and older fault systems) (Jordt et al., 2000; Dmitrieva et al., 2012).

2.2 Cenozoic sedimentation in the northern North Sea

The Cenozoic succession in the northern North Sea represents post-rift infill, which resulted from subsidence, in response to thermal (lithospheric) cooling following the Late Jurassic – Early Cretaceous rifting event (Scalater &Christie, 1980; Nottvedt et al., 1995). The present-day sedimentary architecture within the northern North Sea is related largely to the uplifting of surrounding clastic source areas (i.e., Shetland Platform, southern Norway, and British Isles) in the Paleogene (Paleocene – Eocene) due to tectonic control on sediment supply (Jordt et al., 2000; Faleide et al., 2002). However, sedimentation in the northern North Sea have been documented to be affected by other factors (e.g., climate, climate change and eustatic sea level) asides tectonism, all of which influence sediment production and distribution (Goledowski et al., 2012).

More than 2 km of clastic sediments were deposited along the axis of the northern North Sea in the Cenozoic, with the deposition of hemi-pelagic, smectite-rich mudstones in the deeper parts of the basin (Huuse & Mickelson, 2004). Uplift of sediment source areas due to igneous activity and the North Atlantic rifting, resulted in the supply of large amount of coarse clastic sediments from the East Shetland Platform, British highlands and lesser from southern Norway resulting to the deposition of large prograding sand-rich fans and channel lobe systems in the Late Paleocene – Early Eocene (Ziegler, 1990; Hartog et al., 1993; Jordt et al., 1995; Ahmadi et al., 2003; Huuse & Mickelson, 2004)

Table 2.1 and Fig. 2.2 summarizes the processes leading to Cenozoic sedimentation at each time in the Paleogene, shows the direction of sediment influx into the northern North Sea and the major depocentres at each time based on the work by Faleide et al. (2002).

2.3 Litho-stratigraphic Framework

The lithostratigraphic framework of the North Sea is diverse and has been described by several authors till date, such as Deegan & Scull (1977), Isaksen & Tonstad (1989), Jordt et al. (1995, 2000), Faleide et al. (2002), Rundberg & Eidvin (2005) and Annel et al. (2012). The lithostratigraphy of the central and northern North Sea was extensively described by Deegan & Scull (1977), while Isaksen & Tonstad (1989) published a revised edition of the Cretaceous and Cenozoic succession based on the previous work by Deegan & Scull (1977). However, the Norwegian Offshore Stratigraphic Lexicon (NORLEX) project has led to the adoption of an updated regional offshore lithostratigraphy of the northern North Sea which was based on updated geologic information.

The northern North Sea Basin comprises of post-rift sequences of Cenozoic age (c. 2 km thick) which are characterized by coarse grain, deep water deposits along the eastern margin, and hemi-pelagic, smectite-rich mudstone-dominated succession in the distal part of the basin (Jordt et al., 2000; Dmitrieva et al., 2012). The post-rift sequences have been subdivided into (Fig. 2.3): (a) Cretaceous age: Cromer Knoll and Shetland Groups, and (b) Cenozoic age: Rogaland, Hordaland, and Nordland Groups (Isaksen & Tonstad, 1989).
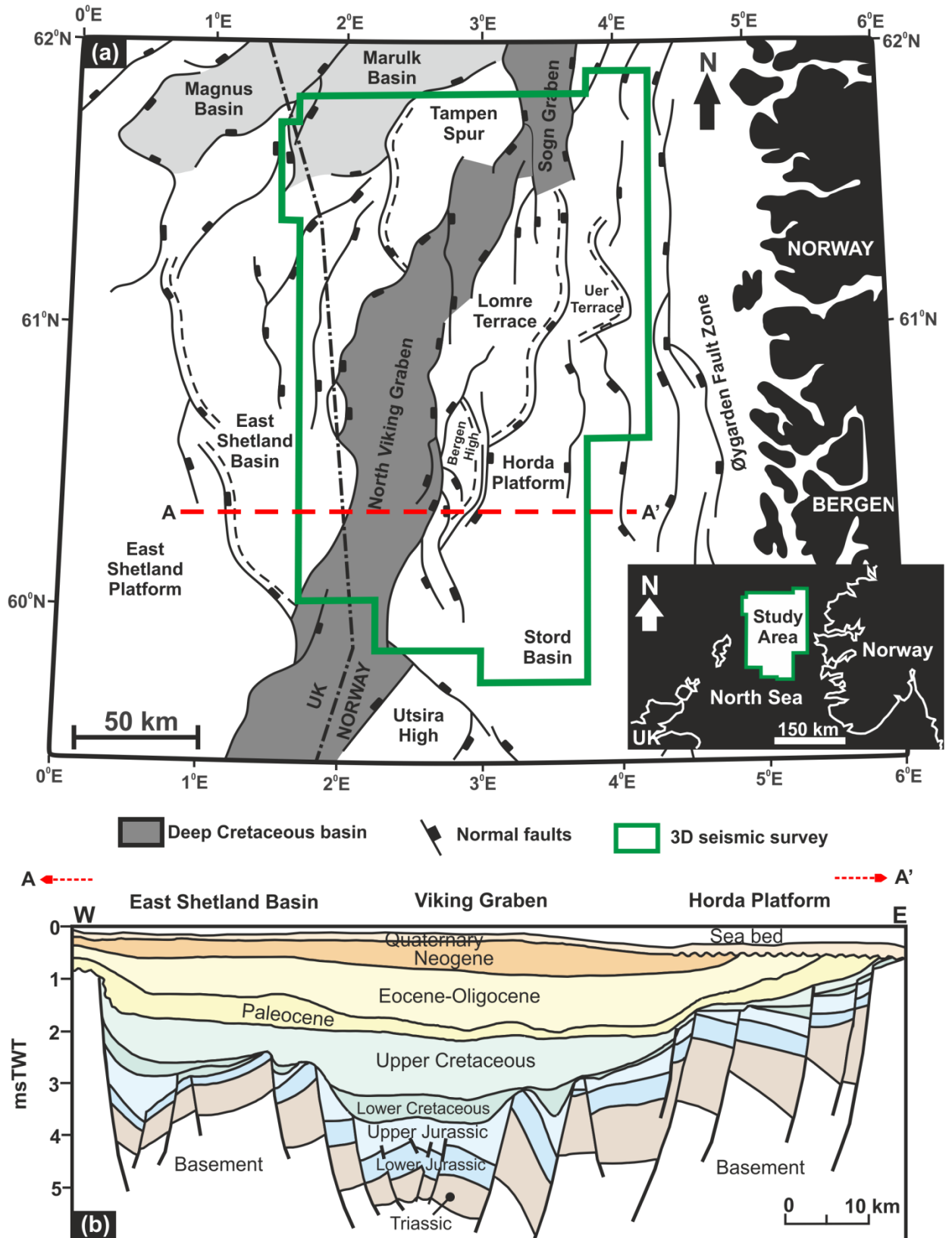
Fig. 2.1: (a) Map showing the major structural elements of the northern North Sea (modified after Nottvedt et al., 1995). (b) Regional cross-section through the study area showing faults and half-grabens related the Mesozoic rift structures. This also shows the chronostratigraphic division of the sedimentary succession in the study area (modified after Husmo et al., 2003).

Table 1.1: General summary of stages of rifting and events within the northern North Sea Basin, leading up to its present-day geomorphology and sedimentary infill.

	AGE	ASSOCIATED EVENTS/OCCURRENCE
Uplift	Pleistocene	**Glaciation** (Sejrup et al., 1996; Fyfe et al., 2003; Anell et al., 2012)
	Pliocene	**Stacking/progradation of clinoforms i.e., outbuilding of thick clastic wedges** (Faleide et al., 2002; Anell et al., 2012)
	Miocene	**Uplift and Erosion; tectonic subsidence** (Kyrkjebo et al., 1999; Faleide et al., 2002)
	Oligocene	**Transition from greenhouse to icehouse environment, uplift and sedimentation continued** (Jordt et al., 2000; Zachos et al., 2001; Anell et al., 2012)
Uplift	Eocene	**Opening of the Norwegian – Greenland Sea and North Atlantic, uplift along eastern margins and sedimentation with development of depocentres** (Den Hartog Jager et al., 1993; Jordt et al., 2000; Faleide et al., 2002; Ahmadi et al., 2003; Jones et al. 2003; Goledowski et al., 2012)
Uplift	Palaeocene	**Uplift and massive volcanism associated with North Atlantic rifting, tectonic subsidence, and sedimentation with development of depocentres** (Martinsen et al., 1999; Jordt et al., 2000; Brekke et al., 2001; Faleide et al., 2002; Dmitrieva et al., 2012)
Post-rift subsidence	Cretaceous	**Post-rift thermal subsidence and infill; continuous sediment loading** (Badley et al., 1984; Gabrielsen et al., 1990; Ziegler, 1990; Jordt et al., 2000; Gabrielsen et al., 2001; Bugge et al., 2001; Goledowski et al., 2012)
	Late Jurassic	**Second rift phase i.e., extensive rifting** (Badley et al., 1988; Ziegler, 1990; Gabrielsen et al., 1990; Roberts et al., 1990, 1995; Faerseth et al., 1996, 1997)
Rifting	Early – Mid Jurassic	**Thermal doming/subsidence** (Ziegler 1982; Badley et al., 1988; Gabrielsen et al., 1986, 1990)
Rifting	Late Palaeozoic - Triassic	**First rift phase; terrestrial to marine sedimentation** (Badley et al., 1988; Ziegler, 1990; Gabrielsen et al., 1990; Roberts et al., 1990, Jordt et al., 1995; Faerseth et al., 1996, 1997)
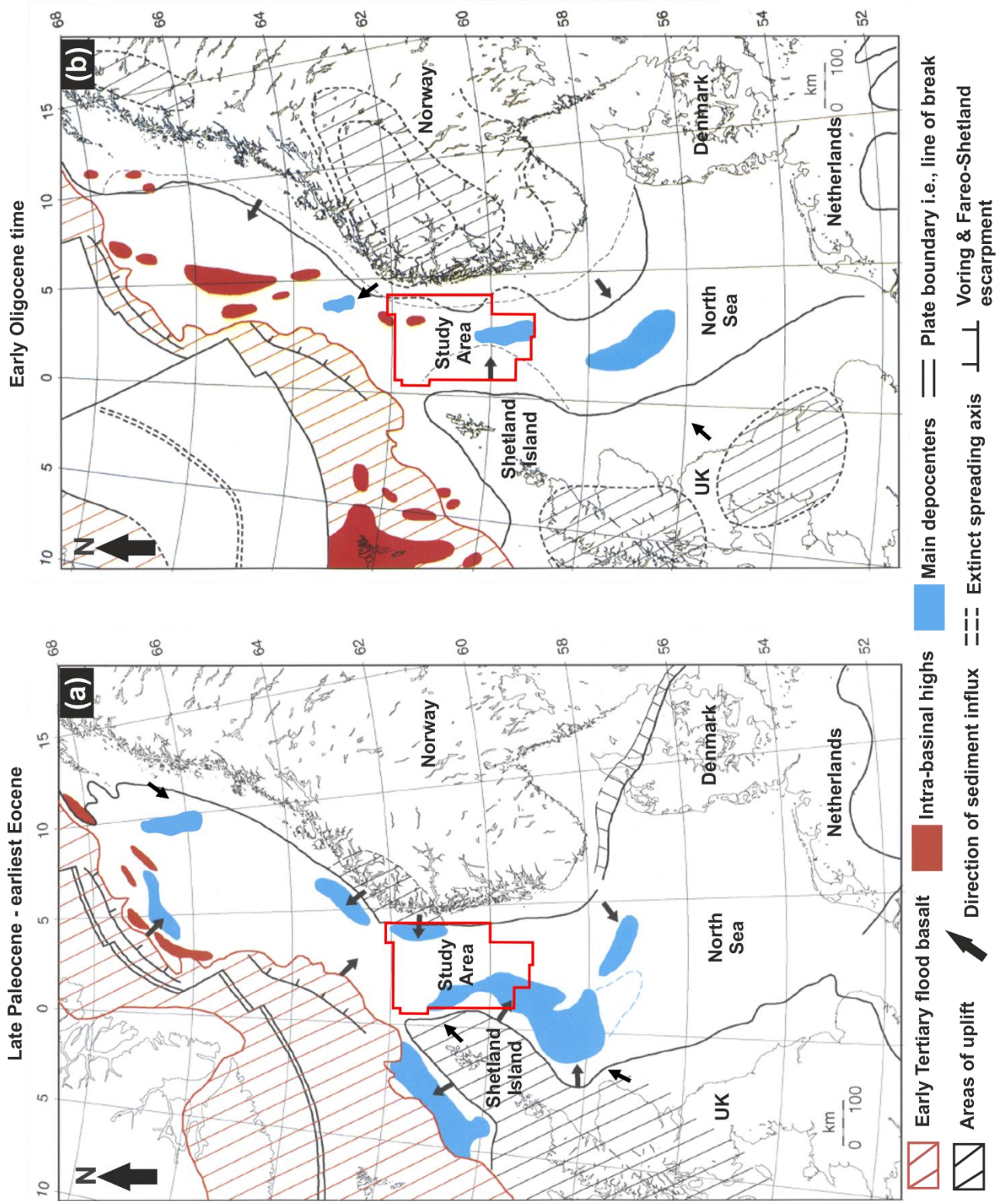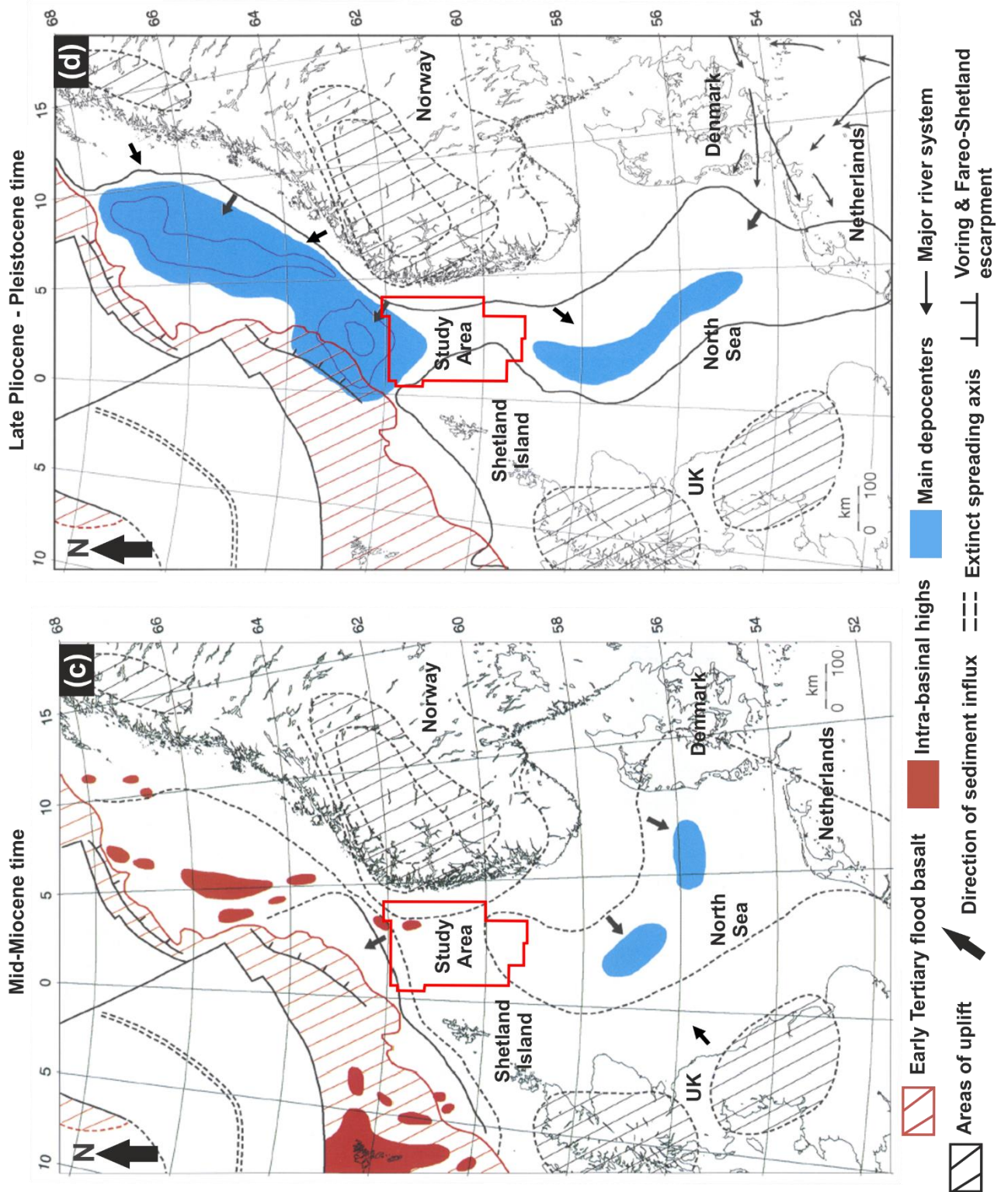
Fig. 2.2: Regional setting of the northern North Sea in the: (a) Late Paleocene to earliest Eocene time, (b) Early Oligocene time, (c) Mid-Eocene time, (d) Late Pliocene to Pleistocene time. Red outlines show the location of the study area (modified after Faleide et al., 2002).

A) Cromer Knoll and Shetland Groups

The Cromer Knoll Group, which is of Early Cretaceous age, consists of fine grained, argillaceous, marine sediments with varying content of calcareous material (calcareous claystone, siltstone, and marlstone) (Deegan & Scull, 1977; NPD, 2018). The group is widely distributed in the Norwegian sector of the North Sea but varies in thickness and are absent in the Lomre Terrace (in the Troll area) and Tampen Spur. However, it is of greater thickness in the Sogn Graben, northern North Sea with an approximate thickness of about 400 m (Deegan & Scull, 1977; NPD, 2018).

The Shetland Group, which is of Late Cretaceous age, consists of mainly chalky-limestone, limestone, marls, and calcareous shales & mudstones. The group are typically developed in the central and northern North Sea (Fig. 2.3) and are present throughout the Norwegian sector of the North Sea (Deegan & Scull, 1977; NPD, 2018). Its chalk facies occur mainly in the central North Sea while its siliciclastic facies are more developed in the northern North Sea (Deegan & Scull, 1977), with its thickness ranging between 1 – 2 km in the graben areas (Deegan & Scull, 1977; Isaksen & Tonstad, 1989; NPD, 2018)

B) Rogaland Group

This overlies the Shetland Group and consists of a 900 m thick interval in the Norwegian sector of the North Sea (Isaksen & Tonstad, 1989; Dmitrieva et al., 2018). The group is of Paleocene – Lower Eocene age and overlies the Shetland Group across a major unconformity (Fig. 2.3) suggested to have formed in relation to tectonic uplift of the Norwegian mainland during the Early Paleocene (Mudge & Bliss, 1983; Martinsen et al., 1999; Faleide et al., 2002; Annel et al., 2012; Dmitrieva et al., 2012). The Rogaland Group is widely distributed in the central and northern North Sea, and generally consists of argillaceous marine sediments (Deegan & Scull, 1977; NPD, 2018). In the Norwegian sector of the North Sea, the group consists of mainly proximal sediments (sandstone inter-bedded with shales) in the west and are sub-divided into the Vale and Lista Formations (Fig. 2.3), which are Paleocene in age, and the Sele and Balder Formations which are Eocene in age (Deegan & Scull, 1977; Dmitrieva et al., 2012, 2018).

The upper boundary of the Rogaland Group which is a well-known regional marker horizon across the North Sea Basin is represented by the top of the Balder Formation of Ypresian age. The Balder Formation comprises of tuffaceous deposits (Fig. 2.3) consisting of laminated tuffaceous shales and thin limestones (Jordt et al., 1995, 2000; Anell et al., 2012; Dmitrieva et al., 2012). In the North Viking Graben, thick sandstones are developed within the Vale and Lista Formations. The sandstone member of the Vale Formation is informally ascribed to the Egga Sandstone Member (Fig. 2.3) while that of the Lista Formation is the Sotra Sandstone Member (see Dmitrieva et al., 2012: their Fig 3a; Dmitrieva et al., 2018: their Fig 3).

C) Hordaland Group

This overlies the Rogaland Group, and it is of Eocene to Early Miocene age both in the North Sea and Norwegian Sea (Deegan & Scull, 1977; NPD, 2018). The group is widely distributed over most of the North Sea Tertiary Basin but are incomplete along basin margins due to erosion and non-deposition (Deegan & Scull, 1977; NPD, 2018). It is bounded above and below by the well-known Mid-Miocene Unconformity (MMU) and the Top tuffaceous Balder Formation respectively (Fig. 2.3). In the northern North Sea (e.g., North Viking Graben), the group reaches a thickness of a few hundred meters and consists of light grey to brown marine claystones with inter-bedded sandstones (NPD, 2018). The Hordaland Group is sub-divided into four formations which are: the Frigg sandstone, Grid, Skade and Vade Formations. The Grid and Skade Formations are found mainly in the Viking Graben area, while the Vade Formation is widely distributed in the central Graben (Isaksen & Tonstad, 1989; NPD, 2018). Along the western basin margin, large sand-rich units were supplied into the basin from the Shetland Isles in the Early Eocene time (Jordt et al., 2000; Anell et al., 2012; Goledowski et al., 2012). One of such sandstone forms the sand reservoir in the Frigg Field.

However, based on the Norwegian Offshore Stratigraphic Lexicon (NORLEX), the Hordaland Group within the east Viking Graben area is divided into the Lark Formation (comprising of two sandstone members: the Skade Sandstone Member and an unnamed Sandstone Member) and the Horda Formation (Rasmussen et al., 2008; Goledowski et al., 2012; Olobayo, 2014). The Horda Formation forms the most abundant Eocene formation in the North Sea (Goledowski et al., 2012).

Era	Period	Epoch	Groups	Cenozoic Seismic Units (modified after Jordt et al., 2000)	Northern North Sea Lithostratigraphy	Geologic events	Post-depositional remobilization and fluid flow products
CENOZOIC	QUATERNARY	Holocene	Nordland	H12 / CSU-9	Naust Fm	Sedimentation & Glaciation	
		Pleistocene 2.6		H11 / CSU-8 / H10	Unnamed	Glaciation with increase in sedimentation rate	
	NEOGENE	Pliocene 5.3		CSU-7 / H9	Unnamed / Unnamed	Erosion	
		Miocene 23		CSU-6 / H8 (MMU) / CSU-5 / H7	Utsira / Skade	Miocene compression with the NNS exposed and eroded	Sand intrusions
	PALEOGENE	Oligocene 34	Hordaland	CSU-4 / H6 Opal A/CT / H5 / CSU-3 / H4	Lark Fm / Ull	Deposition of Paleocene to Lower Miocene mudstones and sandstones	
		Eocene 56		CSU-2 / H3	Grid / Horda Fm / Frigg / Balder Fm / Sele Fm		
		Paleocene 65	Rogaland	CSU-1 / H2	Lista Fm / Sotra / Vale Fm / Egga	Uplift and Volcanism / Thermal subsidence & Sedimentation	Polygonal faults
MESOZOIC	CRETACEOUS	Upper 100.5	Shetland	KSU-1	Jorsalfare Fm / Kyrre Fm / Tryggvason Fm / Svarte Fm	Post rift thermal subsidence and continuous sediment loading	
		Lower 145	Cromer Knoll	BCU (H1)	Rodby Fm / Sola Fm / Agat / Asgard Fm / Mime Fm	Jurassic to Cretaceous rift phase (2nd Rift Phase)	

Legend: Mudstone, Sandstone, Tuff, Unconformity, Carbonate stringers, Remobilized & injected Sandstone

Fig. 2.3: Simplified lithostratigraphic column through the studied succession (modified after Jordt et al., 2000; Olobayo, 2014). Also highlighted are the significant geologic events and post-depositional remobilization and fluid flow products identified in the study area.

D) Nordland Group

The Nordland Group is the topmost and youngest of the post-rift lithostratigraphic group in the North Sea. It is suggested to be of Middle Miocene to Recent age in the North Sea, Early Miocene to Recent in the Norwegian Sea and Late Pliocene to Pleistocene/Holocene in the Hammerfest Basin (NPD, 2018). In the North Sea, the group is dominated by marine claystones with its uppermost part consisting of unconsolidated clays, sands, and glacier deposits (Deegan & Scull, 1977; NPD, 2018). Its lower boundary is represented by the Mid-Miocene Unconformity (MMU) which represents a significant period (approx. 15 Ma) of non-deposition and erosion (Isaksen & Tonstad, 1989; Martinsen et al., 1999; Jordt et al., 2000; Runberg & Eidvin, 2005; Løseth et al., 2013; Olobayo, 2014). The MMU forms a pronounced surface both in deep water basins and on basin margins of the North Sea (Brekke, 2000; Løseth & Henriksen, 2005; Goledowski et al., 2012). In the northern North Sea, the MMU (Fig. 2.3) is directly overlain by the shallow marine, shelf sandstone of the Utsira Formation (Late Miocene – Early Pliocene age) and marks the base of the Nordland Group (Deegan & Scull, 1977; Isaksen & Tonstad, 1989; Martinsen et al., 1999; Runberg & Eidvin, 2005).

2.4 Petroleum System

The North Sea Basin is known as one of the most petroliferous basins in the world, and it is a well-known hydrocarbon province with a petroleum system which has been active throughout the Cenozoic (Huuse & Mickelson, 2004; Olobayo, 2014). The petroleum system elements within the northern North Sea are described below and Fig. 2.4 shows their relative ages.
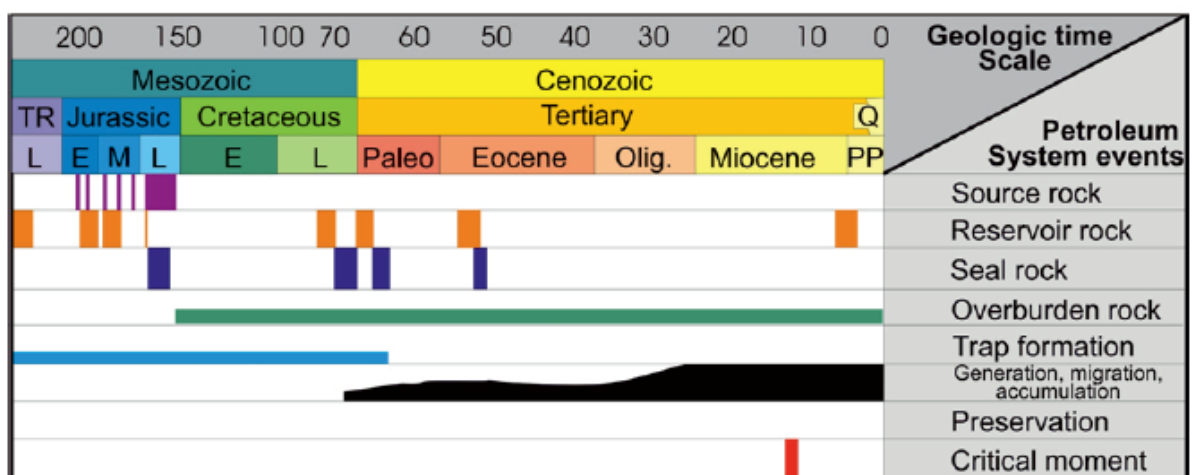
Fig. 2.4: Event chart of the northern North Sea (Northern Viking Graben) Petroleum system (After Kubala et al., 2003 and Schlakker et al., 2012).

a) Source Rock

Basically, all significant oil and gas accumulations in the northern North Sea, which hosts a vast productive hydrocarbon province, are believed to have been generated by the fine-grained, organic carbon-rich marine shales of the Late Jurassic and earliest Cretaceous age (Goff, 1983; Ulmishek & Klemme, 1991). The main source rock in the North Sea is the Kimmeridge Clay Formation of Late Jurassic age (Late Oxfordian - Ryazanian) in the UK sector of the North Sea, which also has its age equivalent referred to as the Draupe Formation in the Norwegian sector (Kubala et al., 2003; Olobayo, 2014). The organic carbon-rich Kimmeridge shales accumulated in a low oxygen rift basin, with a total organic carbon (TOC) content of approximately 2 – 15% and are easily identified from their high gamma ray log signature (Kubala et al., 2003). Other known potential source rocks include the Heather Shale Formation, the lean organic shales of the Dunlin (Mid Plensbachian) and the middle Jurassic coal-bearing Brent Group, all of which have a high potential for gas and limited potential for oil (Coward et al., 2003; Kubala et al., 2003)

Most of the organic carbon-rich source rocks became thermally mature for oil/gas generation between the Early Cretaceous to Neogene age (Fig. 2.4). Maturity modelling of the North Sea has shown that the primary source rock (Jurassic Kimmeridge Clay Fm) actively generated hydrocarbons in the deepest parts of the central and northern North Sea in the Paleogene, and as such providing hydrocarbon charge to the basin (Conford, 1998; Johnson & Fisher, 1998; Lonergan et al., 2000). The Paleogene is suggested to have been characterized by early oil generation with peak oil and gas generation in the Late Paleogene – Early Neogene and Late Neogene – Quaternary respectively (Huuse & Mickelson, 2004).

b) Reservoir

The most important reservoir rocks in the North Sea are the Triassic and Lower – Middle Jurassic sandstone reservoirs, as well as the Brent Group deposited prior to the Late Jurassic rifting (Gautier, 2005). In the Northern Viking Graben, the main reservoirs constitute mainly Middle to Late Jurassic shallow marine sandstones which are suggested to be sourced by either the Draupe Formation or Heather Formation (for oil) and/or the Brent Group (for gas) (Kubala et al., 2003; Olobayo, 2014). Some authors like Johnson & Fisher (1998), Pegrum & Spenser (1991) and Gautier (2005) grouped the North Sea reservoirs into four groups with respect to the timing of major rift episodes in the basin. They include:

- **Pre-rift Reservoirs of Pre Jurassic age:** these pre-rift Jurassic reservoirs of Pre-Jurassic age are suggested to contain a little fraction of the North Sea hydrocarbon (Gautier, 2005). These pre-rift reservoirs (Triassic to Lower Jurassic) consist of thick fluvial sandstones of the Upper Jurassic Lunde Formation and the Upper Triassic – Lower Jurassic Statfjord Formation. The largest producing hydrocarbon field in the North Sea which produces from Pre-Jurassic reservoirs is the Snorre Oil Field (Fig. 2.5), located in

the Norwegian sector of the northern Viking Graben whose reservoirs are found in tilted fault blocks (Pegrum & Spenser, 1990; Gautier, 2005)

- **Pre-rift Reservoirs of Early & Middle Jurassic age:** these pre-rift reservoirs of Early and Middle Jurassic age are known to contain high accumulation of hydrocarbon in the vast productive hydrocarbon province in the Viking Graben (Gautier, 2005). These reservoirs constitute the marginal marine to non-marine fluvial sandstones and the upper shore-face/shallow marine/delta front/delta-top sandstones of the Statfjord Formation and the Brent group respectively (Gautier, 2005). The Brent Group sandstone constitute the main producing Middle Jurassic reservoir in most fields (e.g., Fig. 2.5: Brent, Dunlin, Gullfaks, Heather, Hutton, and Statfjord) in the North ViKing Graben (Gautier, 2005).

- **Syn-rift reservoirs of Late Jurassic age:** these constitute reservoir rocks deposited during maximum extension and are well developed in areas like the Central Graben, Southern Viking Graben (submarine fans of the Brae Formation) and Outer Moray Firth/Witch Ground (shallow marine transgressive sandstones of the Piper Formation) (Gautier, 2005). They form producing reservoirs in the Troll Field and Magnus Field in the Viking Graben (see Fig. 2.5)

- **Post-rift reservoirs:** they include reservoirs of Early Cretaceous to Eocene age, with Cretaceous and earliest Paleocene reservoirs composed of mainly chalk with high porosity and low permeabilities (Scholle, 1977; Gautier, 2005). However, Paleocene sandstone reservoirs are known to occur in the Central Graben and South Viking Graben which were deposited as massive, channelized gravity flow deposits (Gautier, 2005). Some well-known fields with Paleocene reservoirs include (Fig. 2.5): the Forties, Maureen, Frigg, Montrose, Heidal and Arbroath (Abbots, 1991; Gautier, 2005).

c) Traps & Seals

The main traps consist of structural traps: horst/graben structures and fault-related structures (e.g., tilted fault blocks), formed during the rifting episode. These structures form most of the well-known hydrocarbon fields such as: Snorre, Troll, Gullfaks, Stratfjord and Brent (Fraser et al., 2003; Olobayo, 2014). However, some hydrocarbons are trapped in submarine channels and fan complexes deposited during the syn-rift and post-rift sedimentation periods (Gautier, 2005).

The sealing lithology comprises of thick, fine-grained, marine Jurassic to Cretaceous mudstones, marls, and chalk (?). The Cretaceous shales/mudstones are known to provide regional seal which is believed to coincide with the development of overpressure above deep graben centres reflecting restricted pore water escape (Burley, 1993).
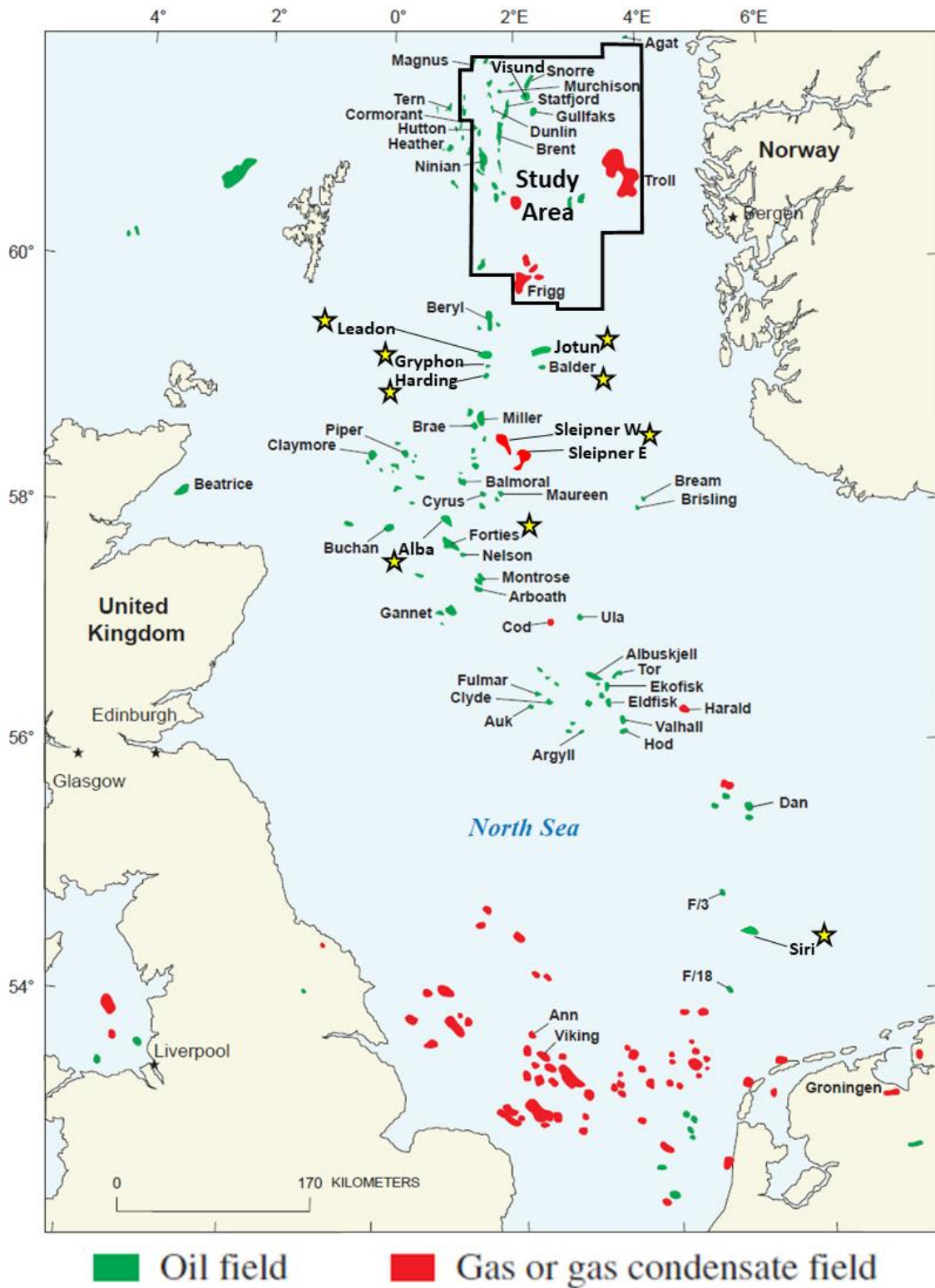
Fig. 2.5: North Sea prominent oil and gas fields, with yellow star showing fields (see Table 2) with documented occurrence of sand injectite reservoirs (modified from Gautier, 2005). Black outline shows the outline of the 3D seismic survey in the study area.

d) Migration

Oil and gas migration within the northern North Sea is believed to have occurred either laterally, stratigraphically downwards and vertically upward through high permeable rocks and fractures of pre-rift, syn-rift, and post-rift ages (Gautier, 2005), with the timing of oil generation and migration ranging from the Late Cretaceous to Recent (Barnard & Bastow, 1991). Huuse & Mickelson (2004) suggested that migration pathways range from strike-slip faults and fractures which are related to underlying structures. It is also believed that the main mechanism for migration in the northern North Sea involves short distance migration due to juxtaposition of source rocks and reservoirs, as well as migration in the rotated fault blocks and along the major half-graben bounding faults (Barnard & Bastow, 1991; Gautier, 2005).

2.5 Review of literature on sediment remobilization and fluid flow in the northern North Sea

2.5.1 Introduction to sediment remobilization and injection

The term remobilization refers to the deformation of clastic sediments in the subsurface during early burial, which usually involves the vigorous or rapid injection of sandy sediments into fine-grained host rock (i.e., mudstone) (Lonergan et al., 2000). In a broader sense, this includes the various processes involved in the redistribution of sand by injection, and the potential extrusion of sand on the sea floor after they were previously deposited (Brooke et al., 1995; Lonergan et al., 2000; Hurst et al., 2011). Post-depositional sand remobilization and injection is recognized to be an important process in deep water clastic systems (Huuse et al., 2007), and features associated with these process have been documented in sedimentary basins globally, especially in the Paleogene of the central and northern North Sea where large-scale sand intrusions are well documented and are known to have significant impact on reservoir geometries and fluid flow within the interval they occupy (Huuse at al., 2007; Lonergan et al., 2000). Previously, the North Sea Tertiary deep water sandstone bodies were interpreted as low-stand fans, mounded fans, and isolated channel complexes based on the assumption that they reflect a primary depositional origin (Fig. 2.6; Den Hartog Jager et al., 1993; Lonergan et al., 2000). However, detailed study and investigation based on high resolution seismic data, with integration of well data and outcrop data has revealed that some of these Paleogene deep water sandstone reservoirs have undergone post-depositional remobilization and injection, with the intrusions impacting on the morphology and distribution of important reservoir units (like in the Alba, Forth/Harding, Balder, Gryphon and Volund fields) (Dixon et al., 1995; Lonergan & Cartwright, 1999; Lonergan et al., 2000; Duranti et al., 2002; Huuse et al., 2003; Huuse & Mickelson, 2004; Huuse et al., 2007). As such, it has been realized that remobilization produces a range of

complex sand geometries which are distinctly different from those predicted by traditional depositional models (Lonergan et al., 2000).

The products derived from post-depositional remobilization and injection in the North Sea are generally classified as: remobilized, injected and/or extruded sandstones as shown in Fig. 2.7 which illustrates the three suggested models for the occurrence of sandstone in the North Sea Basin (Lonergan et al., 2000; Huuse et al., 2009: AAPG). Sand intrusions and extrusions form part of the organized forms of subsurface sediment remobilization and fluid flow products (Fig. 2.8) as described by Huuse et al. (2010). These sand intrusion and extrusions, together with other products (such as mud volcanoes, mass transport deposits, focused fluid-flow pipes and polygonal fault systems, etc.) are collectively referred to as fluid flow features because their formation require that a significant volume of fluid (either pore water or hydrocarbon) be added to unconsolidated sediments to facilitate fluidization, resulting to the remobilization and injection of sediments (Løseth et al., 2003; Cartwright, 2007; Løseth et al., 2009; Huuse et al., 2010; Andresen, 2012; Olobayo, 2014).

Some of these remobilization and fluid flow products are discussed in detail below with particular emphasis on those found within the Palaeogene succession in the study area.
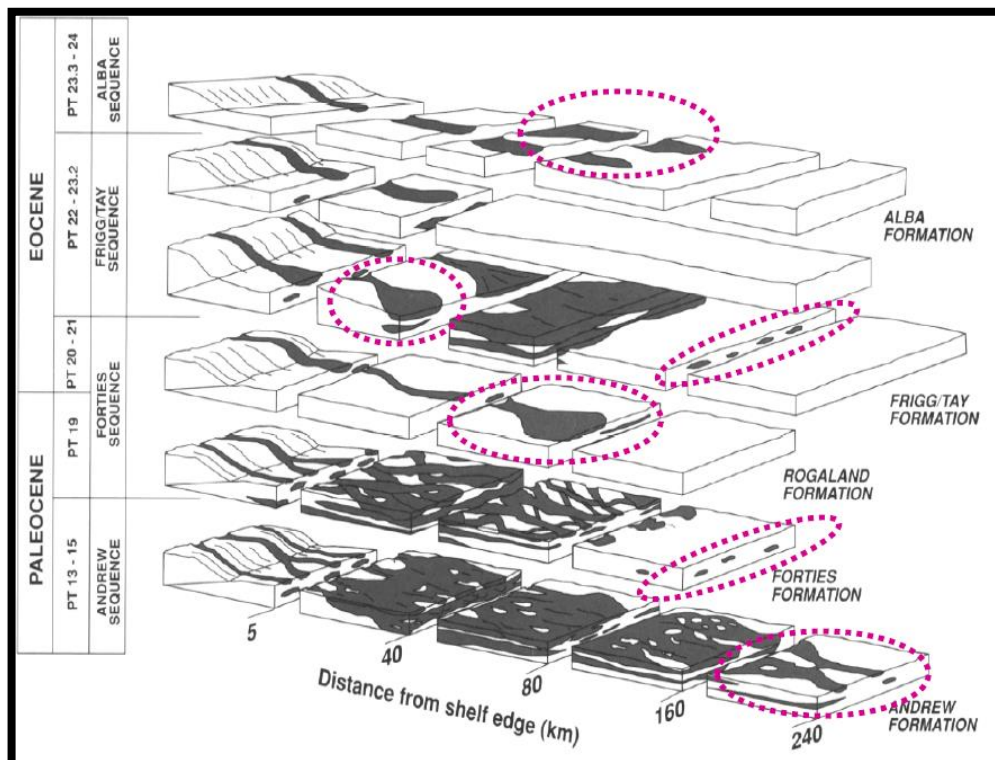
Fig. 2.6: Previous interpretation of North Sea Paleogene sandstone reservoirs as low-stand fans, mounded fan, and isolated channel complexes (Huuse et al., 2009, AAPG).
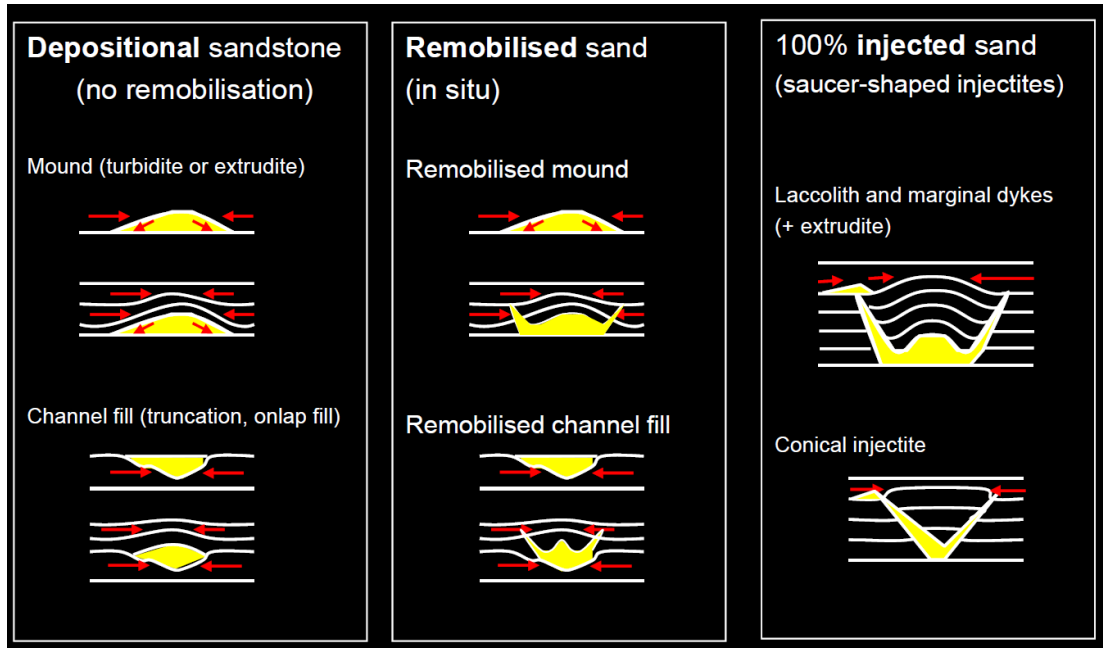
Fig. 2.7: Seismic stratigraphy models for the occurrence of sandstone in the North Sea Basin. Ranges from depositional model formed by gravity driven processes to remobilized and injected model formed due to sandstone remobilization and injection caused by post-depositional processes (Huuse et al., 2009, AAPG).
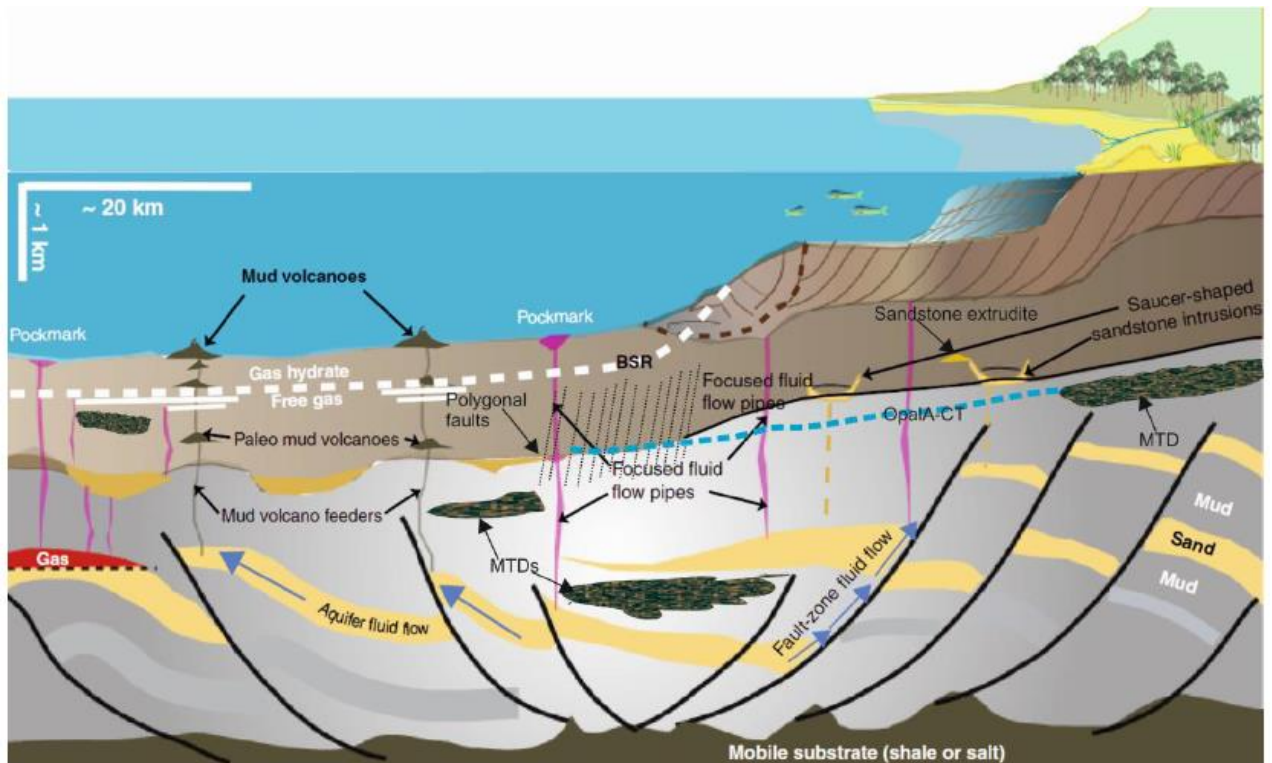
Fig. 2.8: Sediment remobilization and fluid flow products associated with typical continental basin margins. MTD – Mass Transport Deposits, BSR – Bottom Simulating Reflector (Huuse et al., 2010; modified by Olobayo, 2014).

2.5.2 Sand Injectites or Sandstone Intrusions

2.5.2.1 Introduction and Early Recognition

Sand injection is known to occur when fluidized sand is forcibly injected into a mudstone host stratum, resulting to the formation of a network of intrusions (Hurst et al., 2003; Hurst et al., 2011). They are suggested to form by fluidization of sand, usually in response to the failure of a low permeable sealing lithology caused by hydraulic fracturing, which results to either upward and/or lateral escape of fluid (Hurst et al., 2005). Sand dikes and sills (also referred to as sand injectites) are recognized in outcrop and subsurface data in several geodynamic and geological settings globally within the stratigraphic record (Fig. 2.9; Hurst et al., 2011). They are found in almost all sedimentary environments but have been mostly reported or documented in deep water settings and comprises mainly of fine to medium grained siliciclastic sand (Hurst & Cartwright, 2007; Hurst et al., 2011). Sand injectites comprises of mostly clastic dikes and sills, as well as irregular shaped sands some of which are genetically related and are formed within depositional sand bodies during sand remobilization (Hurst et al., 2003; Hurst et al., 2005; Hurst & Cartwright, 2007). These sandstone intrusions occur in centimetres to several kilometres in scale, and exhibit different geometries ranging from the normal dikes and sills which cross-cut beddings at different angles, to lensoid bodies with interconnected sill-like protrusions referred to as 'Wings' (Huuse et al., 2003), which are fundamentally different in morphology and geometry from most known depositional clastic reservoirs (Hurst et al., 2003, 2005; Cartwright et al., 2008)

They were first recognized as far back as the 19th Century and have been studied by many authors till date (e.g., Jenkins 1930; Braccini et al., 2008; Hurst et al., 2011: see their Appendix A - F). These sand injectites were previously considered as mere geological oddities and ignored by E&P companies until the mid-1980s when it was realized through further extensive studies that they may have significant impact on hydrocarbon exploration and production (Braccini et al., 2008; Hurst & Cartwright, 2007). In the early stage of their observation, these clastic intrusions were believed to have formed only when large cracks which open to the surface get filled by sediments from above, as was the case for Neptunian dikes formed when high pressure from glaciers or other depositional loads force sediments downward into underlying layers (Braccini et al., 2008). However, an investigation of sandstone dikes in northern California in 1899 brought about the conclusion that these intrusions may have intruded from below (Braccini et al., 2008).

Sand injection occurs from a few meters burial depth to about 700 m burial, but usually between 300 – 350 m burial depths (Hurst et al., 2003). Sand injectites are known to occur in millimetre to kilometre scale, and have been observed in borehole cores, borehole image logs, aerial photographs, satellite images and above all in high resolution seismic data (Huuse & Mickelson, 2004; Braccini et al., 2008). Due to improved resolution, high resolution seismic imaging now makes it possible for geoscientists to visualize the three-dimensional (3D) geometries of subsurface intrusions, revealing sand-rich reservoir features that cross-cut

stratigraphy and appear as an extension of other deeper depositional (parent) sand bodies (Hurst & Cartwright, 2007). Sand injectite facies were previously either unidentified or misidentified or misinterpreted (e.g., as debris flow deposits: Anderton, 1997), which led to their effect on reservoir geology (i.e., architecture, properties, and connectivity) and reserve distribution to be largely ignored. However, the criteria for the identification of sand injectites in seismic (e.g., Huuse et al., 2003), core (e.g., Duranti & Hurst, 2004), and outcrop data (e.g., Duranti et al., 2002; Hurst et al., 2011: see their Appendix A - F) has become widespread, and the reserve associated with them being considered as exploration targets (e.g., in the North Sea Paleogene).

Outcrop exposures of injectites have been used by geologists and E&P professionals as analogs to model possible occurrences of injectite features observed in the subsurface (Braccini et al., 2008; Hurst et al., 2011). Some well-known outcrop analogs of sand injectites which are comparable to the scale observed in the subsurface occur in: **(a) the Cretaceous dike and sill complex exposed in the Moreno Formation of the Panoche Hill in California (Fig. 14a: G & H), also referred to as the Panoche Giant Injectite Complex** (Braccini et al., 2008; Hurst et al., 2011)**; (b) near the Santa Cruz coast in California** (Boehm & Moore, 2002; Thompson et al, 2007; Huuse et al., 2007)**; (c) at Tabarka, Tunisia; and (d) the Magallanes Basin (Upper Cretaceous Cerro Toro Fm), southern Chile** (Braccini et al., 2008)**; (d) Tumey Giant Injectite Complex, Kreyenhagen Shale (Eocene) of the Tumey Hill, western United States; and (e) the ''Amphitheatre of Injectites''** within **the Tierra Loma Member, Dosados Canyon.** Other analogs for large-scale sandstone intrusions are found in: **The Blue Marl Formation (Aptian-Albian) Southern France** (Pavize & Fries, 2003; Huuse et al., 2007)**, Ordovician in Ireland** (Lonergan et al., 2000)**, Cretaceous sequence in the Sacramento Basin, California, Upper Jurassic Hareelv Formation of southwest Greenland** (Surlyk & Noe-nygaard, 2001; Surlyk et al., 2007; Huuse et al., 2007), **Miocene Frimmersdorf Seam in the Lower Rhine Embayment** (Prinz & McCann, 2019) and **the Tertiary clastic dikes of the Chilean fold and thrust belt** (Winslow, 1983).

The significance of clastic intrusions in sedimentary basin analysis is progressively becoming obvious. For example, they can give an insight on the possible timing of basin scale fluid flow events, as well as periods of overpressure development and catastrophic release (Cartwright, 2010; Jackson & Sømme, 2011). It has also been observed that most depositional sand bodies have connections to injectite and as such, injected sandstones can: (1) add volume to a reservoir; (2) can improve connectivity or inter-reservoir communication; (3) can indicate seal failure; (4) act as a new style of trap (intrusive trap); and (5) also serve as a high porosity fluid migration pathway (Dixon et al., 1995; Lonergan et al., 2000; Braccini et al., 2008). Overall, large scale sand remobilization and injection can lead to significant changes in reserves estimation and risking, as well as have both positive and negative impact on hydrocarbon prospectivity. This have been proven to a very large extent by observations in several Paleogene reservoirs in some North Sea oil fields such as Alba (Duranti et al, 2002; Braccini et al., 2008), Balder (Bergslien 2002; Bergslien et al., 2005), Gryphon (Purvis et al, 2002; Braccini et al., 2008), Gamma (Huuse et al., 2004) and Forth/Harding (Dixon et al., 1995).

The general review presented here tries to cover a bit of more than a century-old published literature and research (e.g. Hurst et al., 2011: see their Appendix A - F) on the occurrence of sand injectite. More detail about their formation, recognition (outcrop & subsurface), mechanics and implication for hydrocarbon exploration and production is further discussed below.
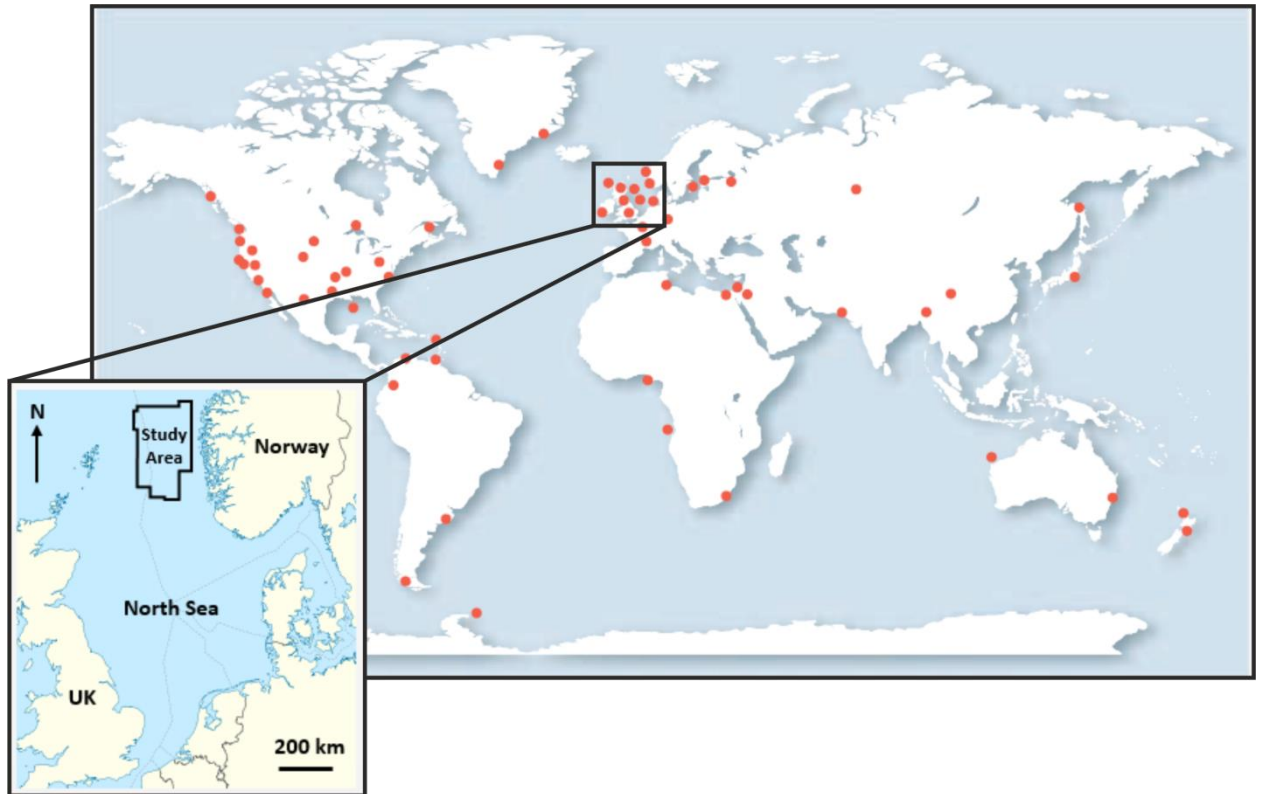
Fig. 2.9: Global occurrence of sand intrusions observed from both outcrop and subsurface data (modified after Braccini et al., 2008). The location of study is shown in the inset map.

2.5.2.2 Geological settings in which Clastic Intrusions occur (North Sea Example)

Clastic intrusions (especially dikes) are found across a range of sedimentary environments and are well documented in all sedimentary environments in many basins globally. This range of environments includes (Fig. 2.10; Jolly & Lonergan, 2002): fluvial (Oomkens, 1966; Plint, 1985); lacustrine (Martel & Giblings, 1993); deltaic, tidal & coastal (Dionne 1976; Hardie, 1999); glacial (Johnston, 1993); offshore shallow marine (Johnson, 1977); and deep-water marine channel fans and turbiditic successions (Truswell, 1972; Parize, 1988). In glacial environments, dikes are commonly injected downwards due to the overburden downward loading force exerted on unconsolidated sediments beneath the glacier (Von Brunn & Talbot, 1986; Jolly & Lonergan, 2002). While within other sedimentary environments they are generally believed to intrude either upwards or laterally (Jolly & Lonergan, 2002; Braccini et al., 2008).

Based on extensive published literature and research, sandstone intrusion appears to be a very common occurrence in deep water marine (channel & turbidites) environment compared to other sedimentary environments (Fig. 2.10; Jolly & Lonergan, 2002). However, from a tectonic point of view, large-scale sandstone intrusion networks are more commonly documented in tectonically active basins characterized by high sedimentation rate, presence of mud-dominated succession and where associated tectonic stress expedite development of high in-situ fluid pressures which in turn facilitates the fluidization process required for sediment injection to occur (Lonergan et al., 2000; Jolly & Lonergan, 2002). Some examples include the dikes and sill complexes described from fold and thrust belt settings by Winslow (1983), and those found in the strike-slip basins along the San Andreas Fault System (see Newsom, 1903; Thompson et al., 1999; Jolly & Lonergan, 2002).
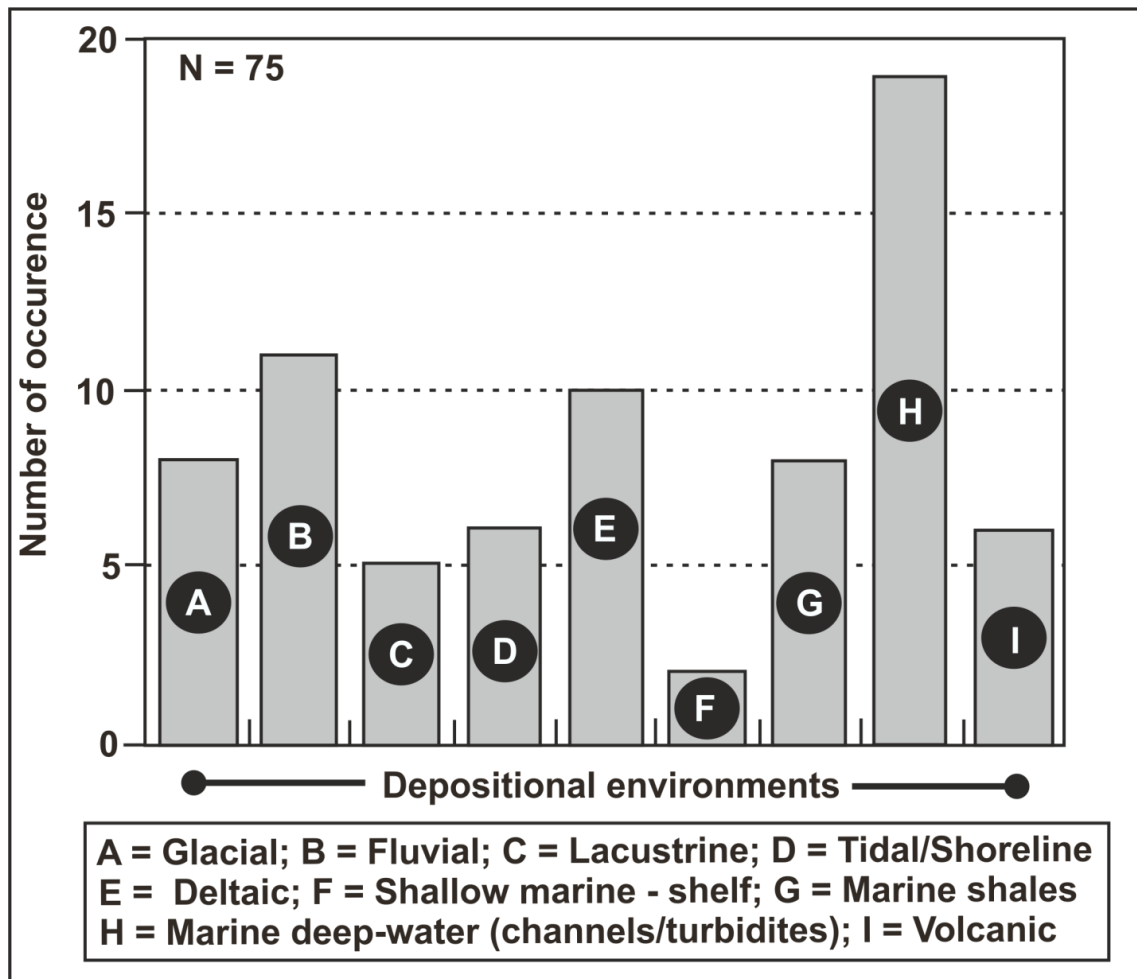
Fig. 2.10: Sedimentary environments where clastic intrusions have been documented. Deep water marine (channel & turbidites) environment shows the highest documented occurrence (modified after Jolly & Lonergan, 2002).

In the north-west European Continental Shelf, sand injectite have been documented to occur within the deep-water clastic reservoirs of the Upper Jurassic, Lower Cretaceous, Paleogene (Paleocene, Eocene and Oligocene) and Aeolian reservoirs of Permian age (Huuse & Mickelson, 2004; Hurst et al., 2005). In the North Sea Basin, sand intrusions are widespread in the deep-water sandstone reservoirs of Late Paleocene – Early Eocene (Fig. 2.11) within hemi-pelagic smectite-rich fine-grained mudstone which are pervasively polygonally faulted (Cartwright, 1994; Cartwright & Lonergan, 1996). The interval within the North Sea most susceptible to remobilization consists of depositionally restricted deep water sandstone bodies (e.g., narrow, elongate channels or gully-filled sands) and isolated/localized sand rich fan lobes which accumulated in mud-dominated basinal settings (Lonergan et al., 2000). The intrusions within the North Sea Basin are observed to be most abundant in the Lower Eocene succession and then become less frequent in the Oligocene and Lower Miocene (Lonergan et al., 2000; Huuse & Mickelson, 2004; Cartwright et al., 2008). The occurrence of large-scale sandstone within the Lower – Middle Eocene have been documented in the following areas in the northern North Sea (Fig. 2.11 & 2.12): North Viking Graben (e.g., Gras & Cartwright, 2002; Løseth et al., 2003; Huuse et al., 2004); South Viking Graben: Norwegian Quad. 9 & 25 (e.g., Løseth et al., 2003; Huuse & Mickelson, 2004); Tampen Spur: Norwegian Quad 34 (e.g., Huuse & Mickelson, 2004); Outer Moray Firth (e.g., Lonergan et al., 2000; Molyneux et al., 2002); and the southern part of Tampen Spur (e.g., Løseth et al., 2003).

2.5.2.3 Architectural Elements

Sand injectites (or sandstone intrusions) are commonly identified by their relationship with the host strata since they are known to form discordant or concordant elements that either split, branch, or form a network of other bedding discordant geometries (Fig. 2.13; Diggs, 2007; Hurst et al., 2011). Sand intrusions and remobilized sandstones exhibit a range of geometries and have several components which are sub-divided into four basic elements: sills, dikes (low- and high-angle), extrudites, parent units & host strata (Thompson et al., 1999; Hurst et al., 2006; Thompson et al., 2007; Vigorito et al., 2008; Hurst et al., 2011). Based on this, one can say that sand injectites have a tri-partite organization comprising of the parent sandstone unit that source sand and fluid for sand injection, the intrusive complex (mainly dikes and sills) and the extrudite complex which is basically sandstone extrusion sourced from the underlying intrusive complex (Fig. 2.13; Hurst et al., 2011). The above components of sand intrusions are all genetically related, and dikes and sills combine to form irregular geometries such as conical or saucer-shaped (or flat-based) intrusions of Km-scale, composed of 10's of meters of sandstone which often cross-cut the stratigraphy (Huuse et al., 2005, 2007; Vigorito et al., 2008; Vigorito & Hurst, 2010; Hurst et al., 2011). These main elements of sand injectites are further discussed in detail below.
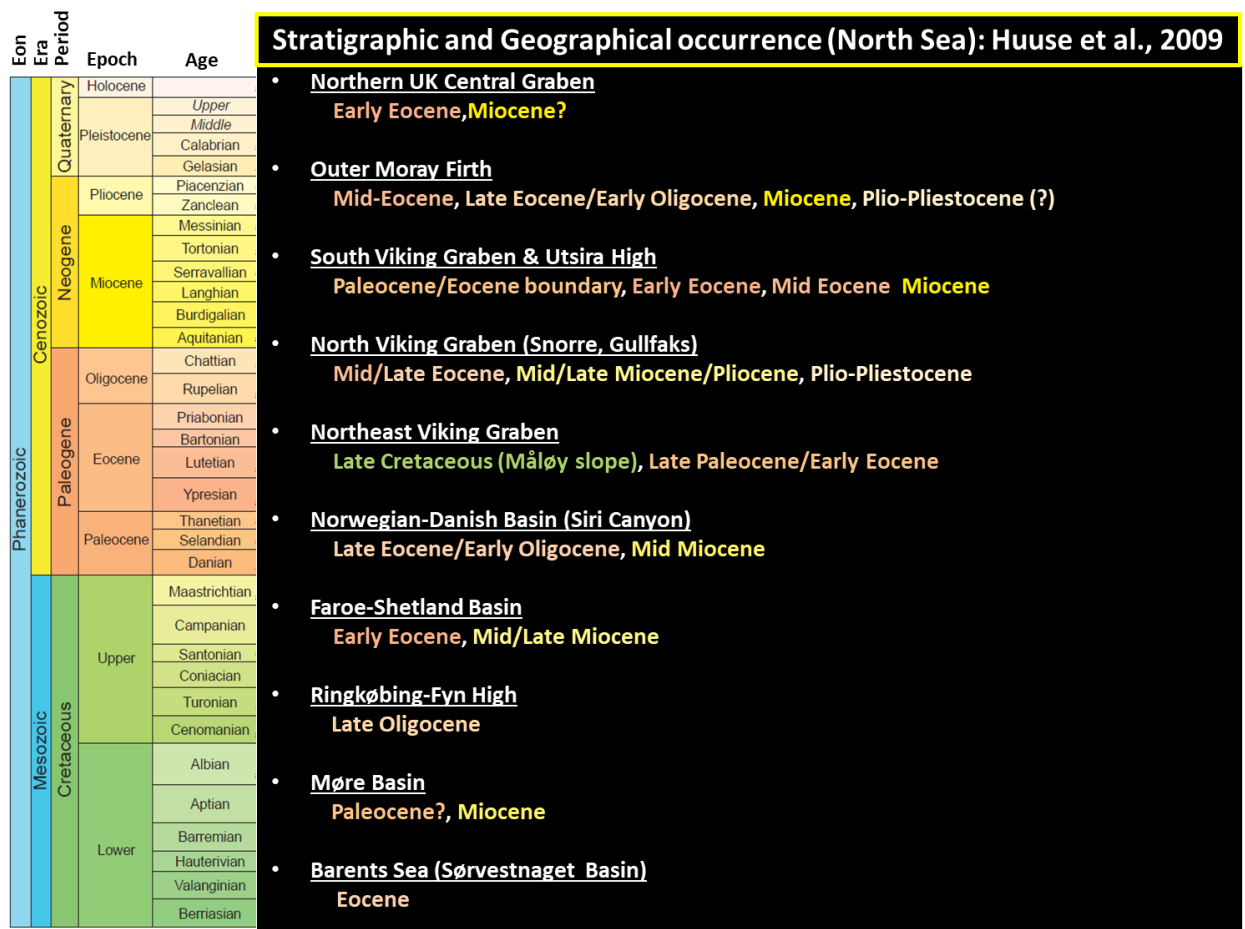
Fig. 2.11: Stratigraphic and geographical occurrence of Sand injectites in the North Sea Basin (Huuse et al, 2009, AAPG).

a) Sandstone Dikes (or dykes)

Sandstone dikes (Fig. 2.13a & b) are discordant features or tubular sandstone bodies which over majority of its length cross-cut sedimentary bedding either at low (< 20°) or high (> 20°) angles (Hurst et al., 2011). They are often recognized by their discordance with bedding in the host strata. Clastic dikes are a major occurrence in sedimentary basin deposits worldwide and they are typically produced either by seismic disturbance or liquefaction of fluid containing sediments (Obermeier, 1989; Boehm & Moore, 2002). They are usually obvious when present in cores of fine-grained strata (Fig. 2.14d) and can occur in millimetre to centimetre scale. They are commonly vertical (planar) or near vertical (Fig. 2.13a) and may display other range of geometries from highly irregular to bulbous and curved geometries (Parize et al, 2007; Hurst et al., 2011). The planar – curvilinear geometry of sandstone dikes have been described by several authors (e.g., Surlyk & Noe-Nygaard, 2001; Hurst et al., 2001: Appendix A - F), and the common planar geometry is believed to be suggestive of sand injection along planar fractures while the irregular curved geometries are attributed to the anisotropy in the host strata as well as due to post-injection folding and boudinage (Truswell, 1972; Hurst et al., 2011).

In outcrops, clastic dikes are observed to be characterized by distinct internal sedimentary structures such as deformation bands (Jonk et al., 2003) or flow laminae (Hubbard et al, 2007; Thompson et al., 1999; Hurst et al., 2011) which are typically parallel to dike margins. Also, they have been found to consist of mainly fine-grained sand which is preferentially fluidized (Lowe, 1975). Well known outcrop occurrence of clastic dikes occurs in the Panoche Giant Injectite Complex in California (Fig. 2.14a: G & H) and in the Columbia Basin.

Field/Structure	Reservoir Interval and Age	Depositional Environment	Reservoir Style and Scale of Intrusion	Reserves (× 10^6 BOE**)	Key References
Harding (UK)	Mid-Eocene	Deep-water basin-floor setting	Intrareservoir shales crosscut by intrusions; crestal intrusions	280	Dixon et al. (1995); Bergslien (2002)
Gryphon (UK)	Balder Formation (early Eocene)	Deep-water slope setting	Intrareservoir shales crosscut by intrusions; crestal intrusions	117	Purvis et al. (2002); Lonergan et al. (2007)
Chestnut (UK)	Alba/Chestnut sequence (upper Eocene)	Deep-water slope and basin-floor setting	Remobilized depositional sandstones; conical intrusions in reservoir underburden	25	Huuse et al. (2005)
Volund (Norway)	Sele, Balder, Horda formations (early Eocene)	Deep-water slope setting	Saucer-shape sandstone intrusion	NA**	Szarawarska et al. (2010)
Balder (Norway)	Lista, Hermod, Balder formations (Paleocene–early Eocene)	Deep-water basin-floor setting	Low-angle dikes at channel margins; crestal intrusions; conical intrusions	186	Briedis et al. (2007); Wild and Briedis (2010)
Nini area (Denmark)	Våle, Lista, Balder formations (late Paleocene–early Eocene)	Deep-water slope setting	Low-angle dikes at margins of remobilized sandstone; intrachalk sands; fault-zone injectites	NA	Svendsen et al. (2010)
Alba (UK)	Alba Formation (upper Eocene)	Deep-water slope setting	Low-angle dikes at channel margins; crestal intrusions	460	Duranti and Hurst (2004); Fretwell et al. (2007); Huuse et al. (2007)
Sleipner Øst (Norway)	Ty Formation (lower Paleocene)	Deep-water basin-floor setting	Intrareservoir shales crosscut by intrusions	NA	Satur and Hurst (2007)
Danica (UK)	Sele, Balder, Horda formations (early Eocene)	Deep-water slope setting	Low-angle dikes at channel margins; crestal intrusions	NA	Szarawarska et al. (2010)
Jotun (Norway)	Heimdal Formation (Paleocene)	Deep-water basin-floor setting	Intrareservoir shales crosscut by intrusions; crestal intrusions	203	Guargena et al. (2007)
Hamsun (Norway)	Sele, Balder formations (early Eocene)	Deep-water slope and basin-floor setting	Sandstone-injectite complex of low-and high-angle dikes and sills	NA	De Boer et al. (2007)
Cecile (Denmark)	Våle Formation (late Paleocene–early Eocene)	Deep-water slope setting	Dome-shape sandstone injection; crestal intrusions	NA	Hamberg et al. (2007)

*Reserve estimates are compiled from Hurst et al. (2005, table 1) and may not represent present-day estimates.
**BOE = barrels of oil equivalent; NA = not applicable.

Fig. 2.12: Fields in the North Sea (UK/Norway) and adjourning area with post-depositional remobilized sandstone and sand injectite reservoirs (Scott et al., 2013).

b) Sandstone Sills

Sandstone sills (Fig. 2.13a & b) are referred to as tabular sheet-like bodies of injected clastic materials whose boundaries appear concordant with beddings of the host strata but may be slightly discordant (localized discordance) with bedding along their lower and upper margins (Vigorito et al., 2008; Hurst et al., 2011). Since they are concordant with bedding (Fig. 2.13a & b) they may appear similar to some depositional sandstone especially when the latter are modified by sand injection (Hurst et al., 2005; Hurst et al., 2011). This similarity poses a problem when trying to differentiate between them in cores, resulting to many sills being misinterpreted in subsurface analysis (Hurst et al., 2011: see their Appendix B).

Sand sills have been described at outcrops by several authors, and of particular interest is that documented at the approximately 350 km² exposure of the Panoche Giant Injectite Complex (Fig. 2.14a: G & H) characterized by three distinct geometries ranging from staggered, stepped, and multi-layered geometries (Vigorito et al., 2008; Vigorito & Hurst, 2010; Hurst et al., 2011: see their Fig 6). Generally, in outcrops, sandstone sills have been recorded to commonly exhibit rapid lateral change in thickness (e.g., Surlyk & Noe-Nygaard, 2001) with either planar, curved, or irregular margins. However, on seismic, sills are usually associated with sudden lateral terminations and sometimes low-angle bedding discordance (Hurst et al., 2005).

c) Sand Extrusions

Sand extrusion also referred to as extrudites (Fig. 2.13a & b) are known to occur in a variety of stratigraphic setting and are suggested to have formed by venting of sand onto paleo-surfaces (such as the seafloor) (Hurst et al., 2006; Hurst et al., 2011). They are thought to be connected to and fed by underlying individual sandstone dikes (Hurst et al., 2011). They occur mainly as sand volcanoes (their simplest form) and have been identified as a new class of stratigraphic traps associated with sand injectites (Hurst et al., 2006). They have a four-way dip closure (Table 2.2) in map view and are connected to the parent sand body by sandstone dikes or transgressive sills through underlying fine-grained low permeability injectite host strata. Outcrop observations show that they have a thickness range between 0.1 – 0.75 m with diameter ranging between 0.3 – 3.0 m (Hurst et al., 2011). These extruded sandstone sheets may however exceed a thickness of 3 m and can extend laterally for several hundreds of metres (Boehm & Moore, 2002; Hurst et al., 2006; Hurst et al., 2011). Well known outcrop examples are recorded on the flood plain of the Mississippi Valley (Hurst et al., 2006); Ross Formation (Carboniferous) County Clare (Gill & Kuene, 1957) and near the Santa Cruz area (Hurst et al., 2006). Seismic evidence has also identified possible extrudites as documented by Hurst et al., (2011), Shoulder & Cartwright (2004), and Hurst et al., (2005): Eocene of Chestnut Field, Outer Moray Firth.

d) Parent Units

Parent units refer to depositional sandstone bodies that sourced the injected sands and served as reservoir and conduits for the fluid (pore water or hydrocarbon) that facilitated the injection process (Hurst et al., 2011). They are associated with features formed by both depositional process and post-depositional sand and fluid remobilization and form a network of interconnected systems with sandstone dikes and sills (Fig. 2.13a & b; Hurst & Cartwright, 2007; Hurst et al., 2011). An outcrop example of parent sandstone unit modified by sand remobilization and injection is the sandstone body within the Miocene Santa Cruz Mudstone of central California (Thompson et al, 1999; Hurst et al., 2007; Hurst et al., 2011: see their Fig 12).
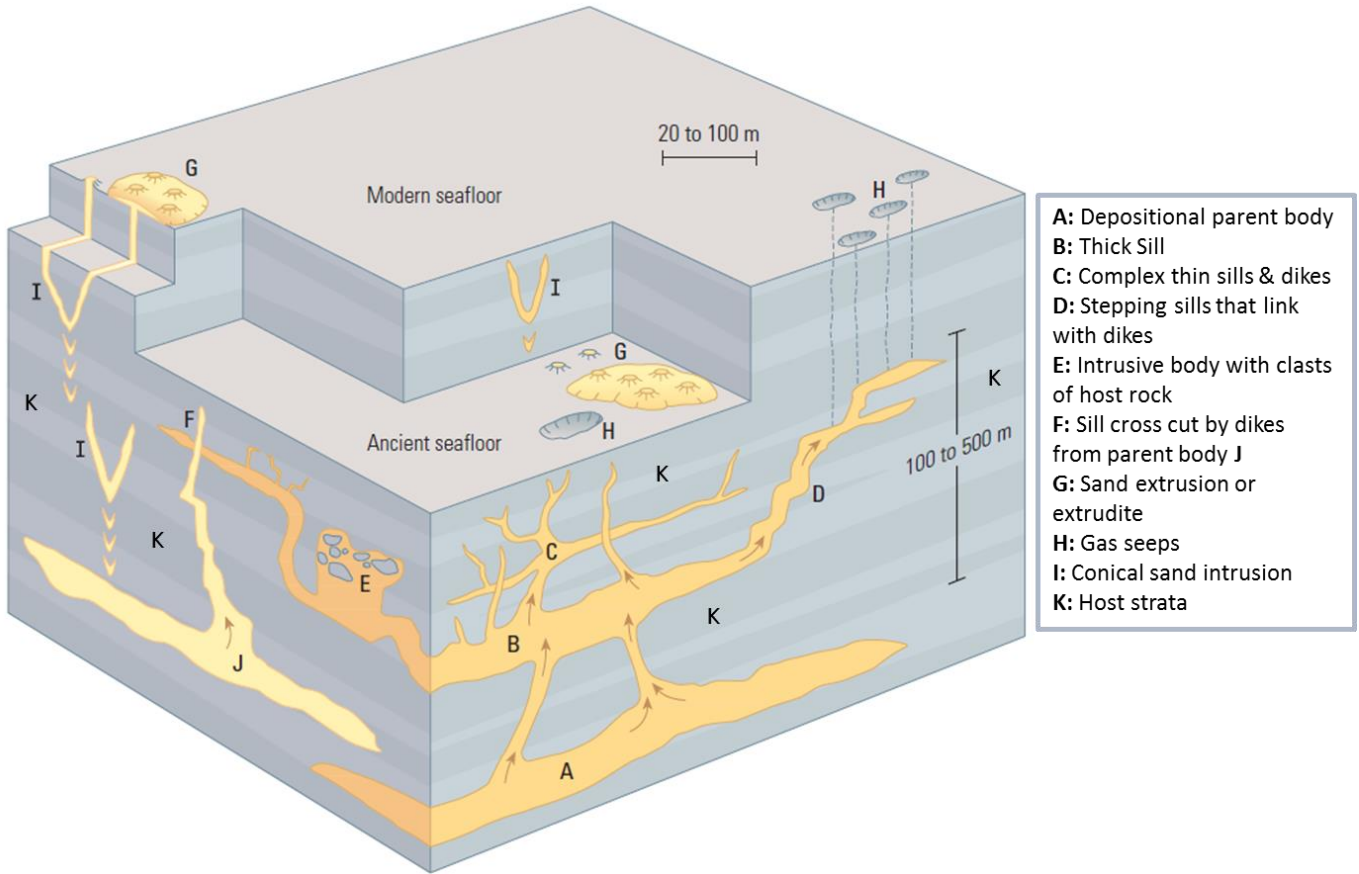
Fig. 2.13a: 3D schematic representation of sand injectites complex showing the architectural elements (modified after Braccini et al., 2008).

Legend:
- **A:** Depositional parent body
- **B:** Thick Sill
- **C:** Complex thin sills & dikes
- **D:** Stepping sills that link with dikes
- **E:** Intrusive body with clasts of host rock
- **F:** Sill cross cut by dikes from parent body **J**
- **G:** Sand extrusion or extrudite
- **H:** Gas seeps
- **I:** Conical sand intrusion
- **K:** Host strata
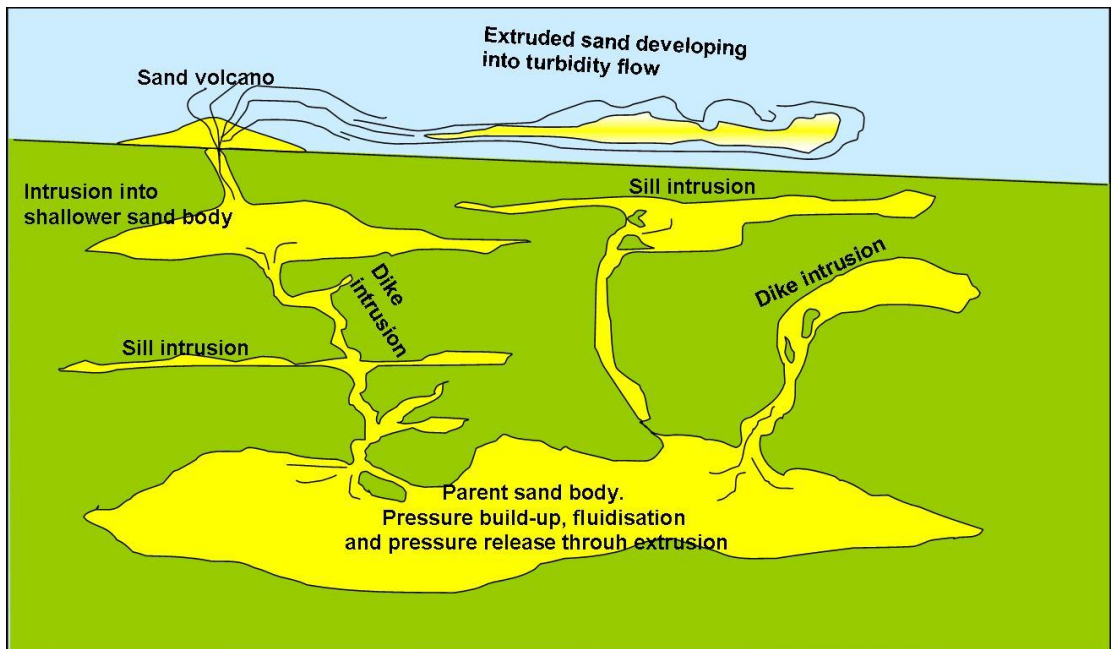
Fig. 2.13b: Schematic diagram showing an interconnected network of dikes and sills with the parent sand bodies and extrudites (Brunstad et al., 2009).

e) Host Strata

Sand injectites are commonly found in host sequences that are fine-grained, which is itself a sealing lithology or aquitard (Hurst et al., 2011). For sand injection to occur, elevated pore fluid pressure is required (Lonergan et al., 2000; Jolly & Lonergan, 2002; Hurst et al., 2003). To achieve this, a seal (aquitard) is required to prevent or reduce upward flow of fluid towards the earth's surface, which in turn maintains the required elevated pore pressure for hydro-fracturing and subsequent injection to occur. For example, sand injectites in the North Sea Basin are found within smectite-rich, fine-grained, low permeability mudstone dominated Paleogene host strata.

2.5.2.4 Detection and Recognition of sand injectites in the subsurface

Sand injectites occur in sizes ranging from millimetre – kilometre scale and exhibit different geometries. These features have been recognized in borehole cores, borehole image logs, outcrops, aerial photographs, satellite images and seismic section (Braccini et al., 2008).

a) Borehole Cores

Sand injectites have been identified in cores from oil fields in some sedimentary basins e.g., North Sea, Gulf of Guinea, and offshore Australia (Braccini et al., 2008). Dikes are much easier to recognize on cores than sills due to their clear and obvious discordance with host rock bedding (Fig. 2.14d). However, for sills which are concordant to host rock bedding, additional criteria (also applicable to dikes) may be applied for their recognition. Some of these criteria include homogeneity or lack of primary depositional structures resulting from fluidization; likely presence of internal stratification inconsistent with bedding but consistent with remobilized sand (i.e., flow laminae and alignment of grains); presence of clasts in the host rock; and contrast in grain packing between the parent depositional sand body and the sand injectite (Fig. 2.14d; Hurst et al., 2003; Braccini et al., 2008; Briedis et al., 2007).

Core studies from the Paleogene succession (Late Paleocene – Early Eocene) of the central and northern North Sea show features which indicate the presence of extensive injection complexes above the main reservoir sands. These are observed mainly in reservoirs in Alba, Balder, Gryphon and Forth/Harding fields. Lonergan et al. (2000) outlined some of the key features of the injected interval as observed from core photographs from the Gryphon (Quad. 9) and Alba Field (Fig. 2.14d), and they include: (1) complex dike (sub-parallel) and sill geometries resulting from processes such as dilation and/or brecciation during injection; (2) abundance of angular host-rock (mudstone) clasts which suggest host sediment cohesivity during injection (Fig. 2.14d); (3) near sharp margins of intrusions which suggests host strata cohesivity or fast flow velocities during injection; (4) oil-bearing intrusions which are rarely calcite cemented; and (5) ptygmatic folding which indicates plasticity of the host strata during intrusion. It is however, to

be noted that borehole cores sample a relatively small volume of the subsurface, and as such under sample injectite volume (Braccini et al., 2008).

b) Well Logs

The identification of injectites in borehole logs are usually not straight forward (Braccini et al., 2008), since they do not exhibit any unique log signature on gamma ray or resistivity logs and are usually misinterpreted as either thin or ratty sands. Some of these injectites are widely calibrated in the North Sea Basin by both exploration and development wells (e.g., Huuse & Mickelson, 2004: see their Fig. 9; Jackson & Sømme, 2011: see their Fig. 3 and 4). Possible indicators of sand injectites on well logs include: (a) occurrence of thin sands above a massive sand body (see Fig. 2.14b) and (b) presence of sand in unusual stratigraphic setting (Braccini et al., 2008). However, Borehole imaging tools such as Ultrasonic Borehole Imager (UBI); Full-bore Formation Micro-Imager (FMI) and Oil-Base Micro-Imager (OBMI) have been used to image injectites in the subsurface (e.g., in the Gulf of Guinea by Total E&P Angola) and these logs provide a crucial link between core-scale and large-scale log measurements (Braccini & Penna, 2005; Braccini et al., 2008).

c) Seismic Expression

Improvement in subsurface 3D seismic imaging, resulting from the application of new acquisition technology, has led to the widespread recognition of sand injectites associated with mostly deep-water sandstone reservoirs, especially on the north-west European continental margin (MacLeod et al., 1999; Huuse & Mickelson, 2004; Hurst et al., 2004, 2005; Bergslien et al., 2005). A large number of these sand injectites have been identified using seismic data from offshore petroleum provinces such as the North Sea, offshore West African basins and offshore mid-Norway (Lonergan et al., 2000; Duranti et al., 2002; Davies, 2003; Hurst et al., 2003). The seismic expression of large-scale sand injectites is largely determined by the interplay between the acoustic properties of the sand and the host strata mudstones (determined by factors such as porosity, mineralogy, and diagenesis), geometry of the sand body and the factors which influence seismic wave propagation and energy attenuation (Huuse et al., 2007). They usually produce ''hard'' reflections (high acoustic impedance contrast) that terminate abruptly laterally and have varying degree of discordance with bedding (Hurst et al., 2005). However, sand intrusions can either be acoustically soft or hard, which is dependent on whether the acoustic impedance of the intrusion is lower than or greater than that of the host strata respectively (Cartwright et al., 2008). One of the key recognition criteria for intrusions in seismic reflection data are their discordant nature to bedding.

3D seismic studies of large scale injectites in the Paleogene of the North Sea Basin have revealed a variety of geometrical types which occur in metre to kilometre scale (Fig. 2.14c;

Dixon et al., 1995; Jolly & Lonergan, 2002; Hurst et al., 2005). These large-scale intrusions have been grouped into three main categories by Huuse et al. (2007) based on their inferred seismic characteristics (e.g., size and morphology) and relationship to their inferred parent depositional sand body. These three types of intrusions are described in detail below (Fig. 2.15).

i) Wing-like Sandstone Intrusions

They are characterized by large, concordant central segment (i.e., flat-based bowel) which is flanked by a discordant margin consisting of a single or segmented inclined sheet with a wing-like appearance (Huuse et al., 2007). This type of sandstone intrusions in the subsurface were first documented in the Alba Field, located in the Eocene succession of the Outer Moray Firth, northern North Sea (Lonergan & Cartwright, 1999; MacLeod et al., 1999). They appear as discordant reflections inclined a few tens of degree with respect to bedding (Fig. 2.14c & 2.15). These wing-like intrusions have been calibrated (using well logs) in the North Sea Paleogene to represent tens-of-meter thick steep-sided remobilized sands of excellent reservoir properties (Dixon et al., 1995; Lonergan & Cartwright, 1999; Duranti et al., 2002; Huuse et al., 2003, 2004), with intrusions ranging between 10 – 40 m in thickness, 50 – 250 m vertical extent and inclination of wings of the order 10 – 35° (Huuse et al., 2007).

ii) Conical Sandstone Intrusion

This is the most common geometry of discordant sandstone intrusion seen on seismic. They exhibit high amplitudes and have V-shaped reflections referred to as 'V-bright' by Molyneux et al. (2002) and Løseth et al. (2003) due to their V-shaped geometry (Fig. 2.14c & 2.15). In 3D, the reflections form reversed conical structures (apical cones) and are commonly circular or sub-circular to polygonal in map view (Molyneux et al., 2002; Løseth et al., 2003; Huuse et al., 2003, 2004; Huuse & Mickelson, 2004). They were at some point previously misinterpreted as channel bodies with erosive inclined margins but can easily be differentiated from channel bodies due to their circular/polygonal planform geometry (Huuse & Mickelson, 2004; Cartwright et al., 2008). Their unique conical geometry with well-defined apex clearly distinguishes them from the wing-like intrusions. Conical intrusions typically have diameters in the range 0.5 – 2 km and height between 50 – 300 m, while their calibrated thickness may be of the order of 10 – 50 m or greater (Huuse et al., 2007). Several well calibration of these conical amplitude anomalies have been carried out, which have successfully tied them to tens-of-meters of thick sandstones. They have been documented to be abundant in the Lower Eocene succession of the South Viking Graben, North Viking Graben (Løseth et al., 2003; Huuse et al., 2003, 2004; Huuse & Mickelson, 2004), the Outer Moray Firth (Lonergan et al., 2000; Molyneux et al., 2002; Gras & Cartwright, 2002) and in the Fareo-Shetland Basin (Huuse et al., 2001; Shoulder & Cartwright, 2004; Cartwright et al., 2008). For example, Huuse & Mickelson (2004) documented the occurrence of conical amplitude anomalies in the Lower – Middle Eocene (Fig. 2.14c & 2.15) in the northern part of the Tampen Spur area (Norwegian North Sea – Quad 34), which they interpreted as tens-of-meters of thick sandstone penetrated by two exploration wells.

OUTCROP EXAMPLES OF SAND INTRUSIONS (DYKES & SILLS)

(A) Santa Cruz (Huuse et al, 2009, AAPG)

(B) & (C) Vocontian Basin, SE France (Ravier et al., 2015)

(D) Vocontian Basin, Le Puy Hill, SE France (Parize et al., 2007)

(E) & (F): San Joaquin Valley (Huuse et al, 2009, AAPG)

(G) Panoche Hill (Vigorito et al., 2008; Vigorito & Hurst, 2010)

(H) Panoche Hills (Lonergan et al., 2000)
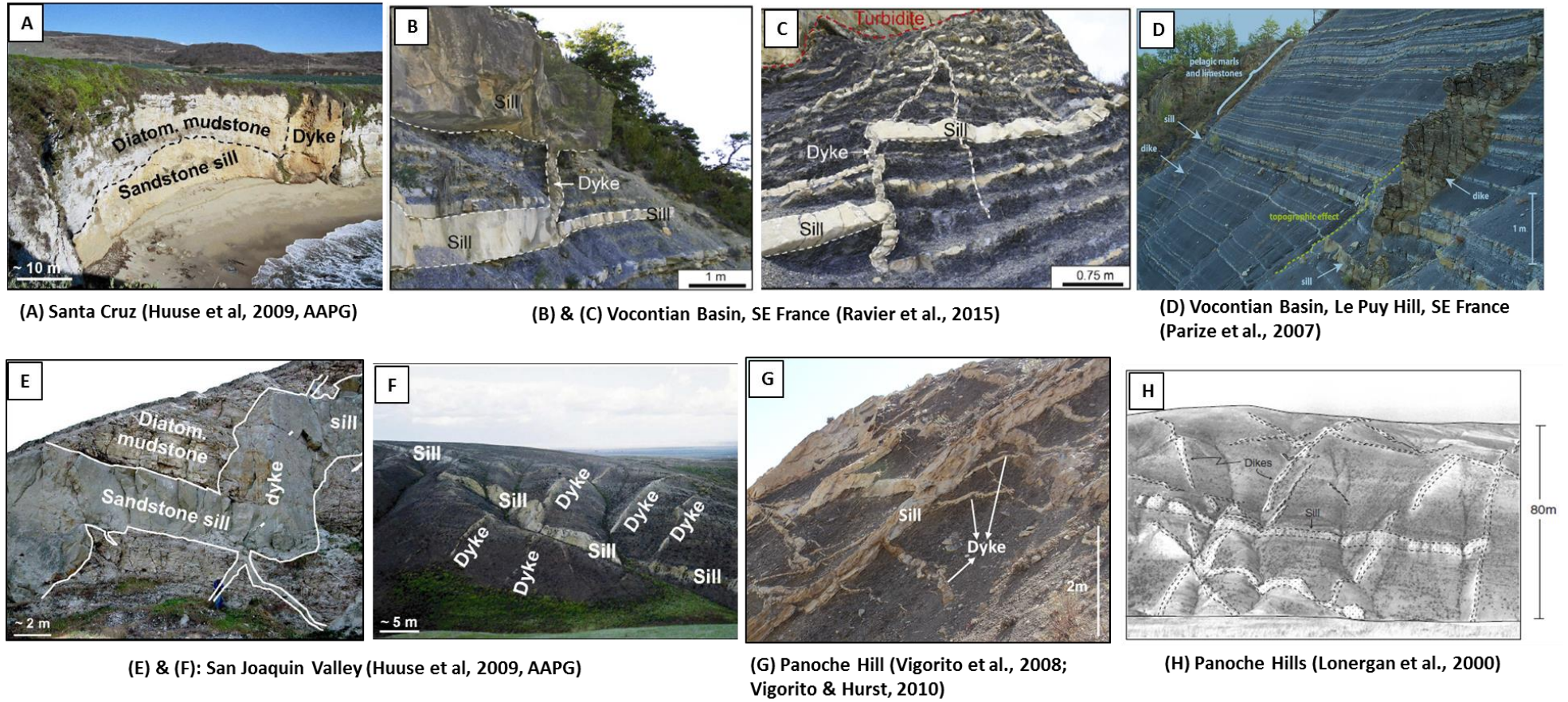
Fig. 2.14a: Outcrop examples of known sand intrusion complexes (dikes and sill complexes)
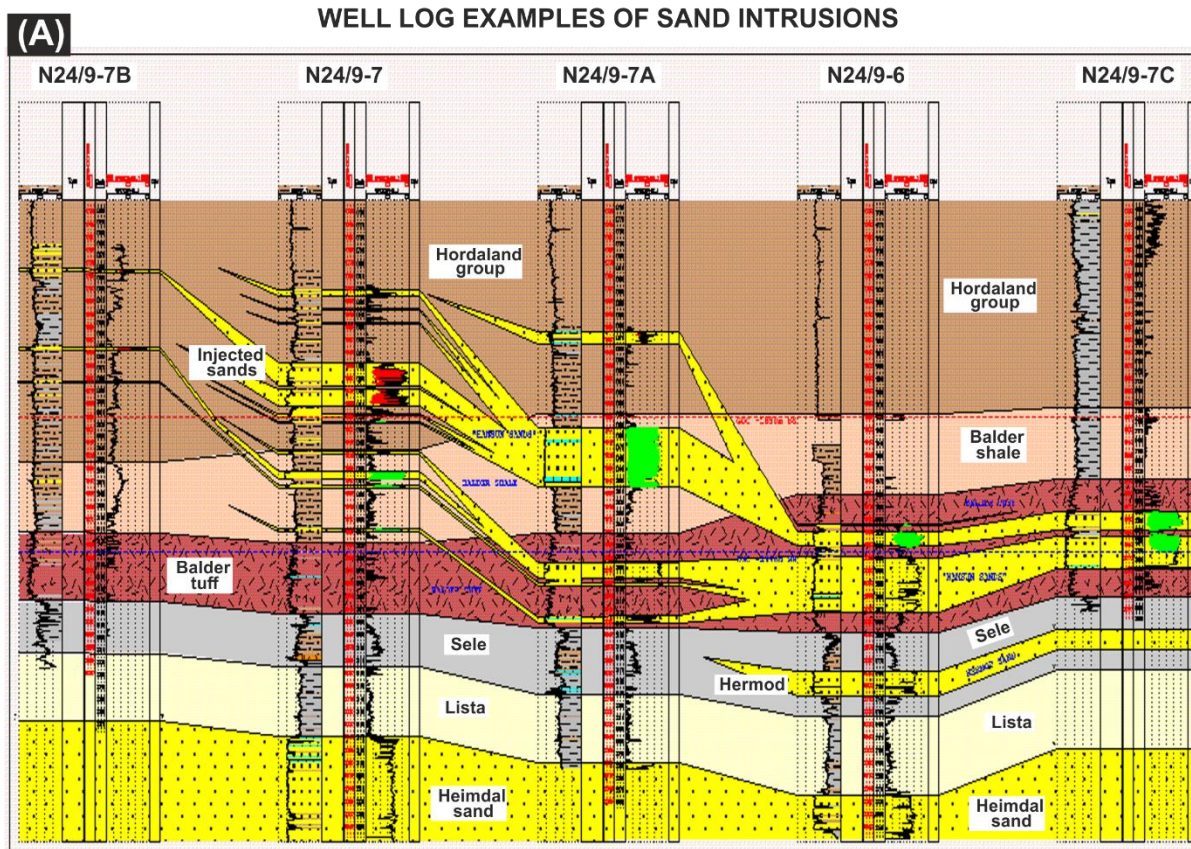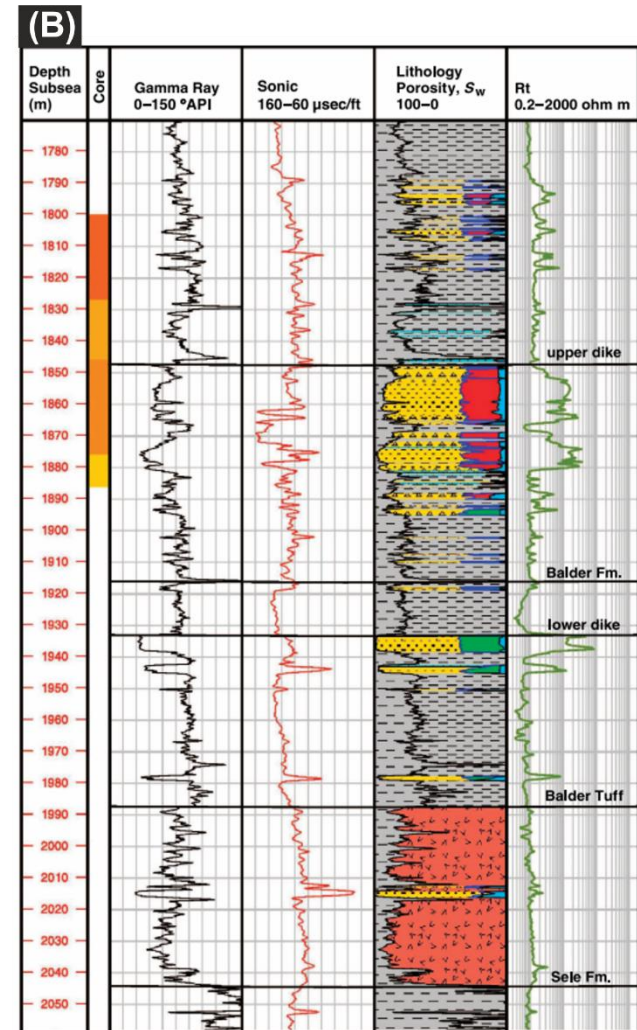
Fig. 2.14b: Subsurface example of sand intrusion in well logs

SEISMIC EXPRESSION OF SAND INTRUSIONS

(A), (B) & (C) Faeroe-Shetland (Cartwright et al., 2008)

Alba Field (Huuse et al., 2007)

Faeroe-Shetland (Cartwright et al., 2008)

Tampen Spur (Norwegian North Sea Quad. 34): Huuse & Mickelson, 2004

Alba Field (Huuse et al., 2003)

Volund Field (Huuse et al., 2009)

Maløy Slope (Jackson et al., 2007, AAPG)

Gamma Field (Huuse et al., 2007)
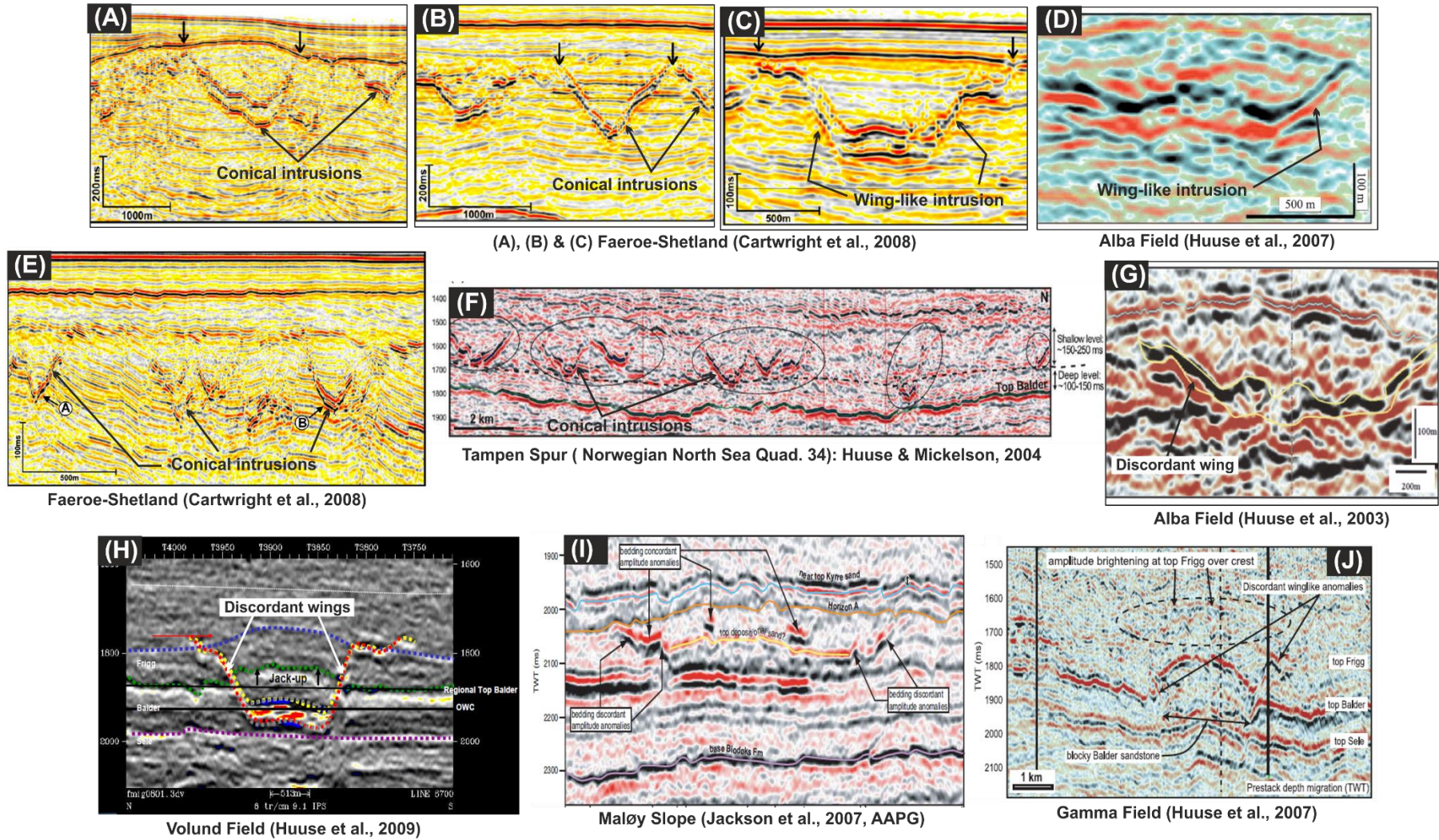
Fig. 2.14c: Subsurface example of sand intrusion in 3D seismic data

CORE EXAMPLES OF SAND INTRUSIONS
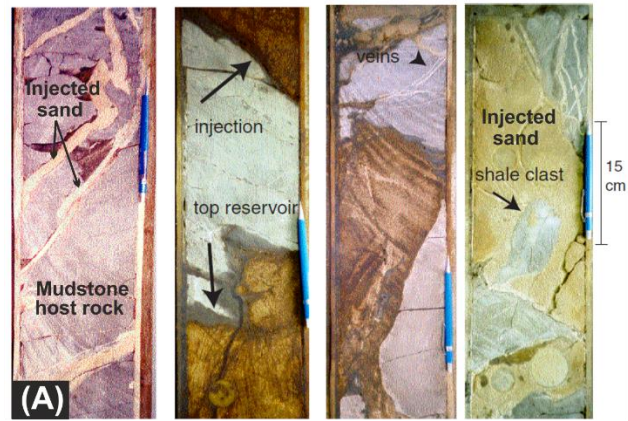
Gryphon Field (Lonergan et al., 2000)
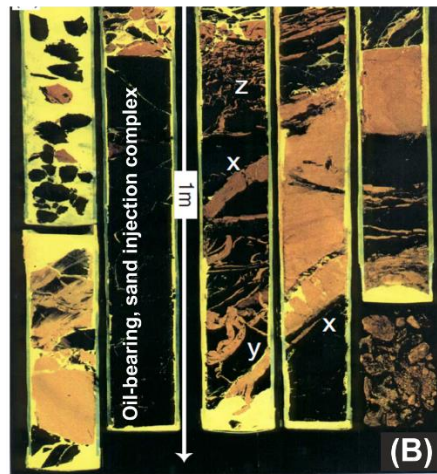
Alba Field (Lonergan et al., 2000)

x = sub-parallel dikes
y = ptygmatic dikes
z = brecciated facies
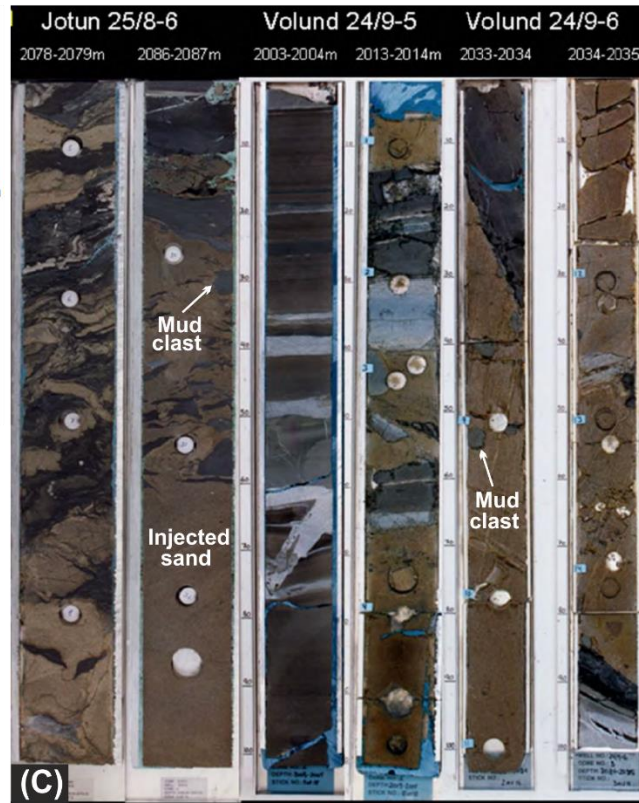
Jotun & Volund Field (Huuse, 2008; World Oil)
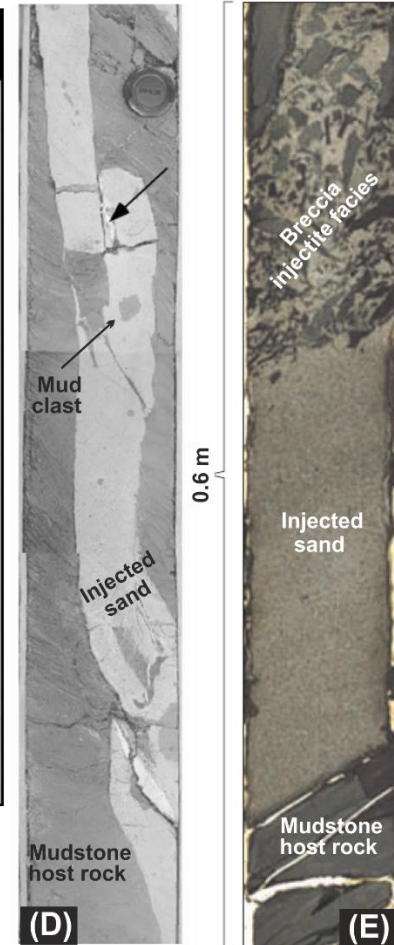
South Viking Graben
(Jonk et al., 2005)

Volund Field
(Braccini et al., 2008)

Fig. 2.14d: Subsurface example of sand intrusion in borehole cores

iii) Crestal Intrusion Complexes

This is also referred to as crestal intrusion fringes. The intrusions which make up crestal intrusion complexes (Fig. 2.15) are usually of centimetre to metre scale and they are frequently encountered in borehole cores (e.g., in the North Sea Paleogene) few hundreds of meters above massive depositional sand bodies (Lonergan et al., 2000; Duranti et al., 2002; Duranti & Hurst, 2004; Huuse et al., 2007). Based on their small thickness and complex geometries, they are not readily interpreted on seismic but are considered because they form an important component of reservoir volume and may enhance vertical connectivity between strati-graphically separate reservoirs (Dixon et al., 1995; Lonergan et al., 2000; Huuse et al., 2007).
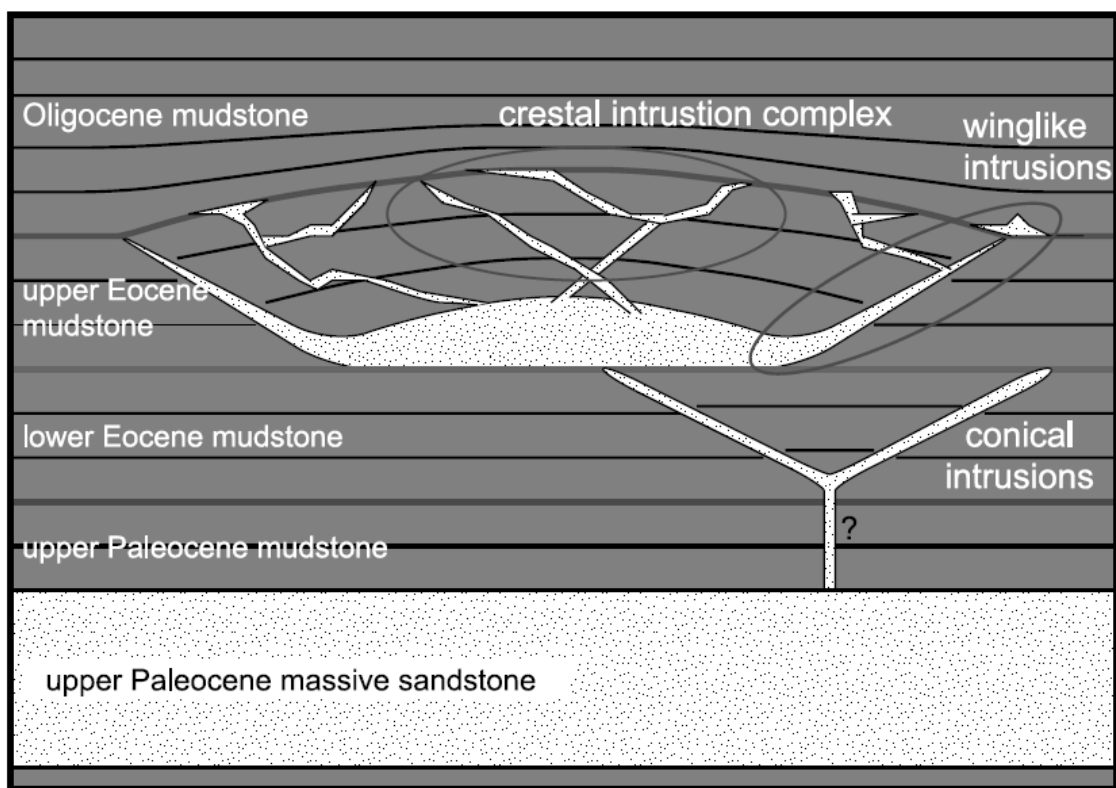
Fig. 2.15: Three main geometrical types of sand intrusions detected in the Paleogene of the North Sea basin by subsurface 3D seismic data (Huuse et al., 2007)

2.5.2.5 Oil Fields with Sand Injectites (North Sea Case)

Several oil fields in the North Sea Basin have been documented to contain reservoirs affected by one or more episodes of sand remobilization and injection (see Fig. 2.5, 2.12). Often these fields constitute deep water sandstone reservoir units which were deposited as either turbidites or channel fans. Some of these intrusive sands were previously identified in cores from early exploration wells but were ignored or considered insignificant (Braccini et al., 2008). The first seismic scale example of sand remobilization and injection in the North Sea Basin was

from the Balder Field and the Forth/Harding Field (Jenssen et al., 1993; Dixon et al., 1995). However, the best and well-known example of the North Sea (UK sector) reservoir affected by sand injection is found in the highly porous turbidite channel sand reservoir of the Alba Field; where sand injection features were observed in cores but was initially not considered important like in the case of the Balder Field. Other fields in the North Sea Basin and adjacent basins which contain injectites and remobilization features include Chestnut, Grane, Gryphon, Jotun, Leadon, Sleipner Ost, Forties, Catcher, Siri (Norwegian-Danish Basin), Solan (West Shetland Basin), Nini, Kraken and Volund (Lonergan & Cartwright, 1999; Duranti et al., 2002; Braccini et al., 2008; Olobayo, 2014).

2.5.2.6 Sand intrusion trigger mechanisms, mechanics, and process of sand injection

In other to understand the mechanics or processes involved in sand injection, it is necessary to consider both the priming mechanism (i.e., conditions which facilitate the remobilization and injection of sand) and the actual trigger mechanisms that lead to remobilization and injection. However, the generation of large-scale sand intrusion require three main ingredients to be present and this includes:

- The occurrence of deep-water sedimentary system characterized by clean, unconsolidated source sand bodies encased in low permeable sealing mudstones (Lonergan et al., 2000; Huuse & Mickelson, 2004; Braccini et al., 2008; Huuse et al., 2007).

- Overpressure condition caused by one or a combination of mechanisms (Fig. 2.16) such as disequilibrium compaction (due to rapid sediment loading), lateral or deep pressure transfer, fluid (hydrocarbon) migration and/or buoyancy, and possibly salt diapirism (Osborne & Swarbrick, 1997; Molyneux et al., 2002; Huuse & Mickelson, 2004; Braccini et al., 2008; Huuse et al., 2007).

- A triggering event such as large magnitude earthquake, tectonic shaking, bolide (meteorite) impact, volcanic eruption, landslide, or widespread faulting episode (Dore et al., 1999; Lonergan & Cartwright, 1999; Jolly & Lonergan, 2002; Molyneux et al., 2002; Huuse & Mickelson, 2004; Braccini et al., 2008; Huuse et al., 2007; Hermanrud et al., 2019).

2.5.2.6a Sand intrusion & injection trigger mechanisms

The series of processes which lead to the formation of sand injectites (e.g., high pore pressure, hydro fracturing of sealing strata, fluidization and then injection of sand) are well known. But the exact or precise detail of what triggers sand fluidization and the process for the development of discordant complex geometries are still speculative (Davies et al., 2006; Hurst et al., 2011). This trigger may be internally or externally driven. Based on more than a century

of research, several triggering mechanisms have been suggested to be associated with the formation of sand injectites and these include (Fig. 2.17):

- Tectonic activity/stress (Peterson, 1966; Winslow, 1983; Huuse et al., 2010)
- Seismicity induced liquefaction (Obermeier, 1989, 1996; Boehm & Moore, 2002; Obermeier et al., 2005; Hurst et al., 2011)
- Over pressuring caused by rapid loading i.e., localized excess pore fluid pressure related to depositional process (Truswell 1972; Allen 1985; Hurst et al., 2011)
- Thermal pressurization (Ujiie et al., 2007; Hurst et al., 2011)
- Fluid (hydrocarbon or pore water) migration (Jenkins 1930; Thompson et al., 1999; Lonergan et al., 2000; Jolly & Lonergan, 2002; Molyneux et al., 2002; Davies et al., 2006)
- Slab sliding due to slope instability (Hermanrud et al., 2019)

Overpressure in the subsurface may result from one or a combination of mechanisms (Fig. 2.16) Load-induced overpressuring is believed to be the main source of overpressuring which drives sand injection. This can result from gravitational instability along submarine slopes leading to large-scale mass movement of sediments (i.e., slides & slump) (Truswell 1972; Jonk et al., 2007), which may produce localized sand injection and/or extrusion. Earthquake activity has been linked as a trigger for sand injection and possible extrusion at the earth's surface (Obermeier, 1996; Obermeier et al., 2005). Sand injectites have been reported to occur at a high frequency in seismically active areas which thus suggests that earthquake forms an effective mechanism for the liquefaction of sands (Obermeier, 1996; Boehm & Moore, 2002). But earthquake engineering studies have shown that liquefaction will only occur for earthquakes with high magnitudes (i.e., > 5) (Ambraseys, 1988; Jolly & Lonergan, 2002). However, when considering earthquake-induced liquefaction as a possible trigger for sandstone intrusion, it is crucial to also consider the intrusion scale & depth, and the possibility that an earthquake of magnitude greater than five (> 5) occurred at the time of intrusion or if the basin was tectonically active at any time (Lonergan et al., 2000).

Generally, seismicity and rapid loading have been suggested to be the most typical triggering mechanisms for sand injection and intrusion (Jonk, 2010). However, some authors (e.g. Brooke et al., 1995; Lonergan et al., 2000; Molyneux et al., 2001; Jolly & Lonergan, 2002; Molyneux et al., 2002; Hurst et al., 2011) have inferred that the extensive development of sandstone intrusions within the Paleogene (Lower Paleocene - Eocene) of central and northern North Sea may be linked to the early migration and expulsion of hydrocarbon (gas) from deep Mesozoic structures, since it is believed that the Paleogene of the North Sea was tectonically quiescent and as such earthquake induced liquefaction would be an unlikely trigger for sand remobilization and injection in the North Sea during the Paleogene time (Jolly & Lonergan, 2002; Huuse & Mickelson, 2004).
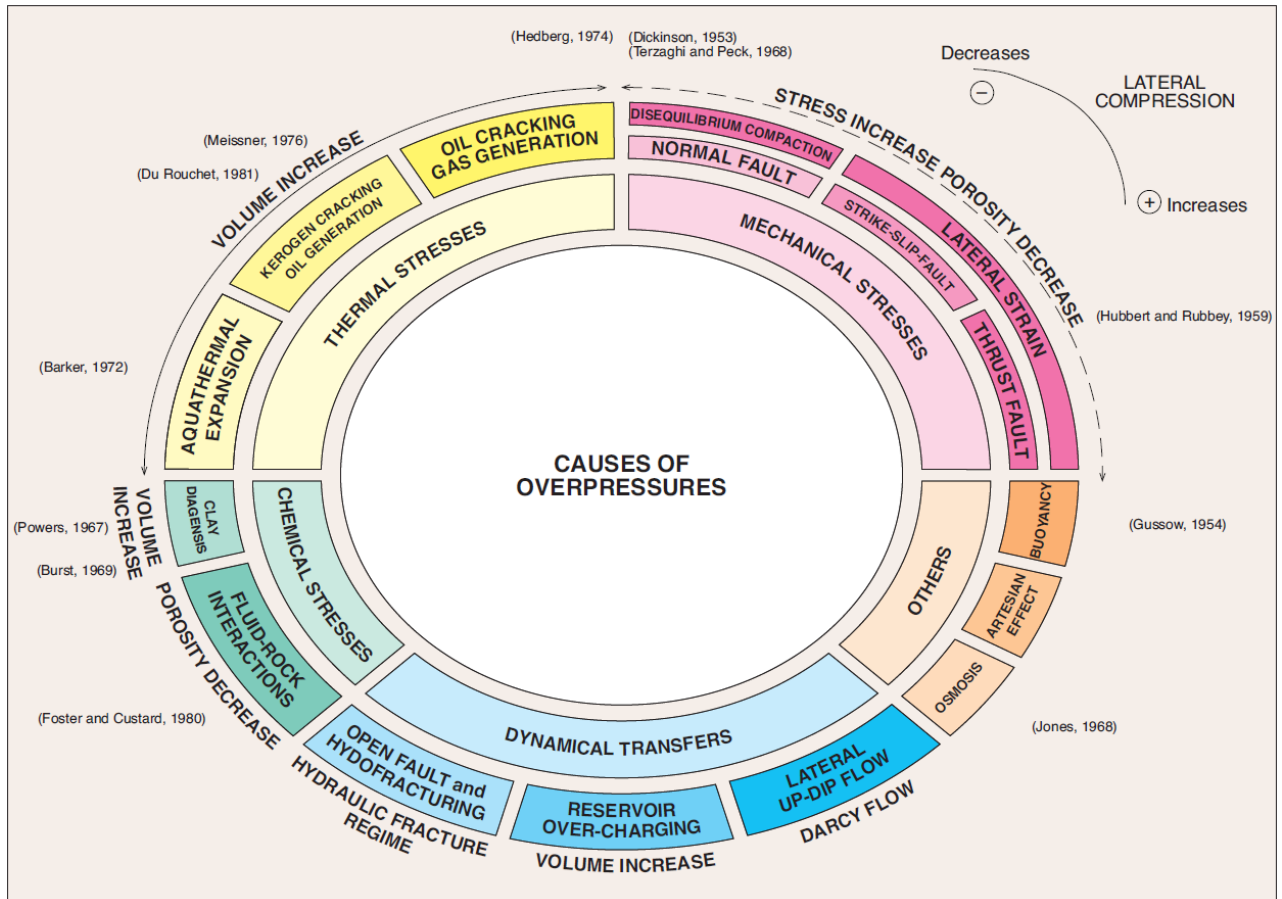
Fig. 2.16: Overpressure generation mechanisms in the subsurface (Moss et al., 2003).

2.5.2.6b Mechanics and process of sand injection

Clastic dikes and sills may be considered as a natural Mode-1 hydraulic fracture (Lorenz et al., 1991) and the intrusion of clastic dikes and sills require that the host rock fails (i.e., by hydraulic fracturing), and that a fracture propagates which then gets filled with injecting sediments. For Mode-1 failure to occur in the host rock, it needs to have tensile strength, and as such cohesion of the host strata is a critical factor for clastic intrusion to form (Lonergan et al., 2000)

If one considers a tectonically quiescent basin (passive margin or intra-cratonic basin) that is not under any form of applied tectonic stress, the direction of the maximum principal stress will be vertical due to overburden load. For a dike to propagate in such basin, the fluid pressure (P_f) must exceed the horizontal or minimum principal stress (σ_h) and the tensile strength of the host strata parallel to the bedding (T_h) (Lonergan et al., 2000; Jolly & Lonergan, 2002):

$$P_f > \sigma_h + T_h \quad \ldots\ldots\ldots\ldots\ldots. (1)$$

While for a sill to form, the fluid pressure must exceed the vertical stress (σ_v) and the tensile strength of the host strata perpendicular to the bedding (T_v) (Lonergan et al., 2000; Jolly & Lonergan, 2002):
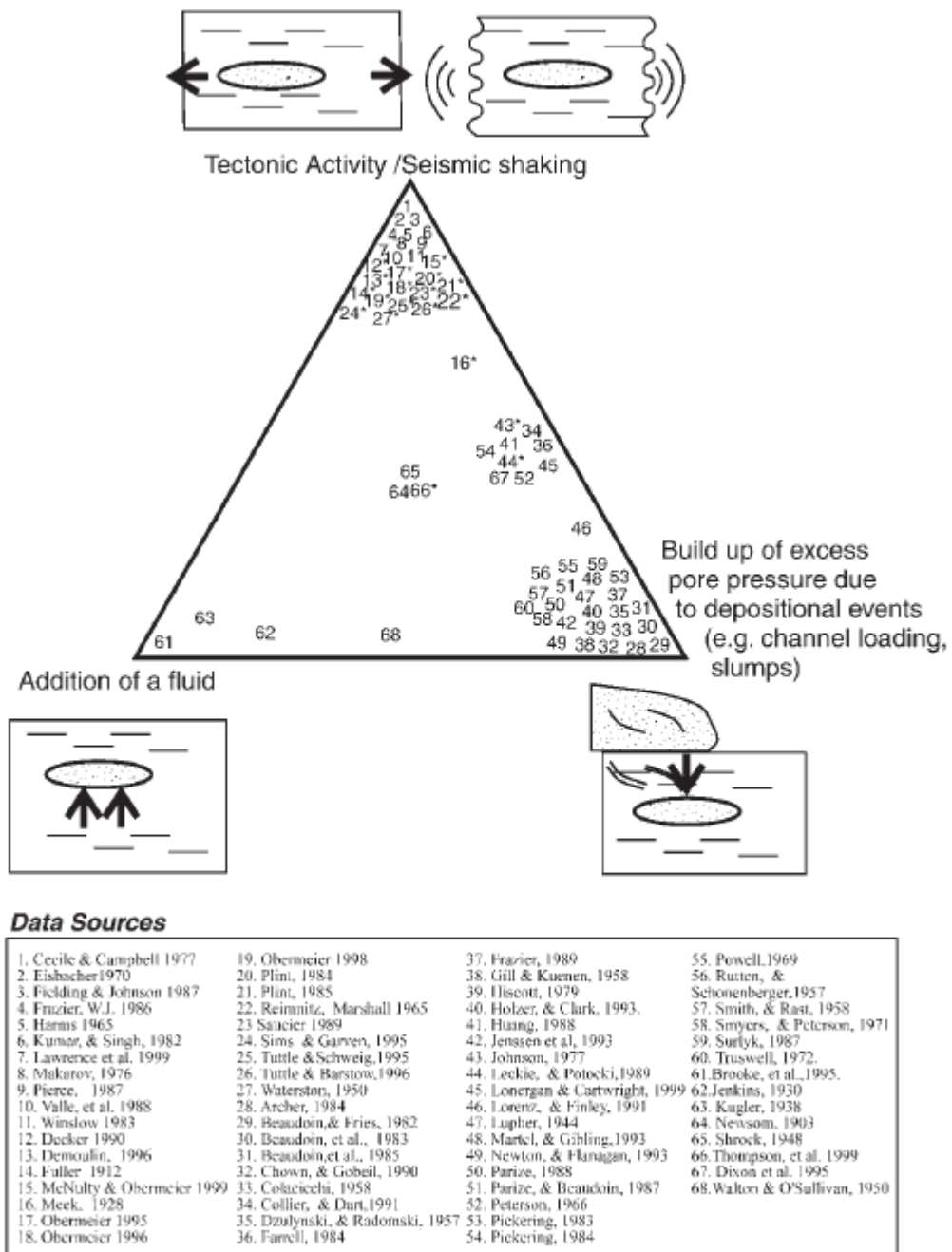
Fig. 2.17: Most cited sand intrusion trigger mechanism. Marked in asterisks are those that specifically mentioned earthquake induced liquefaction as a trigger (from Jolly & Lonergan, 2002).

$$P_f > \sigma_v + T_v \quad \dots\dots\dots\dots\dots (2)$$

The above (equation 1 & 2) suggest that the formation of either dike or sill is largely dependent on the fluid pressure (P_f), the maximum (σ_v) or minimum (σ_h) principal stress, the tensile strength (T_h or T_v) and burial depth of the host strata (i.e., sealing lithology)

The processes leading to the formation of clastic intrusion (dikes or sills) are subdivided into four stages and discussed briefly: (a) Overpressure development (build-up of excess fluid pressure); (b) Liquefaction; (c) Hydrofracturing (seal failure); and (d) Fluidization (Jolly & Lonergan, 2002; Hurst et al., 2011).

a) Overpressure Development:

Fluid overpressure is of critical importance (priming mechanism) for sand injection to occur since it initiates hydrofracturing and drives subsequent fluid flow (Hurst et al., 2011). Overpressure development is usually linked to disequilibrium compaction during rapid burial (Osborne & Swarbrick, 1997) but other mechanisms such as lateral and deep transfer (Yardley & Swarbrick, 2000; Reily & Flemmings, 2010), hydrocarbon generation and migration of basinal fluids (Jolly & Lonergan, 2002), mineral transformation i.e. silica diagenetic transformation (Davies et al, 2006; Olobayo, 2014) and possibly drop in water table (Hermanrud et al., 2013), can account for overpressure development in the subsurface (see Fig. 2.16).

Excess fluid pressure (or overpressure) is generated in sandstones when the rate of compaction-induced expulsion of fluid is reduced by low-permeability sealing strata. The moment sandstone gets effectively sealed (X_1, Fig. 2.18a) the pore fluid pressure (P_f) becomes greater than the hydrostatic pressure gradient ($X_1\_X_2$, Fig. 2.18a). At this point, the pore fluid pressure tends to resist mechanical compaction due to the overburden and then maintains a metastable grain fabric (see stage 2: Fig. 2.18b) which results in the breakdown of grain contacts under shear (stage 3: Fig. 2.18b) and this transfers grain support of the overburden to the pore fluids leading to a rapid increase in pore fluid pressure ($X_2\_X_3$, Fig. 2.18a) and liquefaction of the sand (Hurst et al., 2011). If the pore fluid pressure reaches the fracture pressure (X_3, Fig. 2.18a), it initiates hydro-fracture propagation, giving rise to a pressure differential between the sandstone unit and the propagating fracture, which results to the injection of fluidized sand into the fracture (stage 4: Fig. 2.18b) (Hurst et al., 2011).

It is to be noted that the scale of sandstone remobilization and injection is largely dependent on the operating mechanisms of overpressure generation and development which in turn depends on other factors such as the burial history of the basin, tectonism, sedimentation, and diagenesis (Osborne & Swarbrick, 1997; Hurst et al., 2011).
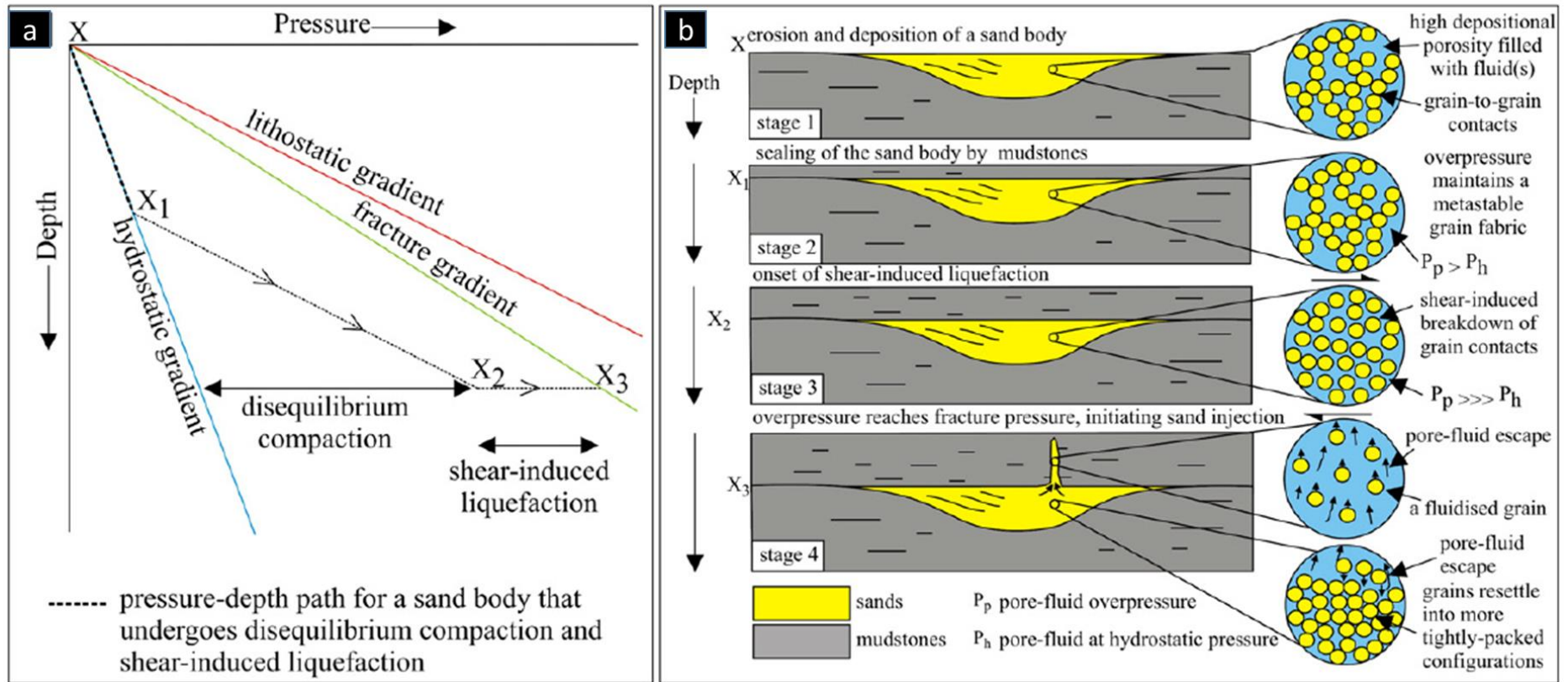
Fig. 2.18: (a) Relationship between overpressure development and increase in burial depth resulting from disequilibrium compaction, and the subsequent initiation of sand injection by shear-induced liquefaction; (b) summary of stages involved in the initiation and injection of overpressured parent sand body through a propagating fracture resulting from overpressure development, liquefaction, hydro-fracturing, and fluidization (from Hurst et al., 2011).

b) Liquefaction

According to Allen (1984), liquefaction refers to: 'the breakdown of the fabric of a material, to a degree that the grains are no longer mutually supported but are temporarily separated and dispersed in a pore fluid'. In essence, it simply involves the rapid rise in pore fluid pressure and occur when grains are no longer supported by inter-granular friction but are temporarily suspended by the surrounding pore fluid (Leeder, 1982; Hurst et al., 2011). This initiates localized sand fluidization and drives pore fluid upward (Hurst et al., 2003a; Hurst et al., 2011). Liquefaction of sand materials usually results from seismically induced shearing (Takahama et al., 2000) and is associated with both sand intrusion and extrusion (Obermeier, 1996; Hurst et al., 2011). However, Hurst et al. (2003) have argued that liquefaction alone may not be able to account for large scale remobilization and injection of sand (such as those in the North Sea) because the volume of fluid liberated may be insufficient to sustain fluidization and thus, an external fluid source may be required.

c) Hydro-fracturing (Seal failure)

Seal failure is believed to be caused by hydraulic fracturing that occur when pore fluid pressure exceeds the fracture gradient (X_3, Fig. 2.18b) within the sealing lithology or near the contact between the seal and underlying parent sandstone unit (Jolly & Lonergan, 2002; Hurst et al., 2011). The above causes the propagation of fracture within the host sediment, leading to the upward injection of fluidized sand. The presence of sandstone intrusion and other fluid flow products such as pockmarks, pipes and polygonal faults are all evidence of seal failure and are generally termed **'Seal By-pass Systems'** (Løseth et al., 2009; Cartwright, 2010; Huuse et al., 2010).

d) Fluidization

This is the final stage of the sand injection process and involves the suspension of grains by drag force due to upward migration of fluid (DiFelice, 1995; Hurst et al., 2011). It is regarded as the main process responsible for the transportation of sand from the parent sandstone units into hydraulic fractures (Duranti & Hurst, 2004; Gallo & Woods, 2004; Hurst et al., 2011). Sand grains fluidize when the upward movement of pore fluid exceeds the minimum fluidization velocity (V_{mf}) which is estimated as (Lowe, 1975):

$$V_{mf} = \frac{[0.00081(\rho_s - \rho_f)]d^2 g}{\mu} \quad …………………… (3)$$

Where ρ_s = density of solid; ρ_f = fluid density; d = mean diameter of particles (in mm); g = acceleration due to gravity; μ = viscosity. The V_{mf} for fine grained sediments range between 0.001 – 0.01 ms^{-1} (Duranti & Hurst, 2004; Hurst et al., 2011) and they are preferentially fluidized

due to their very low minimum fluidization velocity (Richardson, 1971; Lowe, 1975; Hurst et al., 2011). For effective fluidization to occur, significant volume of fluid (hydrocarbon or pore fluid) derived either internally or externally may be required. It is suggested that upward migrating fluids (especially gas) from deeper parts of the basin in well-known large scale intrusion provinces (such as the North Sea, Fareo- Shetland and San Joaquin Basin: Panoche & Tumey hills) may have partly contributed to the fluid required to drive sand remobilization and injection (Lonergan et al., 2000; Jolly & Lonergan, 2002; Huuse et al., 2010; Wild & Briedis, 2010).

2.5.2.7 Implications of sand remobilization and injection for Hydrocarbon Exploration and Production

The implications of large-scale sandstone intrusions on deep water clastic systems are well documented and known for more than a decade. Over the years, it has emerged and have been documented that many deep-water reservoirs of the North Sea Paleogene were subject to episodes of large-scale sand remobilization and injection resulting to obvious modifications to reservoir geometry and connectivity (Dixon et al., 1995; Lonergan et al., 2000; Duranti et al., 2002; Huuse et al., 2003). Since sand injectites form highly porous and permeable conduits in low- permeability mudstone units, they therefore act as a seal risk, facilitates the expulsion of basinal fluids, as well as mitigating timing and rate of fluid migration (Huuse & Cartwright, 2004; Huuse & Cartwright, 2007). Therefore, one can say that the development of sand intrusion may be significant in sedimentary basin analysis because they may provide an insight into the possible timing and location of basin scale fluid flow events and possible periods of overpressure development (Cartwright, 2010; Jackson & Sømme, 2011).

Based on the North Sea experience, the occurrence of large-scale sandstone has obvious significance in the context of hydrocarbon exploration and production for several reasons which include:

- They may constitute volumetrically significant reservoirs for hydrocarbon (Huuse et al., 2007; Jackson & Sømme, 2011)
- They impact reservoir geometry and properties i.e., reservoir quality, distribution, and connectivity (Lonergan et al., 2000; Hurst et al., 2005; Huuse et al., 2007; Hurst & Cartwright, 2007)
- They provide both vertical and lateral connectivity between reservoirs over long distances (Lonergan et al., 2000; Huuse et al., 2007)
- They can also constitute drilling hazards (Hurst et al., 2005; Huuse et al., 2007)

2.5.2.7a Implications for Hydrocarbon Exploration

In the exploration context, sand intrusions influence traps, reservoirs, seal, and fluid migration. As such the knowledge of their impact play an important role in developing and modifying new and existing play concepts respectively (Hurst & Cartwright, 2007).

a) Traps

Sandstone intrusions are known to form a separate class of traps referred to as 'intrusive trap' (Hurst et al., 2003; Hurst & Cartwright, 2007), which are distinct from the conventional structural and stratigraphic traps because sand injectites form both the structure (trap) and the reservoir. These traps consist of a combination of dikes, sills and irregular intrusions that have intruded into low-permeable mudstones which typically act as seals for the intrusive traps (Hurst & Cartwright, 2007). Five main intrusive trap geometries have been identified, which may occur individually or in combination: (i) Dikes; (ii) Intrusive sills; (iii) Emergent sills or Extrudites or sand sheets; (iv) Scalloped tops; (v) irregular bodies (Table 2.2; Hurst et al., 2005)

b) Reservoir

Experience from North Sea fields (e.g., Alba, Balder, Gryphon and Forth/Harding) modified by sand injectites show that sand injectites form excellent reservoirs and usually contain substantial volume of sand (Hurst et al., 2003; Hurst & Cartwright, 2007). Well calibrations of discordant high amplitude anomalies on seismic data interpreted as sand injectites have also identified thick sandstone reservoir intervals (e.g., Huuse & Mickelson, 2004; Jackson & Sømme, 2011). Reservoir quality of sand injectites is typically homogenous and good, with recorded porosity ranging between 25 – 35% and permeability in the Darcy scale (Fig. 2.19 & 2.20; Duranti et al., 2002; Duranti & Hurst, 2004; Briedis et al., 2007; Lonergan et al., 2007). Since injected sand are derived from depositional sand, the features they form and their petrophysical properties are largely dependent on the composition/mineralogy of the parent sand and grain redistribution and re-packing during fluidization (Jonk et al, 2003; Hurst et al., 2005). Therefore, sand remobilization and injection have obvious effect on reservoir geology which is summarized in (Table 2.3).

c) Seal & Migration

The injection of sand through a low permeable mudstone host strata may compromise the integrity of the sealing lithology (Hurst & Cartwright, 2007), and there is evidence to show that sand injectites may be linked with fluid (gas) leakage and seepage to modern and paleo-sea floors (Jonk et al., 2003; Mazzini et al., 2003; Hurst et al., 2005). Therefore, sand injection through a sealing unit may increase the risk associated with underlying reservoirs but provides an avenue for fluid migration to shallower intervals (Hurst & Cartwright, 2007). However, if the injectite reservoirs are overlain by subsequent deposition of another sealing lithology, seal integrity may not be an issue like in the Alba Field (MacLeod et al., 1999; Hurst et al., 2005; De Boer et al., 2007; Hurst & Cartwright, 2007). In essence, sand injectites have the potential to

improve the gross permeability of an otherwise low-permeability interval and increase the rate of fluid migration and escape in hydrocarbon basins (Hurst & Cartwright, 2007)

2.5.2.7b Implications for Hydrocarbon Production

Based on the common occurrence of injectites in deep water clastic reservoirs in the North Sea Paleogene, a substantial history of production and prediction of field performance for clastic reservoirs affected by sand intrusion is well known (Braccini et al., 2008; Hurst & Cartwright, 2007). One well-known example of the positive impact of sand injectites is in the Gryphon Field where wells which targeted sand injectite wings doubled oil production (Fig. 2.21; Jackson et al., 2011: see their Fig. 2). Sand injectites enhance intra-reservoir communication and sweep efficiency (i.e., aquifer support) between isolated reservoirs. Although this natural enhancement of aquifer drive may result to rapid water break through during production (Hurst & Cartwright, 2007). They also constitute potential drilling hazards due to their large pore volumes and occurrence in polygonally faulted mudstone successions usually drilled with overbalanced mud weight; they can result to loss of drilling fluid when encountered by wells (Huuse et al., 2007).
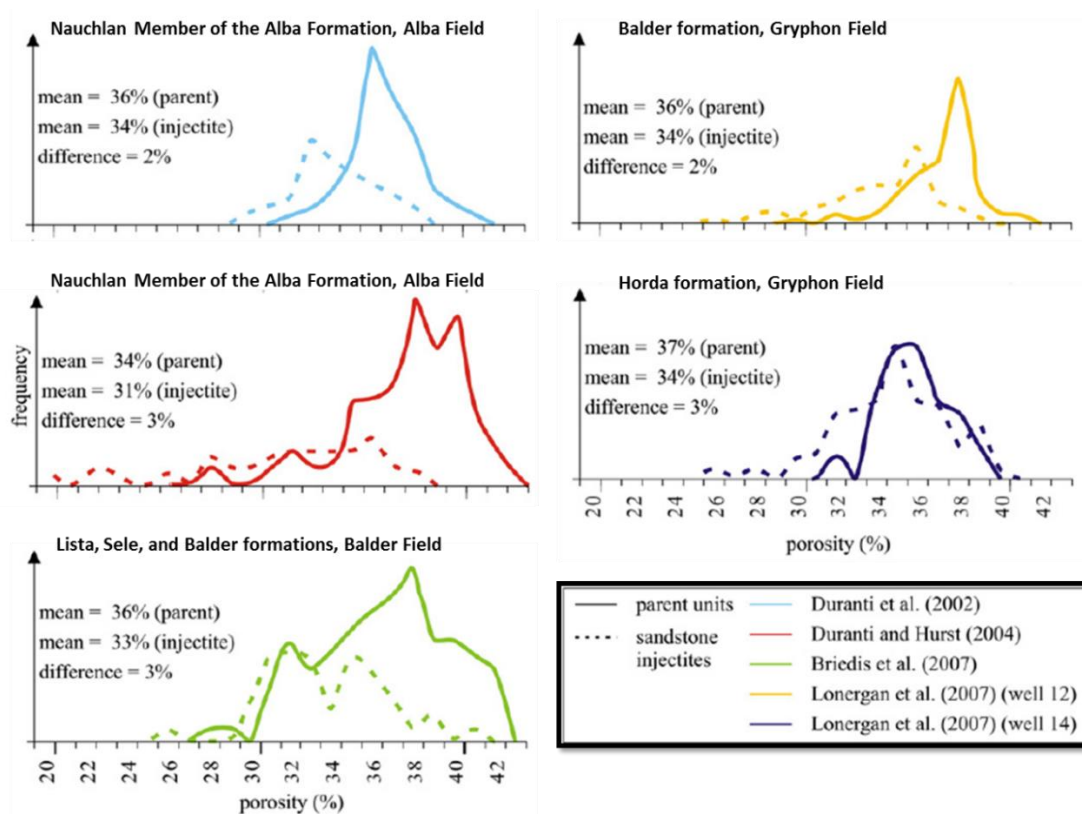
Fig. 2.19: Frequency distribution of porosity in sand injectite reservoirs of some fields (e.g., Alba, Balder and Gryphon Field) in the North Sea Basin showing the observed high porosity values of sand injectite reservoirs (from Hurst et al., 2011).
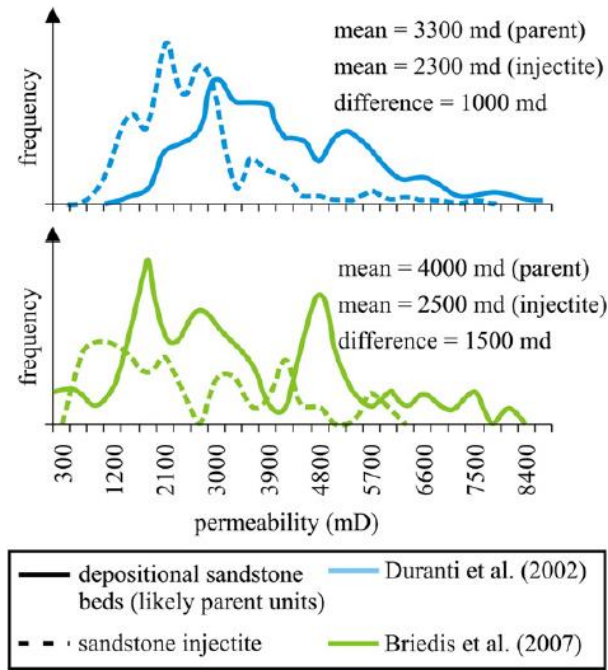
Fig. 2.20: Frequency distribution of permeability (milli-Darcy) in sand injectite reservoirs of the Alba (blue) and Balder (green) Fields showing the high permeability values of injectite reservoirs (from Hurst et al., 2011).
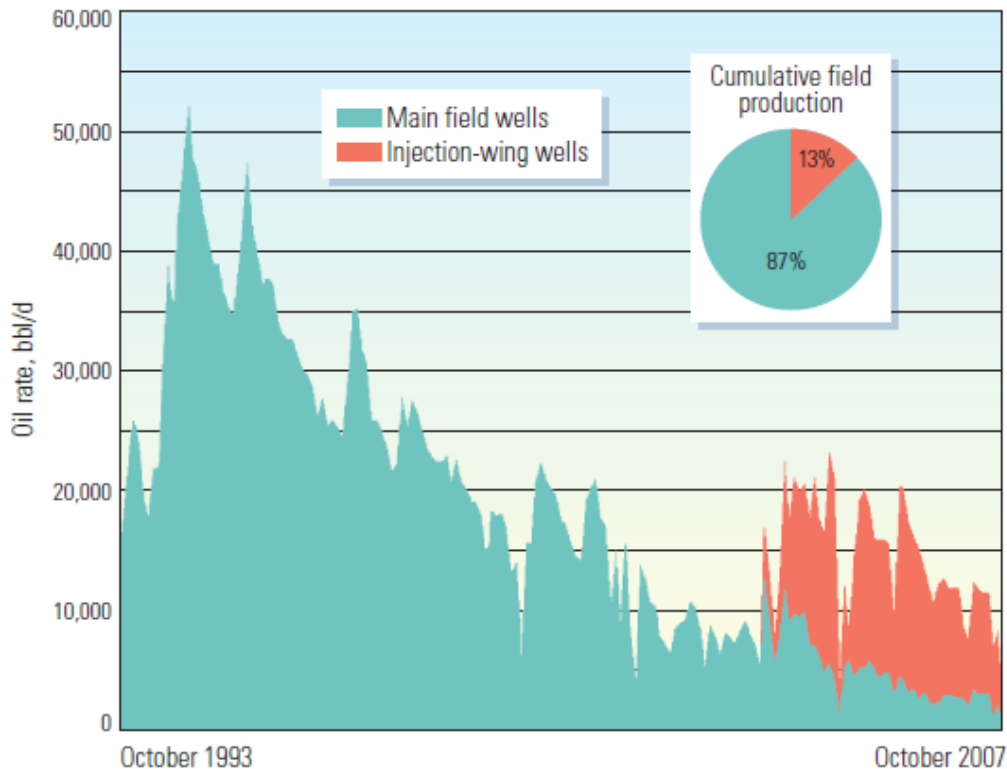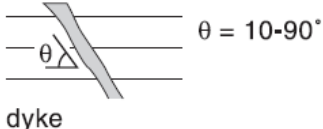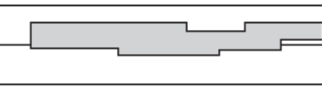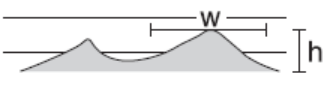
Fig. 2.21: Sand injectite impact on production. Production increased by seven horizontal wells in injectites wings (by 13%) in the Gryphon Field (UK 9/18b), North Sea Basin (from Braccini et al., 2008).

Table 2.2: An illustration of sand injectites as a new class of traps (intrusive trap styles) which are known to occur in a broad scale from centimetres to hundreds of meters in plan view and millimetres to tens of metres in vertical scale (modified from Hurst et al., 2005).

S/N	CROSS SECTION	PLAN VIEW	APPROX. DIMENSION (METRES)
a	$\theta = 10\text{-}90°$ dyke		x 700 y >200 z >20
b	sill (intrusive)		x 5 y >1000 z >15
c	sea-level sill (emergent)		x - y >250 z 5
d	w h scalloped tops	dependent on pre- and post-injection faulting	h 20 w 50
e	irregular bodies		x >30 y >500 z >30
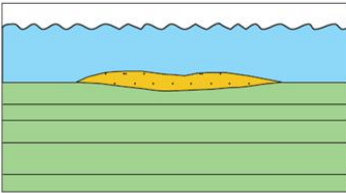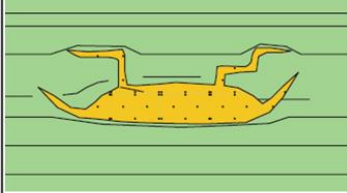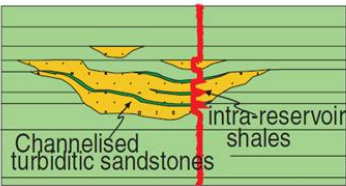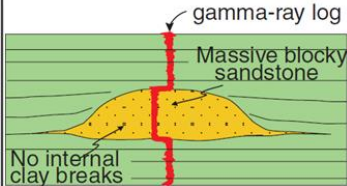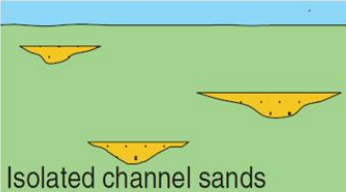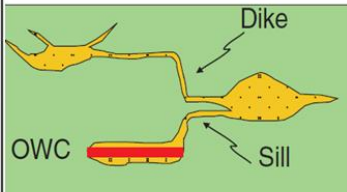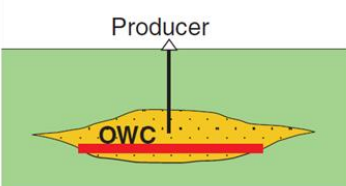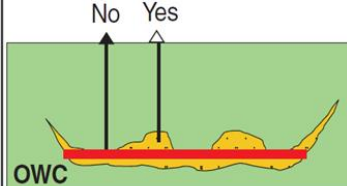
EFFECT ON RESERVOIR GEOLOGY (Lonergan et al., 2000)	DESCRIPTION	DEPOSITIONAL GEOMETRY (Prior to remobilization/injection)	POST-DEPOSITIONAL GEOMETRY (After remobilization/injection)
Change in reservoir geometry	- Steeping of original depositional geometries (e.g. Balder Field) - Development of pod-like sand bodies (e.g. Balder &Alba Fields) - Vertical intrusion of clastic dikes & sills above the reservoir (e.g. Alba, Gryphon and Forth/Harding Fields)		
Change in reservoir properties	- Homogenization of sand texture and reservoir properties - Obliteration of original sedimentary structures leading to a massive sandstone facies	Channelised turbiditic sandstones / intra-reservoir shales	gamma-ray log / Massive blocky sandstone / No internal clay breaks
Change in connectivity	- Alter transmissivity by allowing connectivity between previously isolated reservoir units	Isolated channel sands	Dike / OWC / Sill
Change in top reservoir structure/ depth surface and in reservoir volumetric	- Modification to the top reservoir surface (e.g. Alba - Uncertainty associated with the prediction of net sand volume and recovery efficiency	Producer / OWC	No Yes / OWC

Table 2.3: Summary of the effect of remobilization and injection on reservoir geology (modified from Lonergan et al., 2000).

2.5.3 Polygonal Fault Systems (PFS)

Polygonal faults are defined as an array of extensional, early compaction-related, non-tectonic, intra-formational, low-displacement (< 100 m throw) normal faults that form within layer-bound or confined stratigraphic units known as ''Tiers'' (Fig. 2.22c; Cartwright & Lonergan, 1996; Lonergan et al., 1998; Sun et al., 2010; Cartwright, 2011). This polygonal fault tiers usually vary in thickness between a few tens-of-meters to about 1 km or more and are characterized by very fine-grained sediments composed of smectite-rich claystone and/or biogenic mudstones (Sun et al., 2010). They exhibit a polygonal geometry in map view (Fig. 2.22d & e) which may be related to the fact that the faults usually intersect bedding planes (e.g., Fig.2.22b) with a variety of azimuth that define random polygons when viewed in map view.

Their occurrence was first recorded from conventional 2D seismic data from the Southern North Sea and in the Lower Tertiary Leper Claystone in Belgium (Henriet et al., 1989, 1991). However, their polygonal geometry was not recognized at that time because 3D seismic data was not available. At present, polygonal fault systems have been recorded and described globally (see Fig. 2.22a) in several sedimentary basins (e.g. North Sea Basin; Voring basin – offshore Norway; Offshore Angola; Nankai Trough – offshore Japan; Eromanga Basin – Australia; Baffin Bay – offshore west Greenland), with majority occurring in slope settings along passive continental margins and usually associated with hemipelagic sediments dominated by clay-sized grains (Cartwright & Dewhurst, 1998; Dewhurst et al., 1999; Cartwright, 2011). Polygonal faults are known to be widespread throughout the deep-water Paleogene succession of the North Sea (i.e., central and northern – Early Cretaceous to Miocene interval) and within the study area (Cartwright & Lonergan 1996; Lonergan et al., 1998; Dewhurst et al., 1999; Lonergan & Cartwright, 1999)

Cartwright & Dewhurst (1998) outlined seven important criteria for the identification of polygonal fault systems:

- **Map geometry:** they show polygonal plan view fault pattern
- **Vertical extent:** they are usually layer-bound and delimited by regionally correlatable stratigraphic surfaces
- **Areal extent:** usually distributed over large area of > 150,000 km^2 up to 200,000 km^2
- **Fault type:** all normal faults with throws between 5 – 100 m
- **Fault spacing:** faults are usually closely spaced (100 – 1000 m spacing)
- **Tiers:** deformed intervals and usually occur in two or more tiers
- **Fault polarity:** the faults tend to switch from synthetic to antithetic fault pattern

In general, their formation has been linked to compacting-related early-stage dewatering of fine-grained sediments, indicating their formation is associated with fluid remobilization and discharge (Cartwright et al., 2003; Cartwright, 2011). However, the exact driving mechanism for their formation remains a subject of debate. Several mechanisms have been documented by different authors, although most of the mechanisms are insufficient to account for all documented instances of polygonal fault occurrence. Some of these mechanisms include:

- **Hydraulic fracturing** due to differential compaction and overpressure development (Cartwright, 1994)
- **Syneresis** of fine-grained sediments which involves compaction by spontaneous volumetric contraction resulting from gravitational loading in slope settings (Cartwright & Lonergan 1996; Cartwright & Dewhurst, 1998; Dewhurst et al., 1999)
- **Density inversion** caused by differential compaction between their host strata and the overlying strata (Henriet et al., 1989; Wrona et al., 2017)
- Particle dissolution during diagenesis, which in turn induces tensile stress of sufficient magnitude for normal faulting (Shin et al., 2008; Cartwright, 2011; Wrona et al., 2017)
- Internal layer parallel extension of host strata caused by downslope gravitational sliding (Clausen et al., 1999; Cartwright et al., 2007); and
- Residual friction on fault plane (Goultry, 2001, 2002, 2008; Wrona et al., 2017a)

Polygonal fault systems have been documented as potential fluid flow pathway (Cartwright & Dewhurst, 1998; Hustoft et al, 2010). They have potential to serve as migration pathways for ascending fluid and may provide a vertical fluid plumbing system with the fault acting as permeable pathway through low porosity and permeability sediments (Gay et al., 2007). Therefore, their occurrence may be important for hydrocarbon migration and leakage. Some notable examples are in the Ormen Lange gas field in Norway, Hammerfest Basin and SW Barents Sea where their occurrence is suggested to have an implication for fluid migration and gas leakage. Finally, they may act as a seal-bypass systems which can compromise seal integrity, and they can result to reservoir compartmentalization when they occur at intervals where thin sandstone reservoirs are inter-bedded with thick interval of fine-grained mudstones, which raises an issue for consideration during risk analysis and development planning.

2.5.4 Silica Diagenetic Boundaries

Diagenetic reactions in siliceous sediments within most sedimentary basin, leading to the transformation of biogenic silica (Opal A - amorphous) to Crytocrystallne Opal-CT (cristobalite and tridymite a metastable intermediate phase) and subsequent transition of Opal-CT to quartz is well known (Runberg, 1991; Thyberg et al., 1999). This results to the formation of a silica diagenetic boundary (e.g., Fig. 2.23). Silica diagenetic boundaries have been recognized in many basins globally, e.g., in the Paleocene to Oligocene succession of the northern North Sea (e.g., Fig. 2.23h; Rundberg 1991; Olobayo, 2014; Wrona et al., 2017b: see their Fig. 2 & 8), North Sakhalian Basin (Meadow & Davies, 2009), and IODP drilling sites. The transformation occurs by dissolution and precipitation reactions which results to the alteration of the acoustic/physical (e.g., porosity, seismic velocity, and density) and chemical properties of the host sediment (Davies & Cartwright, 2002). This silica phase transformation is controlled by factors such as time, temperature, pressure, pore water chemistry, presence of clays & carbonate minerals, and the host rock lithology; with temperature and time playing a major role (Hein et al., 1978; Tada 1991; Davies & Cartwright 2002). The temperature requirement for Opal A to Opal-CT

phase transformation ranges between 2 – 56°C (Hein et al., 1978) while the temperature required for Opal-CT to quartz transformation range from 46 – 110°C (Hesse, 1990; Nobes et al., 1992). Lithology can however affect the rate and mode of transformation due to its direct influence on pore water chemistry, porosity, permeability, fracture formation and detrital mineral concentration. Silica phase transformation results to an abrupt collapse of pore framework, marked reduction in porosity, rapid sediment compaction leading to increase in density, decrease in water content due to significant expulsion of water, increase in thermal conductivity and generation of abnormally high pore pressure (Davies et al., 2006; Davies & Clark, 2006). Based on this, they are believed to facilitate the formation of polygonal faults & sand intrusion and can result to marine slope failure (Davies et al., 2006; Davies & Clark, 2006; Cartwright 2007; Huuse et al., 2010; Cartwright, 2011). X-ray diffraction (XRD) and scanning electron microscopy (SEM) analysis in the northern North Sea has shown evidence of diagenetic transformation within the Paleogene succession (i.e., Paleocene to Oligocene), which is the interval affected by sand intrusions and polygonal faulting (see Runberg 1991; Thyberg et al., 1999; Olobayo, 2014).

The changes in physical properties (e.g. density) resulting from the phase transformation, cause an increase in the acoustic impedance at the diagenetic boundaries compared to the surrounding sediments giving rise to a strong, high amplitude (normal polarity) reflection which can cover areas of about 10^4 – 10^5 km^2 of sedimentary basin (Davies & Cartwright, 2002; Meadow & Davies, 2007; Meadow & Davies, 2009) and cross-cut background stratal reflection (Davies & Cartwright, 2002; Hein et al., 1978). Most documented silica diagenetic boundaries on seismic are usually parallel to the present-day seafloor (Hein et al., 1978), while some others are not (e.g., Davies & Cartwright, 2002; Meadow & Davies, 2007), but instead are parallel to important unconformities. Due to the large dependence of silica phase transformation on temperature, Opal-A to Opal-CT diagenetic boundaries can be used as low-temperature present-day isothermal markers to reconstruct thermal history of basins, in order to determine the timing of maturation and maturity of source rocks (Brekke et al., 1999; Meadow & Cartwright, 2009). Also due to their observed tendency to follow unconformities, they can serve as potential paleo-thermometers (Kuramoto et al., 1992; Meadow & Davies, 2009).
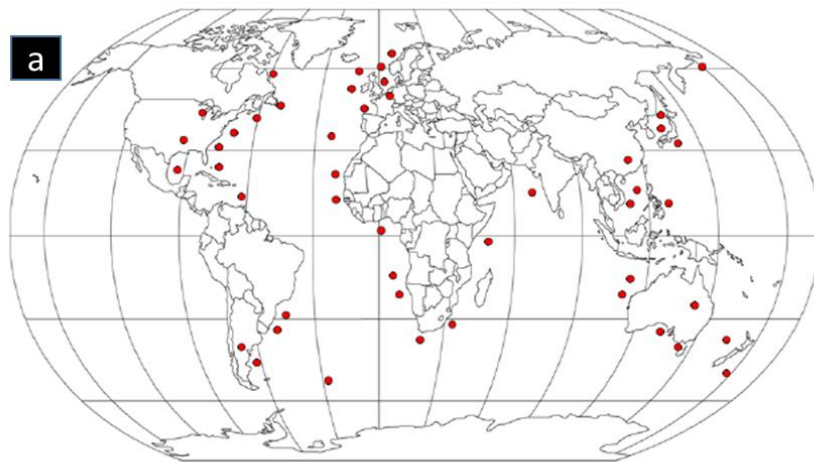
Global distribution of polygonal fault systems (PFS). Red dots are basins where PFS have been identified using 2D and 3D seismic data (after Cartwright, 2011)
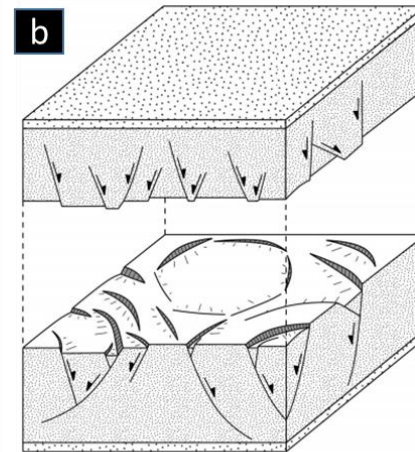
PFS showing layer-bound, low-displacement normal faults (after Wrona et al., 2017)
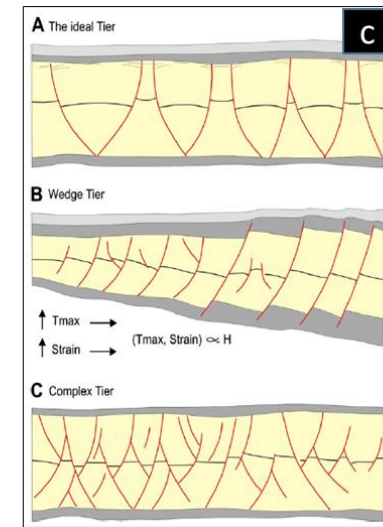
Polygonal faults tiers (Cartwright, 2011)
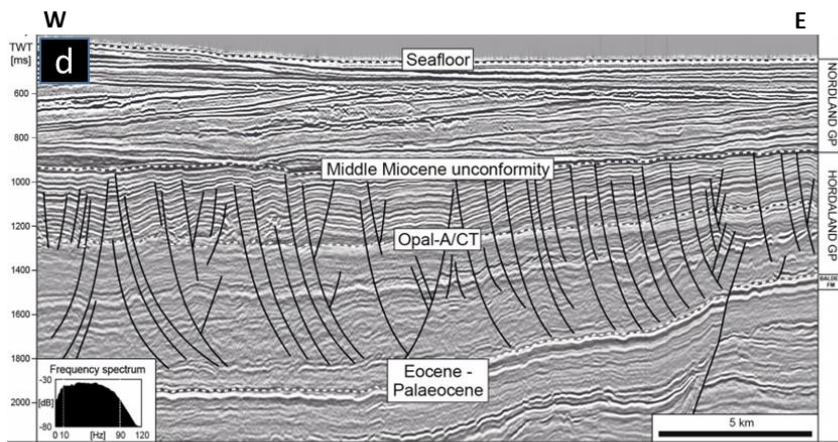
PFS in seismic cross section in the northern North Sea (after Wrona et al., 2017)
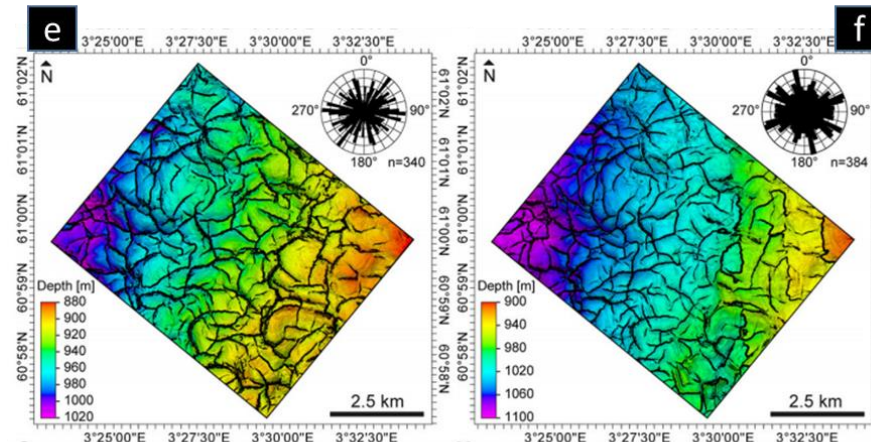
PFS in plan view from the northern North Sea (after Wrona et al., 2017)

Fig. 2.22: Polygonal fault occurrence, distribution, and its seismic characteristics. Also show is the Opal-A/CT diagenetic boundary.
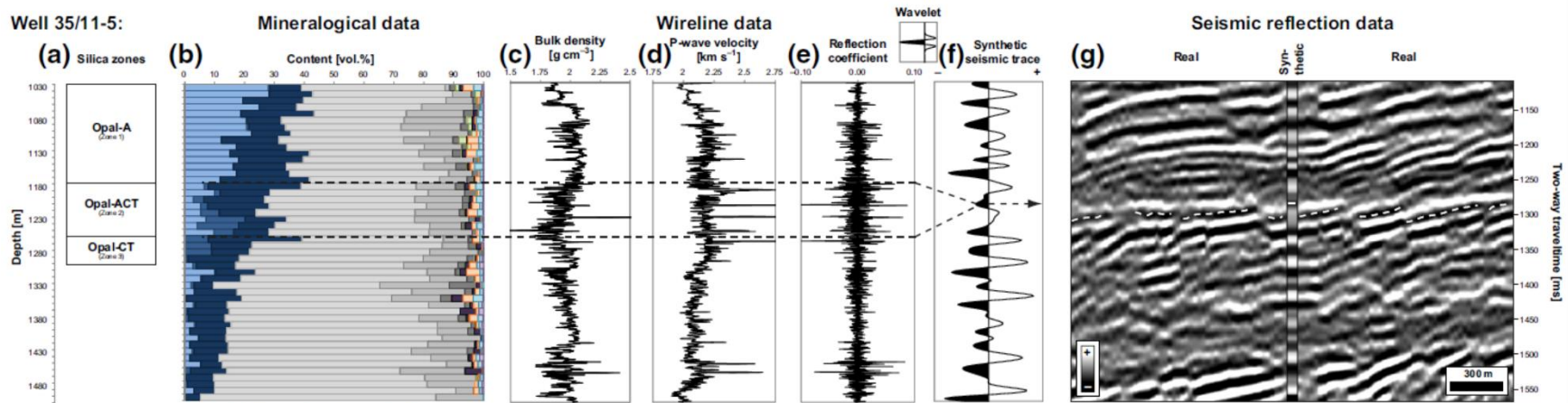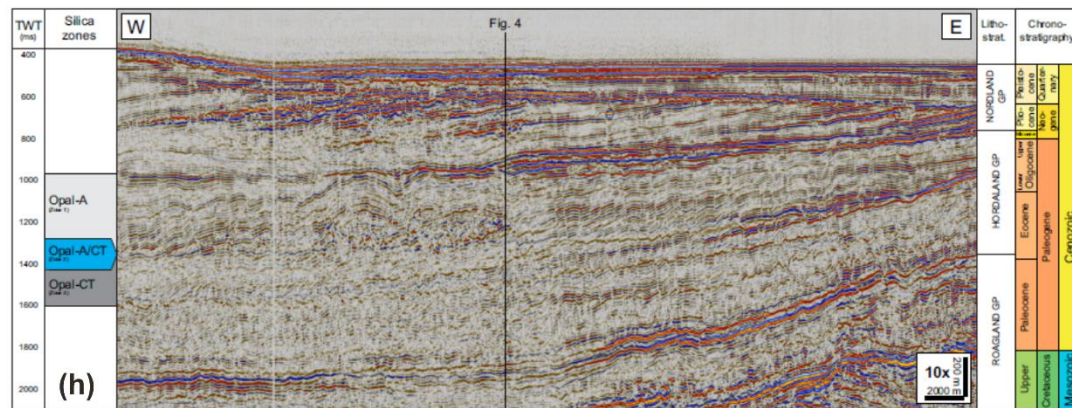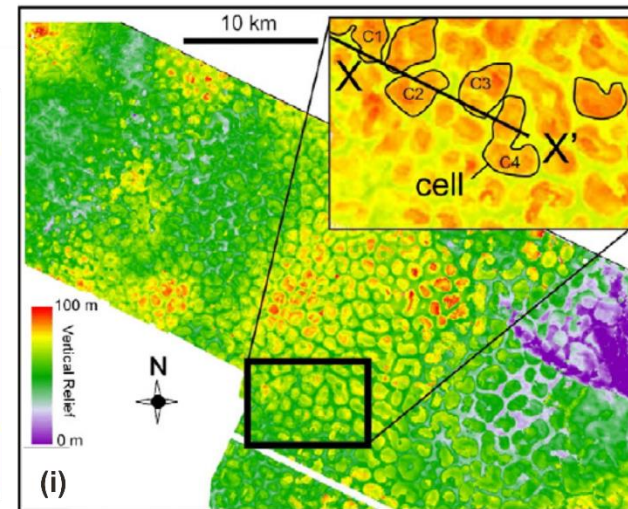
Fig. 2.23: An illustraion of opal-A/CT diagenetic boundary in wireline log data and 3D seismic data from the North Sea and Møre Basin

References (Chapter 1 & 2)

ABBOTTS, I.L. 1991. United Kingdom oil and gas fields 25 Years commemorative volume. *Geological Society Memoir*, **14**, 573.

AHMADI, Z.M., SAWYERS, M., KENYAN-ROBERTS, S., STANWORHT, C.W., KUGLER, K.A., KRISTENSEN, J. & FUGELLI, E.M.G. (2003). Palaeocene. In: *The Millennium Atlas: Petroleum geology of the central and northern North Sea* (Ed. by D. Evans, C. Graham, A. Armour & P. Bathurst). *The Geological Society of London, London,* 235–259.

ALLEN, J.R.L, 1985, Principles of Physical Sedimentology. *London, George Allen & Unwin*.

ALLEN, J.R.L. 1984. Sedimentary structures: their character and physical basis. Unabridged and corrected one-volume edition. *Sedimentary structures: their character and physical basis. Unabridged and corrected one-volume edition.*

AMBRASEYS, N.N. 1988. Engineering seismology: Part I. *Earthquake Engineering & Structural Dynamics*, **17**, 1–50, https://doi.org/10.1002/eqe.4290170101.

ANDERTON, R. 1993. Sedimentation and basin evolution in the Paleogene of the Northern North Sea and Faeroe–Shetland basins. *In*: *Petroleum Geology of Northwest Europe: Proceedings of the 4th Conference*. Geological Society of London, 31–31., https://doi.org/10.1144/0040031.

ANDRESEN, K.J. 2012. Fluid flow features in hydrocarbon plumbing systems: What do they tell us about the basin evolution? *Marine Geology*, **332**–**334**, 89–108, https://doi.org/10.1016/j.margeo.2012.07.006.

ANDRESEN, K.J., HEILMANN-CLAUSEN, C., CLAUSEN, O.R. & FRIIS, H. 2019. Deposition or remobilization of the enigmatic Hefring Member sand, eastern North Sea – A multidisciplinary approach. *Marine and Petroleum Geology*, https://doi.org/10.1016/j.marpetgeo.2019.06.001.

ANELL, I., THYBO, H. & RASMUSSEN, E. 2012. A synthesis of Cenozoic sedimentation in the North Sea. *Basin Research*, **24**, 154–179, https://doi.org/10.1111/j.1365-2117.2011.00517.x.

BADLEY, M.E., PRICE, J.D., RAMBECH DAHL, C. & AGDESTEIN, T. 1988. The structural evolution of the northern Viking Graben and its bearing upon extensional modes of basin formation. *Journal of the Geological Society*, **145**, 455–472, https://doi.org/10.1144/gsjgs.145.3.0455.

BARNARD, P.C. & BASTOW, M.A. 1991. Hydrocarbon generation, migration, alteration, entrapment and mixing in the Central and Northern North Sea. *Geological Society, London, Special Publications*, **59**, 167–190, https://doi.org/10.1144/GSL.SP.1991.059.01.12.

BERGSLIEN, D. 2002. Balder and Jotun - two sides of the same coin? A comparison of two Tertiary oil fields in the Norwegian North Sea. *Petroleum Geoscience*, **8**, 349–363, https://doi.org/10.1144/petgeo.8.4.349.

BERGSLIEN, D., KYLLINGSTAD, G., SOLBERG, A., FERGUSON, I.J. & PEPPER, C.F. 2005. Jotun Field reservoir geology and development strategy: pioneering play knowledge, multidisciplinary teams and partner co-operation – key to discovery and successful development. *Petroleum Geology: North-West Europe and Global Perspectives – Proceedings of the 6th Petroleum Geology Conference*, 99–110, https://doi.org/10.1144/0060099.

BOEHM, A. & MOORE, J.C. 2002. Fluidized sandstone intrusions as an indicator of Paleostress orientation, Santa Cruz, California. *Geofluids*, **2**, 147–161, https://doi.org/10.1046/j.1468-8123.2002.00026.x.

BRACCINI, E., DE BOER, W., HURST, A., HUUSE, M., VIGORITO, M. & TEMPLETON, G. 2008. Sand Injectites. *Oilfield Review*, 34–49.

BREKKE, H., DAHLGREN, S., NYLAND, B. & MAGNUS, C. 1999. The prospectivity of the Voring and More basins on the Norwegian Sea continental margin. *Petroleum Geology Conference Series*, **14**, 261–274, https://doi.org/10.1144/0050261.

BREKKE, H. & SJULSTAD, H. 2001. Sedimentary environments offshore Norway—an overview. *Norwegian Petroleum …*, 7–37.

BREKKE, H. 2000. The tectonic evolution of the Norwegian Sea Continental Margin with emphasis on the Vøring and Møre Basins. *Geological Society, London, Special Publications*, **167**, 327–378, https://doi.org/10.1144/GSL.SP.2000.167.01.13.

BRIEDIS, N. A, BERGSLIEN, D., HJELLBAKK, A, HILL, R.E. & MOIR, G.J. 2007. Recognition Criteria, Significance to Field Performance, and Reservoir Modelling of Sand Injections in the Balder Field, North Sea. *Sand injectites: Implications for hydrocarbon exploration and production*, 91–102, https://doi.org/-.

BROWN, A.R. 1996. Seismic attributes and their classification. *Leading Edge*, **15**, 1090, https://doi.org/10.1190/1.1437208.

BROWN, A.R. 2001. Understanding seismic attributes. Geophysics, 66, 47–48, https://doi.org/10.1190/1.1444919.

BROOKE, C.M., TRIMBLE, T.J. & MACKAY, T. a. 1995. Mounded shallow gas sands from the Quaternary of the North Sea: analogues for the formation of sand mounds in deep water Tertiary sediments? *Geological Society, London, Special Publications*, **94**, 95–101, https://doi.org/10.1144/GSL.SP.1995.094.01.08.

BRUNSTAD, H., GRADSTEIN, F., VERGARA, L., LIE, J.E. & HAMMER, Ø. 2009. A Revision of the Rogaland Group, Norwegian North Sea.

BUGGE, T., TVEITEN, B. & BACKSTROM, S. 2001. The depositional history of the Cretaceous in the north-eastern North Sea. *In*: *Sedimentary Environments Offshore Norway - Palaeozoic to Recent*. 279–291., https://doi.org/10.1016/S0928-8937 (01)80018-7.

BURLEY, S.D. 1993. Models of burial diagenesis for deep exploration in Jurassic fault traps of the Central and Northern North Sea. *In*: *Petroleum Geology of Northwest Europe: Proceedings of the 4th Conference on Petroleum Geology of NW. Europe, at the Barbican Centre, London*. Geological Society of London, 1353–1376., https://doi.org/10.1144/0041353.

CALVÈS, G., SCHWAB, A.M., HUUSE, M., VAN RENSBERGEN, P., CLIFT, P.D., TABREZ, A.R. & INAM, A. 2010. Cenozoic mud volcano activity along the Indus Fan: offshore Pakistan. *Basin Research*, **22**, 398–413, https://doi.org/10.1111/j.1365-2117.2009.00448.x.

CARTWRIGHT, J. 2010. Regionally extensive emplacement of sandstone intrusions: A brief review. *Basin Research*, **22**, 502–516, https://doi.org/10.1111/j.1365-2117.2009.00455.x.

CARTWRIGHT, J.A. & DEWHURST, D.N. 1998. Layer-bound compaction faults in fine-grained sediments. *Bulletin of the Geological Society of America*, **110**, 1242–1257, https://doi.org/10.1130/0016-7606 (1998)110<1242: LBCFIF>2.3.CO; 2.

CARTWRIGHT, J.A. & LONERGAN, L. 1996. Volumetric contraction during the compaction of mudrocks: A mechanism for the development of regional-scale polygonal fault systems. *Basin Research*, **8**, 183–193, https://doi.org/10.1046/j.1365-2117.1996.01536.x.

CARTWRIGHT, J., HUUSE, M. & APLIN, A. 2007. Seal bypass systems. *AAPG Bulletin*, **91**, 1141–1166, https://doi.org/10.1306/04090705181.

CARTWRIGHT, J., JAMES, D. & BOLTON, A. 2003. The genesis of polygonal fault systems: a review. *Geological Society, London, Special Publications*, **216**, 223–243, https://doi.org/10.1144/GSL.SP.2003.216.01.15.

CARTWRIGHT, J., JAMES, D., HUUSE, M., VETEL, W. & HURST, A. 2008. The geometry and emplacement of conical sandstone intrusions. *Journal of Structural Geology*, **30**, 854–867, https://doi.org/10.1016/j.jsg.2008.03.012.

CARTWRIGHT, J.A. 1994. Episodic basin-wide hydrofracturing of overpressured Early Cenozoic mudrock sequences in the North Sea Basin. *Marine and Petroleum Geology*, **11**, 587–607, https://doi.org/10.1016/0264-8172 (94)90070-1.

CHRISTIANSSON, P., FALEIDE, J.I. & BERGE, A.M. 2000. Crustal structure in the northern North Sea: an integrated geophysical study. *Geological Society, London, Special Publications*, **167**, 15–40, https://doi.org/10.1144/GSL.SP.2000.167.01.02.

CLAUSEN, O.R., GREGERSEN, U., MICHELSEN, O. & SØRENSEN, J.C. 1999. Factors controlling the Cenozoic sequence development in the eastern parts of the North Sea. *Journal of the Geological Society*, 156, 809–816, https://doi.org/10.1144/gsjgs.156.4.0809.

CORNFORD, C. 2009. Source rocks and hydrocarbons of the North Sea. *In*: *Petroleum Geology of the North Sea: Basic Concepts and Recent Advances: Fourth Edition*. Oxford, UK, Blackwell Science Ltd, 376–462., https://doi.org/10.1002/9781444313413.ch11.

COWARD, M.P., DEWEY, J.F., HEMPTON, M., HOLROYD, J. (2003). Tectonic evolution. In: The Millennium Atlas: *Petroleum geology of the central and northern North Sea* (Ed. by D. Evans, C. Graham, A. Armour & P. Bathurst). *The Geological Society of London*, 17–33.

DAVIES, R.J. & CARTWRIGHT, J. 2002. A fossilized Opal A to Opal C/T transformation on the northeast Atlantic margin: Support for a significantly elevated palaeo-geothermal gradient during the Neogene? *Basin Research*, **14**, 467–486, https://doi.org/10.1046/j.1365-2117.2002.00184.x.

DAVIES, R.J. 2003. Kilometer-scale fluidization structures formed during early burial of a deep-water slope channel on the Niger Delta. *Geology*, **31**, 949–952, https://doi.org/10.1130/G19835.1.

DAVIES, R.J., BRUMM, M., MANGA, M., RUBIANDINI, R., SWARBRICK, R. & TINGAY, M. 2008. The East Java mud volcano (2006 to present): An earthquake or drilling trigger? *Earth and Planetary Science Letters*, **272**, 627–638, https://doi.org/10.1016/j.epsl.2008.05.029.

DAVIES, R.J. & CLARK, I.R. 2006. Submarine slope failure primed and triggered by silica and its diagenesis. *Basin Research*, **18**, 339–350, https://doi.org/10.1111/j.1365-2117.2006.00297.x.

DAVIES, R.J., HUUSE, M., HIRST, P., CARTWRIGHT, J. & YANG, Y. 2006. Giant clastic intrusions primed by silica diagenesis. *Geology*, **34**, 917–920, https://doi.org/10.1130/G22937A.1.

DE BOER, W., RAWLINSON, P.B. & HURST, A. 2007. Successful Exploration of a Sand Injectite Complex: Hamsun Prospect, Norway Block 24/9. *Sand injectites: Implications for hydrocarbon exploration and production: AAPG Memoir 87*, 65–68, https://doi.org/10.1306/1209850M873256.

DEEGAN, C.E. & SCULL, B.J. 1977. A standard lithostratigraphic nomenclature for the Central and Northern North Sea. *Norwegian Petroleum Directorate Bulletin*, **1**, 36.

DEWHURST, D.N., CARTWRIGHT, J.A. & LONERGAN, L. 1999. The development of polygonal fault systems by syneresis of colloidal sediments. *Marine and Petroleum Geology*, **16**, 793–810, https://doi.org/10.1016/S0264-8172 (99)00035-5.

DI FELICE, R. 1995. Hydrodynamics of liquid fluidisation. *Chemical Engineering Science*, **50**, 1213–1245, https://doi.org/10.1016/0009-2509(95)98838-6.

DIGGS, T.N. 2007. An Outcrop Study of Clastic Injection Structures in the Carboniferous Tesnus Formation, Marathon Basin, Trans-Pecos Texas. *AAPG Memoir*, 209–219, https://doi.org/10.1306/1209864M873266.

DIONNE, J.-C. 1976. Miniature mud volcanoes and other injection features in tidal flats, James Bay, Quebec. *Canadian Journal of Earth Sciences*, **13:422-428**, 422–428, https://doi.org/10.1139/e76-043.

DIXON, R.J., SCHOFIELD, K., ANDERTON, R., REYNOLDS, A.D., ALEXANDER, R.W.S., WILLIAMS, M.C. & DAVIES, K.G. 1995. Sandstone diapirism and clastic intrusion in the Tertiary submarine fans of the Bruce-Beryl Embayment, Quadrant 9, UKCS. *Geological Society, London, Special Publications*, **94**, 77–94, https://doi.org/10.1144/GSL.SP.1995.094.01.07.

DMITRIEVA, E., JACKSON, C.A.-L., HUUSE, M. & MCCARTHY, A. 2012. Paleocene deep-water depositional systems in the North Sea Basin: a 3D seismic and well data case study, offshore Norway. *Petroleum Geoscience*, **18**, 97–114, https://doi.org/10.1144/1354-079311-027.

DMITRIEVA, E., JACKSON, C.A.-L., HUUSE, M. & KANE, I.A. 2018. Regional distribution and controls on the development of post-rift turbidite systems: insights from the Paleocene of the eastern North Viking Graben, offshore Norway. *Geological Society, London, Petroleum Geology Conference series*, **8**, PGC8.31, https://doi.org/10.1144/PGC8.31.

DORÉ, A.G., LUNDIN, E.R., JENSEN, L.N., BIRKELAND, Ø., ELIASSEN, P.E. & FICHLER, C. 1999. Principal tectonic events in the evolution of the northwest European Atlantic margin. *In*: *Petroleum Geology of Northwest Europe: Proceedings of the 5th Conference*. 41–61., https://doi.org/10.1144/0050041.

DURANTI, D., HURST, A., BELL, C., GROVES, S. & HANSON, R. 2002. Injected and remobilized Eocene sandstones from the Alba Field, UKCS: core and wireline log characteristics. *Petroleum Geoscience*, **8**, 99–107, https://doi.org/10.1144/petgeo.8.2.99.

DURANTI, D. & HURST, A. 2004. Fluidization and injection in the deep-water sandstones of the Eocene Alba Formation (UK North Sea). *Sedimentology*, **51**, 503–529, https://doi.org/10.1111/j.1365-3091.2004.00634.x.

FAERSETH, R.B., GABRIELSEN, R.H. & HURICH, C.A. 1995. Influence of basement in structuring of the North Sea Basin, offshore southwest Norway. *Norsk Geologisk Tidsskrift*, **75**, 105–119.

FAERSETH, R.B., KNUDSEN, B.-E., LILJEDAHL, T., MIDBØE, P.S. & SØDERSTRØM, B. 1997. Oblique rifting and sequential faulting in the Jurassic development of the northern North Sea. *Journal of Structural Geology*, **19**, 1285–1302, https://doi.org/10.1016/S0191-8141(97)00045-X.

FALEIDE, J.I., KYRKJEBØ, R., KJENNERUD, T., GABRIELSEN, R.H., JORDT, H., FANAVOLL, S. & BJERKE, M.D. 2002. Tectonic impact on sedimentary processes during Cenozoic evolution of the northern North Sea and surrounding areas. *Geological Society, London, Special Publications*, **196**, 235–269, https://doi.org/10.1144/GSL.SP.2002.196.01.14.

FJELDSKAAR, W., TER VOORDE, M., JOHANSEN, H., CHRISTIANSSON, P., FALEIDE, J.I. & CLOETINGH, S.A.P.L. 2004. Numerical simulation of rifting in the northern Viking Graben: The mutual effect of modelling parameters. *Tectonophysics*, **382**, 189–212, https://doi.org/10.1016/j.tecto.2004.01.002.

RICHARDSON, J.R. 1971. Incipient fluidization and particulate systems. *ci.nii.ac.jp*.

FRASER, S., ROBINSON, A., JOHNSON, H, UNDERHILL, J., & KADOLSKY, D. (2003). Palaeocene. In: *The Millennium Atlas: Petroleum geology of the central and northern North Sea* (Ed. by D. Evans, C. Graham, A. Armour & P. Bathurst). *The Geological Society of London, London,* 157–189.

FYFE, J.A., GREGERSEN, U., JORDT, H., RUNDBERG, Y., EIDVIN, T., EVANS, D., STEWART, D., HOVLAND, M. & ANDERSEN, P. (2003) Oligocene to Holocene. In: *The Millenium Atlas: Petroleum Geology of the Central and Northern North Sea* (Ed. by D. Evans, C. Graham, A. Armour & P. Bathurst. *Geological Society London, London,* 279-287

GABRIELSEN, R.H. & SPENCER, A.M. 1986. Structural elements in graben systems and their influence on hydrocarbon trap types. Habitat of hydrocarbons on the Norwegian continental shelf; proceedings of an international conference. *In*: *Norwegian Petroleum Society* …. 55–60.

GABRIELSEN, R.H., KYRKJEBO, R., FALEIDE, J.I., FJELDSKAAR, W. & KJENNERUD, T. 2001. The Cretaceous post-rift basin configuration of the northern North Sea. *Petroleum Geoscience*, **7**, 137–154, https://doi.org/10.1144/petgeo.7.2.137.

GABRIELSEN, R.H., FOERSETH, R.B., STEEL, R.J., IDIL, S. & KLOVJAN, O.S. 1990. *Architectural Styles of Basin Fill in the Northern Viking Graben*.

GALLO, F. & WOODS, A.W. 2004. On steady homogeneous sand-water flows in a vertical conduit. *Sedimentology*, **51**, 195–210, https://doi.org/10.1111/j.1365-3091.2004.00608.x.

GAMBERI, F. & ROVERE, M. 2010. Mud diapirs, mud volcanoes and fluid flow in the rear of the Calabrian Arc Orogenic Wedge (southeastern Tyrrhenian Sea). *Basin Research*, **22**, 452–464, https://doi.org/10.1111/j.1365-2117.2010.00473.x.

GAUTIER, D.L. 2005. Kimmeridgian Shales Total Petroleum System of the North Sea Graben Province. *U.S. Geological Survey Bulletin*, **2204–C**, 29.

GAY, A., LOPEZ, M., COCHONAT, P., SÉRANNE, M., LEVACHÉ, D. & SERMONDADAZ, G. 2006. Isolated seafloor pockmarks linked to BSRs, fluid chimneys, polygonal faults and stacked Oligocene-Miocene turbiditic palaeochannels in the Lower Congo Basin. *Marine Geology*, **226**, 25–40, https://doi.org/10.1016/j.margeo.2005.09.018.

GAY, A., LOPEZ, M. & AL., E. 2007. Geological controls on focused fluid flow associated with seafloor seeps in the Lower Congo Basin. *Elsevier*.

GILL, W.D. & KUENEN, P.H. 1957. Sand volcanoes on slumps in the Carboniferous of County Clare, Ireland. *Quarterly Journal of the Geological Society,* **113**, 441–460, https://doi.org/10.1144/GSL.JGS.1957.113.01-04.19.

GOFF, J.C. 1983. Hydrocarbon generation and migration from Jurassic source rocks in the E Shetland Basin and Viking Graben of the northern North Sea. *Journal of the Geological Society*, **140**, 445–474, https://doi.org/10.1144/gsjgs.140.3.0445.

GOŁĘDOWSKI, B., NIELSEN, S.B. & CLAUSEN, O.R. 2012. Patterns of Cenozoic sediment flux from western Scandinavia. *Basin Research*, **24**, 377–400, https://doi.org/10.1111/j.1365-2117.2011.00530.x.

GOULTY, N.R. 2001. Mechanics of layer-bound polygonal faulting in fine-grained sediments. *Journal of the Geological Society, London*, **159**, 239–246, https://doi.org/10.1144/0016-764901-111.

GOULTY, N.R. 2001. Polygonal fault networks in fine-grained sediments - An alternative to the syneresis mechanism. *First Break*, **19**, 69–73, https://doi.org/10.1046/j.1365-2397.2001.00137.x.

GOULTY, N.R. 2008. Geomechanics of polygonal fault systems: a review. *Petroleum Geoscience*, **14**, 389–397, https://doi.org/10.1144/1354-079308-781.

GRAUE, K. 2000. Mud volcanoes in deep-water Nigeria. *Marine and Petroleum Geology*, **17**, 959–974, https://doi.org/10.1016/S0264-8172(00)00016-7.

HARDIE, J. 1999. Clastic dikes intruding Cretaceous coals of western Colorado.

HARTOG JAGER, D. Den, GILES, M.R. & GRIFFITHS, G.R. 1993. Evolution of Paleogene submarine fans of the North Sea in space and time. *In*: *Petroleum Geology of Northwest Europe: Proceedings of the 4th Conference*. Geological Society of London, 59–71., https://doi.org/10.1144/0040059.

HEGGLAND, R. 1998. Gas seepage as an indicator of deeper prospective reservoirs. A study based on exploration 3D seismic data. *Marine and Petroleum Geology*, **15**, 1–9, https://doi.org/10.1016/S0264-8172(97)00060-3.

HEIN, J.R., SCHOLL, D.W., BARRON, J.A., JONES, M.G. & MILLER, J. 1978. Diagenesis of late Cenozoic diatomaceous deposits and formation of the bottom simulating reflector in the southern Bering Sea. *Sedimentology*, **25**, 155–181, https://doi.org/10.1111/j.1365-3091.1978.tb00307.x.

HENRIET, J.P., DE BATIST, M., VAN VAERENBERGH, W. & VERSCHUREN, M. 1989. Seismic facies and clay tectonic features in the southern North Sea. *Bulletin of the Belgian Geological Society*, **97**, 457–472.

HENRIET, J.P., DE BATIST, M. & VERSCCHUREN, M. 1991. Early Fracturing of Palaeogene clays, southernmost North Sea: relevance to mechanisms of primary hydrocarbon migration. *Generation, accumulation, and production of Europe's hydrocarbons, Special Publication of the European Association of Petroleum Geoscientists No.1*, 217–227.

HERMANRUD, C., VENSTAD, J.M., CARTWRIGHT, J., RENNAN, L., HERMANRUD, K. & NORDGÅRD BOLÅS, H.M. 2013. Consequences of Water Level Drops for Soft Sediment Deformation and Vertical Fluid Leakage. *Mathematical Geosciences*, **45**, 1–30, https://doi.org/10.1007/s11004-012-9435-0.

HERMANRUD, C., CHRISTENSEN, E., HAUGVALDSTAD, M., RØYNESTAD, L.M., TJENSVOLD, I.T. & WATSEND, L. 2019. Triggers of sand remobilization in deep marine deposits. *Geological Society, London, Special Publications*, https://doi.org/10.1144/sp493-2018-35.

HESSE, R. 1988. Diagenesis No.13. Origin of chert: diagenesis of biogenic siliceous sediments. *Geoscience Canada*, **15**, 171–192.

HOVLAND, M., GARDNER, J. V. & JUDD, A.G. 2002. The significance of pockmarks to understanding fluid flow processes and geohazards. *Geofluids*, **2**, 127–136, https://doi.org/10.1046/j.1468-8123.2002.00028.x.

HUBBARD, S.M., ROMANS, B.W. & GRAHAM, S.A. 2007. An Outcrop Example of Large-scale Conglomeratic Intrusions Sourced from Deep-water Channel Deposits, Cerro Toro Formation, Magallanes Basin, Southern Chile. *American Association of Petroleum Geologists*, 199–207, https://doi.org/10.1306/1209863M873265.

HURST, A. & CARTWRIGHT, J. 2005. Sand injectites: an emerging global play in deep-water clastic environments. *In*: *Petroleum Geology: North-West Europe and Global Perspectives— Proceedings of the 6th Petroleum Geology Conference*. 133–144., https://doi.org/10.1144/0060133.

HURST, A., CARTWRIGHT, J., HUUSE, M., JONK, R., SCHWAB, A., DURANTI, D. & CRONIN, B. 2003. Significance of large-scale sand injectites as long-term fluid conduits: Evidence from seismic data. *Geofluids*, **3**, 263–274, https://doi.org/10.1046/j.1468-8123.2003.00066.x.

HURST, A. & CARTWRIGHT, J. 2007. Relevance of Sand Injectites to Hydrocarbon Exploration and Production. *In*: *Sand Injectites: Implications for Hydrocarbon Exploration and Production: AAPG Memoir 87*. 1–19., https://doi.org/10.1306/1209846M871546.

HURST, A., CARTWRIGHT, J. & DURANTI, D. 2003. Fluidization structures produced by upward injection of sand through a sealing lithology. *Geological Society, London, Special Publications*, **216**, 123–138, https://doi.org/10.1144/GSL.SP.2003.216.01.09.

HURST, A., CARTWRIGHT, J., HUUSE, M. & DURANTI, D. 2006. Extrusive sandstones (extrudites): a new class of stratigraphic trap? *The Deliberate Search for the Stratigraphic Trap. Geological Society, London, Special Publications, 254*, 289–300, https://doi.org/10.1144/gsl.sp.2006.254.01.15.

HURST, A., SCOTT, A. & VIGORITO, M. 2011. Physical characteristics of sand injectites. *Earth-Science Reviews*, **106**, 215–246, https://doi.org/10.1016/j.earscirev.2011.02.004.

HUSMO, T., HAMAR, G. P., HØILAND, O., JOHANNESSEN, E., RØMULD, A., SPENCER, A. M., & TITTERTON, R. 2003. Lower and Middle Jurassic. In: *The Millennium Atlas: Petroleum geology of the central and northern North Sea* (Ed. by D. Evans, C. Graham, A. Armour & P. Bathurst). *The Geological Society of London, London,* 129–155.

HUSTOFT, S., BÜNZ, S. & MIENERT, J. 2010. Three-dimensional seismic analysis of the morphology and spatial distribution of chimneys beneath the Nyegga pockmark field, offshore mid-Norway. *Basin Research*, **22**, 465–480, https://doi.org/10.1111/j.1365-2117.2010.00486.x.

HUUSE, M., CARTWRIGHT, J.A., GRAS, R. & HURST, A. 2005. Kilometre-scale sandstone intrusions in the Eocene of the Outer Moray Firth (UK North Sea): migration paths, reservoirs, and potential drilling hazards. *In*: *Petroleum Geology: North-West Europe and Global Perspectives – Proceedings of the 6th Petroleum Geology Conference*. Geological Society of London, 1577–1594., https://doi.org/10.1144/0061577.

HUUSE, M., JACKSON, C.A.L., OLOBAYO, O., DMITRIEVA, E. & ANDRESEN, K.J. 2012. A sand injectite stratigraphy for the North Sea. *In*: *74th European Association of Geoscientists and Engineers Conference and Exhibition 2012 Incorporating SPE EUROPEC 2012: Responsibly Securing Natural Resources*, https://doi.org/10.3997/2214-4609.20148702.

HUUSE, M., LYKKE-ANDERSEN, H. & MICHELSEN, O. 2001. Cenozoic evolution of the eastern Danish North Sea. *Marine Geology*, **177**, 243–269, https://doi.org/10.1016/S0025-3227(01)00168-2.

HUUSE, M. 2008. Sandstone intrusions: Implications for exploration and production. *World Oil*, **229**, 87–91.

HUUSE, M., CARTWRIGHT, J., HURST, A. & STEINSLAND, N. 2007. Seismic Characterization of Large-scale Sandstone Intrusions. *Sand injectites: Implications for hydrocarbon exploration and production: AAPG Memoir 87*, 21–35, https://doi.org/10.1306/1209847M873253.

HUUSE, M., DURANTI, D., STEINSLAND, N., GUARGENA, C. G., PRAT, P., HOLM, K., CARTWRIGHT, J., & Hurst, A. 2004. Seismic Characteristics of Large-Scale Sandstone Intrusions in the Paleogene of the South Viking Graben, UK and Norwegian North Sea. *Geological Society, London, Memoirs*, **29**, 263–278, https://doi.org/10.1144/GSL.MEM.2004.029.01.25.

HUUSE, M., JACKSON, C., CARTWRIGHT, J. & HURST, A. 2009. Large-Scale Sand Injectites in the North Sea: Seismic and event Stratigraphy and Implications for Hydrocarbon Exploration. *AAPG Search & Discovery*, **40481**, https://doi.org/10.1306/1209847M873253.

HUUSE, M., JACKSON, C.A.-L., VAN RENSBERGEN, P., DAVIES, R.J., FLEMINGS, P.B. & DIXON, R.J. 2010. Subsurface sediment remobilization and fluid flow in sedimentary basins: An overview. *Basin Research*, **22**, 342–360, https://doi.org/10.1111/j.1365-2117.2010.00488.x.

HUUSE, M. & MICKELSON, M. 2004. Eocene sandstone intrusions in the Tampen Spur area (Norwegian North Sea Quad 34) imaged by 3D seismic data. *Marine and Petroleum Geology*, **21**, 141–155, https://doi.org/10.1016/j.marpetgeo.2003.11.018.

JACKSON, C.A.-L. & SØMME, T.O. 2011. Borehole evidence for wing-like clastic intrusion complexes on the western Norwegian margin. *Journal of the Geological Society*, **168**, 1075–1078, https://doi.org/10.1144/0016-76492011-035.

JACKSON, C.A.-L. 2007. The geometry, distribution, and development of clastic injections in slope systems: seismic examples from the Upper Cretaceous Kyrre Formation, Måløy Slope, Norwegian Margin. *Sand injectites: implications for hydrocarbon exploration and production*, 37–48, https://doi.org/-.

JACKSON, C.A.L., HUUSE, M. & BARBER, G.P. 2011. Geometry of wing-like clastic intrusions adjacent to a deep-water channel complex: Implications for hydrocarbon exploration and production. *AAPG Bulletin*, 95, 559–584, https://doi.org/10.1306/09131009157.

JENKINS, O.P. 1930. Sandstone dikes as conduits for oil migration through shales. *AAPG bulletin*, **14**, 411–421.

JENSSEN, A.., BERGSLIEN, D., RYE-LARSEN, M. & LINDHOLM, R. 1993. Origin of complex mound geometry of Paleocene submarine-fan sandstone reservoirs, Balder Field, Norway. *Petroleum Geology of Northwest Europe: Proceedings of the 4th Conference on Petroleum Geology of NW. Europe, at the Barbican Centre, London*, **1**, 135–143, https://doi.org/10.1144/0040135.

JOHNSON, H.D. & FISHER, M.J. 2009. North Sea plays: Geological controls on hydrocarbon distribution. *In*: *Petroleum Geology of the North Sea: Basic Concepts and Recent Advances: Fourth Edition*. Oxford, UK, Blackwell Science Ltd, 463–547., https://doi.org/10.1002/9781444313413.ch12.

JOHNSON, H.D. 1977. Sedimentation and water escape structures in some late Precambrian shallow marine sandstones from Finnmark, North Norway. *Sedimentology*, **24**, 389–411, https://doi.org/10.1111/j.1365-3091.1977.tb00129.x.

JOHNSTON, J.D. 1993. Ice wedge casts in the Dalradian of south Donegal - evidence for subaerial exposure of the Boulder Bed. *Irish Journal of Earth Sciences*, **12**, 13–26.

JOLLY, R.J.H. & LONERGAN, L. 2002. Mechanisms and controls on the formation of sand intrusions. *Journal of the Geological Society*, **159**, 605–617, https://doi.org/10.1144/0016-764902-025.

JONK, R., CRONIN, B.T. & HURST, A. 2007. Variation in Sediment Extrusion in Basin-floor, Slope, and Delta-front Settings: Sand Volcanoes and Extruded Sand Sheets from the Namurian of County Clare, Ireland. *The American Association of Petroleum Geologist*, **87**, 221–226, https://doi.org/10.1306/1209865M873267.

JONK, R., DURANTI, D., PARNELL, J., HURST, A & FALLICK, A. E. 2003. The structural and diagenetic evolution of injected sandstones: examples from the Kimmeridgian of NE Scotland. *Journal of the Geological Society*, **160**, 881–894, https://doi.org/10.1144/0016-764902-091.

JONK, R. 2010. Sand-rich injectites in the context of short-lived and long-lived fluid flow. *Basin Research*, **22**, 603–621, https://doi.org/10.1111/j.1365-2117.2010.00471.x.

JORDT, H., THYBERG, B.I. & NØTTVEDT, A. 2000. Cenozoic evolution of the central and northern North Sea with focus on differential vertical movements of the basin floor and surrounding clastic source areas. *Geological Society, London, Special Publications*, **167**, 219–243, https://doi.org/10.1144/GSL.SP.2000.167.01.09.

KUBALA, M., BASTOW, M., THOMPSON, S., SCOTCHMAN, I., OYGARD, K. (2003). Geothermal regime, petroleum generation and migration. In: Evans, D., Armour, C.G.A., Bathurst, P. (Eds.), The Millennium Atlas: Petroleum Geology of the Central and Northern North Sea. The Geological Society of London, London, pp. 289–315.

KURAMOTO, S. 1992. Can opal-A/opal-CT BSR be an indicator of the thermal structure of the Yamato Basin, Japan Sea? *Proc., scientific results, ODP, Legs 127/128, Japan Sea*, 1145–1156.

KYRKJEBO, R., GABRIELSEN, R.H. & FALEIDE, J.I. 2004. Unconformities related to the Jurassic-Cretaceous synrift-post-rift transition of the northern North Sea. *Journal of the Geological Society*, **161**, 1–17, https://doi.org/10.1144/0016-764903-051.

LEEDER, M.R. 1982. *Sedimentology: Process and Product*. Springer Netherlands.

LONERGAN, L. & CARTWRIGHT, J.A. 1999. Polygonal faults and their influence on deep-water sandstone reservoir geometries, Alba field, United Kingdom central North Sea. *AAPG Bulletin (American Association of Petroleum Geologists)*, **83**, 410–432, https://doi.org/10.1306/00AA9BBA-1730-11D7-8645000102C1865D.

LONERGAN, L., CARTWRIGHT, J. & JOLLY, R. 1998. The geometry of polygonal fault systems in Tertiary mudrocks of the North Sea. *Journal of Structural Geology*, **20**, 529–548, https://doi.org/10.1016/S0191-8141 (97)00113-2.

LONERGAN, L., LEE, N., JOHNSON, H.D., CARTWRIGHT, J. A & JOLLY, R.J.H. 2000. Remobilization and Injection in Deepwater Depositional Systems: Implications for Reservoir Architecture and Prediction. *Deep-Water Reservoirs of the World: 20th Annual GCSSEPM Foundation Bob F. Perkins Research Conference*, **15**, 515–532, https://doi.org/10.5724/gcs.00.15.0515.

LORENZ, J.C., TEUFEL, L.W. & WARPINSKI, N.R. 1991. Regional fractures I: a mechanism for the formation of regional fractures at depth in flat-lying reservoirs. *American Association of Petroleum Geologists Bulletin*, **75**, 1714–1737, https://doi.org/10.1306/0C9B29E3-1710-11D7-8645000102C1865D.

LØSETH, H. & HENRIKSEN, S. 2005. A Middle to Late Miocene compression phase along the Norwegian passive margin. *In*: *Petroleum Geology: North-West Europe and Global Perspectives – Proceedings of the 6th Petroleum Geology Conference*. 845–859., https://doi.org/10.1144/0060845.

LØSETH, H., RAULLINE, B. & NYGARD, A. 2013. Late Cenozoic geological evolution of the northern North Sea: development of a Miocene unconformity reshaped by large-scale Pleistocene sand intrusion. *Journal of the Geological Society*, **170**, 133–145, https://doi.org/10.1144/jgs2011-165.

LØSETH, H., WENSAAS, L., ARNTSEN, B. & HOVLAND, M. 2003. Gas and fluid injection triggering shallow mud mobilization in the Hordaland Group, North Sea. *Geological Society, London, Special Publications*, **216**, 139–157, https://doi.org/10.1144/gsl.sp.2003.216.01.10.

LØSETH, H., GADING, M. & WENSAAS, L. 2009. Hydrocarbon leakage interpreted on seismic data. *Marine and Petroleum Geology*, **26**, 1304–1319, https://doi.org/10.1016/j.marpetgeo.2008.09.008.

LOWE, D.R. 1975. Water escape structures in coarse grained sediments. *Sedimentology*, **22**, 157–204, https://doi.org/10.1111/j.1365-3091.1975.tb00290.x.

MACLEOD, M.K., HANSON, R.A., BELL, C.R. & MCHUGO, S. 1999. The Alba Field Ocean bottom cable seismic survey: Impact on development. *The Leading Edge*, **18**, 1306–1312, https://doi.org/10.1190/1.1438206.

MARK J. OSBORNE AND RICHARD E. SWAR. 1997. Mechanisms for Generating Overpressure in Sedimentary Basins: A Re-evaluation. *AAPG Bulletin*, **81 (1997)**, https://doi.org/10.1306/522B49C9-1727-11D7-8645000102C1865D.

MARTINSEN, O.J., BØEN, F., CHARNOCK, M.A., MANGERUD, G. & NØTTVEDT, A. 1999. Cenozoic development of the Norwegian margin 60–64°N: sequences and sedimentary response to variable basin physiography and tectonic setting. *In*: *Petroleum Geology of Northwest Europe: Proceedings of the 5th Conference*. 293–304., https://doi.org/10.1144/0050293.

MAZZINI, A. 2009. Mud volcanism: Processes and implications. *Marine and Petroleum Geology*, **26**, 1677–1680, https://doi.org/10.1016/j.marpetgeo.2009.05.003.

MAZZINI, A., DURANTI, D., JONK, R., PARNELL, J., CRONIN, B.T., HURST, A. & QUINE, M. 2003. Palaeo-carbonate seep structures above an oil reservoir, Gryphon Field, Tertiary, North Sea. *Geo-Marine Letters*, **23**, 323–339, https://doi.org/10.1007/s00367-003-0145-y.

MEADOWS, D. & DAVIES, R.J. 2007. Morphological development of basin-scale silica diagenetic fronts revealed with 2D seismic reflection data: offshore Sakhalin, Russian Far East. *Journal of the Geological Society*, **164**, 1193–1206, https://doi.org/10.1144/0016-76492006-163.

MEADOWS, D. & DAVIES, R.J. 2009. Predicting porosity reduction due to silica diagenesis using seismic reflection data. *Marine and Petroleum Geology*, **26**, 1543–1553, https://doi.org/10.1016/j.marpetgeo.2008.09.006.

MILKOV, A. V. 2000. Worldwide distribution of submarine mud volcanoes and associated gas hydrates. *Marine Geology*, **167**, 29–42, https://doi.org/10.1016/S0025-3227 (00)00022-0.

MILTON, N.J. 1993. Evolving depositional geometries in the North Sea Jurassic rift. *In*: Petroleum Geology of Northwest Europe: *Proceedings of the 4th Conference*. 425–442., https://doi.org/10.1144/0040425.

MOLYNEUX, S. 2001. Sandstone remobilisation in the Eocene to Miocene of the central and northern North Sea. (*Doctoral dissertation, Imperial College London*)

MOLYNEUX, S., CARTWRIGHT, J. & LONERGAN, L. 2002. Conical sandstone injection structures imaged by 3D seismic in the central North Sea, UK. *First Break*, **20**, 383–393, https://doi.org/10.1046/j.1365-2397.2002.00258.x.

NEWSOM, J.F. 1903. Clastic dikes. *Bulletin of the Geological Society of America*, **14**, 227–268, https://doi.org/10.1130/GSAB-14-227.

NOBES, D.C., MURRAY, R.W., KURAMOTO, S., PISCIOTTO, K.A. & HOLLER, P. 1992. 1. Impact of Silica Diagenesis on Physical property variations. *Proceedings of the Ocean Drilling Program, Scientific Results*, **127/128**, 3–31.

NORDGÅRD BOLÅS, H.M. & HERMANRUD, C. 2003. Hydrocarbon leakage processes and trap retention capacities offshore Norway. *Petroleum Geoscience*, **9**, 321–332, https://doi.org/10.1144/1354-079302-549.

NOTTVEDT, A., GABRIELSEN, R.H. & STEEL, R.J. 1995. Tectonostratigraphy and sedimentary architecture of rift basins, with reference to the northern North Sea. *Marine and Petroleum Geology*, 12, 881–901, https://doi.org/10.1016/0264-8172(95)98853-W.

NPD. 2018. Fact Pages: Norwegian Petroleum Directorate. http://factpages.npd.no. Accessed 20th February, 2018

OBERMEIER, S.F. 1989. *The New Madrid Earthquakes; an Engineering-Geologic Interpretation of Relict Liquefaction Features*.

OBERMEIER, S.F. 1996. Use of liquefaction-induced features for paleo-seismic analysis — An overview of how seismic liquefaction features can be distinguished from other features and how their regional distribution and properties of source sediment can be used to infer the location. *Engineering Geology*, **44**, 1–76, https://doi.org/10.1016/S0013-7952 (96)00040-3.

OBERMEIER, S.F., OLSON, S.M. & GREEN, R.A. 2005. Field occurrences of liquefaction-induced features: A primer for engineering geologic analysis of paleo-seismic shaking. *Engineering Geology*, **76**, 209–234, https://doi.org/10.1016/j.enggeo.2004.07.009.

OLOBAYO, O. 2014. Deposition, Remobilization and Fluid flow in Sedimentary Basins – case studies in the Northern North Sea and Nigeria Transform Margin. A thesis submitted to The University of Manchester for the degree of Doctor of Philosophy in the Faculty of Engineering. *PhD Thesis*.

OOMKENS, E. 1966. ENVIRONMENTAL SIGNIFICANCE OF SAND DIKES. *Sedimentology*, **7**, 145–148, https://doi.org/10.1111/j.1365-3091.1966.tb01585.x.

PARIZE, O. 1988. Sills et dykes gréseux sédimentaires: paléomorphologie, fracturation précoce, injection et compaction.

PARIZE, O. & FRIES, G. 2003. The Vocontian clastic dykes and sills: a geometric model. *Geological Society, London, Special Publications*, **216**, 51–72, https://doi.org/10.1144/GSL.SP.2003.216.01.05.

PARIZE, O., BEAUDOIN, B., ET AL. 2007. The Vocontian Aptian and Albian Syn-depositional Clastic Sills and Dikes: A Field-based Mechanical Approach to Predict and Model the Early Fracturing of Marly-limy Sediments. *In*: *Sand Injectites: Implications for Hydrocarbon Exploration and Production: AAPG Memoir 87*. 163–172., https://doi.org/10.1306/1209860M873262.

PEGRUM, R.M. & SPENCER, A.M. 1990. Hydrocarbon plays in the northern North Sea. *Geological Society, London, Special Publications*, **50**, 441–470, https://doi.org/10.1144/GSL.SP.1990.050.01.27.

PETERSON, G.L. 1966. Structural interpretation of sandstone dikes, northwest Sacramento Valley, California. *Bulletin of the Geological Society of America*, **77**, 833–842, https://doi.org/10.1130/0016-7606 (1966)77[833: SIOSDN] 2.0.CO; 2.

PLINT, A.G. 1985. Possible earthquake-induced soft-sediment faulting and remobilization in Pennsylvanian alluvial strata, southern New Brunswick, Canada. *Canadian Journal of Earth Sciences*, **22**, 907–912, https://doi.org/-.

PRINZ, L. & McCANN, T. 2019. Sand injectites: from source to emplacement – an example from the Miocene age Frimmersdorf Seam, Garzweiler Open-cast Mine, Lower Rhine Embayment. *Geological Society, London, Special Publications*, https://doi.org/10.1144/sp493-2017-289.

PURVIS, K., KAO, J., FLANAGAN, K., HENDERSON, J. & DURANTI, D. 2002. Complex reservoir geometries in a deep-water clastic sequence, Gryphon Field, UKCS: Injection structures, geological modelling, and reservoir simulation. *Marine and Petroleum Geology*, **19**, 161–179, https://doi.org/10.1016/S0264-8172 (02)00003-X.

RASMUSSEN, E.S., HEILMANN-CLAUSEN, C., WAAGSTEIN, R. & EIDVIN, T. 2008. The tertiary of Norden. *Episodes*, **31**, 66–72.

RAVIER, E., GUIRAUD, M., GUILLIEN, A., VENNIN, E., BUONCRISTIANI, J.F. & PORTIER, E. 2015. Micro- to macro-scale internal structures, diagenesis and petrophysical evolution of injectite networks in the Vocontian Basin (France): Implications for fluid flow. *Marine and Petroleum Geology*, **64**, 125–151, https://doi.org/10.1016/j.marpetgeo.2015.02.040.

REILLY, M.J. & FLEMINGS, P.B. 2010. Deep pore pressures and seafloor venting in the Auger Basin, Gulf of Mexico. *Basin Research*, **22**, 380–397, https://doi.org/10.1111/j.1365-2117.2010.00481.x.

ROBERTS, A.M., YIELDING, G. & BADLEY, M.E. 1990. A kinematic model for the orthogonal opening of the late Jurassic North Sea rift system, Denmark - mid Norway. *In*: *Tectonic Evolution of the North Sea Rifts*. 180–199.

ROBERTS, A.M., YIELDING, G., KUSZNIR, N.J., WALKER, I.M. & DORN-LOPEZ, D. 1995. Quantitative analysis of Triassic extension in the northern Viking Graben. *Journal of the Geological Society*, **152**, 15–26, https://doi.org/10.1144/gsjgs.152.1.0015.

ROBERTS, K.S., DAVIES, R.J. & STEWART, S.A. 2010. Structure of exhumed mud volcano feeder complexes, Azerbaijan. *Basin Research*, **22**, 439–451, https://doi.org/10.1111/j.1365-2117.2009.00441.x.

RUNDBERG, Y. (1991) Tertiary sedimentary history and basin evolution of the Norwegian North Sea between 60 – 62 degrees N – an Integrated Approach. *PhD Thesis, University of Trondheim*

RUNDBERG, Y. & EIDVIN, T. 2005. Controls on depositional history and architecture of the Oligocene-Miocene succession, northern North Sea Basin. *Norwegian Petroleum Society Special Publications*, **12**, 207–239, https://doi.org/10.1016/S0928-8937 (05)80050-5.

SCHLAKKER, A., CSIZMEG, J., POGÁCSÁS, G. & HORTI, A. 2012. Burial, Thermal and Maturation History in the Northern Viking Graben (North Sea). **50545**, 1–3, https://doi.org/10.1016/0264-8172 (95)98852-V.

SCHOLLE, P.A. 1977. Chalk Diagenesis and Its Relation to Petroleum Exploration: Oil from Chalks, a Modern Miracle?' *The American Association of Petroleum Geologists Bulletin*, **61**, 982–1009, https://doi.org/10.1306/C1EA43B5-16C9-11D7-8645000102C1865D.

SCLATER, J.G. & CHRISTIE, P.A.F. 1980. Continental stretching: An explanation of the Post-Mid-Cretaceous subsidence of the central North Sea Basin. *Journal of Geophysical Research: Solid Earth*, **85**, 3711–3739, https://doi.org/10.1029/JB085iB07p03711.

SCOTT, A., HURST, A. & VIGORITO, M. 2013. Outcrop-based reservoir characterization of a kilometer-scale sand-injectite complex. *AAPG Bulletin*, **97**, 309–343, https://doi.org/10.1306/05141211184.

SEJRUP, H.P., KING, E.L., AARSETH, I., HAFLIDASON, H. & ELVERHØI, A. 1996. Quaternary erosion and depositional processes: western Norwegian fjords, Norwegian Channel and North Sea Fan. *Geological Society, London, Special Publications*, **117**, 187–202, https://doi.org/10.1144/GSL.SP.1996.117.01.11.

SHIN, H., SANTAMARINA, C.J. & CARTWRIGHT, J.A. 2008. Contraction-driven shear failure in compacting uncemented sediments. *Geology*, **36**, 931–934, https://doi.org/10.1130/G24951A.1.

SHOULDERS, S.J. & CARTWRIGHT, J. 2004. Constraining the depth and timing of large-scale conical sandstone intrusions. *Geology*, **32**, 661–664, https://doi.org/10.1130/G20654.1.

STEEL, R.J. 1995. Tectonostratigraphy and sedimentary architecture of rift basins, with reference to the northern North Sea Tectonostratigraphy and sedimentary architecture of rift basins, with reference to the northern North. *Elsevier*, https://doi.org/10.1016/0264-8172 (95)98853-W.

STEWART, S.A. & DAVIES, R.J. 2006. Structure and emplacement of mud volcano systems in the South Caspian Basin. *AAPG Bulletin*, **90**, 771–786, https://doi.org/10.1306/11220505045.

SUN, Q., WU, S., LÜ, F. & YUAN, S. 2010. Polygonal faults and their implications for hydrocarbon reservoirs in the southern Qiongdongnan Basin, South China Sea. *Journal of Asian Earth Sciences*, **39**, 470–479, https://doi.org/10.1016/j.jseaes.2010.04.002.

SURLYK, F., GJELBERG, J. & NOE-NYGAARD, N. 2007. The Upper Jurassic Hareelv Formation of East Greenland: A Giant Sedimentary Injection Complex. *Sand injectites: Implications for hydrocarbon exploration and production*, 141–149, https://doi.org/-.

SURLYK, F. & NOE-NYGAARD, N. 2001. Sand remobilisation and intrusion in the Upper Jurassic Hareelv Formation of East Greenland. *Bulletin of the Geological Society of Denmark*, **48**, 169–188.

SZARAWARSKA, E., HUUSE, M., HURST, A., DE BOER, W., LU, L., MOLYNEUX, S. & RAWLINSON, P. 2010. Three-dimensional seismic characterisation of large-scale sandstone intrusions in the lower Palaeogene of the North Sea: completely injected vs. in situ remobilised sand-bodies. *Basin Research*, **22**, 517–532, https://doi.org/10.1111/j.1365-2117.2010.00469.x.

TADA, R. 1991. Compaction and cementation in siliceous rocks and their possible effect on bedding enhancement. *In*: *Cycles and Events in Stratigraphy*. Springer, 480–491.

TAKAHAMA, N., OTSUKA, T. & BRAHMANTYO, B. 2000. A new phenomenon in ancient liquefaction--the draw-in process, its final stage. *Sedimentary Geology*, **135**, 157–165, https://doi.org/Doi: 10.1016/s0037-0738(00)00069-5.

THOMAS MARTEL, A. & GIBLING, M.R. 1993. Clastic dykes of the Devono-Carboniferous Horton Bluff Formation, Nova Scotia: storm-related structures in shallow lakes. *Sedimentary Geology*, **87**, 103–119, https://doi.org/10.1016/0037-0738 (93)90038-7.

THOMPSON, B.J., GARRISON, R.E. & MOORE, J.C. 2007. A Reservoir-scale Miocene Injectite near Santa Cruz, California. *Sand injectites: Implications for hydrocarbon exploration and production*, 151–162, https://doi.org/-.

THOMPSON, B.J., GARRISON, R.E. & MOORE, J.C. 1999. A late Cenozoic sandstone intrusion west of Santa Cruz, California; fluidized flow of water- and hydrocarbon-saturated sediments. *Guidebook - Pacific Section, American Association of Petroleum Geologists*, **76**, 53–74.

THYBERG, B.I., STABELL, B., FALEIDE, J.I. & BJØRLYKKE, K. 1999. Upper Oligocene diatomaceous deposits in the northern North Sea - silica diagenesis and paleogeographic implications. *Norsk Geologisk Tidsskrift*, **79**, 3–18, https://doi.org/10.1080/002919699433870.

TRUSWELL, J.F. 1972. Sandstone sheets and related intrusions from Coffee Bay, Transkei, South Africa. *Journal of Sedimentary Petrology*, **42**, 578–583, https://doi.org/10.1306/74d725c2-2b21-11d7-8648000102c1865d.

UJIIE, K., YAMAGUCHI, A., KIMURA, G. & TOH, S. 2007. Fluidization of granular material in a subduction thrust at seismogenic depths. *Earth and Planetary Science Letters*, **259**, 307–318, https://doi.org/10.1016/j.epsl.2007.04.049.

ULMISHEK, G. & KLEMME, H.D. 1990. Depositional controls, distribution, and effectiveness of world's petroleum source rocks. *USGS bulletin*, 66.

VAN RENSBERGEN, P., HILLIS, R.R., MALTMAN, A.J. & MORLEY, C.K. 2003. Subsurface sediment mobilization: introduction. *Geological Society, London, Special Publications*, **216**, 1–8, https://doi.org/10.1144/GSL.SP.2003.216.01.01.

VIGORITO, M. & HURST, A. 2010. Regional sand injectite architecture as a record of pore-pressure evolution and sand redistribution in the shallow crust: insights from the Panoche Giant Injection Complex, California. *Journal of the Geological Society*, **167**, 889–904, https://doi.org/10.1144/0016-76492010-004.

VIGORITO, M., HURST, A., CARTWRIGHT, J.A. & SCOTT, A. 2008. Regional-scale subsurface sand remobilization: geometry and architecture. *Journal of the Geological Society*, **165**, 609–612, https://doi.org/10.1144/0016-76492007-096.

VON BRUNN, V. & TALBOT, C.J. 1986. Formation and deformation of subglacial intrusive clastic sheets in the Dwyka Formation of northern Natal, South Africa. *Journal of Sedimentary Petrology*, **56**, 35–44, https://doi.org/10.1306/212F8878-2B24-11D7-8648000102C1865D.

WILD, J. & BRIEDIS, N. 2010. Structural and stratigraphic relationships of the Palaeocene mounds of the Utsira High. *Basin Research*, **22**, 533–547, https://doi.org/10.1111/j.1365-2117.2010.00479.x.

WINSLOW, M.A. 1983. Clastic dike swarms and the structural evolution of the foreland fold and thrust belt of the southern Andes (Chile). *Geological Society of America Bulletin*, **94**, 1073–1080, https://doi.org/10.1130/0016-7606 (1983)94<1073: CDSATS>2.0.CO; 2.

WRONA, T., MAGEE, C., JACKSON, C.A.-L., HUUSE, M. & TAYLOR, K.G. 2017a. Kinematics of Polygonal Fault Systems: Observations from the Northern North Sea. *Frontiers in Earth Science*, **5**, https://doi.org/10.3389/feart.2017.00101.

WRONA, T., JACKSON, C.A.L., HUUSE, M. & TAYLOR, K.G. 2017b. Silica diagenesis in Cenozoic mudstones of the North Viking Graben: physical properties and basin modelling. *Basin Research*, **29**, 556–575, https://doi.org/10.1111/bre.12168.

YARDLEY, G.S. & SWARBRICK, R.E. 2000. Lateral transfer: A source of additional overpressure? *Marine and Petroleum Geology*, **17**, 523–537, https://doi.org/10.1016/S0264-8172 (00)00007-6.

ZACHOS, J., PAGANI, M., SLOAN, L., THOMAS, E. & BILLUPS, K. 2001. Trends, Global Rhythms, Aberrations in Global Climate 65Ma to Present. *Science*, **292**, 686–693, https://doi.org/10.1126/science.1059412.

ZIEGLER, P.A. 1990. Tectonic and palaeogeographic development of the North Sea rift system. In: Blundell, D.J. & Gibbs, A.D. (eds) Tectonic evolution of the North Sea rifts. *Oxford University Press*, 1–36.

ZIEGLER, P.A. 1982. Triassic rifts and facies patterns in Western and Central Europe. *Geologische Rundschau*, **71**, 747–772, https://doi.org/10.1007/BF01821101.

ZIEGLER, P.A. 1992. North Sea rift system. *Tectonophysics*, **208**, 55–75, https://doi.org/10.1016/0040-1951 (92)90336-5.
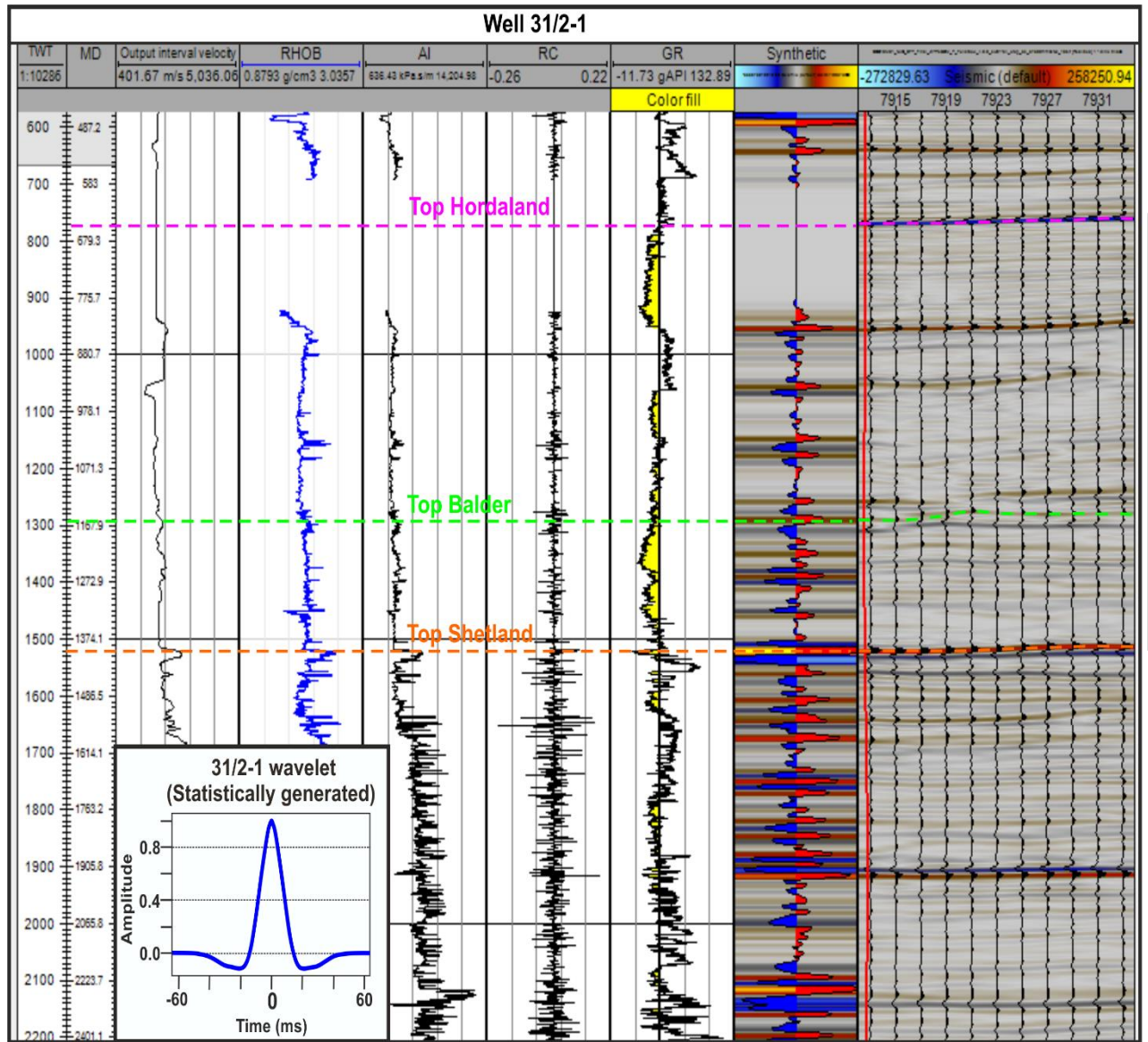
Appendix A

Appendix A.1: Synthetic seismogram for Well 31/2-1 using a statistically extracted wavelet by extracting the required wavelet parameter from the available seismic data. Well location is shown in Fig. 1.2. Key stratigraphic boundaries (Top Shetland, Top Balder and Top Hordaland Groups) are highlighted in different colours on both the generated synthetic seismogram and real seismic data.

Appendix A.2: Complete list of wells used in this study showing their individual formation top depths and associated field/discovery. Formation top depths were obtained from NPD website, TGS Facies Map browser and CGG wells-to seismic study. CALI - Calliper, DRHO - Density correction, DT - Interval transit time, GR - Gamma ray, NPHI - Neutron porosity, ILD - Deep resistivity, ILM - Shallow resistivity, RHOB - Bulk density, SP- Spontaneous Potential, PEF- Photoelectric Factor, TD – Total depth, TNG – Top Nordland Group, THG – Top Hordaland Group, TB – Top Balder, TSG – Top Shetland Group

Quadrant	Well	TD (MD)	Wireline Data	Top Depth (from CGG, TGS_FMB & NPD)				Field/Discovery
				TNG (m)	THG (m)	TB (m)	TSG (m)	
3	UK 3/15-2		CALI, DT, GR, ILD, NPHI, RHOB, SP	158	641.2	1883.3	2250	ELLON
	UK 3/25a-4		CALI, DT, DRHO, GR, ILD, NPHI, RHOB	136?	551	2079.5	2516.1	N/A
	UK 3/29-2		CALI, DT, GR, ILD, NPHI, RHOB, SP	135	440.5	2018.3	2585.5	RHUM
25	NO 25/2-3	2795	CALI, DT, GR, ILD, NPHI, RHOB, SP	138	1008	2211	2726	N/A
	NO 25/2-17	2193	CALI, DT, GR, ILD, NPHI, RHOB, SP	142	645	2112		
	NO 25/3-1	3922	DT, GR, ILD, NPHI, RHOB	136	731.5	2123.4	2470	
26	NO 26/4-2	2302	CALI, DT, DRHO, GR, ILD, NPHI, RHOB	160	979.5	1983	2253	N/A
	NO 26/5-1	1910	CALI, DT, GR, DRHO, ILD, ILM, NPHI, PEF, RHOB	292	874	1495	1857	
29	NO 29/3-1	4427	CALI, DT, GR, ILD, NPHI, RHOB, SP	156	788	1726	2032.5	N/A
	NO 29/6-1	4832	CALI, DT, GR, DRHO, ILD, NPHI, RHOB, PEF	149	679.2	1946.3	2366.5	MARTIN LINGE
	NO 29/9-1	4703	CALI, DT, GR, ILD, NPHI, RHOB, SP	129	636	2003	2390	
30	NO 30/2-2	955	CALI, DT, DRHO, GR, ILD, NPHI, RHOB	152	892	1964.8	2224	HULDRA
	NO 30/3-2R	3567	CALI, DT, GR, DRHO, ILD, NPHI, RHOB, PEF	211	907.5	1923	2203	VESLEFRIKK
	NO 30/3-3	3419	CALI, DT, GR, ILD, NPHI, RHOB, SP	208	883	1916	2213	N/A
	NO 30/3-4	3287	CALI, DT, DRHO, GR, ILD, NPHI, RHOB	186.5	903	1989.3	2269	VESLEFRIKK
	NO 30/3-9	4015	CALI, DT, GR, ILD, NPHI, RHOB, SP	141	930	1968	2228	N/A
	NO 30/4-1	5454	CALI, DT, GR, ILD, NPHI, RHOB	144.8	722	1917	2262	N/A
	NO 30/4-2	4775	CALI, DT, GR, ILD, NPHI, RHOB, SP	148	690	1976	2337	MARTIN LINGE
	NO 30/5-1	4124	CALI, DT, GR, ILD, NPHI, RHOB, SP	131	796	1994.5	2304	N/A
	NO 30/6-2	2890	CALI, DT, GR, ILD, NPHI, RHOB, SP	131	869.5	1918	2165	OSEBERG
	NO 30/6-5	3550	CALI, DT, GR, ILD, NPHI, RHOB, SP	181	879	1909	2202.5	OSEBERG OST
	NO 30/6-14	2900	CALI, DT, GR, ILD, NPHI, RHOB, SP	171	854	1853	2123	
	NO 30/6-16	3300	CALI, DT, GR, ILD, NPHI, RHOB, SP	137	902.5	2001	2301	N/A
	NO 30/6-18	3690	CALI, DT, GR, ILD, NPHI, RHOB, SP	133	893	2047	2383	OSEBERG
	NO 30/6-20	3046	CALI, DT, GR, ILD, NPHI, RHOB, SP	134	922	1984	2280.8	N/A
	NO 30/6-24S	3986	CALI, DT, GR, ILD, NPHI, RHOB, SP	145	923	2107	2442	
	NO 30/6-28S	4064	CALI, DT, GR, ILD, NPHI, RHOB	135	857	1952	2231	OSEBERG
	NO 30/7-7	5127	CALI, DT, GR, NPHI, RHOB, SP	134	675.5	2150	2537	N/A
	NO 30/9-14	3680	CALI, DT, GR, NPHI, RHOB	130	840	2141	2438	OSEBERG SØR
	NO 30/9-22	3255	CALI, DT, DRHO, GR, ILD, NPHI, RHOB	118	883.4	2139	2430	
	NO 30/9-23	2872	CALI, DT, DRHO, GR, ILD, NPHI, RHOB	140	832	1860	2119	N/A
	NO 30/10-6	5250	CALI, DT, DRHO, GR, ILD, NPHI, RHOB	109	1158	2161	2581	
	NO 30/11-3	4662	CALI, DT, GR, NPHI, RHOB	112	653.9	2092.6	2601	
	NO 30/11-5	3726	CALI, DT, GR, ILD, NPHI, RHOB	128	705	2169	2561	STEINBIT
	NO 30/11-6S	3550	CALI, DT, GR, DRHO, ILD, NPHI, RHOB, PEF	132	749	2270.6	2639	N/A
	NO 30/11-7	4067	CALI, DT, GR, ILD, NPHI, RHOB	129	673.6	2102.9	2626	FULLA
	NO 30/11-8S	4043	CALI, DT, GR, DRHO, ILD, NPHI, RHOB	130	767	2180	2567	KRAFLA
	NO 30/11-10	4079	CALI, DT, GR, DRHO, ILD, NPHI, RHOB	128	777	2187.7	2544	KRAFLA NORD
	NO 30/12-1	3641	CALI, DT, GR, DRHO, ILD, NPHI, RHOB	135	772	2156	2429	N/A
31	NO 31/2-1	2433	CALI, DT, GR, ILD, NPHI, RHOB, SP	348	828	1169		TROLL
	NO 31/2-3	2601	CALI, DT, GR, ILD, NPHI, RHOB, SP	359	779.9	1145		
	NO 31/2-4R	5035	CALI, DT, GR, ILD	361	724	1200		
	NO 31/2-5	2532	CALI, DT, GR, ILD, NPHI, RHOB, SP	365	815	1346	1533	
	NO 31/2-6	1760	CALI, DT, DRHO, GR, ILD, NPHI, RHOB, SP	368	698	1107	1463	
	NO 31/2-7	1660	CALI, DT, GR, ILD, NPHI, RHOB, SP	363	813	1327		
	NO 31/2-8	3375	CALI, DT, GR, ILD, NPHI, RHOB, SP	371	831	1420	1808	N/A
	NO 31/2-10	1833	CALI, DT, GR, ILD, NPHI, RHOB	356	802	1305	1539	TROLL
	NO 31/2-11	1744	CALI, DT, GR, ILD, NPHI, RHOB, SP	361	805	1367	1537	
	NO 31/2-12	1615	CALI, DT, GR, ILD, NPHI, RHOB, SP	359	769	1204		
	NO 31/2-14	1725	CALI, DT, GR, ILD, NPHI, RHOB, SP	365	809	1326	1530	
	NO 31/2-15	1677	CALI, DT, GR, ILD, NPHI, RHOB, SP	368	804.5	1201		
	NO 31/2-17S	2220	CALI, DT, GR, ILD, NPHI, RHOB, SP	365	803	1540		
	NO 31/2-18	1711	CALI, DT, GR, ILD, NPHI, RHOB	366	670	1220		
	NO 31/2-18A	2005	CALI, DT, GR, ILD, NPHI, RHOB	366	670	1220		
	NO 31/2-19S	4114	CALI, DT, GR, ILD, NPHI, RHOB, SP	367	840	1585	1983	N/A
	NO 31/3-1	2374	CALI, DT, GR, ILD, NPHI, RHOB, SP	357	531	931	1235	TROLL
	NO 31/3-2	2090	CALI, DT, GR, ILD, NPHI, RHOB, SP	365	604	1123	1471	
	NO 31/3-3	2573	CALI, DT, GR, ILD, NPHI, RHOB, SP	358	540	826	1230	N/A
	NO 31/4-3	4981	CALI, DT, GR, ILD, NPHI, RHOB, SP	195	843	1723	1965	BRAGE

31	NO 31/4-7	2505	CALI, DT, GR, ILD, NPHI, RHOB, SP	161	771	1769	1987	BRAGE
	NO 31/4-8	2611	CALI, DT, GR, ILD, NPHI, RHOB, SP	149	827	1830	2024	
	NO 31/5-2	2500	CALI, DT, GR, ILD, NPHI, RHOB, SP	342	670	1210	1432	TROLL
	NO 31/5-5	1930	CALI, DT, GR, ILD, NPHI, RHOB, SP	348	741	1295	1529	N/A
	NO 31/5-6	2370	BS, CALI, DENC, GR, ILD, NPHI, RHOB, PEF	354	494	1528	1790	TROLL
	NO 31/6-1	4070	CALI, DT, GR, ILD, NPHI, RHOB, SP	327	522	972	1231	N/A
	NO 31/6-3	2250	CALI, DT, GR, ILD, NPHI, RHOB, SP	326		508	809	
	NO 31/6-5	2082	CALI, DT, GR, ILD, NPHI, RHOB, SP	327	455	816	1144	TROLL
	NO 31/6-6	2290	CALI, DT, GR, ILD, NPHI, RHOB, SP	336	532	650	1014	
	NO 31/8-1	2629	CALI, DT, GR, NPHI, RHOB, SP	336	715	1253	1494	N/A
	NO 31/10-1	2388	CALI, DT, GR, NPHI, RHOB, SP	152	820	2085	2348	
32	NO 32/4-1	3186	CALI, DT, GR, NPHI, RHOB, SP	336		535	837	N/A
33	NO 33/5-1	3829	CALI, DT, DRHO, GR, NPHI, RHOB, SP	365	1064	1495	1650	N/A
	NO 33/5-2	4520	CALI, DT, DRHO, GR, ILD, NPHI, RHOB, SP	335	1098	1558	1717	
	NO 33/6-1	3900	CALI, DT, GR, ILD, NPHI, RHOB, SP	331	1138	1723	1893	
	NO 33/6-2	3950	CALI, DT, GR, ILD, NPHI, RHOB, SP	342	1162.4	1732	1933	
	NO 33/9-1	3126	CALI, DT, GR, ILD, NPHI, RHOB, SP	171	821	1662	1871	STATFJORD
	NO 33/9-3	2992	CALI, DT, GR, ILD, NPHI, RHOB, SP	171	926	1662	1860	STATFJORD
	NO 33/9-4	3076	CALI, DT, GR, ILD, NPHI, RHOB, SP	169	1011	1667	1855	STATFJORD
	NO 33/9-6	3354	CALI, DT, GR, ILD, NPHI, RHOB, SP	179	1062	1670	1890	STATFJORD
	NO 33/9-7	3127	CALI, DT, GR, ILD, NPHI, RHOB, SP	181	980	1651	1851	STATFJORD ØST
	NO 33/9-10	3715	CALI, DT, GR, ILD, NPHI, RHOB, SP	188	1054	1666	1895	N/A
	NO 33/9-11	3528	CALI, DT, GR, ILD, NPHI, RHOB, SP	312	1123	1673	1900	
	NO 33/9-12	2959	CALI, DT, GR, ILD, NPHI, RHOB, SP	170	1075	1683	1871	STATFJORD ØST
	NO 33/9-13S	3077	CALI, DT, GR, ILD, NPHI, RHOB, SP	313	1135	1707	1940	STATFJORD NORD
	NO 33/9-15	3007	CALI, DT, GR, ILD, NPHI, RHOB	279	1057	1688	1935	N/A
	NO 33/9-16	2870	CALI, DT, GR, ILD, NPHI, RHOB, SP	249	1073	1663	1911	
	NO 33/9-17	3233	CALI, DT, GR, ILD, NPHI, RHOB, SP	254	1054	1668	1916	
	NO 33/9-18	3253	CALI, DT, GR, ILD, NPHI, RHOB	168	998	1729	1933	
	NO 33/12-6	4612	CALI, DT, GR, ILD, NPHI, RHOB, SP	164	940.7	1774.5	2028	
	NO 33/12-7	3703	CALI, DT, GR, ILD, NPHI, RHOB, SP	163	946.5	1784	2027	
34	NO 34/2-4	4107	DT, DRHO, GR, ILD, NPHI, RHOB, SP	424	1520	1946	2081	N/A
	NO 34/3-1S	4221	CALI, DT, GR, NPHI, RHOB, SP	436	1563	2004	2141	KNARR
	NO 34/3-2S	4331	CALI, DT, GR, NPHI, RHOB, SP	427	1529	1984	2121	N/A
	NO 34/4-5	3917	CALI, DT, GR, ILD, NPHI, RHOB, SP	405	1332	1802	1936	
	NO 34/4-7	2950	CALI, DT, GR, ILD, NPHI, RHOB, SP	380	1200	1700	1824	SNORRE
	NO 34/4-10R	4246	DT, DRHO, GR, ILD, NPHI, RHOB, SP	381	1249	1741	1910	N/A
	NO 34/4-11	4327	DT, DRHO, GR, ILD, ILM, NPHI, RHOB, SP	404	1289	1763	1937	
	NO 34/5-1S	3900	CALI, DT, GR, NPHI, RHOB, SP	412	1449	1890	2010	
	NO 34/6-2S	4335	CALI, DT, GR, ILD, NPHI, RHOB, SP	417	1187	1849	2034	GARANTIANA
	NO 34/7-1	2905	CALI, DT, GR, ILD, NPHI, RHOB, SP	353	1170	1673	1823	SNORRE
	NO 34/7-4	3115	DT, GR, ILD, ILS, NPHI, RHOB, OWT	345	1187	1685	1848	
	NO 34/7-6	3685	CALI, DT, GR, ILD, NPHI, RHOB, SP	333	1036	1677.5	1846	
	NO 34/7-8	2766	CALI, DT, GR, ILD, NPHI, RHOB, SP	312	1105	1658	1833	VIGDIS
	NO 34/7-9	3240	CALI, DT, GR, ILD, NPHI, RHOB, SP	356	1172	1657	1807	SNORRE
	NO 34/7-10	3000	CALI, DT, DRHO, GR, ILD, NPHI, RHOB, SP	326	1093	1682	1863	
	NO 34/7-21	3015	CALI, DT, GR, ILD, NPHI, RHOB, SP	218	1025	1711	1900	TORDIS
	NO 34/8-1	3610	CALI, DT, GR, ILD, NPHI, RHOB, SP	349	1136	1826	2006	VISUND
	NO 34/8-3A	3230	CALI, DT, GR, ILD, NPHI, RHOB, SP	405	1180	1873	2088	
	NO 34/8-6	3950	CALI, DT, GR, ILD, NPHI, RHOB, SP	400	1178	1891	2145	N/A
	NO 34/8-10S	3470	CALI, DT, GR, NPHI, RHOB, SP	349	1145	1815	1994	VISUND
	NO 34/10-1	2460	CALI, DT, GR, ILD, NPHI, RHOB, SP	163	915	1513	1678	GULLFAKS
	NO 34/10-2	3729	CALI, DT, GR, ILD, NPHI, RHOB, SP	158	1015	1795	2017	GULLFAKS SØR
	NO 34/10-3R	2802	CALI, DT, GR, ILD, NPHI, RHOB, SP	162	894	1575	1745	GULLFAKS
	NO 34/10-6	2363	CALI, DT, GR, ILD, NPHI, RHOB, SP	248	982	1578	1757	
	NO 34/10-16	4042	CALI, DT, GR, ILD, NPHI, RHOB, SP	163	1002	1855	2062	GULLFAKS SØR
	NO 34/10-16R	4042	CALI, DT, GR, ILD, NPHI, RHOB, SP	160	1042	1852	2059	
	NO 34/10-19	2218	CALI, DT, GR, ILD, NPHI, RHOB, SP	215	905	1470	1661	GULLFAKS
	NO 34/10-23	4764	CALI, DT, GR, ILD, OWT	164	1052	1892	2136	VALEMON
	NO 34/10-30	3785	CALI, DT, GR, ILD, NPHI, RHOB, SP	158	951	1785	2006	GULLFAKS SØR
	NO 34/10-34	2410	CALI, DT, GR, ILD, NPHI, RHOB, SP	163	923	1600	1806	GULLFAKS
	NO 34/10-36	3640	CALI, DT, GR, ILD, NPHI, RHOB, SP	159	953	1843	2066	GULLFAKS SØR

34	NO 34/10-38S	3940	CALI, DT, GR, ILD, NPHI, RHOB, SP	160	936.3	1822	2030	GULLFAKS SØR
	NO 34/11-2S	4743	CALI, DT, GR, ILD, NPHI, RHOB, SP	286	1026.5	1820	2033	NØKKEN
	NO 34/11-3	4482	CALI, DT, GR, NPHI, RHOB, SP	233	986	1904	2118	KVITEBJØRN
	NO 34/12-1	4713	CALI, DT, GR, NPHI, RHOB, SP	396	973	1815	2007	AFRODITE
35	NO 35/1-1	4540	CALI, DT, GR, ILD, NPHI, RHOB, SP	431	1581	2015	2147	N/A
	NO 35/2-3	1640	CALI, DT, GR, ILD, NPHI, RHOB, SP	386	848	1324.5	1591	
	NO 35/3-1	4475	CALI, DT, DRHO, GR, ILD, NPHI, RHOB	330	743	1350	1580	
	NO 35/3-2	4400	CALI, DT, DRHO, GR, ILD, NPHI, RHOB, SP	272	726.5	1332	1537	
	NO 35/3-5	4114	CALI, DT, DRHO, GR, ILD, NPHI, RHOB, SP	295	582.5	975	1410	
	NO 35/3-7S	4051	CALI, DT, GR, ILD, NPHI, RHOB	282	654.5	1231.5	1518	
	NO 35/4-1	4936	CALI, DT, GR, ILD, NPHI, RHOB, SP	404	1116	1721	1912	
	NO 35/6-2S	3700	CALI, DT, DRHO, GR, ILD, ILM, NPHI, RHOB	366	600	627	1355	
	NO 35/7-1S	4825	CALI, DT, DRHO, GR, NPHI, RHOB	426	1062	1780	1991	
	NO 35/8-1	4345	CALI, DT, GR, ILD, NPHI, RHOB, SP	402	964	1683	1893	VEGA
	NO 35/8-2T2	4356	CALI, DT, GR, ILD, NPHI, RHOB, SP	406	964	1675	1941	
	NO 35/8-3	3944	CALI, DT, GR, ILD, NPHI, RHOB, SP	396	792	1468	1792.5	AURORA
	NO 35/9-1	2350	CALI, DT, GR, ILD, NPHI, RHOB, SP	384		588	1238	GJOA
	NO 35/9-2	2885	CALI, DT, GR, ILD, NPHI, RHOB, SP	392	573	658	1341	
	NO 35/9-3	2783	CALI, DT, GR, ILD, NPHI, RHOB, SP	377		622	1247	N/A
	NO 35/9-5	3531	CALI, DT, GR, ILD, NPHI, RHOB, SP	384	605	860	1464	
	NO 35/9-6S	3740	CALI, DT, GR, DRHO, ILD, NPHI, RHOB	394	605	1229	1688	
	NO 35/9-7	3006	CALI, DT, GR, DRHO, ILD, NPHI, RHOB, PEF	397	706	1288	1767	NOVA
	NO 35/9-8	3256	CALI, DT, GR, DRHO, ILD, NPHI, RHOB	392	695	1221	1738.5	
	NO 35/9-10A	3203	CALI, DT, GR, DRHO, ILD, NPHI, RHOB, PEF	389	656	1263	2001	
	NO 35/9-10S	3619	CALI, DT, GR, DRHO, ILD, NPHI, RHOB, PEF	389	660	1277	2040	
	NO 35/10-1	3986	CALI, DT, GR, ILD, NPHI, RHOB	384	912	1755	2000	N/A
	NO 35/10-2	4677	CALI, DT, GR, ILD, NPHI, RHOB	397	946	1877	2106	
	NO 35/10-3	2250	CALI, DT, GR, ILD, NPHI, RHOB	387	933	1881	2199	
	NO 35/11-1	3361	CALI, DT, GR, ILD, NPHI, RHOB, SP	385	696	1307	1765	
	NO 35/11-2	4025	CALI, DT, GR, ILD, NPHI, RHOB, SP	395	824	1663	1950	VEGA
	NO 35/11-3S	4040	CALI, DT, GR, ILD, NPHI, RHOB, SP	383	866	1728	2063	N/A
	NO 35/11-4	3127	CALI, DT, GR, ILD, NPHI, RHOB, SP	372	735	1397	1835	FRAM
	NO 35/11-5	3769	CALI, DT, GR, ILD, NPHI, RHOB, SP	382	845	1702	2044	N/A
	NO 35/11-6	3995	CALI, DT, GR, ILD, NPHI, RHOB, SP	396	843	1625	1955	VEGA
	NO 35/11-7	2895	CALI, GR, ILD, NPHI, SP	384	715	1295	1735	FRAM
	NO 35/11-8S	3624	CALI, DT, GR, ILD, NPHI, RHOB, SP	387	785	1618	2124	
	NO 35/11-9	2830	CALI, DT, GR, ILD, NPHI, RHOB	386	783	1534	1973	
	NO 35/11-10	2950	CALI, DT, GR, ILD, NPHI, RHOB, SP	376	756	1414	1858	
	NO 35/11-11	3225	CALI, DT, GR, NPHI, RHOB, SP	383	763	1466	1914	
	NO 35/11-12	3378	CALI, DT, GR, NPHI, RHOB	388	896	1727	2019	N/A
	NO 35/11-13	3292	CALI, DT, DRHO, GR, ILD, NPHI, RHOB	387	763	1541	1938	BYRDING
	NO 35/11-14S	3306	CALI, DT, GR, DRHO, ILD, NPHI, RHOB	387	800	1548	1950	
	NO 35/11-16S	3554	CALI, DT, GR, ILD, NPHI, RHOB	392	750	1647	2192	N/A
	NO 35/11-15ST5	3250	CALI, DT, GR, NPHI, RHOB	389	798	1531	1947	FRAM H-NORD
	NO 35/11-16ST2	3554	CALI, DT, GR, ILD, NPHI, RHOB	392	750	1629		N/A
	NO 35/12-1	3020	CALI, DT, GR, ILD, NPHI, RHOB, SP	377		573	1434	
36	NO 36/1-1	1596	CALI, DT, GR, ILD, NPHI, RHOB	191	586	650	888	N/A
	NO 36/1-2	3256	CALI, DT, GR, ILD, NPHI, RHOB	251.5	614	960	1315	
	NO 36/4-1	2717	CALI, DT, GR, ILD, NPHI, RHOB	284	625	850	1253	
	NO 36/7-2	1435	CALI, DT, GR, ILD, NPHI, RHOB, SP	291		648		
	NO 36/7-3	2947	CALI, DT, GR, ILD, NPHI, RHOB, SP	373		580	1249	
211	UK 211/13-5A		CALI, DT, GR, ILD, NPHI, RHOB, SP	201	994.5	1498.5	1724	PENGUIN
6204	NO 6204/10-1	2709	CALI, DT, GR, ILD, NPHI, RHOB, SP	211	636	744	1202	N/A

Section 2:

Result chapters: Journal format

General reviews, Observations, Analysis and Discussions

Chapter 3

CHAPTER 3   Hydrocarbon reserve and resource distribution of sand injectite fields in the UK & Norwegian sectors of the North Sea Basin

Theme: Sand Injectites as attractive exploration targets: Implications for Exploration & Production

Hydrocarbon reserve and resource distribution of sand injectite fields in the UK & Norwegian sectors of the North Sea Basin

(A short overview)

Sebastian Nnorom & Mads Huuse

Basins Research Group, Department of Earth and Environmental Sciences, University of Manchester, Oxford Road, Manchester M13 9PL, UK

Abstract

The modification of deep-water sand reservoirs in the North Sea have been studied over a decade, with some well-known hydrocarbon fields with associated injectite reservoirs documented. These fields are affected by either small-scale or large-scale injection resulting to moderate to very complex reservoir geometries, which have important implications for exploration and production. Over the years, studies have shown that these injectites or intrusions contain substantial volumes of sand and can act as standalone hydrocarbon reservoirs. They have excellent reservoir properties, constitute potential drilling hazards, and can improve both lateral and vertical connectivity between isolated reservoirs which in turn provide pressure communication and aquifer support. North Sea (UK & Norwegian sectors) fields with deep-water reservoirs modified by sand remobilization and injection processes have been documented here by outlining their reserve and resource distribution in both sectors, their age distribution, reservoir properties, including the style and scale of their associated injectite complexes. This was carried out with the aid of different tables and plots to understand their contribution to the hydrocarbon reserves and resources in the North Sea Basin.

3.1 Introduction

Here we attempt to provide a summary of the cumulative reserves and resource potential of fields associated with sand injectite complexes in the North Sea, giving details of estimated reserves for known and recently discovered injectite fields. This study provides more information and updated details in addition to the work done by Willett (2015) which covers reserves and resources estimates for UK and Norwegian North Sea fields with reservoirs affected by sand remobilization and injection from 1967 – 2014. The database provided in his study is updated with recent figures and information to show the viability of injectite complexes as potential exploration targets which can help increase the productivity and reserves of existing fields. More emphasis is however laid on the injectite fields in the Norwegian sector of the North Sea with the Northern North Sea (Fig. 3.1) forming the study area in subsequent chapters.

The remobilization and injection of sand into low permeable mudstone host strata create clastic reservoirs with complex geometries, comprising of highly porous and permeable sills and dikes, which are often concordant to discordant to bedding (Fig. 3.2; Hurst et al., 2011). Many deep- water oil and gas depositional sandstone reservoirs have connections to sand injectites. In the past, the possible influence of clastic remobilization and injection on deep-water clastic reservoirs were not considered because they were either misinterpreted (e.g., as processing artefacts), undervalued, completely ignored, and overlooked or unidentified due to poor data quality (Hurst et al., 2005; Huuse et al., 2007). Recent advances in data acquisition techniques, improved data resolution and the recent understanding of their implication for hydrocarbon

exploration and production (e.g., Lonergan et al., 2000; Duranti et al., 2002; Duranti & Hurst, 2004; Hurst et al., 2005; Briedis et al., 2007; Huuse et al., 2007; Hurst & Cartwright, 2007; Lonergan et al., 2007; Hurst et al., 2011) based on lessons from a few North Sea fields have led to several studies to further understand them.   However, their complexity and difficulty to integrate into subsurface reservoir modelling remains the greatest barrier. Their recognition (on seismic, borehole & core data) and study have shown that sand injectites can increase the total recoverable reserves in fields with hydrocarbon reservoirs associated with injectite complexes (e.g., Alba, Balder, Gryphon, Volund fields) and as such proven to potentially constitute attractive exploration targets (Braccini et al., 2008; Dixon et al., 1995; Jackson et al., 2011: see their Fig. 2). This is supported by their exceptionally high porosity and permeability from cases of known North Sea Tertiary injectite fields (Table 3.1 & 3.2; Hurst et al., 2011: see their Fig. 17 & 18).

3.2 Data/ Information Gathering and Methods

The current cumulative recoverable reserves and resource distribution of fields in the UK and Norwegian sector of the North Sea affected by sand remobilization and injection are presented here covering from 1967 – 2019 (Table 3.1 & 3.2). Field names, discovery date, production start date, recoverable reserves/resource figures, reservoir interval & age, reservoir type (style & scale of intrusion), depositional setting, hydrocarbon type, reservoir properties (porosity & permeability), number of wells drilled (includes exploration, appraisal & production wells) and total investments ($mm) are considered with more emphasis on the Norwegian fields (Table 3.1 & 3.2). The above details are derived mainly from published sources (e.g., published papers, reports, press releases/media publications, oil/gas company websites, etc.) and scout data (from Norwegian Petroleum Directorate: NPD and UK Oil & Gas Authority: OGA). The reserve and resource history of these injectite fields/discoveries were then investigated with the aid of creaming curves and charts to clearly understand how they have varied over time from 1997 – 2019.
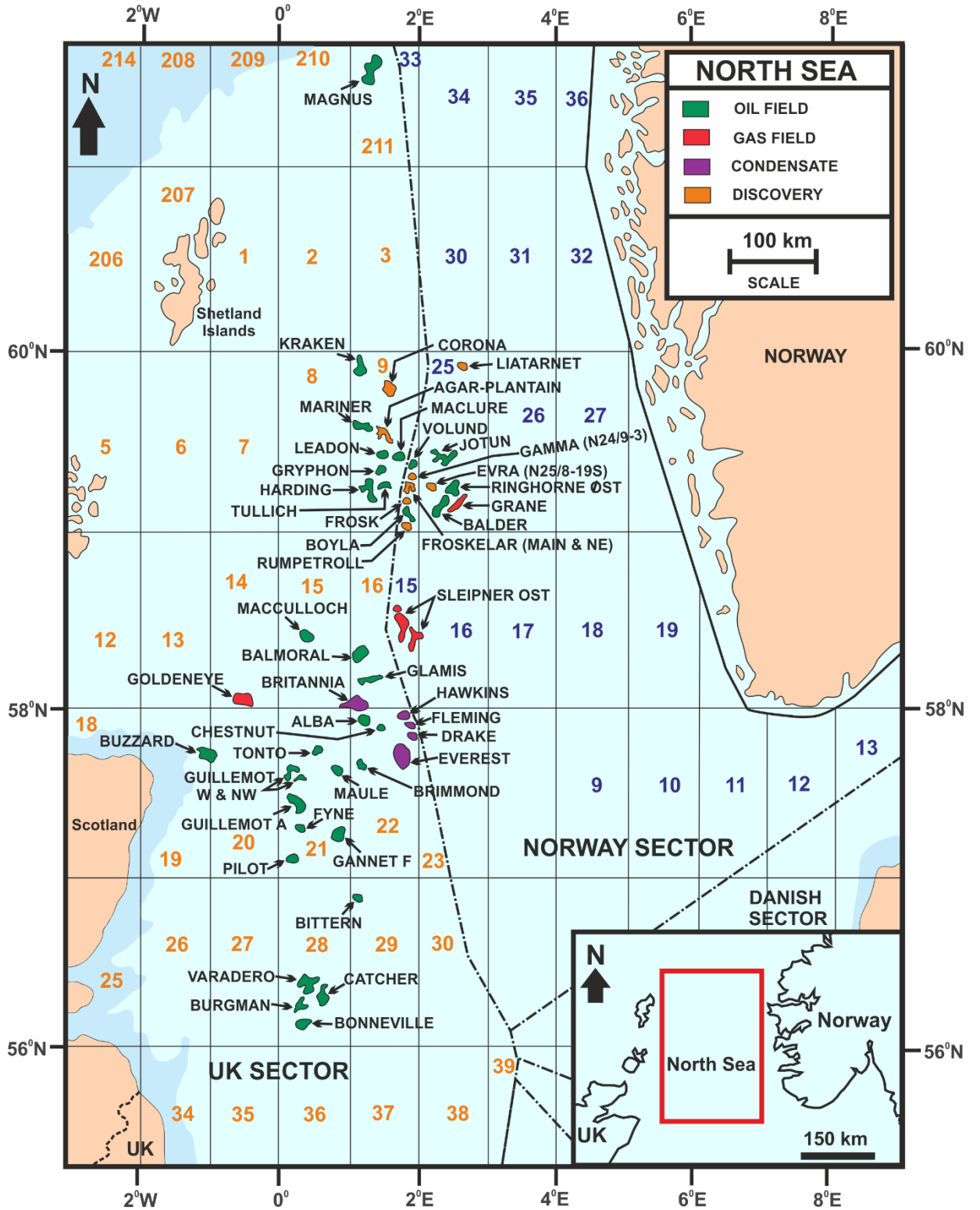
Fig. 3.1: Map showing the location of study. Location of oil, gas and condensate fields with reservoirs affected by sand remobilization and injection are also highlighted within the different quadrants in the UK and Norwegian sectors of the North Sea Basin.
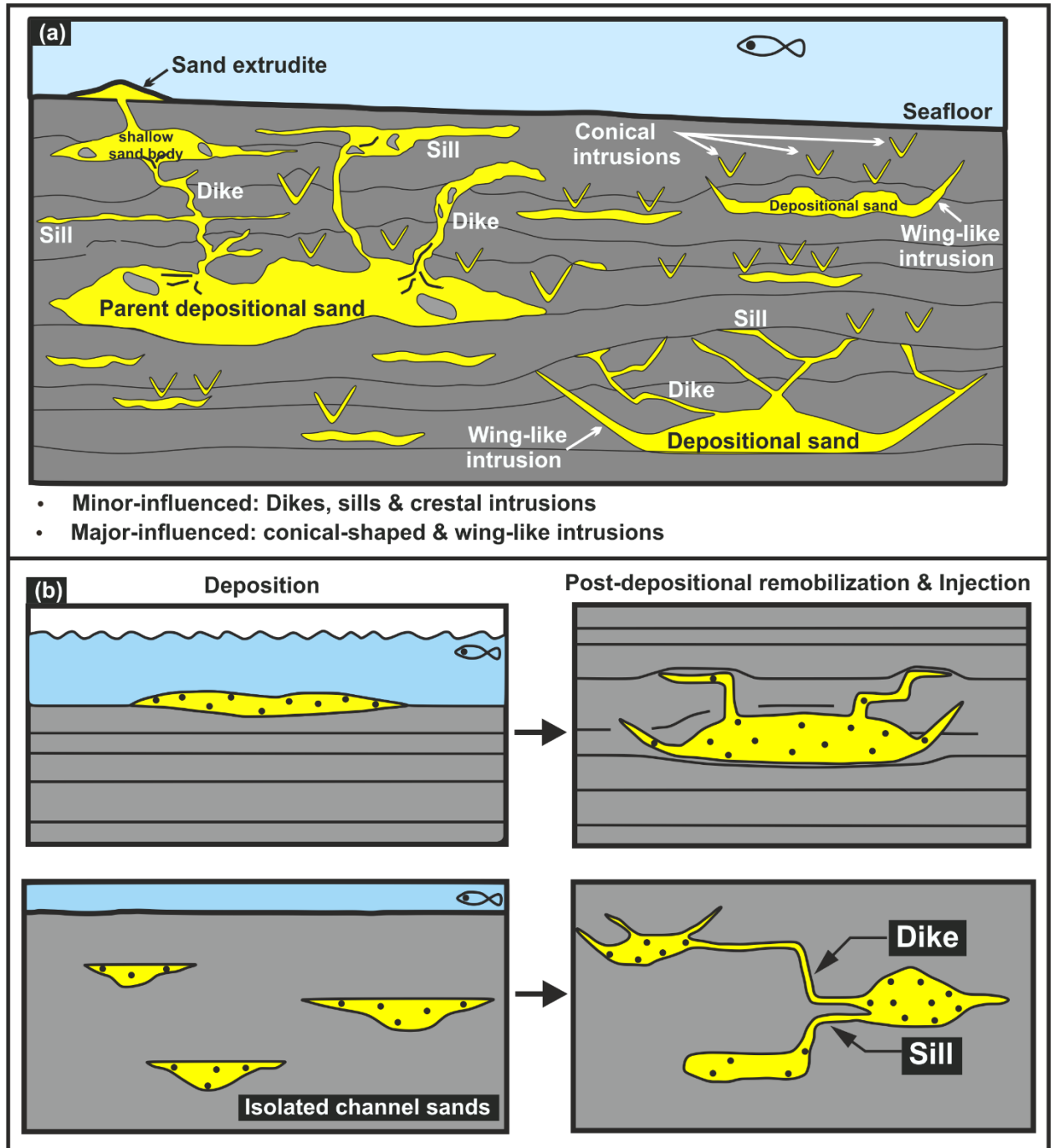
Fig. 3.2: (a) Schematic representation of sand injectite complexes illustrating their associated architectural elements and geometries ranging from small-scale to large-scale intrusions. The figure also defines the two reservoir types: minor-influenced and major-influenced reservoirs (see text in section 3.2 for definition) associated with sand injectite fields in the North Sea Basin (redrawn and modified from Huuse et al., 2007; Brunstad et al., 2009). (b) Schematic representation of the effects of post-depositional remobilization and injection on deep-water sandstone reservoirs. The process clearly alters the geometry of the reservoirs and can also enhance connectivity between initially isolated sand reservoirs (redrawn and modified from Lonergan et al., 2000).
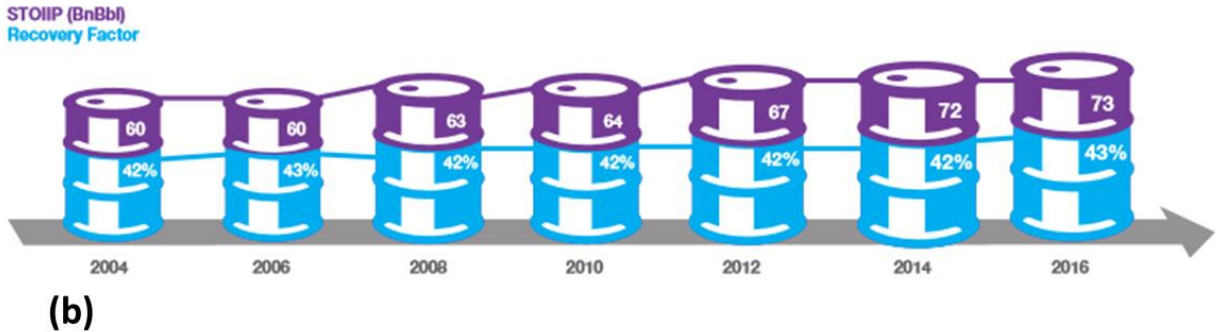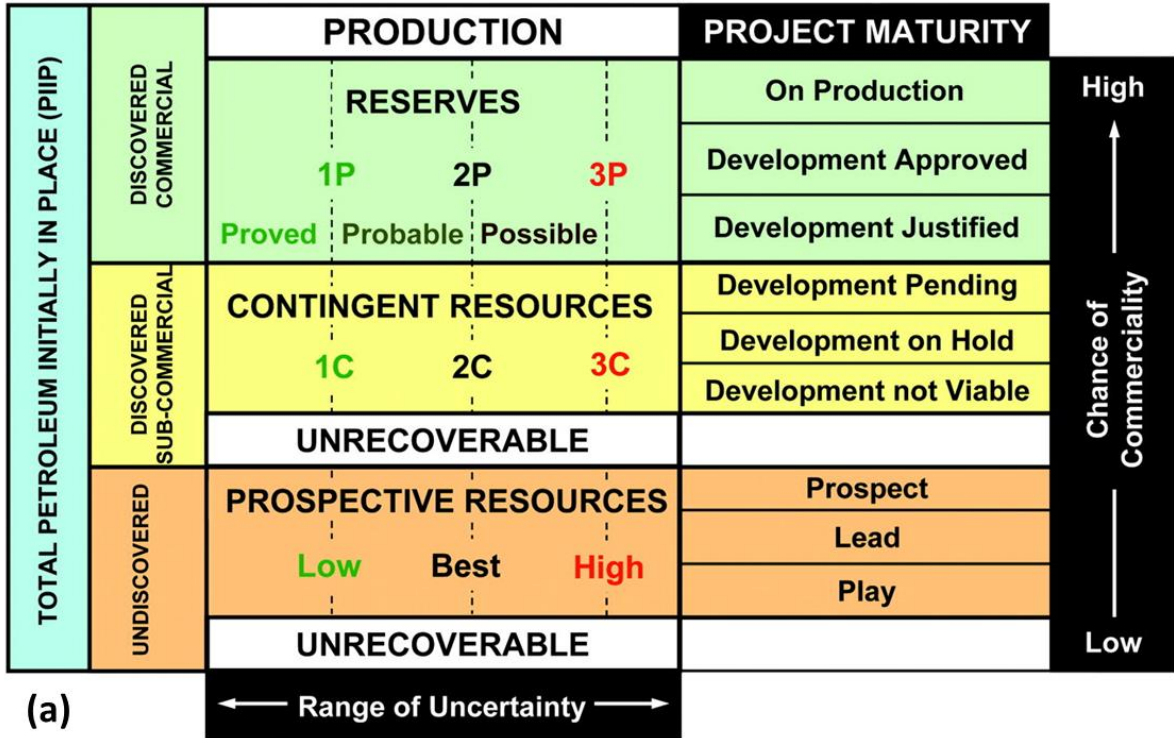
Fig. 3.3: (a) Hydrocarbon reserve/resource classification criteria based on the SPE Petroleum Resource Management System (Worthington, 2007). Only probable reserves (2P) and contingent resources (2C) are documented in Table 3.1 & 3.2. Here reserves refer to the quantity of hydrocarbon anticipated to be commercially recoverable while contingent resources refer to potentially recoverable volumes of hydrocarbon which are not yet considered as commercially recoverable. (b) UKCS Oil recovery factor over time from 2004 – 2016 which have been used to estimate reserves where only STOIIP estimates are available for UK injectite fields (OGA, 2017b). Note that in Fig. b, increase in STOIIP values is cumulative while recovery factors are per-year values.

The extent of post-depositional remobilization and injection on the reservoirs has been considered by divided the reservoirs into two types: minor-influenced and major-influenced reservoir types based on Willett (2015) which considers the style and scale of the injectite complexes. The minor-influenced reservoirs refer to high and low angle small-scale intrusion complexes (e.g., dikes, sills, crestal intrusions) above the main reservoir sands which may be unresolvable on seismic but could be visible on cores and has the capability of providing vertical & lateral connectivity and communication between previously isolated depositional reservoir units (Fig. 3.2; Willett, 2015). The major-influenced reservoirs however refer to large-scale intrusion complexes comprising of low-angle dikes at channel margins, conical and wing-like intrusions (e.g., Alba Field: Lonergan et al., 2000 – their Fig. 4a; Volund Field: Pernin et al., 2019 – their Fig. 10) which are resolvable on seismic and consists of deep-water reservoirs which may have gone through field development and production phase (Willett, 2015).

It is to be noted that access to required information for the Norwegian fields were readily available on the Norwegian Petroleum Directorate (NPD) website. However, there is limited access to information on the UK fields because some of the required information (e.g., number of wells drilled, total investment till date) do not exist in the public domain and some of the available data may be outdated. Only probable (2P) reserves and contingent resources were considered and do not include prospective resources (Fig. 3.3a). Therefore, some of the figures quoted for some fields/discoveries (e.g., Fyne, Gamma, Pilot) are presented as resources. All recoverable reserves and resources in million standard cubic meters (mmSm^3) are converted to million barrels of oil equivalent (mmbbloe) using the conversion factors in Table 3.3 for all the Norwegian injectite fields. Some of the UK fields (e.g., Bonneville) have their reserves estimated by applying a benchmark recovery factor (RF) of 43% since the UKCS (UK Continental Shelf) oil recovery factor have been consistent between 42 – 43% from 2004 -2016 (Fig. 3.3b). This was then applied to STOIIP (stock-tank-oil-initially-in-place) values obtained from press releases/published sources to derive estimated reserves (STOIIP *RF) in million barrels of oil equivalent (mmbbloe). Also, the mean value for reserves presented as a range of values have been used for analysis and calculation where needed. Total investment value for the Norwegian fields were documented in million Norwegian Krone (mmkr) on NPD website but have been converted to million US dollars ($mm) using the NOK to USD exchange rate as the 24th of March, 2020 ($1 = 10.41 NOK). The total investment recorded for the Norwegian injectite fields include the cumulative total sum of the investment in each field up until the end of 2018.

Table 3.1: UK North Sea Sand Injectite Fields & Discoveries (modified after Willett, 2015)

Fields & Discoveries	Discovery Date	Production Start	Recoverable Reserves/Resources (mmbbloe)	Reservoir Type	Reservoir Interval and Age	Reservoir properties Porosity (%)	Reservoir properties Permeability (mD)	Depositional Environment	Hydrocarbon Type	Key References
Gannet F	1969	1997	19 - 21.2	Major	Andrew, Lista, Forties, Rogaland, Tay Fm. (Palaeocene)	22 - 34	N/A	Deep-water slope & basin-floor setting	Oil	https://www.offshore-technology.com/projects/gannet/
Balmoral	1975	1986	110**	Minor	Andrew Formation (Upper Paleocene)	17 - 28 (25§)	700 - 3300	Deep-water basin-floor setting	Oil	Tokin & Fraser (1991); Gambaro & Currie (2003)
Guilletmot A	1979	1996	26.3?	Major	Forties, Rogaland Fm. (Pal. - Eocene)	27 - 31?	N/A	Deep-water slope & basin-floor setting	Oil & Gas	http://www.databydesign.co.uk/energy/ukdata/fields/guillemt.htm; https://www.offshore-technology.com/projects/anasuria-cluster-central-north-sea/
Leadon	1979	2001	120 - 170	Major	Balder Formation (Lower Eocene)	35	N/A	Deep-water basin-floor setting	Oil	https://www.offshore-mag.com/production/article/16759844/leadon-fpso-delivered-on-time-complete-within-budget
Mariner	1981	2019	250 - 300	Major	Maureen, Heimdal Fm. (Paleocene)	34	2000 - 10000	Deep-water slope & basin-floor setting	Oil	Søreide et al. (2013); https://www.equinor.com/en/what-we-do/mariner.html
Everest	1982	1993	162.9	Minor	Maureen, Andrew, Forties Fm. (Paleocene)	15 - 20	30 - 420	Deep-water slope & basin-floor setting	Gas & Condensate	O'Connor & Walker (1993); http://abarrelfull.wikidot.com/everest-oil-and-gas-field
Fleming	1982	1997	200.6	Minor	Maureen Formation (Paleocene)	15 - 22 (18§)	30 - 400 (200§)	Deep-water slope & basin-floor setting	Condensate	O'Connor & Walker (1993); Stuart (2003)
Guillemot W & NW	1979; 1985	2000	58?	Major	Forties Sst. Mbr., Rogaland Fm. (Pal. - Eocene)	27 - 31?	N/A	Deep-water slope & basin-floor setting	Oil	http://www.databydesign.co.uk/energy/ukdata/fields/guillewt.htm; https://www.offshore-technology.com/projects/triton/
Alba	1984	1994	430$^+$	Major	Alba Formation (Upper Eocene)	31 - 34	2300 - 3000	Deep-water slope setting	Oil	Hurst et al. (2011); Scott et al. (2013)
Brimmond	1985	1996	3.4	Minor	Balder Formation (Lower Eocene)	33 - 34	1100	Deep-water basin-floor setting	Oil	Carter & Heale (2003); van Oorschot et al. (2019)
Kraken	1985	2017	137	Minor	Heimdal Fm. (Paleocene)	30 - 38	3700	Deep-water slope setting	Oil	Dangfa et al. (2012); https://www.offshore-technology.com/projects/kraken-oil-field-north-sea/
Chestnut	1986	2008	17.2 - 25.8	Major	Nauchlan Formation (Middle Eocene)	30	2000	Deep-water slope & basin-floor setting	Oil	Wood & Coghlan (2010); Scott et al. (2013)
Fyne	1987	Relinquished	10.6	Minor	Tay Sst. Member (Eocene)	33	2500	Deep-water slope & basin-floor setting	Oil	OGA (2017a)
Gryphon	1987	1993	177.2$^+$	Minor	Balder Formation (Lower Eocene)	33 - 38 (34§)	2000 - 10000 (7000§)	Deep-water slope & basin-floor setting	Oil	Lonergan et al. (2007); Braccini et al. (2008); Hurst et al. (2011); Scott et al. (2013); Berthereau (2014); Pernin et al. (2019)
Harding	1988	1996	278	Major	Balder Formation (Lower Eocene)	35	8000 - 10000	Deep-water basin-floor setting	Oil	Beckly et al. (2003); Scott et al. (2013); Pernin et al. (2019)
Pilot	1989	N/A	143	Unknown	Tay Sst. Member (Eocene)	35	2000 - 8000	Deep-water slope setting	Oil	https://pharis.energy/pilot
MacCulloch	1990	1997	119**	Minor	Balmoral Fm. (Upper Paleocene)	24 - 32 (28§)	200 - 2000	Deep-water basin-floor setting	Oil	https://www.offshore-technology.com/projects/macculloch/; Gunn et al. (2003)

Maclure	1991	2002	38**	Major	Balder Formation (Lower Eocene)	33	4500	Deep-water basin-floor setting	Oil & Gas	Pernin et al. (2019)
Bittern	1997	2000	145	Major	Cromarty Sst. Member (Lower Eocene)	33	1000	Deep-water basin-floor setting	Oil	McCormick & Leisham (2004); Willett (2015)
Tullich	2001	2002	42	Minor	Balder Formation (Lower Eocene)	27 - 36 (30§)	500 - 5000	Deep-water basin-floor setting	Oil	Rodriguez et al. (2005)
Tonto	2007	2013	2.5	Major	Brimmond Formation (Eocene)	30 - 35	N/A	Deep-water basin-floor setting	Oil	Byerley et al. (2014)
Maule	2009	2010	3.0**	Major	Brimmond Formation (Eocene)	30 - 35	N/A	Deep-water basin-floor setting	Oil	Pyle et al. (2011); Morton et al. (2014); van Oorschot et al. (2019)
Catcher	2010	2017	38.6	Major	Cromarty, Tay Sst. Mbr. (Upper Pal. - Eocene)	35	N/A	Deep-water slope & basin-floor setting	Oil	Premier Oil (2014)
Varadero	2011	2018	21.7	Minor	Tay Sst. Member (Eocene)	35	N/A	Deep-water slope & basin-floor setting	Oil	Premier Oil (2014)
Burgman	2011	2018	23.3	Minor	Tay Sst. Member (Eocene)	35	N/A	Deep-water slope & basin-floor setting	Oil	Premier Oil (2014)
Bonneville	2013	N/A	12.9^{+}	Minor	Tay Sst. Member (Eocene)	30	N/A	Deep-water slope & basin-floor setting	Oil	https://www.premier-oil.com/premieroil/media/press/exploration-drilling-update-3
Agar-Plantain Discovery	2014	Expected by 2021	50 - 98	Minor	Frigg Sst. Mbr. - Balder Fm. (Lower Eocene)	30	N/A	Deep-water basin-floor setting	Oil	https://expronews.com/exploration/revival-of-the-injectite-play/
Corona Discovery	2015	N/A	9 - 19	Unknown	Frigg Sst. Mbr. - Balder Fm. (Lower Eocene)	N/A	N/A	Deep-water basin-floor setting	Oil	Pernin et al. (2019); Apache (2015)
Britannia	1975	1998	131	Minor	Britannia Formation (Lower Cretaceous)	15	30 - 60 (50§)	Deep-water basin-floor setting	Condensate	Jones et al. (1999); Blackbourn & Thomson (2000); Hill & Palfrey (2003)
Goldeneye	1996	2004	124$^{\pi}$	Major	Captain Sst. Mbr. (Lower Cretaceous)	25	700 - 1500	Deep-water basin-floor setting	Gas & Condensate	Marshall et al. (2018)
Magnus	1974	1983	665 - 869	Major	Magnus Sst. Mbr. (Upper Jurassic)	18 - 24 (21§)	950	Deep-water basin-floor setting	Oil	Shepherd (1991); Goodall et al. (1999); https://en.wikipedia.org/wiki/Magnus_oilfield
Drake	1980	1997	77	Minor	Fulmar Formation (Upper Jurassic)	22	60	Shallow marine - shoreface	Condensate	Stuart (2003)
Hawkins	1980	2001	27.8	Unknown	Fulmar Formation (Upper Jurassic)	17	5	Shallow marine - shoreface	Condensate	Stuart (2003)
Glamis	1982	1989	19**	Unknown	Glamis Sst. (Upper Jurassic)	7 - 18 (15§)	1500	Shallow marine	Oil	Fraser & Tonkin (1991); Gambaro & Currie (2003)
Buzzard	2001	2007	700	Minor	Buzzard Sst. Mbr. (Upper Jurassic)	15 - 34	200 - 18000	Deep-water basin-floor setting	Oil	Dore & Robbins (2005); Ray et al. (2010); https://www.offshore-technology.com/projects/buzzard-field-expansion-north-sea/

Table 3.2: Norwegian North Sea Sand Injectite Fields & Discoveries (modified after Willett, 2015)

Fields & Discoveries	Discovery Date	Production Start	Recoverable Reserves & Resources (mmbbloe)	Total Investment ($mm)	Reservoir			Reservoir properties		Depositional Environment	Hydrocarbon Type	No. of wells	Key References
					Type	Interval	Age	Avg. Porosity (%)	Permeability (mD)				
Balder	1967	1999	692.5	3313	Major	Lista, Hermod, Balder Fm.	Paleocene - Early Eocene	33	2500	Deep-water basin-floor setting	Oil	128	Briedis et al. (2007); Scott et al. (2013); NPD, 2020
Sleipner Øst	1981	1993	761	2762	Minor	Ty, Hugin, Heimdal Fm.	Lower Paleocene & Jurassic	22	400	Deep-water basin-floor setting	Gas & condensate	41	Østvedt, (1987); Scott et al. (2013); Willett (2015); NPD, 2020
Gamma (N24/9-3) #	1981	N/A	21	N/A	Major	Frigg Formation	Lower Eocene	39	2000 - 4000	Deep-water basin-floor setting	Oil	2	Hurst et al. (2005); Huuse et al. (2007); NPD, 2020
Grane	1991	2003	946	2767	Minor	Heimdal Formation	Paleocene	34.5	N/A	Deep-water slope setting	Oil	178	NPD, 2020
Jotun	1994	1999	151.1	912	Minor	Heimdal Formation	Paleocene	30	1500 - 3000	Deep-water basin-floor setting	Oil & Gas	43	Scott et al. (2013); NPD, 2020
Volund	1994	2009	87	508	Major	Hermod, Balder Fm.	Paleocene - Early Eocene	32	1000 - 6000	Deep-water slope setting	Oil & Gas	30	Szarawarska et al. (2010); Schwab et al. (2015); NPD, 2020
Ringhorne Øst	2003	2006	105	94.8	Minor	Statfjord Grp.	Early Jurassic	N/A	200	Fluvial & Shallow marine	Oil	9	NPD, 2020
Bøyla	2009	2015	17.6	513	Minor	Hermod Formation	Paleocene - Early Eocene	27	N/A	Deep-water basin-floor setting	Oil	9	NPD, 2020
Frosk Discovery	2018	2019	30 - 60 (50*)	359?	Major	Heimdal, Hermod Fm.	Paleocene - Early Eocene	N/A	N/A	Deep-water basin-floor setting?	Oil	7	NPD, 2020; https://expronews.com/exploration/revival-of-the-injectite-play/
Froskelår Discovery (Main & NE)	2019	N/A	45 - 153 (92*)	N/A	Major	Heimdal, Hermod Fm.	Paleocene - Early Eocene	N/A	N/A	Deep-water basin-floor setting?	Oil & Gas	2	NPD, 2020; https://expronews.com/exploration/revival-of-the-injectite-play/
Rumpetroll Discovery	2019	N/A	45 - 148 (93*)	N/A	Minor	Heimdal, Hermod Fm.	Paleocene - Early Eocene	N/A	N/A	Deep-water basin-floor setting?	Gas	2	NPD, 2020; https://expronews.com/wells/ncs-gas-at-rumpetroll/
Evra (N25/8-19S) Discovery	2019	N/A	Appraisal required	N/A	Unknown	Heimdal Fm.	Paleocene - Eocene	N/A	N/A	N/A	Oil & Gas	3	https://www.offshore-technology.com/news/lundin-discovery-north-sea-iving-evra/

Note:

+ - reserve estimated using published STOIIP (mmbbl) and recovery factor (43%); ***** - means most likely reserve /resource based on some published sources; **?** – author not sure of given value, investment figure and depositional environment; **N/A** – unknown, no information available, no information found, no record available; **π** - field abandoned and final cumulative production total used as reserve figure; **#** - field development may be unlikely; ****** - production has exceeded original reserve estimate and the current cumulative production figures or updated reserve figure have been used;

§ - average values for porosity (ø) and permeability (K). See Fig. 3.1 for the location of sand injectite fields and discoveries in the UK & Norwegian sectors of the North Sea Basin

Table 3.3: Conversion factors used to convert reserve and resource estimates from published sources e.g., conversion from standard cubic meter (Sm^3) to barrels (bbl) and then to barrel-of-oil-equivalent (bbloe).

Conversion Factors Used	
Conversions to oil equivalent	
1 Sm^3 oil	= 1.0 Sm^3 o.e.
1 Sm^3 condensate	= 1.0 Sm^3 o.e.
1000 Sm^3 gas	= 1.0 Sm^3 o.e.
Conversion factors for Liquid (Oil, Condensate)	
1 Sm^3	= 6.2898 barrels (bbl)
1 bbl	= 0.1590 Sm^3
Conversion factors for Gas	
1 Sm^3	= 35.315 SCF (standard cubic feet)
1 SCF	= 0.028317 Sm^3

3.3 Results

3.3.1 Reserves and resource distribution of injectite fields in the UK/Norway North Sea

A total of forty-seven (47) sand injectite fields/discoveries have been documented for the UK/Norwegian North Sea with the UK sector (Table 3.1) accounting for thirty-five (35) fields and twelve (12) for the Norwegian sector (Table 3.2, Fig. 3.1). The recoverable reserves and resources in both sectors give 4578.4 mmbbloe and 3021.7 mmbbloe for the UK and Norwegian sector respectively, with a total cumulative reserves and resources (TCRR) of 7600.1 mmbbloe (Fig. 3.4 & 3.5). The graph in Fig. 3.5 shows that sand injectite complexes were discovered throughout the history of hydrocarbon exploration and production in the North Sea leading to the overall increase in recoverable reserves and resources. The years from 1979 – 1997 recorded the highest increase in reserves with a plateau recorded beyond 1997.

In both sectors, sand injectite are associated with deep-water sandstone reservoirs (e.g., turbidites, submarine fans) and often contain low gravity oil of less than 25 API (Hurst et al., 2005). The injected reservoirs have very high porosities generally ranging between 15 – 38%, high permeability in the Darcy scale (0.3 – 18D) and occur mainly in deep-water basin-floor settings (Table 3.1 & 3.2). The Paleogene interval contains 74.3% (5649.3 mmbbloe) of the total cumulative reserves and resources in thirty-nine (39) injectite fields consisting of

Paleocene – Eocene reservoirs. Cretaceous sand injectite reservoirs are found in two (2) fields and they both contain 3.36% (255 mmbbloe) of the cumulative reserves and resources. While Jurassic injectite reservoirs are found in six (6) fields and accounts for the remaining 22.35% (1695.8 mmbbloe) (Table 3.4, Fig. 3.6). This implies that sand injectite reservoirs are largely distributed in the Paleogene succession of the North Sea and as such the Paleogene contributes hugely to the reserve and resource figures in both sectors. This is evidenced from 1983 – 2019 with majority of discoveries made within the Paleogene (Paleocene – Eocene), except for the Ringhorne Øst, Buzzard and Goldeneye fields (Table 3.1 & 3.2).

Considering the reservoir type based on the style and scale of injection, we observe that the minor-influenced reservoirs with small-scale intrusions form majority of the reservoirs in the injectite fields. They occur in 46.8% (22 fields) of the fields while the major-influenced reservoirs with large-scale intrusions and the unknown-reservoir type occur in 46.6% (20 fields) and 10.6% (5 fields) of the North Sea fields respectively (Fig. 3.7). The minor-influenced reservoirs contain recoverable reserves and resources in the three (3) stratigraphic intervals in both sectors which sum up to 4079.8 mmbbloe and forms 53.68% of the total cumulative reserves and resources (Table 3.4). The major-influenced reservoirs contain 3316.5 mmbbloe which forms 43.63% while the unknown accounts for 203.8 mmbbloe which forms just 2.68% of the total cumulative reserves/resources (Table 3.4). 42.9%, 54.29% and 2.78% of the total cumulative recoverable reserves and resources in the Paleogene are found in major-influenced, minor-influenced, and unknown reservoir types respectively (Table 3.4, Fig. 3.8). Also 51.37% of the total cumulative reserve and resources in the Cretaceous are contained in injectite reservoirs affected by small-scale (minor) remobilization and injection while 48.63% are found in reservoirs affected by large-scale (major) sand remobilization and injection (Table 3.4, Fig. 3.8). Finally, 52.01%, 45.23% and 2.76% of the total Jurassic reserves/resources are housed in minor-influenced, major-influenced, and unknown reservoir types respectively (Table 3.4, Fig. 3.8).

Fields discovered after 2001 were mainly associated with small-scale injectite complexes with a few large-scale injectite complexes (Table 3.1 & 3.2). Among fields with minor-influenced reservoirs in the UK sector, the Buzzard Field (700 mmbbloe) discovered in 2001 contains the highest recoverable reserves followed by the Fleming Field (200.6 mmbbloe). While in the Norwegian sector the Grane Field (946 mmbbloe) contains the highest followed by the Sleipner Øst Field (761 mmbbloe). However, for the major-influenced reservoirs the Magnus Field (767 mmbbloe) has the highest recoverable reserve in the UK sector followed by the Alba Field (430 mmbbloe). While in the Norwegian sector it is the Balder Field (692.5 mmbbloe) followed by the recent Froskelår discovery (99 mmbbloe).
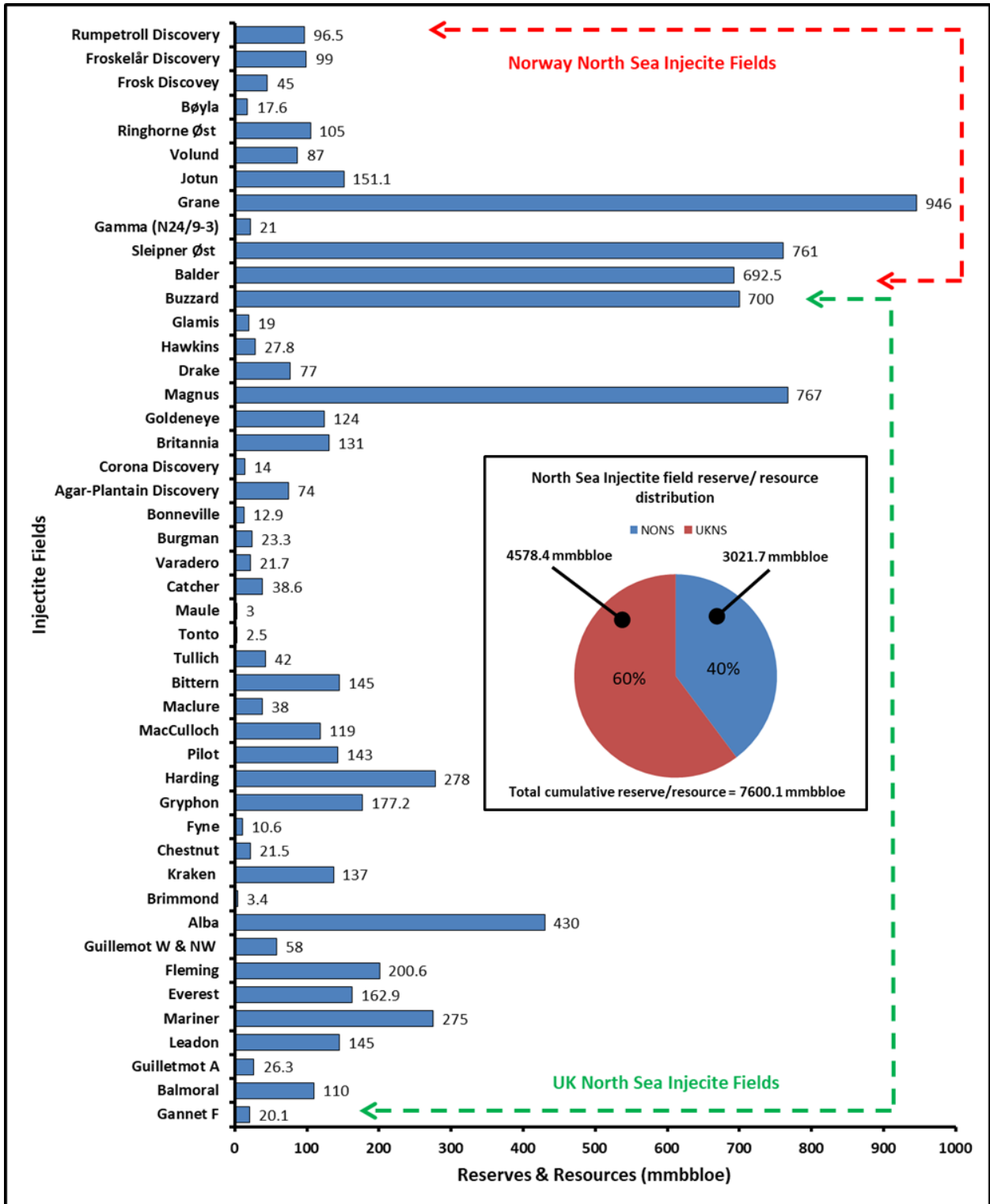
Fig. 3.4: Bar chart showing the distribution of reserves and resources in the sand injectite fields & discoveries of the UK and Norwegian sectors of the North Sea Basin. In the UK sector, we have a total of thirty-five (35) injectite fields with a total reserves/resource of 4578.4 mmbbloe, while the Norwegian sector consists of twelve (12) fields with a total reserves/resources of 3021.7 mmbbloe (See table 3.1 & 3.2). UKNS – UK North Sea; NONS – Norwegian North Sea. See Fig. 3.1 for location of sand injectite fields and discoveries.
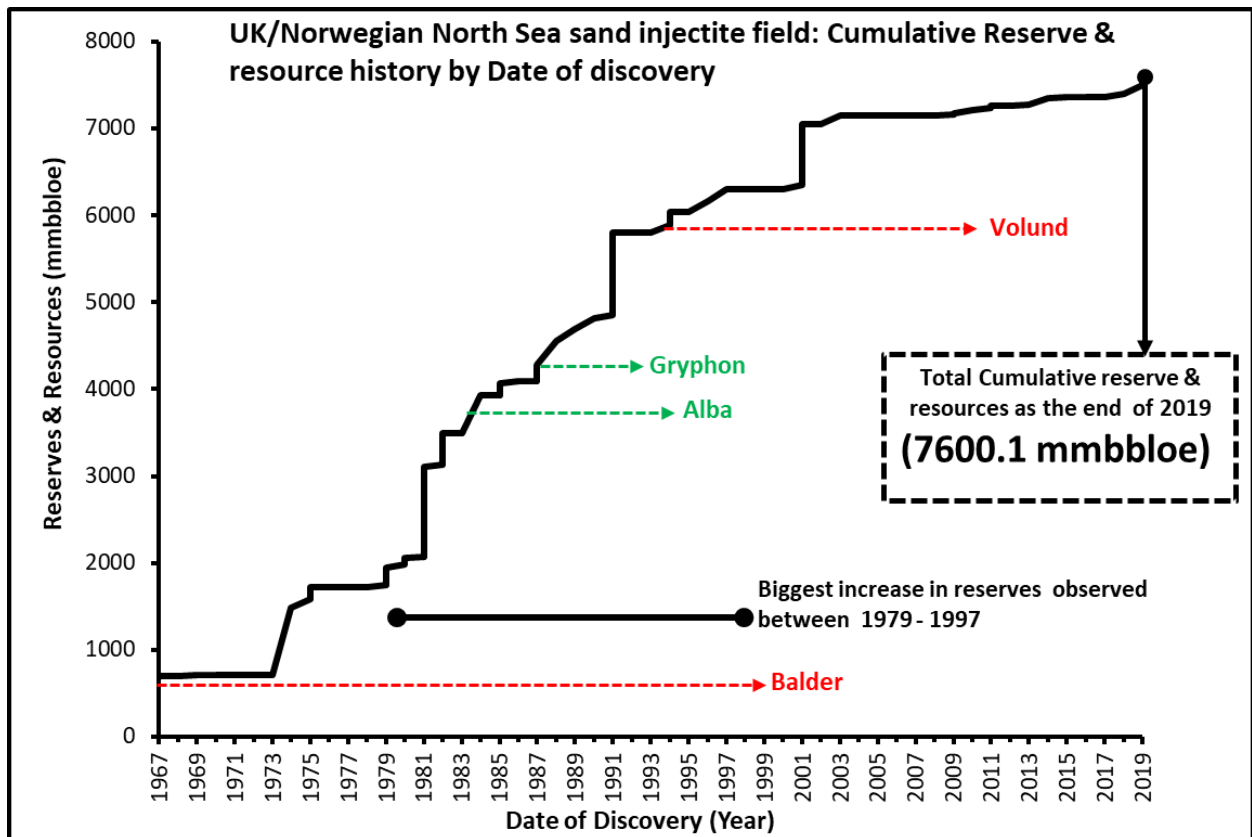
Fig. 3.5: Graph showing the cumulative reserve/resource distribution for injectite fields/discoveries versus year of discovery in both sectors of the North Sea basin. 1979 – 1997 saw the largest increase in reserves with a uniform increase in reserves after 1997. The green arrows shows the length of time between discovery and start of production for the two prominent injectite fields (Alba & Gryphon) in the UK sector while the red arrow shows same for the two most prominent (Balder & Volund) in the Norwegian sector.

Table 3.4: Reserve and resource distribution in the UK & Norwegian North Sea injectite fields/discoveries by reservoir type and stratigraphic age.

No. of fields & discoveries	Age of Reservoirs	No. of Reservoir Type			Reserve & Resource total
		Major	**Minor**	**Unknown**	
39	**Paleogene (Paleocene - Eocene)**	18	18	3	5649.3
	Reserve/ Resources (mmbbloe)	**2425.5**	**3066.8**	**157**	
	Reserve/ Resources %	42.9	54.29	2.78	
2	**Cretaceous**	1	1	0	255
	Reserve/ Resources (mmbbloe)	**124**	**131**	**0**	
	Reserve/ Resources %	48.63	51.37	0	
6	**Jurassic**	1	3	2	1695.8
	Reserve/ Resources (mmbbloe)	**767**	**882**	**46.8**	
	Reserve/ Resources %	45.23	52.01	2.76	
Total reserves/resources (mmbbloe)		3316.5	4079.8	203.8	7600.1
% Total		43.64	53.68	2.68	

(The top of the table spans the title: UK/Norwegian North Sea injectite field Reserves/Resources by reservoir types and age)
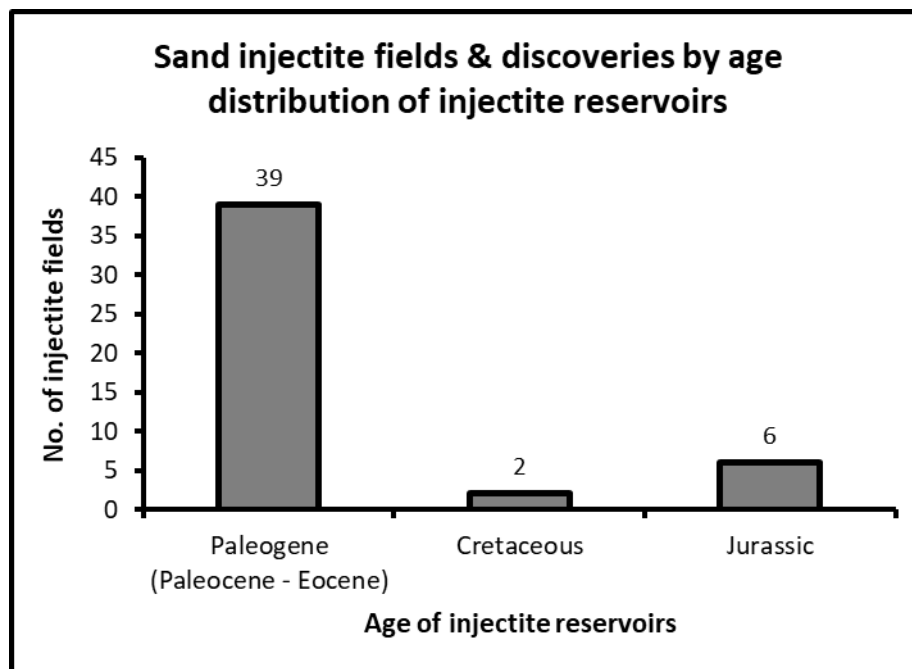
Fig. 3.6: Stratigraphic age distribution and number of fields with sand injectite reservoirs at different stratigraphic intervals in the North Sea Basin. Majority of the fields (39 out of 47) are associated with reservoirs of Paleogene (Paleocene – Eocene) age.
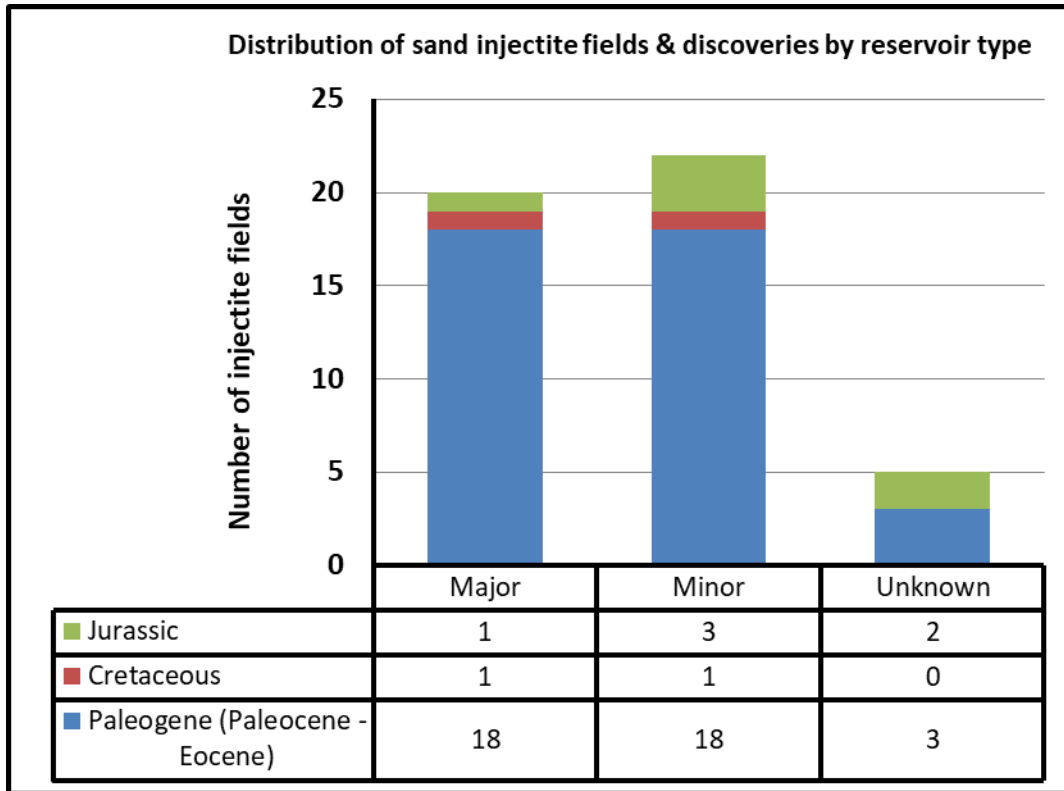
Fig. 3.7: Summary bar chart illustrating the number of injectite fields associated with minor-influenced, major-influenced, and unknown reservoir types according to the ages of the reservoir interval.
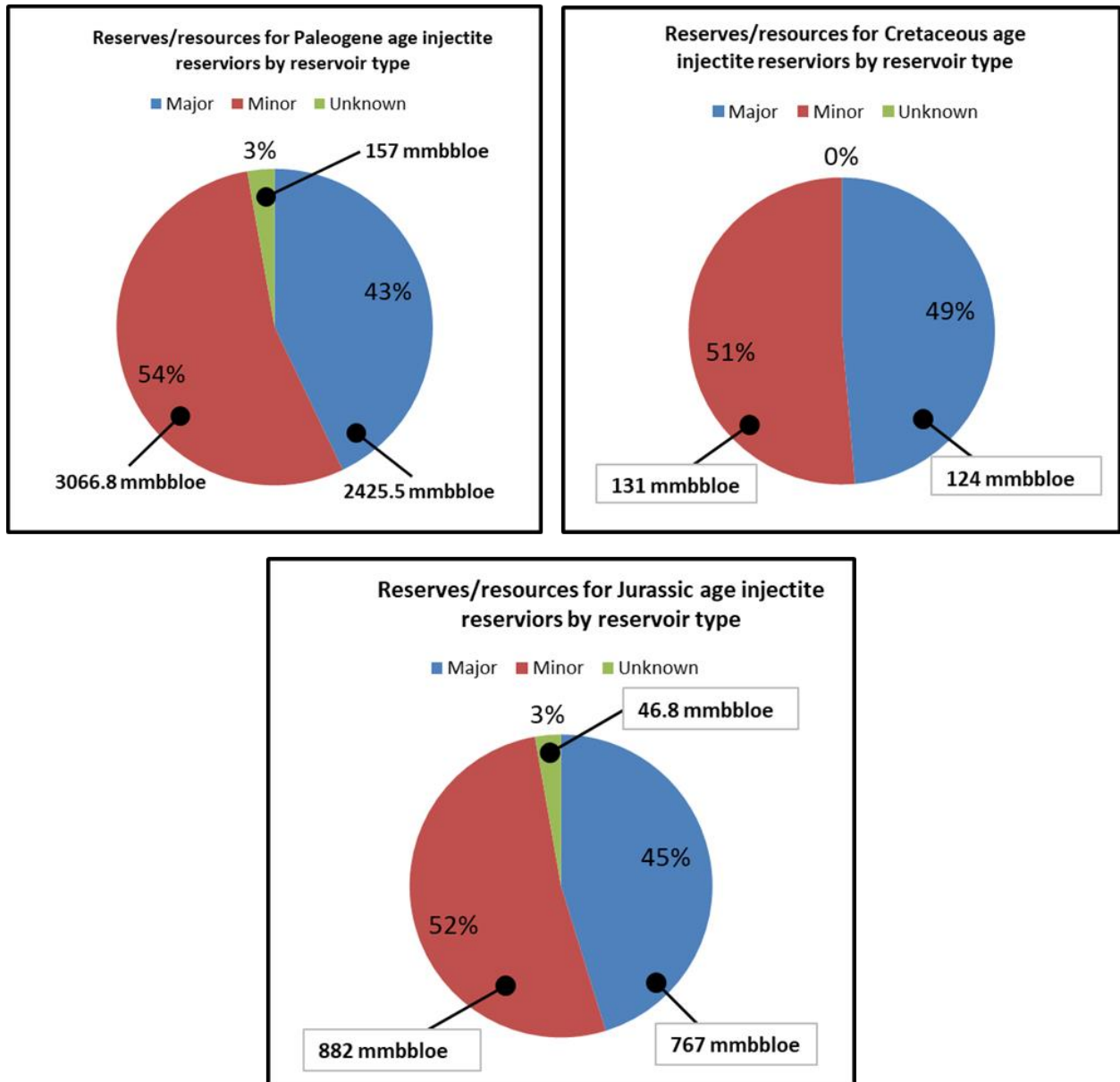
Fig. 3.8: Percentage reserve and resource distribution by reservoir type and age of injectite complexes in the UK & Norwegian North Sea (See Table 3.4: values in pie charts have been rounded up).

3.3.2 Reserve and resource history and distribution of injectite fields in the Norwegian sector of the North Sea

Sand injectites fields in the Norwegian North Sea accounts for 39.8% (3021.7 mmbbloe) of the total cumulative reserves/resources associated with injectite complexes in the North Sea (Fig. 3.4; Table 3.5). This part of the North Sea contains eight (8) fields and four (4) recent discoveries of sand injectite complexes out of the forty-seven (47) fields/discoveries documented here (Table 3.2, Fig. 3.9). The reservoirs in these Norwegian fields consist of gravity flow (turbidites) and submarine fans sands deposited in deep-water slope and basin-floor settings. The injectite complexes have excellent reservoir quality with porosities ranging from 22 – 39% and permeability from 200 – 6000 mD (Table 3.2). Here the injectites are associated with mainly Paleogene (Paleocene – Eocene) reservoirs with only one case in the Jurassic. The injectite complexes in the Paleogene of the Norwegian North Sea accounts for 96.5% (2916.7 mmbbloe) of the total recoverable reserves/resources (Table 3.5), while only the Ringhorne Øst Field with Jurassic injectite reservoir accounts for the remaining 3.5% (105 mmbbloe). The Froskelår and Rumpetroll discoveries in 2019 are both expected to go into development and production subsequently (i.e., say between 2021 and 2022) while the Gamma (N24/9-3) development may be unlikely (Willett, 2015). In the Paleogene of the Norwegian North Sea, major-influenced injectite complexes account for 31.3% (944.5 mmbbloe) of the total recoverable reserves/resources while the minor small-scale injectite complexes account for the remaining 68.7% (2077.2 mmbbloe). No major-influenced injectite complexes are however present in the Jurassic (Table 3.5). A total of 454 wells, which includes exploration, appraisal, and production wells, have been drilled in the Norwegian North Sea injectite fields with 282 wells drilled in minor injectite complexes compared to the 169 wells drilled in major injectite complexes. Three (3) wells comprising of a discovery well and two (2) side-tracks were drilled in the unknown reservoir type for the Evra (N25/8-19S) discovery. However, the number of wells shown in Table 3.5 for the Gamma Field, Froskelår and Rumpetroll discoveries are only exploration and appraisal wells because they are yet to undergo development and production. It is to be noted that Aker BP currently considers the Rumpetroll discovery to be non-commercial. The total capital investment (in $mm) for each of the Norwegian North Sea injectite fields/discoveries up to the end of 2018 is outlined in Table 3.2 & Fig. 3.10 and sums up to $11.23 billion dollars. This brings the amount invested on major-influenced injectite fields to $4.18 billion dollars which is 37% of the total capital investment. While the minor-influenced injectite complexes accounts for the remaining 63% ($7.05 billion dollars or $7048.8 million dollars).
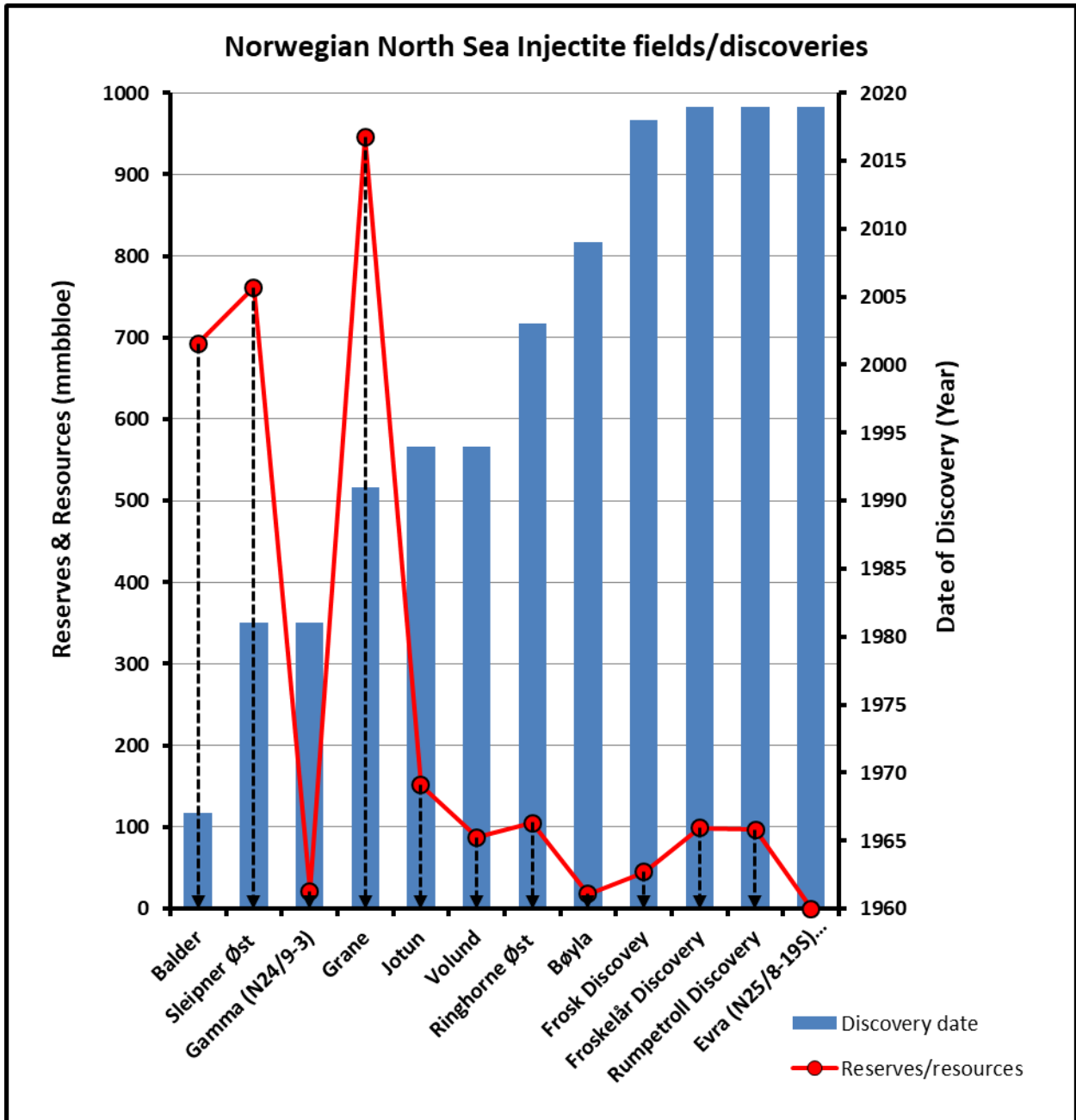
Fig. 3.9: Graph showing the twelve (12) Norwegian North Sea sand injectite fields and discoveries by their hydrocarbon reserve and resource distribution together with their year of discovery. See Fig. 3.1 for location of sand injectite fields and discoveries.

Table 3.5: Reserve and resource distribution of Norwegian North Sea injectite field/discoveries by reservoir type and interval.

Norwegian North Sea injectite field Reserves/Resources by reservoir types and age				
Age of Reservoirs	**No. of Reservoir Type**			**Reserve/Resource total**
	Major	**Minor**	**Unknown**	
Paleogene (Paleocene - Eocene)	5	5	1	**2916.7**
Reserve/ Resources (mmbbloe)	944.5	1972.2	N/A	
Reserve/ Resources %	32.4	67.6	N/A	
Jurassic	N/A	1	N/A	**105**
Reserve/ Resources (mmbbloe)	N/A	105	N/A	
Reserve/ Resources %	N/A	100	N/A	
Total reserves/resources (mmbbloe)	944.5	2077.2	N/A	**3021.7**
% Total	31.3	68.7	N/A	

3.4 Conclusion

This brief review has shown that sand injectite complexes contain substantial amount of hydrocarbon and contributes significantly to the total cumulative hydrocarbon reserves and resources in the North Sea Basin. This has also shown that the few recorded success (e.g., Alba, Balder, Gryphon & Volund) in targeting these reservoirs have yielded positive results and have led to the increase in search for near-field accumulations above producing fields because the injection of sand into low permeable sealing mudstones can enhance the migration of fluids to shallower intervals. Therefore, the North Sea Basin is likely to contain more near-field accumulations of hydrocarbon (e.g., the recent Liatårnet 25/2-21 discovery) which are yet to be discovered. Furthermore, this study has also shown that injectite complexes are viable exploration targets which should be embraced, although their mechanisms of formation is not yet fully understood. It is also evident that the Paleogene succession of the North Sea Basin is the most susceptible to sand remobilization and injection because majority of the injectite fields have their reservoirs hosted in the Paleocene – Eocene deep-water sediments. This may suggest that the Paleogene holds significant potential for accumulation of hydrocarbons in injectite reservoirs and there is a tendency for future discoveries in new and existing fields within the Paleogene interval. Even though majority of the reserves and resources reported here are hosted in small-scale injection complexes, the large-scale injection complexes also contribute significant volumes of reserves and resources.

Finally, it is important that the potential influence of sand remobilization and injection on the geometry of deep-water sandstone reservoirs is considered in all phases of hydrocarbon

exploration, development, and production especially in reserve/resource evaluation and reservoir modelling by considering their possible implications on the overall recoverable reserves. Also, it may be worthwhile to re-evaluate previous reservoir models for producing Paleogene – Jurassic fields by revisiting seismic, borehole and core data for possible influence of remobilization and injection. Their identification may in turn add more reserves and improve future drilling success.
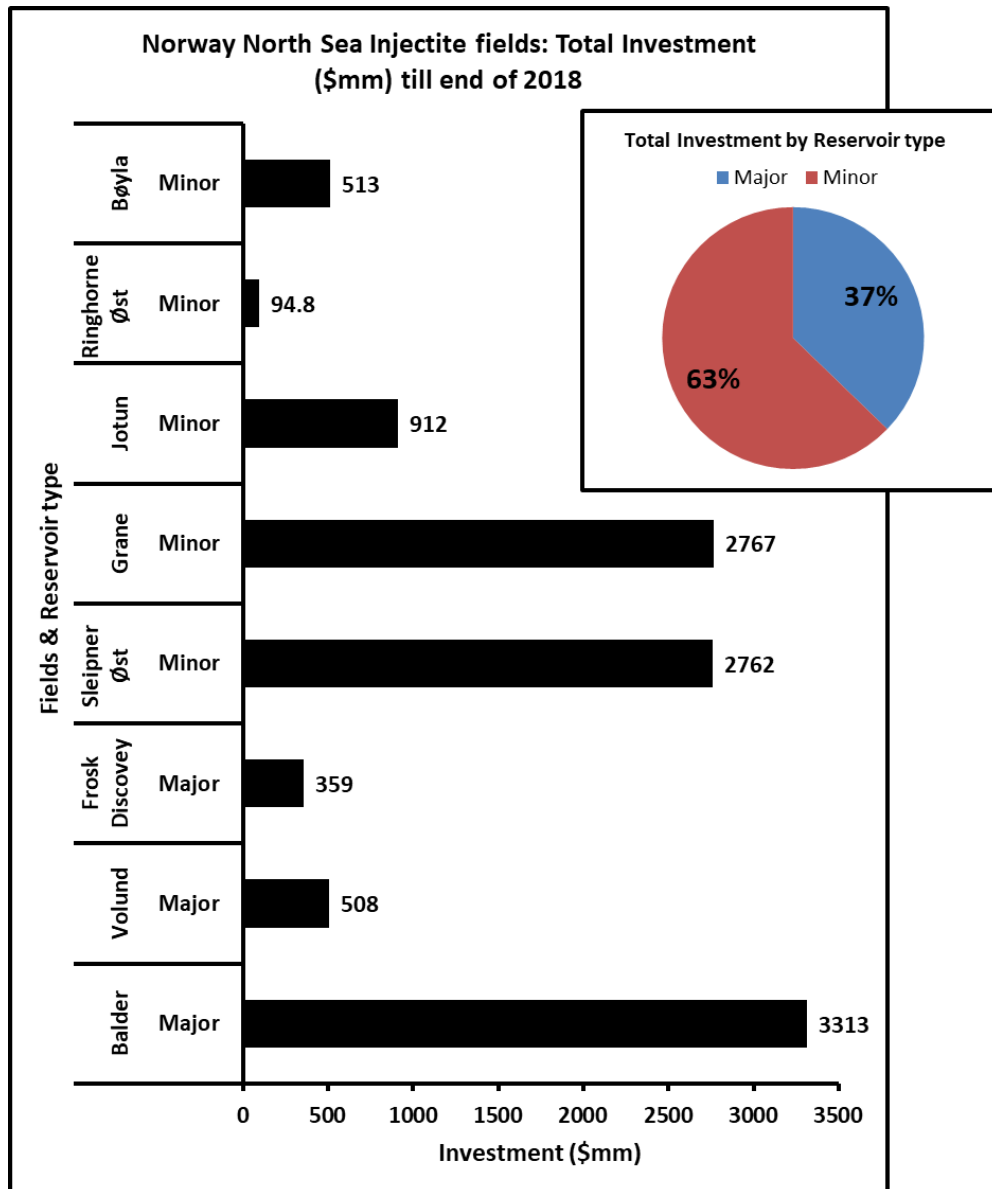
Fig. 3.10: A bar chart showing the total capital investment (in $mm) for the Norwegian North Sea injectite fields and discoveries up till the end of 2018. The Balder field ($3313mm) clearly has the highest expenditure compared to the Ringhorne øst ($94.8mm) with the least capital investment which may be related to the number of wells drilled in both fields. Total investment estimates gotten from NPD (accessed April 2020).

References

APACHE. 2015. *Forward-Looking Statements*. https://oilandgasuk.co.uk/wp-content/uploads/2015/10/Oil-Gas-UK-Presentation-Dec-2015-16-by-9.pdf

BECKLY, J., NASH, T., POLLARD, R., BRUCE, C., FREEMAN, P. & PAGE, G. 2003. The Harding Field, Block 9/23b. *Geological Society Memoir*, **20**, 283–290, https://doi.org/10.1144/GSL.MEM.2003.020.01.24.

BERTHEREAU, G. 2014. *Maximize Chance of Drilling Injected Sand: Examples from Gryphon Area*.

BLACKBOURN, G.A. & THOMSON, M.E. 2000. Britannia Field, UK North Sea: Petrographic constraints on Lower Cretaceous provenance, facies and the origin of slurry-flow deposits. *Petroleum Geoscience*, **6**, 329–343, https://doi.org/10.1144/petgeo.6.4.329.

BRACCINI, E., DE BOER, W., HURST, A., HUUSE, M., VIGORITO, M. & TEMPLETON, G. 2008. Sand injectites. *Oilfield Review*, **20**, 34–49, https://doi.org/10.1306/m871209.

BRIEDIS, N. A, BERGSLIEN, D., HJELLBAKK, A, HILL, R.E. & MOIR, G.J. 2007. Recognition Criteria, Significance to Field Performance, and Reservoir Modelling of Sand Injections in the Balder Field, North Sea. *Sand injectites: Implications for hydrocarbon exploration and production*, 91–102, https://doi.org/-.

BRUNSTAD, H., GRADSTEIN, F., VERGARA, L. & LIE, J.E. 2009. A Revision of the Rogaland Group, Norwegian North Sea. *Norwegian Stratigraphic Lexicon*, 1–157.

BYERLEY, G., PYLE, J. & TOWART, J. 2014. Tonto field -The application of AVO inversion to fast-track development of a new small field at forties. *In*: *76th European Association of Geoscientists and Engineers Conference and Exhibition 2014: Experience the Energy - Incorporating SPE EUROPEC 2014*. EAGE Publishing BV, 3610–3614., https://doi.org/10.3997/2214-4609.20141021.

CARTER, A. & HEALE, J. 2003. The Forties and Brimmond Fields, Blocks 21/10, 22/6a, UK North Sea. *Geological Society Memoir*, **20**, 557–561, https://doi.org/10.1144/GSL.MEM.2003.020.01.45.

DANGFA, D.N., ISLAM, A.I., WHITE, J., DATIR, H., MUKHERJEE, B. & SIMS, A. 2012. Innovative Approach to Characterizing a Heavy Oil North Sea Reservoir drilled with OBM , using Multi-Depth of Investigation NMR , Dielectric Dispersion and Sonic Anisotropy Data acquisition and job planning. *In*: *World Heavy Oil Congress*. 1–12.

DIXON, R.J., SCHOFIELD, K., ANDERTON, R., REYNOLDS, A.D., ALEXANDER, R.W.S., WILLIAMS, M.C. & DAVIES, K.G. 1995. Sandstone diapirism and clastic intrusion in the Tertiary submarine fans of the Bruce-Beryl Embayment, Quadrant 9, UKCS. *Geological Society Special Publication*, **94**, 77–94, https://doi.org/10.1144/GSL.SP.1995.094.01.07.

DORÉ, G. AND ROBBINS, J., 2005. The Buzzard Field. In *Geological Society, London, Petroleum Geology Conference series* (Vol. 6, No. 1, pp. 241-252). Geological Society of London.

DURANTI, D. & HURST, A. 2004. Fluidization and injection in the deep-water sandstones of the Eocene Alba Formation (UK North Sea). *Sedimentology*, **51**, 503–529, https://doi.org/10.1111/j.1365-3091.2004.00634.x.

DURANTI, D., HURST, A., BELL, C., GROVES, S. & HANSON, R. 2002. Injected and remobilized Eocene sandstones from the Alba Field, UKCS: core and wireline log characteristics. *Petroleum Geoscience*, **8**, 99–107, https://doi.org/10.1144/petgeo.8.2.99.

FRASER, A.R. & TONKIN, P.C. 1991. The Glamis Field, Block 16/21a, UK North Sea. *Geological Society Memoir*, **14**, 317–322, https://doi.org/10.1144/GSL.MEM.1991.014.01.39.

GAMBARO, M. & CURRIE, M. 2003. The Balmoral, Glamis and Stirling Fields, Block 16/21, UK Central North Sea. *Geological Society Memoir*, **20**, 395–413, https://doi.org/10.1144/GSL.MEM.2003.020.01.33.

GOODALL, I., LOFTS, J., MULCAHY, M., ASHTON, M. & JOHNSON, S. 1999. A sedimentological application of ultrasonic borehole images in complex lithologies: The Lower Kimmeridge Clay Formation, Magnus Field, UKCS. *Geological Society Special Publication*, **159**, Vol.6 No.1 pp. 203-225, https://doi.org/10.1144/GSL.SP.1999.159.01.11.

GUNN, C., MACLEOD, J.A., SALVADOR, P. & TOMKINSON, J. 2003. The MacCulloch Field, Block 15/24b, UK North Sea. *Geological Society Memoir*, **20**, 453–466, https://doi.org/10.1144/GSL.MEM.2003.020.01.37.

HILL, P.J. & PALFREY, A.J. 2003. The Britannia Field, Blocks 15/29a, 15/30, 16/26, 16/27a, 16/27b, UK North Sea. *Geological Society Memoir*, **20**, 415–429, https://doi.org/10.1144/GSL.MEM.2003.020.01.34.

HURST, A., CARTWRIGHT, J.A., DURANTI, D., HUUSE, M. & NELSON, A. 2005. Sand injectites: an emerging global play in deep-water clastic environments. *Geological Society of London*, **6**, 133–144.

HURST, A. & CARTWRIGHT, J. 2007. Relevance of Sand Injectites to Hydrocarbon Exploration and Production. *In*: *Sand Injectites: Implications for Hydrocarbon Exploration and Production: AAPG Memoir 87*. 1–19., https://doi.org/10.1306/1209846M871546.

HURST, A., SCOTT, A. & VIGORITO, M. 2011. Physical characteristics of sand injectites. *Earth-Science Reviews*, **106**, 215–246, https://doi.org/10.1016/j.earscirev.2011.02.004.

HUUSE, M., CARTWRIGHT, J., HURST, A. & STEINSLAND, N. 2007. Seismic Characterization of Large-scale Sandstone Intrusions. Sand injectites: Implications for hydrocarbon exploration and production: AAPG Memoir 87, 21–35, https://doi.org/10.1306/1209847M873253

JACKSON, C.A.L., HUUSE, M. & BARBER, G.P. 2011. Geometry of wing-like clastic intrusions adjacent to a deep-water channel complex: Implications for hydrocarbon exploration and production. *AAPG Bulletin*, **95**, 559–584, https://doi.org/10.1306/09131009157.

JONES, L.S., GARRETT, S.W., MACLEOD, M., GUY, M., CONDON, P.J. & NOTMAN, L. 1999. Britannia Field, UK Central North Sea: Modelling heterogeneity in unusual deep-water deposits. *In*: *Petroleum Geology Conference Proceedings*. 1115–1124., https://doi.org/10.1144/0051115.

LONERGAN, L., BORLANDELLI, C., TAYLOR, A. & QUINE, M. 2007. The three-dimensional geometry of sandstone injection complexes in the Gryphon field, United Kingdom North Sea. *AAPG Memoir*, 103 112. https://doi.org/10.1306/1209854M873260

LONERGAN, L., LEE, N., JOHNSON, H.D., CARTWRIGHT, J.A. & JOLLY, R.J.H. 2000. Remobilization and Injection in Deepwater Depositional Systems: Implications for Reservoir Architecture and Prediction. *In*: *Deep-Water Reservoirs of the World: 20th Annual*, https://doi.org/10.5724/gcs.00.15.0515.

MARSHALL, J.D., TUCKER, O.D., LOVELOCK, C.E., DARKER, S.J., ANNIA, C.E. & HOGNESTAD, J.B. 2018. Goldeneye: Tomorrow Never Dies (or a field only Lives Twice). *Petroleum Geology Conference Proceedings*, **8**, 547–560, https://doi.org/10.1144/PGC8.18.

MCCORMICK, D. & LEISHMAN, M. 2004. The Bittern Field: Topographic Control of an Eocene Aged "Channel- Fill' Turbidite Reservoir in the U.K. Central North Sea*. *North*, **20016**, 1–6.

MORTON, A., MCFADYEN, S., HURST, A., PYLE, J. & ROSE, P. 2014. Constraining the origin of reservoirs formed by sandstone intrusions: Insights from heavy mineral studies of the Eocene in the Forties area, United Kingdom central North Sea. *AAPG Bulletin*, **98**, 545–561, https://doi.org/10.1306/06141312191.

NPD. 2020. Field - Fact pages – NPD, https://factpages.npd.no/en/field. Accessed: 2020-04-15

O'CONNOR, S.J. & WALKER, D. 1993. Paleocene reservoirs of the Everest trend. *In*: *Petroleum Geology Conference Proceedings*. 145–160., https://doi.org/10.1144/0040145.

OGA. 2017a. *UKCS Licence P.077 Block 21/28a Relinquishment Report*. https://itportal.ogauthority.co.uk/web_files/relinqs/P077_21_28a.pdf

OGA. 2017b. *Recovery Factor Benchmarking*. https://www.ogauthority.co.uk/media/4155/recovery-factor-report-7-september.pdf

ØSTVEDT O.J. 1987. Sleipner Øst. *Geology of the Norwegian oil and gas fields: London, Graham*, 243–252.

PERNIN, N., FEUILLEAUBOIS, L., BIRD, T. & REISER, C. 2019. Identifying and de-risking near-field opportunities through reliable pre-stack broadband attributes: examples from the Paleocene North Sea (UK–Norway) injectites play. *Geological Society, London, Special Publications*, SP494-2019–11, https://doi.org/10.1144/sp494-2019-11.

PREMIER OIL. 2014. *Capital Markets Presentation*. https://www.premier-oil.co.uk/sites/default/files/presentation/CMD_Presentation.pdf

RAY, F.M., PINNOCK, S.J., KATAMISH, H. & TURNBULL, J.B. 2010. The Buzzard Field: Anatomy of the reservoir from appraisal to production. *In*: *Petroleum Geology Conference Proceedings*. 369–386., https://doi.org/10.1144/0070369.

RODRIGUEZ, J.M., SCHOLEY, H. & FLANAGAN, K.P. 2005. Tullich Field. *In*: *Petroleum Geology Conference Proceedings*. 111–121., https://doi.org/10.1144/0060111.

SCHWAB, A.M., JAMESON, E.W. & TOWNSLEY, A. 2015. Volund Field: Development of an Eocene sandstone injection complex, offshore Norway. *In*: *Geological Society Special Publication*. 247–260., https://doi.org/10.1144/SP403.4.

SCOTT, A., HURST, A. & VIGORITO, M. 2013. Outcrop-based reservoir characterization of a kilometer-scale sand-injectite complex. *AAPG Bulletin*, **97**, 309–343, https://doi.org/10.1306/05141211184.

SHEPHERD, M. 1991. The Magnus Field, Blocks 211/7a, 12a, UK North Sea. *Geological Society, London, Memoirs*, **14**, 153–157.

SØREIDE, I., SILCOCK, S. & THOMSON, I. 2013. *Mariner Field: A Challenging UK Heavy Oil Development*. https://www.spe-uk.org/aberdeen/knowledgefiles/SPE_Aberdeen_Mariner-250913- Final.pdf

STUART, I.A. 2003. The Armada development, UK Central North Sea: The Fleming, Drake and Hawkins Gas-Condensate Fields. *Geological Society Memoir*, **20**, 139–151, https://doi.org/10.1144/GSL.MEM.2003.020.01.12.

SZARAWARSKA, E., HUUSE, M., HURST, A., DE BOER, W., LU, L., MOLYNEUX, S. & RAWLINSON, P. 2010. Three-dimensional seismic characterisation of large-scale sandstone intrusions in the lower Palaeogene of the North Sea: completely injected vs. in situ remobilised sand bodies. *Basin Research*, **22**, 517–532, https://doi.org/10.1111/j.1365-2117.2010.00469.x.

TONKIN, P.C. & FRASER, A.R. 1991. The Balmoral Field, Block 16/21, UK North Sea. *Geological Society Memoir*, **14**, 237–244, https://doi.org/10.1144/GSL.MEM.1991.014.01.29.

VAN OORSCHOT, L.A., PYLE, J.R., BYERLEY, G.W. & ROSE, P.T.S. 2019. Development of the Brimmond Sand Fairway. *Geological Society, London, Special Publications*, SP493-2017–2350, https://doi.org/10.1144/sp493-2017-350.

WILLET MAGNUS. 2015. *Sand Injectites: A Review of Reserves and Resource Potential for the North Sea, UK and Norwegian Sectors. BSc. Thesis, University of Aberdeen*, https://www.researchgate.net/publication/329074747

WOOD, P. & COGHLAN, G. 2010. Chestnut - A successful, innovative development of a small, marginal North Sea oilfield. *In*: *Proceedings - SPE Annual Technical Conference and Exhibition*. 2157–2165.

WORTHINGTON, P.F. 2007. A road map for improving the technical basis for the estimation of petroleum reserves. *Petroleum Geoscience*, **13**, 291–303, https://doi.org/10.1144/1354-079306-732.

WEBSITES:

https://www.offshore-technology.com/projects/gannet/. Accessed: 2020-04-13

http://www.databydesign.co.uk/energy/ukdata/fields/guillemt.htm. Accessed: 2020-04-13

https://www.offshore-technology.com/projects/anasuria-cluster-central-north-sea/. Accessed: 2020-04-13

https://www.offshore-mag.com/production/article/16759844/leadon-fpso-delivered-on-time-complete-within-budget. Accessed: 2020-04-14

https://www.equinor.com/en/what-we-do/mariner.html. Accessed: 2020-04-14

http://abarrelfull.wikidot.com/everest-oil-and-gas-field. Accessed: 2020-04-14

http://www.databydesign.co.uk/energy/ukdata/fields/guillewt.htm. Accessed: 2020-04-15

https://www.offshore-technology.com/projects/triton/. Accessed: 2020-04-15

https://www.offshore-technology.com/projects/kraken-oil-field-north-sea/. Accessed: 2020-04-15

https://www.offshore-technology.com/projects/macculloch/. Accessed: 2020-04-15

https://www.premier-oil.com/premieroil/media/press/exploration-drilling-update-3. Accessed: 2020-04-16

https://expronews.com/exploration/revival-of-the-injectite-play/. Accessed: 2020-04-16

https://en.wikipedia.org/wiki/Magnus_oilfield. Accessed: 2020-04-16

https://www.offshore-technology.com/projects/buzzard-field-expansion-north-sea/. Accessed: 2020-04-16

https://expronews.com/exploration/revival-of-the-injectite-play/. Accessed: 2020-04-17

https://expronews.com/wells/ncs-gas-at-rumpetroll/. Accessed: 2020-04-17

https://www.offshore-technology.com/news/lundin-discovery-north-sea-iving-evra/. Accessed: 2020-04-17

Chapter 4

CHAPTER 4   Three-dimensional seismic and quantitative geometrical characterization of sandstone intrusions in the Paleogene succession of the northern North Sea Basin

Three-dimensional seismic and quantitative geometrical characterization of sandstone intrusions in the Paleogene succession of the northern North Sea Basin

(Northern North Sea Sand Injectite Framework)

Sebastian Nnorom & Mads Huuse

Basins Research Group, Department of Earth and Environmental Sciences, University of Manchester, Oxford Road, Manchester M13 9PL, UK

A revised version of this chapter will be submitted to Journal of Basin Research for publication

Abstract

High resolution three-dimensional seismic data integrated with well data have been used to investigate the occurrence of discordant high amplitude anomalies within the Paleogene succession of the northern North Sea. These discordant anomalies, which are found within the Paleocene – mid Miocene, exhibit varying simple to complex geometries in cross-section and occur predominantly as isolated discreet anomalies characterized by circular/sub-circular to elliptical map view form, or as amalgamated or stacked complexes characterized by irregular cross-sectional geometry and map view form. The discordant amplitude anomalies are interpreted as large-scale sand injectites or sandstone intrusions by well calibration of anomalies intersected by available wells at different depth and interval which yielded tens-of-meters of thick sandstone. All aspects of the remobilization and injection process have been constrained from the parent source sands, potential feeder conduits and timing of injection to their priming and trigger mechanisms. The injectites/intrusions are distributed mainly in the east, west, and south-western parts of the study area, and vary in geometry from conical-shaped, wing-like or saucer-shaped to highly irregular and complex-shaped intrusions with the conical-shaped intrusions being the most predominant. The conical intrusions are here suggested to represent injected sands while the wing-like intrusions may represent in-situ depositional sand bodies which were subjected to post-depositional remobilization and injection leading to the formation of their marginal wings. Measurements of the geometrical parameters for the best resolved conical and wing-like intrusions show their dimensions range from 24 to 226 m in height, 239 to 3294 m in width and 2 to 30° for the dip of their discordant limbs or wings. We suggest that the injectites formed due to post-depositional remobilization and injection of the source sands into their sealing mudstone-dominated succession, facilitated by overpressure caused by disequilibrium compaction, differential loading and lateral transfer of pressure combined with possible migration of fluid from deeper Mesozoic successions and fluid release from silica (Opal-A to Opal-CT) and Smectite-to-Illite diagenetic transformations. In addition, the injection of fluidized sand is suggested to have been triggered by differential compaction or when the threshold of the encasing mudstones was reached. This study has important implications for hydrocarbon exploration and production because it clearly demonstrates the possible impact of sand intrusions on deep-water sand reservoirs and fluid flow in the subsurface since their propagation into low permeable sealing mudstones can modify sand reservoir geometries, compromise seal integrity and they can act as long-lived permeable pathway for fluid flow and migration.

4.1 Introduction

The occurrence of sand intrusions (or injectites) has been described as far back as the 19th century (e.g., Murchison, 1827) but their importance was only recently recognized (Monnier et al., 2014). These intrusions were previously either unidentified, misidentified or misinterpreted which led to their effect on reservoir geometry (i.e., architecture, properties, and connectivity) and reserve distribution to be largely ignored. Availability of high-resolution seismic imaging have made it possible to visualize the three-dimensional geometries of these intrusions, revealing sand-rich deep-water reservoir features that cross-cut stratigraphy and appear as an extension of other depositional parent sand bodies (Dixon et al., 1995; Molyneux et al., 2002; Hurst and Cartwright, 2007; Cartwright, 2010). Sand injection involves the forced emplacement of sand in an adjacent lithology (Duranti and Hurst, 2004), and this occur when fluidized sand is forcibly injected into a host stratum, resulting to the formation of networks of intrusions (Hurst et al., 2003; Hurst et al., 2011). These networks of intrusions are suggested to form in response to the failure of a low permeable sealing lithology caused by hydraulic fracturing, which results to either upward and/or lateral escape of fluidized sand (Hurst et al., 2005). Sand intrusions occur in centimetres to several kilometres scale and exhibit varying geometries ranging from dikes and sills to conical and wing-like intrusions which are typically recognized as discordant amplitude anomalies in 3D seismic cross section (Huuse and Mickelson, 2004; Cartwright et al., 2008; Jackson et al., 2011; Andresen and Clausen, 2014).

The occurrence of sandstone intrusions has been documented by several authors (e.g., Huuse and Mickelson, 2004; Huuse et al., 2005, 2007; Hurst et al., 2011; Jackson et al., 2011, etc.) with the North Sea Basin forming a global type-area for large-scale sandstone intrusion complexes. In the North Sea Basin, sand intrusions are widespread in the Paleogene deep-water sandstone reservoirs within hemi-pelagic smectite-rich and polygonally faulted fine-grained mudstones which form the host strata (Cartwright, 1994; Cartwright and Lonergan, 1996). The interval within the North Sea most susceptible to the processes of sediment remobilization and injection is documented to consists of depositionally restricted deep-water sandstone bodies (e.g., narrow, elongate channels or gully-filled sands) and isolated/localized sand-rich fan-lobes which accumulated in mud-dominated basinal settings (Lonergan et al., 2000). In the North Sea, the occurrence and distribution of large-scale sand injectites have been previously documented within the Lower – Middle Eocene succession in the following areas: North Viking Graben (e.g., Løseth et al., 2003; Huuse at al., 2004, Olobayo, 2014; Cobain et al., 2019), Outer Moray Firth (e.g., Lonergan et al., 2000; Molyneux et al., 2002) and South Viking Graben: Norwegian Block 9 and 25 (e.g., Løseth et al., 2003; Huuse and Mickelson, 2004). Even though North Sea sandstone intrusions have been studied extensively, some aspects (e.g., parent source sands, timing & depth of emplacement, and priming & trigger mechanisms) of their formation and distribution are still poorly understood. For instance, the exact details of the processes which trigger seal failure and sand fluidization, and the series of factors which determine their resultant

simple to complex geometries remain speculative (Davies et al., 2006; Hurst et al., 2011). In addition, the controls on their location, sourcing and architecture from both pore-scale and mineralogical standpoint still need to be addressed. In the northern North Sea area, Olobayo (2014: PhD thesis) has presented an in-depth documentation of the distribution of sandstone intrusions including potential mechanisms for their formation. We however extend or expand the above studies southwards by taking a dip dive into the origin of Paleogene sandstone intrusions in the northern North Sea using the most regionally extensive and complete 3D seismic data available for the northern North Sea, enabling a more regional studies and documentation of their distribution and formation. The current data enabled all aspects of the intrusion process to be revisited and re-evaluated (because the intrusions are well imaged), with new findings used to validate pre-existing conceptual models. Previous documentation of sandstone intrusions in the North Sea have demonstrated that the occurrence of large-scale sandstone intrusion complexes has obvious implications for hydrocarbon exploration and production because: (i) they may constitute volumetrically significant reservoir for hydrocarbon (Huuse et al., 2007; Jackson and Sømme, 2011), and (ii) they can influence reservoir architecture, connectivity and pore-scale reservoir properties (Lonergan and Cartwright, 1999; Lonergan et al., 2000; Duranti et al., 2002; Jackson, 2007).

This study uses an integration of 3D seismic data and well data to describe and analyse the occurrence of discordant high amplitude anomalies in the Paleogene succession of the northern North Sea which we have interpreted as the seismic expression for large-scale sandstone intrusions. The aim of this study is to: (i) document their occurrence, geometries, distribution, and dimensions; (ii) consider mechanisms responsible for their formation (i.e., priming and triggering mechanisms) and discuss other aspects of the intrusion process such as the location of their parent source sands, timing of intrusion; and (iii) highlight their potential implications for hydrocarbon exploration and production.

4.2 Geological Setting

The study area is in the Norwegian sector of the northern North Sea Basin (which hosts several oil and gas discoveries) between Longitude 1 – 4°E and latitude 59 – 62°N (Fig. 4.1a). It covers the whole of the Horda Platform, Tampen Spur, North Viking Graben, Måløy Slope, Uer Terrace, Lomre Terrace, and part of the Sogn Graben. The study area is bounded to the west by the East Shetland Basin, to the north by the Marulk Basin, to the south by the Central & South Viking Graben and to the east by the Norwegian mainlands separated by the Øygarden Fault Zone (Fig. 4.1a).

This part of the North Sea Basin was affected by two main rifting episodes which took place in the Permian to Early Triassic and Late Jurassic to Early Cretaceous (Badley et al., 1988; Ziegler, 1990). Its present-day geometry is associated with the above two rifting episodes.

Rifting during the Permo-Triassic and Late Jurassic – Early Cretaceous led to the formation of half graben as well as series of south striking and west dipping normal faults which are cross-cut by other large NE – SW and NW – SE trending normal faults with variable dip directions (Fig. 4.1; Faerseth et al., 1995, 1997; Dmitrieva et al., 2018). The rift axis of the Permian –Triassic rifting phase is presumed to lie beneath the areas around the Viking Graben (e.g., Horda Platform and Magnus Basin – Unst Basin) while that of the Late Jurassic – Early Cretaceous rifting phase lie beneath the present-day Viking Graben and Sogn Graben (Christiansson et al., 2000). Rifting ceased in the Early Cretaceous and as such majority of the rift-related normal faults became inactive (Dmitrieva et al., 2018). The post-rift phase which commenced in the Early Cretaceous was marked by thermally controlled subsidence due to thermal relaxation of the crust (Gabrielsen et al., 1990; Ziegler, 1990; Jordt et al., 2000; Wrona et al., 2017b; Dmitrieva et al., 2018). This was accompanied by uplift events along basin margins which are speculated to have been associated with igneous activity and break-up or opening of the North Atlantic (Jordt et al., 2000; Bugge et al., 2001; Gabrielsen et al., 2001). Studies indicate that this uplift occurred during the Late Cretaceous – Early Paleocene, Late Eocene – Early Oligocene and Late Pliocene – Pleistocene times (Jordt et al., 2000). This uplift along the basin margins caused abundant supply of coarse clastic sediments from surrounding clastic source areas (i.e., Shetland Platform, British Isles, and west Norway) to be deposited as sand-rich fans and channel-lobe systems forming depocentres during the Late Paleocene, Early Eocene, Early Oligocene, and Early Miocene (Martinsen et al., 1999; Brekke et al., 2001; Ahmadi et al., 2003). The deposited sediments in-filled the relict bathymetry associated with the Mesozoic rift-related structures forming depocentres along boundary faults.

The present sedimentary architecture of the northern North Sea comprises of Cenozoic post-rift infill which were sourced from the uplifted clastic source areas due to tectonic control on sediment supply (Christiansson et al., 2000). This resulted to the deposition of more than 2 km thick siliciclastic sediments along the axis of the northern North Sea. Sedimentation in the Cenozoic was influenced by a combination of factors such as the Atlantic and European tectonic events, climate change, eustatic sea level, differential tilting and subsidence, and variable sediment supply (Ziegler, 1990; Dmitrieva et al., 2012; Goledowski et al., 2012). The Cenozoic post-rift sequence is characterized by coarse grained, deep-water deposits along the eastern margin while the distal part of the basin comprises of hemi-pelagic smectite-rich mud-dominated succession (Jordt et al., 2000; Dmitrieva et al., 2012). This has been subdivided into the Rogaland, Hordaland, and Nordland Groups (Fig. 4.2).
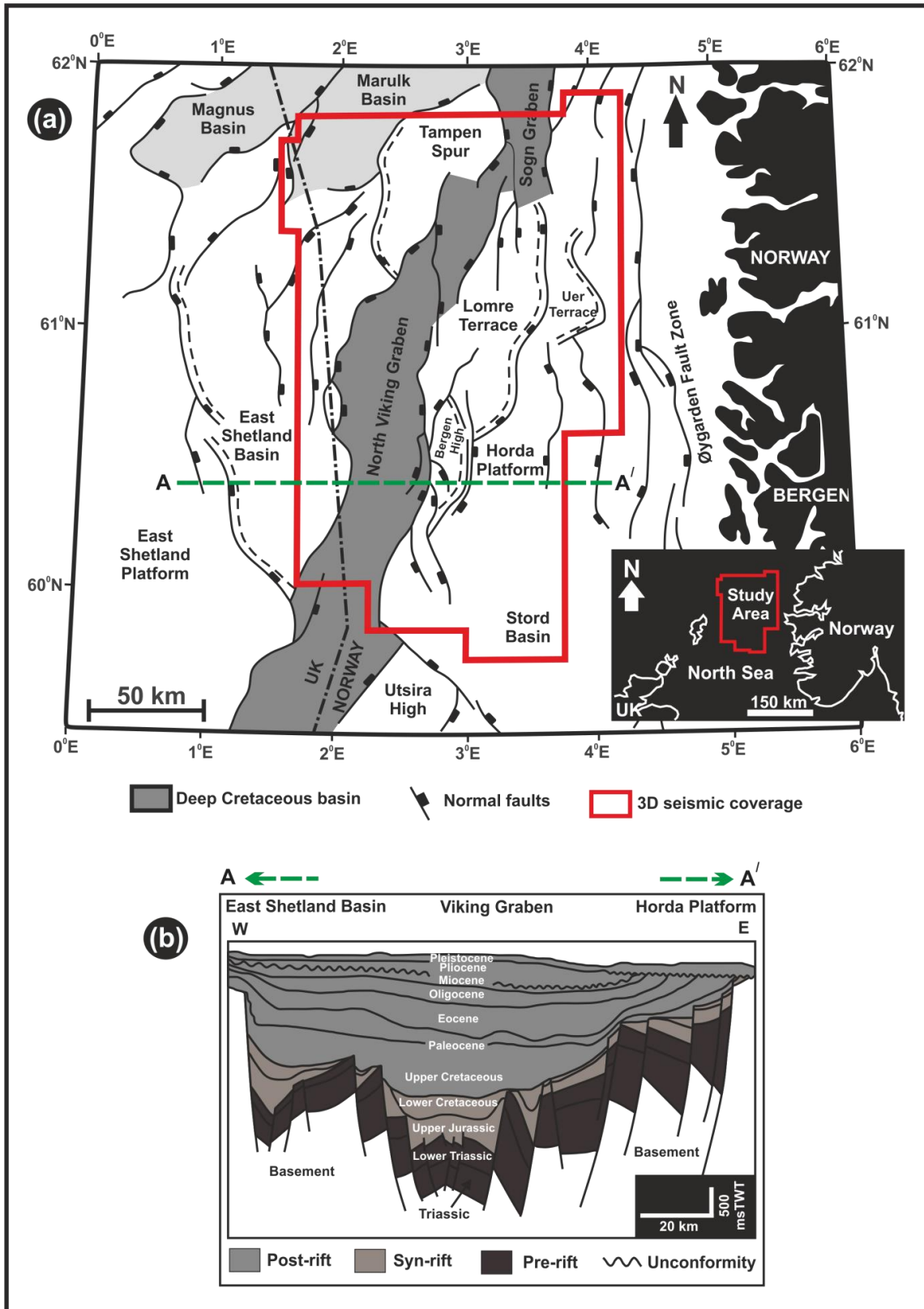
Fig. 4.1: (a) Location map of the study area in the northern North Sea (in red outline) highlighting the main structural elements (modified after Nottvedt et al., 1995). (b) East-west regional cross-section (A – A′) through the northern North Sea showing the chronostratigraphic units and normal faults associated with the Mesozoic rift episodes in the study area (modified after Wrona et al., 2017b).
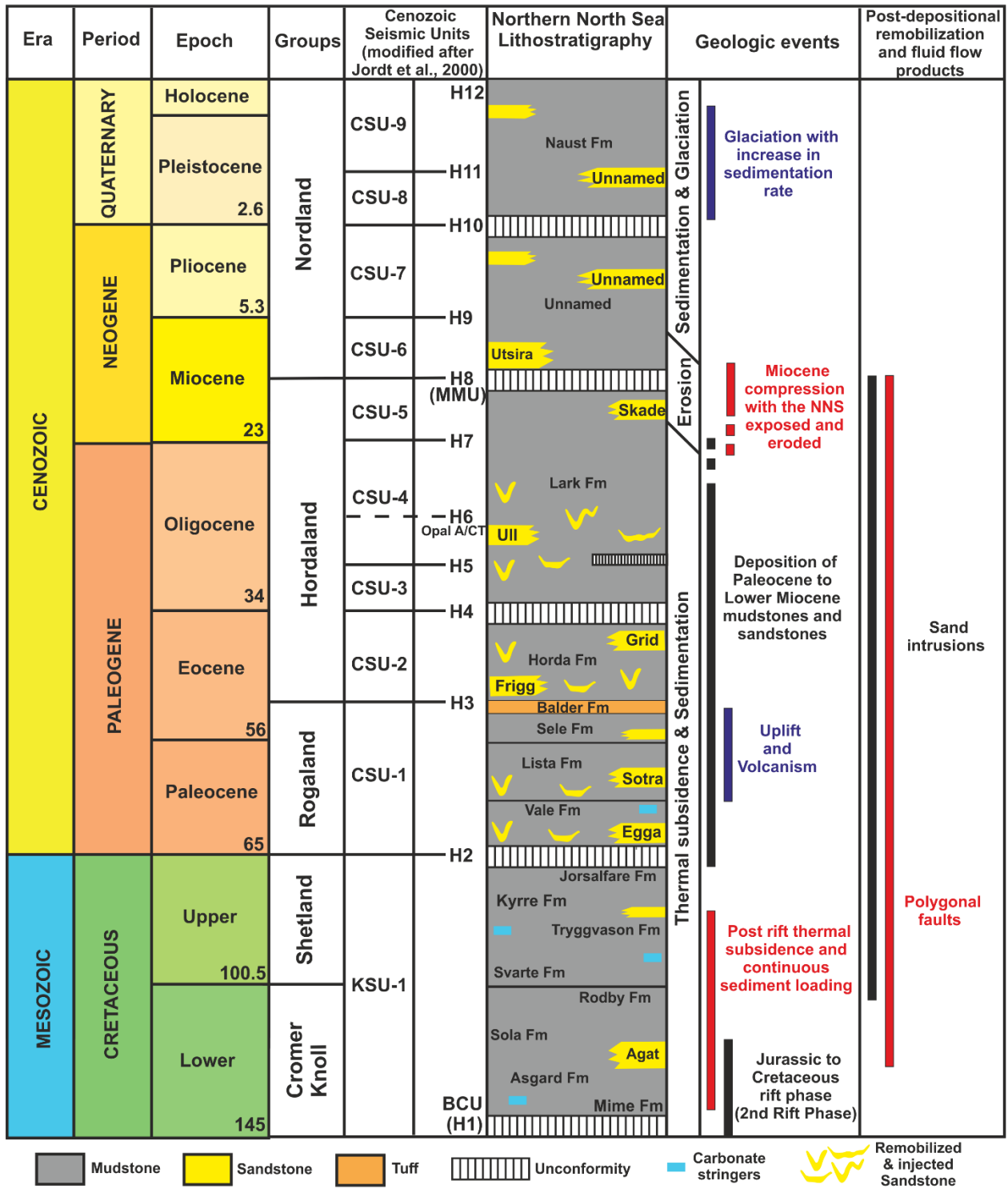
Fig. 4.2: Simplified chronostratigraphic and lithostratigraphic framework of the studied Paleogene interval in the northern North Sea showing major stratigraphic units and their boundaries (modified after Jordt et al., 2000 and Olobayo, 2014). BCU: Base Cretaceous Unconformity; KSU: Cretaceous Seismic Unit; CSU: Cenozoic Seismic Unit; MMU: Mid-Miocene Unconformity.

4.3 Data and Methods

4.3.1 Data

This study involves the interpretation of a high-resolution 3D BroadSeis Broadsource seismic reflection survey (CGG18M01_NVG) covering an area of about 36,400 km^2 in the northern North Sea Basin (Horda/Tampen) provided by CGG (Fig. 4.3). The survey covers: (i) the Norwegian sector of the northern North Sea (Quadrant: 29 – 36), (ii) part of the Norway southern North Sea (Quadrant: 25 & 26), (iii) part of mid-Norway (Quadrant: 6203 & 6204), and (iv) part of the UK sector of the northern North Sea (Quadrant: 003 & 211). The seismic data is time-migrated and extends downward to a depth of 5000 msTWT. It has a sub-sampled line spacing of 37.5 m and a dominant frequency of 50 Hz. The survey is zero-phase processed and displayed with SEG normal polarity which means that a downward decrease in acoustic impedance with depth represents a negative reflection event (displayed in blue), while a downward increase in acoustic impedance represents a positive reflection event (displayed in red). Based on available data from wells, the average interval velocity within the studied interval is around 2000 m/s. This implies that vertical measurements in milliseconds two-way-time (msTWT) can be converted directly to depth in metres. With the average interval velocity and dominant frequency, we estimate that the studied interval which lies between 500 – 2200 msTWT has a vertical resolution ($\lambda/4$) and horizontal resolution ($\lambda/2$) of approximately 10 m and 20 m, respectively.

A total of 115 wells were available for this study (Fig. 4.3) and they all contain complete suite of well logs (e.g., Gamma ray, GR; Density, RHOB; Sonic, DT) and formation top data. Deviation surveys and checkshot data were also available for most of the wells.

4.3.2 Methods

To ensure an accurate tie between the available 3D seismic data (in time domain) and well data (in depth domain), synthetic seismogram was calculated for some selected wells in the study area (e.g., Fig. 4.4b). The synthetic seismogram for the selected wells were computed by the convolution of a statically extracted wavelet from the seismic traces around the well paths with the reflectivity logs for the individual wells derived from their bulk density (RHOB) and sonic (DT) logs. The generated synthetic seismogram enabled: (i) proper age constraints to be placed on observed seismic reflection events and interpreted seismic horizons, (ii) a good correlation across the study area, (iii) identification of key stratigraphic boundaries, and (iv) the evaluation of the lithological significance of the observed discordant high amplitude anomalies within the studied Paleogene interval.

Based on the generated synthetic seismogram, four (4) key stratigraphic boundaries or horizons characterized by high seismic amplitude reflections were identified and mapped across the study area. The mapped boundaries correspond to the Top Shetland Group (TSG

or Base tertiary), Top Rogaland Group (or Top Balder: TB), Eocene-Oligocene boundary (EOB) and the Top Hordaland Group (THG or Mid-Miocene Unconformity). The interval of study lies between the Top Hordaland Group and the Top Shetland Group characterized by varying degree of discordant high amplitude anomalies related to soft sediment remobilization and injection processes.

The discordant amplitude anomalies are present in restricted intervals bounded by the mapped horizons (see Fig. 4.2 & 4.4a). Their 3D seismic geometries were investigated using the mapped horizons and along cross sections. Mapping was carried out by horizon auto-tracking and generation of iso-proportional slices between the horizons. Time thickness maps were also generated to evaluate variation in thickness of the studied intervals and provide insight into the topography at different stages of deposition. Furthermore, the quantitative geometrical measurements of the discordant amplitude anomalies interpreted as sand injectites or intrusions was carried out to document their geometrical parameters (e.g., dip of intrusion limbs/wings and intrusion height).
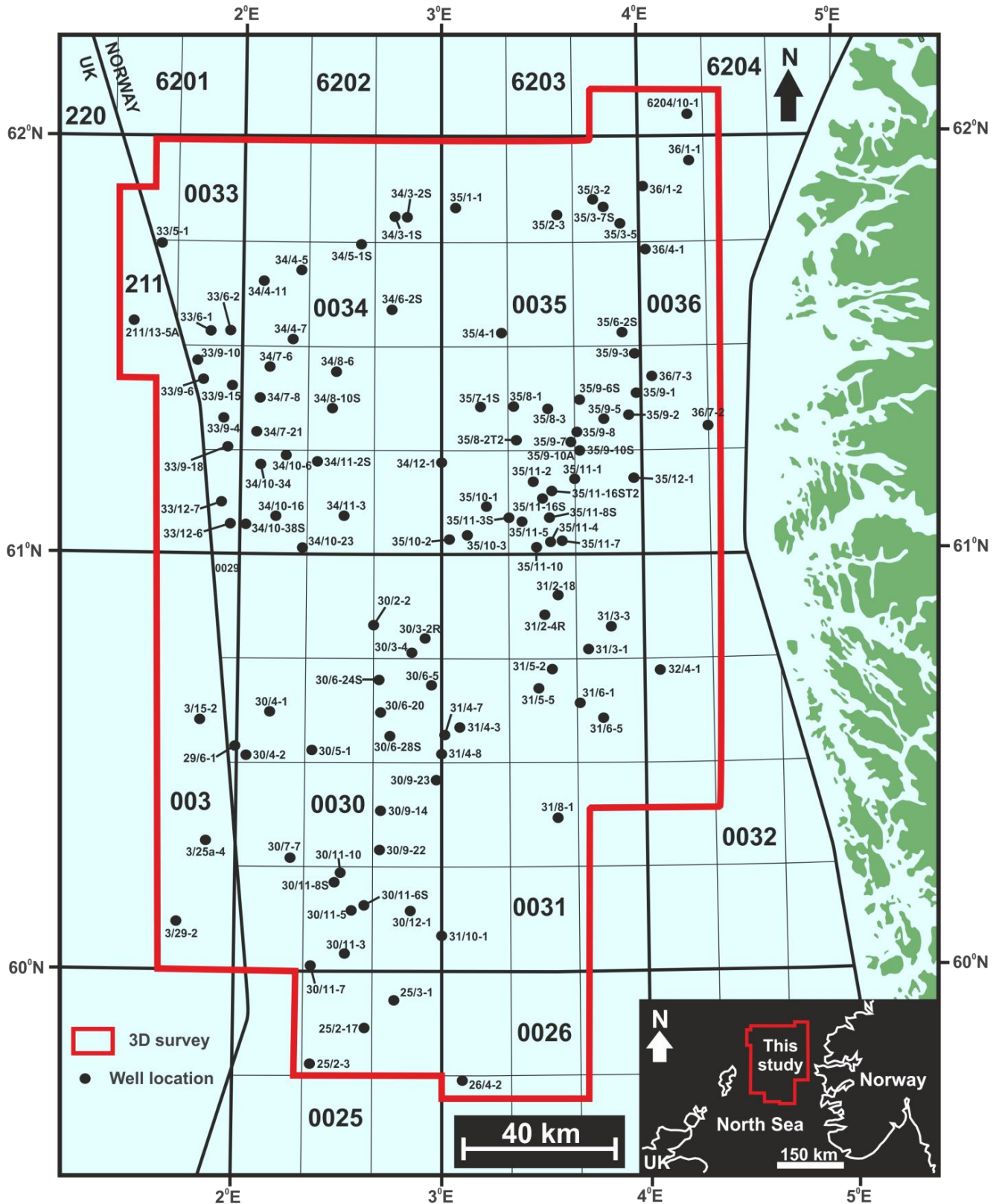
Fig. 4.3: Map showing the outline (in red) of the 3D broadband seismic survey and surface location of some available wells in the northern North Sea used for this study. Seismic data courtesy of CGG and well data from TGS Facies Map Browser.
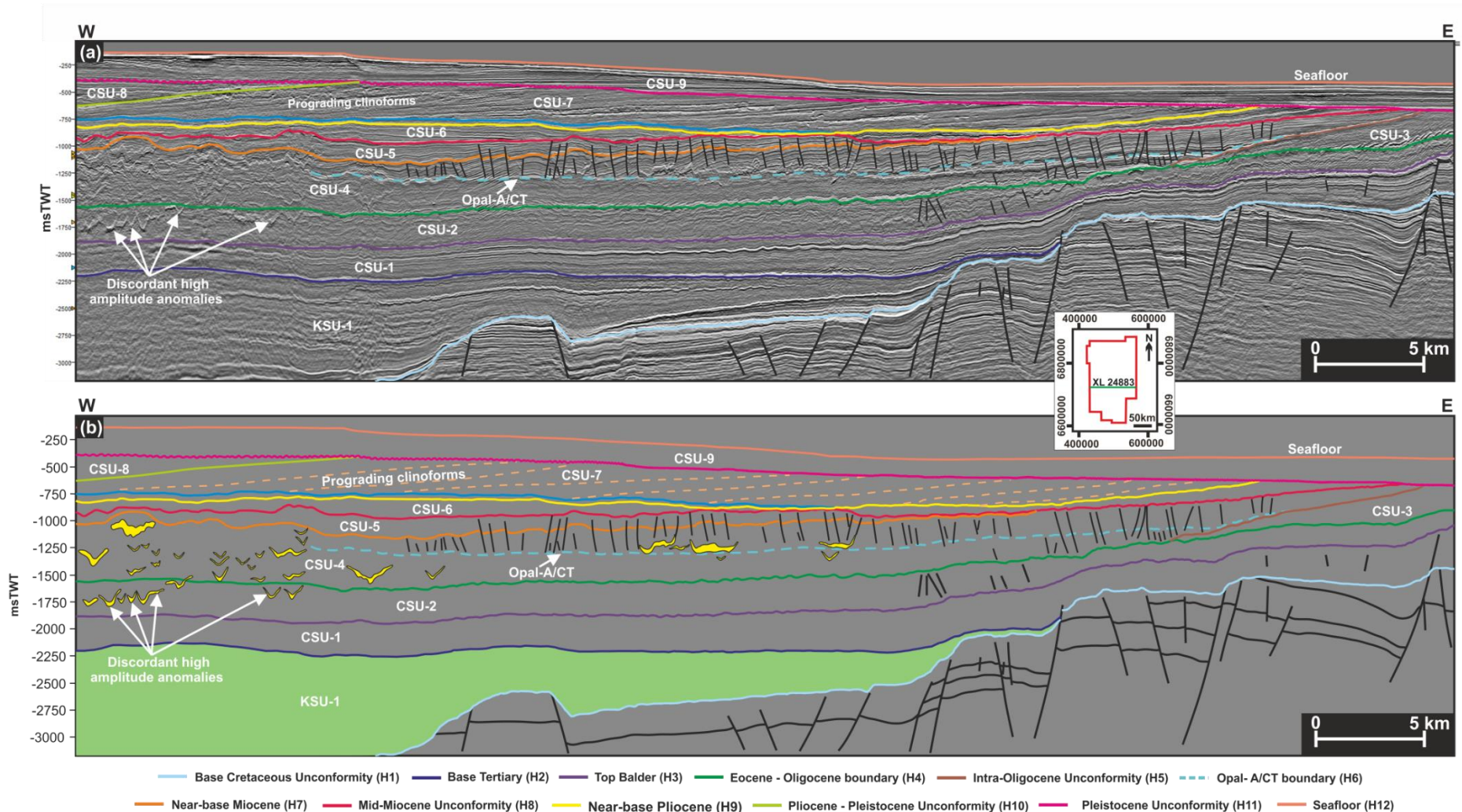
Fig. 4.4a: (a) West to east trending seismic section in dip direction showing the identified Cenozoic seismic units (CSU-1 to CSU-9), their bounding surfaces (H1 to H12) and discordant high amplitude anomalies within the units. (b) Geoseismic section showing the discordant amplitude anomalies interpreted as the seismic expression of large-scale sand intrusions. Insert map shows the location of the cross-section. Seismic data courtesy of CGG.
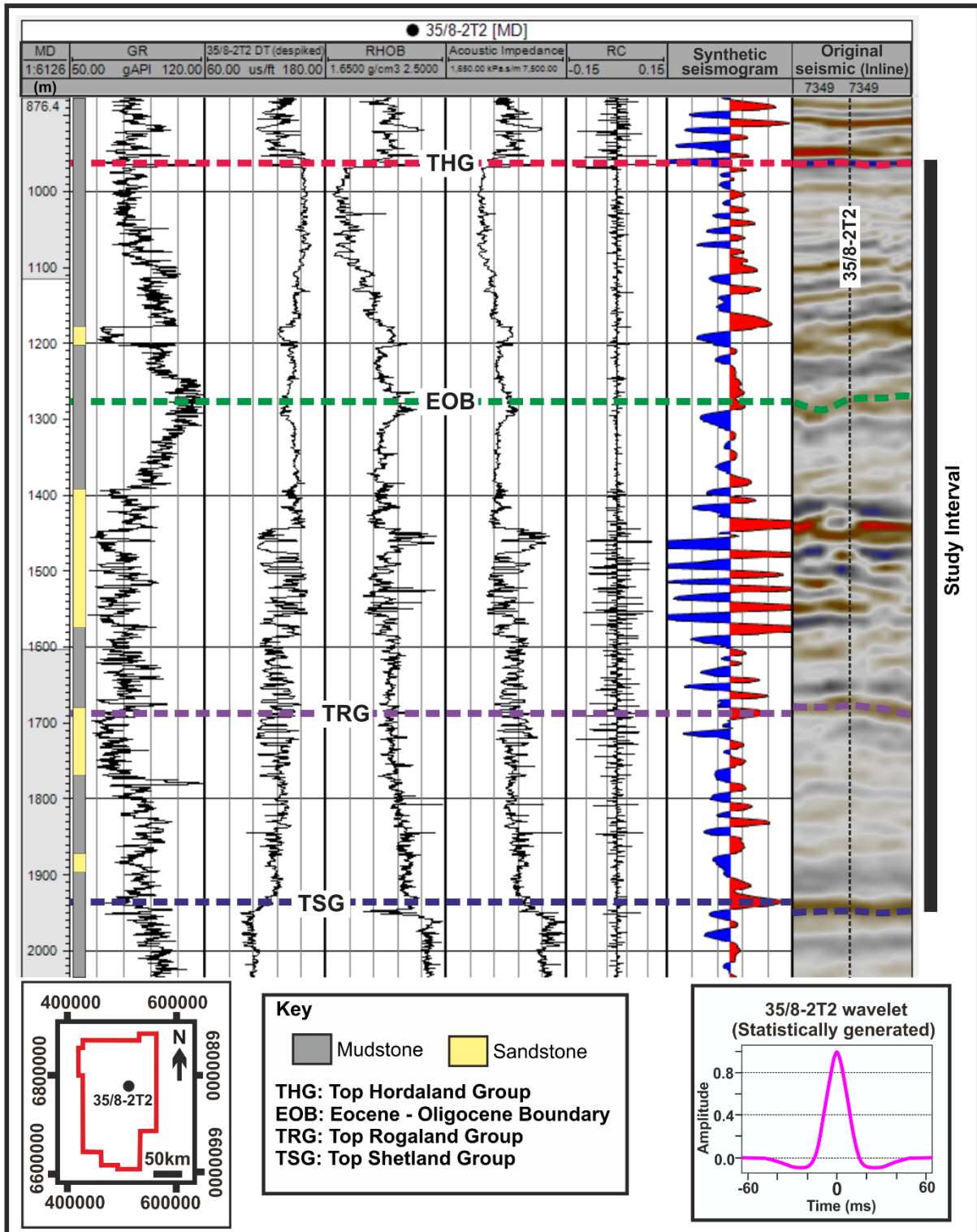
Fig. 4.4b: Synthetic seismogram generated for Well 35/8-2T2. The study interval is indicated, with the key stratigraphic boundaries highlighted. The interpretation of the lithology is shown using the gamma-ray (GR) and sonic log (DT). Well location is shown by the insert map. Seismic data courtesy of CGG and well data from TGS facies Map Browser.

4.4 Results

4.4.1 Seismic stratigraphy and Facies Description

The seismic used in this study have been divided into nine (9) Cenozoic Seismic Units (CSU) labelled CSU-1 to CSU-9 following the seismic stratigraphic division of Jordt et al. (2000) and Olobayo (2014). The Cretaceous unit have been labelled KSU-1 to differentiate it from the Cenozoic units which form the interval of interest (Fig. 4.2 & 4.4a). Based on available well formation top data, calculated synthetic seismograms for some key wells (Fig. 4.4b) and because detailed description and studies of the stratigraphic evolution of these Cenozoic units in the North Sea have been described by several authors (e.g. Jordt et al., 1995, 2000; Faleide et al., 2002; Anell et al., 2012; Goledowski et al., 2012 and Olobayo, 2014), twelve (12) mappable horizons which includes the Opal-A/CT diagenetic boundary (see Wrona et al., 2017b) were identified and have been labelled H1 to H12. H1 and H12 represent the Base Cretaceous Unconformity (BCU) and the seafloor respectively (Fig. 4.2 & Table 4.2). These horizons were identified based on their distinct top seismic characteristics which are described in Table 4.2 while age constrain were assigned using available well data.

Four key stratigraphic boundaries were mapped, and they include (Fig. 4.5): (i) Top Shetland Group or Base Tertiary (H2), (ii) Top Rogaland Group or Top Balder (H3), (iii) Top Hordaland Group or Mid-Miocene Unconformity (H8), and (iv) Top Nordland Group or seafloor (H12). However, the interval of interest lies between the Top Hordaland Group (THG) and Top Shetland Group (TSG). The THG which correlates to the Mid-Miocene Unconformity (MMU) occurs as a high amplitude – continuous trough reflection and defines a well-known regional unconformity in the study area (Jordt et al., 2000; Løseth et al., 2003). It separates the underlying smectite-rich mudstones of the Hordaland Group from the overlying Nordland Group sediments comprising of glauconitic sands, silts, and clays (Løseth et al., 2013). The boundary is irregularly mounded in the NW, ENE, and central parts of the study area with elongate escarpments. This mounded topography of the THG have been related to differential compaction by Rundberg and Eidvin (2005, 2016) and occur above discordant high amplitude anomalies.

Two-way-time structure maps have been created for the mapped key boundaries (Fig. 4.5) with which Isochron/time thickness maps were created to give an insight into the syn-depositional geometry of the basin during the Oligocene – Mid Miocene, Eocene and Paleocene – Early Eocene times (Fig. 4.6). Table 4.1 gives a detailed seismic facies description for the Cenozoic Seismic Units (CSU-1 to CSU-9) based on observed reflection geometry (i.e., reflection configuration and continuity), amplitude characteristics and features within the units.

4.4.2 Occurrence, Distribution and Geometry of observed anomalies and their relationships to their host strata

4.4.2.1 Occurrence

Numerous high amplitude anomalies are observed within the Paleogene interval (between the TSG and THG) of the study area. These anomalies are clearly distinguishable from their surrounding low-amplitude strata, are characterized by even high amplitude through much of their extent and often characterized by a top moderate – high amplitude peak reflection and a base moderate – high amplitude trough reflection (i.e., peak-trough pair) and in very rare cases a top moderate – high amplitude trough reflection and a base moderate – high amplitude peak reflection (i.e., trough-peak pair). The top and base reflections are often roughly parallel and have varying amplitude and continuity in cross-section. The anomalies are generally observed to be discordant to the host stratification (i.e., cross-cut overlying reflections) and exhibit varying simple to complex-shaped geometries (see Fig. 4.8 – 4.14, Fig. 4.17 – 4.21, and Table 4.4) with some occurring within polygonally faulted intervals. They commonly either crosscut or exploits the pervasive polygonal faults. In some cases, they are also comprised of some bedding-concordant anomalies which are often found to develop at the upper tips of the bedding-discordant amplitude anomalies (e.g., Fig. 4.9b).

The high amplitude anomalies are found to occur between the Paleocene to Miocene interval (see Table 4.5) within: (i) CSU-1 (Paleocene – Early Eocene), (ii) CSU-2 (Eocene), and (iii) CSU-4 (Oligocene). They occur predominantly within the Eocene and Oligocene interval, both of which are highly perturbed by these anomalies.

4.4.2.2 Seismic expression and geometry of discordant amplitude anomalies

The discordant amplitude anomalies observed in the study area occur predominantly as either isolated discrete anomalies (about 70%) characterized by circular/sub-circular to elliptical form in map view (e.g., see Fig. 4.10, 4.14 & 4.21) or as amalgamated and stacked complexes (about 30%) characterized by irregular to complex 3D cross-sectional geometry and plan view form (Andresen and Clausen, 2014). The discrete discordant amplitude anomalies exhibit varying geometries consisting of: (i) apical cones or conical-shaped anomalies characterized by U/V/W-shaped reflections with fairly sharp apexes, steeply dipping limbs in cross-section and circular to sub-circular plan view geometry (e.g. see Fig. 4.8 & 4.11); (ii) flat-based bowls/ saucer-shaped or wing-like anomalies characterized by a concordant central base (i.e. basal sill or laccolith) flanked by inclined marginal wings (i.e. dikes), with occasional crestal anomalies or fringes above their concordant bases(e.g. see Fig. 4.9, 4.11d, 4.18, & 4.35a), and (iii) irregular and complex-shaped anomalies (e.g. zig-zag shaped; see Fig. 4.19). Outer concordant elements (i.e., sill) which appear to extend laterally from the top of the inclined wings or limbs of the conical and saucer-shaped anomalies are often observed (e.g., see Fig. 4.18a - d). The amalgamated and stacked complexes are

characterized by a combination of several conical-shaped, wing-like and irregular to complex shaped anomalies which sometimes crosscut one another (e.g., see Fig. 4.20). Some of the amalgamated complexes occasionally consist of saucer-shaped or wing-like anomalies with smaller conical-shaped anomalies observed above their concordant bases. Another type of anomaly observed consist of mound-shaped anomaly with steep flanks which occur mainly above the THG unconformity but are sometimes observed above the Top Balder.

Common to some of the observed discordant amplitude anomalies is the pronounced deformation of the host strata which occur as forced-folds or jack-up of overburden above the discordant anomalies (e.g., see Fig. 4.17a - b, 4.20 & 4.31). This is linked to the significant relief observed on the top host surfaces (e.g., Top Hordaland Group – THG and Top Rogaland Group – TRG) which are in the order of 10 – 90 msTWT high (not de-compacted) above the regional trend of the top host surfaces. Some of the marginal wings and limbs associated with the anomalies tend to follow existing polygonal fault planes within the mudstone host strata. This is however not observed for all the anomalies and there is no evidence for an obvious relationship between the polygonal faults and the discordant amplitude anomalies.
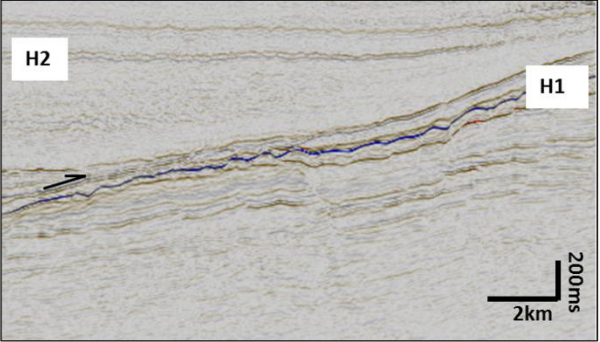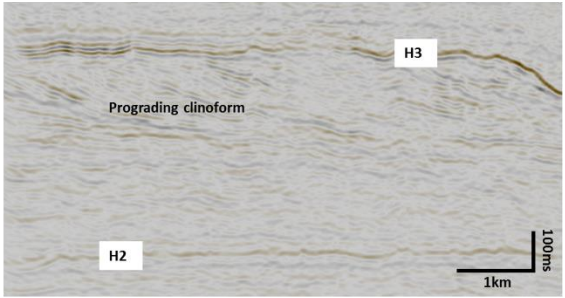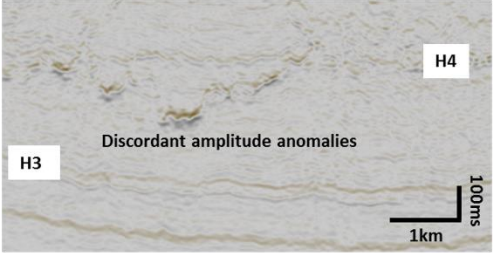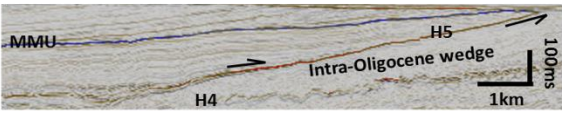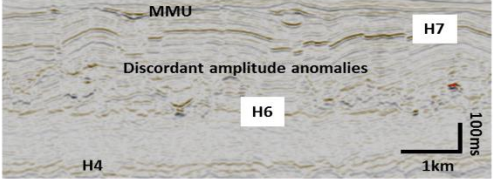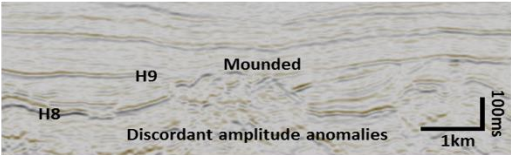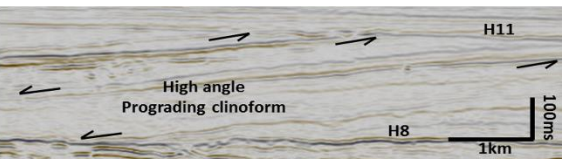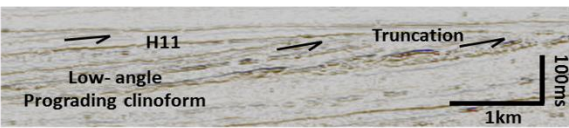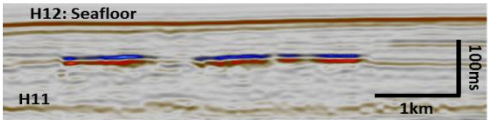
Era	Period	Epoch	Groups	Seismic Units	Boundary		Example	Internal Facies Description
					Top	Base		
MESOZOIC	CRETACEOUS	Lower	Cromer Knoll	KSU-1	H2	H1		KSU-1: Low to transparent amplitude, parallel and semi continuous reflection. Has variable thickness and offset by major Mesozoic tilted fault blocks. Polygonally faulted at the eastern margin
		Upper	Shetland					
CENOZOIC	PALEOGENE	Paleocene	Rogaland	CSU-1	H3	H2		CSU-1: Low to medium, continuous to semi-continuous, semi-parallel amplitude reflection. Prograding clinoform (Donorch Delta) in the SW part of the study area. Localized polygonal faulting with chaotic reflections to the eastern part of the study area. Has uniform thickness across the basin. Truncated by H11 (Pleistocene unconformity) along the eastern basin margin
		Eocene	Hordaland	CSU-2	H4	H3		CSU-2: Low to medium discontinuous amplitude reflections. Intensely modified by remobilized and injected facies. Presence of high amplitude discordant anomalies. Polygonally faulted interval. Truncated by H11 (Pleistocene unconformity) along the eastern basin margin

Table 4.1: Seismic facies description of observed Cenozoic Seismic Units (CSU) labelled CSU-1 to CSU-9. Also shown are seismic examples illustrating some of the features observed within the units. Refer to Fig. 4.2. Seismic data courtesy of CGG

Era	Period	Epoch	Groups	Seismic Units	Boundary		Example	Internal Facies Description
					Top	Base		
CENOZOIC	PALEOGENE	Oligocene	Hordaland	CSU-3	H5	H4		**CSU 3:** Semi-continuous, low amplitude reflection. Intra-Oligocene wedge which down-laps onto H4 towards the basin centre. Truncates beneath H11 (Pleistocene unconformity) at the eastern basin margin
				CSU-4	H7	H4		**CSU-4:** Semi-parallel, low to medium amplitude reflection. The lower section consists of very low to transparent discontinuous facies while the upper section is characterized by medium and discontinuous (polygonally faulted interval) reflection. Both are separated by a high amplitude non-stratigraphic surface (H6) which marks the opal-A/CT diagenetic boundary. Intensely modified/distorted by remobilization and injected facies which results to a very chaotic reflection character at the central and western part of the study area
	NEOGENE	Miocene	Nordland	CSU-5	H8	H7		**CSU-5:** Low to medium amplitude, semi-parallel and discontinuous reflection. Polygonally faulted interval. Conformable with underlying stratal reflection. Not easily identifiable along the eastern margin due to remobilized/injected facies
				CSU-6	H9	H8		**CSU-6:** High to medium amplitude, semi-parallel and continuous reflections. Characterized by mounded/undulating geometry resulting from the underlying discordant amplitude facies in the SW part of the study area. Characterized by onlap unto the underlying (H8—MMU) bounding surface.
		Pliocene		CSU-7	H10	H9		**CSU-7:** Low to medium amplitude and parallel prograding high angle clinoform reflections. Characterized by downlap onto the underlying (H9) surface in a west dipping direction and by a toplap beneath the overlying (H10 - Pleistocene Unconformity) surface
	QUATERNARY	Pleistocene		CSU-8	H11	H10		**CSU-8:** Parallel, semi-continuous , low to medium amplitude, low angle prograding clinoform reflection similar to that observed in the adjacent CSU-7 unit. Restricted to the north-western part of the study area. Presence of isolated high amplitude reflections and acoustic masking of reflection
				CSU-9	H12	H11		**CSU-9:** Parallel, low to medium, continuous amplitude reflections. Isolated high amplitude anomalies which may be related to shallow gas pockets. Presence of acoustic masked reflections related to shallow gas charged sediments
		Holocene						

Era	Period	Epoch	Groups	Seismic Units	Surfaces	DESCRIPTION OF IDENTIFIED SEISMIC SURFACES
CENOZOIC	QUATERNARY	Holocene	Nordland	CSU-9	H12	**H1 (Base Cretaceous Unconformity: BCU):** Continuous high amplitude trough reflection offset by underlying tilted fault blocks. Well established regional unconformity
		Pleistocene 2.6		CSU-8	H11	**H2 (Base Tertiary / Top Shetland Group: TSG):** Continuous amplitude peak reflection. Forms the base of the Cenozoic seismic units and correlates to the Top Shetland Group.
	NEOGENE	Pliocene 5.3		CSU-7	H10	**H3 (Top Balder Surface: TB):** High amplitude continuous peak reflection. Well established regionally extensive marker horizon which resulted from Paleocene - Early Eocene volcanic activity associated with the North Atlantic rifting. Correlates to the top of the Rogaland Group and also referred to as a wide spread chronostratigraphic surface (Jordt et al., 2000; Huuse et al., 2001; Goledowski et al., 2012)
		Miocene 23		CSU-6	H9	**H4 (Eocene - Oligocene boundary: EOB):** High amplitude peak reflection offset by series of polygonal faults between the central to the eastern part of the study area. Difficult to identify towards the western basin margin due to intense remobilization/injection of sediments.
			Hordaland	CSU-5	H8	**H5 (Intra Oligocene Unconformity):** Forms the top of an intra-Oligocene wedge. High amplitude wedge surface. Restricted to the eastern basin margin and downlap onto the H4 surface.
	PALEOGENE	Oligocene 34		CSU-4	H7 / H6 / H5	**H6 (Opal-A/CT boundary):** High amplitude peak reflection, westward dipping diagenetic reflection which cuts across CSU-4 and divides the unit into two zones with distinct seismic character. Onlap onto the intra-Oligocene Unconformity (H5)
				CSU-3	H4	**H7 (Base Miocene/Top Oligocene surface):** Medium and discontinuous amplitude peak reflection offset by polygonal faults within the underlying seismic unit
		Eocene 56		CSU-2	H3	**H8 (MMU: Mid-Miocene Unconformity):** High amplitude trough reflection which forms a regionally semi-continuous and widespread hiatus in the North Sea and correlates with the top of the Hordaland Group. Characterized by channel incisions notably in the northern part of the study area and is mounded and severely affected by underlying injected and remobilized facies. Characterized by low-angle truncations and top-lap of the underlying strata.
		Paleocene 65	Rogaland	CSU-1	H2	**H9 (Base Pliocene/Top Miocene surface):** Medium amplitude reflection with undulating/mounded topography at the western margin of the study area. Forms the base surface for the down-lapping Pliocene (CSU-7) prograding clinoform
MESOZOIC	CRETACEOUS	Upper 100.5	Shetland	KSU-1		**H10 (Late Pliocene - Early base Pleistocene Unconformity):** High amplitude peak reflection which is restricted to the NW part of the study area and truncates beneath the H11. Characterized by top-lap of underlying low-angle clinoform
		Lower 145	Cromer Knoll		H1	**H11 (Pleistocene Unconformity):** High amplitude regionally continuous peak reflection with truncation of underlying units/surfaces in the eastern basin margin

H12 (Seafloor): Parallel, continuous, peak reflection with slight variation in topography. Marks the top of the Nordland Group

Table 4.2: Description of all observed horizons labelled H1 to H12. Their seismic reflection character, geometry and features associated with them are also highlighted. See location of surfaces/horizons in Fig. 4.4a
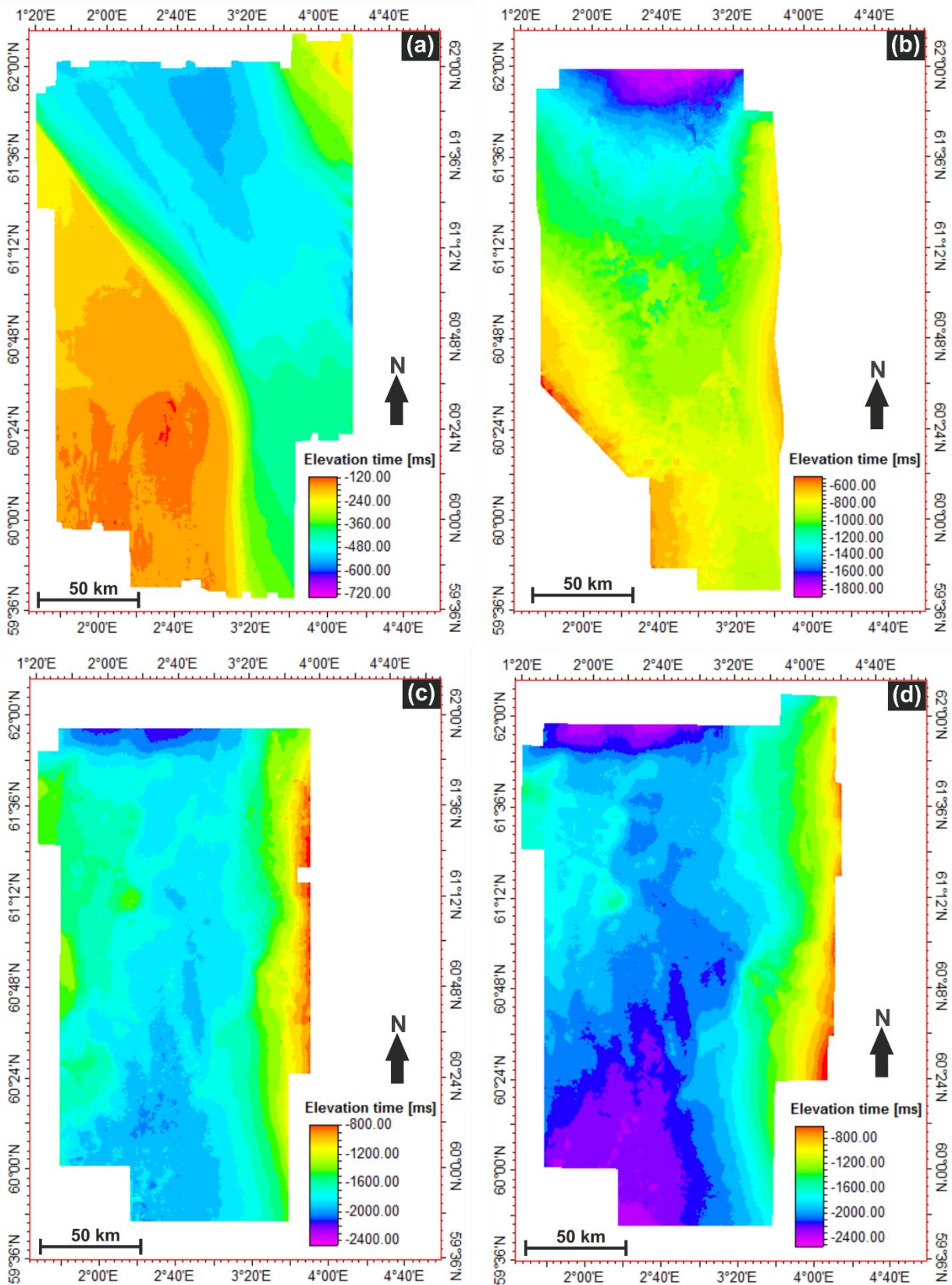
Fig. 4.5: Two-way-time structure map of mapped key stratigraphic boundaries: (a) Top Nordland Group (TNG: H12) or seafloor, (b) Top Hordaland Group (THG: H8) or mid-Miocene Unconformity (MMU), (c) Top Rogaland Group or Top Balder (TB: H3), and (d) Top Shetland Group (TSG: H2) or Base Tertiary. See outline of seismic data in Figure 4.3. Seismic data courtesy of CGG.
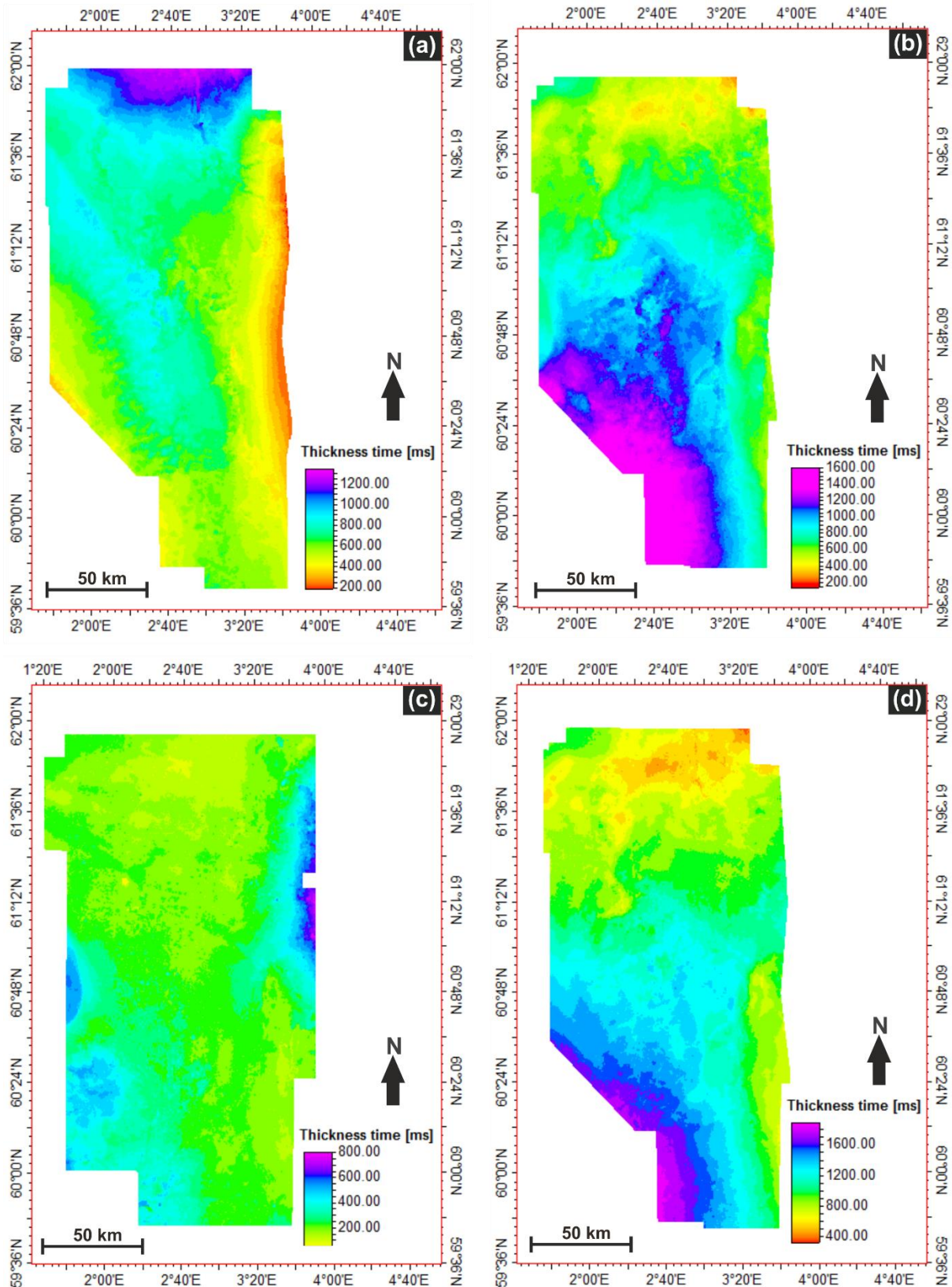
Fig. 4.6: Isochron (thickness) maps between mapped key horizons: (a) Top Nordland and Top Hordaland Group, (b) Top Hordaland and Top Rogaland Group, (c) Top Rogaland and Top Shetland Group, and (d) Top Hordaland and Top Shetland Group. See outline of seismic data in Figure 4.3. Seismic data courtesy of CGG.

4.4.3 Cenozoic seismic units and their distribution of discordant amplitude anomalies

4.4.3.1 CSU-1 (Paleocene – Early Eocene) discordant amplitude anomalies

The CSU-1 which represents the Rogaland Group interval is bounded at the top and base by the Top Rogaland Group/Top Balder (H3) and Top Shetland Group/Base Tertiary (H2) respectively (Fig. 4.2 & Table 4.2). The unit has a relatively uniform thickness of c. 150 – 200 msTWT in the basin centre, the north, south-east and north-western parts of the study area with the thickness increasing to c. 400 – 800 msTWT along the eastern (West Norway) and western (East Shetland Platform) basin margins (Fig. 4.6c). Overall, the unit thins westwards and is pervasively polygonally faulted in the north, east and south-eastern parts of the study area. The unit is further sub-divided into three (3) sub-seismic units based on differences in seismic facies and generated synthetic seismogram. The lower unit consists of low-amplitude, discontinuous to chaotic reflections, as well as high amplitude discordant reflections. This unit have been interpreted to coincide with the Våle Formation (Fig. 4.8; also see Dmitrieva et al., 2012: see their Fig. 3, 10). The middle sub-unit is defined by discontinuous to semi-discontinuous and discordant reflections and interpreted to correspond to the Lista Formation (Fig. 4.8a & b, Dmitrieva et al., 2012: see their Fig. 3, 10). However, the uppermost unit, which is characterized by continuous to semi-continuous, semi-parallel and moderate to high amplitude reflections (Fig. 4.7b & 4.8) have been interpreted to correspond to the Sele and Balder Formations (see Dmitrieva et al., 2012: see their Fig. 3). Detailed description of the regional basin morphology, seismic stratigraphy, and distribution of the Rogaland Group in the study area have been documented by Jordt et al. (1995, 2000), Faleide et al. (2002), Brunstadt et al. (2009), Anell et al. (2012), Dmitrieva et al. (2012), Olobayo (2014) and Dmitrieva et al. (2018).

Isolated, laterally discontinuous, high amplitude anomalies are observed within the CSU-1 in the eastern and north-eastern parts of the study area, forming a north-south trend like the orientation of the underlying Mesozoic faults and structures (Table 4.5). The high amplitude anomalies observed in cross-section are characterized by: (i) channel-like anomalies which are irregular-based, continuous to discontinuous, and are 0.5 – 1.8 km wide with discordant margins (Fig. 4.7a); (ii) sheet-like amplitude anomalies which are continuous to semi-continuous, flat-based, comprising of a top (peak) and base (trough) reflections, 40 – 70 msTWT thick and 1.5 – 5 km long (Fig. 4.7b; Dmitrieva et al., 2012: see their Fig. 7, 10); and (iii) discordant amplitude anomalies consisting of conical (U,V,W) shaped (Fig. 4.8) and saucer-shaped/wing-like anomalies (Fig. 4.9). The conical-shaped anomalies are predominant (about 85%) and have steep dipping limbs which crosscut up to 150 msTWT of adjacent strata reflection. Some of the V-shaped anomalies have bedding-concordant anomalies (i.e., sill) extending laterally from the tip of their discordant limbs (i.e., dikes) for about 0.6 – 1.2 km long (Fig. 4.9b & 4.10d).

The discordant high amplitude anomalies occur at 50 – 100 msTWT above the TSG (H2) within the Paleocene mudstones of the Lista and Våle Formation (Dmitrieva et al., 2018). Most of the anomalies are associated with jack-up of the overburden above them (Fig. 4.9a [ii, iv] & 4.9b [i]) and are characterized by circular to sub-circular (up to 3 km in diameter) and elongate (up to 2 km long and 0.5 km wide) map view geometries on time slices and iso-proportional slices through the interval (Fig. 4.10). Onlap of overlying reflections are also observed above the jack-up associated with the anomalies.

4.4.3.2 CSU-2 (Eocene) discordant amplitude anomalies

The CSU-2 of Eocene age forms part of the Hordaland Group (see Fig. 4.2 & Table 4.2; Isaken and Tonstad, 1989) and corresponds to the PAL 2, CSS 2, MU2 and CSS-2 of Anell et al. (2012), Jordt et al. (2000), Rundberg (1991) and Kyrkjebo et al. (2001) respectively. It is bounded at the top and base by the Eocene-Oligocene boundary (EOB: H4) and the Top Rogaland Group/Top Balder (TRG/TB: H3) respectively. The unit consists primarily of the Horda Formation, the Frigg, and Grid Sandstone Members (Knox and Holloway, 1992; Faleide et al., 2002; Goledowski et al., 2012). The unit has a maximum thickness of up to 600 msTWT along the basin margins with a uniform thickness of c. 300 msTWT within the basin centre. It is truncated along the eastern basin margin by the Pleistocene unconformity (H11) and thickens towards the west. The interval is characterized by fine-grained smectite-rich mudstones and sands sourced from the uplifted basin margins (Jordt et al., 2000). It consists of mainly low amplitude reflections, some isolated high amplitude reflections, and is pervasively modified by polygonal faulting (e.g., Fig. 4.12c). The polygonal faults are usually not easily observed in the western part of the study area due to the very chaotic nature of the reflections observed there due to intense post depositional remobilization and injection. Detailed description of this unit, its composition and sedimentary evolution can also be referred to in the studies by Rundberg (1991); Knox and Holloway, 1992; Galloway et al. (1993); Jordt et al. (1995, 2000), Faleide et al. (2002); Anell et al. (2012); Goledowski et al. (2012) and Olobayo (2014).

Several isolated discordant amplitude anomalies are observed in cross-section within the CSU-2. These anomalies are spatially distributed in the western (Quadrant 29, 30 & 34) and north-eastern (part of Quadrant 35) parts of the study area with a NE-SW trend (Table 4.5). In both areas, the anomalies appear to occur mainly along the flanks of underlying structures formed above the Mesozoic tilted fault blocks. The anomalies are in cross-section characterized by: (i) mainly V, W and occasionally U-shaped discordant amplitude anomalies with distinct apexes (Fig. 4.11 & 4.12), and (ii) a few wing-like anomalies (Fig. 4.13). In map view, they are characterized by circular to sub-circular, oval to elliptical and occasionally polygonal geometries due to their occurrence within polygonally faulted Eocene mudstone host strata (Fig. 4.14). The above observations are consistent with documented observations in previous studies of the Tampen Spur area (Quadrant 34) by Huuse and

Mickelson (2004). Seismic cross-section through the CSU-2 interval indicate that the anomalies appear to occur at two different levels (Fig. 4.12a & d); (i) in the lower part of the unit (i.e. Lower Eocene) where their apexes terminate directly on or above (approx. 50 – 100 msTWT) the Top Rogaland/Top Balder, and (ii) in the upper part of the unit where their apexes terminate at a boundary 180 – 200 msTWT above the Top Rogaland which likely corresponds to the base of the Upper Eocene (Huuse and Mickelson, 2004). However, the anomalies in the lower part of CSU-2 sometimes have their limbs/wings extending into the upper part, while the limbs of anomalies in the upper level terminate beneath the Eocene – Oligocene boundary (EOB) which marks the global transition from greenhouse to icehouse climatic condition (Rundberg and Eidvin, 2005).

In the western and south-western parts of the study area, the Upper Eocene to Oligocene is characterized by intensely mobilized sediments with chaotic reflections which makes it difficult to identify the Eocene – Oligocene boundary, although some distinct discordant amplitude anomalies within the upper Eocene can be identified. Some of the anomalies are in some cases associated with jack-up of the overburden or the EOB above the individual anomalies (Fig. 4.12d, & 4.13a), while the limbs of some anomalies in the upper level extend into the Lower Oligocene interval (see Fig. 4.31)

In the east to north-eastern part of the study area around Block 35/8, the CSU-2 interval consists of two large sand-rich packages of Lower to Middle Eocene age interpreted as upper Fan-A and lower Fan-B basin floor fans which terminate westwards (Fig. 4.15a & b). Both fans form low mounds with lengths of up to a few tens of kilometres (Jordt et al., 2000; Jones et al., 2003; Olobayo, 2014). Fan-A consists of relatively high amplitude, semi-continuous to chaotic internal reflections with discordant high amplitude anomalies observed at the margin of its western termination (Fig. 4.15a). Fan-B is however distinguished from Fan-A by its moderate – low amplitude semi-continuous reflection which downlap onto the Top Rogaland/Top Balder boundary (Fig. 4.15). Wireline log data through both fans indicate the presence of c. 180 m and c. 200 m thick sandstone units inter-bedded within mudstone units for both Fan-A and Fan-B respectively (Fig. 4.15b). Another large sand-rich basin floor fan (i.e., Fan-C) of Lower to Middle Eocene age is observed in the south-western part of the study area (Fig. 4.16).
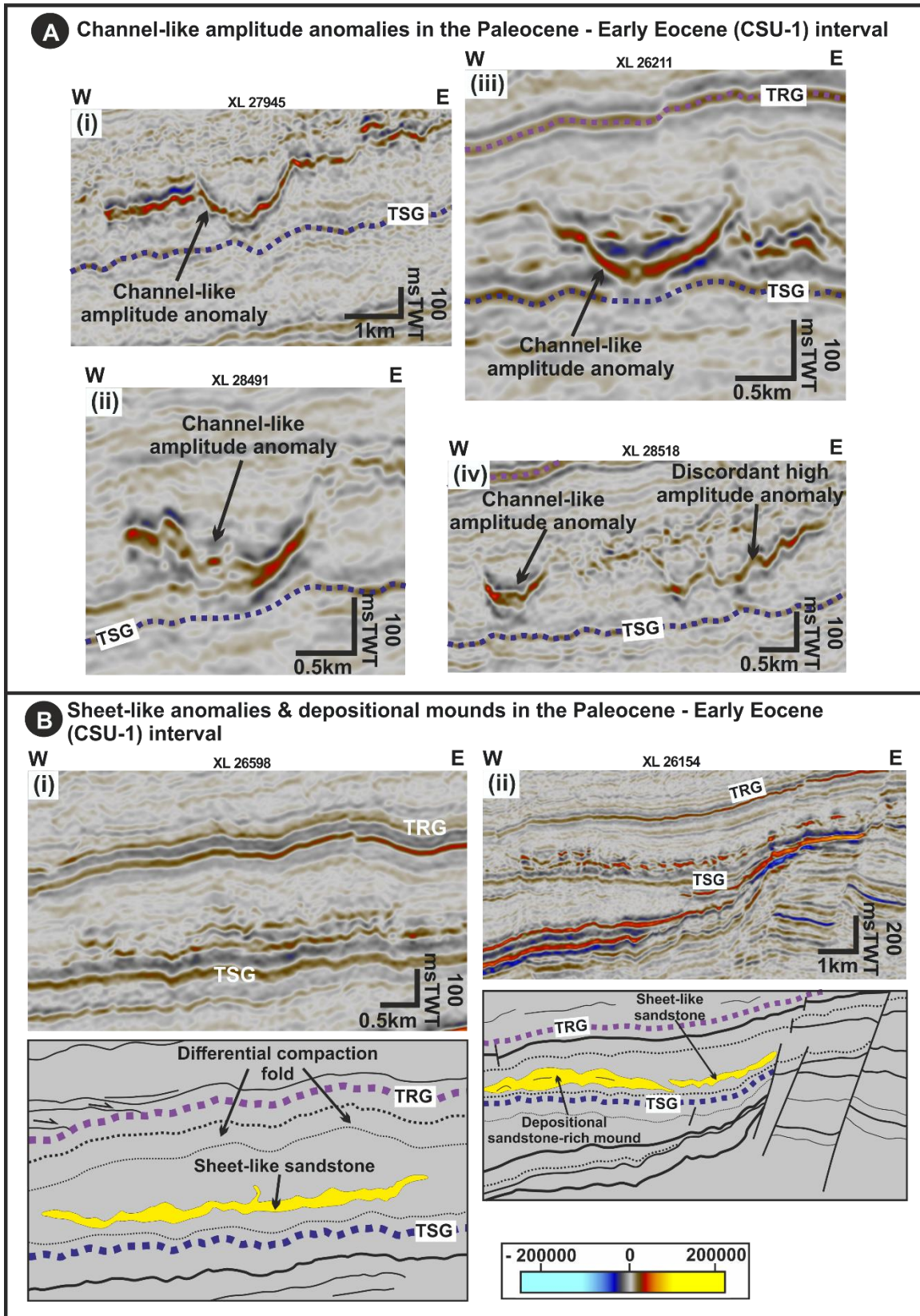
Fig. 4.7: Paleocene – Early Eocene (CSU-1) high amplitude anomalies: (a) Channel-like amplitude anomalies (i - iv) and (b) Sheet-like anomalies and depositional mounds interpreted as sheet-like sandstones and depositional sandstone-rich mounds (i – ii). TRG: Top Rogaland Group, TSG: Top Shetland Group. Seismic data courtesy of CGG.
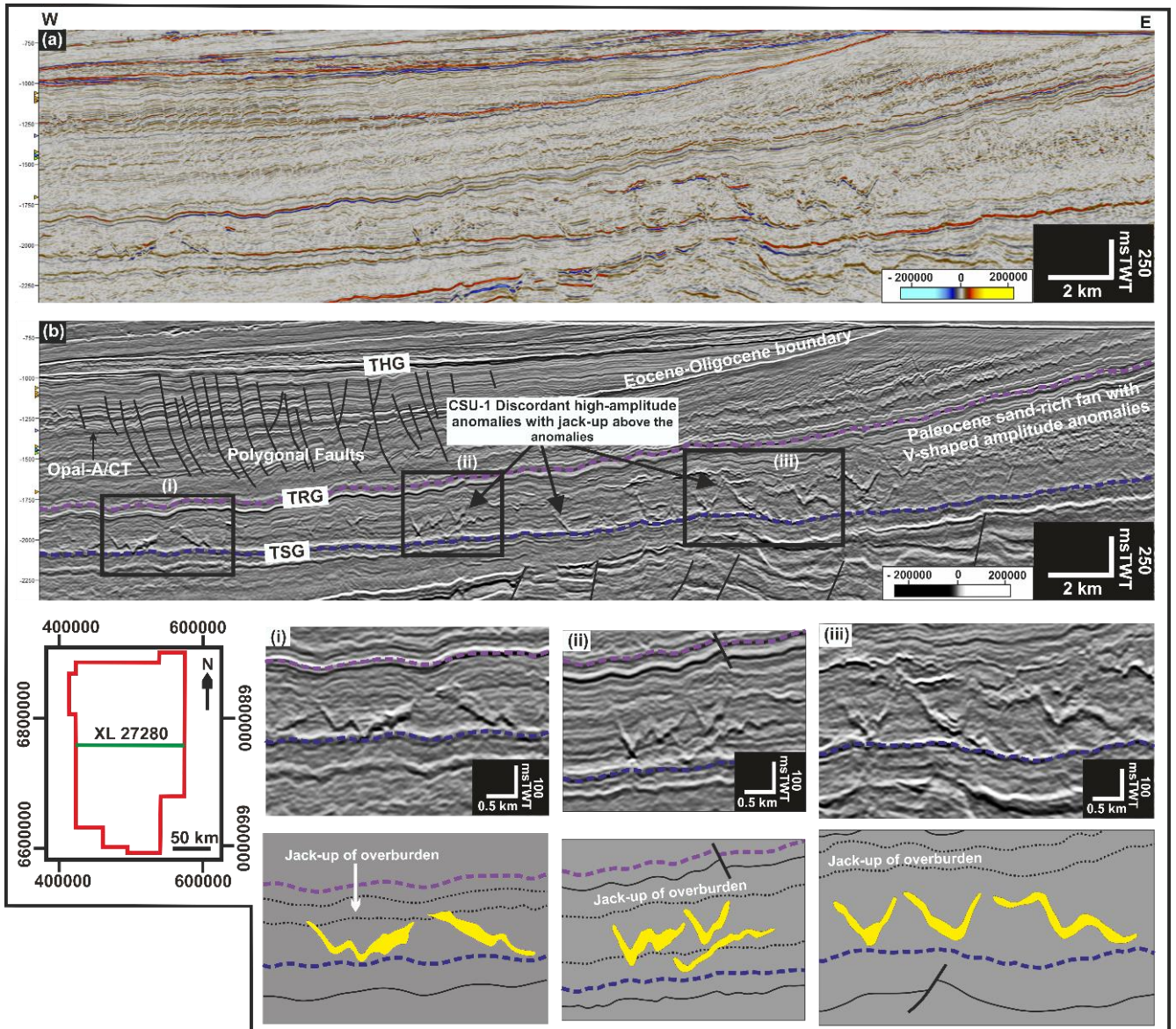
Fig. 4.8: Paleocene – Early Eocene (CSU-1) high amplitude anomalies: (a) East-west trending seismic line in dip direction. (b) Interpreted seismic line in dip direction showing the presence of V/W-shaped discordant amplitude anomalies within the CSU-1. Some of the anomalies are associated with jack-up of overburden. THG: Top Hordaland Group, TRG: Top Rogaland Group, TSG: Top Shetland Group. Seismic data courtesy of CGG.
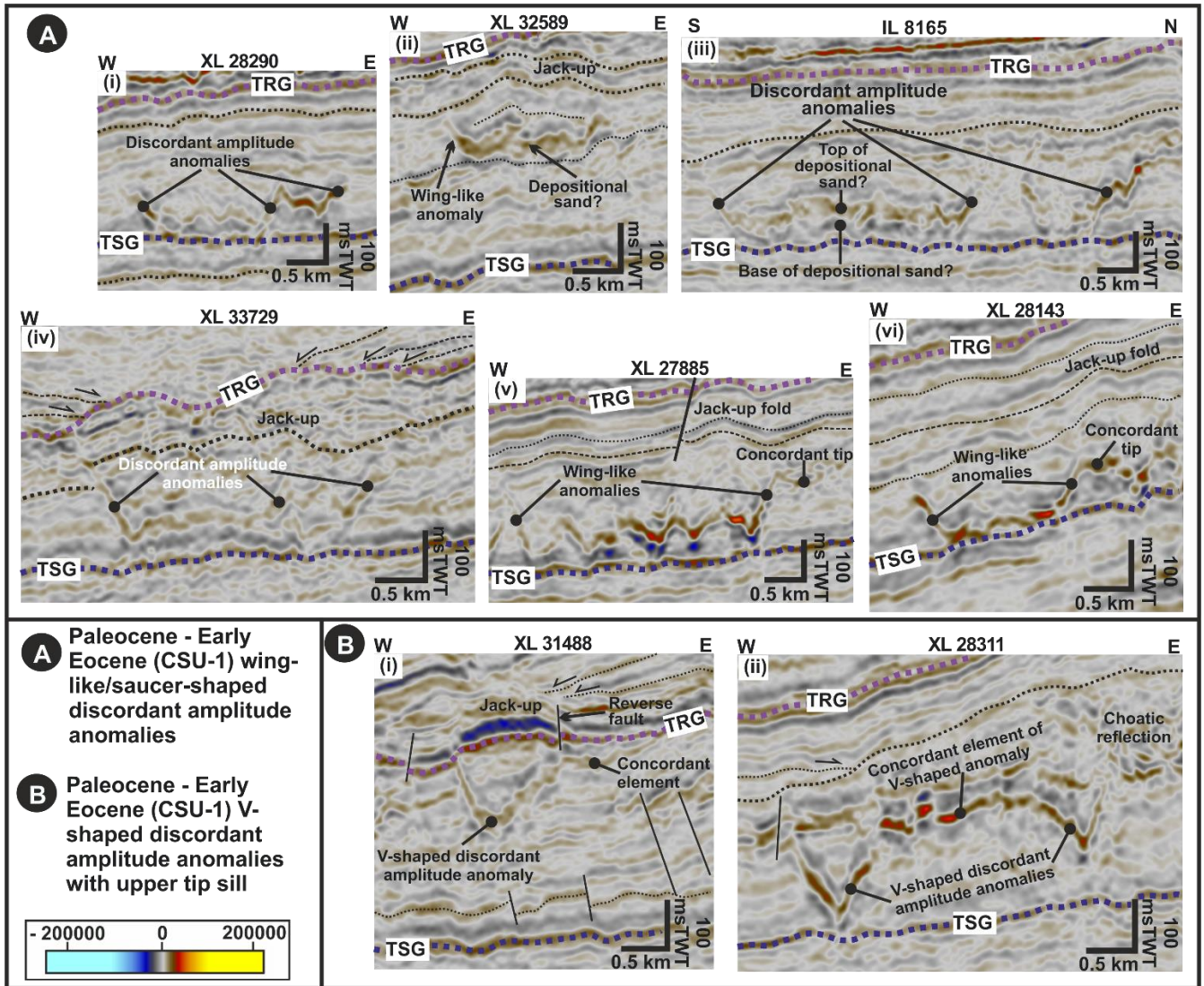
Fig. 4.9: Paleocene – Early Eocene (CSU-1) discordant high amplitude anomalies: (a) Wing-like/saucer-shaped discordant amplitude anomalies (i – vi) and (b) Conical-shaped discordant amplitude anomalies (i – ii). TRG: Top Rogaland Group, TSG: Top Shetland. Seismic data courtesy of CGG.
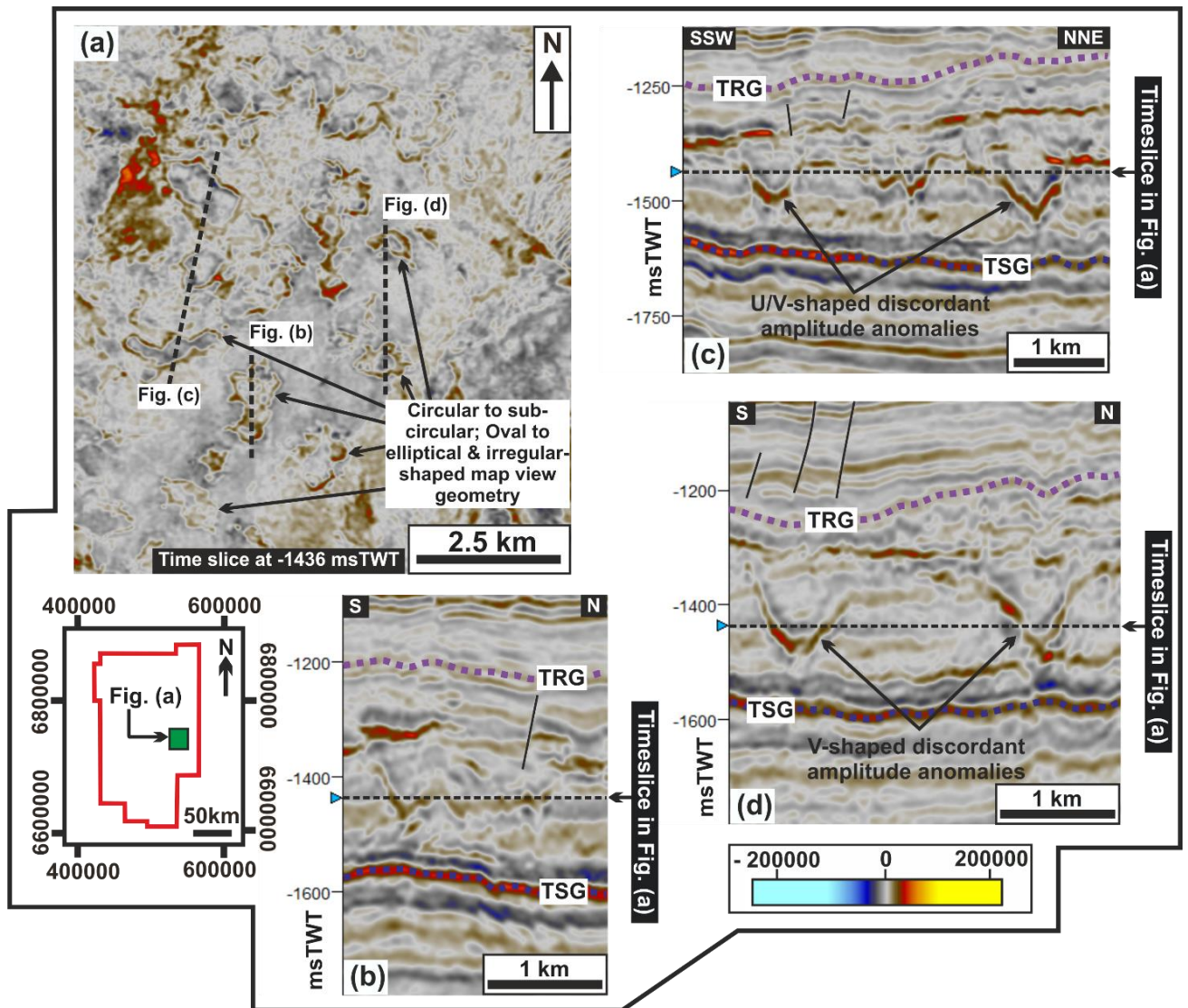
Fig. 4.10: Paleocene – Early Eocene (CSU-1) conical discordant amplitude anomalies observed as U/V-shaped anomalies in cross sections and as circular to sub-circular and elongate to irregular amplitude anomalies in time slice (1436 msTWT). TRG: Top Rogaland Group, TSG: Top Shetland. Seismic data courtesy of CGG.
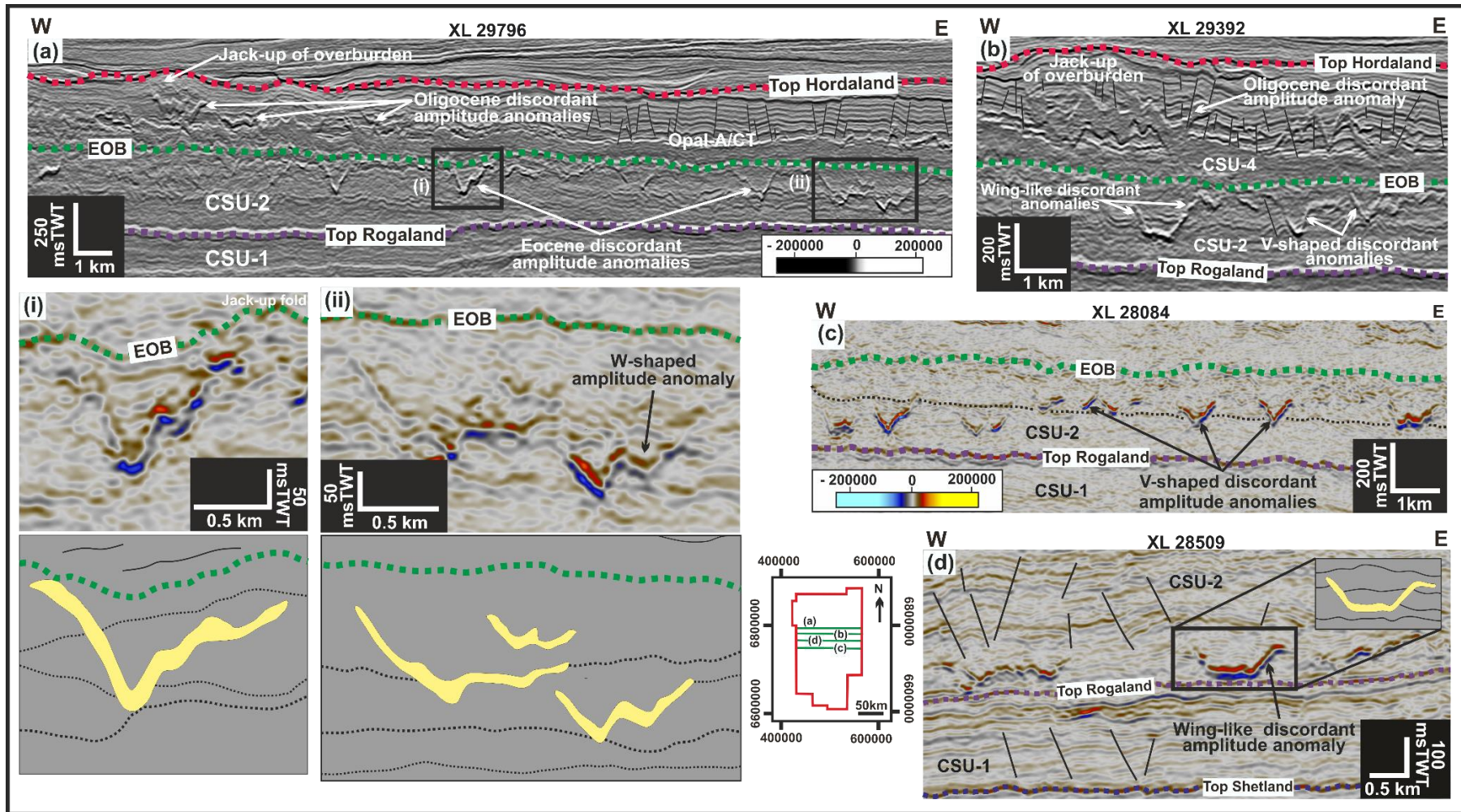
Fig. 4.11: Eocene conical-shaped [in (a) to (c)] and wing-like [in (d)] discordant high amplitude anomalies with some of their limbs terminating beneath the Eocene – Oligocene boundary (EOB). The anomalies in (c) display two levels of downward termination with the boundary between both levels shown by the dotted black line. Seismic data courtesy of CGG.
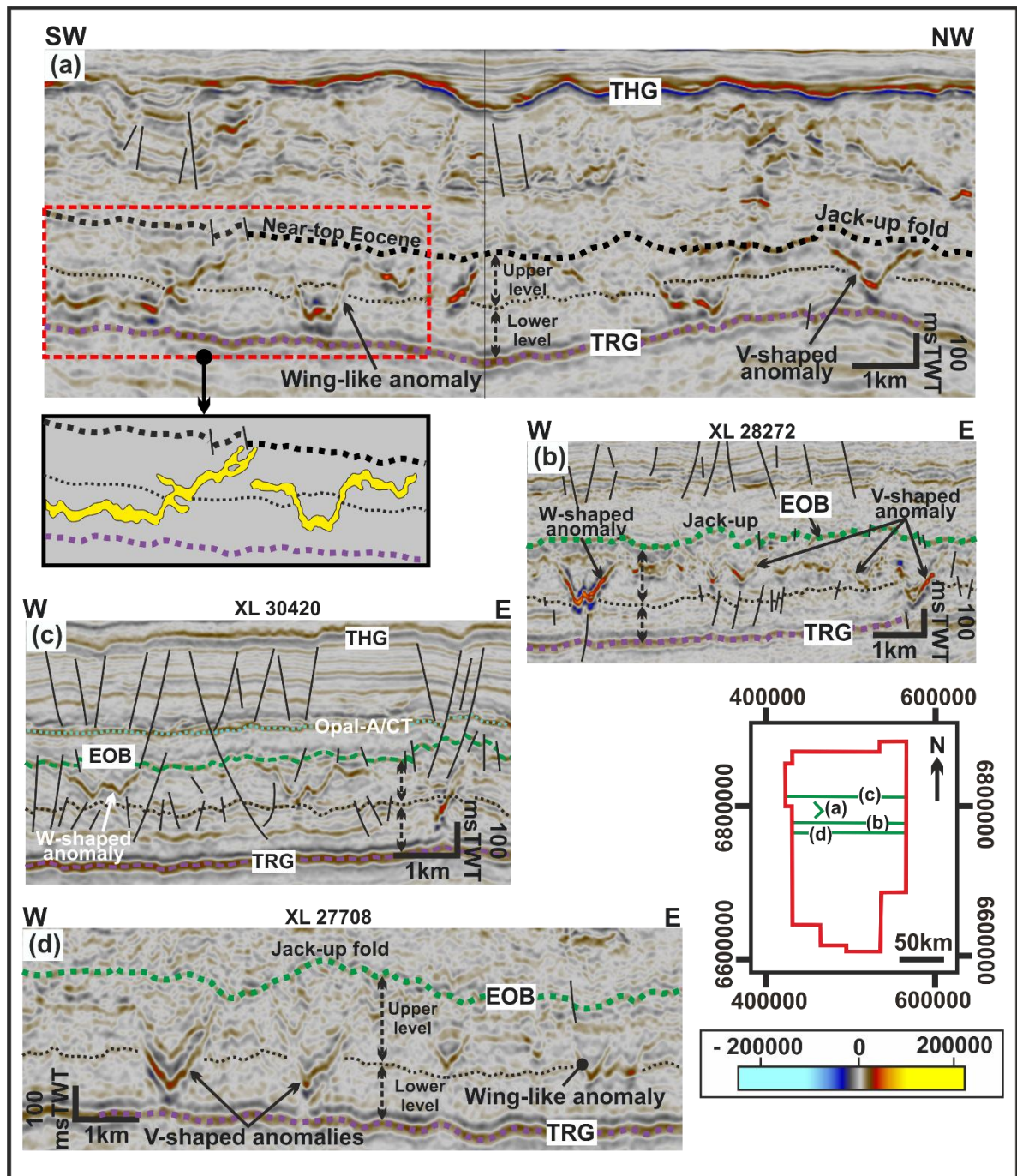
Fig. 4.12: Eocene (CSU-2) conical discordant high amplitude anomalies observed as V/W-shaped anomalies in cross section: (a) to (d). Wing-like anomalies are also observed in (a) and (d). Some of the anomalies have limbs with concordant anomalies (i.e., sill) at their upper tips. The discordant amplitude anomalies also show two (upper and lower) different levels of downward termination of their apexes or bases. THG: Top Hordaland, TRG: Top Rogaland Group, EOB: Eocene – Oligocene boundary. Data courtesy of CGG.

Fig. 4.13: Eocene (CSU-2) wing-like or saucer-shaped discordant amplitude anomalies observed as anomalies characterized by concordant central bases (i.e., basal sill) flanked by inclined marginal wings (i.e., dikes): (a) to (e). These have been interpreted as depositional sand bodies modified by sand remobilization and injection leading to their marginal sand dikes. TRG: Top Rogaland Group, EOB: Eocene – Oligocene boundary. Seismic data courtesy of CGG.
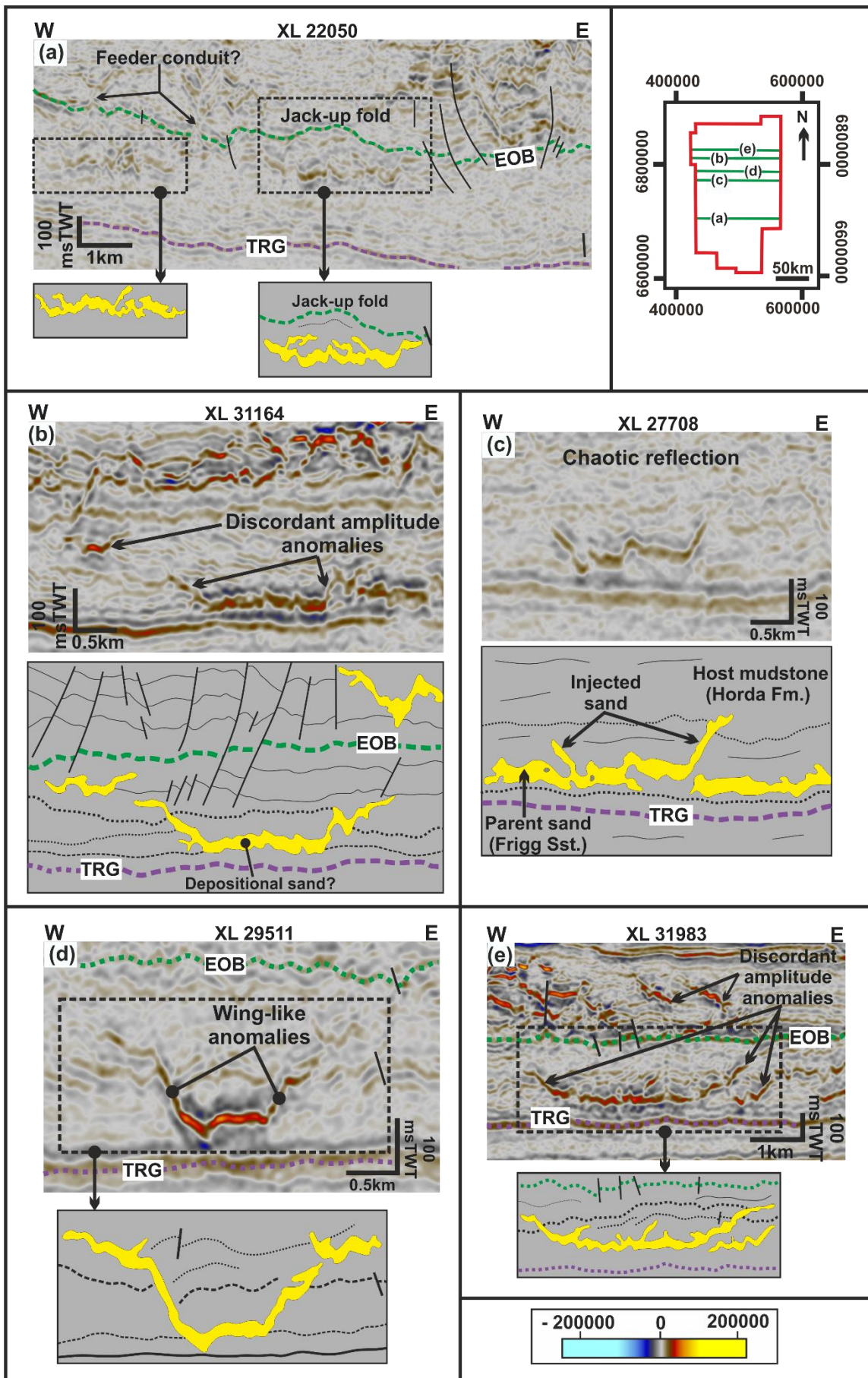
Fig. 4.14: (a) East-west oriented seismic section showing the occurrence of discordant high amplitude anomalies within the Eocene (CSU-2) succession. Figure (b) to (e) are time slices at different depth (msTWT) for an Eocene (CSU-2) discordant amplitude anomaly which shows varying irregular-shaped amplitude anomaly at different depth. THG: Top Hordaland, TRG: Top Rogaland Group, EOB: Eocene – Oligocene boundary. Seismic data courtesy of CGG.
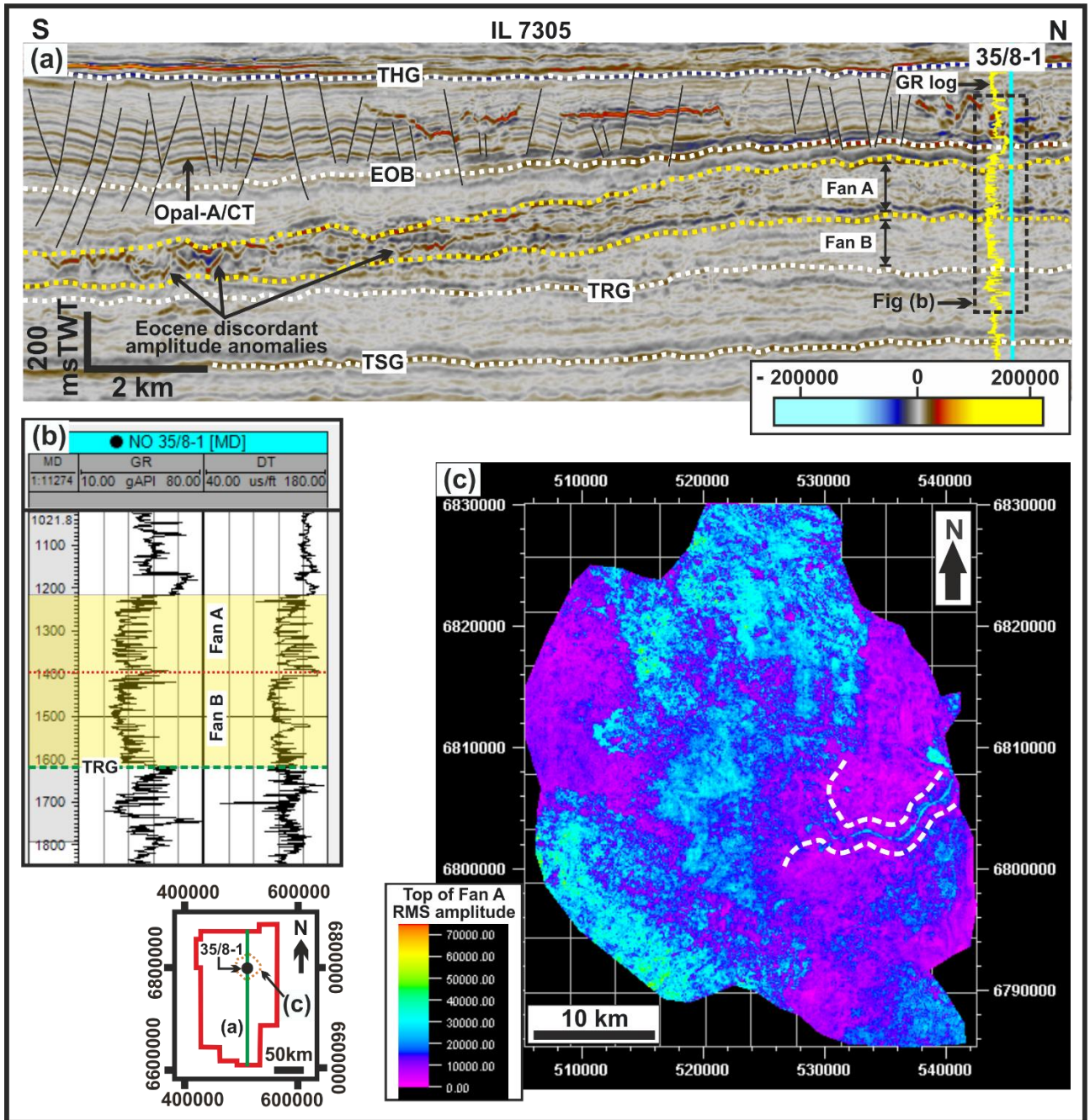
Fig. 4.15: (a) Lower to Middle Eocene sand-rich Fan A & B in the east/north-eastern part of the study area with discordant amplitude anomalies at the western margin of the fans. (b) Well section for well 35/8-1 through the fan showing the presence of sandstone. (c) RMS amplitude map for the mapped Top of Fan A showing the presence of high amplitudes indicative of the presence of sand. Well location is shown by the insert map. THG: Top Hordaland, TRG: Top Rogaland Group, EOB: Eocene – Oligocene boundary, TSG: Top Shetland Group. Seismic data courtesy of CGG and well data from TGS Facies Map Browser.
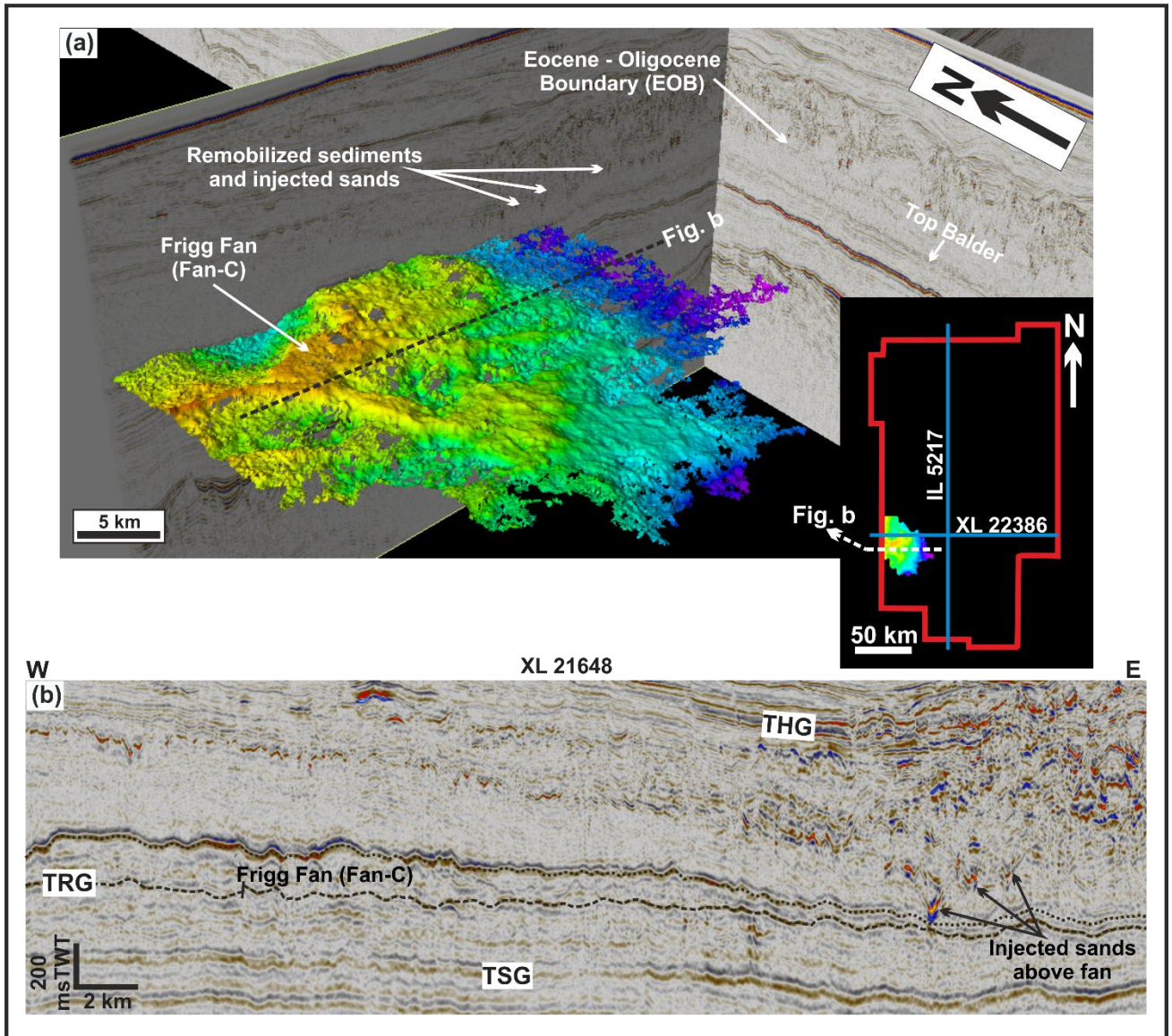
Fig. 4.16: (a) Middle Eocene (CSU-2) large sand-rich basin-floor fan (Fan C: Frigg Fan) in the south-western part of the study area. (b) East-west oriented seismic cross section across the fan showing discordant high amplitude anomalies above the fan complex which have been interpreted to represent injected sandstones sourced from the fan. THG: Top Hordaland, TRG: Top Rogaland Group, TSG: Top Shetland. Seismic data courtesy of CGG.

4.4.3.3 CSU-4 (Oligocene) discordant amplitude anomalies

The CSU-4 which is of Oligocene age is bounded at the top and base by the Base Miocene (H7) and the Eocene – Oligocene Boundary (H4) respectively (Fig. 4.2 & Table 4.2). The interval corresponds to the Cenozoic Seismic Sequence (CSS) reported by Jordt et al. (1995, 2000), Anell et al. (2012) and Rundberg (1991) as CSS 4, part of PAL 3 and Mu5, respectively. In the northern North Sea, the Oligocene time is noted to be associated with a transition from deep-water pelagic sediments to shallow marine sediments with abundant supply of clastic sediments (Huuse and Clausen, 2001; Rundberg and Eidvin, 2005). The unit thickens westwards (Fig. 4.4a) and has thickness in the range 400 – 680 msTWT in the southern part of the study area which reduces to about 150 – 300 msTWT in the northern part. The CSU-4 unit is generally characterized by varying amplitudes ranging from low amplitude, isolated and amalgamated high amplitude reflections and it is pervasively modified by polygonal faulting which terminate upward beneath the Top Hordaland Group (e.g., see Fig. 4.18d & 4.19b).

The CSU-4 which forms part of the Lark Formation (Fig. 4.2) can be sub-divided into two distinct sub-seismic units: the Lower Oligocene and Upper Oligocene sub-units which are both distinguished by their remarkably different reflection amplitude characteristics. However, both sub-units are well defined and easily distinguishable in the eastern parts of the study area where the reflection pattern are parallel to sub-parallel and continuous to semi-continuous, while they are difficult to define in the western part due to the intense post-depositional remobilization of sediments in that area. The lower sub-unit which directly overlies the Eocene – Oligocene Boundary, pinches out eastwards (Fig. 4.4a) and is documented to consist of sediments sourced from the East Shetland Platform due to the Late Eocene – Early Oligocene uplift along the basin margins (Rundberg and Eidvin, 2005). Its internal reflection is characterized by semi-continuous to discontinuous, sub-parallel to chaotic and low amplitude reflections (Table 4.1). The top of the Lower Oligocene sub-unit is defined by a strong, high amplitude, semi-continuous peak reflection (Fig. 4.17d, 4.18e) which have been described or interpreted as the Opal-A/CT diagenetic boundary by Rundberg (1989), Thyberg et al. (1999), Olobayo (2014) and recently by Wrona et al. (2017b). This reflection represents the boundary between Opal-A zone and Opal-CT zone. As such the lower Oligocene sub-unit represents the Opal-CT zone which consists of Opal-CT-rich sediments which were subjected to Opal-A/CT transformation (Wrona et al., 2017b: their Fig 3 & 4). The upper sub-unit is however characterized by medium to high, discontinuous, and chaotic amplitude reflections. This sub-unit have been documented by Wrona et al. (2017b) to represent the Opal-A zone which consists of Opal-A rich sediments. The upper sub-unit is considerably thicker than the lower sub-unit and onlap onto the top CSU-3 succession (H5 – Intra Oligocene Unconformity) along the eastern basin margin (Fig. 4.4a).

Numerous discordant high amplitude anomalies are observed within the CSU-4. These anomalies are spatially distributed throughout the study area except in the north-western part (Table 4.5). The geometry of the observed anomalies varies from isolated conical (V/W) shaped anomalies, saucer-shaped/wing-like anomalies characterized by bedding concordant bases and steeply dipping marginal limbs/wings, to irregular and complex-shaped discordant amplitude anomalies which crosscut their host strata (Fig. 4.17, 4.18 & 4.19). Some amalgamated and stacked complexes are also observed within the CSU-4 in the western and north-eastern parts of the study area (Fig. 4.20). The anomalies in the southern and western parts generally consist of stacked/amalgamated and some isolated V/W-shaped anomalies within highly mobilized sediments and are observed to occur within the upper and lower Oligocene sub-units with some having their apexes terminating directly on the Eocene-Oligocene boundary (Fig. 4.17a). However, in the north-east and eastern parts, the anomalies comprise of mainly wing-like and irregular to complex-shaped anomalies which occur within the upper Oligocene sub-unit and either occur directly on or a few milliseconds TWT above the Opal-A/CT diagenetic boundary (Fig. 4.19a & b). Some of the anomalies in this area appear connected to other anomalies above or adjacent to them with some observed to crosscut each other in seismic cross-section (e.g., Fig. 4.17b & 4.20c). Some isolated V/W-shaped anomalies were also observed within the lower Oligocene sub-unit in the eastern part.

In plan view, the anomalies are observed to have circular to sub-circular, lobate to elliptical and elongate geometries with diameters of up to 2 km and length of up to 4.5 km (Fig. 4.21a). The wing-like discordant amplitude anomalies are often associated with pronounced deformation of their host strata which occur as forced-folds and/or jack-up of the overburden (up to 100 msTWT) above the anomalies, with the edges of the folds or jack-up on the Top Hordaland Group Unconformity found to coincide with the tip of the discordant margins of the wing-like anomalies. This close spatial correlation between the folds on the unconformity and the underlying discordant anomalies are clearly illustrated in Fig. 4.17d, 4.18e and 4.20a. Overburden deformation are also found to be more pronounced above the irregular and complex-shaped discordant amplitude anomalies compared to those observed above the conical-shaped amplitude anomalies.

Fig. 4.17: Oligocene (CSU-4) conical discordant high amplitude anomalies. Isolated U/V-shaped amplitude anomalies with some characterized by concordant tips and observed in (a), (c) and (d). While vertically and laterally connected V-shaped amplitude anomalies are observed in (b). EOB: Eocene – Oligocene boundary, THG: Top Hordaland Group. Seismic data courtesy of CGG.
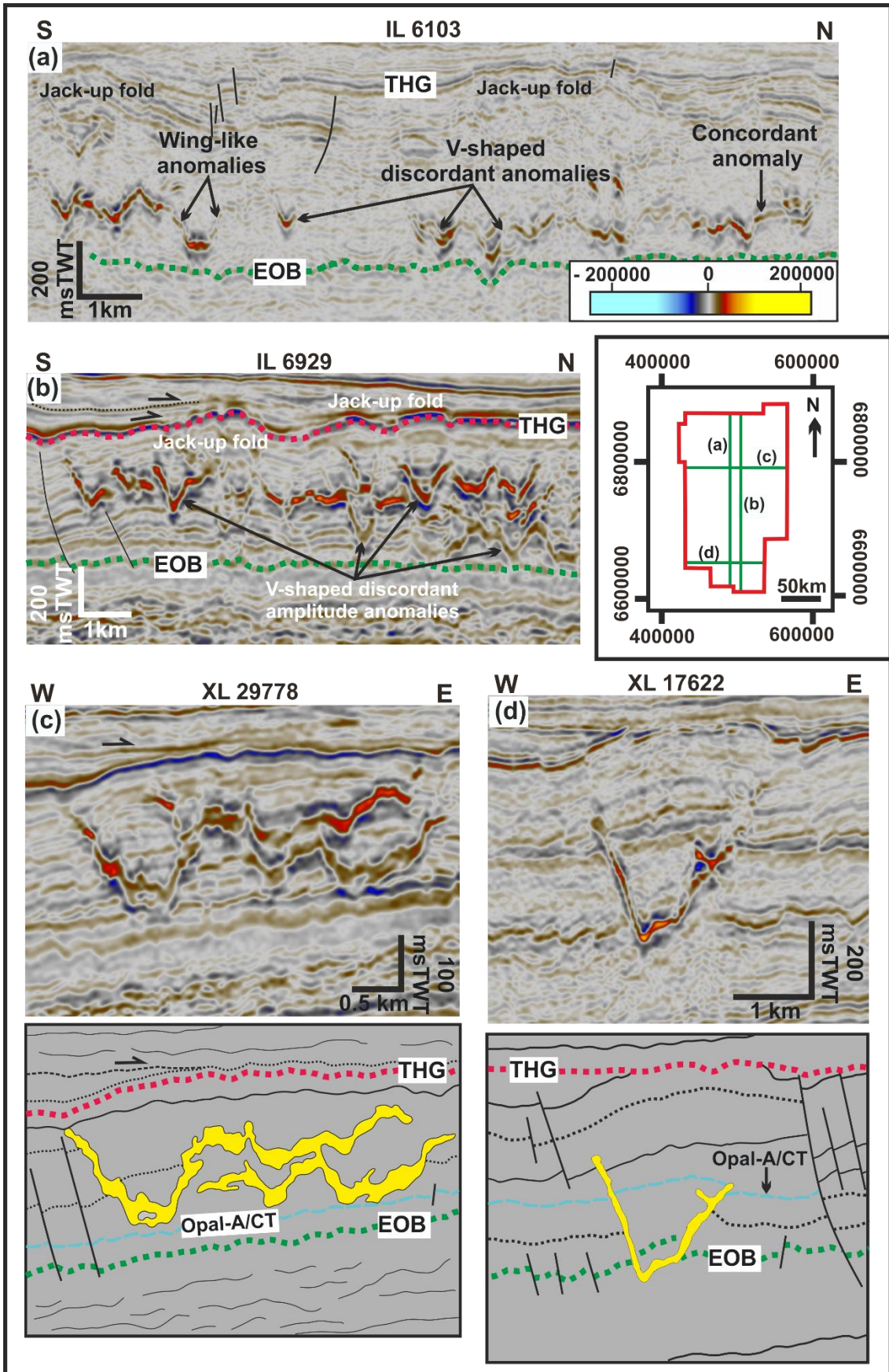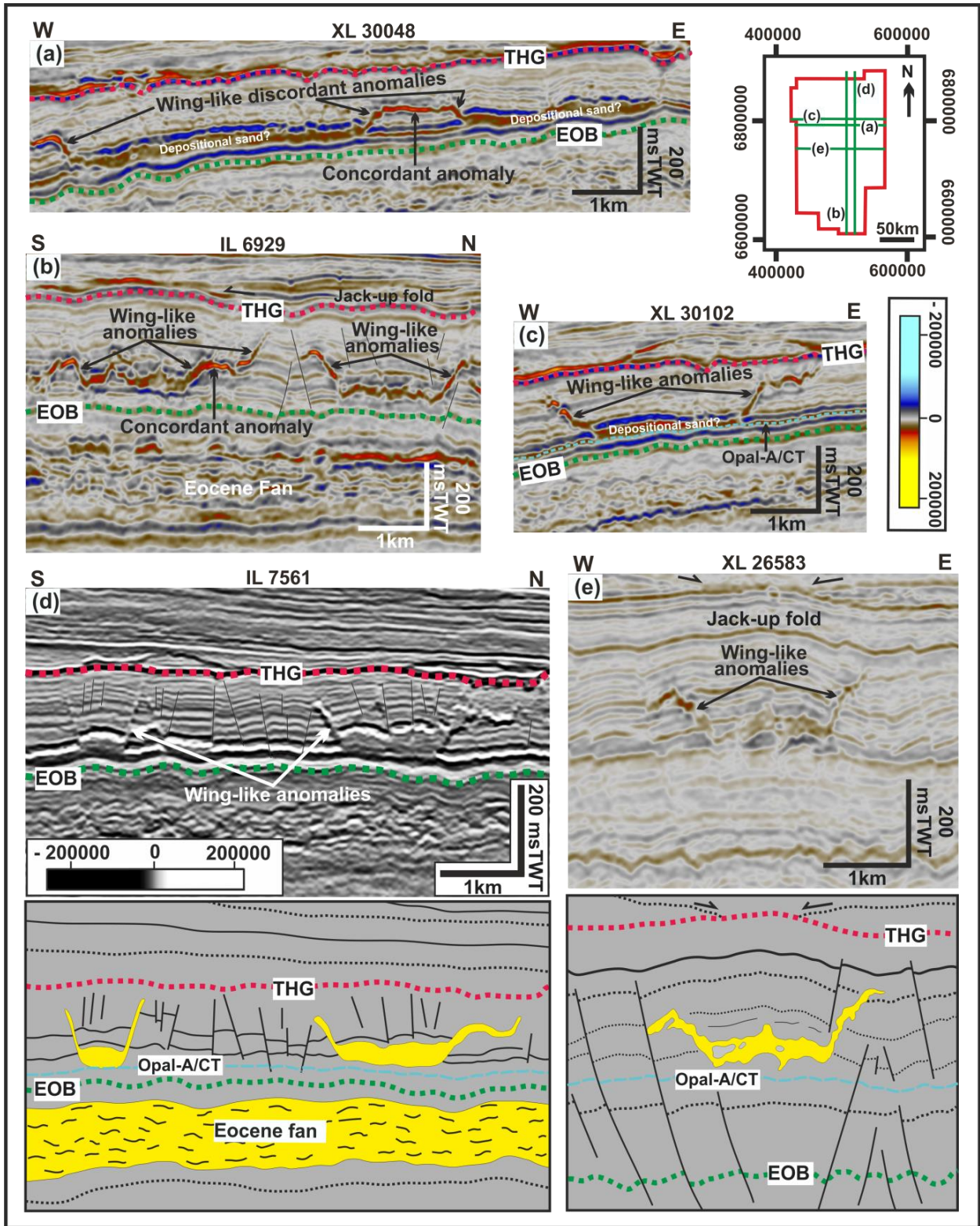
Fig. 4.18: Oligocene (CSU-4) wing-like or saucer-shaped discordant amplitude anomalies characterized by concordant bases (i.e., basal sill) with steeply dipping marginal discordant anomalies (i.e., dikes) which sometimes have concordant anomalies at their tips: (a) to (e). Some of the anomalies are associated with jack-up of the overburden above them. THG: Top Hordaland Group, EOB: Eocene – Oligocene boundary. Seismic data courtesy of CGG.
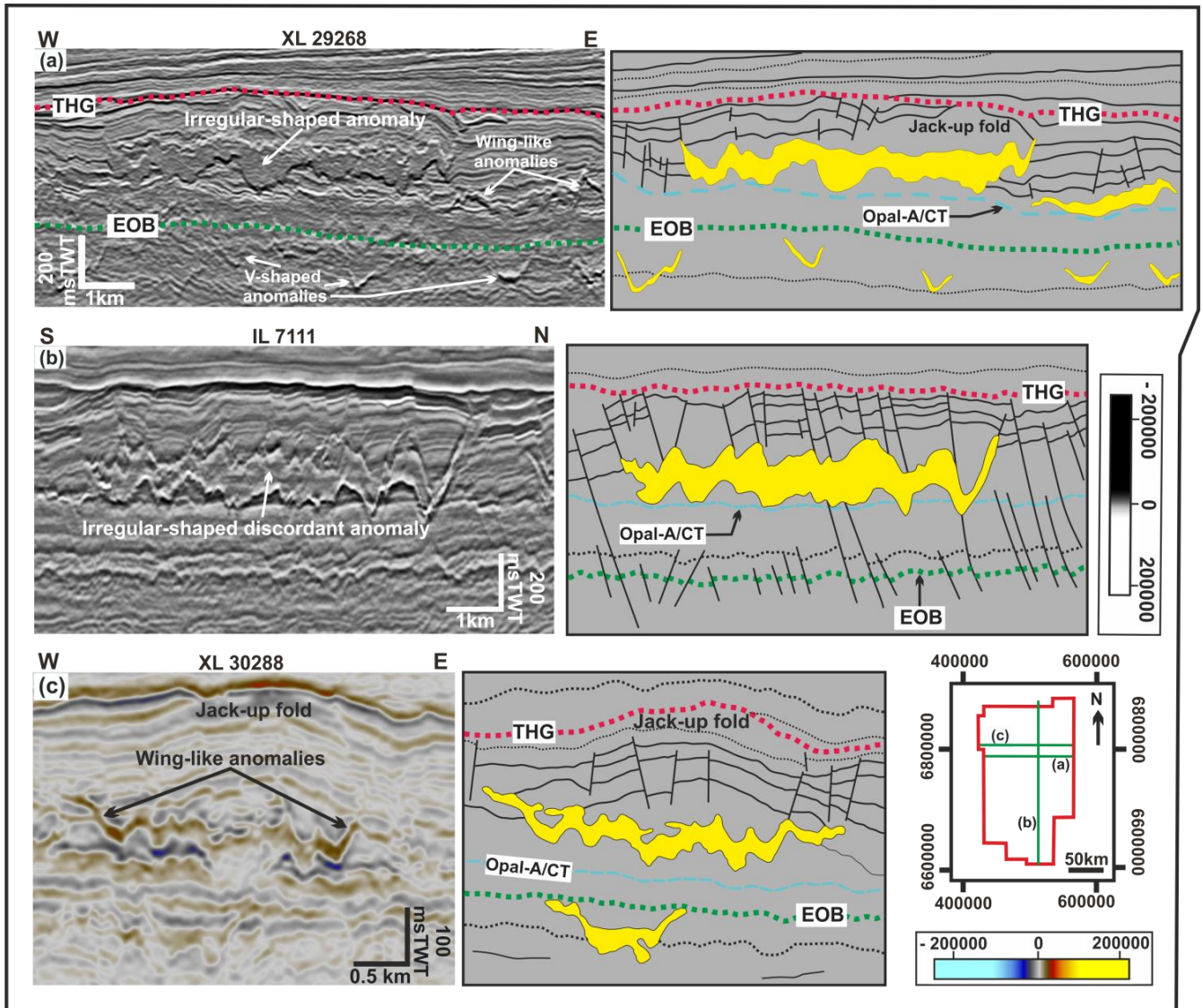
Fig. 4.19: Oligocene (CSU-4) irregular to complex-shaped discordant amplitude anomalies: (a) to (c). The anomalies are characterized by zig-zag cross sectional geometry and observed to occur on or directly above a high amplitude peak reflection interpreted as the Opal-A/CT diagenetic boundary (see Wrona et al., 2017b). THG: Top Hordaland Group, EOB: Eocene – Oligocene boundary. Seismic data courtesy of CGG.
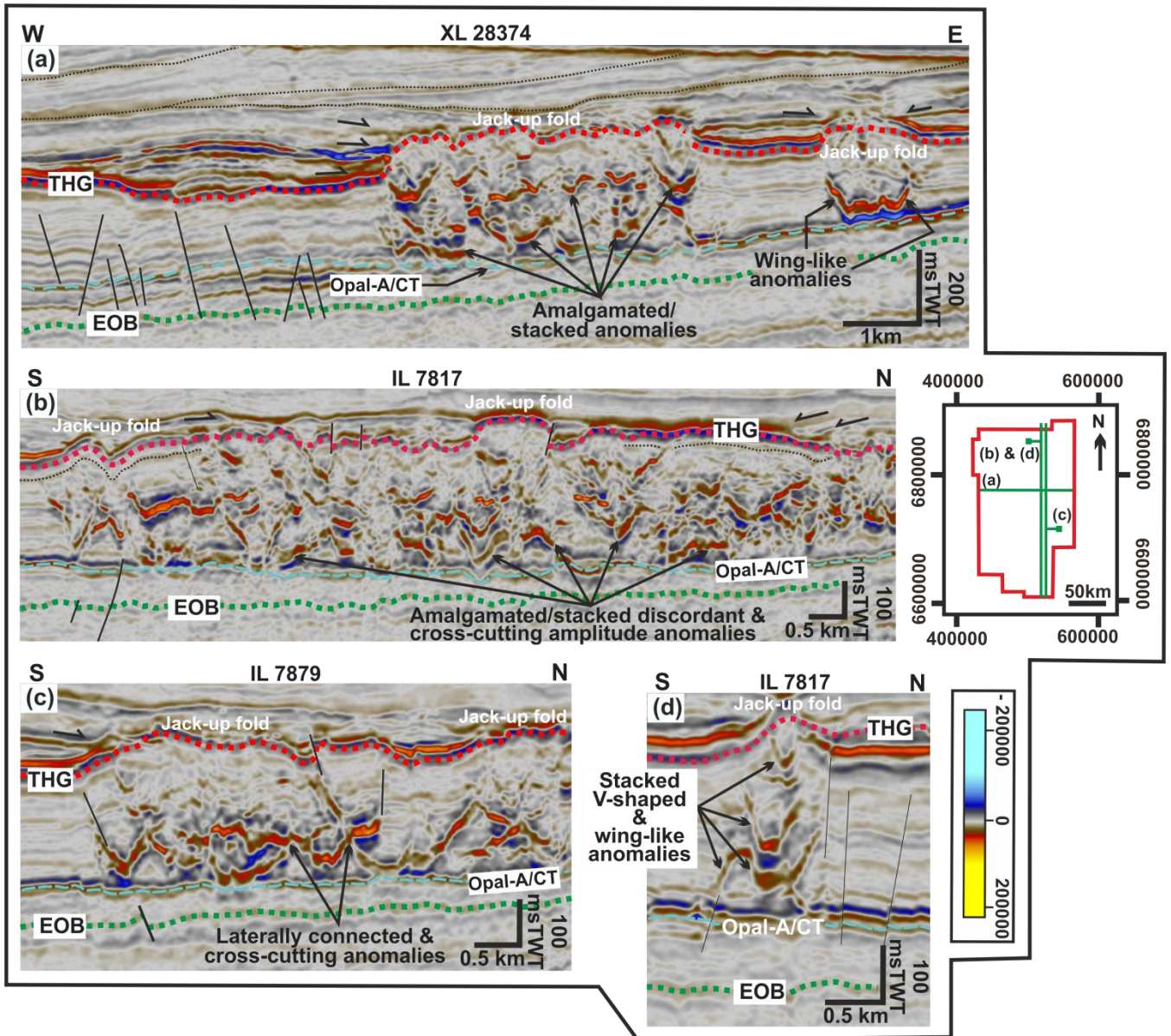
Fig. 4.20: Oligocene (CSU-4) amalgamated or stacked amplitude anomalies: (a) Vertical stacking of U/V shaped amplitude anomalies. (b) Juxtaposition of several amplitude anomalies comprises of V/W-shaped and irregular-shaped amplitude anomalies. (c) Laterally connected and cross-cutting stacked amplitude anomalies. (d) Stacked isolated U-shaped discordant anomalies. EOB: Eocene – Oligocene boundary, THG: Top Hordaland Group. Seismic data courtesy of CGG.
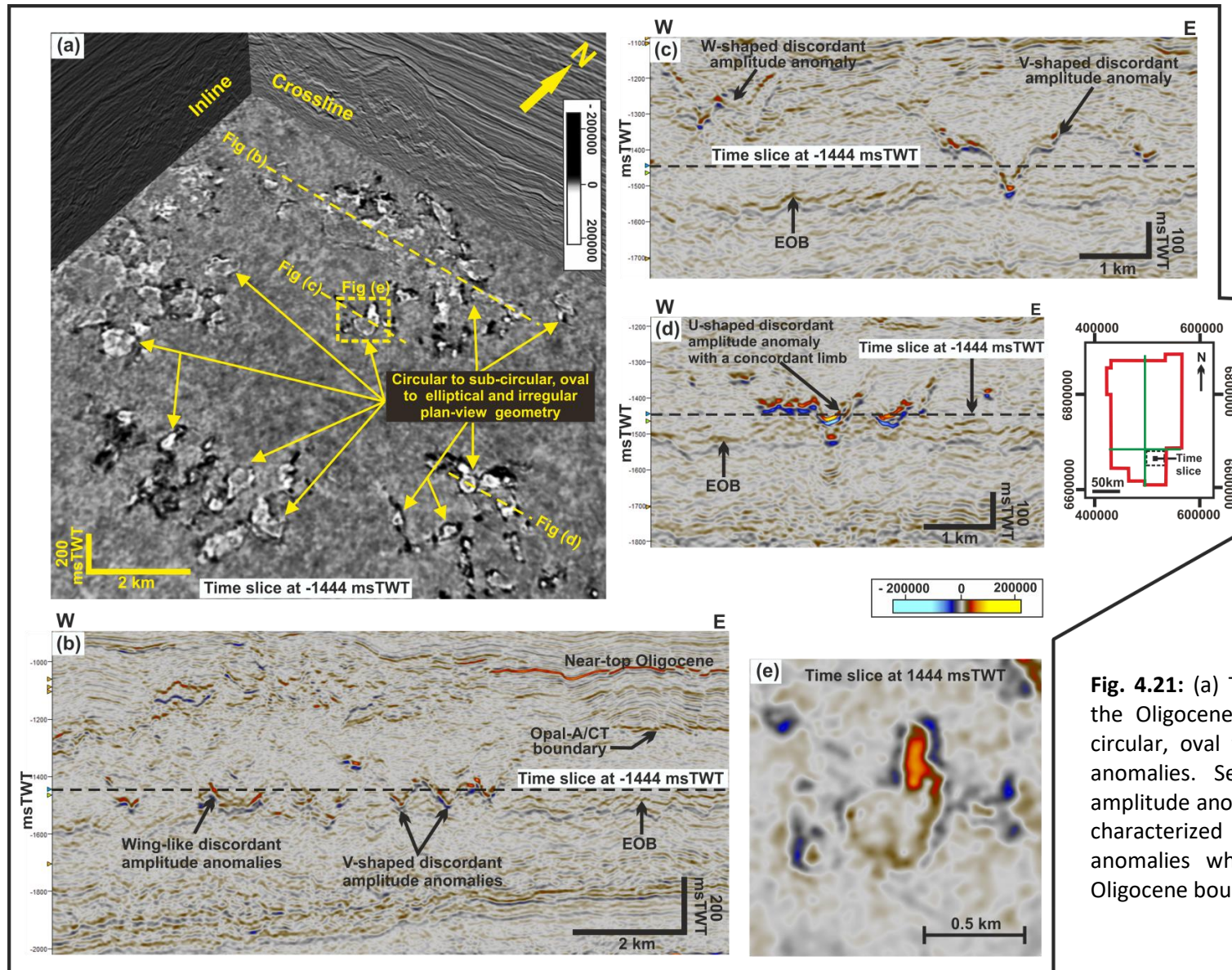
Fig. 4.21: (a) Time slice (at 1444 msTWT) through the Oligocene (CSU-4) which shows circular/sub-circular, oval to elliptical and irregular amplitude anomalies. Seismic lines across some selected amplitude anomalies [(b) to (d)] are in cross section characterized by V-shaped discordant amplitude anomalies which directly overlie the Eocene – Oligocene boundary. Data courtesy of CGG.

4.4.4 Well Calibration of Discordant Amplitude Anomalies

Wells in quadrants 34 and 35 were observed to have intersected some of the discordant and concordant high amplitude anomalies at various depths and interval. The wireline log (gamma-ray and sonic log) signature of the anomalies intersected by these wells show the presence of tens-of-meters of sandstone which are either thick sandstone units encased in their host mudstone strata or inter-bed of sandstone and thin mudstone units. Some of the wells are observed to intersect the anomalies at different levels and mainly at the discordant or concordant margin of the anomalies. The observed acoustic signal for the top and base reflection of most of the discordant amplitude anomalies compared to their surrounding mudstone-dominated host strata clearly indicates that they are characterized by a high velocity and/or high density compared to their host strata. Their acoustic signal is however also dependent on fluid content and degree of cementation. As such the sandstones encountered by these wells are all suggested to be partially cemented and water wet giving rise to their observed high amplitude reflection with no significant velocity effects. Table 4.3 gives a list of wells which intersected the anomalies within the seismic units where they occur, and the approximate thickness of the sand units encountered.

Table 4.3: List of wells which intersected the observed discordant high amplitude anomalies and the approximate thickness of the sandstone units encountered. See Fig. 4.22 for seismic illustration of well intersection of discordant amplitude anomalies and their calibration to sand using GR-log signature.

Seismic Unit	Well name	Approximate thickness (m) of sandstone encountered
Palaeocene – Early Eocene (CSU-1)	35/11-10	45
	35/11-3S	95
Eocene (CSU-2)	34/7-8	20
	34/10-34	15
Oligocene (CCU-4)	35/8-2T2	25

Well calibration of Paleocene – Early Eocene (CSU-1) anomalies

- **Well 35/11-10 (Fram Field):** the well encountered c. 45 m thick sandstone unit some 141 m above the Top Shetland Group horizon (Fig. 4.22a), where it intersected a concordant anomaly (possibly depositional sand body) with discordant – winglike anomalies at its margins. The sandstone shows a blocky gamma-ray log signature. From the well completion report, the sandstone encountered at this interval (1712.5 – 1776.5 m) was documented to belong to the Heimdal Sandstone Member and comprises of fine to very coarse, loose, and poorly sorted sandstone, with thin mudstone beds and stringers of limestone (NPD, 2019). Due to the direct connection of the marginal discordant anomalies to the concordant anomaly calibrated as sandstone, they are inferred to represent intruded sandstones developed at the margins of their depositional concordant sandstone (Fig. 4.22a).

- **Well 35/11-3S:** the well encountered c. 95 m thick sandstone unit where it intersected a W-shaped discordant amplitude anomaly about 28 m above the Top Shetland Group horizon (Fig. 4.22c). The intersected thick sandstone package is expressed by a blocky low-value gamma-ray log signature suggesting that the sandstone is homogenous with thin/ratty sandstone units found above it. The top and base of the thick sandstone unit is sharp, and the sandstone is characterized by high sonic log velocity (> 95 us/ft). Core photo of a 9 m core taken at the base of the thick sandstone shows a clean and structureless sandstone unit belonging to the Sotra Sandstone Member of the Lista Formation (see Dmitrieva et al., 2018: their Fig. 4). However, angular clasts of the host mudstone are observed within the massive sandstone (see Dmitrieva et al., 2018: their Fig. 4). The absence of sedimentary structures within the sandstone is suggested to indicate that the sand may be part of a depositional sand body which was subsequently modified by remobilization leading to the lack of any primary sedimentary structures as observed in the core photo (Hurst et al., 2011; Olobayo, 2014; Dmitrieva et al., 2018). The intersection of the thick sandstone is however used to infer that the discordant margins of the anomaly may represent intruded sandstone (Fig. 4.22c).

Well calibration of Eocene (CSU-2) anomalies

- **Well 34/7-8 (Vigdis Field):** the well encountered c. 20 m thick sandstone unit where it intersected the margin of a V-shaped (conical) discordant amplitude anomaly about 190 m above the Top Rogaland Group (Fig. 4.22b). The conical shape of the anomaly and its calibration to sandstone implies it represents injected sandstone which may have been source from the Eocene Grid Sandstone Member of the Horda Formation.

- **Well 34/10-34 (Gullfaks Field):** the well encountered c. 15 m thick sandstone unit where it intersected a laterally extensive concordant tip (or sill) of a V-shaped discordant amplitude anomaly some 235 m above the Top Rogaland Group (Fig. 4.22d). The direct connection of the concordant sandstone to the tip of the V-shaped discordant anomaly suggests that the V-shaped anomaly may represent injected sand dikes which formed concordant sandstone sills at its upper tips. The encountered sandstone may have been source from the Eocene Grid Sandstone Member of the Horda Formation. Other additional sandstone units are developed above the intersected sand and are characterized by alternating sandstone and mudstone beds (Fig. 4.22d).

Well calibration of Oligocene (CSU-4) anomalies

- **Well 35/8-2T2 (Vega Field):** the well encountered c. 25 m thick sandstone unit where it intersected the base of a V-shaped discordant amplitude anomaly (Fig. 4.22e). The anomaly is characterized by: (i) a steeply dipping limb (or dike) which passes upwards into a concordant anomaly (or sill) and back into a discordant anomaly, and (ii) a limb which passes into a concordant anomaly. The anomaly lies about 60 msTWT above the Eocene – Oligocene Boundary and directly overlies the Opal-A/CT diagenetic boundary. The calibration of the base of the anomaly to sandstone and its apparent connection to the concordant and discordant parts of the anomaly implies the anomaly represent an intruded sand body (Fig. 4.22e).

4.4.5 Interpretation of the discordant amplitude anomalies

The discordant and concordant high amplitude anomalies described in this study are interpreted as sand injectites/intrusions and may represent sandstone dikes and sills which are formed due to the fluidization and injection of sands into low-permeable host mudstone strata. The above interpretation is based on: (i) their isolated distribution, (ii) their discordant relationship with their host strata and reflection character, (iii) their varying geometries as observed in 3D cross-section and map view, and (iv) their calibration to tens-of-meters of thick sand-bearing units where they are intersected by wells in the study area. Their discordant nature implies that they are not genetically related to their host strata but were formed after the deposition of the host strata. The clear jack-up and gentle doming of the overburden above most of the intrusions is suggested to be indicative of intrusion, forced-folding and differential compaction above depositional sand bodies (Andresen and Clausen, 2014; Dmitrieva et al., 2012; Huuse et al., 2012). However, the absence of forced folds or jack-up above some of the intrusions may partly be due to low thickness of the parent sand body (Szarawarska et al., 2010; Safronova et al., 2012). The high seismic amplitude associated with their top and base reflections indicates an acoustically hard (high impedance) body encased within low-impedance host mudstone-dominated strata (Shoulders and Cartwright, 2004). Discordant high amplitude anomalies with similar acoustic properties, scale and three-dimensional geometries have previously been recognized and documented in the North Sea and other basins e.g. Faroe-Shetland Basin (Shoulders et al., 2007; Cartwright et al., 2008), Tampen Spur- Q34 (Huuse and Mickelson, 2004), South Viking Graben (Huuse et al, 2004), Luna Graben (Andresen and Clause, 2014), Outer Moray Firth (Gras and Cartwright, 2002; Molyneux et al., 2002), Måløy Slope (Jackson, 2007; Jackson et al., 2011), North Viking Graben (Olobayo, 2014; Dmitrieva et al., 2018; Cobain et al., 2019), and Norwegian-Danish Basin (Andresen et al., 2019). These were interpreted as sand intrusions with some calibrated to wells indicating tens-of-meters of sandstone of up to 60m in thickness (e.g., Huuse and Mickelson, 2004; Jackson and Sømme, 2011). The anomalies

characterised by concordant bases with marginal wings are suggested to likely represent depositional sand bodies which were subjected to post-depositional remobilization and injection leading to the formation of their marginal wings; while anomalies characterized by irregular and complex-shaped geometries are interpreted as depositional sands which were probably remobilized in-situ. On the other hand, the conical anomalies are suggested to represent injected sand bodies. The mound-shaped anomalies with steep flanks (e.g., see Fig. 4.18c, 4.34a/b & 4.35) which occur mainly above the Top Hordaland Group unconformity but also observed above the Top Rogaland Group/Top Balder have been interpreted as sand extrudites due to the clear onlap of overlying strata rather than depositional mounds which are usually characterized by draping of overlying sediments (see Løseth et al., 2013; Rundberg and Eidvin, 2016).

The interpreted sand intrusions found within the Paleogene (CSU-1, CSU-2 & CSU-4) succession in the study area have been grouped into three (3) geometrical types based on the classification by Huuse et al. (2007) and Cartwright et al. (2008). This grouping is achieved based on their observed varying seismic characteristics (e.g., scale, geometry, and morphology) and the nature of their interaction with their mudstone-dominated host strata. The intrusion types include:

- **Type-1 Intrusions:** Conical (U, V, W) shaped sandstone intrusions
- **Type-2 Intrusions:** (i) Saucer-shaped (flat-based) or wing-like sandstone intrusions and (ii) Crestal sandstone intrusions or intrusion fringes
- **Type-3 Intrusions:** Irregular and complex-shaped intrusions

Table 4.4 gives a schematic summary representation of the various geometries exhibited by the intrusion types observed. In general, Type-1 and Type-3 intrusions are the most common in the study area. The variability in the conical geometry of the Type-1 intrusions as observed in Table 4.4 may suggest a direct control on geometry related to burial depth. While Table 4.5 gives a summary description of intrusion types, their spatial distribution, cross sectional geometries and plan view geometry within the seismic units.

4.4.6 Quantitative geometrical characterization of observed sandstone intrusions or injectites

4.4.6.1 Measured parameters and Limitations

The interpreted sandstone intrusions observed within the Paleogene succession in this study are generally characterized by high amplitude reflections relative to their encasing mudstone-dominated host strata. Due to the wide range of geometries exhibited by the observed intrusions, geometrical measurements have been taken for 167 sandstone intrusions/injectites comprising of only Type-1 and Type-2 intrusions within the Paleocene – Early Eocene (CSU-1: 44 injectites), Eocene (CSU-2: 58 injectites) and Oligocene (CSU-4: 65

injectites). The key geometrical parameters measured are listed below based on Bureau et al. (2013):

- $\Theta1$, $\Theta2$ – True dip of discordant limbs or wings (in degrees with no vertical exaggeration)
- H1, H2 – Height or vertical extent of discordant limbs or wings from the base of the intrusion (in metres)
- Z – Depth of intrusion from the present seafloor reflection (in metres)
- Td – Top diameter or upper width or maximum lateral extent of intrusion (in metres)
- Bd – Base diameter or lower width or minimum lateral extent of intrusion (in metres)
- Th – Thickness between the top and base reflection of Type-2 sandstone intrusions (in metres)

The above parameters were measured across the study area on the best resolved sandstone intrusions. Measurements were made at a vertical exaggeration, VE = 5. However, for the dip measurements, the dip values were converted to an unexaggerated true dip (at scale of approximately 1:1 aspect ratio) using the relationship (tan $\ddot{\Theta}$ = VE tan Θ) by Stewart (2011), where $\ddot{\Theta}$ represents the exaggerated dip and Θ represents the unexaggerated dip (true dip). It is also worth noting that the actual dip of limbs/wings of conical and wing-like intrusions are presumably smaller than their original angle of emplacement due to subsequent compaction of surrounding sediments (Huuse et al., 2004; Monnier et al., 2014). Fig. 4.23 shows a schematic drawing which illustrates the principle for measurement of the above parameters for Type-1 & -2 sand intrusions. It is to be noted that conversion from depth in milliseconds two-way travel time (msTWT) to depth in meters was carried out using the average interval velocities obtained from wells for the intervals of interest (see Appendix B.1). Based on the measured parameters, Table 4.6 summarizes the range and average values obtained for measurements of Type-1 & 2 sand intrusions within the three Cenozoic seismic units where they have been observed. The values obtained for each Type-1 intrusion give some level of indication about the possible shape and geometry of the measured intrusion with regards to whether they are U, V or W-shaped in geometry.

A potential source of uncertainty in the measured parameters is associated with the average interval velocity data used to convert measurements in vertical domain (e.g., height, thickness, and depth of intrusion) from milliseconds two-way travel time (msTWT) to meters. This is because the selected interval velocity values from wells may not be representative of the velocity within the interval across the study area due to both vertical and horizontal heterogeneity. This, however, will only have a minor effect on the estimated parameters and do not affect the interpretation presented here. Another possible source of uncertainty is related to the accuracy of measurements (by user) using the available measurement tool in Petrel software. For instance, for the measurement of intrusion length (Top diameter/Upper width and Base diameter/Lower width), the uncertainty is estimated to be c. 37.5 m, which is constrained by the inline and crossline spacing of the seismic data. While for vertical measurements (height, thickness, and depth of intrusion) the uncertainty

is estimated to be 4 ms which is also constrained by the 4 ms sampling interval of the seismic data. The variation in values obtained for measurements of intrusion height (H1 & H2) may be related to underestimation of intrusion height due to detectability which limits the identification of reflection termination especially in cases where intrusion tips cannot be resolved or are crosscut by polygonal faults. Also, the estimated thickness for Type-2 (wing-like) intrusions derived from measurement of the vertical distance between the top (peak) and base (trough) reflection associated with the intrusions may not accurately represent the true thickness of the intrusions measured (Huuse et al., 2007; Jackson et al., 2011).
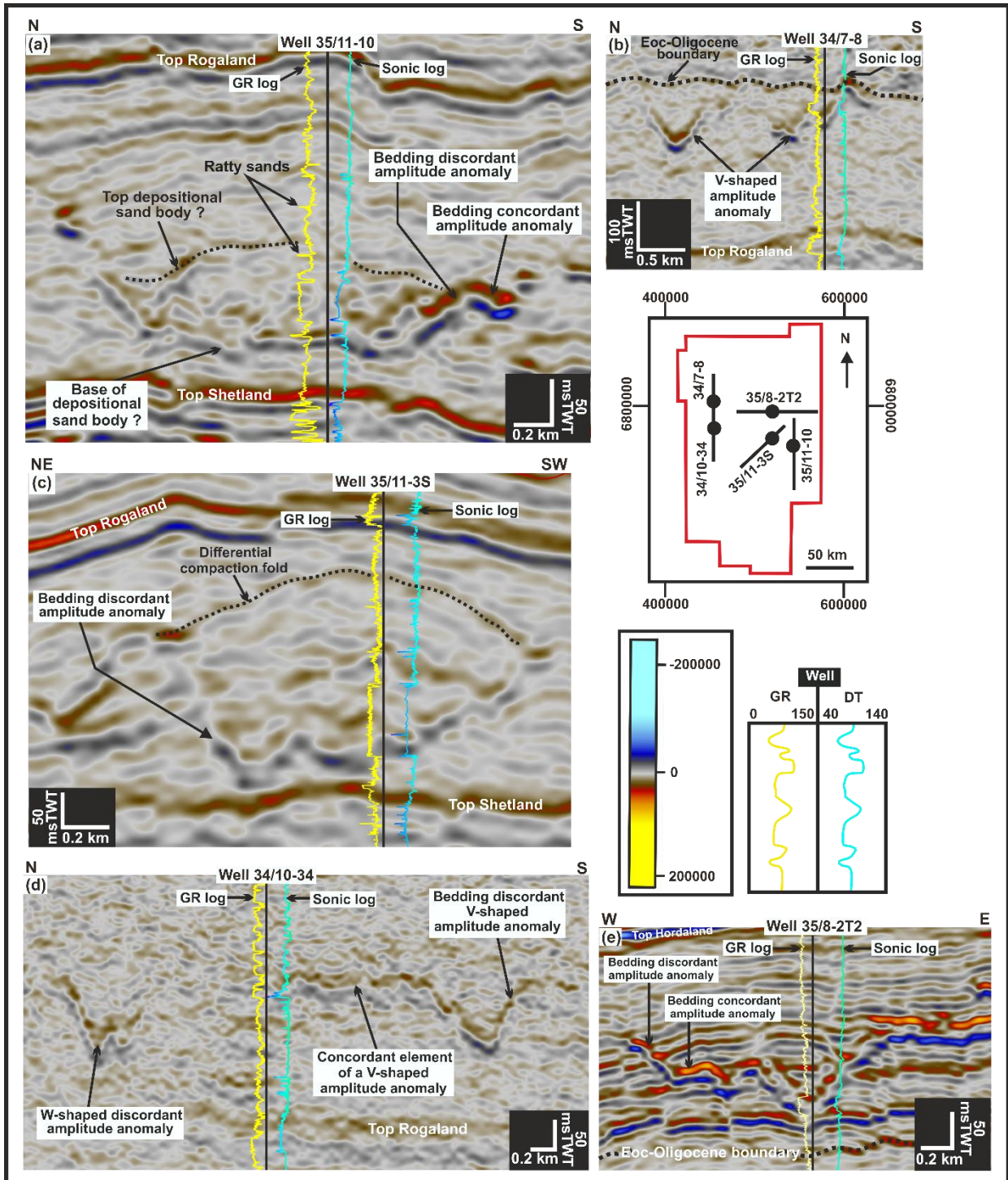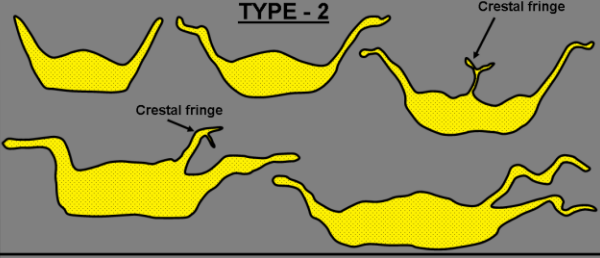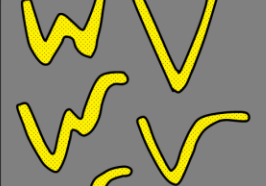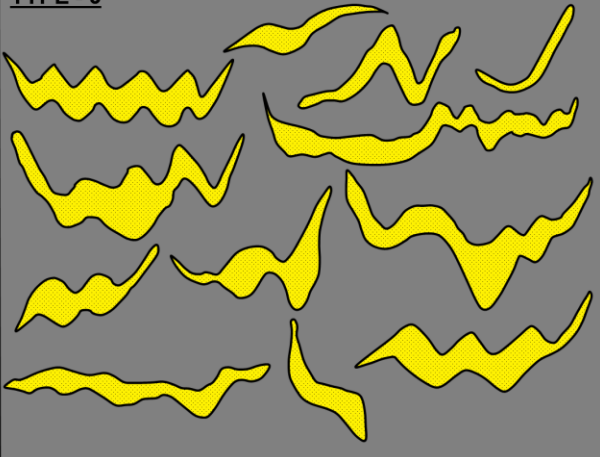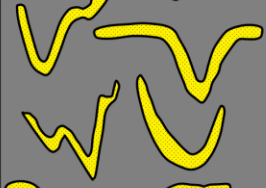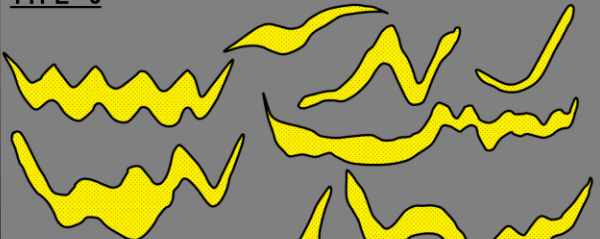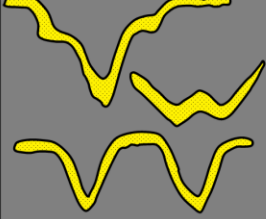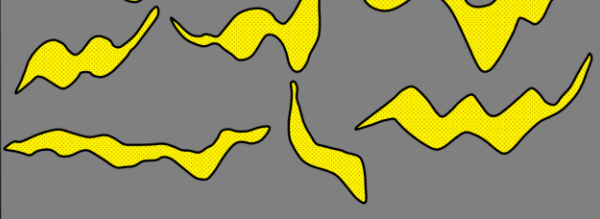
Fig. 4.22: Calibration of anomalies intersected by wells in the study area. (a) Well 35/11-10 encountered c. 45 m thick sandstone unit where it intersected a concordant anomaly with discordant margins in the CSU-1 interval. (b) Well 34/7-8 encountered c. 20 m thick sandstone unit where it intersected the margin of a V-shaped amplitude anomaly in the CSU-2 interval. (c) Well 35/11-3S encountered c. 95 m thick sandstone unit where it intersected the margin of a W-shaped discordant anomaly in the CSU-1 interval. (d) Well 34/10-34 encountered c. 15 m thick sandstone unit where it intersected a laterally extensive concordant tip of a V-shaped discordant amplitude anomaly in the CSU-2 interval. (e) Well 35/8-2T2 encountered c. 25 m thick sandstone unit where it intersected the base of a V-shaped discordant amplitude anomaly in the CSU-4 interval. Seismic data courtesy of CGG and well data courtesy TGS Facies Map Browser.

Table 4.4: Classification and schematic illustration of the varying geometries exhibited by the intrusion found within the Paleogene succession (CSU-1, CSU-2 & CSU-4) in the study area.

Intrusion Type	Description	Schematics of sandstone intrusion geometries observed
Type 1	Conical (U, V, W) shaped sandstone intrusions	
Type 2	Flat based-bowl (saucer-shaped) or wing-like sand-stone intrusions	
	Crestal sandstone intrusion or intrusion fringes	
Type 3	Irregular/complex shaped sandstone intrusions	

4.4.6.2 Variability of measured intrusion parameters within the seismic units

The estimated quantitative data for Type-1 & -2 intrusions (Table 4.6, Appendix B.1) indicate a moderate variability in the overall key geometrical parameters for the intrusions within the seismic units. The geometrical variability within each unit is further described below and we suggest that the inherent variability in the measured parameters may be attributed to the level of burial, compaction, and mechanical heterogeneity within each of the host sequence.

i) Geometrical variability of Paleocene – Early Eocene (CSU-1) intrusions

The sand intrusions observed within the Paleocene to Early Eocene CSU-1 seismic unit consists of both Type-1 & 2 sandstone intrusions with the Type-1 being the most predominant. The intrusions are restricted to the eastern and north-eastern part of the study area (within Paleocene mudstones of the Lista Formation) along the eastern basin margin characterized by Paleocene sand-rich fan complexes (see Table 4.5). Within this interval, the geometrical parameters of forty-four (44) sandstone intrusions were measured comprising of thirty-three (33) Type-1 and eleven (11) Type-2 intrusions.
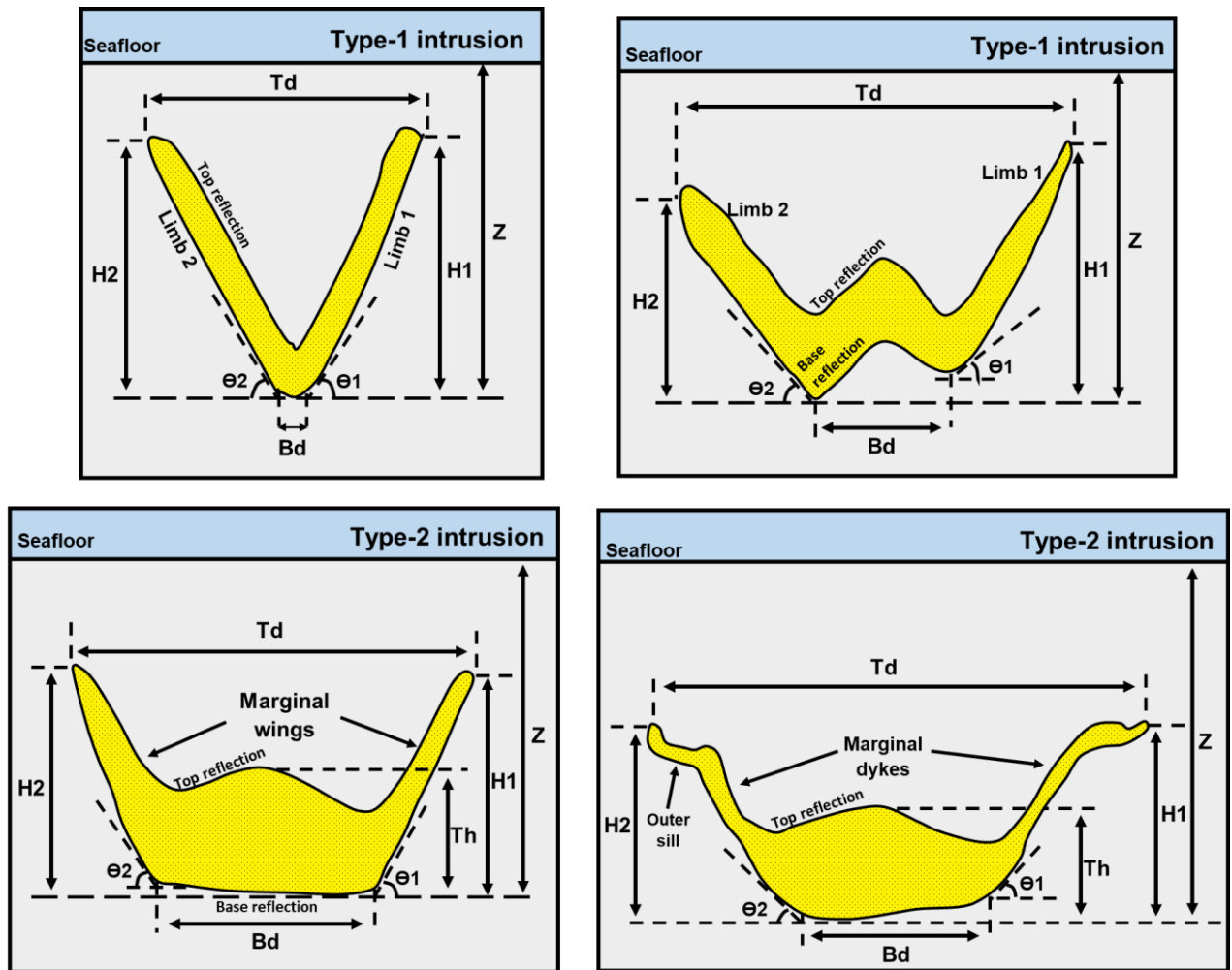
Fig. 4.23: Schematic drawings illustrating the principles for the geometrical characterization and measurement of conical-shaped (Type-1) and flat-based/wing-like (Type-2) sandstone intrusions. See definition of measured parameters (Ө1, Ө2, H1, H2, Z, Td, Bd & Th) in the text.

The limbs of Type-1 intrusions display dips (Ө1, Ө2) ranging from 2 – 30° with a mean dip value of 18°± 1°. The height or vertical extent (H1, H2) of the limbs range from 24 – 124 m; the top diameter/upper width/maximum horizontal extent (Td) of the intrusions ranges from 239 – 1265 m with a mean value of 702 m, while the base diameter/ lower width/minimum horizontal extent (Bd) of the intrusions ranges from 62 – 727 m with a mean value of 178 m (Table 4.6, Appendix B.1). Type-2 intrusions display dips (Ө1, Ө2) ranging from 7 – 30° with a mean dip value of 17°; height or vertical extent (H1, H2) ranging from 56 – 127 m; top diameter of 687 – 1739 m with a mean value of 1047 m; base diameter of 289 – 1006 m with a mean value of 548 m, and thickness (Th) ranging from 35 – 78 m with a mean value of 61 m (Table 4.6, Appendix B.1).

To establish a link between some of the measured geometrical parameters, cross-plots of the Paleocene – Early Eocene (CSU-1) average intrusion dips have been plotted against the average limb height/vertical extent (H) and top diameter/upper width (Td), while the

average limb height was also plotted against the top diameter/upper width (Fig. 4.24). The plots indicate a very poor correlation (R^2 = 0.02 to 0.04) exists between dip and top diameter of both Type-1 & 2 Paleocene intrusions (Fig. 4.24a). In addition, a weak correlation (R^2 = 0.10 to 0.22) is observed between intrusion dip and height for both intrusion types (Fig. 4.24b). Finally, there appears to be a similar weak relationship (R^2 = 0.18 to 0.20) between height and top diameter (Fig. 4.24c), which implies that the shortness or tallness of an intrusion do not necessarily determine its top diameter/lateral extent.

ii) Geometrical variability of Eocene (CSU-2) intrusions

The sand intrusions found within the CSU-2 unit also comprise of Type-1 & -2 intrusions with Type-1 intrusions forming the predominant intrusion type (see Fig. 4.11). The intrusions were observed to be distributed mainly in the western, north-east, and north-western parts of the study area and are rarely found in the eastern and central part (Table 4.5). Measurement of geometrical parameters of fifty-eight (58) injectites was taken comprising of forty-nine (49) Type-1 and nine (9) Type-2 intrusions.

The limbs of Type-1 intrusions display dips (Ɵ1, Ɵ2) ranging from 10 – 30° with a mean dip value of 20 ± 1°; height/vertical extent (H1, H2) ranging from 33 – 226 m; top diameter/upper width (Td) ranging from 303 – 2118 m with a mean value of 707m; base diameter/lower width (Bd) ranging from 60 – 483 m with a mean value of 129 m (Table 4.6, Appendix B.1). However, the wings/marginal dikes of Type-2 intrusions display dips ranging from 10 – 30° with a mean value of 19 ± 2°, vertical extent ranging from 33 – 85 m, upper width ranging from 560 – 3294 m with a mean value of 1063 m, lower width ranging from 255 – 1834 m with a mean value of 610 m and thickness (Th) ranging from 34 – 99 m with a mean value of 49 m (Table 4.6, Appendix B.1). Cross-plot of their measured geometrical parameters show similar relationship as that obtained for the Paleocene (CSU-1) intrusions, and the variability in the intrusion types explains the scatter in these plots (Fig. 4.25). The cross plots also indicate a very poor correlation (R^2 = 0.04 to 0.06) exist between dip and top diameter for both Eocene intrusion types (Fig. 4.25a), while similar correlation (R^2 = 0.02 to 0.05) exist between their dip and height (Fig. 4.25b). However, the Type-1 intrusions show a moderate correlation (R^2 = 0.40) between intrusion height and top diameter, while Type-2 intrusions show extremely poor correlation (R^2 = 0.002) between both parameters (Fig. 4.25c).

Table 4.5: Summary description of intrusion types with their spatial distribution, cross sectional geometries and plan view geometry within the Cenozoic seismic units (CSU-1, CSU-2 & CSU-4).

Seismic units	Age	Intrusion type present	Spatial distribution	Cross-sectional geometry	Plan view geometry	Host rock deformation	Study area map view distribution
CSU-7/8/9	Pliocene to Pleistocene	Not present					
CSU-6	Miocene	Sand extrudites	Distributed above the MMU in the central and eastern part of the study area	Mounded and anticlinal geometry	Circular	Onlap , downlap & truncations against the mounds	
CSU-5	Miocene	No present					
CSU-4	Oligocene	Type 1 – 3	Distributed throughout the study area with most of the intrusions lying immediately above the Opal-A/CT diagenetic boundary. Type-2 & 3 intrusions are the most abundant within this interval	U, V, W, wing-like/saucer/flat-bowl shaped, irregular to complex-shaped discordant and concordant high amplitude anomalies	Circular to sub-circular, oval to elliptical, and irregular	Forced-folds, domal folds, mounded top and jack-up of overburden above the intrusion. Host rock intensely deformed by intrusions	
CSU-3	Oligocene	Not present					
CSU-2	Eocene	Type 1 & 2	Distributed mainly in the western, NE & SW parts of the study area and are rarely or not found at the basin centre and eastern parts. Type-1 intrusions are the most predominant.	U, V, W and saucer/flat-bowl shaped discordant and concordant high amplitude anomalies	Circular to sub-circular, oval to elliptical	Forced-folds and jack-up of overburden above the intrusion. Host rock intensely deformed by intrusions	
CSU-1	Paleocene to Early Eocene	Type 1 & 2	Restricted to the eastern and north-eastern part of the study area along the basin margin. Type-1 intrusions are the most common.	Symmetrical/asymmetrical conical and flat-bowl shaped discordant high amplitude anomalies with V/W and wing-like shapes	Circular to sub-circular, oval to elliptical	Forced-folds and jack-up of overburden above the intrusion	

iii) Geometrical variability of Oligocene (CSU-4) intrusions

The sandstone intrusions observed within the CSU-4 unit comprises of Type-1 to Type-3 intrusions which are distributed almost throughout the study area, with most of them occurring just above the Opal-A/CT diagenetic boundary (common datum e.g., Fig. 4.17c & 4.18d). The CSU-4 unit is predominantly occupied by Type-2 and Type-3 intrusions occurring in combination with polygonal faults.

Measurements of geometrical parameters for sixty-five (65) injectites were taken, comprising of forty-four (44) Type-1 intrusions and twenty-one (21) Type-2 intrusions. The limbs of Type-1 intrusions display dips (Θ_1, Θ_2) ranging from 7 – 30°; intrusion height (H1, H2) of 29 – 196 m; upper width (Td) ranging from 309 – 1650 m with a mean value of 771 m; lower width (Bd) ranging from 41 – 959 m with a mean value of 123 m. While the wings of Type-2 intrusions display dips ranging from 10 – 30°; intrusion height of 48 – 176 m; upper width of 468 – 3264 m with a mean value of 1340 m and base diameter of 199 – 2336 m with a mean value of 730 m and thickness (Th) between the top and base reflection ranging from 23 – 128 m with a mean value of 56 m (Table 4.6, Appendix B.1). Cross plots of key geometrical parameters are shown in Fig. 4.26. The plots show a very poor correlation (R^2 = 0.01 to 0.05) exist between dip and top diameter which is consistent with that observed for the Paleocene and Eocene intrusions (Fig. 4.26a). A weak correlation (R^2 = 0.15 to 0.24) is also observed between dip and height for both intrusion types (Fig. 4.26b). Finally, Type-1 intrusions show a weak correlation (R^2 = 0.26) between height and top diameter while Type-2 intrusions show a moderate correlation (R^2 = 0.56) exist between both parameters (Fig. 4.26c).

Fig. 4.27a shows an illustration of the frequency of occurrence for specific range of dip values for both Type-1 and Type-2 intrusions, while Fig. 4.27b also shows the frequency of occurrence of specific range of dips within the Paleocene – Early Eocene (CSU-1), Eocene (CSU-2) and Oligocene (CSU-4) seismic units. The above conclusively illustrated that there are more sand intrusions with their limbs/wings dipping between 11 – 20°. The measured geometrical parameters shown in Appendix B.1 may be useful as input parameters when modelling the emplacement of sand injectite in the subsurface and gives a clue about attainable scale and simple to complex geometries of the intrusions.

Table 4.6: Summary of values obtained for geometrical measurements taken for Type-1 & 2 sandstone intrusions. See text and Appendix B.1 for details on how the values were derived.

Age	CSU	Intrusion type	Range of measured geometrical parameters					No. of intrusions measured
			Limb true dip (○)	Height H(m)	Top diameter Td(m)	Base diameter Bd(m)	Thickness Th(m)	
Pal. - Early Eocene	CSU-1	Type-1	2- 30	24 – 214	239 – 1265	62 – 727	-	33
		Type-2	7 - 30	56 - 127	687 - 1739	289 - 1006	35 - 78	11
Eocene	CSU-2	Type-1	10 - 30	33 – 226	303 - 2118	60 – 483	-	49
		Type-2	10 - 30	33 – 85	560 - 3294	255 – 1834	34 - 99	9
Oligocene	CSU-4	Type-1	7 - 30	29 - 196	309 – 1650	41 – 959	-	44
		Type-2	10 - 30	48 - 176	486 - 3264	199 - 2336	23 - 128	21
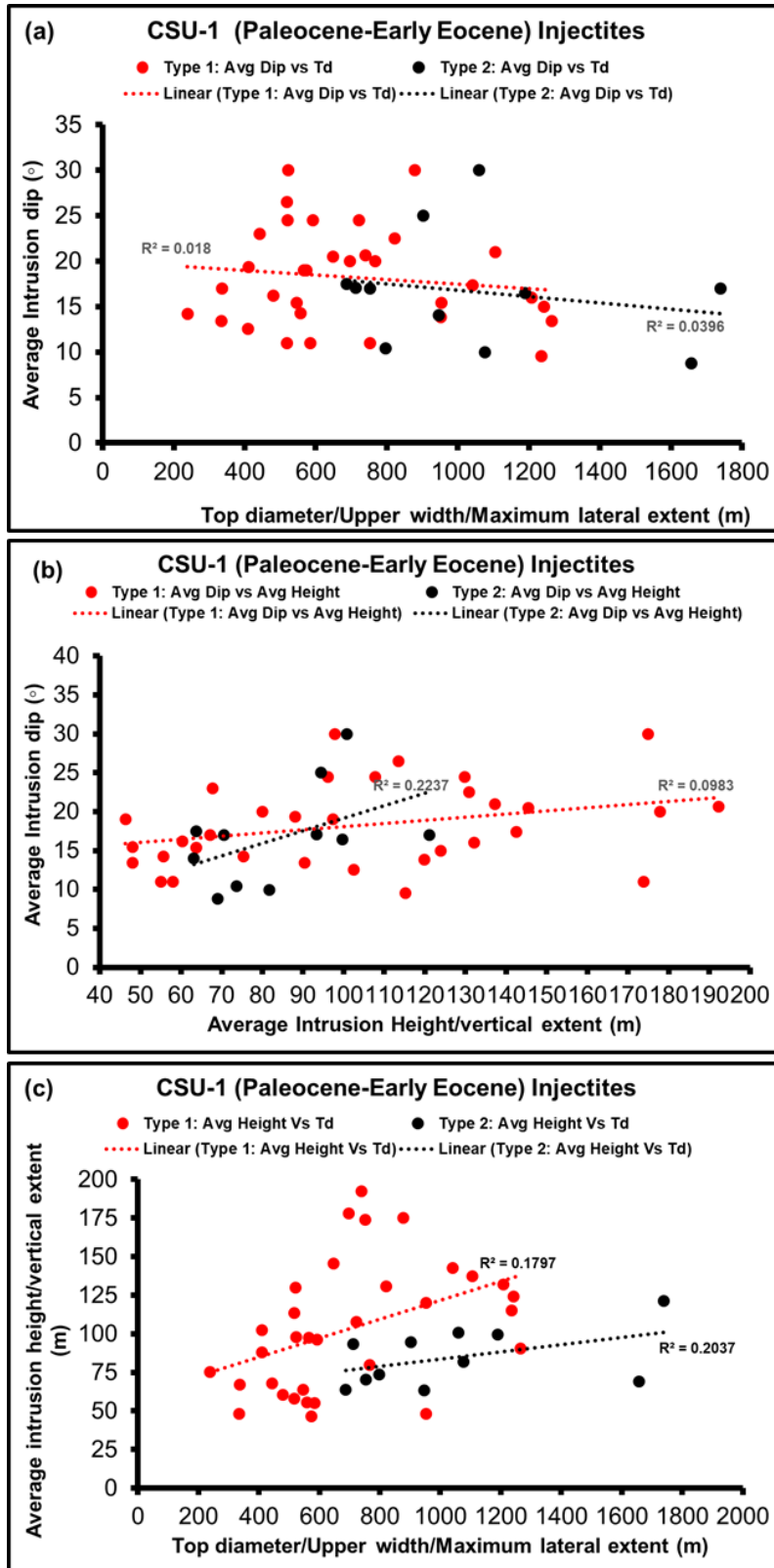
Fig. 4.24: Cross-plot of geometric parameters associated with Type-1 and Type-2 sandstone intrusions in the Paleocene – Early Eocene (CSU-1) interval. Red circles and red dotted trend line are associated with measurements for Type-1 (conical) intrusions while the black circles and black dotted trend line are associated with measurements for Type-2 (wing-like) intrusions. See text for full discussion and Appendix B.1 for the plotted values.
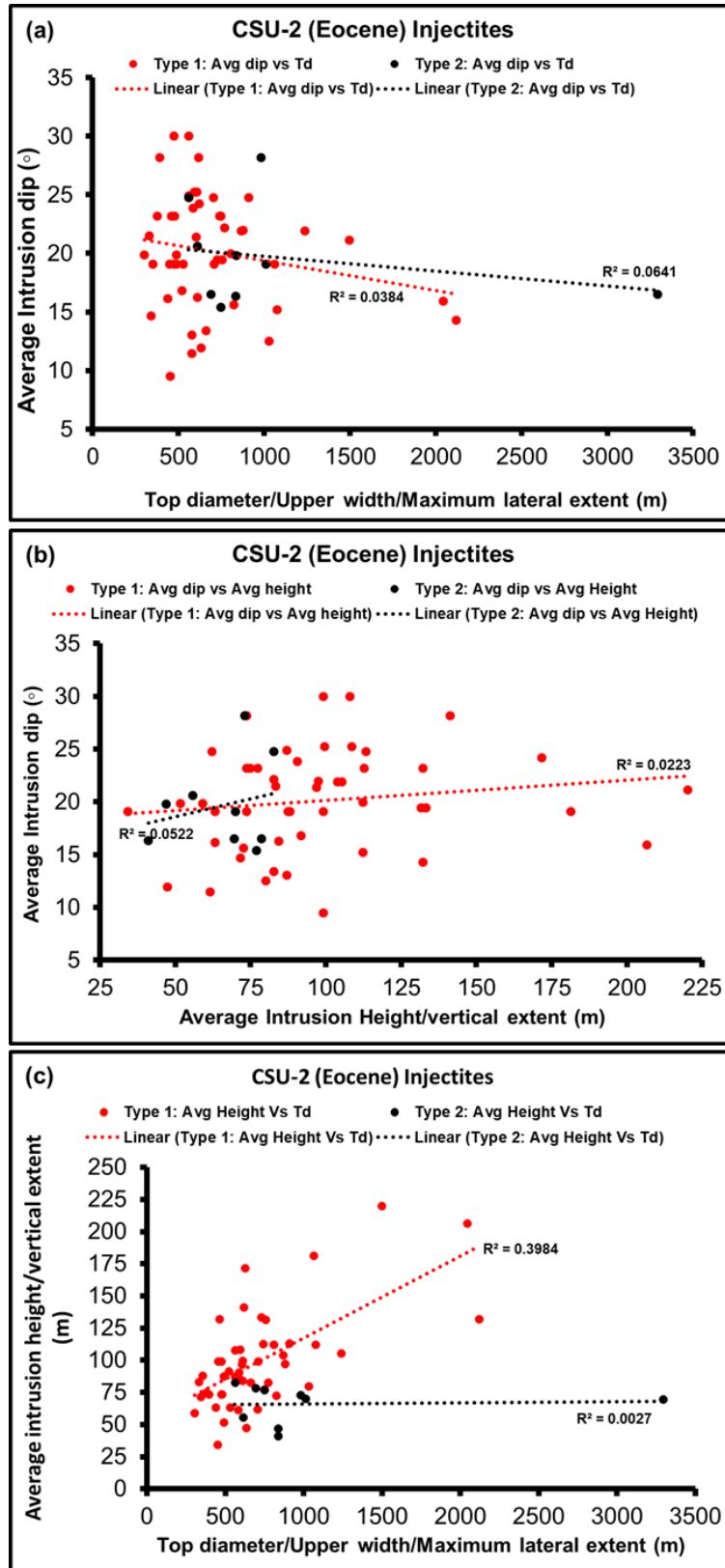
Fig. 4.25: Cross-plot of key geometric parameters associated with Type-1 and Type-2 sandstone intrusions in the Eocene (CSU-2) interval. Red circles and red dotted trend line are associated with measurements for Type-1 (conical) intrusions while the black circles and black dotted trend line are associated with measurements for Type-2 (wing-like) intrusions. See text for full discussion and Appendix B.1 for the plotted values.
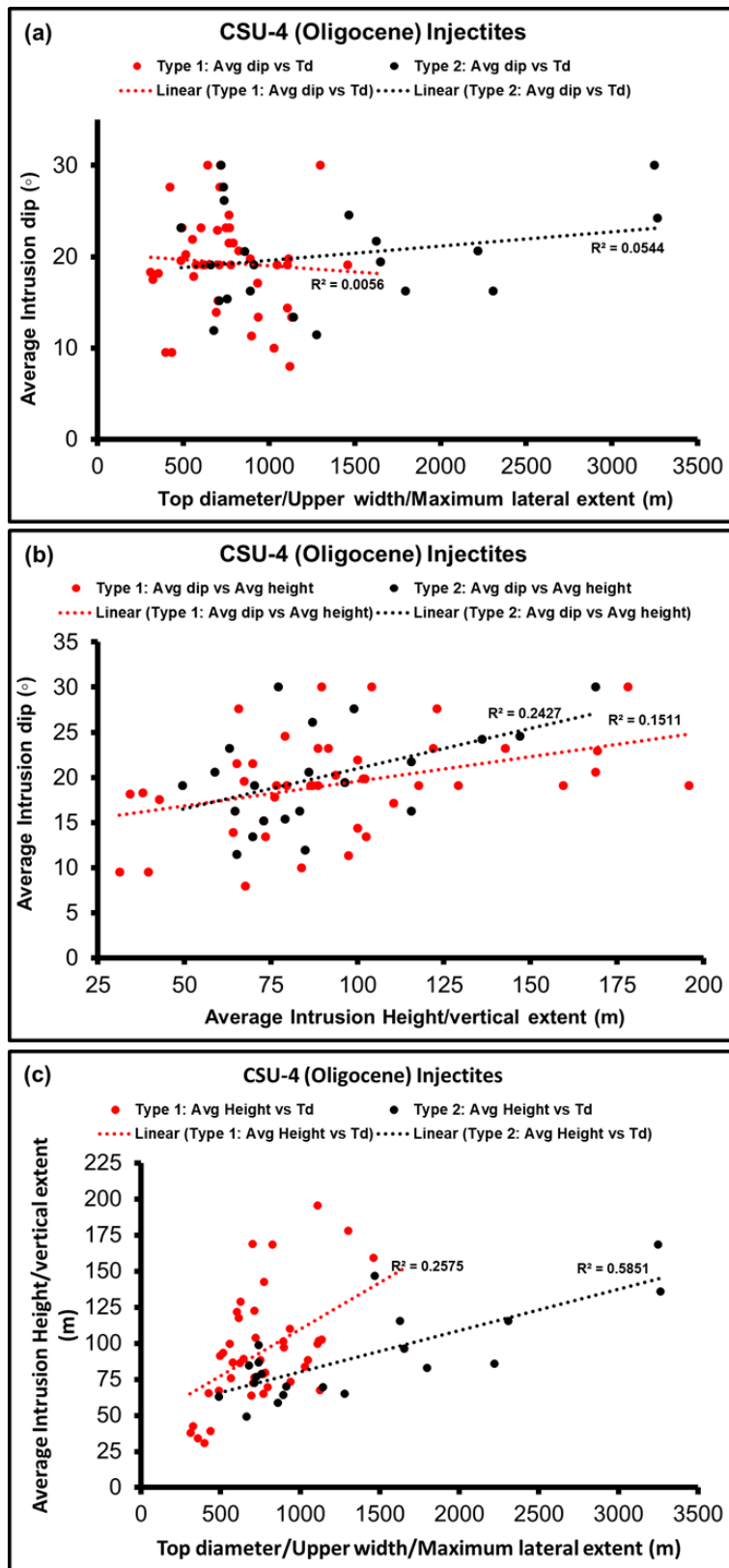
Fig. 4.26: Cross-plot of key geometric parameters associated with Type-1 and Type-2 intrusions within the Oligocene (CSU-4) succession. Red circles and red dotted trend line are associated with measurements for Type-1 (conical) intrusions while the black circles and black dotted trend line are associated with measurements for Type-2 (wing-like) intrusions. See text for full discussion and Appendix B.1 for the plotted values.
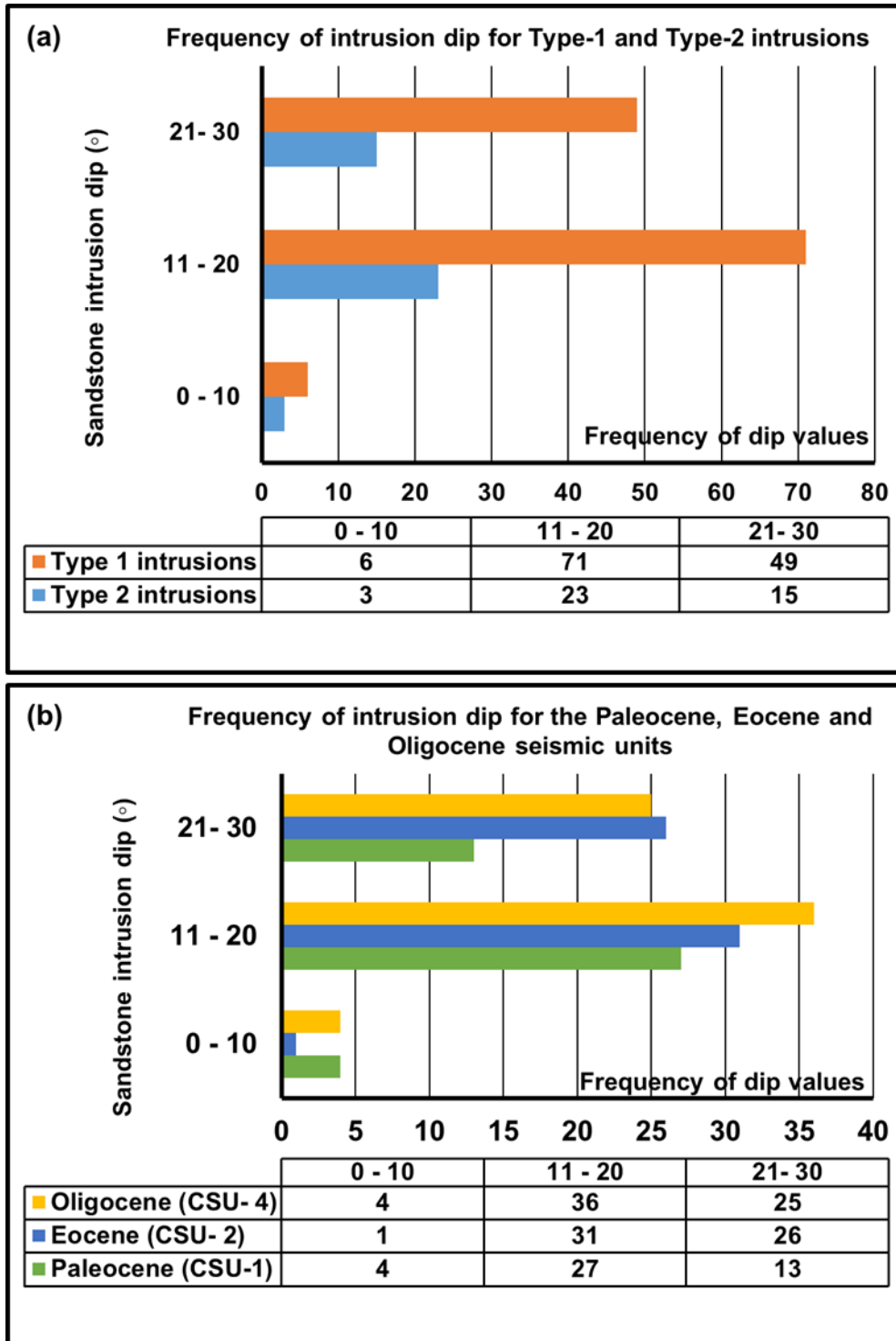
Fig. 4.27: Dip distribution of sandstone intrusions in the northern North Sea Basin based on Type-1 and Type-2 intrusion styles. (a) A histogram showing the frequency of occurrence for specific range of dip values for both intrusion types. (b) A histogram showing the frequency of occurrence of specific range of dip values for sandstone intrusions within the Paleocene – Early Eocene (CSU-1), Eocene (CSU-2) and Oligocene (CSU-4) seismic units. Both plots shows that majority of the intrusions have dip values in the range 11 – 20°.

4.5 Discussion

4.5.1 Location of source sands

Identifying and constraining the parent source sand bodies for the observed intrusions injected into the Paleocene (Vale & Lista Fm.), Eocene (Horda Fm.) and Oligocene (Lark Fm.) mudstones is a bit challenging because a first-hand requirement for injection to occur is the occurrence of a deep-water sedimentary system characterized by unconsolidated source sand bodies encased in low permeable sealing mudstones (Lonergan et al., 2000; Huuse and Mickelson, 2004; Huuse et al., 2007; Braccini et al., 2008). Well calibration have confirmed the presence of tens-of-meters of sandstone which may imply that part or the whole of an initial depositional sand body may have undergone intense remobilization and injection resulting to the modification of their original depositional geometries. Therefore, we suggest that the conical (V/W)-shaped intrusions are injected sand bodies which may be linked to depositional sand bodies at their apexes or fed by much deeper underlying sand bodies; while the U-shaped and wing-like intrusions may represent in-situ depositional sand bodies subjected to post-depositional remobilization and injection leading to the formation of their marginal wings (Lonergan and Cartwright, 1999; Lonergan et al., 2000; Huuse et al., 2004; Safronova et al., 2012; Andresen and Clause, 2014; Monnier et al., 2014; Andresen et al., 2019).

i) Paleocene – Early Eocene (CSU-1) intrusions: based on observation and spatial distribution of the studied intrusions, the CSU-1 injectites which are restricted to the eastern and north-eastern part of the study area are suggested to be sourced by the Paleocene sand-rich channel-fills and fans found in that area deposited by sediment gravity flows processes (Fig. 4.7 & 4.8). Previous and recent studies (e.g., Ahmadi et al., 2003: see their Fig. 14.5 & 14.9; Brunstadt et al., 2009; Dmitrieva et al., 2012, 2018; Sømme et al., 2019) have documented the existence of sand-rich, deep-marine depositional systems comprising of series of sand-rich channel-fills and large stacked submarine fans developed in a slope to proximal basin-floor settings along the eastern margin of the North Sea Basin during the Early Tertiary (i.e., Paleocene) uplift along basin margins. The location (Quadrant 35) of the sand intrusions coincides with the spatial and temporal distribution of deep-water sandstones described in detail by Dmitrieva et al., (2012: their Fig. 7 – 14; 2018: their Fig. 9 – 13), which were documented to be associated with high-amplitude reflections characterized by channel-like packages, sheet-like packages of reflection and discordant amplitude reflections. All the above reflection characteristics were also observed in cross-section (Fig. 4.7 & 4.28) in the north-eastern part of the study area and well data confirms the presence of 20 – 100 m thick sandstones which gives credence to the interpretation that the source sands for the CSU-1 intrusions are the Paleocene sandstones of the Sotra and Egga Sandstone Members (Fig. 4.28; also see Dmitrieva et al., 2012: see their Fig. 3) sourced from the Norwegian mainland. Both sand intervals are suggested to have undergone large scale

remobilization and injection leading to the modification of their initial depositional geometries.

Alternative source sands from the underlying Cretaceous succession have also been considered based on suggestions by some authors (e.g., Huuse et al., 2004; Szarawarska et al., 2010; Wild and Briedis, 2010) that the Paleocene – Eocene sands in the central part of the northern North Sea do not represent sediment gravity flow deposits but represent sandstone laccoliths which were intruded/injected in the subsurface (Dmitrieva et al., 2012). However, this is very unlikely because the Paleocene sandstones overlie thick Cretaceous mud-dominated successions (Jorsalfare & Kyrre Formations). The next reasonably thick potential source sand unit lie either in the Lower Kyrre Formation (in Quadrant 35) documented as remobilized slope channel and fan complexes by Jackson (2007) and Jackson et al. (2011) or within the middle Jurassic Brent Group (Dmitrieva et al., 2012). In both cases, the deeply buried sands lie beneath thick mudstone successions and are therefore presumed to be well lithified prior to the emplacement of the Paleocene sandstones intrusions.

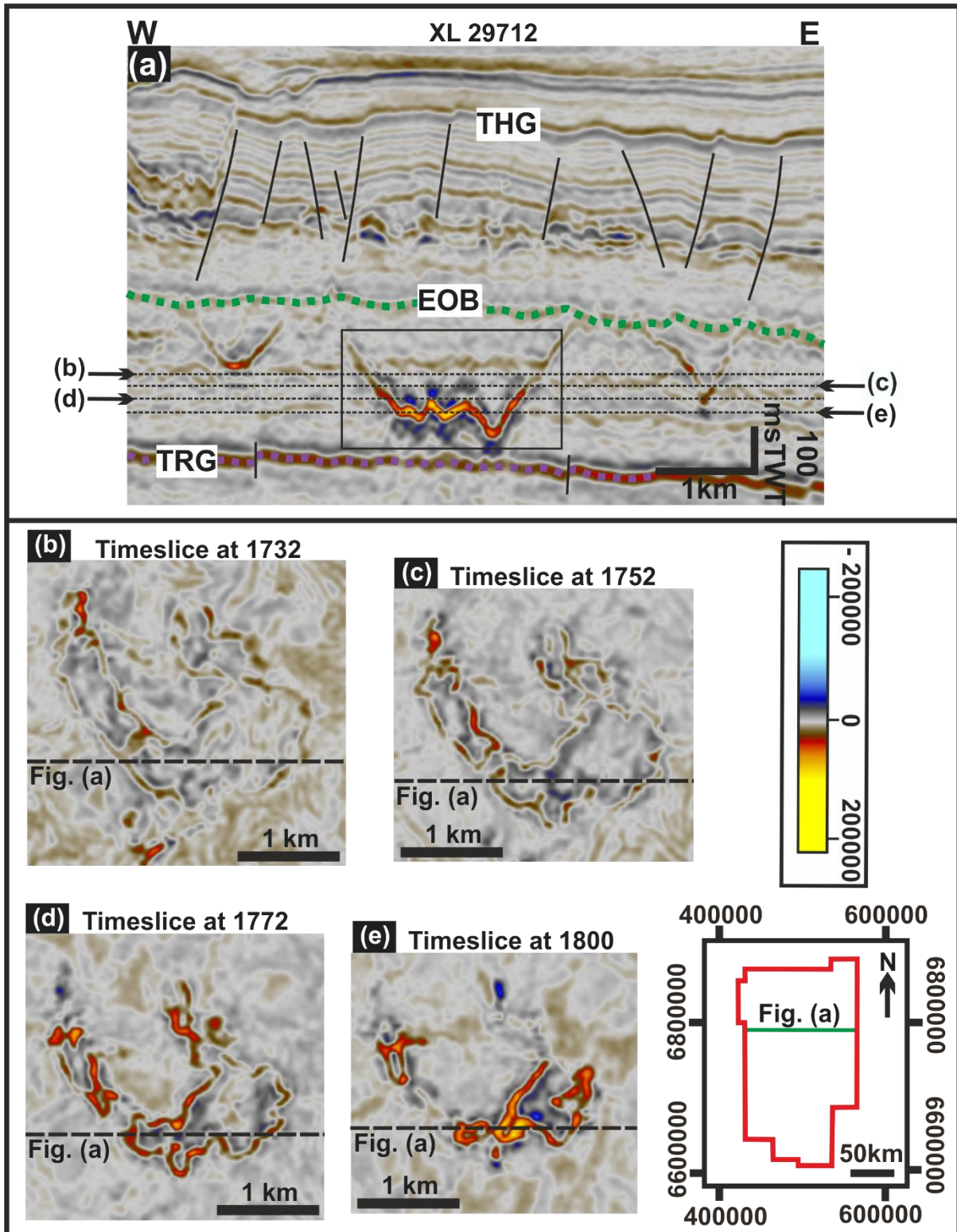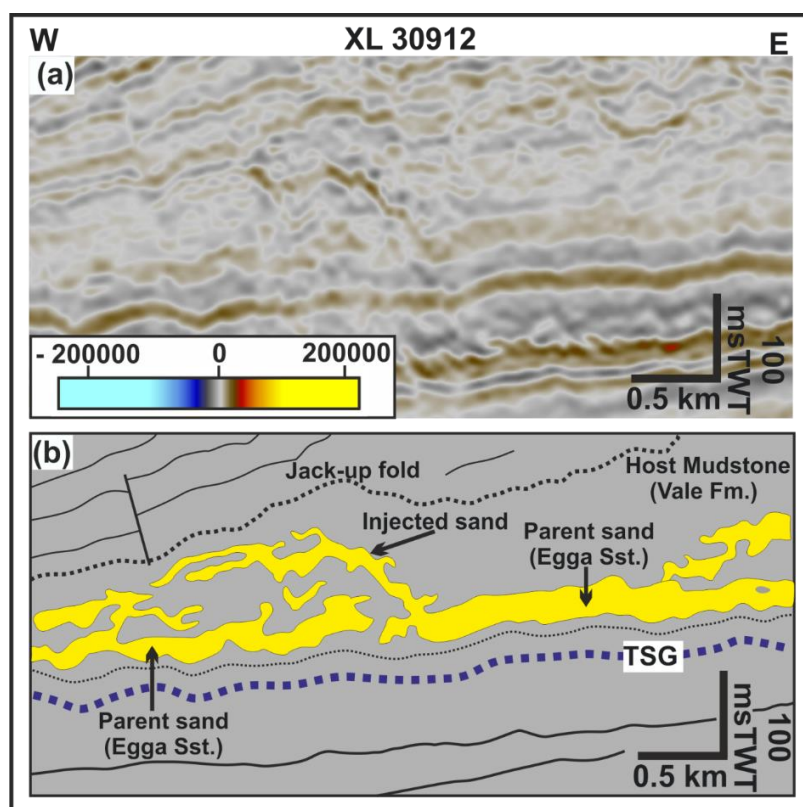**Fig. 4.28:** (a) East-west oriented seismic section showing the occurrence of discordant amplitude anomaly within the Paleocene – Early Eocene (CSU-1) interval just above the Top Shetland Group. (b) Simplified interpretation of the location of the potential parent fan sand (Egga Sandstone Member) and the resultant sand intrusion, injected into the host mudstone strata (Vale Fm.). Also, present is the associated jack-up of the overburden above the intrusion. See Fig. 4.29 for location of seismic line. TSG: Top Shetland Group. Seismic data courtesy of CGG.
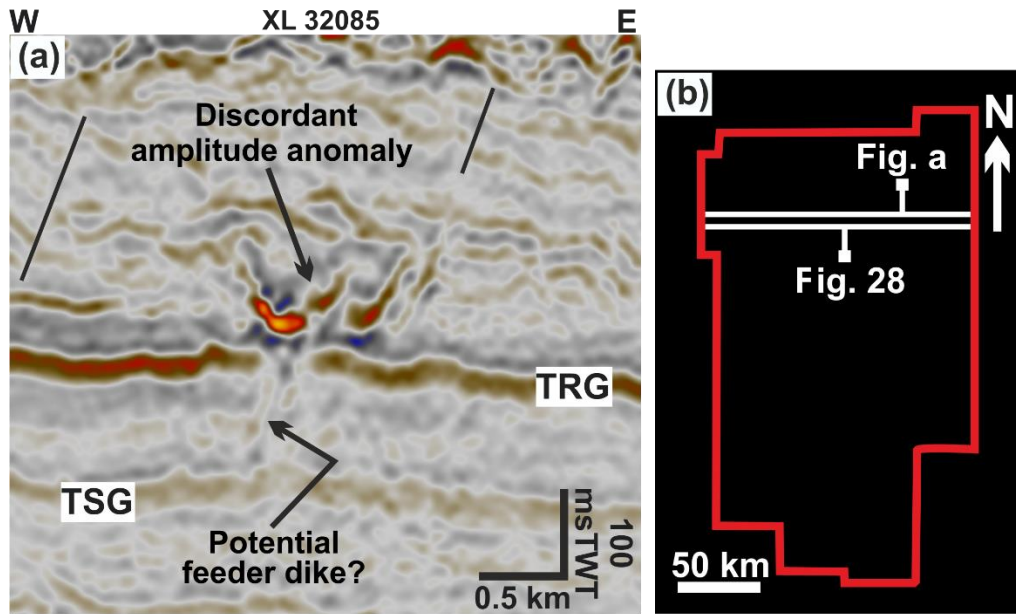
Fig. 4.29: Potential feeder dike within the Upper Paleocene which is suggested to have sourced the overlying isolated Eocene sand intrusion. This may support our interpretation that some isolated Eocene (CSU-2) sand intrusions recorded at far distances (10 – 20 km) away from the Eocene submarine fan A to C may have been sourced from Upper Paleocene parent depositional sands. TRG: Top Rogaland Group, TSG: Top Shetland. Seismic data courtesy of CGG.

 ii) Eocene (CSU-2) intrusions: seafloor spreading in the Early Eocene time related to the opening of the Norwegian-Greenland Sea and North Atlantic brought about compression in the North Sea which in turn led to uplift along basin margins (Knott et al., 1993; Hartog Jager et al., 2003; Jones et al., 2003). This uplift led to the deposition of several hundred meters of deep submarine-fans and hemi-pelagic sediments in the depocentres of the Viking and Central graben, sourced from the East-Shetland Platform and the Scottish Highlands in the west, and the Norwegian mainland in the east (Jordt et al., 2000; Faleide et al., 2002; Jones et al., 2003). A greater number of the submarine fan systems deposited in the early Eocene were deposited as localised fans while that of the mid – late Eocene were more channelized (Jones et al., 2003). These Eocene sand-rich systems belong to the Frigg Sandstone Member and the Grid Sandstone Member of the Horda Formation (Deegan and Scull, 1977; Knox and Holloway, 1992). The presence of numerous discordant high amplitude anomalies within the CSU-2 and their calibration to sandstones suggest that part of these Eocene sandstones may have undergone large-scale remobilization and injection into their host Horda Formation mudstones. We suggest that the Eocene sandstone intrusions distributed in the western and south-western parts of the study area were sourced by the Frigg fan (i.e., Fan-C: comprising of Frigg Sandstone Member) classified as a sand-rich, point-sourced submarine fan deposited in the south-western part of the study area (see Fig. 4.16; Jones et al., 2003). This is because the distribution pattern of the discordant anomalies connects to the top of the sand-rich fan (see Fig. 4.16). While the Eocene sand intrusions in the north-eastern part are thought to be derived from submarine Fan-A and Fan-B described previously within the

CSU-2 unit due to observation of discordant high amplitude anomalies at the toe of the fans (see Fig. 4.15).

Some Eocene sand intrusions are however recorded at distances of up to 10 – 20 km away from the edges of the submarine fans and as such we can say the distribution of the sand intrusions do not completely match the extent of the Lower – Middle Eocene fans (Bureau et al., 2013). It is therefore, suggest that these isolated intrusions may have been sourced either by: (i) lateral migration of fluidized sands (e.g. Shoulders et al., 2007; Bureau et al., 2013); (ii) from Upper Paleocene parent depositional sand bodies (see Fig. 4.29, Huuse and Mickelson, 2004: their Fig. 1; Olobayo, 2014: their Fig. 4.14g); (iii) from isolated Lower to Middle Eocene sand bodies (see Jones et al., 2003: their Fig. 15.8) deposited in the western basin margin and the basin centre which may not be well imaged on seismic data but are identified in wireline log data in quadrant 34 (see Fig. 4.30); and (iv) from isolated channel-shaped anomalies which are abundant in the south and south-western part of the study area within the Lower Eocene, as well as in the northern part and basin centre within the Upper Eocene.

Further analysis (e.g., heavy mineral provenance studies/analysis, fluid inclusion analysis, garnet geochemical analysis, see Hurst et al., 2017) of sandstone samples from the intrusions and potential parent sand bodies will provide additional clue to the source sand for the intrusions within the CSU-2.

iii) Oligocene (CSU-4) intrusions: post-Eocene uplift along basin margins led to the deposition of sand-rich sediments into the North Sea (Fyfe et al., 2003; Rundberg and Eidvin, 2005). The Early – Late Oligocene saw the deposition of gravity flow sands into the northern North Sea sourced mainly from the uplifted East Shetland Platform (west source area) and to a lesser degree from West Norway (east source) and South Fennoscandia (southern source). The approximate outline of these Oligocene sand depositional systems is presented in the work by Rundberg and Eidvin (2005: their Fig. 7a) and Eidvin et al. (2014: their Fig. 1) and they are documented to belong to the Skade and Uil Sandstone Members of the Lark Formation (Fyfe et al., 2003; Eidvin et al., 2014; Rundberg and Eidvin, 2016). These sandstones are difficult to map on seismic due to the very chaotic nature of the Oligocene interval in the western part of the study area but are confirmed by thick sandstone units in wireline log data (e.g., Fig. 4.30, also see Rundberg and Eidvin, 2016: their Fig. 6).

It is therefore reasonable to suggest that the sandstone intrusions within the Oligocene were sourced from the above depositional sand bodies by sediment remobilization and injection processes. In the western and southern parts of the study area were the apexes of conical (V/W)-shaped intrusions are found to lie directly above the Eocene – Oligocene boundary (EOB), some V-shaped intrusions are however observed to have their apexes emanating from or extending down into the Upper Eocene interval (Fig. 4.31) with potential

feeder dikes within the Upper Eocene (Fig. 4.32). Based on the above observations, we therefore suggest that: (i) the Oligocene intrusions distributed in the western and southern parts of the study area were sourced from the Lower and Upper Oligocene depositional sand system derived from the East Shetland Platform, in combination with some underlying Middle – Upper Eocene sandstones, and (ii) the Oligocene intrusions in the north and north-eastern part which occur in the Middle - Upper Oligocene above the Opal-A/CT boundary were sourced from a Middle – Late Oligocene sandy depositional system derived from the uplifted eastern basin margin and partly from Lower Oligocene sands due to observation of V-shaped intrusions with limbs extending across the Opal-A/CT boundary into the Upper Oligocene from the Lower Oligocene (see Fig. 4.17d).

4.5.2 Sand Intrusions and Polygonal Fault Systems

Polygonal faults and sandstone intrusions co-exist within the studied Paleogene succession in the study area; with the interval between the Paleocene - Oligocene pervasively modified by polygonal faults. The co-occurrence of both features has been reported in many cases in the subsurface e.g., Lonergan et al. (2000), Gras and Cartwright (2002), Molyneux et al. (2002), Huuse and Mickelson (2004), Jackson (2007), Shoulders et al. (2007), Szarawarska et al. (2010), and Bureau et al. (2013). This have led to the suggestion that polygonal faulting may likely control the occurrence, timing, and geometry of sand intrusions (Lonergan et al., (1998; 2000); Lonergan and Cartwright, 1999; Cosgrove and Hillier, 2000; Gras and Cartwright, 2002; Hillier and Cosgrove, 2002; Szarawarska et al. 2010). Contrary to the above, some authors (e.g., Huuse et al., 2004; Huuse and Mickelson, 2004; Bureau et al., 2013) have argued that although sand intrusions and polygonal faults may display some geometrical similarities and/or sometimes coincide in cross-section, the intrusions tend to achieve their unique and distinct geometries regardless of the presence of polygonal faults. However, the polygonal faults may be exploited by the sand intrusions in cases where they are favourably oriented and may likely form a crucial part of the feeder system by contributing to seal failure and preferential rapid transport of fluidized sands along the fault planes (Gay, 2002; Huuse and Mickelson, 2004).

Here, no close spatial relationship is observed between some of the Paleocene - Oligocene sand injectites and the polygonal faults developed in their surrounding mudstone-dominated host strata (e.g., see Fig. 4.8b & 4.15a). However, three (3) main kinds of interaction are observed: (i) a scenario where a limb/wing of an intrusion appear to be fully or partially intruded along fault plane and as such exploit the polygonal faults (Fig. 4.19b), (ii) cases where the intrusions cross-cut polygonal faults and the other way round (Fig. 4.19b), and (iii) other cases where the propagation of an intrusion limb terminates against a fault plane (Fig. 4.18b). Since no close spatial correspondence exist between the observed sandstone intrusions and polygonal faults, we therefore suggest the non-existence of a clear evidence that the polygonal faults controlled the resultant simple to complex geometries of

the intrusions, and that their co-existence is largely dependent on the rheology of the host mudstone strata (Huuse et al., 2004; Huuse and Mickelson, 2004; Szarawarska et al., 2010). A comprehensive analysis of the interaction between both features (refer to Chapter 7) will provide better insight and understanding about their co-existence within the studied interval, but this is beyond the scope of this study.

4.5.3 Timing of Injection

The ability to tie seismic to well data do not only provide proper age constrains for seismic reflection events, but also serve as a tool for addressing timing of injection and intrusion depth for clastic intrusion complexes. Previous studies (e.g., Shoulders and Cartwright, 2004; Cartwright et al., 2008; Safronova et al., 2012, Andresen and Clause, 2014) of sand intrusions have estimated timing of injection based on one or a combination of criteria (Fig. 4.33). One of such criteria is based on an indirect technique which involves the seismic stratigraphic analysis of domal folds and jack-up of overburden developed in response to hydraulic elevation of the overburden and differential compaction. This technique was introduced by Shoulders and Cartwright (2004) using the sandstone intrusions in the Faeroe-Shetland Basin as the case study. The technique is based on defining the paleo-seafloor and dating onlap of sediments onto the flanks of the forced folds (Fig. 4.33) with which an estimate of timing of injection is made (Shoulders and Cartwright, 2004; Cartwright et al., 2008). A second criterion considered is the upward termination of the upper tips of intrusion wings or limbs at a common stratigraphic datum over an extensive area, which is a common observation in the central and northern North Sea Basin (Cartwright et al., 2008). This has led to the suggestion by previous authors that this datum may represent the paleo-seafloor at the time of injection (Molyneux et al., 2002; Huuse and Mickelson, 2004). Therefore, the ability to map and date this datum can provide an indication for the timing of injection as well as the added benefit of defining the paleo-seafloor. The last criteria are the recognition of sand extrudites (or sand volcano). Authors (e.g., Molyneux (2001), Boehm and Moore (2002), Huuse et al. (2004), Hurst et al. (2006, 2011), Løseth et al. (2013)) have argued that some intrusions get to the seafloor and get vented onto the seafloor in the form of extrudite deposits. Their identification therefore helps in defining the position of the seafloor at the time of intrusion and extrusion since the seafloor at that time pre-dates the extrudites. The sediments which onlap onto the extrudites also post-date them suggesting the timing of intrusion falls between the age of the seafloor and the onlapping sediments. Nonetheless, extrudites may be difficult to recognize in the subsurface because they are not often preserved due to erosion and strong bottom currents (Hurst et al., 2006; Andresen and Clausen, 2014, Olobayo, 2014).
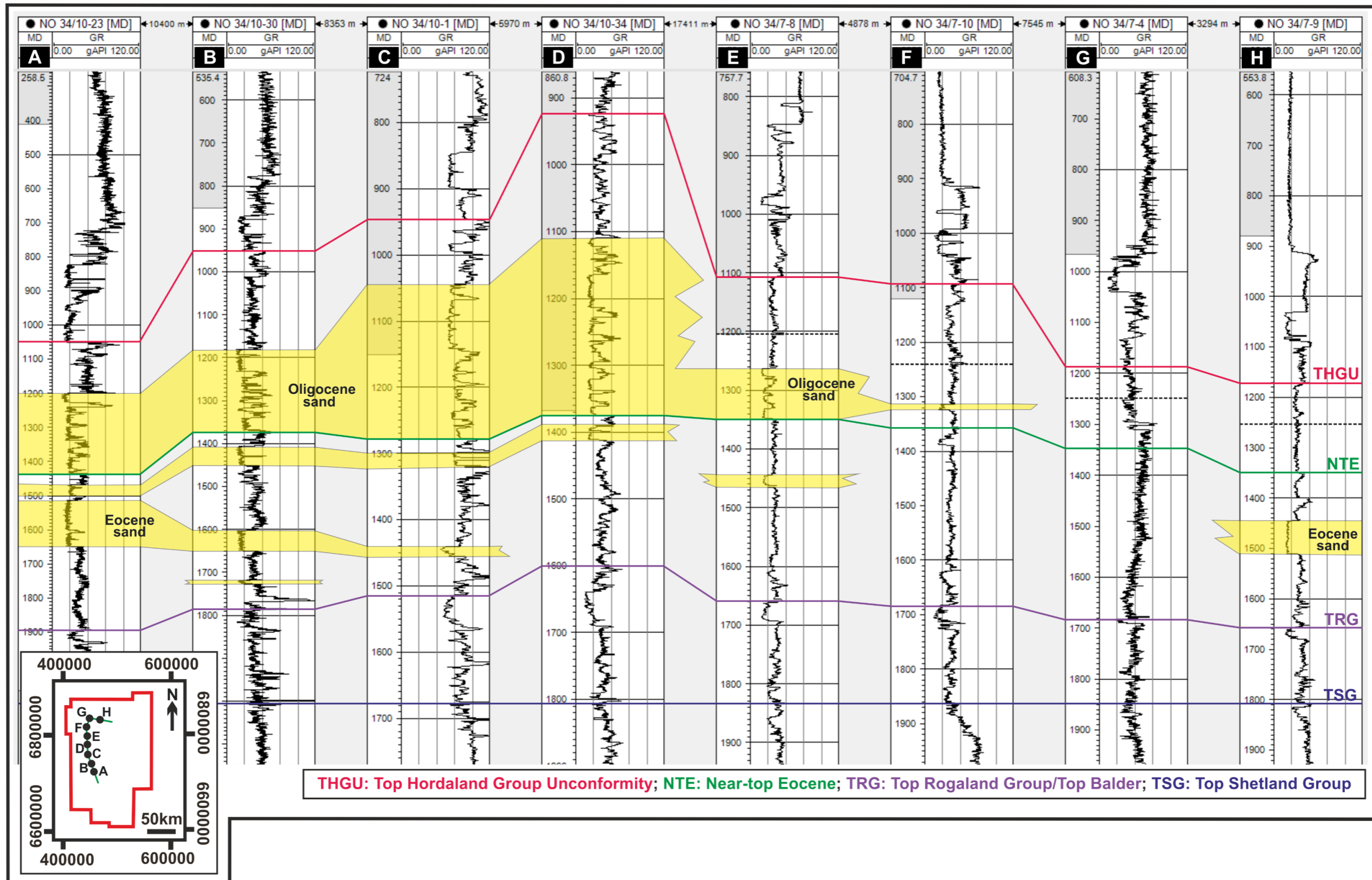
Fig. 4.30: Lithostratigraphic well log correlation diagram of the Eocene to Oligocene section in wells 34/10-23, 34/10-30, 34/10-1, 34/10-34, 34/7-8, 34/7-10, 34/7-4 and 34/7-9. The correlation indicates the distribution of Eocene and Oligocene deep-water sand bodies highlighted in yellow where they are penetrated by wells in the western part of the study area. The correlation shown is flattened at the Top Shetland Group or Base Tertiary. Wells from TGS Facies Map Browser.
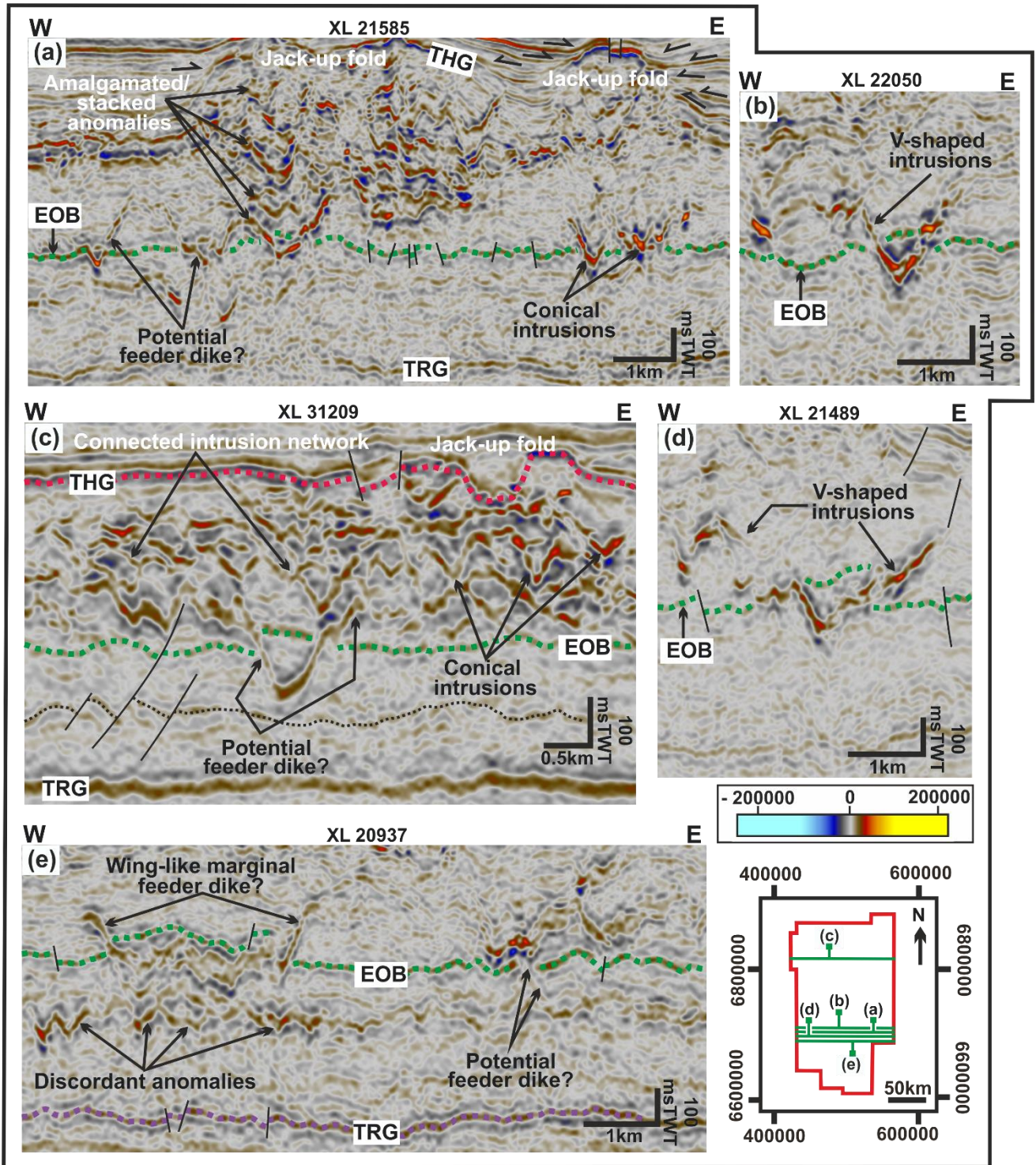
Fig. 4.31: (a) to (d) are V-shaped conical intrusions with their apexes lying within or emanating from the Upper Eocene (CSU-2) interval. (e) Wing-like intrusions interpreted to have been injected into the Oligocene (CSU-4) from Upper Eocene parent depositional sands. The injected sands with limbs across the EOB are suggested to be feeder dikes which partly sourced some of the Oligocene sand intrusions in the western and southern parts of the study area. THG: Top Hordaland Group, EOB: Eocene – Oligocene boundary, TRG: Top Rogaland Group. Seismic data courtesy of CGG.
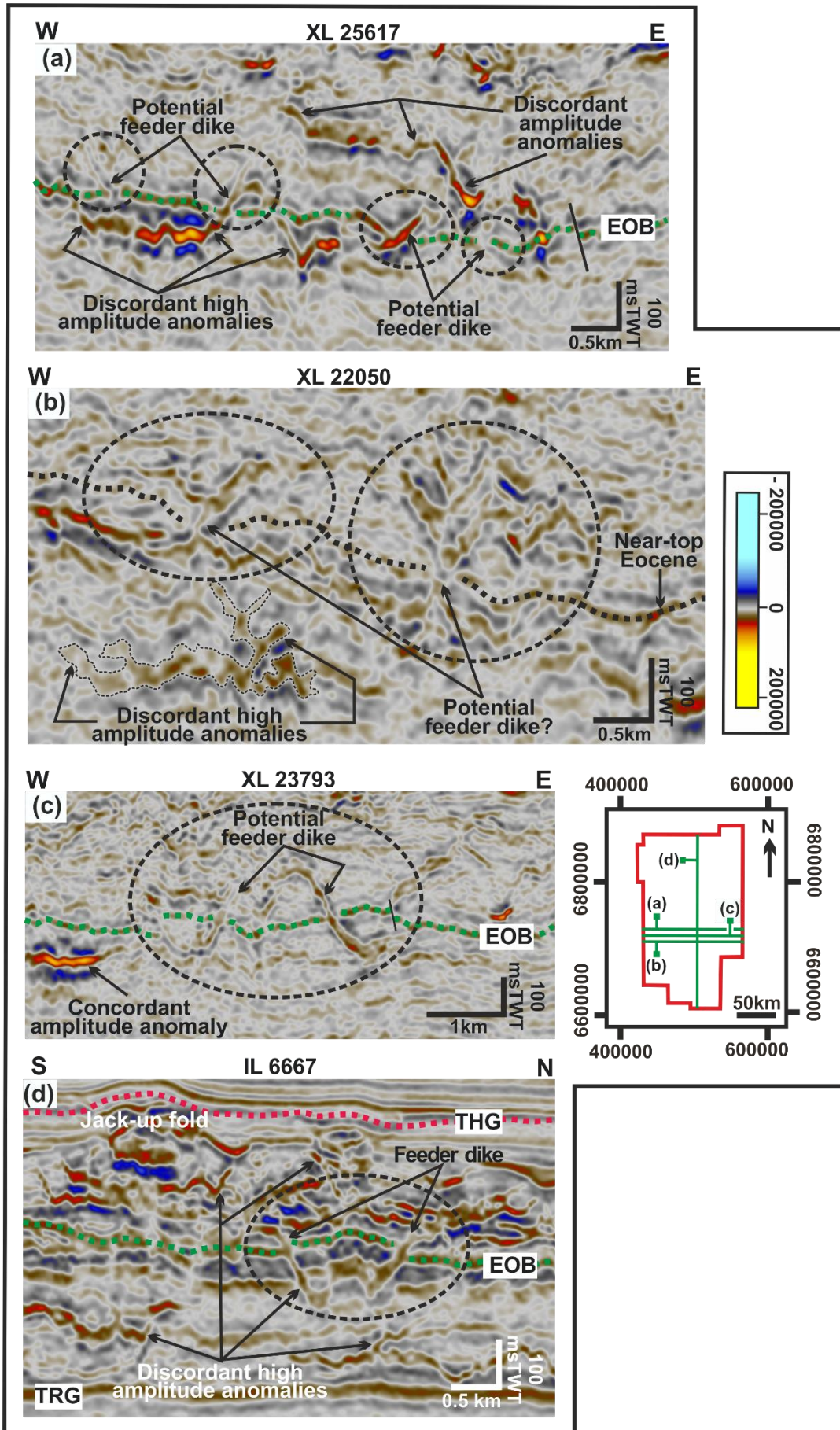
Fig. 4.32: (a) to (d) are seismic cross-sections showing potential feeder dikes emanating from the Middle - Upper Eocene (CSU-2) into the Oligocene (CSU-4) interval. We have interpreted these to represent Middle - Upper Eocene sand dikes which partly sourced some of the Oligocene sand intrusions in the western and southern parts of the study area. THG: Top Hordaland Group, EOB: Eocene – Oligocene boundary, TRG: Top Rogaland Group. See text for full discussion. Seismic data courtesy of CGG.
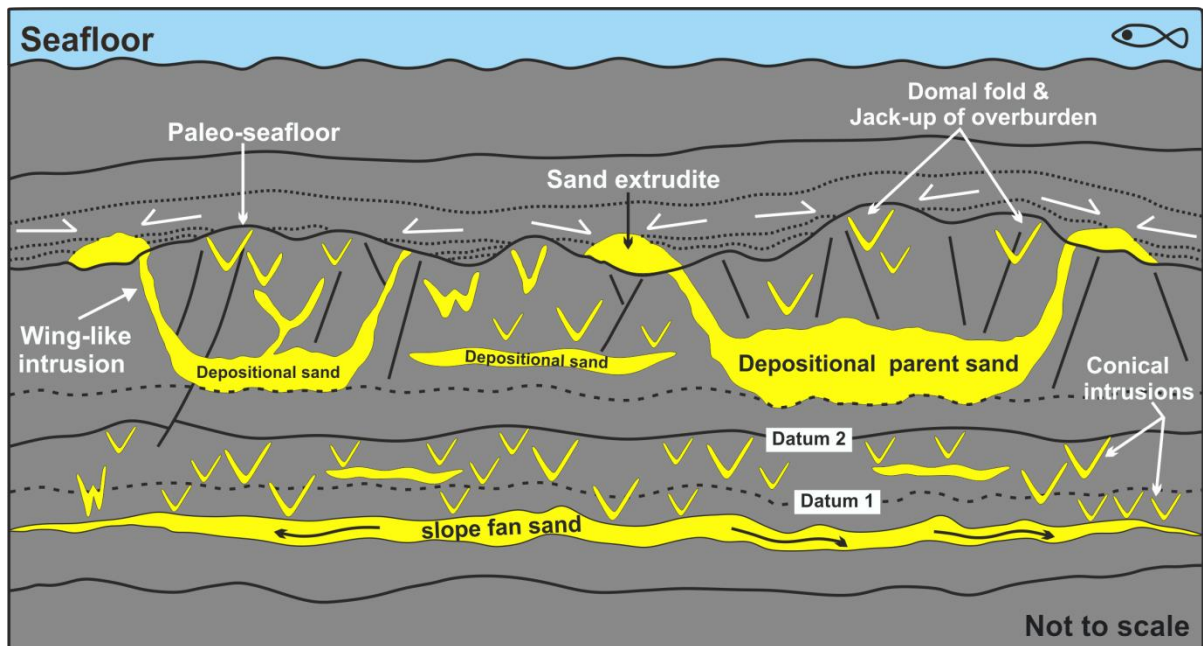
Fig. 4.33: Schematic representation of the key criteria considered in estimating timing of emplacement of sandstone intrusions: (i) seismic stratigraphic analysis of onlapping and down-lapping sediments onto domal folds and jack-up of overburden developed above the intrusions, (ii) upward termination of upper tips of intrusion limbs or wings at a common stratigraphic datum, and (iii) the recognition of sand extrudites. See text for full discussion.
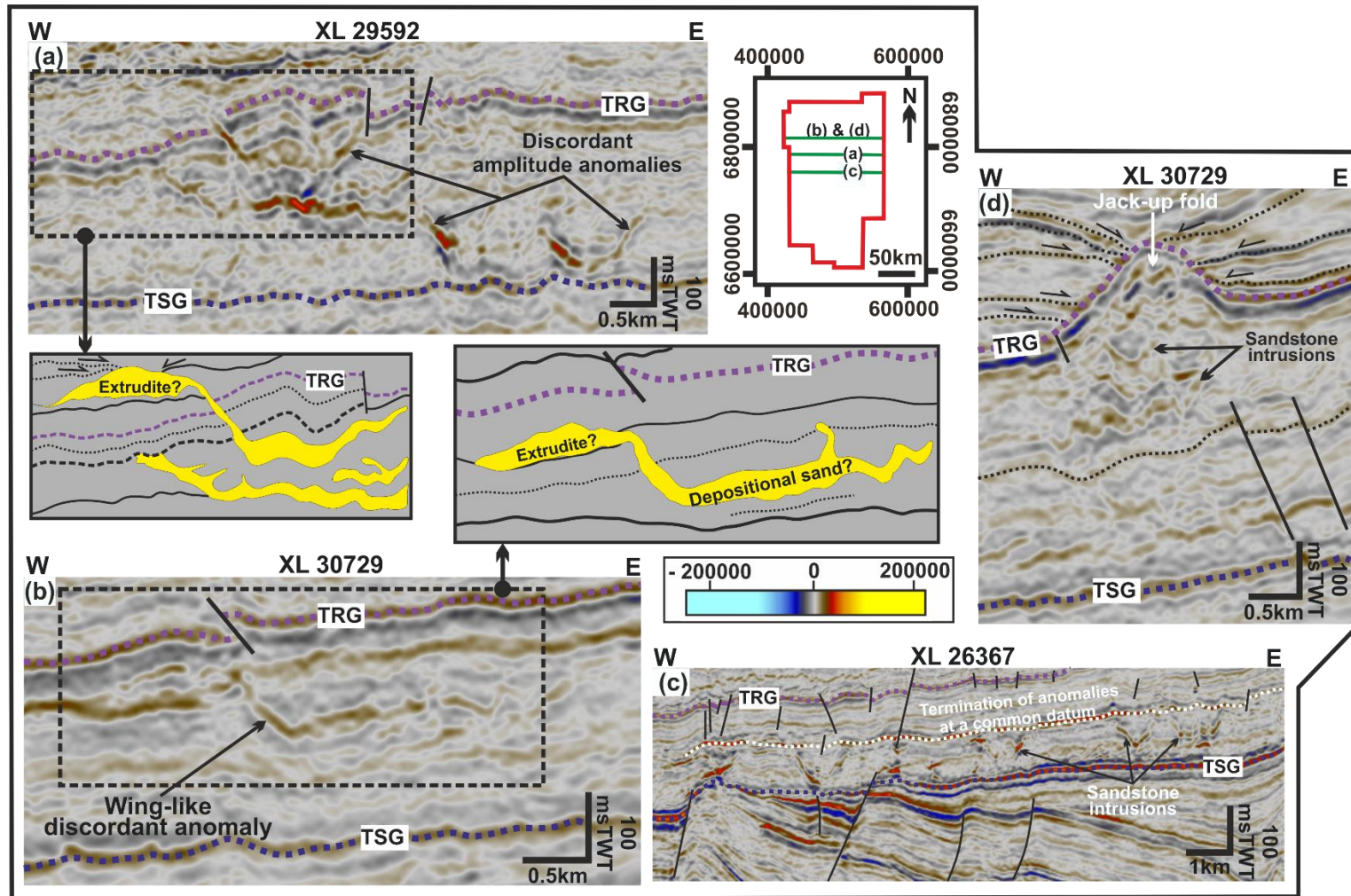
Fig. 4.34: Observations used in estimating the timing of emplacement of the Paleocene – Early Eocene (CSU-1) sandstone intrusions to have occurred in the mid/late Paleocene to Early Eocene time. (a) & (b): recognition of potential extrudites which defines the position of the paleo-seafloor at that time, (c) termination of upper tips of conical-shaped intrusions at a common datum, and (d) onlap and downlap of younger sediments onto jack-up fold above the wing-like intrusions. TRG: Top Rogaland Group, TSG: Top Shetland. Seismic data courtesy of CGG.
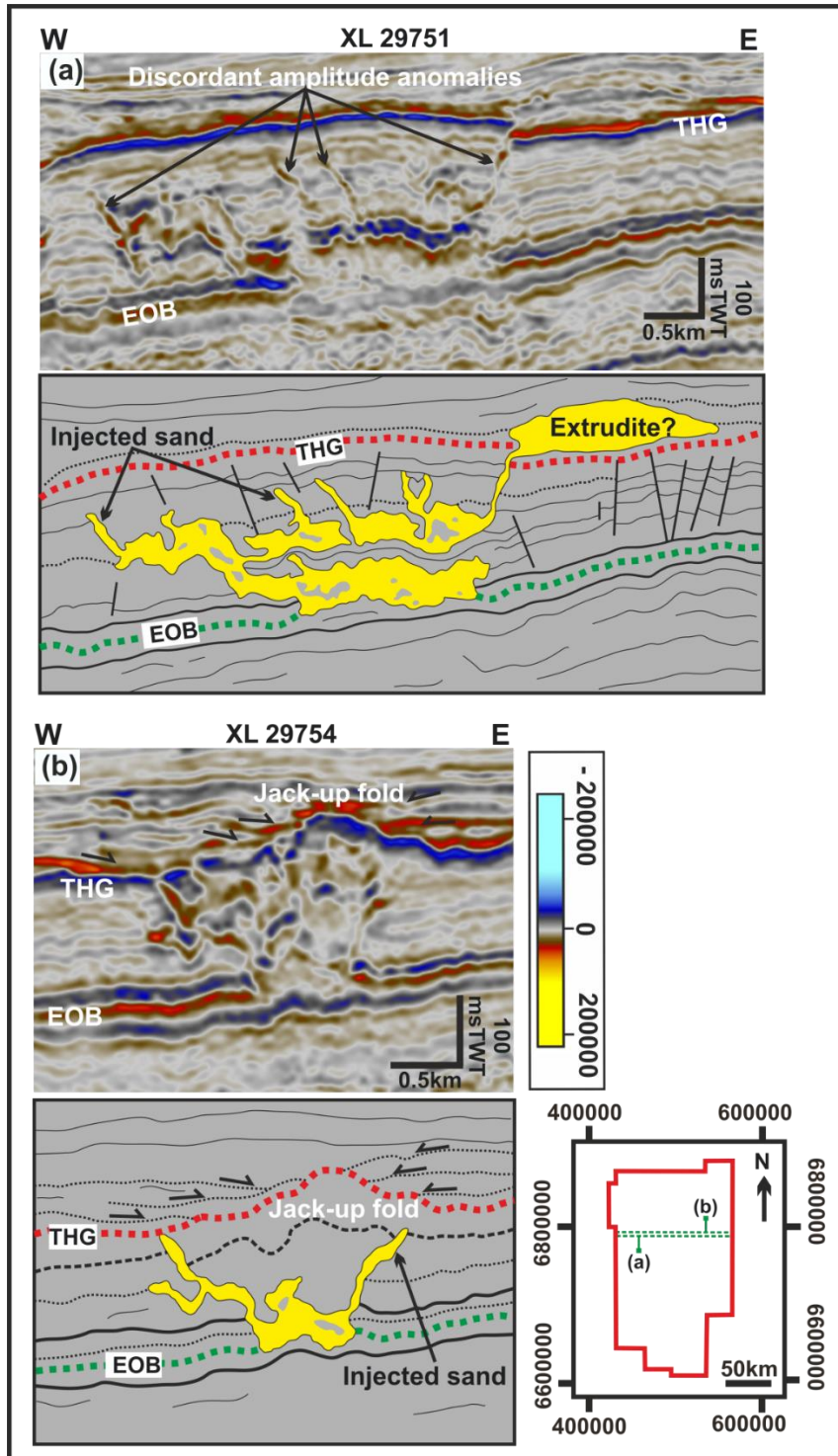
Fig. 4.35: Example observations used in estimating the timing of emplacement of the Oligocene (CSU-4) sandstone intrusions to have occurred in Late Miocene to Early Pliocene time. (a) recognition of potential extrudites above the paleo-seafloor defined by the Top Hordaland Group Unconformity at that time of emplacement, and (b) onlap of younger sediments onto the jack-up fold above an Oligocene wing-like sand intrusion. THG: Top Hordaland Group, EOB: Eocene – Oligocene boundary. Seismic data courtesy of CGG.

The Paleocene – Early Eocene (CSU-1) intrusions in the lower Paleocene unit are also found to have their limbs terminate upward at a common datum 231 – 324 m above the Top Shetland Group horizon (Fig. 4.34c). Well data indicates that this datum corresponds to the top Lista Formation of mid – late Paleocene age (see Dmitrieva et al., 2012: their Fig 3, 2018: their Fig. 13). Other intrusions within the upper unit are found to be characterized by onlap and downlap onto domal folds and jack-up formed on the Top Rogaland Group or Top Balder horizon above the intrusions (Fig. 4.34b), which implies it may have defined the seafloor at that time. In addition, we recognized potential sand extrudites (Fig. 4.34a & b) above the Top Rogaland Group which may also provide an indication of the timing of intrusion. Based on these outlined observations, we suggest that the CSU-1 intrusions may have formed during the Mid /Late Paleocene to Early Eocene time.

The Eocene (CSU-2) intrusions comprising of mainly conical-shaped intrusions, which occur at two levels (see Fig. 4.12), in most cases have their limbs terminate upwards at a common stratigraphic datum corresponding to the Eocene – Oligocene boundary (Fig. 4.11a, 4.12a & 4.12c). While a few within the Lower Eocene unit are found to terminate at the base of the Upper Eocene unit (Fig. 4.11c). Biostratigraphy data from well 35/11-1 (see Jordt et al., 2000; Faleide et al., 2002) indicate a hiatus between the Eocene and the Oligocene succession which implies the Eocene – Oligocene boundary represents an unconformity. Hence, the observed upward termination of conical-shaped intrusions below the boundary may imply it was the seafloor at the time of intrusion. We, however, do not recognize extrudites above the boundary as their preservation would be unlikely due to erosion associated with the hiatus or sand from the intrusions did not reach the seafloor at that time. We therefore suggest that sand injection would have occurred in the Mid – Late Eocene time.

The Oligocene (CSU-4) intrusions documented here are characterized by onlap and downlap of sediments onto the domal folds and jack-up formed on the Top Hordaland Group Unconformity (THGU) or Mid-Miocene Unconformity (MMU) surface above the intrusions (e.g., Fig. 4.20a, 4.35b). This implies that the relief of the THGU reflects the seafloor topography during the deposition of the overlying succession and as such the THGU defines the paleo-seafloor. This is supported by the recognition of potential sand extrudites above the THGU as shown in Fig. 4.35a and those previously documented above the THGU by Løseth et al. (2013: see their Fig. 11 & 12). The mid-Miocene time represents a period of widespread hiatus in the North Sea characterized by substantial erosion, leading to the non-preservation of mid-Miocene sediments (Ahmadi et al., 2003; Rundberg and Eidvin, 2005; Goledowski et al., 2012). Previous studies have documented the sediments overlying the unconformity to be Late Miocene to Early Pliocene in age (Løseth et al., 2013; Eidvin et al., 2014). Taken together, we constrain the timing of the Oligocene intrusions to the Middle – Late Miocene using similar approach as Shoulders and Cartwright (2004) because the folding post-dates the erosional sculpturing of the THGU surface (i.e., because the unconformity is folded and/or mounded) and pre-dates the onlapping younger sediments. Having

established that the Top Hordaland Group Unconformity represents the seafloor at the time of intrusion, we also estimate the depth of intrusion to be c. 104 – 417 m (not de-compacted) which equates to the distance between the top of the wing-like intrusions or the apex of the conical intrusions to the THGU surface (Shoulders and Cartwright, 2004; Safronova et al., 2012).

4.5.4 Priming and triggering mechanisms for Sand remobilization and Injection

Large-scale remobilization and intrusion of sand in the subsurface form by injection of fluidized sand (Duranti and Hurst, 2004). This process is generally considered to require: (i) the presence of an unconsolidated deep-water source sand body encased in low permeable sealing mudstones (Lonergan et al., 2000; Huuse and Mickelson, 2004), (ii) significant overpressure in the sealed sand body (Jolly and Lonergan, 2002) with large volumes of fluid to transport the sand in a fluidized flow (Szarawarska et al., 2010), and (iii) a triggering event which results to seal breaching, sand fluidization and injection (Jolly and Lonergan, 2002, Huuse and Mickelson, 2004; Hermanrud et al., 2019). Thus, the formation of large-scale sand intrusion complexes requires a sealing lithology and a volumetrically significant aquifer both of which account for overpressure build-up and fluid availability (Szarawarska et al., 2010). Several priming mechanisms which facilitate overpressure development have been suggested by different authors such as: (i) disequilibrium compaction (e.g. Swarbrick and Osborne, 1998; Jolly and Lonergan, 2002), (ii) lateral transfer of pressure (e.g. Osborne and Swarbrick, 1997), (iii) fluid release from silica diagenetic transformation (Davies et al., 2006; Huuse et al., 2007), (iv) fluid (i.e. gas or pore water) migration into sealed depositional sand bodies (Jolly and Lonergan, 2002), and (v) sea-level fluctuations (Andresen and Clausen, 2014; Andresen et al., 2019). Several triggering mechanisms for large-scale sand remobilization and injection have also been suggested by a number of authors which include: (i) earthquake activity (e.g Obermeier, 1996, 1998; Lonergan et al., 2000; Jolly and Lonergan, 2002; Huuse and Mickelson, 2004; Briedis et al., 2007; Huuse et al, 2007, 2010; Szarawarska et al., 2010, Wild and Briedis, 2010; Hurst et al., 2011), (ii) propagation of polygonal faults (e.g. Lonergan et al., 1998; Lonergan and Cartwright, 1999; Cosgrove and Hillier, 2000; Gras and Cartwright, 2002; Molyneux et al., 2002; Hurst et al., 2003; Jackson, 2007), (iii) tectonic stress (e.g. Winslow 1983; Scholz et al., 2009), (iv) influx of fluid from deep over-pressured reservoirs into shallow sand bodies (e.g. Jenkins, 1930; Brooke et al., 1995; Jolly and Lonergan, 2002; Duranti and Mazzini, 2005; Andresen et al., 2009; Wild and Briedis, 2010; Monnier et al., 2014), (v) propagation of fractures due to differential compaction (e.g. Huuse et al, 2004; Jackson, 2007; Jackson et al., 2011; Safronova et al., 2012), (vi) bolide or meteoric impact (e.g. Alvarez et al., 1998; Huuse et al, 2007, 2010; Cartwright., 2010; Hurst et al., 2011), and (vii) recently slab sliding due to slope instability (Hermanrud et al., 2019). The very high abundance of large-scale intrusions within the Paleogene succession of the northern North Sea suggests that a regional and inclusive

explanation should be sought in determining the possible priming and trigger mechanisms for the intrusions rather than localized mechanisms which however should not be ruled out.

In the following section we discuss some of the above listed priming and triggering mechanisms and how they may single-handedly or in combination be linked to the localized and regional large-scale sand remobilization and injection in the study area.

4.5.4.1 Generation of Overpressure

The sources of overpressure build-up in the North Sea remain a subject of debate (Osborne and Swarbrick, 1997; Swarbrick and Osborne, 1998). However, it has been recently agreed by authors to be caused by two main processes which are disequilibrium compaction (i.e., due to rapid loading and effective sealing of sand bodies) and gas generation (Moss et al., 2003). Other mechanisms such as lateral transfer, diagenesis, hydrocarbon buoyancy, aqua-thermal expansion and others have also been proposed (see Osborne and Swarbrick, 1997; Moss et al., 2003: their Fig. 18.18). These mechanisms are thought to be capable of generating high overpressures which can exceed or approach fracture gradients in most basins worldwide. We discuss below some of the main mechanisms which we favour as overpressure contributing mechanisms in the study area.

a) Disequilibrium compaction and Load-Induced over-pressuring (or Differential loading)

In deep-water sedimentary environments, overpressure development has been largely linked to disequilibrium compaction which occur when mudstones are rapidly buried during deposition such that pore fluids (i.e., pore water) do not have enough time to escape (or fluid expulsion is impeded) for the pore pressure to remain hydrostatic (Ramdhan and Goulty, 2011). This incomplete dewatering of sediments results to disequilibrium compaction. Disequilibrium compaction usually occurs during rapid burial of fine-grained sediments, and the rate of dewatering is primarily controlled by their permeability (Moss et al., 2003). The rapid loading and burial of the sediments gives rise to increase in vertical stress while their low permeability results to a decrease in dewatering rate thereby leading to low rate of pressure dissipation. This in turn leads to a build-up of overpressure over time. When sediments of extremely low permeability are buried rapidly, the pore fluids are only partially expelled while the unexpelled pore fluids support all or part of the weight of the overlying sediments leading to the build-up of anomalously high pore fluid pressure (Clausen et al., 1999; Jolly and Lonergan, 2002). However, if the sedimentation or burial rate is slow, an equilibrium is maintained between the increase in overburden stress due to burial and rate of pore fluid expulsion (Osborne and Swarbrick, 1997). Although this mechanism has been documented as the common source of overpressure in basins, recent studies have argued that it is only effective at burial rate of c. 600m/Ma and down to depths

of 2 – 3 km because at greater depths, disequilibrium compaction do not occur since diagenesis leads to the over-consolidation of buried sediments (Duranti and Hurst, 2004; Ramdhan and Goulty, 2010, 2011).

Olobayo (2014: their Table 3.3) estimated the net sedimentation rates for sediments in the northern North Sea using the same approach as Jordt et al. (2000). The Paleogene succession had maximum sedimentation rates ranging from 109.25 m/Ma for the Paleocene – early Eocene (CSU-1), 24.10 m/Ma for the Eocene (CSU-2) to 70.53 m/Ma for the Oligocene (CSU-4) interval. For the CSU-1 interval, the estimated maximum burial rate is relatively high and the observation that the interval is thickest in the eastern and north-eastern part of the study area where the sand intrusions occur may be an indication for rapid loading due to high influx of sediments. This may also apply to the CSU-4 interval which shows an increase in thickness from east to west as well as the CSU-2 interval with maximum thickness at the basin margins. We therefore propose that both disequilibrium compaction and rapid loading form the primary mechanism for overpressure development within the Paleocene – Oligocene source sands for the intrusions supported by: (i) the understanding that the source sands were effectively sealed by very thick fine-grained low permeability smectite-rich mudstones prior to seal breach, and the thick accumulation of low permeable lithology represents suitable conditions for overpressure build-up by disequilibrium compaction (Andresen et al., 2019), (ii) the spatial distribution of the intrusions which mostly correlate to the thickest parts of the studied Paleogene intervals, and (iii) the argument by Davies et al. (2006) that sand intrusions usually form during moderate sedimentation rate of c. 10 – 20 m/ma or when there is a break in sedimentation (hiatus).

b) Addition of fluid and lateral transfer of fluid & pressure

Overpressure development may also result from lateral and vertical fluid (i.e., porewater) drainage into sealed sand bodies from their surrounding less-permeable host mudstone during early-compaction dewatering of sediments (Davies et al., 2006; Safronova et al., 2012) or by vertical fluid migration from deeper sources (Lonergan et al., 2000; Jolly and Lonergan, 2002). This lateral fluid transfer may also result from uneven lateral sediment loading (Flemings et al., 2002; Cartwright, 2010; Hermanrud et al., 2019) due to advance of glaciers (e.g., Dreimanis and Rappol, 1997) and prograding clinoforms (e.g., Løseth et al., 2013). Based on the understanding that deep-water mud-dominated sediments usually show a reduction in porosity from about 75% to 40% when buried down to about 0.5 km due to early compaction (Velde 1996, Wrona et al., 2017b), we propose that lateral and vertical fluid drainage from the encasing mudstones into the sealed sand bodies through faults and/or fractures and laterally continuous sand packages may have assisted in overpressure build-up. This may be supported by the pervasive occurrence of polygonal faults in the Paleogene succession which its formation has been linked to compaction-

related early-stage dewatering of fine-grained sediments (Cartwright and Lonergan, 1996; Dewhurst et al., 1999; Lonergan and Cartwright, 1999; Cartwright et al., 2003; Cartwright, 2011). Lateral transfer of pressure will be most effective at the basin margins due to basinward inclination of depositional sands (e.g., Paleocene and Oligocene sands, see Dmitrieva et al., 2012: their Fig. 1, 2018: their Fig. 11a & 13) but would less likely contribute to overpressure build-up at the basin centre where large-scale intrusions occur in abundance in the Eocene and Oligocene (Huuse et al., 2007). Therefore, this is only likely to be a minor source of overpressure build-up.

Migration of hydrocarbon (i.e., gas) into sealed sand bodies from deeper sources have also been suggested by authors (e.g., Jolly and Lonergan, 2002; Molyneux et al., 2002; Mazzini et al., 2003; Huuse and Mickelson, 2004; Monnier et al., 2014) to generate high pore fluid pressures in the sealed source sands due to buoyancy (Duranti and Hurst, 2004; Andresen et al., 2009). This process is effective in the remobilization and injection of large volumes of unconsolidated sands similar in scale to that in the Paleogene of the northern North Sea because gas involved in the upward transport of fluidized sand would expand and therefore help drive the injection process (Lonergan et al., 2000; Jolly and Lonergan, 2002; Huuse and Mickelson, 2004). Basin and maturity modelling of the North Sea has shown that hydrocarbon generation occurred between early Cretaceous – Neogene with the Paleogene in the northern North Sea marked by early peak oil generation from the Jurassic Draupe Formation (age equivalent of the Kimmeridge Clay Formation in the UK sector) which forms the primary sources rock, with peak oil and gas generation occurring in the Late Paleogene/Early Neogene and Late Neogene/Quaternary respectively (Conford, 1998; Johnson and Fisher, 1998; Lonergan et al., 2000; Huuse and Mickelson, 2004). The migration of the generated hydrocarbons is considered to have occurred both laterally and vertically upwards along fractures, rotated/tilted fault blocks and half-graben bounding faults related to underlying Mesozoic rift structures (Huuse and Mickelson, 2004, Gautier, 2005). Faults are believed to aid fluid leakage from deep overpressured compartments, and therefore produce overpressure in overlying shallower sediments. This mechanism is quite compelling and may be supported by: (i) the fact that these large-scale intrusions occur within hydrocarbon mature area of the North Sea Basin which hosts well-known oil and gas discoveries and the documentation of deep-water sandstone reservoirs affected by one or more episodes of sand remobilization and injection in North Sea oil and gas fields such as the Alba, Balder, Volund, etc. (Lonergan and Cartwright, 1999; Braccini et al., 2008); (ii) the spatial distribution of the Paleocene – Early Eocene (CSU-1) intrusions and some Eocene - Oligocene intrusions in areas above structural highs associated with half-graben and Mesozoic faults, which may represent hydrocarbon (i.e., gas) focusing zones; and (iii) the observation of vertical acoustically distorted zones and gas chimneys on seismic cross section (see Fig. 4.36) above the Mesozoic structures. However, some of the intrusions are observed within structural low areas or are entirely absent above structural highs such as the absence of the Paleocene – Early Eocene intrusions above the Troll area (Quadrant 31:

Blocks 2, 3, 5 & 6). We therefore suggest that upward migration of hydrocarbon (gas) along the half-graben bounding faults, tilted fault blocks and fracture systems may have significantly contributed to overpressure build-up in the Paleocene sands which directly overlie Mesozoic (Jurassic) sediments and structures in the eastern (Quadrant 31) and north-eastern (Quadrant 35) parts of the study area (see Dmitrieva et al., 2018: their Fig. 11a & 13). This mechanism may have also contributed to overpressure build-up in the Eocene and Oligocene sands (see Fig. 4.36) but to a lesser extent due to the partial correlation between the underlying Mesozoic structures and the spatial distribution of the sand intrusions within both intervals (Olobayo, 2014). Nonetheless, it is very likely that lateral migration of expelled gas into connected source sand bodies may account for the distribution of some of the studied intrusions in structural low areas adjacent and away from the structural highs.
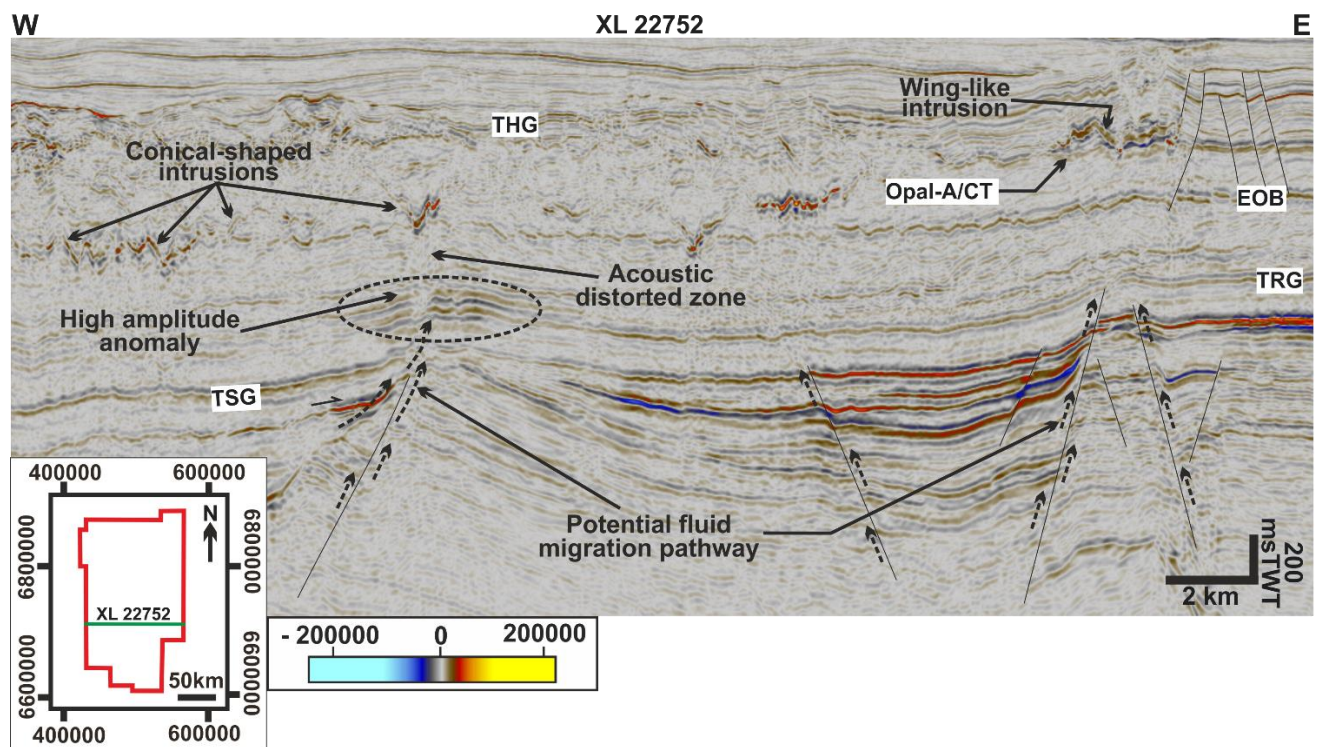
Fig. 4.36: Example evidence for potential fluid (i.e., gas) migration from deeper sources along Mesozoic faults into shallow succession which may have contributed to overpressure build-up within the parent depositional sands which sourced the sandstone intrusions in the study area. THG: Top Hordaland Group, EOB: Eocene – Oligocene boundary, TRG: Top Rogaland Group, TSG: Top Shetland Group. See text for full discussion. Data courtesy of CGG.

c) Fluid release from Smectite – to – Illite and silica (Opal-A to Opal-CT) diagenetic transformations

The diagenetic clay reaction which results to the transformation of smectite to Illite, usually at depths of 2 – 3 km, have been documented to result to the release of pore water which in turn can contribute to overpressure build-up (Osborne and Swarbrick, 1997; Moss et al., 2003). This clay mineralogical reaction is known to occur in smectite-rich sediments during burial diagenesis and can also be referred to as 'Smectite Illitization' (see Lanson et al., 2009). This mechanism has been proposed as a possible contributing factor to overpressure build-up in the smectite-rich Hordaland Group (Eocene & Oligocene) mudstones in the northern North Sea (Clausen et al., 1999; Moss et al., 2003; Marcussen et al., 2009). X-ray diffraction (XRD) clay fraction analysis of washed drill-bit cuttings from selected wells in the northern North Sea indicate that the Rogaland Group mudstones of Paleocene – Early Eocene age contain relatively high quantity of smectite clay of up to 60 – 70% with about 10 – 20% Illite; while the Hordaland Group mudstones have substantial amount of smectite in the range of 40 – 80% with up to 10 – 40% Illite (see Thyberg et al., 2000: their Fig. 4; Marcussen et al., 2009: their Fig. 9 & Table 2). We therefore suggest a possible contribution to overpressure development by this mechanism with the assumption that the major controlling factor for compaction of Paleocene to Early Miocene mudstones in the northern North Sea is dependent on their smectite content (Marcussen et al., 2009). However, this mechanism may only contribute limited amount of overpressure usually less than 0.7 MPa or 100 psi (Moss et al., 2003).

The documentation of large-scale sand intrusions within biosiliceous opal-rich mudstones (e.g. Faeroe Shetland Basin: Davies and Cartwright, 2002; North Viking Graben: Rundberg, 1991, Davies et al., 2006) have led to the suggestion that the process involved in the diagenetic transformation of biogenic silica (Opal-A) to cryptocrystalline Opal – CT (Cristobalite and Tridymite) could be a potential priming mechanism for sand remobilization and injection (Davies et al., 2006; Wrona et al., 2017b). This phase transformation process is known to result to significant expulsion of pore water, considerable reduction in porosity, rapid sediment compaction and formation of abnormal high pore pressure which have led to the suggestion that it may aid the formation of sand intrusions and polygonal fault systems and could cause marine slope failure (Davies et al., 2006; Davies and Clark, 2006; Cartwright, 2007, 2011, Ireland et al., 2011). The phase transformation from Opal-A to Opal-CT is primarily controlled by temperature, pressure, presence of clay & carbonate minerals, pore water chemistry and the host rock lithology (Hein et al., 1978; Ireland et al., 2010; Davies and Cartwright, 2002). Recent study by Wrona et al. (2017b) which used a basin modelling approach to simulate the spatial and temporal evolution of the Opal-A to Opal-CT transformation in the northern North Sea indicate the transformation process commenced sometime around the Middle – Late Eocene time corresponding to the proposed timing of injection for the Eocene sand intrusions, and then migrated upwards with increased burial until it fossilized at its present-day location. Seismic cross section (Fig. 4.17c & d, 4.18d & e,

and Fig. 4.20) through the study area indicates the presence of a high amplitude reflection separating the upper and lower Oligocene units which have been interpreted as the Opal-A/CT diagenetic boundary (see Thyberg et al., 1991; Olobayo, 2014 and Wrona et al., 2017b). The interval (mid/late Oligocene – early/mid Miocene) above the boundary have been interpreted to represent Opal-A zone which contains Opal-A-rich sediments while the interval (mid/late Eocene – lower Oligocene) below the boundary represent Opal-CT zone which contains Opal-CT-rich sediments (Rundberg, 1989; Rundberg and Eidvin, 2005: see their Fig. 11; Thyberg et al., 1991; Olobayo, 2014: see their Fig. 5.15; Wrona et al., 2017b: see their Fig. 2 – 4). We therefore suggest that expulsion of pore water and the associated reduction of porosity due to Opal-A to Opal-CT transformation in the Hordaland Group mudstones may have resulted to build-up of overpressure within the Eocene and Oligocene source sands perhaps leading to sand remobilization and injection. This may be supported by: (i) the documentation that Eocene and Oligocene mudstones contain variable proportions of biogenic silica (Rundberg, 1989; Wrona et al., 2017b); (ii) evidence of regional silica phase transformation in the northern North Sea documented by previous studies (e.g. Rundberg, 1991; Thyberg et al., 1991; Olobayo, 2014 & Wrona et al., 2017b) from seismic, well data and petrophysical analysis; (iii) presence of Eocene – Oligocene intrusions and their potential source sands within opal-rich zones; (iv) the observation that Oligocene intrusions in the eastern and north-eastern part of the study area, lie directly or slightly above the present-day position of the conversion boundary characterized by a positive high amplitude reflection; (vi) documented evidence for c. 20% (49% down to 20%) porosity reduction in Hordaland Group mudstones (see Wrona et al., 2017b: their Fig. 11) which is usually associated with the conversion process; and (vii) the extensive development of polygonal faults within the Hordaland Group which have recently been attributed to silica diagenesis and the understanding that diagenesis can cause shear fracturing (i.e. seal failure) in fine grained mudstones which is a requirement for sand injection to occur (e.g. Davies and Clark, 2006; Huuse et al., 2010; Cartwright, 2011).

d) Other potential overpressure generating mechanisms

Other possible mechanisms which may have very minor contribution to overpressure development include: aquathermal expansion (e.g., Barker, 1972; Magara, 1974; Mouchet and Mitchell, 1989; Osborne and Swarbrick, 1997; Moss et al., 2003) and sea-level fluctuations (e.g., Andresen and Clausen, 2014). Aquathermal expansion have been proposed as a pressure generating mechanism in sedimentary sequences and results from the thermal expansion of water due to increase in temperature in a closed system. This occur mainly in low permeable sediments and the amount of pressure associated with the expansion effect is dependent on the extent to which the rate of expansion due to increase in temperature matches the rate of dewatering by compaction (Mouchet and Mitchell, 1989; Osborne and Swarbrick, 1997). We propose this may have contributed to minor over-

pressuring prior to the breaching of the Paleocene – Early Miocene sealing mudstones by polygonal faults because the mechanism requires an impermeable seal and its effect on fluid volume is quickly dissipated by fluid flow (Osborne and Swarbrick, 1997). This may also account for overpressure development in isolated sand-rich channels and lobes prior to their remobilization and injection since their isolation may act as a closed system which favours this mechanism.

Deposition of Paleogene sediments in the North Sea was characterized by episodes of sea-level variation with the most significant occurring in the Oligocene caused by the climatic induced sea-level changes due to the transition from greenhouse to ice-house environment (Clausen et al., 1999; Jordt et al., 2000; Huuse and Clausen, 2001; Huuse, 2002; Zachos et al., 2001; Miller et al., 2005; Anell et al., 2012; Andresen and Clausen, 2014). Sea-level fluctuations can influence subsurface pressures with periods of sea-level fall associated with lower subsurface pressures, while periods of seal-level high results to high subsurface pressures (Andresen and Clausen, 2014). Therefore, this may have also contributed to overpressure build-up in the parent source sand for the intrusions.

4.5.4.2 Trigger mechanisms for the sandstone intrusions

For sand remobilization and injection to occur, an internally or externally driven trigger mechanism is required to cause seal failure which leads to the remobilization and injection of an overpressured source sand into the host strata. This seal failure is usually caused by hydraulic fracturing which occur when the pore fluid pressure exceeds the fracture gradient (i.e., the threshold of the seal is reached) within or near the contact between the seal and underlying source sand unit (Jolly and Lonergan, 2002; Hurst et al., 2011). We therefore consider some potential trigger mechanisms which may favour the formation of the large-scale intrusions in the study area.

The propagation of polygonal faults has been suggested as a plausible mechanism which can trigger the formation of sand intrusions and control their resultant geometries by several authors (e.g., Lonergan and Cartwright, 1999; Lonergan et al., 2000; Gras and Cartwright, 2002; Molyneux et al., 2002; Hurst et al., 2003). This was largely based on the co-occurrence of both features, and it is thought that propagation of polygonal faults into an over-pressured parent sand body can trigger sand remobilization and injection by establishing a pressure differential leading to the flow of fluidized sand (Huuse and Mickelson, 2004). However, some authors (e.g., Huuse et al., 2004; Huuse and Mickelson, 2004; Jackson, 2007) have opposed this notion. Although some of the sandstone intrusions are observed to coincide with polygonal fault planes, which may lead to an inference that the propagation of polygonal faults may have triggered intrusions, we also observe several cases where the intrusions do not follow the fault planes but crosscut the polygonal faults and vice versa. The intrusions also do not show polygonal plan view geometries. Based on this inconsistent

or partial correlation between both features, we suggest that the propagation of polygonal faults is unlikely to have triggered sandstone intrusion. However, the intrusions may have exploited the faults (e.g., Eocene and Oligocene intrusions) when they are favourably oriented and the polygonal faults may have contributed to seal failure and served as a preferential pathway for upward injection of fluidized sand (Gay, 2002; Huuse et al., 2004, 2005). This may be supported by the proposed timing for polygonal faulting (Eocene – early Oligocene with reactivation in the late Oligocene – mid Miocene) in the study area by Wrona et al. (2017a) which differ from our suggested timing of intrusion. This means that polygonal faulting occurred prior to sand injection which results to the observed partial correlation between both features.

Differential compaction across thick depositional sand bodies encased in mudstone will lead to doming/folding of the overlying mudstones (Huuse et al., 2004). This may also bring about faulting and fracturing at the margins and above the sand bodies near the sand/mudstone interface (Cosgrove and Hillier, 2000; Huuse et al., 2004). Differential compaction and its associated faulting and fracturing adjacent to depositional sand bodies have been proposed as a possible trigger for sand injection (e.g., Jackson, 2007; Jackson et al., 2011; Safronova et al., 2012). Differential compaction would lead to the formation of regions of maximum extensional strain at the edges of the parent sand bodies which favours the development of small-scale faults and fractures, leading to the localization of large-scale wing-like intrusions at the margins of the sand bodies (e.g., Fig. 4.9a, 4.11d & 4.18; Cosgrove and Hillier, 2000; Huuse et al., 2004; Jackson, 2007; Jackson et al., 2011). Differential compaction also results to the formation of regions of maximum compressional strain above the sand bodies which also favours the formation of small-scale dykes and sills at the crest of the sand bodies (Cosgrove and Hillier, 2000; Huuse et al., 2004; Jackson, 2007). The diagenetic transformation of Opal-A to Opal-CT have been linked to large scale (i.e., kilometre-scale) differential compaction and subsidence in clastic sediments (refer to Davies, 2005) due to the rapid sediment compaction associated with the conversion process (Davies et al., 2006; Davies and Clark, 2006). We therefore propose that the diagenetic conversion of Opal-A to Opal-CT mentioned earlier as a priming mechanism may have also resulted to large-scale differential compaction which probably triggered the formation of Eocene and Oligocene sand intrusions. This may be supported by: (i) the observation of differential compaction folds or jack-up above most of the intrusions together with their associated differential compaction faults like those formed at the top Hordaland Group Unconformity (e.g. Fig. 4.20b & c; Fig. 4.31c), (ii) the presence of wing-like intrusions which are most abundant in the Oligocene (CSU-4) interval, interpreted to form at the margins of their in-situ depositional sand bodies, and (iii) the evidence that the edges of the compaction folds spatially coincide with the upper tip of the wing-like sandstone intrusions (e.g. Fig. 4.18e & 4.20a). Therefore, this mechanism seems to have a significant control on the formation of wing-like intrusions studied here and as such forms the main trigger for sand remobilization and injection in the study area.

Due to the large-scale distribution of sandstone intrusions within different intervals in the Paleogene succession in the study area, one possible idea to consider is that for some cases, no external triggers were probably required. Meaning that sand injection may have occurred when the threshold or capacity of the encasing mudstones were reached (Andresen and Clausen, 2014). This implies that pore fluid pressure would have exceeded the fracture gradient within the sealing mudstones and some of the suggested priming mechanisms (i.e., disequilibrium compaction, load-induced over-pressuring, addition of fluid and mineral diagenesis) may have over time triggered sand remobilization (Andresen and Clausen, 2014). Therefore, it is possible that as soon as the capacity (or fracturing limit) of the seal was reached, seal failure (i.e., hydro-fracturing) occurred leading to the propagation of hydraulic fractures within the host sediments, which in turn led to the upward injection of fluidized sands (Jolly and Lonergan, 2002; Duranti and Hurst, 2004; Hurst et al., 2011). Seal failure may have been augmented by the presence of polygonal faults within the Paleogene interval. Although it may be difficult to ascertain if sufficient overpressure was generated by the suggested priming mechanisms to exceed the threshold of the seal and initiate injection, we suggest that access to the IHS Markit Formation Pressure Database which contains detailed pressure case study for the North Viking Graben (2008) and provides pressure distribution maps and pressure plots for key stratigraphic boundaries, may provide more insight into the regional pressure distribution and trends within the Paleogene interval in the study area. This is however beyond the scope of this study. Because Paleocene sand-rich channel-fills and fans were developed on the submarine slope and basinward on the toe of slope in the east and north-eastern parts of the study area (see Dmitrieva et al., 2018), it is possible to suggest that load-induced overpressuring due to rapid loading and subsequent deposition may have led to gravitational instability along the submarine slope resulting to possible mass movement of Paleocene sediments (see Sømme et al., 2019: their Fig. 4) which may produce localized sand remobilization and injection. This may be evidenced by the chaotic reflection pattern of some Paleocene sediment and the restricted formation of the Paleocene – Early Eocene (CSU-1) sand intrusions in the east and north-eastern parts of the study area where the interval is thickest.

Earthquakes and bolide impact are not thought to represent possible trigger mechanisms for the formation of sandstone intrusions in the study area. Although earthquake activity has been related to sand injection and extrusion by shear-induced liquefaction or dynamic liquefaction, studies have also shown that: (i) liquefaction will occur only at shallower depths (< 100 m) due to rise in overburden stress with depth (Alvarez et al., 1998) and (ii) liquefaction will only occur for earthquakes of high magnitudes (> 5) and will result to centimetre to few meter scale intrusions. Thus, its consideration as a trigger is dependent on the magnitude of the earthquake, intrusion scale and depth of intrusion. Based on the above, it is very unlikely that earthquake triggered the formation of intrusions in the study area because: (i) the intrusions studied here are of meters to kilometre-scale, (ii) the estimated depth of intrusion for the Oligocene (CSU-4) intrusions is too deep for dynamic

liquefaction to occur, and (iii) there is no record of earthquake with the required magnitude in the study area and the Paleogene time is said to tectonically quiescent (Huuse and Mickelson, 2014). However, it is possible that the large-scale tectonic events along the Atlantic margin which took place during the Paleogene (Paleocene – Eocene) and led to several episodes of thermal subsidence and inversion in the North Sea may have acted as an indirect trigger for local earthquakes along faults in the North Sea which could then result to induced liquefaction facilitated by overpressure in the sands (Huuse and Mickelson, 2004). Bolide impact has also been suggested as potential trigger for sand remobilization (Huuse et al., 2007, 2010; Szarawarska et al., 2010; Hurst et al., 2011). We suggest this is unlikely to have played a role in the formation of intrusion in the study area because there is no record of any Paleogene bolide impact in the northern North Sea, and these are usually rare events. Although we do know that the Silverpit Impact Crater (Late Cretaceous – Late Eocene age) in the southern North Sea, the Ries and Steinheim Craters (mid Miocene age) in southern Germany have been suggested as possible triggers for sand intrusion (Cartwright, 2010), they all occur at considerable distances away from the study area and it is very unlikely that their impact reached the northern North Sea (Olobayo, 2014).

4.5.5 Conceptual model for formation of the intrusions in the study area

The large-scale distribution and occurrence of sand intrusions within different intervals in the Paleogene succession of the northern North Sea is an indication that multiple episodes of sand intrusion took place. This is supported by the variation in the proposed timing for the intrusions which we have earlier stated to have occurred during the Mid-Late Paleocene to early Eocene (for CSU-1 intrusions), Mid – Late Eocene (for CSU-2 intrusions) and Late Miocene to Early Pliocene (CSU-4 intrusions). It is however possible that more than one episode of intrusion may have occurred within each individual interval depending on the prevailing conditions within the interval at different parts of the study area, since the available data covers vast area (c. 36, 400 km^2) of the northern North Sea. For example, there is evidence for cross-cutting relationship between some Oligocene intrusions in the north-eastern part of the study area and the observation of potential feeder conduits above the Eocene Fan-C (Fig. 4.31 & 4.32) which may imply that some of the Oligocene conical intrusions may have been sourced from the fan at a time which may vary from our proposed timing of injection for Oligocene intrusion. Thus, a continuous and recurring mechanism is needed and will be efficient to give rise to the scale of remobilization and injection observed. Based on this, we consider disequilibrium compaction & differential loading, introduction of excess fluid due to fluid migration and mineral diagenetic transformation to be the main sources of overpressure build-up while differential compaction and its associated faulting and fracturing constitute the main trigger mechanism. Our proposed model of formation for the Paleogene (Paleocene – Oligocene) sandstone intrusions is shown in Fig. 4.37, Fig. 4.38 and Fig. 4.39 and described in detail below.

In the Early - Middle Paleocene, uplift along basin margins led to the deposition of mudstones and sand-dominated sediments of the Vale (Danian – Early Selandian) and Lista (Late Selandian – Thanetian) Formation which were deposited as sand-rich channel-fill and lobes, as well as stacked sand-rich fans developed in a slope to proximal basin floor settings (Fig. 4.37a). The direction of sediment transport was from east to west due to increased subsidence, leading to the formation of depocentres. This was followed by subsequent deposition of mud-dominated sediments of the Sele and Balder Formation in the Mid-Late Paleocene (Fig. 4.37b), thus burying and forming a seal above the depositional sand bodies. Disequilibrium compaction, depositionally-controlled differential rapid loading, and burial of the sand bodies, fluid (gas & pore water) addition into the sealed sand bodies from deeper sources, fluid drainage from their surrounding mudstones during early dewatering due to compaction, and lateral transfer of pressure during deposition facilitated the development of high pore fluid pressure in the depositional sands (Fig. 4.37c). Differential compaction of the sand and their surrounding mudstone gave rise to the formation of domal folds and jack-up of the overburden above the sands (Fig. 4.37c). Differential compaction and its associated faults and fractures or seal failure when overpressure exceeded the threshold of the seal may have triggered sand remobilization and injection during the Mid/Late Paleocene to Early Eocene forming conical intrusions above and wing-like intrusions at the margins of the depositional source sands (Fig. 4.37d). Further burial and compaction followed, and evened-out the topography above the sand as well as reduced the initial angles of the intrusions (Fig. 4.37d).

Following the deposition of the Balder Formation in the Early Eocene was the deposition of hemipelagic mudstone-dominated sediments of the Horda Formation. This was accompanied by deposition of large deep-water submarine fan systems and isolated channel-fan complexes belonging to the Frigg and Grid Sandstone Members in the Lower to Middle Eocene from a western, south-western, and eastern source areas (Fig. 4.38a). Subsequent deposition of mudstones sealed the fan systems leading to burial and compaction. Overpressure build-up in the fan systems is attributed to disequilibrium compaction, differential loading, lateral pressure transfer and a major contribution from fluid migration into the sealed sand-rich fans from fluids released during early compaction, fluid from deeper sources via syn-sedimentary faults, lateral fluid drainage from surrounding sealing mudstones and fluid released from either or both Smectite-to-Illite and Opal-A to Opal-C diagenetic transformation (Fig. 4.38b). Remobilization of the sandstones within the Eocene submarine fan systems is speculated to have been triggered either by regional tectonic activity related to the opening of the North Atlantic (Huuse and Mickelson, 2004) or when overpressure simply exceeded the seal capacity. This led to the formation of hydro-fractures, with the fluidized sands injected along discrete fractures and potentially exploiting the polygonal fault planes, forming conical-shaped intrusions above or next to their source sand-rich fans in the Mid - Upper Eocene time (Fig. 4.38c). This injection of sand into the Mid to Upper Eocene mudstones led to the formation of domal forced folds and

elevation of the overburden above the conical intrusions (Fig. 4.38c). Wing-like intrusions were also formed at the margins of some isolated Eocene channel-sand bodies with differential compaction folds and jack-up of the overburden above the intrusions (Fig. 4.38c).

Post Eocene uplift along basin margins led to the deposition of gravity flow sands in the Early - Mid Oligocene in a deep-water setting. The sands (i.e., Uil Sandstone Member) were deposited as sand-dominated channel and lobe complexes derived from both western (East Shetland Platform) and eastern (west Norway) source areas (Fig. 4.39a). These were subsequently sealed by deposition of mud-dominated sediments of the upper Lark Formation leading to compaction (Fig. 4.39b). Overpressure development within the sands which primed them for remobilization have been interpreted to be due to disequilibrium compaction, differential loading, and mainly from pore water migration into the sands derived from fluid release during early dewatering of the sealing mudstones and the diagenetic conversion of Opal-A to Opal-CT with possible contribution from Smectite-to-Illite transformation due to the very high Smectite content of the Oligocene mudstones. Differential compaction of the sand bodies and their surrounding mudstone host strata due to further burial led to the formation of compaction folds or domal folds and jack-up of the overburden above the intrusions (Fig. 4.39b). Large-scale differential compaction which may be linked to silica diagenetic transformation (see Davies, 2005) due to rapid sediment compaction associated with the conversion process may have triggered sand remobilization and injection. This led to the development of hydro-fractures at the margins of the sand bodies which resulted to the formation of marginal wing-like intrusions, as well as the formation of conical and crestal intrusions above and next to the depositional parent sand bodies (Fig. 4.39c). Some of the conical-shaped intrusions were probably injected or sourced from the Middle – Upper Eocene fan due to the presence of potential feeder dikes above the fan and some conical intrusions with apexes within the upper Eocene (see Fig. 4.31 & 4.32). Part of the fluidized sands were also extruded at the paleo-seafloor as the fractures propagated to the surface or by exploiting the polygonal faults as conduits, thus forming sand extrudites (Fig. 4.39c). The compaction folds and extrudites formed on the top Hordaland Group Unconformity or Mid-Miocene unconformity were subsequently onlapped and down-lapped by Late Miocene to Early Pliocene deep-water clastic sediments with the topography above the sands slightly evened-out due to further burial (Fig. 4.39c).

A summary model is shown in Fig. 4.40 which integrates the models for formation of sand injectites in the Paleocene to Oligocene interval and shows the present-day morphology of the study area with the further deposition of Pleistocene clinoforms and recent sediments above the Miocene unconformity.
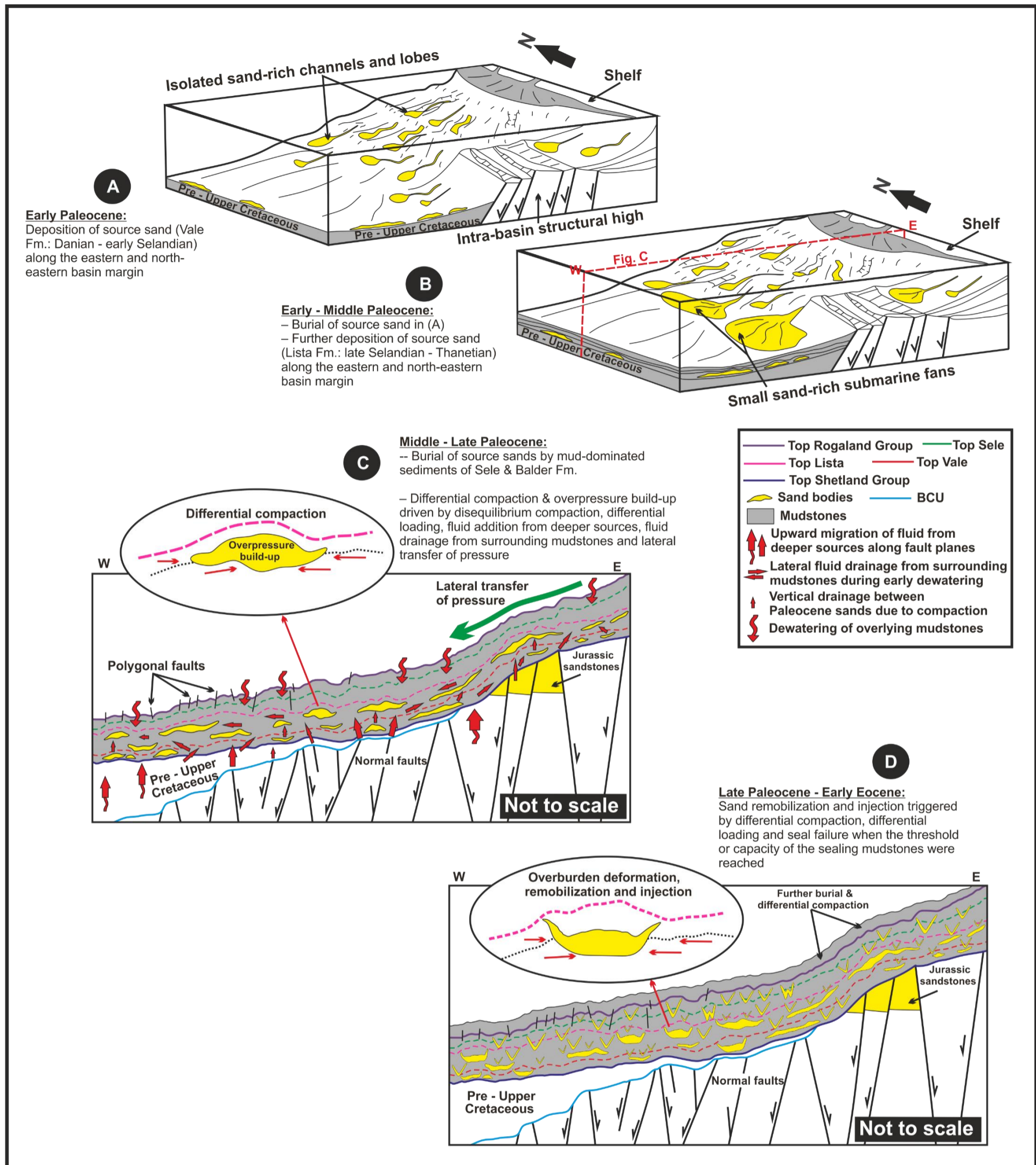
Fig. 4.37: Four-stage conceptual model for formation of the Paleocene – Early Eocene (CSU-1) sand injectites. This includes: (i) deposition of source sands and their sealing by their host mudstones (see stage A & B: modified from Dmitrieva et al., 2018), (ii) overpressure development within the source sands (see stage C), and (iii) post-depositional remobilization and injection (see stage D). See text for full explanation.
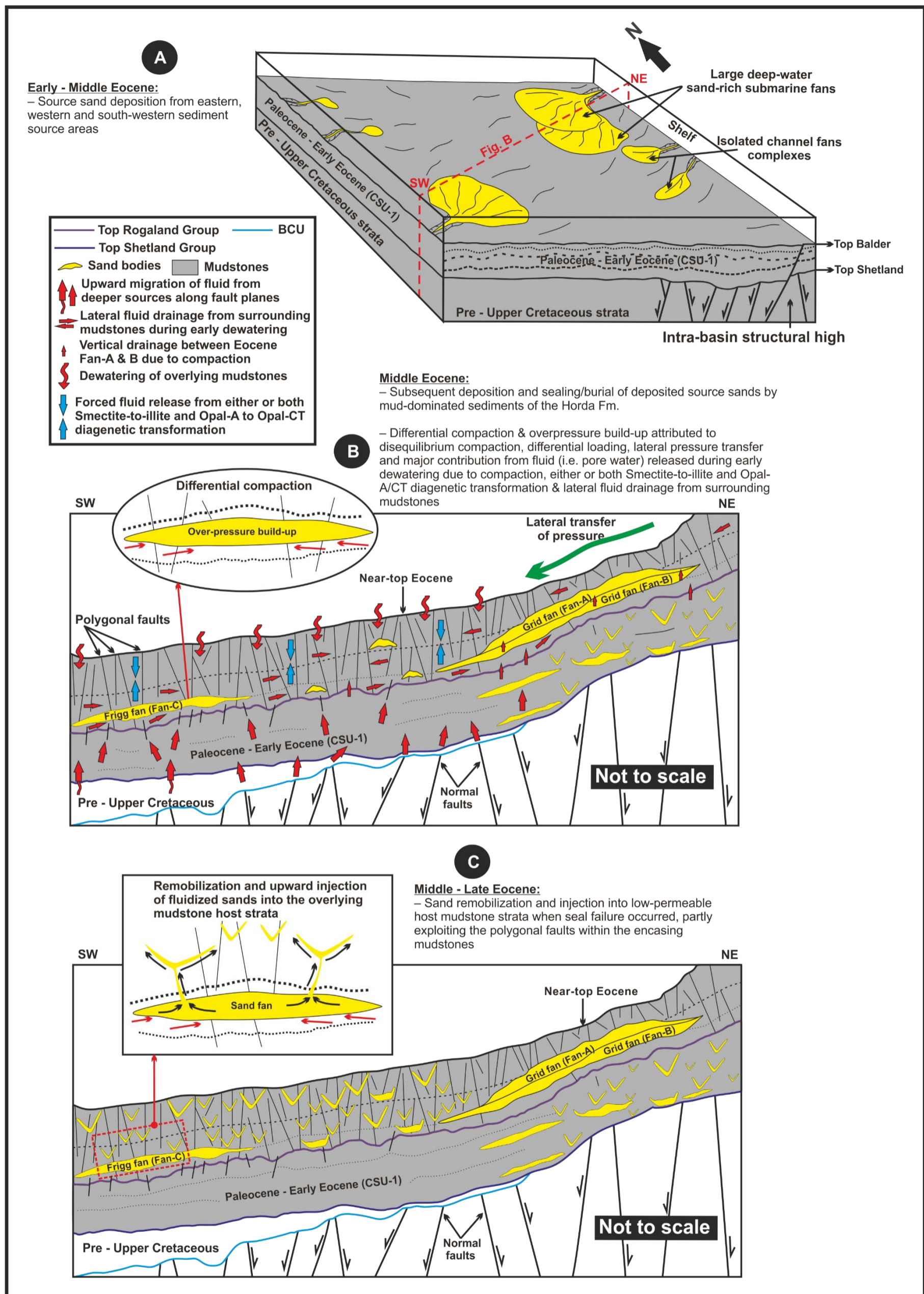
Fig. 4.38: Three-stage schematic model for the formation of Eocene (CSU-2) sand injectites. This includes: (i) deposition of Eocene sands and host rock sediments (stage A); (ii) subsequent burial, sealing of sands by the host mudstone strata and overpressure build-up within the Eocene parent source sands (stage B); and (iii) sand remobilization and injection with overburden deformation and further burial (stage C). See text for full explanation.
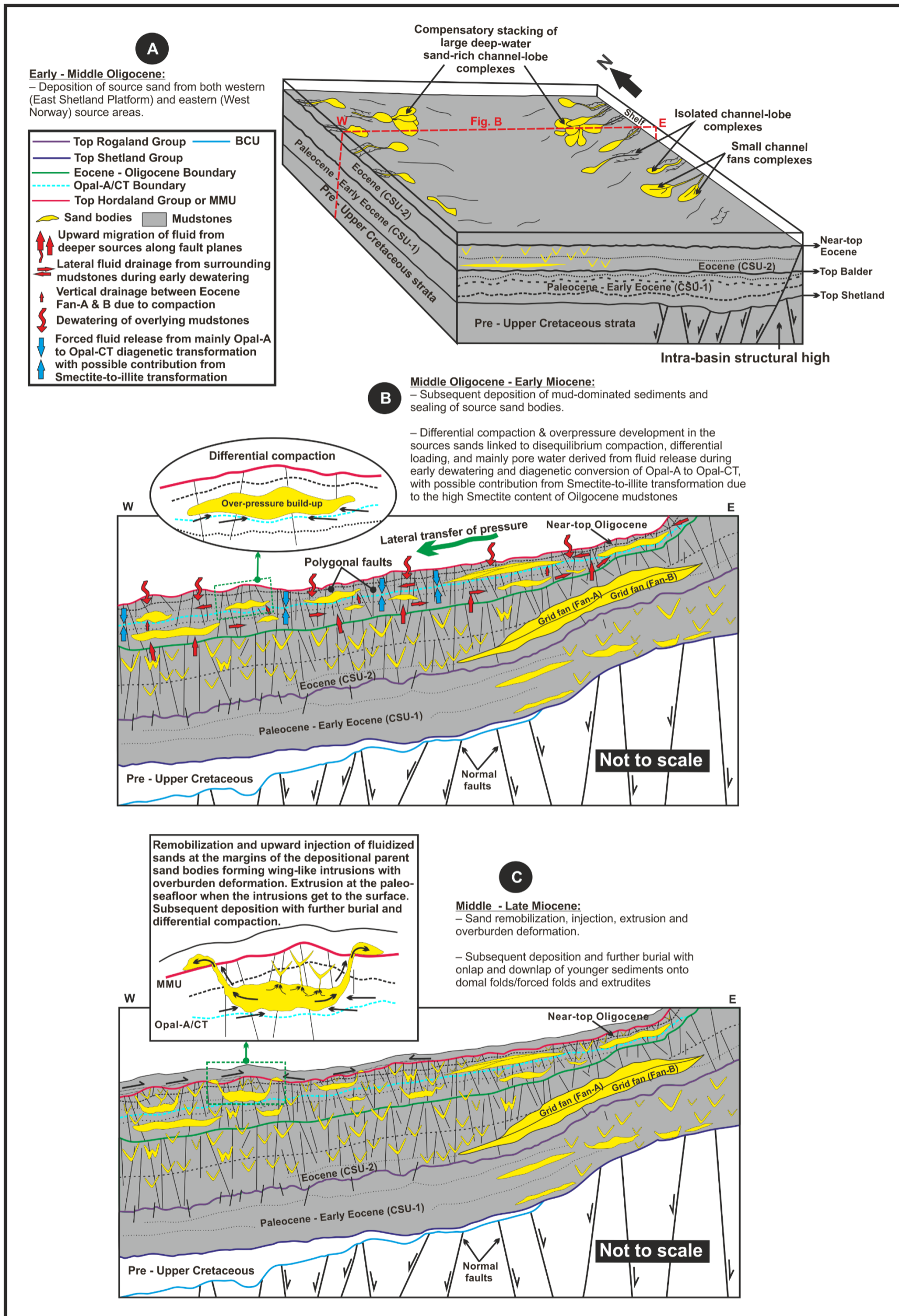
Fig. 4.39: Three-stage schematic model for the formation of Oligocene (CSU-4) sand injectites. Stage A: deposition of Oligocene source sands and host rock sediments. Stage B: their subsequent burial due to further deposition of mud-dominated sediments and initiation of overpressure build-up within the parent source sands. Stage C: post-depositional remobilization and formation of the sand intrusions with overburden deformation and further burial. See text for further explanation.
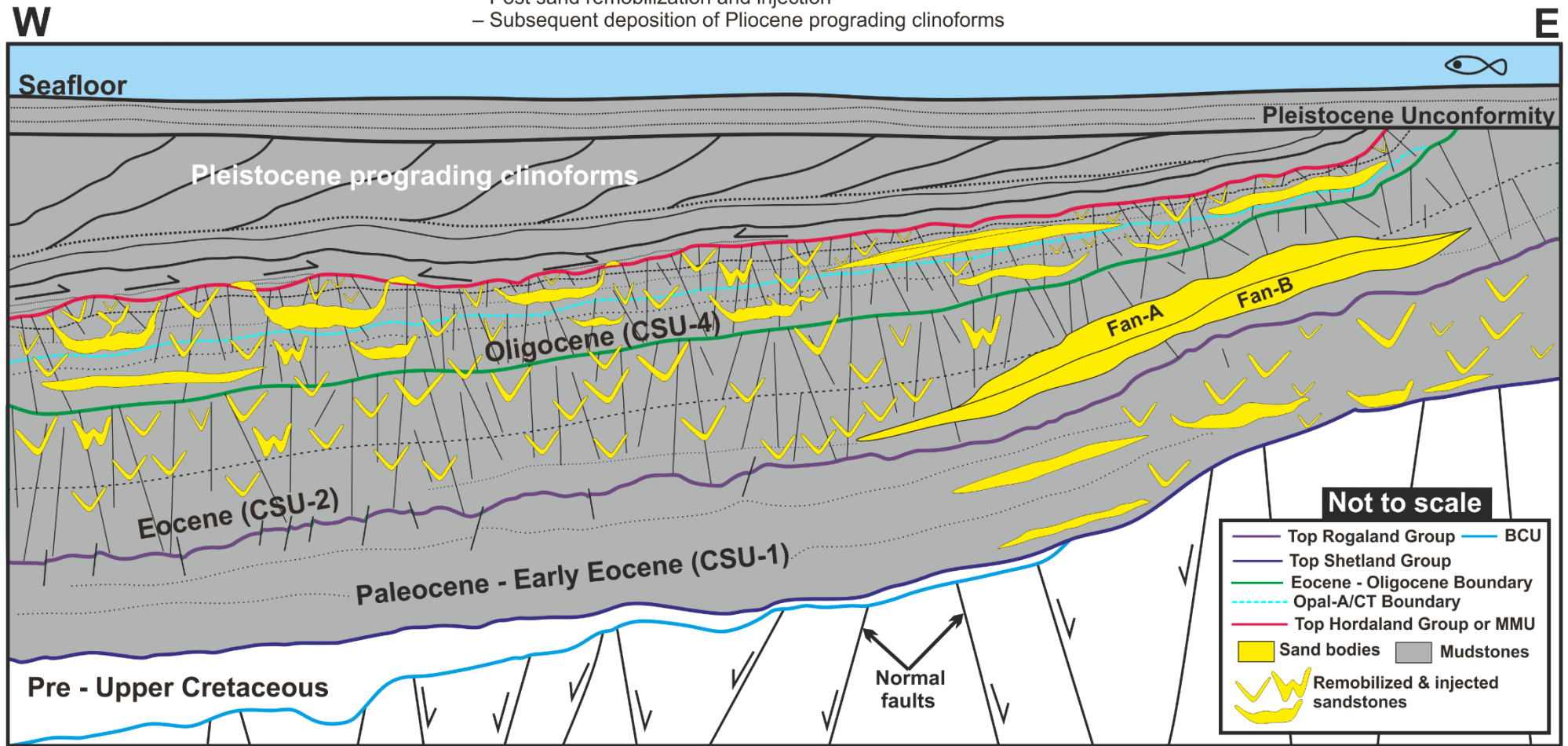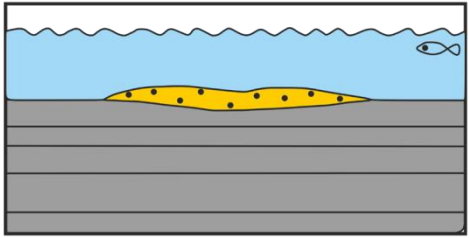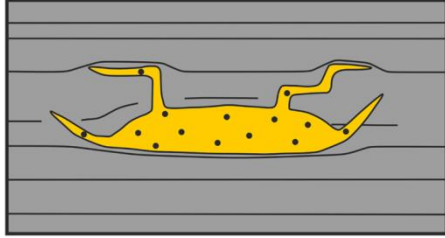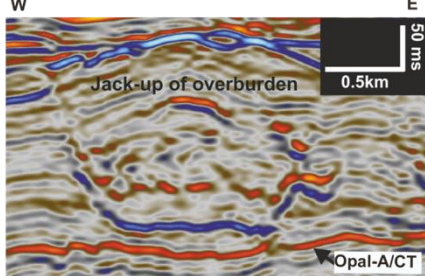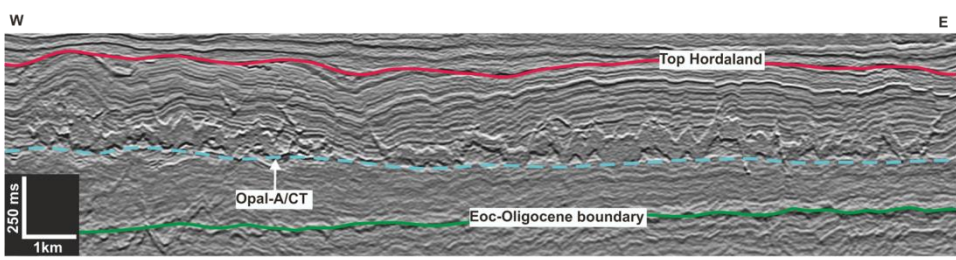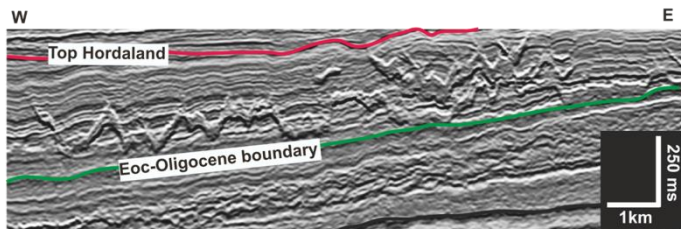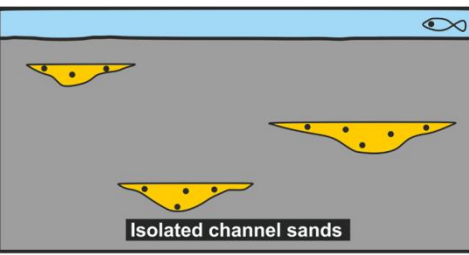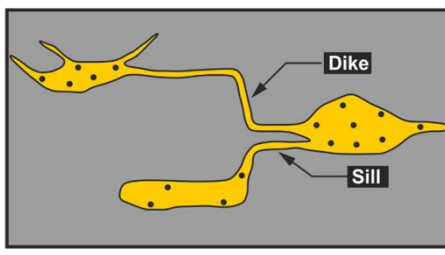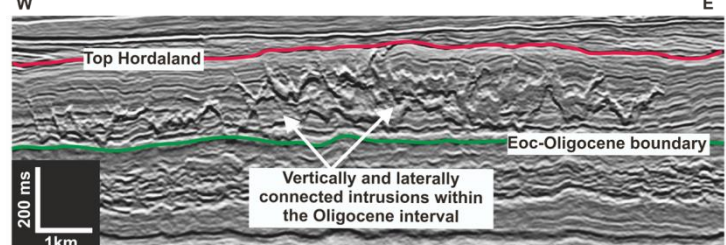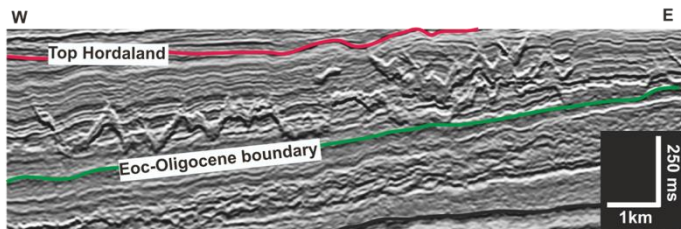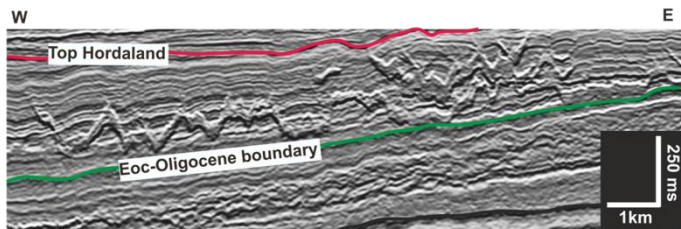
Fig. 4.40: Summary schematic model for the formation of Paleogene (Paleocene – Oligocene) sand intrusions in the study area. This shows the present-day morphology of the study area with its abundant large-scale sandstone intrusions.

4.5.6 Implications of sand remobilization and injection

Previous studies of sand intrusions indicate that the process of sand remobilization and injection can bring about significant changes in reservoir architecture, reservoir properties and enhance connectivity of isolated reservoir units (Lonergan et al., 2000; Jackson, 2007). Sand intrusions can also constitute important hydrocarbon reservoirs (Huuse et al., 2004, 2007). Large-scale sand remobilization and injection in the study area have clearly altered the geometry of depositional sand bodies (e.g., Fig. 4.7 – 4.22, Table 4.7) within the three Cenozoic seismic units where sand injectites occur, with the highest level of modification observed in the Oligocene (CSU-4) interval. For example, remobilization and injection have led to the formation of distinct marginal wings at the edges of the depositional parent sand bodies with the formation of forced folds and elevation of the overburden above the intrusions which in some cases form distinct mounded geometry (e.g., Fig 4.18). The sandstone intrusions observed in this study have similar size and scale (km-scale) as those previously documented and drilled in some North Sea hydrocarbon fields (e.g., Volund, Alba and Balder) with reservoirs modified by sand injection. Thus, the intrusions observed here can represent standalone hydrocarbon reservoirs and can form shallow near-field accumulations of hydrocarbon (e.g., the Liatårnet 25/2-21 discovery) above deeper hydrocarbon reservoirs (Huuse and Mickelson, 2004; Briedis et al., 2007). Post-depositional remobilization and injection may have also enhanced the connectivity of sealed and isolated sand bodies in the study area. This is evidenced by the observed vertical and lateral connectivity of sandstone intrusions mainly in the Eocene and Oligocene intervals (e.g., Fig 4.17b, Table 4.7). The distribution of sand injectites over a large area of the northern North Sea have an important implication for fluid flow. Although the Paleogene mudstones in the study area are known to have very low permeability, the presence of large-scale intrusions and polygonal faults may imply that the seal integrity of the mudstones have been compromised. Thus, both features may constitute long-lived permeable conduit for subsequent fluid flow and migration through the Paleogene succession and therefore represent different episodes of fluid migration and expulsion (Huuse and Mickelson, 2004; Shoulders et al., 2007). The intrusions are also indicative of possible periods of overpressure development in the basin since their formation is largely dependent on the generation of overpressure within the source sands prior to remobilization and injection (Cartwright, 2010; Jackson and Sømme, 2011).

Table 4.7: Summary illustration of the possible implications of remobilization and injection on reservoir geology and seismic examples from the study area (modified after Lonergan et al.,2000).

Effect on reservoir geology (Lonergan et.al., 2000)	Example Description	Depositional geometry (Prior to remobilization and injection)		Post-depositional geometry (After remobilization and injection)
1 **Change in reservoir geometry**	- Leads to the vertical intrusion of clastic dikes & sills above the depositional sand bodies - Modification of original depositional geometries and as such result to the development of complex sand reservoirs		➡	
Seismic Example (data courtesy of CGG)				
2 **Change in connectivity**	- Can enhanced the connectivity of sealed and isolated sand bodies as evidenced by the vertical and lateral connectivity of Oligocene sand intrusions. Therefore may bring about improved pressure communication between reservoirs		➡	
Seismic Example (data courtesy of CGG)				

4.6 Conclusion

This study presents a detailed 3D seismic analysis and characterization of large-scale Paleogene discordant amplitude anomalies in the northern North Sea around the North Viking Graben and adjourning areas. The available broadband seismic data combined with well data were used to map in detail the spatial distribution and geometries of the anomalies, as well as their relationships with their host strata. The discordant amplitude anomalies occur between the Paleocene to mid-Miocene (CSU-1, CSU-2 & CSU-4) interval and were interpreted as sand injectites or sand intrusions formed within Paleogene mudstone dominated succession. The interpretation of the lithology of the injectites as sand has been achieved by well calibration of discordant anomalies intersected by wells in the study area, which yielded tens-of-meters of thick sandstone. The intrusions are characterized by simple to complex seismic geometries forming conical (U, V & W), saucer-shaped/wing-like and irregular to complex-shaped features. These injectites occur either as isolated discrete features or as amalgamated/stacked complexes all characterized by circular to elliptical and irregular map view geometry. Common to the intrusions is the significant deformation of the succession above them which occur as forced folds and/or jack-up of overburden above the intrusions, which we have interpreted to result from differential compaction and the injection process. The injectites have been grouped into Type-1 to Type-3 intrusions based on their 3D seismic geometries following the classification by Huuse et al. (2007) and Cartwright et al. (2008). The intrusions comprising of Type-1 and Type-2 intrusions generally have steep-sided limbs/ marginal wings with dips of 2 – 30°, width from 239 – 3294 m and height from 24 – 226 m. The entire injection system has been addressed from the source sands for the injectites, potential feeder conduit and timing of injection to their priming (overpressure generation) and potential trigger mechanisms. The source sand for the intrusions within the CSU-1 (Paleocene – Early Eocene) unit is suggested to be the Lower – Middle Paleocene sand-rich channel-fills and fans within the Vale and Lista Formations deposited during the Early Tertiary uplift along basin margins. The timing of injection within this unit is estimated to have occurred in the Mid/Late Palaeocene to Early Eocene time. The source sand for the CSU-2 (Eocene) intrusions is also suggested to be Early – Mid Eocene sand-rich submarine fan systems and channel-fills within the Horda Formation. The injection of the CSU-2 injectites is suggested to have occurred in the Mid – Late Eocene time. While the CSU-4 (Oligocene) intrusions were sourced from Early – Mid Oligocene gravity flow sands within the Lark Formation and injection is estimated to have occurred in the Middle – Late Miocene.

The occurrence of sand injectites within three different Paleogene intervals therefore implies that the sand injectites would have been emplaced by three or multiple episodes of sand remobilization and injection. Overpressure development within the sands, which primed them for remobilization and injection is suggested to result from disequilibrium compaction, differential loading, addition of fluid (e.g., lateral fluid drainage and fluid migration from deeper sources), lateral transfer of pressure and fluid release from Smectite-to-Illite and silica (Opal-A to Opal-CT) diagenetic transformations. Other processes such as aqua-thermal expansion and

sea-level fluctuations were also considered as potential overpressure generating mechanisms. The remobilization and injection of fluidized sands into the host mudstones is suggested to have been triggered by differential compaction and its associated small-scale fracturing and faulting or simply when the sealing capacity of the encasing mudstones was exceeded. The pervasive occurrence of polygonal faults within the Paleogene interval may have contributed to seal breach with the polygonal faults exploited by the injectites where favourable. This study just like previous studies of sand injectites have demonstrated the significance of sand injectites and their huge influence on reservoir geology as they can modify subsurface reservoir geometries, are capable of connecting otherwise isolated sand reservoirs and can offer highly permeable fluid flow pathway through low permeable successions. Therefore, their association with most deep-water sand reservoirs cannot be overlooked.

Acknowledgements

References

AHMADI, Z.M., SAWYERS, M., KENYAN-ROBERTS, S., STANWORHT, C.W., KUGLER, K.A., KRISTENSEN, J. & FUGELLI, E.M.G. 2003. Palaeocene. In: *The Millennium Atlas: Petroleum geology of the central and northern North Sea* (Ed. by D. Evans, C. Graham, A. Armour & P. Bathurst). *The Geological Society of London, London,* 235–259.

ALVAREZ, W., STALEY, E., O'CONNOR, D. & CHAN, M.A. 1998. Syn-sedimentary deformation in the Jurassic of south-eastern Utah - a case of impact shaking. Geology, https://doi.org/10.1130/0091-7613(1998)026<0579:SDITJO>2.3.CO;2.

ANDRESEN, K.J., CLAUSEN, O.R., HUUSE, M. 2009. A giant (5.3×10^7 m^3) middle Miocene (c. 15 Ma) sediment mound (M1) above the Siri Canyon, Norwegian–Danish Basin: origin and significance. Marine and Petroleum Geology 26, 1640–1655.

ANDRESEN, K.J., HEILMANN-CLAUSEN, C., CLAUSEN, O.R. & FRIIS, H. 2019. Deposition or remobilization of the enigmatic Hefring Member sand, eastern North Sea – A multidisciplinary approach. *Marine and Petroleum Geology*, https://doi.org/10.1016/j.marpetgeo.2019.06.001.

ANDRESEN, K.J. & CLAUSEN, O.R. 2014. An integrated subsurface analysis of clastic remobilization and injection; a case study from the Oligocene succession of the eastern North Sea. *Basin Research*, 26, 641–674, https://doi.org/10.1111/bre.12060.

ANELL, I., THYBO, H. & RASMUSSEN, E. 2012. A synthesis of Cenozoic sedimentation in the North Sea. *Basin Research*, 24, 154–179, https://doi.org/10.1111/j.1365-2117.2011.00517.x.

BADLEY, M.E., PRICE, J.D., RAMBECH DAHL, C. & AGDESTEIN, T. 1988. The structural evolution of the northern Viking Graben and its bearing upon extensional modes of basin formation. *Journal of the Geological Society*, 145, 455–472, https://doi.org/10.1144/gsjgs.145.3.0455.

BARKER, C. 1972. Aquathermal pressuring: role of temperature in development of abnormal pressure zone. Bulletin of the American Association of Petroleum Geologists, Vol. 56, 2068-2071.

BOEHM, A. & MOORE, J.C. 2002. Fluidized sandstone intrusions as an indicator of Paleostress orientation, Santa Cruz, California. *Geofluids*, 2, 147–161, https://doi.org/10.1046/j.1468-8123.2002.00026.x.

BRACCINI, E., DE BOER, W., HURST, A., HUUSE, M., VIGORITO, M. & TEMPLETON, G. 2008. Sand Injectites. *Oilfield Review*, 34–49.

BREKKE, H., SJULSTAD, H.I., MAGNUS, C. & WILLIAMS, R.W. 2001. Sedimentary environments offshore Norway - an overview. Norwegian Petroleum Society Special Publications, https://doi.org/10.1016/S0928-8937(01)80006-0.

BRIEDIS, N. A, BERGSLIEN, D., HJELLBAKK, A, HILL, R.E. & MOIR, G.J. 2007. Recognition Criteria, Significance to Field Performance, and Reservoir Modeling of Sand Injections in the Balder Field, North Sea. *Sand injectites: Implications for hydrocarbon exploration and production*, 91–102, https://doi.org/-.

BROOKE, C.M., TRIMBLE, T.J. & MACKAY, T. a. 1995. Mounded shallow gas sands from the Quaternary of the North Sea: analogues for the formation of sand mounds in deep water Tertiary sediments. *Geological Society, London, Special Publications*, 94, 95–101, https://doi.org/10.1144/GSL.SP.1995.094.01.08.

BRUNSTAD, H., GRADSTEIN, F., VERGARA, L., LIE, J.E. & HAMMER, Ø. 2009. A Revision of the Rogaland Group, Norwegian North Sea. *Norwegian Stratigraphic Lexicon*

BUGGE, T., TVEITEN, B. & BACKSTROM, S. 2001. The depositional history of the Cretaceous in the north-eastern North Sea. *In*: *Sedimentary Environments Offshore Norway - Palaeozoic to Recent*. 279–291., https://doi.org/10.1016/S0928-8937(01)80018-7.

BUREAU, D., MOURGUES, R., CARTWRIGHT, J., FOSCHI, M. & ABDELMALAK, M.M. 2013. Characterisation of interactions between a pre-existing polygonal fault system and sandstone intrusions and the determination of paleo-stresses in the Faroe-Shetland basin. *Journal of Structural Geology*, 46, 186–199, https://doi.org/10.1016/j.jsg.2012.09.003.

CARTWRIGHT, J. 2010. Regionally extensive emplacement of sandstone intrusions: A brief review. *Basin Research*, 22, 502–516, https://doi.org/10.1111/j.1365-2117.2009.00455.x.

CARTWRIGHT, J. 2011. Diagenetically induced shear failure of fine-grained sediments and the development of polygonal fault systems. *Marine and Petroleum Geology*, 28, 1593–1610, https://doi.org/10.1016/j.marpetgeo.2011.06.004.

CARTWRIGHT, J.A. & LONERGAN, L. 1996. Volumetric contraction during the compaction of mudrocks: A mechanism for the development of regional-scale polygonal fault systems. *Basin Research*, 8, 183–193, https://doi.org/10.1046/j.1365-2117.1996.01536.x.

CARTWRIGHT, J., HUUSE, M. & APLIN, A. 2007. Seal bypass systems. *AAPG Bulletin*, 91, 1141–1166, https://doi.org/10.1306/04090705181.

CARTWRIGHT, J., JAMES, D. & BOLTON, A. 2003. The genesis of polygonal fault systems: a review. *Geological Society, London, Special Publications*, 216, 223–243, https://doi.org/10.1144/GSL.SP.2003.216.01.15.

CARTWRIGHT, J., JAMES, D., HUUSE, M., VETEL, W. & HURST, A. 2008. The geometry and emplacement of conical sandstone intrusions. *Journal of Structural Geology*, 30, 854–867, https://doi.org/10.1016/j.jsg.2008.03.012.

CARTWRIGHT, J.A. 1994. Episodic basin-wide hydrofracturing of overpressured Early Cenozoic mudrock sequences in the North Sea Basin. *Marine and Petroleum Geology*, 11, 587–607, https://doi.org/10.1016/0264-8172(94)90070-1.

CHRISTIANSSON, P., FALEIDE, J.I. & BERGE, A.M. 2000. Crustal structure in the northern North Sea: an integrated geophysical study. *Geological Society, London, Special Publications*, 167, 15–40, https://doi.org/10.1144/GSL.SP.2000.167.01.02.

CLAUSEN, O.R., GREGERSEN, U., MICHELSEN, O. & SØRENSEN, J.C. 1999. Factors controlling the Cenozoic sequence development in the eastern parts of the North Sea. *Journal of the Geological Society*, 156, 809–816, https://doi.org/10.1144/gsjgs.156.4.0809.

COBAIN, S.L., HODGSON, D.M., PEAKALL, J. & SILCOCK, S.Y. 2019. Relationship between bowl-shaped clastic injectites and parent sand depletion: implications for their scale-invariant morphology and composition. *Geological Society, London, Special Publications*, https://doi.org/10.1144/sp493-2018-80.

CORNFORD, C. 1998. Source rocks and hydrocarbons of the North Sea. *In*: *Petroleum Geology of the North Sea: Basic Concepts and Recent Advances: Fourth Edition*, 376–462., https://doi.org/10.1002/9781444313413.ch11.

COSGROVE, J.W. & HILLIER, R.D. 2000. Forced-fold development within Tertiary sediments of the Alba Field, UKCS: evidence of differential compaction and post-depositional sandstone remobilization. *Geological Society, London, Special Publications*, 169, 61–71, https://doi.org/10.1144/gsl.sp.2000.169.01.05.

DAVIES, R.J. & CARTWRIGHT, J. 2002. A fossilized Opal A to Opal C/T transformation on the northeast Atlantic margin: Support for a significantly elevated palaeo-geothermal gradient during the Neogene. *Basin Research*, 14, 467–486, https://doi.org/10.1046/j.1365-2117.2002.00184.x.

DAVIES, R.J. 2005. Differential compaction and subsidence in sedimentary basins due to silica diagenesis: A case study. *Bulletin of the Geological Society of America*, https://doi.org/10.1130/B25769.1.

DAVIES, R.J. & CLARK, I.R. 2006. Submarine slope failure primed and triggered by silica and its diagenesis. *Basin Research*, 18, 339–350, https://doi.org/10.1111/j.1365-2117.2006.00297.x.

DAVIES, R.J., HUUSE, M., HIRST, P., CARTWRIGHT, J. & YANG, Y. 2006. Giant clastic intrusions primed by silica diagenesis. *Geology*, 34, 917–920, https://doi.org/10.1130/G22937A.1.

DEEGAN, C.E. & SCULL, B.J. 1977. A standard lithostratigraphic nomenclature for the Central and Northern North Sea. *Norwegian Petroleum Directorate Bulletin*, 1, 36.

DEWHURST, D.N., CARTWRIGHT, J.A. & LONERGAN, L. 1999. The development of polygonal fault systems by syneresis of colloidal sediments. *Marine and Petroleum Geology*, 16, 793–810, https://doi.org/10.1016/S0264-8172 (99)00035-5.

DIXON, R.J., SCHOFIELD, K., ANDERTON, R., REYNOLDS, A.D., ALEXANDER, R.W.S., WILLIAMS, M.C. & DAVIES, K.G. 1995. Sandstone diapirism and clastic intrusion in the Tertiary submarine fans of the Bruce-Beryl Embayment, Quadrant 9, UKCS. *Geological Society, London, Special Publications*, 94, 77–94, https://doi.org/10.1144/GSL.SP.1995.094.01.07.

DMITRIEVA, E., JACKSON, C.A.-L., HUUSE, M. & MCCARTHY, A. 2012. Paleocene deep-water depositional systems in the North Sea Basin: a 3D seismic and well data case study, offshore Norway. *Petroleum Geoscience*, 18, 97–114, https://doi.org/10.1144/1354-079311-027.

DMITRIEVA, E., JACKSON, C.A.-L., HUUSE, M. & KANE, I.A. 2018. Regional distribution and controls on the development of post-rift turbidite systems: insights from the Paleocene of the eastern North Viking Graben, offshore Norway. *Geological Society, London, Petroleum Geology Conference series*, 8, PGC8.31, https://doi.org/10.1144/PGC8.31.

DREIMANIS, A. & RAPPOL, M. 1997. Late Wisconsinan sub-glacial clastic intrusive sheets along Lake Erie bluffs, at Bradtville, Ontario, Canada. *Sedimentary Geology*, https://doi.org/10.1016/S0037-0738(97)00017-1.

DURANTI, D., HURST, A., BELL, C., GROVES, S. & HANSON, R. 2002. Injected and remobilized Eocene sandstones from the Alba Field, UKCS: core and wireline log characteristics. *Petroleum Geoscience*, 8, 99–107, https://doi.org/10.1144/petgeo.8.2.99.

DURANTI, D. & HURST, A. 2004. Fluidization and injection in the deep-water sandstones of the Eocene Alba Formation (UK North Sea). *Sedimentology*, 51, 503–529, https://doi.org/10.1111/j.1365-3091.2004.00634.x.

DURANTI, D.& MAZZINI, A. 2005. Large-scale hydrocarbon driven sand injection in the Paleogene of the North Sea. Earth and Planetary Science Letters, 239, 327–335.

EIDVIN, T., RIIS, F. & RASMUSSEN, E.S. 2014. Oligocene to Lower Pliocene deposits of the Norwegian continental shelf, Norwegian Sea, Svalbard, Denmark and their relation to the uplift of Fennoscandia: A synthesis. *Marine and Petroleum Geology*, 56, 184–221, https://doi.org/10.1016/j.marpetgeo.2014.04.006.

FAERSETH, R.B., GABRIELSEN, R.H. & HURICH, C.A. 1995. Influence of basement in structuring of the North Sea Basin, offshore southwest Norway. *Norsk Geologisk Tidsskrift*, 75, 105–119.

FAERSETH, R.B., KNUDSEN, B.-E., LILJEDAHL, T., MIDBØE, P.S. & SØDERSTRØM, B. 1997. Oblique rifting and sequential faulting in the Jurassic development of the northern North Sea. *Journal of Structural Geology*, 19, 1285–1302, https://doi.org/10.1016/S0191-8141(97)00045-X.

FALEIDE, J.I., KYRKJEBØ, R., KJENNERUD, T., GABRIELSEN, R.H., JORDT, H., FANAVOLL, S. & BJERKE, M.D. 2002. Tectonic impact on sedimentary processes during Cenozoic evolution of the northern North Sea and surrounding areas. *Geological Society, London, Special Publications*, 196, 235–269, https://doi.org/10.1144/GSL.SP.2002.196.01.14.

FLEMINGS, P., STUMP, B.B., FINKBEINER, T. & ZOBACK, M.D. 2002. Overpressure and flow-focusing in the South Eugene Island 330 field (offshore Lousiana, USA): Theory, examples and implications. *American Journal of Science*, 302, 827–855.

FYFE, J.A., GREGERSEN, U., JORDT, H., RUNDBERG, Y., EIDVIN, T., EVANS, D., STEWART, D., HOVLAND, M. & ANDERSEN, P. 2003. Oligocene to Holocene. In: *The Millenium Atlas: Petroleum Geology of the Central and Northern North Sea* (Ed. by D. Evans, C. Graham, A.Armour & P. Bathurst. *Geological Society London, London, 279-287*

GABRIELSEN, R.H., KYRKJEBO, R., FALEIDE, J.I., FJELDSKAAR, W. & KJENNERUD, T. 2001. The Cretaceous post-rift basin configuration of the northern North Sea. *Petroleum Geoscience*, 7, 137–154, https://doi.org/10.1144/petgeo.7.2.137.

GABRIELSEN, R.H., FOERSETH, R.B., STEEL, R.J., IDIL, S. & KLOVJAN, O.S. 1990. *Architectural Styles of Basin Fill in the Northern Viking Graben*.

GALLOWAY, W.E., GARBER, J.L., XIJIN, L. & SLOAN, B.J. 1993. Sequence stratigraphy and depositional framework of the Cenozoic fill, Central and Northern North Sea Basin. In: Petroleum Geology of Northwest Europe: Proceedings of the 4th Conference (Ed. by J.R. Parker). Geological Society London, London, 33-43

GAUTIER, D.L. 2005. Kimmeridgian Shales Total Petroleum System of the North Sea Graben Province. *U.S. Geological Survey Bulletin*, 2204–C, 29.

GAY, A. 2002. Les Marqueurs Geologiques de la Migration et de l'Expulsion des Fluids Sedimentaires sur le Plancher des Marges Passives Matures. Exemples dans le Bassin du Congo. PhD thesis. Universite ´ des Sciences et Technologies de Lille.

GOŁĘDOWSKI, B., NIELSEN, S.B. & CLAUSEN, O.R. 2012. Patterns of Cenozoic sediment flux from western Scandinavia. *Basin Research*, 24, 377–400, https://doi.org/10.1111/j.1365-2117.2011.00530.x.

GRAS, R.U. AND CARTWRIGHT, J.A. 2002. Tornado Faults-The Seismic Expression of the Early Tertiary on PS-data, Chestnut Field, UK North Sea. *In 64th EAGE Conference & Exhibition*.

HARTOG JAGER, D. Den, GILES, M.R. & GRIFFITHS, G.R. 1993. Evolution of Paleogene submarine fans of the North Sea in space and time. *In*: *Petroleum Geology of Northwest Europe: Proceedings of the 4th Conference*. Geological Society of London, 59–71., https://doi.org/10.1144/0040059.

HEIN, J.R., SCHOLL, D.W., BARRON, J.A., JONES, M.G. & MILLER, J. 1978. Diagenesis of late Cenozoic diatomaceous deposits and formation of the bottom simulating reflector in the southern Bering Sea. *Sedimentology*, 25, 155–181, https://doi.org/10.1111/j.1365-3091.1978.tb00307.x.

HERMANRUD, C., CHRISTENSEN, E., HAUGVALDSTAD, M., RØYNESTAD, L.M., TJENSVOLD, I.T. & WATSEND, L. 2019. Triggers of sand remobilization in deep marine deposits. *Geological Society, London, Special Publications*, https://doi.org/10.1144/sp493-2018-35.

HILLIER, R.D. & COSGROVE, J.W. 2002. Core and seismic observations of overpressure-related deformation within Eocene sediments of the Outer Moray Firth, UKCS. *Petroleum Geoscience*, 8, 141–149, https://doi.org/10.1144/petgeo.8.2.141.

HURST, A. & CARTWRIGHT, J. 2005. Sand injectites: an emerging global play in deep-water clastic environments. *In*: *Petroleum Geology: North-West Europe and Global Perspectives— Proceedings of the 6th Petroleum Geology Conference*. 133–144., https://doi.org/10.1144/0060133.

HURST, A., CARTWRIGHT, J., HUUSE, M., JONK, R., SCHWAB, A., DURANTI, D. & CRONIN, B. 2003. Significance of large-scale sand injectites as long-term fluid conduits: Evidence from seismic data. *Geofluids*, 3, 263–274, https://doi.org/10.1046/j.1468-8123.2003.00066.x.

HURST, A. & CARTWRIGHT, J. 2007. Relevance of Sand Injectites to Hydrocarbon Exploration and Production. *In*: *Sand Injectites: Implications for Hydrocarbon Exploration and Production: AAPG Memoir 87*. 1–19., https://doi.org/10.1306/1209846M871546.

HURST, A., CARTWRIGHT, J. & DURANTI, D. 2003. Fluidization structures produced by upward injection of sand through a sealing lithology. *Geological Society, London, Special Publications*, 216, 123–138, https://doi.org/10.1144/GSL.SP.2003.216.01.09.

HURST, A., CARTWRIGHT, J., HUUSE, M. & DURANTI, D. 2006. Extrusive sandstones (extrudites): a new class of stratigraphic trap? *The Deliberate Search for the Stratigraphic Trap. Geological Society, London, Special Publications, 254*, 289–300, https://doi.org/10.1144/gsl.sp.2006.254.01.15.

HURST, A., SCOTT, A. & VIGORITO, M. 2011. Physical characteristics of sand injectites. *Earth-Science Reviews*, 106, 215–246, https://doi.org/10.1016/j.earscirev.2011.02.004.

HUUSE, M., CARTWRIGHT, J.A., GRAS, R. & HURST, A. 2005. Kilometre-scale sandstone intrusions in the Eocene of the Outer Moray Firth (UK North Sea): migration paths, reservoirs, and potential drilling hazards. *In*: *Petroleum Geology: North-West Europe and Global Perspectives – Proceedings of the 6th Petroleum Geology Conference*. Geological Society of London, 1577–1594., https://doi.org/10.1144/0061577.

HURST, A., MORTON, A., SCOTT, A., VIGORITO, M. & FREI, D. 2017. Heavy-Mineral Assemblages in Sandstone Intrusions: Panoche Giant Injection Complex, California, U.S.A. *Journal of Sedimentary Research*, **87**, 388–405, https://doi.org/10.2110/jsr.2017.22.

HUUSE, M. & CLAUSEN, O.R. 2001. Morphology and origin of major Cenozoic sequence boundaries in the Eastern North Sea Basin: Top Eocene, near-top Oligocene, and the mid-Miocene unconformity. *Basin Research*, 13, 17–41, https://doi.org/10.1046/j.1365-2117.2001.00123.x.

HUUSE, M. 2002. Cenozoic uplift and denudation of southern Norway: Insights from the North Sea Basin. In: Exhumation of the North Atlantic margin: Timing, Mechanisms, and Implications for Petroleum Exploration (Ed. by A.G. Dore´, J.A. Cartwright, M.S. Stoker, J.P. Turner & N. White) Geological Society London, Special. Publication, 196, 271–290.

HUUSE, M., JACKSON, C.A.L., OLOBAYO, O., DMITRIEVA, E. & ANDRESEN, K.J. 2012. A sand injectite stratigraphy for the North Sea. *In*: *74th European Association of Geoscientists and Engineers Conference and Exhibition 2012 Incorporating SPE EUROPEC 2012: Responsibly Securing Natural Resources*, https://doi.org/10.3997/2214-4609.20148702.

HUUSE, M., CARTWRIGHT, J., HURST, A. & STEINSLAND, N. 2007. Seismic Characterization of Large-scale Sandstone Intrusions. *Sand injectites: Implications for hydrocarbon exploration and production: AAPG Memoir 87*, 21–35, https://doi.org/10.1306/1209847M873253.

HUUSE, M., DURANTI, D., STEINSLAND, N., GUARGENA, C.G., PRAT, P., HOLM, K., CARTWRIGHT, J.A., HURST, A. 2004. Seismic Characteristics of Large-Scale Sandstone Intrusions in the Paleogene of the South Viking Graben, UK, and Norwegian North Sea. *Geological Society, London, Memoirs*, 29, 263–278, https://doi.org/10.1144/GSL.MEM.2004.029.01.25.

HUUSE, M., JACKSON, C.A.-L., VAN RENSBERGEN, P., DAVIES, R.J., FLEMINGS, P.B. & DIXON, R.J. 2010. Subsurface sediment remobilization and fluid flow in sedimentary basins: An overview. *Basin Research*, 22, 342–360, https://doi.org/10.1111/j.1365-2117.2010.00488.x.

HUUSE, M. & MICKELSON, M. 2004. Eocene sandstone intrusions in the Tampen Spur area (Norwegian North Sea Quad 34) imaged by 3D seismic data. *Marine and Petroleum Geology*, 21, 141–155, https://doi.org/10.1016/j.marpetgeo.2003.11.018.

IRELAND, M.T., GOULTY, N.R. & DAVIES, R.J. 2010. Influence of pore water chemistry on silica diagenesis: Evidence from the interaction of diagenetic reaction zones with polygonal fault systems. *Journal of the Geological Society*, https://doi.org/10.1144/0016-76492009-049.

IRELAND, M.T., DAVIES, R.J., GOULTY, N.R., CARRUTHERS, T.D. 2011. Structure of a silica diagenetic transformation zone: the Gjallar Ridge, offshore Norway. Sedimentology 58, 424-441.

ISAKSEN, D. AND TONSTAD, K. 1989. A revised Cretaceous and Tertiary lithostratigraphic nomenclature for the Norwegian North Sea. Norwegian Petroleum Directorate. *Norwegian Petroleum Directorate*.

JACKSON, C.A.-L. & SØMME, T.O. 2011. Borehole evidence for wing-like clastic intrusion complexes on the western Norwegian margin. *Journal of the Geological Society*, 168, 1075–1078, https://doi.org/10.1144/0016-76492011-035.

JACKSON, C.A.-L. 2007. The geometry, distribution, and development of clastic injections in slope systems: seismic examples from the Upper Cretaceous Kyrre Formation, Måløy Slope, Norwegian Margin. *Sand injectites: implications for hydrocarbon exploration and production*, 37–48, https://doi.org/-.

JACKSON, C.A.L., HUUSE, M. & BARBER, G.P. 2011. Geometry of wing-like clastic intrusions adjacent to a deep-water channel complex: Implications for hydrocarbon exploration and production. *AAPG Bulletin*, 95, 559–584, https://doi.org/10.1306/09131009157.

JENKINS, O.P. 1930. Sandstone dikes as conduits for oil migration through shales. *AAPG bulletin*, 14, 411–421.

JOHNSON, H.D. & FISHER M.J. 1998. Geological controls of North Sea hydrocarbon plays, in: K.W. Glennie, ed., Petroleum Geology of the North Sea: basic concepts and recent advances Blackwell Scientific Publications, p. 463-547.

JOLLY, R.J.H. & LONERGAN, L. 2002. Mechanisms and controls on the formation of sand intrusions. *Journal of the Geological Society*, 159, 605–617, https://doi.org/10.1144/0016-764902-025.

JONES, E., JONES, R., EBDON, C., EWEN, D., MILNER, P., PLUNKETT, J., HUDSON, G. & SLATER, P. 2003. Eocene. In: The Millennium Atlas, Petroleum Geology of the Central and Northern North Sea (Ed. by D. Evans, C. Graham, A. Armour & P. Bathurst). Geological Society London, London, 261-277

JORDT, H., FALEIDE, J.I., BJØRLYKKE, K. & IBRAHIM, M.T. 1995. Cenozoic sequence stratigraphy of the central and northern North Sea Basin: tectonic development, sediment distribution and provenance areas. *Marine and Petroleum Geology*, 12, 845–879, https://doi.org/10.1016/0264-8172 (95)98852-V.

JORDT, H., THYBERG, B.I. & NØTTVEDT, A. 2000. Cenozoic evolution of the central and northern North Sea with focus on differential vertical movements of the basin floor and surrounding clastic source areas. *Geological Society, London, Special Publications*, 167, 219–243, https://doi.org/10.1144/GSL.SP.2000.167.01.09.

KYRKJEBØ, R., KJENNERUD, T., GILLMORE, G.K., FALEIDE, J.I. & GABRIELSEN, R.H. 2001. Cretaceous-tertiary palaeo-bathymetry in the northern North Sea. *Norwegian Petroleum Society Special Publications*, 10, 321–345, https://doi.org/10.1016/S0928-8937 (01)80020-5.

KNOTT, S D, BURCHELL, M T, JOLLEY, E J, and FRASER, A J, 1993. Mesozoic to Cenozoic plate reconstructions of the North Atlantic and hydrocarbon plays of the Atlantic margins. 953-974 in Petroleum Geology of Northwest Europe: Proceedings of the 4th Conference. PARKER, J R (editor). (London: The Geological Society of London.)

KNOX, R.W.O. & HOLLOWAY, S. 1992. Paleogene of the central and northern North Sea. *In*: *Lithostratigraphic Nomenclature of the UK North Sea*. 206.

LANSON, B., SAKHAROV, B.A., CLARET, F. & DRITS, V.A. 2009. Diagenetic smectite-to-illite transition in clay-rich sediments: A reappraisal of x-ray diffraction results using the multi-specimen method. American Journal of Science, https://doi.org/10.2475/06.2009.03.

LONERGAN, L. & CARTWRIGHT, J.A. 1999. Polygonal faults and their influence on deep-water sandstone reservoir geometries, Alba field, United Kingdom central North Sea. *AAPG Bulletin (American Association of Petroleum Geologists)*, 83, 410–432, https://doi.org/10.1306/00AA9BBA-1730-11D7-8645000102C1865D.

LONERGAN, L., CARTWRIGHT, J. & JOLLY, R. 1998. The geometry of polygonal fault systems in Tertiary mudrocks of the North Sea. *Journal of Structural Geology*, 20, 529–548, https://doi.org/10.1016/S0191-8141 (97)00113-2.

LONERGAN, L., LEE, N., JOHNSON, H.D., CARTWRIGHT, J. A & JOLLY, R.J.H. 2000. Remobilization and Injection in Deepwater Depositional Systems: Implications for Reservoir Architecture and Prediction. *Deep-Water Reservoirs of the World: 20th Annual GCSSEPM Foundation Bob F. Perkins Research Conference*, 15, 515–532, https://doi.org/10.5724/gcs.00.15.0515.

LØSETH, H., RAULLINE, B. & NYGARD, A. 2013. Late Cenozoic geological evolution of the northern North Sea: development of a Miocene unconformity reshaped by large-scale Pleistocene sand intrusion. *Journal of the Geological Society*, 170, 133–145, https://doi.org/10.1144/jgs2011-165.

LØSETH, H., WENSAAS, L., ARNTSEN, B. & HOVLAND, M. 2003. Gas and fluid injection triggering shallow mud mobilization in the Hordaland Group, North Sea. *Geological Society, London, Special Publications*, 216, 139–157, https://doi.org/10.1144/gsl.sp.2003.216.01.10.

MAGARA, K. 1974. Aquathermal Fluid Migration: GEOLOGIC NOTES. *AAPG Bulletin*, 12, 2513-2516, https://doi.org/10.1306/83d91be6-16c7-11d7-8645000102c1865d.

MARCUSSEN, O., THYBERG, B.I, PELTONEN, O., JAHREN, J., BJORLYKKE, K., & FALEIDE J.I. 2009. Physical properties of Cenozoic mudstones from the northern North Sea: Impact of clay mineralogy on compaction trends. AAPG Bulletin, 93, 127–150

MARTINSEN, O.J., BØEN, F., CHARNOCK, M.A., MANGERUD, G. & NØTTVEDT, A. 1999. Cenozoic development of the Norwegian margin 60–64°N: sequences and sedimentary response to variable basin physiography and tectonic setting. *In*: *Petroleum Geology of Northwest Europe: Proceedings of the 5th Conference*. 293–304., https://doi.org/10.1144/0050293.

MAZZINI, A., DURANTI, D., JONK, R., PARNELL, J., CRONIN, B.T., HURST, A. & QUINE, M. 2003. Palaeo-carbonate seep structures above an oil reservoir, Gryphon Field, Tertiary, North Sea. *Geo-Marine Letters*, 23, 323–339, https://doi.org/10.1007/s00367-003-0145-y.

MILLER, K.G., KOMINZ, M.A., BROWNING, J.V., WRIGHT, J.D., MOUNTAIN, G.S., KATZ, M.E., SUGARMAN, P.J., CRAMER, B. S., CHRISTIE-BLICK, N. & PEKAR, S.F. 2005. The Phanerozoic record of global sea-level change. Science, 310, 1293–1298.

MOLYNEUX, S. 2001. Sandstone remobilisation in the Eocene to Miocene of the central and northern North Sea. (*Doctoral dissertation, Imperial College London*)

MOLYNEUX, S., CARTWRIGHT, J. & LONERGAN, L. 2002. Conical sandstone injection structures imaged by 3D seismic in the central North Sea, UK. *First Break*, 20, 383–393, https://doi.org/10.1046/j.1365-2397.2002.00258.x.

MONNIER, D., IMBERT, P., GAY, A., MOURGUES, R. & LOPEZ, M. 2014. Pliocene sand injectites from a submarine lobe fringe during hydrocarbon migration and salt diapirism: A seismic example from the Lower Congo Basin. *Geofluids*, https://doi.org/10.1111/gfl.12057.

MOSS, B. BARSON, D., RAKHIT, K., DENNI, H., & SWARBRICK. R. 2003. Formation pore pressures and formation waters. In: The Millenium Atlas: Petroleum Geology of the Central and Northern North Sea (Ed. by D. Evans, C. Graham, A. Armour & P. Bathurst). Geological Society London, London, 279-287

MOUCHET, J.P. AND MITCHELL, A. 1989. *Abnormal pressures while drilling: origins, prediction, detection, evaluation* (Vol. 2). Editions Technip.

MURCHISON, R.I. 1827. On the coal field of Bora in Sutherland shire and some other stratified deposits in the North of Scotland. Geological Society of London, 2, 293–326.

NOTTVEDT, A., GABRIELSEN, R.H. & STEEL, R.J. 1995. Tectonostratigraphy and sedimentary architecture of rift basins, with reference to the northern North Sea. *Marine and Petroleum Geology*, 12, 881–901, https://doi.org/10.1016/0264-8172(95)98853-W.

NPD. 2019. Fact Pages: Norwegian Petroleum Directorate. http://factpages.npd.no. Accessed 17th September 2019.

OBERMEIER, S.F. 1996. Use of liquefaction-induced features for paleo-seismic analysis — An overview of how seismic liquefaction features can be distinguished from other features and how their regional distribution and properties of source sediment can be used to infer the location. *Engineering Geology*, 44, 1–76, https://doi.org/10.1016/S0013-7952 (96)00040-3.

OBERMEIER, S.F. 1998. Liquefaction evidence for strong earthquakes of Holocene and latest Pleistocene ages in the states of Indiana and Illinois, USA. *Engineering Geology*, 50, 227–254, https://doi.org/10.1016/S0013-7952 (98)00032-5.

OLOBAYO, O. 2014. Deposition, Remobilization, and fluid flow in Sedimentary Basins – case studies in the Northern North Sea and Nigeria Transform Margin. *PhD Thesis*, The University of Manchester, UK

OSBORNE, M.J. & SWARBRICK, R.E. 1997. Mechanisms for Generating Overpressure in Sedimentary Basins: A Re-evaluation. *AAPG Bulletin*, 81 (1997), https://doi.org/10.1306/522B49C9-1727-11D7-8645000102C1865D.

PERNIN, N., FEUILLEAUBOIS, L., BIRD, T. & REISER, C. 2019. Identifying and de-risking near-field opportunities through reliable pre-stack broadband attributes: examples from the Paleocene North Sea (UK–Norway) injectites play. *Geological Society, London, Special Publications*, SP494-2019–11, https://doi.org/10.1144/sp494-2019-11.

RAMDHAN, A.M. & GOULTY, N.R. 2010. Overpressure-generating mechanisms in the Peciko Field, Lower Kutai Basin, Indonesia. *Petroleum Geoscience*, 16, 367–376, https://doi.org/10.1144/1354-079309-027.

RAMDHAN, A.M. & GOULTY, N.R. 2011. Overpressure and mudrock compaction in the Lower Kutai Basin – a radical reappraisal. AAPG Bulletin, 95, 1725–1744.

RUNDBERG, Y. 1989. *Tertiary Sedimentary History and Basin Evolution of the Norwegian North Sea between 60-62 N. An Integrated Approach*. University of Trondheim, Norway.

RUNDBERG, Y. 1991. Tertiary sedimentary history and basin evolution of the Norwegian North Sea between 60 – 62 degrees N – an Integrated Approach. *PhD Thesis, University of Trondheim*

RUNDBERG, Y. & EIDVIN, T. 2005. Controls on depositional history and architecture of the Oligocene-Miocene succession, northern North Sea Basin. *Norwegian Petroleum Society Special Publications*, 12, 207–239, https://doi.org/10.1016/S0928-8937 (05)80050-5.

RUNDBERG, Y. & EIDVIN, T. 2016. Discussion on 'Late Cenozoic geological evolution of the northern North Sea: development of a Miocene unconformity reshaped by large-scale Pleistocene sand intrusion', Journal of the Geological Society, 170, 133–145. *Journal of the Geological Society, London*, 173, 384–393.

SAFRONOVA, P.A., ANDRESSEN, K., LABERG, J.S. & VORREN, T.O. 2012. Development and post-depositional deformation of a Middle Eocene deep-water sandy depositional system in the Sørvestsnaget Basin, SW Barents Sea. *Marine and Petroleum Geology*, 36, 83–99, https://doi.org/10.1016/j.marpetgeo.2012.06.007.

SCHOLZ, H., FRIELING, D. & OBST, K. 2009. Funnel structures and clastic dykes in Cambrian sandstones of southern Sweden - Indications for tensional tectonics and seismic events in a shallow marine environment. *Neues Jahrbuch fur Geologie und Palaontologie - Abhandlungen*, https://doi.org/10.1127/0077-7749/2009/0251-0355.

SHOULDERS, S.J. & CARTWRIGHT, J. 2004. Constraining the depth and timing of large-scale conical sandstone intrusions. *Geology*, 32, 661–664, https://doi.org/10.1130/G20654.1.

SHOULDERS, S.J., CARTWRIGHT, J. & HUUSE, M. 2007. Large-scale conical sandstone intrusions and polygonal fault systems in Tranche 6, Faroe-Shetland Basin. *Marine and Petroleum Geology*, 24, 173–188, https://doi.org/10.1016/j.marpetgeo.2006.12.001.

SØMME, T.O., SKOGSEID, J., EMBRY, P. & LØSETH, H. 2019. Manifestation of Tectonic and Climatic Perturbations in Deep-Time Stratigraphy – An Example from the Paleocene Succession Offshore Western Norway. *Frontiers in Earth Science*, https://doi.org/10.3389/feart.2019.00303.

STEWART, S.A. 2011. Vertical exaggeration of reflection seismic data in geoscience publications 2006-2010. *Marine and Petroleum Geology*, https://doi.org/10.1016/j.marpetgeo.2010.10.003.

SWARBRICK, R.E. & OSBORNE, M.J. 1998. Mechanisms that generate abnormal pressures: an overview. *Abnormal Pressures in Hydrocarbon Environments: AAPG Memoir 70*, 13–34.

SZARAWARSKA, E., HUUSE, M., HURST, A., DE BOER, W., LU, L., MOLYNEUX, S. & RAWLINSON, P. 2010. Three-dimensional seismic characterisation of large-scale sandstone intrusions in the lower Palaeogene of the North Sea: completely injected vs. in situ remobilised sand-bodies. *Basin Research*, 22, 517–532, https://doi.org/10.1111/j.1365-2117.2010.00469.x.

THYBERG, B.I., STABELL, B., FALEIDE, J.I. & BJØRLYKKE, K. 1999. Upper Oligocene diatomaceous deposits in the northern North Sea - silica diagenesis and paleogeographic implications. *Norsk Geologisk Tidsskrift*, 79, 3–18, https://doi.org/10.1080/002919699433870.

THYBERG, B. I., JORDT, H., BJORLYKKE, K., & FALEIDE, J. I. 2000. Relationships between sequence stratigraphy, mineralogy, and geochemistry in Cenozoic sediments of the northern North Sea. In Nottvedt, A. at al. (Eds.), Dynamics of the Norwegian Margin. Geological Society of London, Special Publications, 167, 245-272

VELDE, B. 1996. Compaction trends of clay-rich deep-sea sediments. *Marine Geology*, 133, 193–201, https://doi.org/10.1016/0025-3227 (96)00020-5.

WILD, J. & BRIEDIS, N. 2010. Structural and stratigraphic relationships of the Palaeocene mounds of the Utsira High. *Basin Research*, 22, 533–547, https://doi.org/10.1111/j.1365-2117.2010.00479.x.

WINSLOW, M.A. 1983. Clastic dike swarms and the structural evolution of the foreland fold and thrust belt of the southern Andes (Chile). *Geological Society of America Bulletin*, 94, 1073–1080, https://doi.org/10.1130/0016-7606 (1983)94<1073: CDSATS>2.0.CO; 2.

WRONA, T., MAGEE, C., JACKSON, C.A.-L., HUUSE, M. & TAYLOR, K.G. 2017a. Kinematics of Polygonal Fault Systems: Observations from the Northern North Sea. *Frontiers in Earth Science*, 5, https://doi.org/10.3389/feart.2017.00101.

WRONA, T., JACKSON, C.A.L., HUUSE, M. & TAYLOR, K.G. 2017b. Silica diagenesis in Cenozoic mudstones of the North Viking Graben: physical properties and basin modelling. *Basin Research*, 29, 556–575, https://doi.org/10.1111/bre.12168.

ZACHOS, J., PAGANI, M., SLOAN, L., THOMAS, E. & BILLUPS, K. 2001. Trends, Global Rhythms, Aberrations in Global Climate 65Ma to Present. *Science*, 292, 686–693, https://doi.org/10.1126/science.1059412.

ZIEGLER, P.A. 1990. Tectonic and paleogeographic development of the North Sea rift system. In: Blundell, D.J. & Gibbs, A.D. (eds) Tectonic evolution of the North Sea rifts. *Oxford University Press*, 1–36.

Appendix B

Appendix B.1: Table of values derived for the geometrical measurements of Type-1 and Type-2 sand intrusions within the CSU-1, CSU-2 & CSU-4. See definition of measured parameters (Ө1, Ө2, H1, H2, Z, Td, Bd & Th) in text (section 4.4.6). The average interval velocity used for conversion of measurements taken in depth (msTWT) to depth (in meters) is also highlighted.

Intrusion Type	S/N	Dip (°) θ1	θ2	Avg. Dip (°)	Z (msTWT)	Z (m)	H1 (msTWT)	H1 (m)	H2 (msTWT)	H2 (m)	Avg. H (m)	Td (m)	Bd (m)	Th (msTWT)	Th (m)
					Depth		**Height**							**Thickness**	
PALEOCENE (CSU-1: 44 Injectites)														
Type 2	1	23	11	17	774	897	69	80	53	61	71	753	535	46	53
	2	11	10	10	1358	1573	70	81	57	66	74	797	324	42	49
	3	17	16	16	1528	1770	92	107	80	93	100	1190	872	71	82
	4	8	12	10	1533	1776	66	76	75	87	82	1077	342	64	74
	5	7	11	9	347	402	58	67	61	71	69	1657	754	67	78
	6	15	19	17	1578	1828	110	127	99	115	121	1739	1006	53	61
	7	26	24	25	1505	1744	86	100	77	89	94	903	448	57	66
	8	17	17	17	1455	1686	96	111	65	75	93	712	303	62	72
	9	12	16	14	1156	1339	48	56	61	71	63	946	517	30	35
	10	16	19	17	1148	1330	52	60	58	67	64	687	289	31	36
	11	30	30	30	1022	1184	87	101	87	101	101	1059	638	60	70
	Average	**17**	**17**	**17**		**1412**		**88**		**81**	**85**	**1047**	**548**		**61**
	Range	**7 - 30**					**56 - 127**					**687 - 1739**	**289 - 1006**		**35 - 78**
Type 1	1	13	19	16	641	743	56	65	48	56	60	480	155		
	2	20	2	11	668	774	74	86	21	24	55	585	212		
	3	37	8	22	1248	1446	163	189	63	73	131	822	294		
	4	30	23	27	1260	1460	143	166	53	61	114	518	318		
	5	11	11	11	1114	1291	115	133	185	214	174	752	264		
	6	21	19	20	1263	1463	155	180	152	176	178	697	149		
	7	18	21	19	1071	1241	90	104	62	72	88	411	143		
	8	21	19	20	971	1125	45	52	93	108	80	767	164		
	9	16	15	15	387	448	62	72	48	56	64	546	135		
	10	12	13	13	782	906	110	127	67	78	103	410	73		
	11	19	10	14	960	1112	45	52	51	59	56	558	129		
	12	14	17	15	853	988	42	49	41	47	48	953	249		
	13	16	13	14	845	979	65	75	65	75	75	239	83		
	14	19	11	15	1135	1315	135	156	79	92	124	1243	368		
	15	13	14	13	1065	1234	36	42	47	54	48	334	87		
	16	11	11	11	1078	1249	51	59	49	57	58	518	109		
	17	21	20	21	1010	1170	137	159	114	132	145	648	164		
	18	21	21	21	1260	1460	118	137	119	138	137	1105	194	N/A	
	19	11	23	17	1177	1364	58	67	58	67	67	336	74		
	20	13	14	13	1236	1432	91	105	65	75	90	1265	727		
	21	17	18	17	1207	1398	124	144	122	141	142	1041	185		
	22	19	19	19	2046	2370	86	100	82	95	97	566	268		
	23	16	12	14	1548	1793	97	112	110	127	120	952	94		
	24	19	22	21	1360	1576	165	191	167	193	192	740	126		
	25	15	17	16	1170	1355	124	144	104	120	132	1208	130		
	26	23	23	23	1231	1426	37	43	80	93	68	443	69		
	27	19	19	19	993	1150	41	47	39	45	46	573	79		
	28	30	30	30	1110	1286	151	175	151	175	175	878	87		
	29	30	30	30	1054	1221	86	100	83	96	98	523	74		
	30	30	19	25	1074	1244	93	108	93	108	108	722	84		
	31	10	10	10	1414	1638	118	137	81	94	115	1235	311		
	32	19	30	25	1216	1409	112	130	112	130	130	521	62		
	33	30	19	25	1107	1282	109	126	57	66	96	592	218		
	Average	**19**	**17**	**18**		**1283**		**110**		**97**	**103**	**702**	**178**		
	Range	**2 - 30**					**24 - 214**					**239 - 1265**	**62 - 727**		

Average interval velocity for depth conversion = 2317 m/s

Intrusion Type	S/N	Dip (°)		Avg. Dip (°)	Depth		Height				Avg. H (m)	Td (m)	Bd (m)	Thickness	
		Ө1	Ө2		Z (msTWT)	Z (m)	H1 (msTWT)	H1 (m)	H2 (msTWT)	H2 (m)				Th (msTWT)	Th (m)
							EOCENE (CSU-2: 58 Injectites)								

Intrusion Type	S/N	Ө1	Ө2	Avg. Dip (°)	Z (msTWT)	Z (m)	H1 (msTWT)	H1 (m)	H2 (msTWT)	H2 (m)	Avg. H (m)	Td (m)	Bd (m)	Th (msTWT)	Th (m)
Type 2	1	23	26	25	1689	1780	81	85	76	80	83	560	280	46	48
	2	17	24	21	1152	1214	48	51	58	61	56	613	303	42	44
	3	26	30	28	1293	1363	69	73	69	73	73	981	628	41	43
	4	19	19	19	1293	1363	68	72	65	69	70	1011	782	32	34
	5	20	20	20	1285	1354	43	45	46	48	47	837	573	36	38
	6	17	16	17	1240	1307	65	69	67	71	70	3294	1834	94	99
	7	10	23	16	1129	1190	31	33	47	50	41	836	502	40	42
	8	15	16	15	1314	1385	72	76	74	78	77	747	330	47	50
	9	17	17	17	1584	1670	76	80	73	77	79	691	255	37	39
	Average	18	21	20		1403		65		67	66	1063	610		49
	Range	10 - 30					33 - 85					560 - 3294	255 - 1834		34 - 99
Type 1	1	11	13	12	1348	1421	47	50	43	45	47	633	84		
	2	19	21	20	1334	1406	55	58	57	60	59	303	89		
	3	13	20	16	1350	1423	57	60	63	66	63	438	79		
	4	16	15	16	1392	1467	74	78	64	67	73	822	69		
	5	22	18	20	1341	1413	110	116	103	109	112	807	89		
	6	19	19	19	1306	1377	87	92	79	83	87	488	99		
	7	12	14	13	1263	1331	77	81	88	93	87	579	93		
	8	13	13	13	1289	1359	78	82	74	78	80	1029	85		
	9	23	23	23	1246	1313	71	75	71	75	75	376	118		
	10	20	23	22	1254	1322	70	74	88	93	83	330	60		
	11	21	19	20	1200	1265	41	43	57	60	52	490	63		
	12	16	13	15	1287	1356	71	75	65	69	72	343	71		
	13	19	19	19	1173	1236	77	81	90	95	88	352	69		
	14	20	30	25	1761	1856	81	85	84	89	87	561	81		
	15	10	13	11	1688	1779	68	72	49	52	62	579	112		
	16	19	19	19	1582	1667	46	48	94	99	74	475	80		
	17	23	23	23	1562	1646	141	149	110	116	132	461	74		
	18	23	23	23	1694	1785	133	140	81	85	113	741	102		
	19	25	25	25	1718	1811	82	86	124	131	109	592	64		
	20	21	21	21	1745	1839	124	131	60	63	97	603	89		
	21	19	20	19	959	1011	123	130	130	137	133	728	105		
	22	26	23	25	1606	1693	61	64	57	60	62	704	99		
	23	19	20	19	1624	1712	134	141	116	122	132	755	78		
	24	19	11	15	1597	1683	108	114	105	111	112	1074	483		
	25	23	23	23	1612	1699	52	55	88	93	74	478	69		
	26	30	26	28	1445	1523	134	141	134	141	141	618	64		
	27	30	30	30	1555	1639	94	99	94	99	99	473	81		
	28	25	23	24	1515	1597	163	172	163	172	172	623	78		
	29	21	23	22	1531	1614	102	108	95	100	104	866	379		
	30	20	24	22	1518	1600	86	91	99	104	97	878	392		
	31	23	26	25	1689	1780	105	111	110	116	113	909	373		
	32	13	13	13	1749	1843	81	85	76	80	83	660	280		
	33	19	23	21	1637	1725	204	215	214	226	220	1498	203		
	34	18	30	24	1611	1698	73	77	99	104	91	585	87		
	35	19	25	22	1462	1541	67	71	90	95	83	771	194		
	36	16	18	17	1503	1584	59	62	115	121	92	523	80		
	37	23	23	23	1353	1426	53	56	94	99	77	747	355		
	38	25	25	25	1280	1349	87	92	102	108	100	607	85		
	39	30	30	30	1267	1335	104	110	101	106	108	560	77		
	40	10	10	10	1106	1166	94	99	94	99	99	454	74		
	41	19	19	19	1290	1360	31	33	34	36	34	448	94		
	42	26	30	28	1326	1398	69	73	71	75	74	393	79		
	43	19	19	19	1366	1440	173	182	171	180	181	1061	292		
	44	13	19	16	1411	1487	80	84	80	84	84	610	75		
	45	19	19	19	1507	1588	57	60	63	66	63	529	80		
	46	16	16	16	1550	1634	188	198	204	215	207	2043	99		
	47	23	21	22	1585	1671	87	92	113	119	105	1239	111		
	48	19	19	19	1190	1254	94	99	94	99	99	707	94		
	49	10	19	14	1283	1352	130	137	121	128	132	2118	109	N/A	
	Average	20	21	20		1520		96		100	98	707	129		
	Range	10 - 30					33 - 226					303 - 2118	60 - 483		

Average interval velocity for depth conversion = 2108 m/s

Intrusion Type	S/N	Θ1	Θ2	Avg. Dip (°)	Z (msTWT)	Z (m)	H1 (msTWT)	H1 (m)	H2 (msTWT)	H2 (m)	Avg. H (m)	Td (m)	Bd (m)	Th (msTWT)	Th (m)
		Dip (°)			Depth		Height							Thickness	
Type 2	1	13	19	16	864	900	90	94	132	138	116	2305	1222	55	57
	2	30	30	30	845	880	155	162	169	176	169	3248	2336	123	128
	3	21	20	21	560	584	49	51	64	67	59	859	716	40	42
	4	19	11	15	745	776	79	82	61	64	73	710	224	29	30
	5	19	13	16	840	875	73	76	51	53	65	891	417	41	43
	6	19	19	19	841	876	46	48	49	51	49	660	404	38	40
	7	14	10	12	1427	1487	100	104	63	66	85	676	258	44	46
	8	13	13	13	1348	1405	65	68	69	72	70	1141	643	39	41
	9	30	25	28	946	986	102	106	88	92	99	735	386	62	65
	10	16	15	15	1039	1083	76	79	76	79	79	757	413	58	60
	11	23	23	23	891	928	50	52	71	74	63	486	199	22	23
	12	19	30	25	852	888	129	134	153	159	147	1467	398	94	98
	13	25	23	24	786	819	143	149	118	123	136	3264	2149	90	94
	14	13	10	11	515	537	68	71	57	59	65	1276	538	47	49
	15	30	30	30	1012	1055	74	77	74	77	77	721	434	39	41
	16	22	30	26	1012	1055	78	81	89	93	87	737	382	34	35
	17	20	19	19	1339	1395	83	86	102	106	96	1650	958	44	46
	18	19	19	19	998	1040	62	65	73	76	70	911	240	26	27
	19	21	21	21	704	734	84	88	81	84	86	2219	1043	68	71
	20	30	13	22	682	711	123	128	99	103	116	1627	747	71	74
	21	13	19	16	993	1035	79	82	81	84	83	1794	1226	72	75
	Average	21	20	20		955		90		90	90	1340	730		56
	Range	10 -30					48 - 176					486 - 3264	199 - 2336		23 - 128
Type 1	1	19	19	19	870	907	83	86	84	88	87	573	69		N/A
	2	21	23	22	1055	1099	90	94	102	106	100	554	80		
	3	25	21	23	933	972	149	155	176	183	169	700	147		
	4	21	19	20	841	876	67	70	113	118	94	514	101		
	5	23	20	22	584	609	52	54	73	76	65	766	74		
	6	10	10	10	618	644	31	32	29	30	31	398	99		
	7	13	15	14	601	626	49	51	74	77	64	691	80		
	8	23	23	23	669	697	137	143	137	143	143	769	43		
	9	7	13	10	567	591	67	70	94	98	84	1028	68		
	10	30	30	30	560	584	98	102	102	106	104	716	130		
	11	19	11	15	745	776	79	82	61	64	73	704	74		
	12	23	16	20	751	783	68	71	61	64	67	486	81		
	13	17	19	18	756	788	73	76	73	76	76	561	106		
	14	23	23	23	605	630	88	92	88	92	92	493	50		
	15	16	19	18	491	512	32	33	50	52	43	323	69		
	16	30	30	30	803	837	87	91	85	89	90	641	230		
	17	30	30	30	1435	1495	171	178	171	178	178	1300	132		
	18	23	23	23	1429	1489	77	80	93	97	89	747	41		
	19	13	23	18	1363	1420	35	36	38	40	38	309	44		
	20	11	11	11	1307	1362	91	95	96	100	97	896	60		
	21	10	10	10	1363	1420	32	33	44	46	40	433	69		
	22	19	19	19	1348	1405	75	78	78	81	80	777	224		
	23	19	19	19	1402	1461	124	129	124	129	129	623	69		
	24	13	14	13	1226	1277	109	114	88	92	103	1132	302		
	25	19	19	19	1335	1391	188	196	188	196	196	1108	217		
	26	21	21	21	1209	1260	162	169	162	169	169	822	112		
	27	19	19	19	1001	1043	88	92	82	85	89	1046	66		
	28	30	25	28	959	999	118	123	118	123	123	712	69		
	29	19	19	19	975	1016	155	162	151	157	159	1457	201		
	30	19	30	25	962	1002	69	72	83	86	79	767	78		
	31	13	13	13	470	490	60	63	81	84	73	937	114		
	32	19	19	19	1024	1067	83	86	83	86	86	620	68		
	33	20	17	18	1001	1043	28	29	38	40	34	354	47		
	34	23	20	22	956	996	63	66	71	74	70	792	304		
	35	25	30	28	1302	1357	63	66	63	66	66	423	59		
	36	19	19	19	1277	1331	113	118	113	118	118	613	75		
	37	17	17	17	1187	1237	106	110	106	110	110	932	104		
	38	20	19	19	1312	1367	83	86	102	106	96	1650	959		
	39	20	20	20	1378	1436	110	115	85	89	102	892	84		
	40	23	23	23	1378	1436	117	122	117	122	122	602	64		
	41	8	8	8	1400	1459	65	68	65	68	68	1121	101		
	42	14	14	14	1026	1069	98	102	94	98	100	1106	89		
	43	19	19	19	932	971	77	80	70	73	77	710	54		
	44	20	20	20	973	1014	98	102	98	102	102	1114	116		
	Average	19	19	19		1051		93		97	95	771	123		
	Range	7 - 30					29 - 196					309 - 1650	41 - 959		

Average interval velocity for depth conversion = 2084m/s

Chapter 5

CHAPTER 5   Deposition and subsurface remobilization of a sand-rich deep-water channel-lobe system: a case study from the Oligocene-Miocene of the northern North Sea

Deposition and subsurface remobilization of a sand-rich deep-water channel-lobe system: a case study from the Oligocene-Miocene of the northern North Sea

Nnorom, S. and Huuse, M.

Basins Research Group, Department of Earth and Environmental Sciences, University of Manchester, Oxford Road, Manchester M13 9PL, UK

 *Correspondence (sebastian.nnorom@manchester.ac.uk)

A revised version of this chapter will be submitted to Journal of Marine and Petroleum Geology

Abstract

Integration of broadband 3D seismic data and well data from the eastern North Viking Graben, offshore Norway indicates the development of a Middle – Late Oligocene depositional system. The system comprises a series of NE – SW oriented sediment accumulations with a NNW – SSE trending basinward termination. The depositional system is characterized by sand-rich finger to branch-like lobes encased in hemipelagic mudstones. The Middle – Late Oligocene depositional system displays unusual and complex geometries in cross section and plan view, interpreted to result from post-depositional modification by sediment remobilization and injection processes. In cross section the Middle – Late Oligocene depositional system contains anomalies with discordant high amplitudes and geometries ranging from conical-, wing-like and flat-based to irregular or complex-shaped anomalies interpreted as the seismic expression of sandstone injectites/intrusions. This interpretation is supported by their close spatial relationship to the Middle – Late Oligocene depositional system and the intersection of some of these anomalies by wells revealing up to tens of meters of thick sandstone. The conical (V/W)-shaped intrusions, with limb height of c. 50 – 160 msTWT, are inferred to represent injected sand bodies while the wing-like intrusions characterized by concordant bases with marginal wings, extending upward for c. 50 – 100 msTWT, are inferred to represent in-situ depositional sand bodies with injected sandstones at their margins. The Middle – Late Oligocene depositional system is often associated with folds and jack-up of overburden above the sand bodies, which we relate to differential compaction. The predominant observation of wing-like intrusions and the presence of differential compaction folds above most of the intrusions suggest that differential compaction together with small-scale faulting and fracturing adjacent to the depositional sand bodies may have triggered remobilization and injection. The post-depositional deformation of the Middle – Late Oligocene depositional system is inferred to be associated with overpressure development within the sand bodies as a result of disequilibrium compaction and fluid migration from deeper sources or fluid drainage from surrounding less permeable mudstones during early compaction and silica diagenetic transformation. The post-depositional remobilization and injection of deep-water sandy depositional systems as exemplified in this study has significant implications for hydrocarbon exploration and production because this process has clearly altered the primary reservoir geometries and enhanced connectivity of sand bodies, which may have been deposited as isolated sands.

5.1 Introduction

Clastic intrusions are found across a wide range of sedimentary environment and are well documented in many basins globally (Jolly and Lonergan, 2002). This range of environments include fluvial (Oomkens, 1966; Plint, 1985); lacustrine (Martel and Giblings, 1993); deltaic, tidal and coastal (Dionne, 1976; Hardie, 1999); offshore shallow marine (Johnson, 1977); and deep-water marine channel fans and turbiditic successions (Truswell, 1972; Huuse et al., 2003; Jackson, 2007; Jackson et al., 2011; Safronova et al., 2012). Sand intrusions appear to be a very common occurrence in deep-water marine (channel and turbidites) environments compared to other sedimentary environments (Jolly and Lonergan, 2002). These deep-water depositional systems are known to represent attractive exploration targets and form major hydrocarbon producing reservoirs in basins such as the North Sea, Gulf of Mexico, and the Niger Delta.

Here we document for the 'first time' the occurrence of a Middle – Late Oligocene sand-rich deep-water depositional system modified by subsurface sediment remobilization and injection processes in the eastern margin of the North Viking Graben. Prior to this study, Rundberg and Eidivn (2005) documented and interpreted Oligocene sandstones in the northern North Sea area to consist of in-situ depositional sands representing turbiditic gravity flow sands sourced from uplifted basin margins (East Shetland Platform and west Norway/Southern Fennoscandia) in the Early – Late Oligocene. Contrary to the above, Løseth et al. (2013) have descried these Oligocene sandstones to be intrusive sands sourced from deeper Paleocene parent sands. This study, however, documents the evolution and characteristics of a Middle – Late Oligocene deep-water depositional system which supports a depositional origin for Oligocene sands, while an in-depth scrutiny of both previous models and evidence to support a dual origin for Oligocene sands is presented in Chapter 6.

Post-depositional remobilization of deep-water depositional systems have been documented at different scale; both in outcrops (e.g., Hubbard et al., 2007; Surlyk et al., 2007; Parize et al., 2007; Vigorito et al., 2008; Kane, 2010; Vigorito and Hurst, 2010; Hurst et al., 2011) and on seismic data (e.g., Molyneux et al., 2002; Hurst et al., 2003; Huuse et al., 2003; Huuse and Mickelson, 2004; Huuse et al., 2005, 2007). These studies have generally demonstrated that clastic remobilization and injection have significant implications for the exploration and development of deep-water sand bodies because they can influence reservoir geometry and connectivity, reservoir volumetrics and pore-scale reservoir properties (Lonergan and Cartwright, 1999; Lonergan et al., 2000; Duranti et al., 2002; Jackson, 2007). In addition, large scale sand remobilization can lead to notable changes in reserve estimation and risking and have both positive and negative impact on hydrocarbon prospectivity. This have been proven from experience and observations in several Paleogene reservoirs in some North Sea fields such as the Alba field (Duranti et al., 2002), Balder field (Bergslien, 2002; Bergslien et al., 2005), Gryphon field (Purvis et al., 2002;

Braccini et al., 2008), Gamma field (Huuse et al., 2004) and Forth/Harding (Dixon et al., 1995).

This study is aims to: (1) describe the seismic expression of sand intrusion complexes developed in association with a Middle-Late Oligocene depositional system in the northern North Sea, (2) discuss possible mechanisms and controls on their development, and (3) highlight the implications of sand intrusion complexes developed in deep-water depositional systems for hydrocarbon exploration and production.
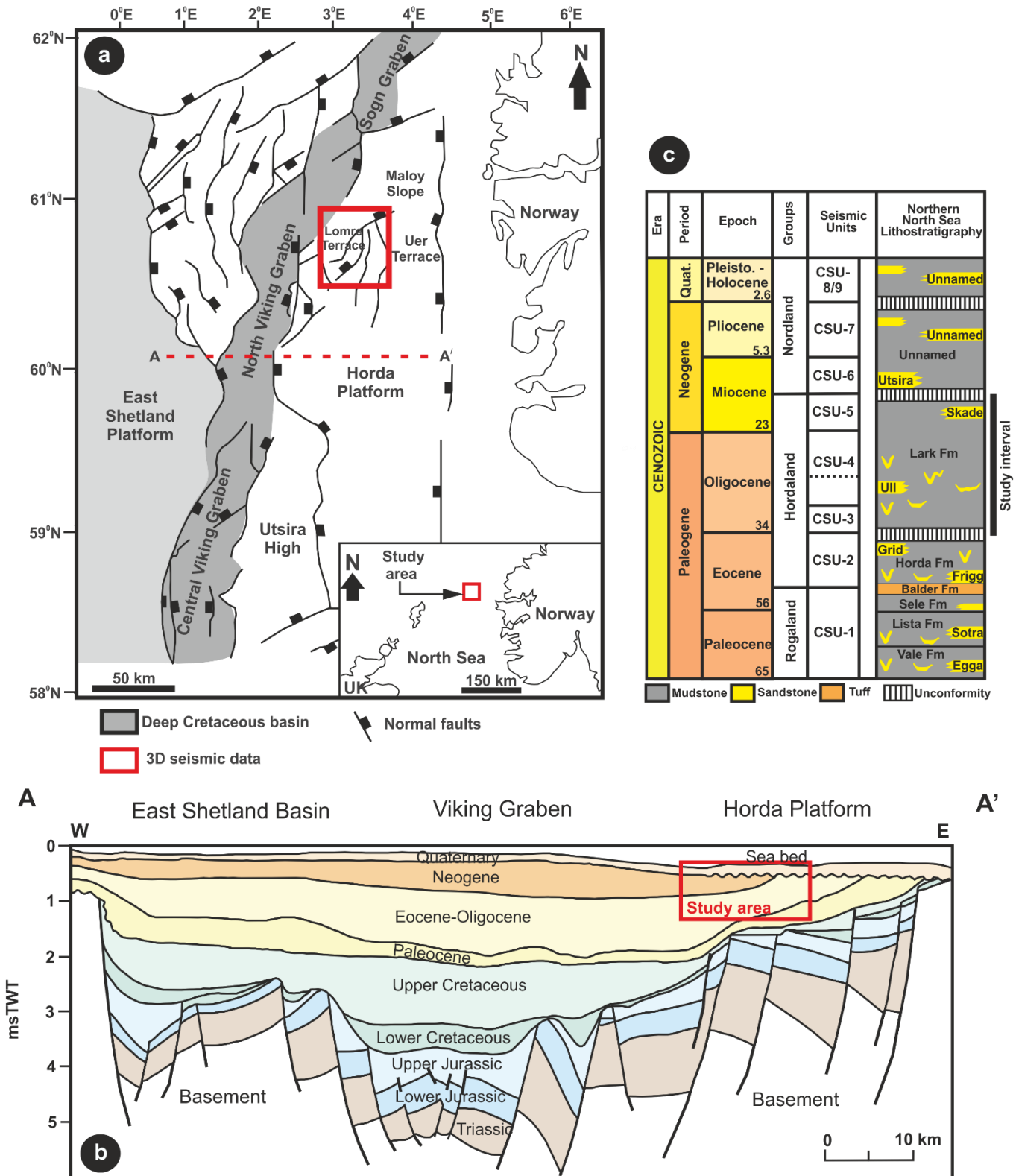
Fig. 5.1: (a) Simplified map of the northern North Sea showing the study area (in red outline) with its associated major faults and structures (modified after Wrona et al. 2017b). (b) Regional cross-section through the northern North Sea illustrating the major faults and chrono-stratigraphic units (modified after Husmo et al., 2003). See Fig. 5.1a for the location of cross-section line A − A′. Study interval and areal extent shown in red outline. (c) Simplified lithostratigraphic framework of the northern North Sea Basin highlighting the studied interval.
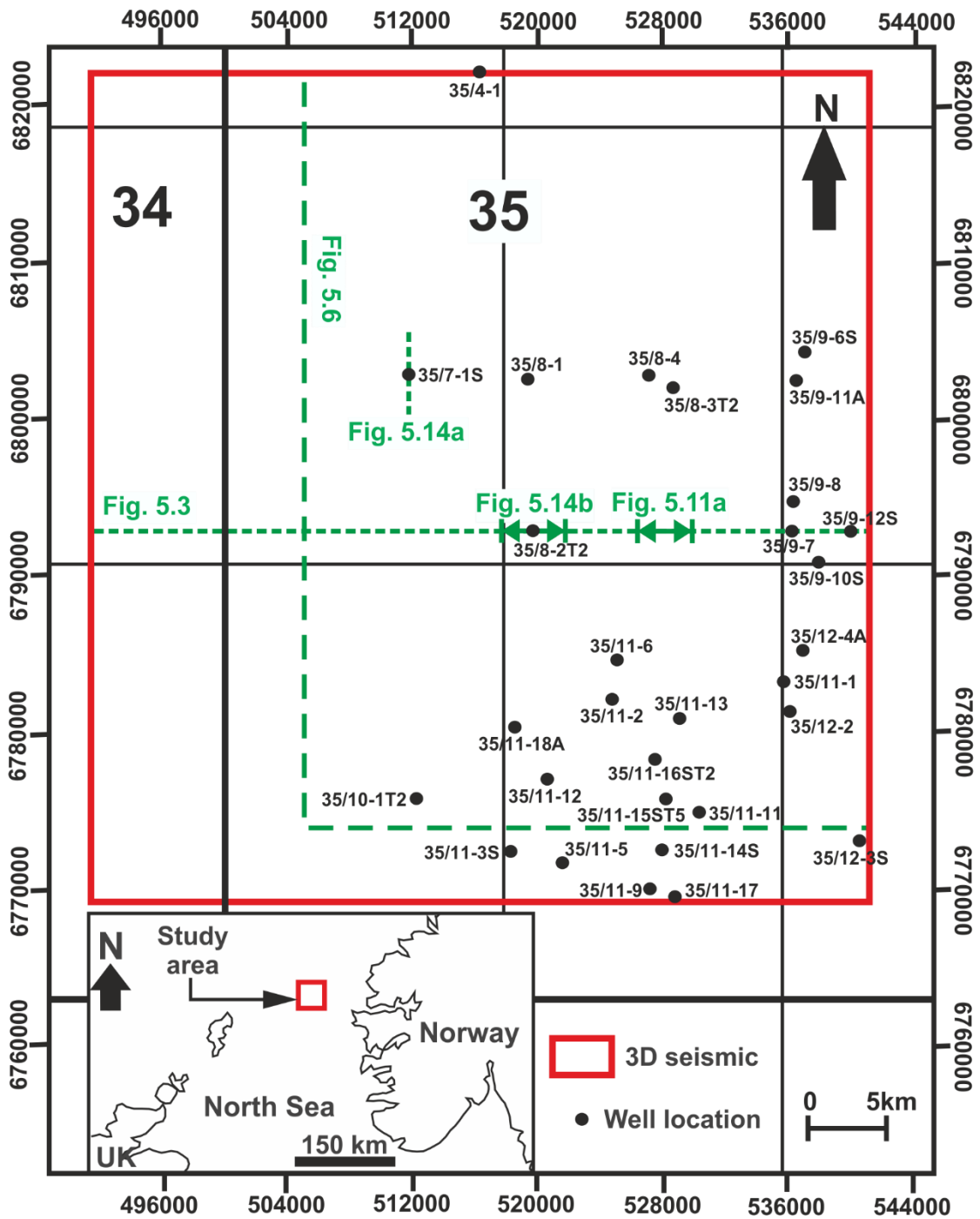
Fig. 5.2: Base map showing the surface locations of wells and 3D seismic survey used in this study. Thirty (30) wells were available for this study, all located in the Norwegian sector of the northern North Sea Basin. Well data from TGS Facies Map Browser.
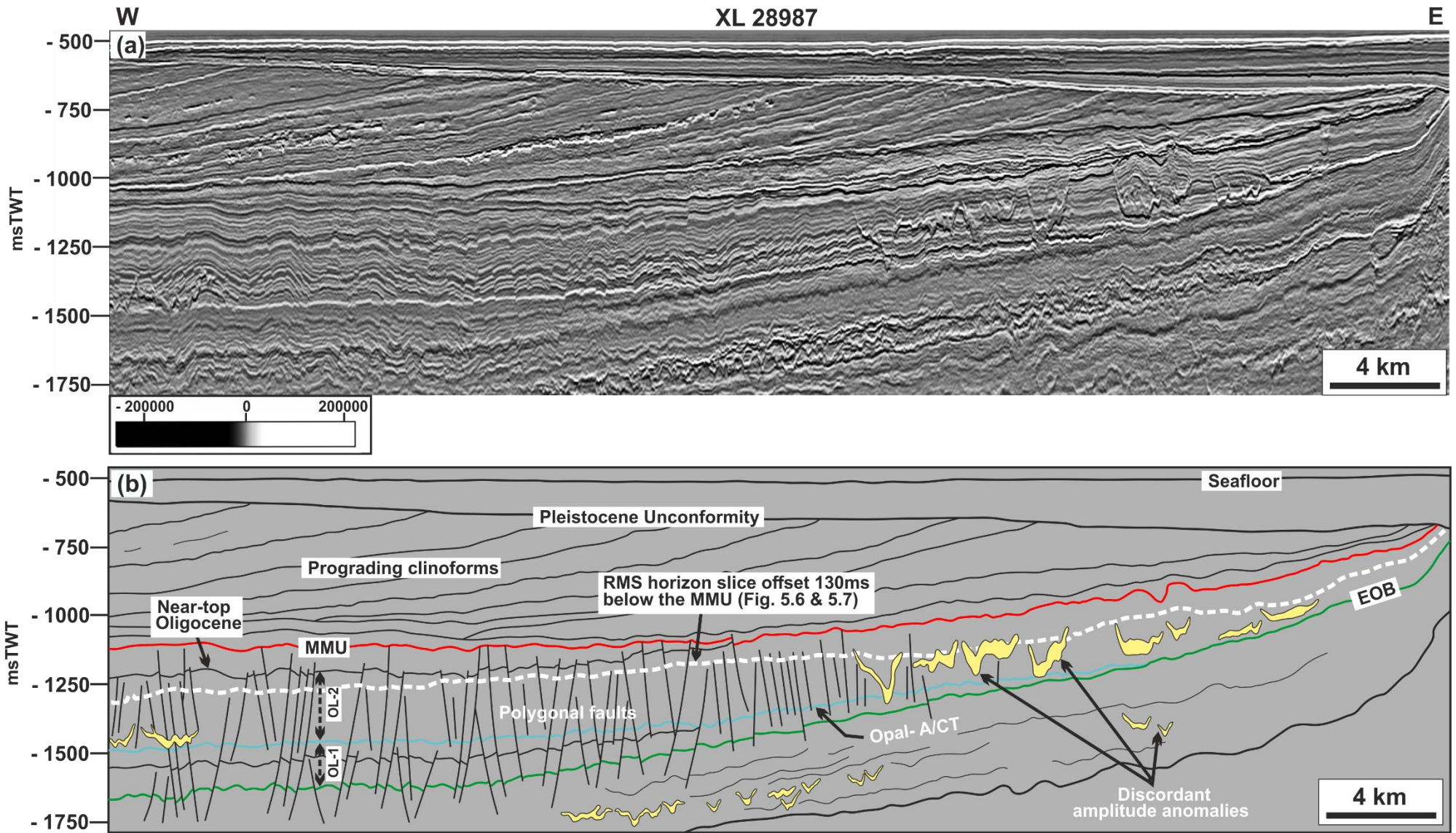
Fig. 5.3: (a) Seismic line in dip direction. (b) Geoseismic section in dip direction showing the discordant amplitude anomalies, Opal-A/CT boundary, and polygonal fault system (PFS) within the Oligocene interval in the study area. See Fig. 5.2 for the location of the seismic line (in green dash line). Dash white line shows the position of the RMS and Chaos attribute maps in Fig. 5.6 & 5.7 generated at a horizon offset of 130 ms (downward shift) below the MMU. MMU = Mid-Miocene Unconformity; EOB = Eocene – Oligocene Boundary; OL-1: Lower Oligocene; OL-2: Upper Oligocene. Seismic data courtesy of CGG.

5.2 Geological setting

5.2.1 Tectonic & stratigraphic evolution

The study area is in the eastern margin of the North Viking Graben and covers part of Quadrant-34 (34/9 and 34/10) and Quadrant-35. The North Viking Graben is bounded by the Norwegian mainland to the east and the East Shetland Platform to the west (Fig. 5.1a). This part of the North Sea Basin had a complex structural development, and its evolution and subsidence history are marked by four major well documented tectonic phases as summarized by Dmitrieva et al (2012): (a) the Caledonian Orogeny (Late Ordovician or Early Silurian); (b) Permian to Triassic rifting and graben formation; (c) Mesozoic (Late Jurassic to Early Cretaceous) rifting and graben formation; and (d) Late Cretaceous to Recent thermal subsidence and inversion. The rift axis of the first rifting phase (Permo-Triassic rifting) is believed to lie beneath the areas marginal to the Viking Graben (e.g., Horda Platform and the Magnus Basin – Unst Basin region) while the Late Jurassic to Early Cretaceous rift is centred mainly along the present-day Viking Graben and Sogn Graben (Badley et al., 1988; Christiansson et al., 2000). The Late Jurassic to Early Cretaceous rift episode was marked by rapid normal fault driven subsidence reactivation of some older Permo-Triassic rift-related structures. It was also marked by the formation of N-S, NE-SW and NW-SE striking normal faults, as well as north-south trending graben and half-graben within the northern North Sea (Ziegler, 1982; Badley et al., 1988; Gabrielsen et al., 1990; Faerseth et al., 1997).

After the Late Jurassic to Early Cretaceous rifting ceased, the post-rift phase which commenced in the Early Cretaceous marked a change from fault- to thermally controlled subsidence (Jordt et al., 2000; Faleide et al., 2002; Wrona et al., 2017b). This was followed by two major uplift events: (1) the Early Paleocene phase related to rifting, igneous activity and the opening of the North Atlantic (Nadin and Kusznir, 1995; Jordt et al., 2000; Bugge et al., 2001), and (2) a middle Miocene phase which may be linked to long wavelength doming during regional compression (Løseth et al., 2013; Wrona et al., 2017b). Studies have shown that most of the uplift occurred along basin margins resulting in large volume of coarse clastic sediments being delivered into the basin, leading to the development of depocentres during the Late Paleocene, Early Eocene, Early Oligocene and Early Miocene time along boundary faults (Jordt et al., 2000; Kyrkjebo et al., 2001; Faleide et al., 2002; Dmitrieva et al., 2012).

The northern North Sea present-day sedimentary architecture is largely related to the uplifting of surrounding clastic source areas (i.e., Shetland Platform, British highlands and Norwegian mainland) which resulted to the deposition of large prograding sand-rich channel-lobe systems in the Late

Paleocene to Oligocene (Jordt et al., 1995; Martinsen et al., 1999; Brekke et al., 2001; Ahmadi et al., 2003). The North Viking Graben comprises of post-rift sequences of up to 3 km thickness, which are dominated by hemi-pelagic, smectite-rich mudstones of the Shetland, Rogaland, Hordaland, and Nordland groups (Isaken and Tonstad, 1989; Jordt et al., 2000; Annel et al., 2012). This study focuses on the discordant high amplitude anomalies in the upper part of the Hordaland Group which are observed to be associated with sand-rich depositional systems of Middle to Late Oligocene age. In the northern North Sea, the Hordaland Group (Early Eocene to Middle Miocene) reaches a thickness of a few hundred meters and comprises of light grey to brown marine mudstones with inter-beds of thick marine sandstones (Marcussen et al., 2009). The top of the Hordaland Group is marked by the well-known Mid-Miocene unconformity (MMU) while its base is defined by the top tuffaceous Balder Formation (Løseth et al., 2013). Three main post-depositional alteration of the Hordaland Group are observed in seismic cross-section within the interval of interest (Fig. 5.3): (1) polygonal faulting (see Cartwright and Lonergan, 1996; Cartwright, 2011; Wrona et al., 2017a), (2) sand remobilization and injection (see Lonergan et al., 2000; Hurst et al., 2011) and (3) silica diagenesis (see Wrona et al., 2017b).

5.2.2 Regional control on Oligocene deep-water deposition

In the Paleogene, large sand-rich, deep-water channel-lobe systems which were fed by sediments sourced from the Norwegian mainland and the British Isles were deposited along the eastern and western basin margins (Ziegler 1990; Ahmadi et al., 2003; Dmitrieva et al., 2012). Their deposition was influenced by a combination of the Atlantic and north-west European tectonic events, differential tilting and subsidence, climate/sea-level change, and variable sediment supply (Ziegler 1990; Dmitrieva et al., 2012). The tectono-stratigraphic framework of the Oligocene-Miocene succession in the northern North Sea Basin is largely linked to the structural evolution of the north-west European passive margin (Rundberg and Eidvin, 2005).

Detailed dating and mapping of the Oligocene interval have been documented by several workers e.g., Jordt et al. (1995), Danielsen et al. (1997), Liu and Galloway (1997), Michelsen et al. (1998), Jordt et al. (2000), Fyfe et al. (2003), Faleide et al. (2002), Gregersen and Johannessen (2007), Goledowski et al. (2012), Rundberg and Eidvin (2005) and Eidvin et al. (2013, 2014). During the Oligocene, the basin configuration changed, with transition from deep-water marine pelagic sediments to shallow marine facies which indicates that the basin progressively shallowed (Rundberg and Eidvin, 2005). The Oligocene period is documented to be associated with global sea level fall and abundant influx of clastic sediments (Huuse and Clausen, 2001, Fyfe et al., 2003; Rundberg and Eidvin, 2005). The deposition of Oligocene sediments took place in a tectonically quiet passive-margin setting and the Early Oligocene marked the onset of large scale progradation southwards from Scandinavia to the Norwegian-Danish Basin (Eidvin et al., 2014). In the northern North Sea, sediments were supplied and prograded eastward from a dominant western source which resulted from uplift of the eastern Shetland Platform. The main Oligocene depocentres in the

northern North Sea are in the Norwegian sector of the North Viking Graben with > 300 m of sediments (Faleide et al., 2002; Annel et al., 2012). The post-Eocene uplift of the East Shetland Platform during the Early Oligocene – Miocene resulted in three different phases (associated with Oligocene – Miocene compressional tectonic phase) of sand influx into the basin. The first phase which occurred in the Early Oligocene (33 – 28 Ma) resulted in the deposition of c. 400 m thick gravity flow sands in the North Viking Graben (Statfjord – Tampen area) (Rundberg and Eidvin, 2005: see their Fig 8C). The second and last phase occurred during the Early Miocene and Late Miocene/earliest Pliocene respectively (Rundberg and Eidvin, 2005). Late Oligocene sand depositional systems of turbiditic origin were also derived from the eastern source areas (west Norway/Southern Fennoscandia) and these sands were interpreted by Rundberg and Eidvin (2005) and Eidvin et al. (2014) to be contemporaneous with sands deposited in the Statfjord area, and are most likely linked to the Early Eocene uplift of the eastern basin margins. Rundberg and Eidvin (2005: see their Fig. 7a) and Eidvin et al. (2014: see their Fig. 1) presented the approximate outline of the Lower/Upper Oligocene sandy systems in the northern North Sea. However, these sands were previously unnamed in the Cenozoic stratigraphic framework of Isaken and Tonstad (1989) but have been suggested as the Ull Formation (Eidvin et al., 2013; Rundberg and Eidvin, 2016).

5.3 Data

5.3.1 3D Seismic data

This study uses approximately 2630 km^2 of high quality three-dimensional BroadSeis^{TM} seismic volume which covers the whole of blocks 35/1, 35/2, 35/4, 35/5, 35/7, 35/8 and partly covers blocks 35/3, 35/6, 35/9, 35/10, 35/11 (Lomre Terrace area), 35/12, 34/3, 34/6, 34/9 and 34/12 (Fig. 5.2). The seismic data is time-migrated, zero-phase processed and displayed with SEG normal polarity which implies that an acoustic impedance increase with depth is represented by a positive reflection event (peak or red) while a decrease in acoustic impedance with depth is represented by a negative reflection event (trough or blue). It extends downward to a depth (in time) of 5000 msTWT (milliseconds two-way-time), has a sub-sampled line spacing of 37.5 m and 4 ms vertical sampling interval. The frequency bandwidth of the processed 3D seismic data is 25 – 55 Hz with a dominant frequency of c. 50 Hz within the interval of interest (Upper Hordaland Group). Check-shot data from available wells indicate that the average seismic velocity immediately above and below the top Hordaland Group is c. 2000 m/s and thus allows depth or vertical measurements in msTWT to be converted directly to depth (in meters). This implies that the interval of interest which lies between 1150 – 1600 msTWT has a vertical resolution (λ\4) of c. 10 m and a horizontal resolution (λ\2) of c. 20 m, determined using wavelength calculated from the dominant frequency and interval velocity.

5.3.2 Well Data

Data from 30 exploration wells were available for this study (Fig. 5.2 and Table 5.1) from the TGS Facies Map Browser (TGS_FMB). The wells contain complete suite of well logs [e.g., gamma ray (GR), density (RHOB), sonic (DT) and neutron porosity (NPHI)] and lithostratigraphic/formation tops data from the Norwegian Petroleum Directorate (NPD). Check-shot and deviation surveys were available for some of the well. All the available wells penetrated the studied interval which lie between the Middle-Late Oligocene and bounded at the top by the Mid-Miocene Unconformity and at the base by the Eocene-Oligocene boundary (Fig. 5.1c and 5.3). The wells allowed the high amplitude seismic expression of the clastic intrusions to be calibrated to the presence of sand (Fig. 5.14).

5.4 Methods

5.4.1 Seismic-to-well tie

To ensure an accurate tie between the 3D seismic data (in time domain) and well data (in depth domain), synthetic seismograms were calculated for some of the key wells within the study area (Fig. 5.4). For this purpose, a statistically computed wavelet (which involves extracting the required wavelet parameters from the seismic data) was extracted for the key wells. The synthetic seismogram for each well was then computed by convolution of the extracted wavelet from the seismic traces surrounding the well path with the acoustic impedance (or reflectivity) log derived from density and sonic logs. The generated synthetic seismogram allowed proper age constraints to be placed on observed seismic reflection events, identification of key stratigraphic boundaries as well as the assessment of lithological significance of observed amplitude anomalies within the interval of interest.

Based on the generated synthetic seismograms, two key horizons characterized by high seismic amplitude were identified and mapped across the study area. The two horizons correspond to the Mid-Miocene unconformity which is equivalent to the Top Hordaland Group Unconformity (THGU), and the Eocene-Oligocene boundary (EOB). Both horizons bound the top and base of the interval of interest respectively (Fig. 5.3 and 5.4). Log data from Well 35/8-2T2 indicate that the top of the sand unit within the interval of interest (Fig. 5.4) correspond to an increase in acoustic impedance and the generated synthetic seismogram show that this corresponds to a high amplitude positive reflection (red peak) which may have resulted from the interference between mudstone and sandstone units within the interval of interest. In contrast to the latter, the log data also show that the base of the sand unit corresponds to a decrease in acoustic impedance which in the generated synthetic seismogram corresponds to a high amplitude negative reflection (blue trough).

5.4.2 Seismic Interpretation

This involved mapping reflection events associated with two main stratigraphic boundaries (MMU & EOB) beginning at the well locations (Fig. 5.5). The geometry of the mapped Mid-Miocene Unconformity horizon provides an insight into the impact of differential compaction across the Middle-Late Oligocene depositional system beneath the horizon over time (Fig. 5.5a). We generated a two-way-time (TWT) thickness map (Fig. 5.5c) which allowed us to assess variation in thickness of the studied interval and provides insight into the syn-depositional geometry of the basin during the Oligocene to Mid-Miocene. Seismic attribute maps (e.g., root-mean-square (RMS) amplitude and chaos attributes; see Brown, 1996, 2001) and time-shifted horizons (e.g., horizon slices) were generated to image features of interest. In generating the attribute maps, we utilized the horizon parallel amplitude extraction methods to ensure the maps follow true geological/stratigraphic timelines as closely as possible (Dmitrieva et al., 2018). To visualize the distribution of the Middle – Late Oligocene depositional system, an RMS amplitude map was created from an RMS attribute volume generated at a 9 ms sample window. Although great caution was taken in generating the attribute maps, it is to be noted that some of the high amplitude anomalies visualized in the north-western part of the study area (see Fig. 5.6) may likely represent sediments of slightly different age. This is largely based on the intrinsic complexity of the studied depositional system due to its associated large-scale post-depositional remobilization and injection. We however, ensured proper cross-referencing between the RMS map and the sections taken through it by ensuring that the high amplitude anomalies in map-view correspond well to anomalies in cross-section.
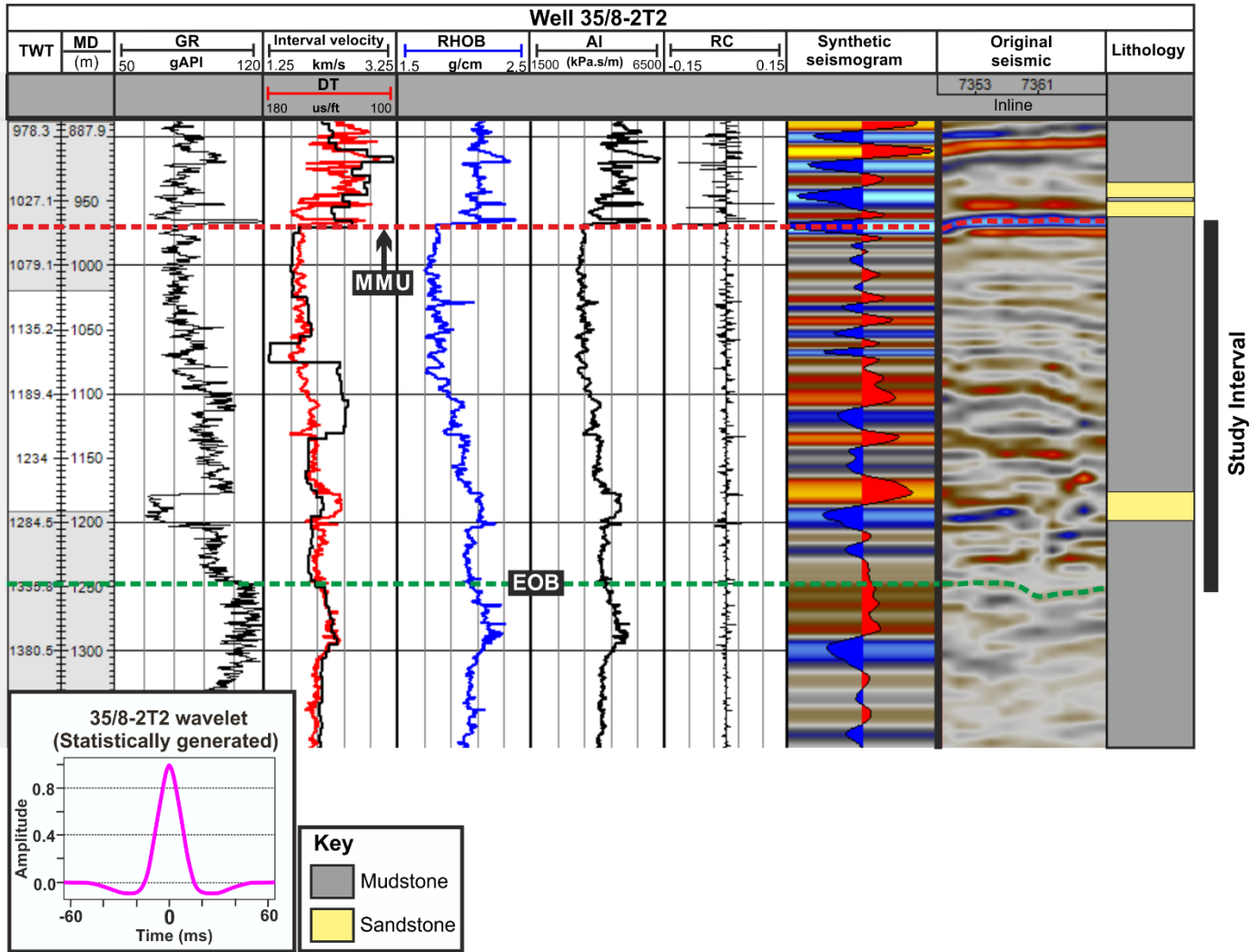
Fig. 5.4: Synthetic seismogram generated for Well 35/8-2T2. Interpretation of the lithology is shown using the gamma-ray and sonic log with the key stratigraphic boundaries highlighted. Well location is shown in Fig. 5.2. MMU – Mid-Miocene Unconformity, EOB – Eocene-Oligocene Boundary. Well data from TGS Facies Map browser.

Table 5.1: Well table with formation tops (CALI-calliper, DRHO-density correction, DT-interval transit time, GR-gamma ray, NPHI-neutron porosity, ILD-deep resistivity, RHOB-bulk density, SP-spontaneous Potential, PEF- Photoelectric Factor). TD – Total depth, TNG – Top Nordland Group, THGU – Top Hordaland Group Unconformity or MMU – Mid-Miocene Unconformity, TRG – Top Rogaland Group, FMB – Facies Map Browser, NPD – Norwegian Petroleum Directorate.

Well	TD (m)	Wireline Data	Top Depth (from TGS_FMB & NPD)		
			TNG (m)	THGU or MMU (m)	TRG (m)
35/4-1	4936	CALI, DT, GR, ILD, NPHI, RHOB, SP	404	1116	1720
35/7-1S	4825	CALI, DT, DRHO, GR, ILD, NPHI, RHOB	426	1062	1780
35/8-1	4345	CALI, DT, GR, ILD, NPHI, RHOB, SP	402	964	1683
35/8-2T2	4356	CALI, DT, GR, ILD, NPHI, RHOB, SP	406	964	1675
35/8-3T2	3944	CALI, DT, GR, ILD, NPHI, RHOB, SP	396	797	1465.7
35/8-4	3719	DT, GR, ILD, NPHI, RHOB	394	815	1528
35/9-6S	3740	CALI, DT, DRHO, GR, ILD, NPHI, RHOB	394	789	1229
35/9-11A	3859	CALI, DT, DRHO, GR, ILD, NPHI, RHOB	393	605	1253
35/9-7	3006	CALI, DT, GR, DRHO, ILD, NPHI, RHOB, PEF	397	706	1288
35/9-8	3256	CALI, DT, DRHO, GR, ILD, NPHI, RHOB	392	695	1221
35/9-10S	3619	CALI, DT, GR, DRHO, ILD, NPHI, RHOB, PEF	389	656	1277
35/9-12S	3556	CALI, DT, DRHO, GR, ILD, NPHI, RHOB	382	624	1000
35/10-1T2	3986	CALI, DT, GR, ILD, NPHI, RHOB	384	948	1755
35/11-1	3361	CALI, DT, GR, ILD, NPHI, RHOB, SP	385	710	1307
35/11-2	4025	CALI, DT, GR, ILD, NPHI, RHOB, SP	395	1081	1663
35/11-3S	4040	CALI, DT, GR, ILD, NPHI, RHOB, SP	383	866	1728
35/11-5	3769	CALI, DT, GR, ILD, NPHI, RHOB, SP	382	855	1701
35/11-6	3995	CALI, DT, GR, ILD, NPHI, RHOB, SP	396	843	1625
35/11-9	2830	CALI, DT, GR, ILD, NPHI, RHOB	386	783	1534
35/11-11	3225	CALI, DT, GR, NPHI, RHOB, SP	383	763	1466
35/11-12	3378	CALI, DT, GR, NPHI, RHOB	388	896	1727
35/11-13	3292	CALI, DT, DRHO, GR, ILD, NPHI, RHOB	387	763	1541
35/11-14S	3306	CALI, DT, DRHO, GR, ILD, NPHI, RHOB	387	800	1548
35/11-15ST5	3250	CALI, DT, GR, NPHI, RHOB	389	798	1531
35/11-16ST2	3554	CALI, DT, GR, ILD, NPHI, RHOB	392	750	1629
35/11-17	2900	CALI, DT, GR, DRHO, ILD, NPHI, RHOB, PEF	382	766	1455
35/11-18A	4020	CALI, DT, GR, ILD, NPHI, RHOB	397	948	1711
35/12-2	2541	CALI, DT, GR, DRHO, ILD, NPHI, RHOB	389	675	1285
35/12-3S	2809	CALI, DT, GR, DRHO, ILD, NPHI, RHOB	381	570	1120
35/12-4A	3413	CALI, DT, GR, DRHO, ILD, NPHI, RHOB	389	650	1305
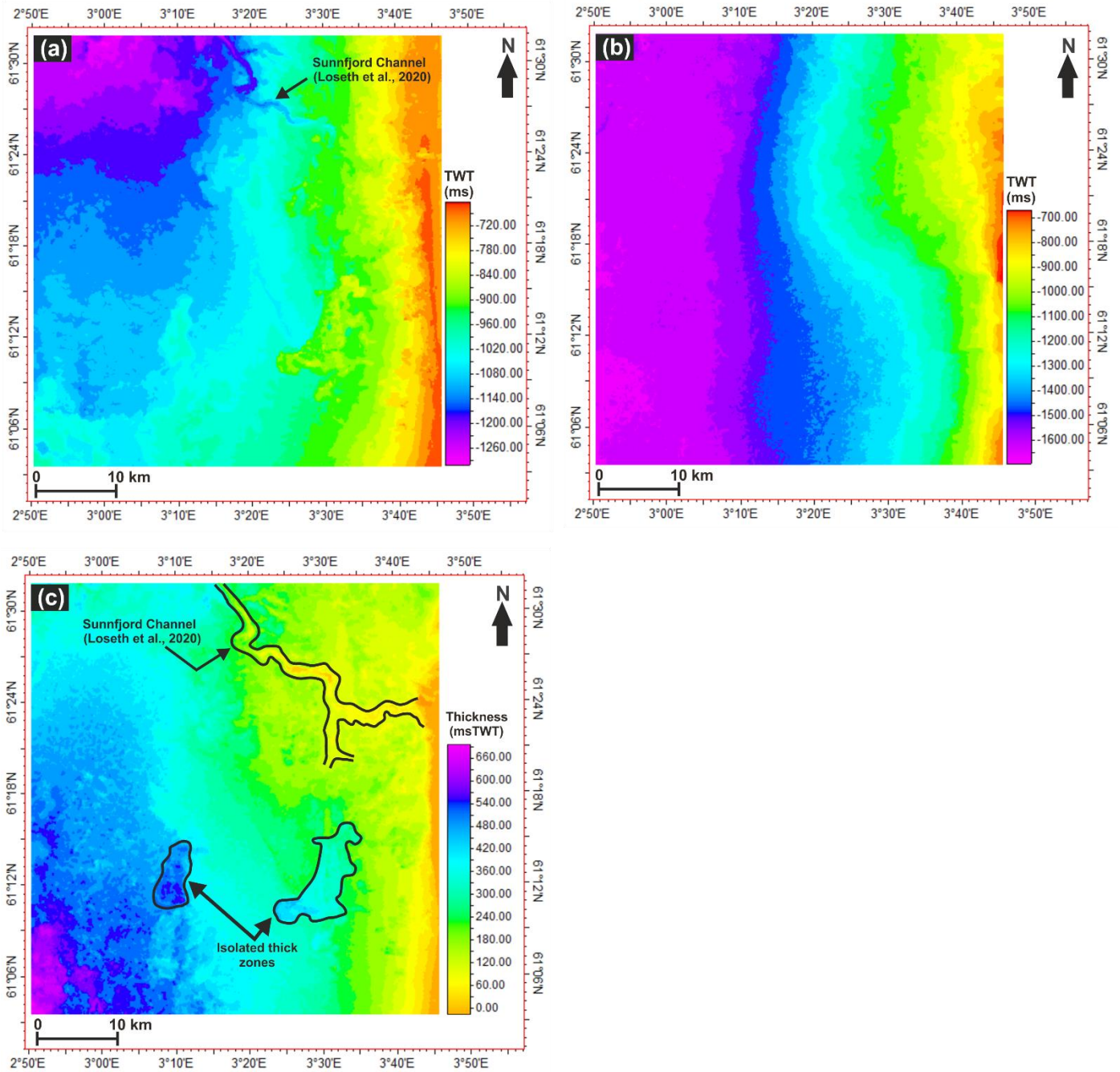
Fig. 5.5: Time structure map of: (a) the Mid-Miocene Unconformity (MMU), (b) Eocene-Oligocene Boundary (EOB), and (c) Time-thickness map between MMU and EOB. Seismic data courtesy of CGG.

5.5 Results

5.5.1 Oligocene Succession

The Oligocene succession which forms part of the Lark Formation (see Fig. 5.1c) shows an overall thickening towards the west and south-west (Fig. 5.5c) and the interval is pervasively affected by intra-formational faulting (see Fig. 5.3a and Fig. 5.7) which have been previously described in detail by Clausen et al. (1999) and Wrona et al. (2017a). The Oligocene succession in the study area can be sub-divided into two distinct seismic units (Fig. 5.3): (a) Lower Oligocene unit (OL-1) and (b) Upper Oligocene unit (OL-2), separated by a moderately-high amplitude semi-continuous reflection which corresponds to the Opal-A/CT diagenetic boundary (see work by Rundberg, 1989; Thyberg et al., 1999; Wrona et al., 2017b), highlighted by a light blue line in Fig. 5.3b & 5.11a. The Lower Oligocene unit overlies the Eocene-Oligocene Boundary (EOB), pinches out eastwards (Fig. 5.3) and has been reported by Wrona et al. (2017b: their Fig. 3 & 4) as the Opal-CT zone which represents Opal-CT-rich sediments that were subjected to Opal-A/CT transformation. On the other hand, the Upper Oligocene unit is polygonally faulted and characterized by the presence of numerous discordant amplitude anomalies (e.g., Fig. 5.3). This unit has also been documented by Wrona et al. (2017b) as the Opal-A zone which represents the earliest stage of silica diagenetic process at which no transformation has occurred.

5.5.2 Distribution and seismic reflection pattern of the Middle – Late Oligocene Depositional System

Available date indicates the development of series of high amplitude anomalies in the Middle – Late Oligocene succession. These anomalies are interpreted as the seismic expression of a deep-water depositional system and are here referred to as the 'Middle – Late Oligocene Depositional System (MLODS). Due to their high seismic amplitude expression, their geometry and distribution have been illustrated here using an RMS amplitude map extracted at a horizon offset of 130 ms below the MMU seismic horizon (Fig. 5.6). The Middle – Late Oligocene depositional system based on the extracted RMS amplitude map is defined by high amplitude anomalies with an east-west and northeast-southwest trend (Fig. 5.6). They are observed to terminate abruptly basinward towards the west and southwest with transition into a low amplitude mudstone dominated section, with associated polygonal faults in the western parts of the study area (Fig. 5.6 and 5.7). For ease of description and characterization, the Middle – Late Oligocene depositional system has been divided into three distinct segments based on the observed lateral variation in seismic reflection pattern using the RMS amplitude map (Fig. 5.6).

Segment-1 (Sg-1) covers an area of c. 580 km^2 in the northern part of the study area (Fig. 5.6, Table 5.2). In cross-section, the seismic pattern of the segment is characterized by continuous – discontinuous high amplitude reflections with series of discordant high amplitude anomalies with varying geometries (Fig. 5.8). The geometries of the observed discordant amplitude anomalies range from a conical (V/W) shaped, bowl-shaped/wing-like reflection with bedding concordant

bases and steeply dipping wings which crosscut the host strata and varying degree of irregular to complex-shaped anomalies (Fig. 5.8). The discordant amplitude anomalies are in cross-section characterized by an upper moderate to high amplitude peak reflection and a lower moderate to high amplitude trough, thereby forming a peak-trough pair. Most of the anomalies appear to be connected to anomalies adjacent and above them. In the northern part of segment-1, bowl-shaped and V-shaped anomalies are observed to be connected and crosscut each other with a general occurrence at different levels (Fig. 5.8 b and c). The network of wing-like reflections associated with the flat-based anomalies extend upward for c. 50 – 100 ms while the V/W-shaped anomalies have limb heights of c. 80 – 160 ms. The western and southern part of Segment-1 comprises of highly irregular shaped anomalies with some well-defined V/W-shaped and bowl-shaped anomalies (Fig. 5.8a, d and e). The discordant anomalies associated with the Middle – Late Oligocene depositional system have dips in the range 7 – 30°. A north-south cross-section through Segment-1 shows a transition from wing-like/bowl-shaped anomalies in the north to conical amplitude anomalies to the south (Fig. 5.8b).

In map view, these amplitude anomalies have lobate and circular to sub-circular plan view geometry which are up to 2 km in diameter or are elongate with length of up to 4.5 km and 1 km wide (refer to Fig. 5.6). A common observation above some of the bowl-shaped and V/W-shaped anomalies is the pronounced deformation of the host rock which occur as forced folds/dome-shaped anticline/jack-up of overburden and steeply dipping mounds developed along the overlying MMU (Fig. 5.8b, e, f and g). The mounds are approximately 30 – 70 ms (not decompacted) high above the regional trend of the MMU surface. The edges of the folds are observed to spatially coincide with the uppermost edges of the wing-like discordant anomalies, with some of the folds down-lapped and on-lapped by overlying younger sediments (Fig. 5.8a and g).

Well 35/7-1S penetrated the south-western edge of Segment-1 where it intersected a discordant high amplitude anomaly in cross section. Well 35/7-1S has excellent wireline logs through the interval of interest and gamma-ray log show the well encountered a c. 25 m thick sandstone unit (encased in mudstone) corresponding to the high amplitude anomaly (see Fig. 5.14a).
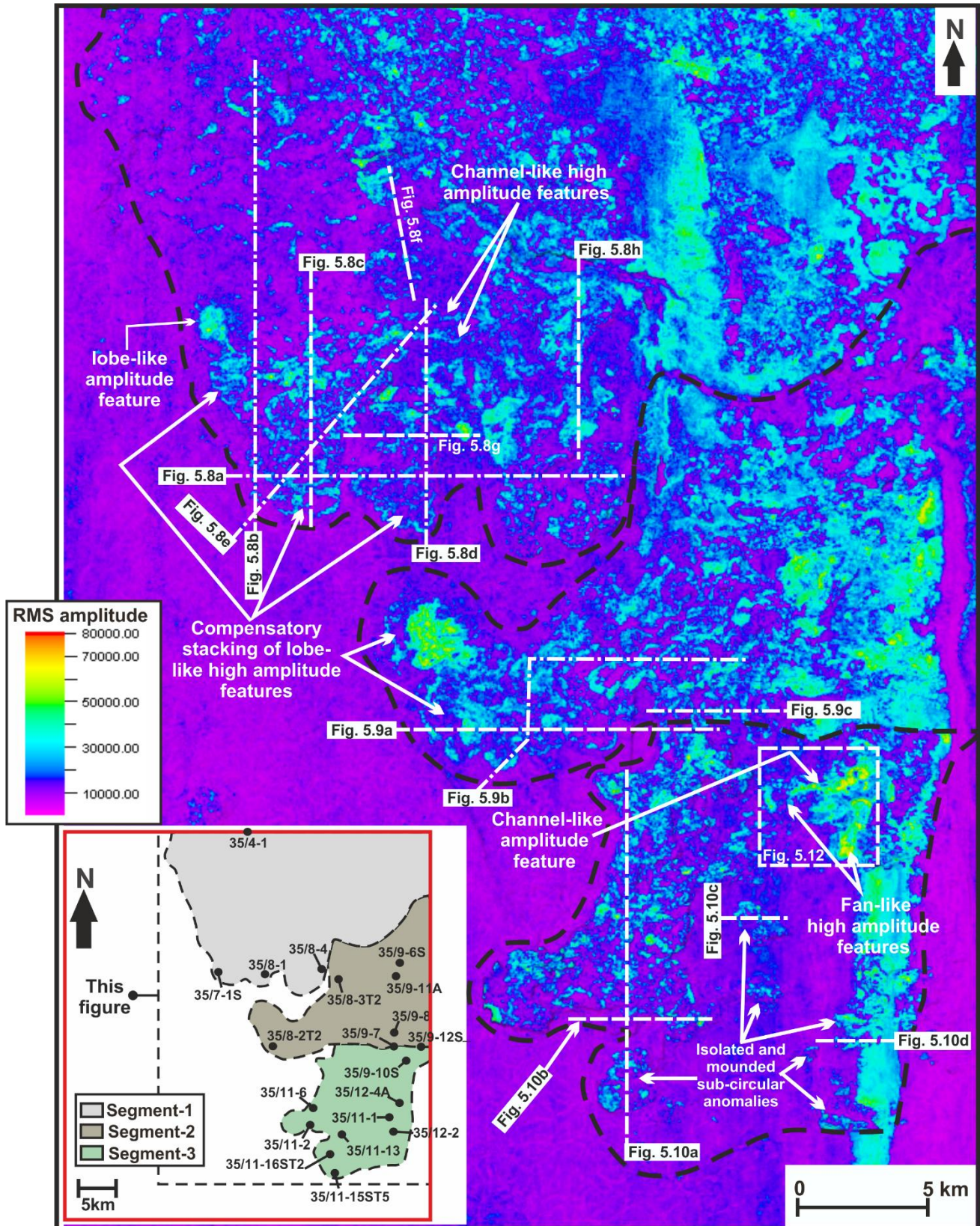
Fig. 5.6: RMS amplitude map generated from an RMS volume at a horizon offset of 130 msTWT (downward shift) below the Mid-Miocene Unconformity (reference horizon) which shows the extent of the Middle – Late Oligocene depositional system. The position of the RMS map is shown in Fig. 5.3b. Its shape is defined by the shape of the MMU, and the RMS amplitudes are extracted where the shifted surface intersects the RMS volume. Black dash line shows the distribution of the three main segments of the Middle-Late Oligocene

depositional system, defined from their reflection character. White dash lines represent cross-sections taken across the segments. The RMS map highlights some depositional features which are in cross-section clearly modified by large-scale post depositional remobilization and injection. The inset map shows the location of wells penetrating the segments of the Middle – Late Oligocene depositional system. See location in Fig. 5.2 and 5.7. Seismic data courtesy of CGG.
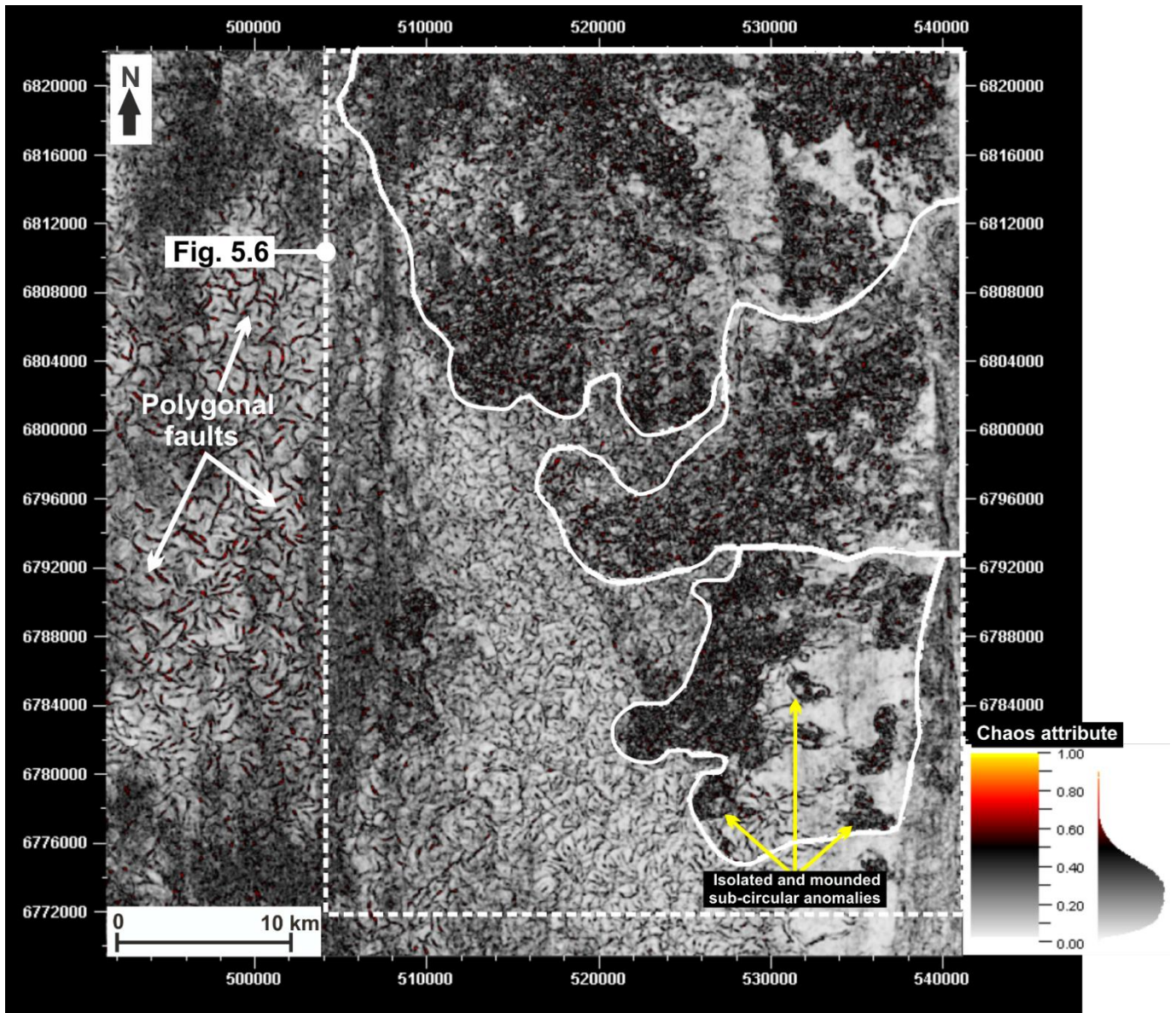
Fig. 5.7: Chaos attribute map generated at a horizon offset of 130 msTWT (downward shift) below the Mid-Miocene Unconformity (reference horizon) which shows the distribution of polygonal faults in the study area. The boundaries of the segments are shown by the white bold outlines. See extent of seismic is shown in Fig. 5.2 and the red outline in the insert map in Fig. 5.6. Seismic data courtesy of CGG.
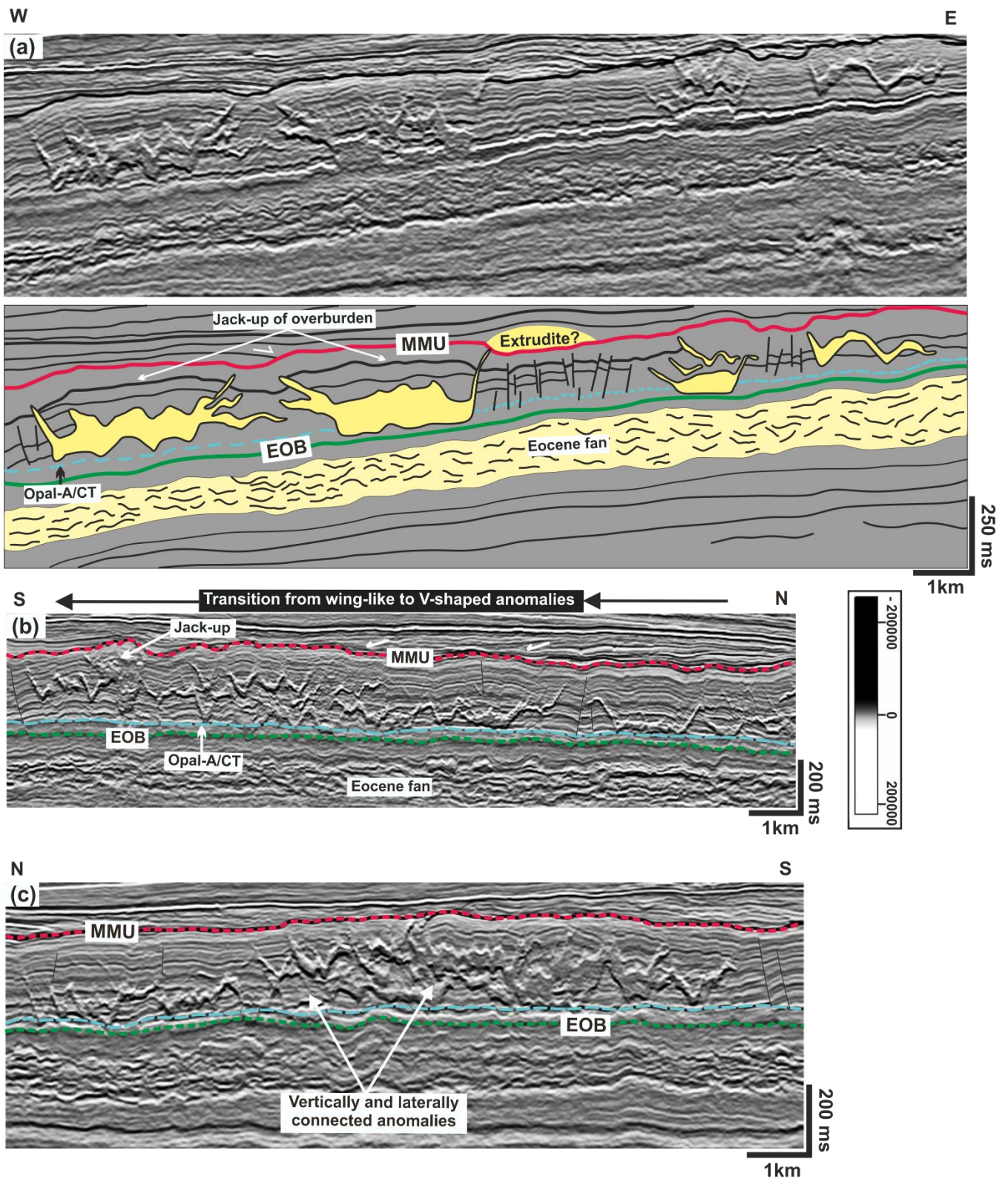
Fig. 5.8: Sand remobilization features observed in seismic cross sections taken across Segment-1. (a) A series of flat-based or bowl-shaped features with wing-like features at their margins. One of the anomalies appear to have extruded at the paleo-seafloor; (b) A north-south seismic section showing a transition from wing-like to V-shaped discordant high amplitude anomalies; (c) Vertically and laterally connected discordant amplitude anomalies. See location of sections in Fig. 5.6. MMU: Mid-Miocene Unconformity, EOB: Eocene – Oligocene Boundary. Seismic data courtesy of CGG.
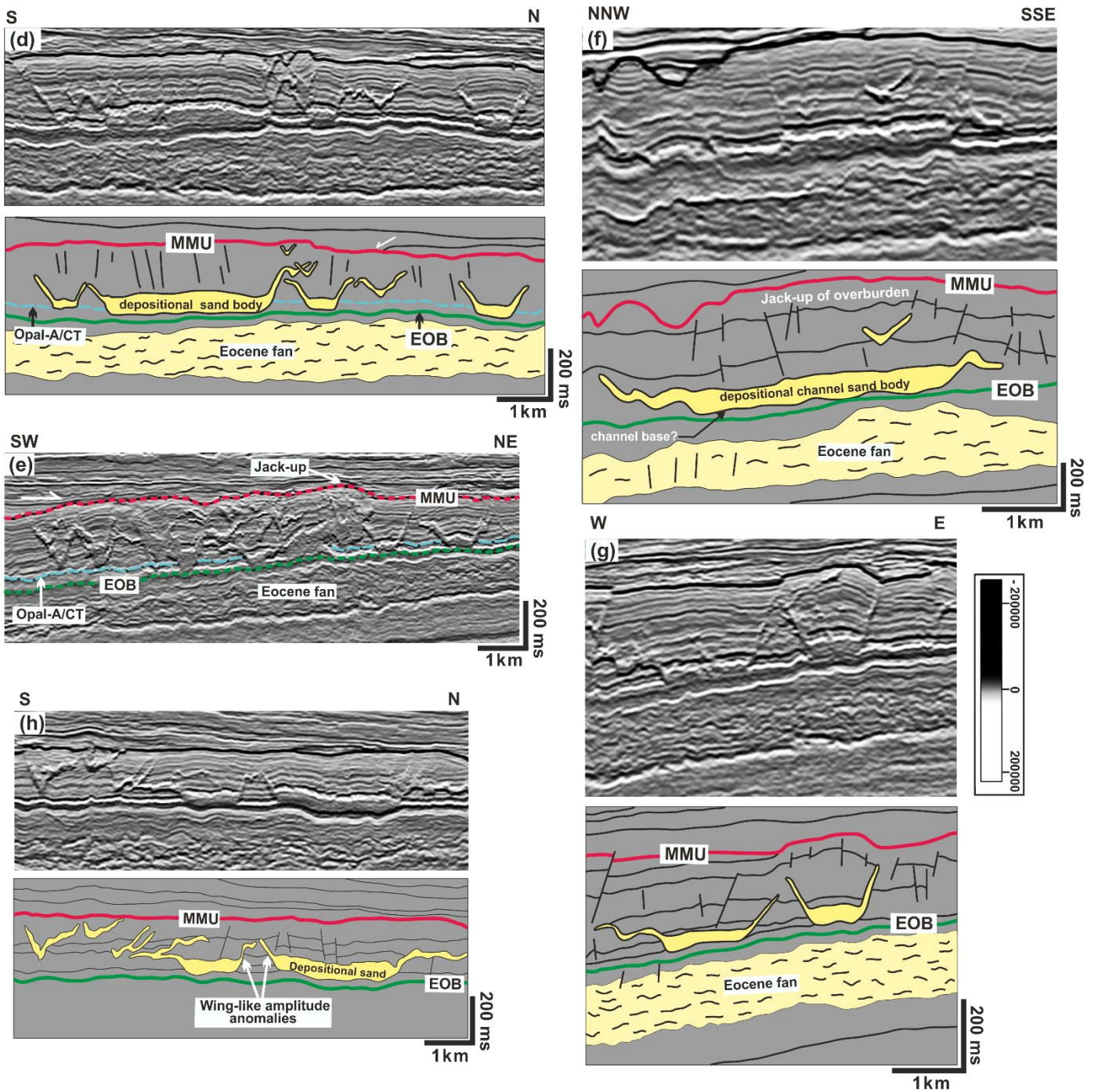
Fig. 5.8 (cont.): (d) Series of adjacent concordant amplitude anomalies with marginal wings interpreted as depositional channel sand bodies with intrusions at their margins; (e) Transition from wing-like anomalies to V-shaped discordant anomalies with some anomalies connected; (f), (g) & (h) Bowl-shaped/wing-like anomalies characterized by jack-up of the overburden above the anomalies related to differential compaction of the sand bodies. See location of sections in Fig. 5.6. MMU: Mid-Miocene Unconformity, EOB: Eocene – Oligocene Boundary. Seismic data courtesy of CGG.

Segment-2 (Sg-2) covers an area of c. 280 km^2 in the central and eastern part of the study area and extends westwards. It is characterized by variation in RMS amplitude with the highest amplitudes observed in the eastern and western margins of the segment (Fig. 5.6). Seismic cross section shows that the Middle – Late Oligocene depositional system in this segment is characterized by numerous high amplitude anomalies (mainly in the western part) consisting of a combination of V/W-shaped, bowl-shaped, sheet-like and abundance of irregular to complex-shaped anomalies (Fig. 5.9, 5.11). Some of the amplitude anomalies also appear connected as observed in Segment-1. The V/W-shaped and wing-like anomalies have limbs/wings extending upwards for c. 50 – 150 ms and c. 80 – 100 ms respectively. While the sheet-like amplitude anomalies have lengths ranging from 1.5 – 3.5 km. In map view, the amplitude anomalies associated with the Middle-Late Oligocene depositional system in Segment-2 have sub-circular (with diameter of up to 1.5 km) and lobate to elliptical plan view geometry (Fig. 5.6). The lobate to elliptical geometries are more pronounced towards the western part of the segment. As observed in Segment-1, dome-shaped anticlines/folds are also observed above some of the anomalies with onlap of younger sediments on the MMU. However, they are more subtle compared to those in Segment-1.

Well 35/8-2T2 penetrated the western edge of Segment-2 (see Fig. 5.6) where it intersected a V-shaped discordant amplitude anomaly with a steeply dipping limb (dike) which passes upwards into a concordant element (sill), and the latter passes back into a discordant element (dike). The V-shaped anomaly lies 60 ms above the Eocene – Oligocene Boundary and appear to be connected to an adjacent V-shaped anomaly by a concordant high amplitude element of c. 1.2 km long (Fig. 5.14b). Well 35/8-2T2 also has excellent wireline coverage through the interval of interest and gamma-ray log data indicates the well intersected a c. 25 m thick sand unit encased in overlying and underlying mudstone units (Fig. 5.4 and 5.14b). The well completion report for the above well described the cuttings sample derived at the depth interval (1175 – 1200 m) of the top and base of the anomaly intersected by the well to consist of a coarse, sub-angular to well rounded, well sorted and unconsolidated sandstone.

Segment-3 (Sg-3) occupies the south-eastern part of the study area and covers an area of c. 230 km^2. It is also characterized by variation in RMS amplitude with the highest amplitudes occurring at the western and eastern part of the segment, while a well-defined dimming in seismic amplitude is observed from the centre down to the southern part of the segment (Fig. 5.6). In map view the Middle – Late Oligocene depositional system consists of sub-circular to irregular shaped anomalies, as well as some isolated sub-circular anomalies which have diameters of 0.7 – 2 km. The isolated anomalies are best imaged on the chaos attribute map in Fig. 5.7. The isolated sub-circular anomalies are observed in cross-section to have similar geometrical characteristics as the bowl-shaped/wing-like anomalies in Segment-1 & 2 (see Fig. 5.10c and 5.13). However, some appear connected to adjacent anomalies and have steep-dipping flanks at the margin of the bowl-shaped anomalies (Fig. 5.10d).

Seismic cross-section through the western part of Segment-3 (Fig. 5.10a) show that the amplitude anomalies consist of amalgamated and/or stacked complexes characterized by a combination of

several conical shaped and irregular to complex-shaped anomalies which occur at different levels within the interval. They are also observed to crosscut each other, with some connected to anomalies above and adjacent to them (Fig. 5.10a). The amplitude anomalies in Segment-3 are associated with more pronounced deformation of the overburden (occurring as steeply dipping mounds) above them compared to that observed for Segment-1 & -2, with associated onlap and downlap of younger sediments above the host strata (Fig. 5.10a – c).

Well 35/11-2 and 35/11-13 penetrated the western part of Segment-3 comprising of the amalgamated/stacked amplitude anomalies (see insert map in Fig. 5.6). They were observed to have intersected two or more discordant amplitude anomalies in cross-section. However, the anomalies crosscut by both wells could not be calibrated due to missing wireline data in the interval of interest. The north-eastern part of the segment shows a very high amplitude anomaly with two distinct channel-shaped geometry (Ch-A & Ch-B) in plan-view (Fig. 5.12a). One of the channel-shaped anomalies (Ch-A) is straight and slightly sinuous, 0.2 – 0.4 km wide and 3.5 km long. The channel-A anomaly trends east-west and terminates down-dip to the west in a fan-shaped anomaly of about 1.4 km wide (Fig. 5.12a). On a north-south oriented seismic cross section through the fan-shaped anomaly, it is observed that the fan comprises of a 20 – 40 ms thick sheet-like high amplitude anomaly with top peak and base trough reflection and discordant margins (Fig. 5.12c). In addition, a north-south oriented cross-section across the channel axis show a flat-based anomaly with discordant wing at one of its margins (Fig. 5.12d).
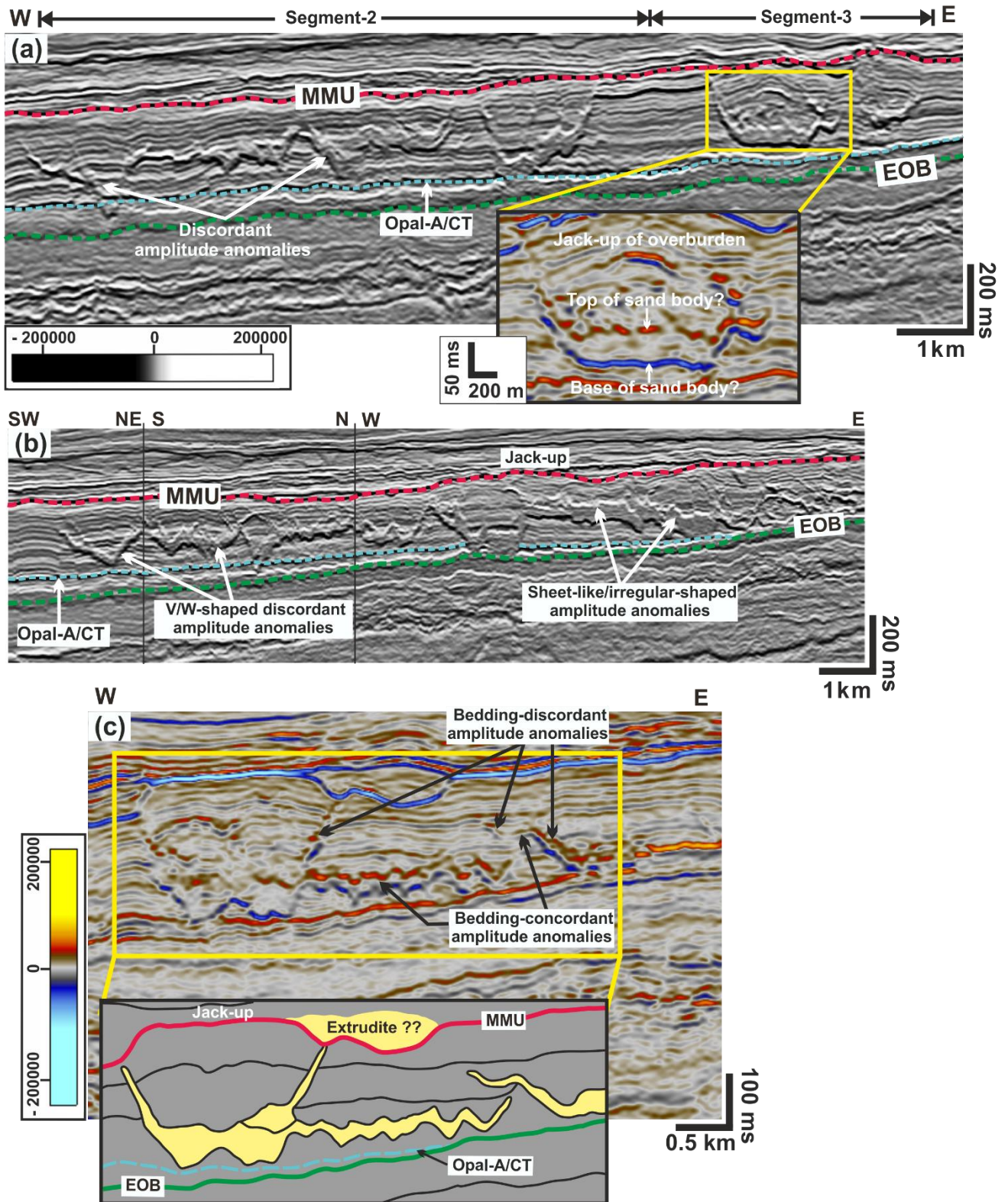
Fig. 5.9: Sand remobilization features observed in seismic cross sections taken across Segment-2. (a) Laterally connected discordant amplitude anomalies, a well-defined channel-like anomaly with marginal wings and jack-up of overburden above the channel sand body (see Fig. 5.11) which may be related to differential compaction; (b) laterally connected V and W-shaped anomalies with adjacent sheet-like amplitude anomalies; (c) Anomalies characterized by bedding concordant and discordant elements. See location of sections in Fig. 5.6. MMU: Mid-Miocene Unconformity, EOB: Eocene – Oligocene Boundary. Seismic data courtesy of CGG.
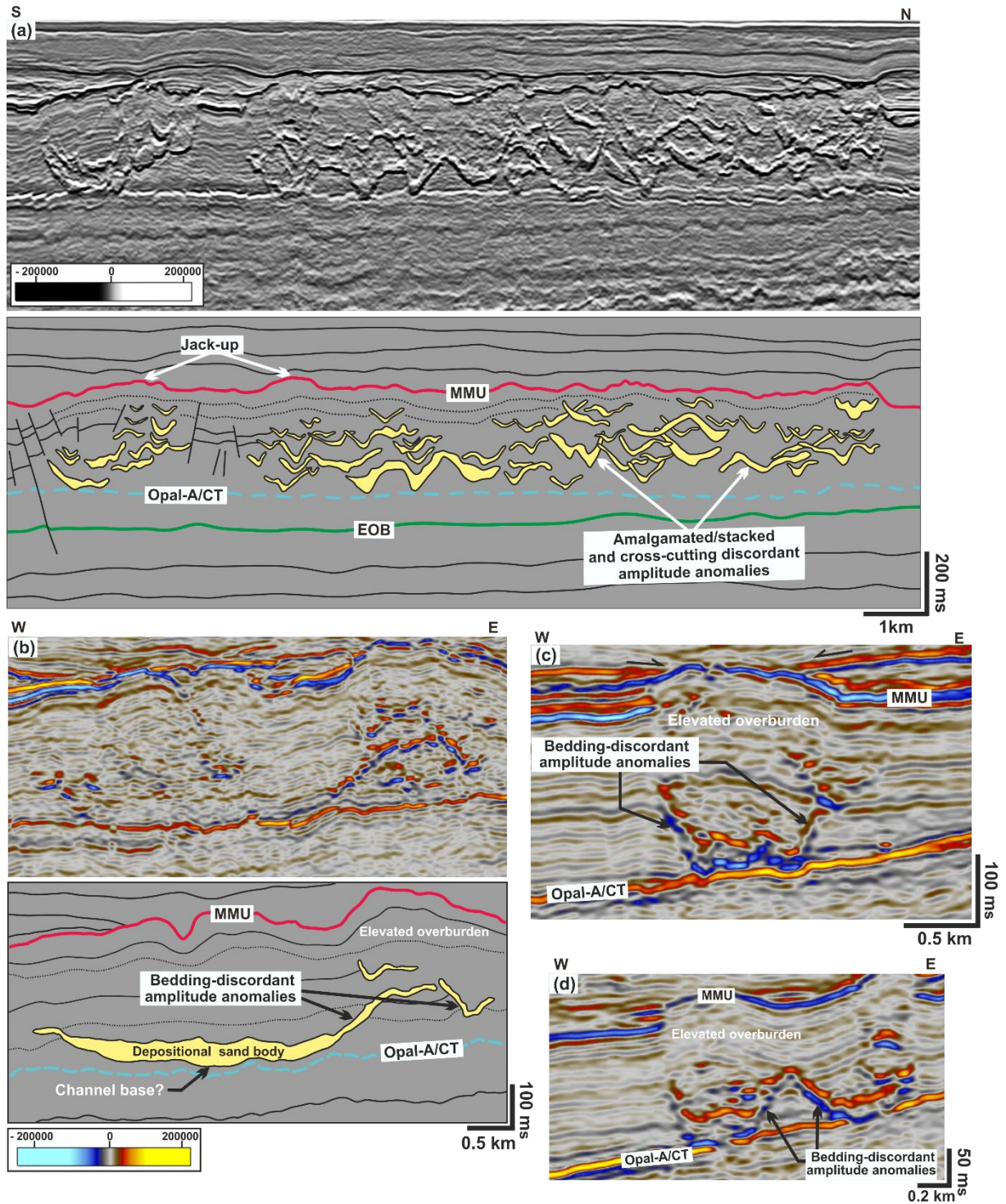
Fig. 5.10: Sand remobilization features observed in seismic cross sections taken across Segment-3. (a) Amalgamated and stacked complexes (covers a major part of Segment-3) characterized by a combination of conical, bowl-shaped, and irregular shaped discordant amplitude anomalies which crosscut each other; (b) a wing-like intrusion emanating from the concordant to bedding depositional sandstone body with jack-up of overburden above the sand body. (c) & (d) Wing-like amplitude anomalies, with pronounced jack-up of overburden, observed in plan-view as isolated sub-circular anomalies in Segment-3. See location of sections in Fig. 5.6. MMU: Mid-Miocene Unconformity, EOB: Eocene – Oligocene Boundary. Seismic data courtesy of CGG.

5.6 Discussion

5.6.1 Middle – Late Oligocene Depositional System and origin of associated amplitude anomalies

Wells in the study area directly penetrate the amplitude anomalies associated with the Middle – Late Oligocene depositional system (Fig. 5.6). Well calibration of the anomalies has yielded tens-of-meters of sand-bearing units at intervals where wells are observed to intersect discordant high amplitude anomalies with varying geometries associated with the Middle – Late Oligocene depositional system (Fig. 5.14). This unequivocally implies that the high amplitude anomalies are caused by sand presence. The amplitude anomalies associated with the Middle – Late Oligocene depositional system (in each segment) is in all cases defined by a top high amplitude peak (red) reflection and a base high amplitude trough (blue) reflection event (e.g., Fig. 5.9c, 5.10c - d and 5.14). The observed dimming in amplitude or decrease in RMS amplitude values to the west, north-west and south-western parts of the study area may imply a transition from sand-bearing units in the east, north-east and south-east to mud-dominated successions. This is supported by pervasive polygonal faulting in the west, north-west and south-western parts of the study area which are known to form in fine-grained mudstone-dominated succession in response to compaction-related-early-stage dewatering of sediments (Cartwright and Dewhurst, 1998; Cartwright, 2011). The network of polygonal faults is well image on a chaos attribute map extracted 130 ms below the Mid-Miocene Unconformity in Fig. 5.7. However, the presence of some isolated high amplitude anomalies outside the outline of the segments which have similar cross-sectional geometry to the discordant high amplitude anomalies in Segment-1 to 3 may indicate that sandstones are present beyond the inferred extent of the Middle – Late Oligocene depositional system.

The bedding-discordant and bedding-concordant amplitude anomalies associated with the Middle – Late Oligocene depositional system is here interpreted as the seismic expression of sand injectites/intrusions, which result from post-depositional remobilization and injection of fluidized sands. This interpretation is based on: (1) their direct connection to the Middle – Late Oligocene depositional system, (2) their discordant relationship with the host strata, (3) their circular to sub-circular plan view and complex cross-sectional geometries, and (4) the calibration of the discordant amplitude anomalies to tens-of-meters of sandstone encased within mudstone-dominated succession. The discordant relationship between the anomalies and their host strata indicates that they are not genetically related but were formed after the deposition of the mudstone-dominated host strata. Their distinct geometry (conical, bowl-shaped, and complex geometries) in cross-section, acoustic properties and scale are comparable to similar features widely documented in the Paleogene of the North Sea. Their three-dimensional geometries are like those described in Tampen Spur (Huuse and Mickelson, 2004), Outer Moray Firth (Gras and Cartwright, 2002; Molyneux et al., 2002); South Viking Graben (Huuse et al., 2004; Løseth et al., 2003), Fareo-Shetland basin (Cartwright et al., 2008) and Måløy slope (Jackson, 2007; Jackson et al., 2011). The dome-shaped anticlines/folds/jack-up of overburden associated with the amplitude anomalies are interpreted to be the result of differential compaction of the Middle – Late Oligocene depositional system sand

bodies and surrounding mudstones. This is also the reason for the mounded nature of the Mid-Miocene Unconformity observed mainly in Segment-3 (Fig. 5.10).
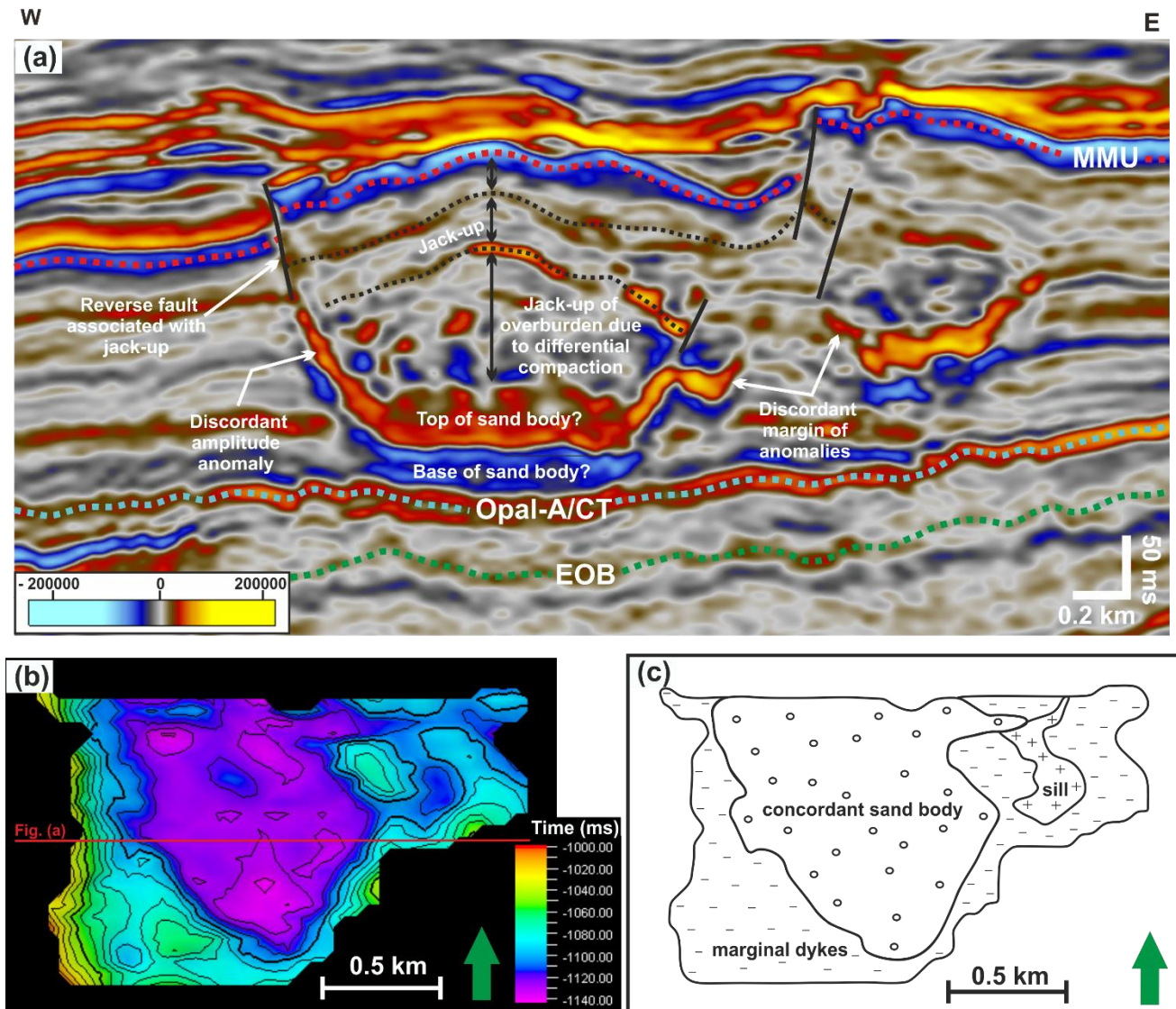
Fig. 5.11: (a) Illustration of jack-up of the overburden above a wing-like discordant amplitude anomaly, with a concordant base and inclined margins emanating from the concordant part at an angle of 13° reaching a height of approximately 70 – 120 msTWT. This demonstrates jack-up related to differential compaction and the reverse aspect of the associated jack-up faults. Location of seismic line is shown in Fig. 5.2 and 5.9a. (b) TWT-structure map of the wing-like sand body, with the bedding-parallel part extending over 0.9 km (E – W). The red line represents the seismic section in Fig. 5.11a. (c) Schematic illustration of the different elements (marginal dikes, concordant base and sills) that make up the mapped isolated Middle-Late Oligocene channel-sand body modified by post-depositional remobilization and injection. MMU: Mid-Miocene Unconformity, EOB: Eocene – Oligocene Boundary. Seismic data courtesy of CGG.
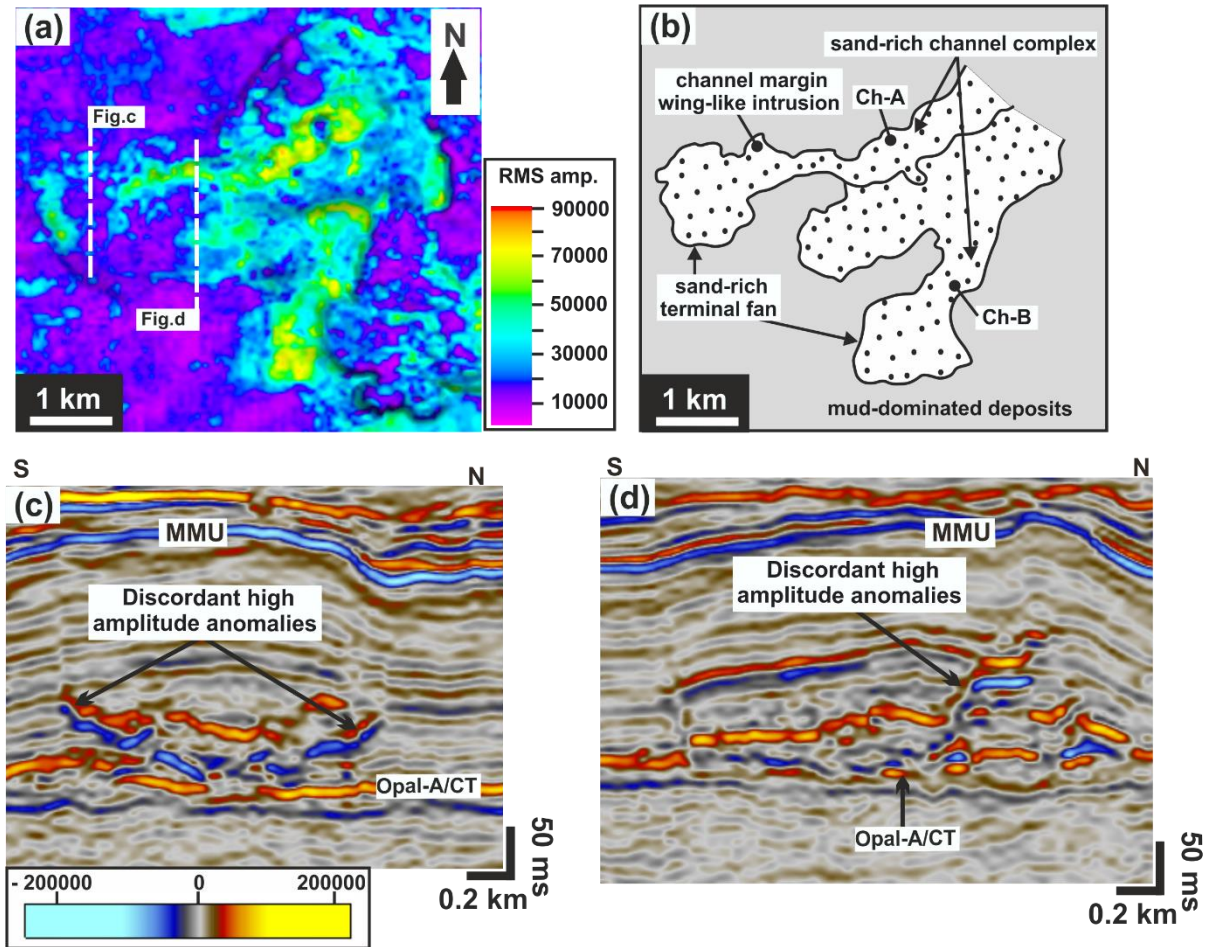
Fig. 5.12: (a) High amplitude anomaly with two distinct channel-shaped geometry (Ch-A & Ch-B) in the north-eastern part of Segment-3. Both channels terminate down-dip into a fan-shaped high amplitude feature; (b) Schematic illustration of the channel and fan-shaped features; (c) Seismic cross-section across the fan-shaped feature (Fan-A) shows a sheet-like (concordant) high amplitude anomaly with discordant margins; (d) Seismic cross-section across the channel-A axis shows a bedding-discordant wing developed adjacent to the submarine channel-A. Location of figure is shown in Fig. 5.6. MMU: Mid-Miocene Unconformity. Seismic data courtesy of CGG.

Table 5.2: Table showing estimated characteristics of the three segments of the Middle – Late Oligocene Depositional System (MLODS). Wells calibrated to anomalies they intersected in each segment are also shown together with the approximate thickness of the sand units encountered. Location of wells within each segment is shown by the insert map in Figure 5.6.

Segments	Area (km²)	% of entire study area	Wells calibrated to anomalies	Approx. sand unit thickness (m)
Segment-1	580	22	35/7-1S	25
Segment-2	280	11	35/8-2T2	25
Segment-2	230	8.6	-	-

.
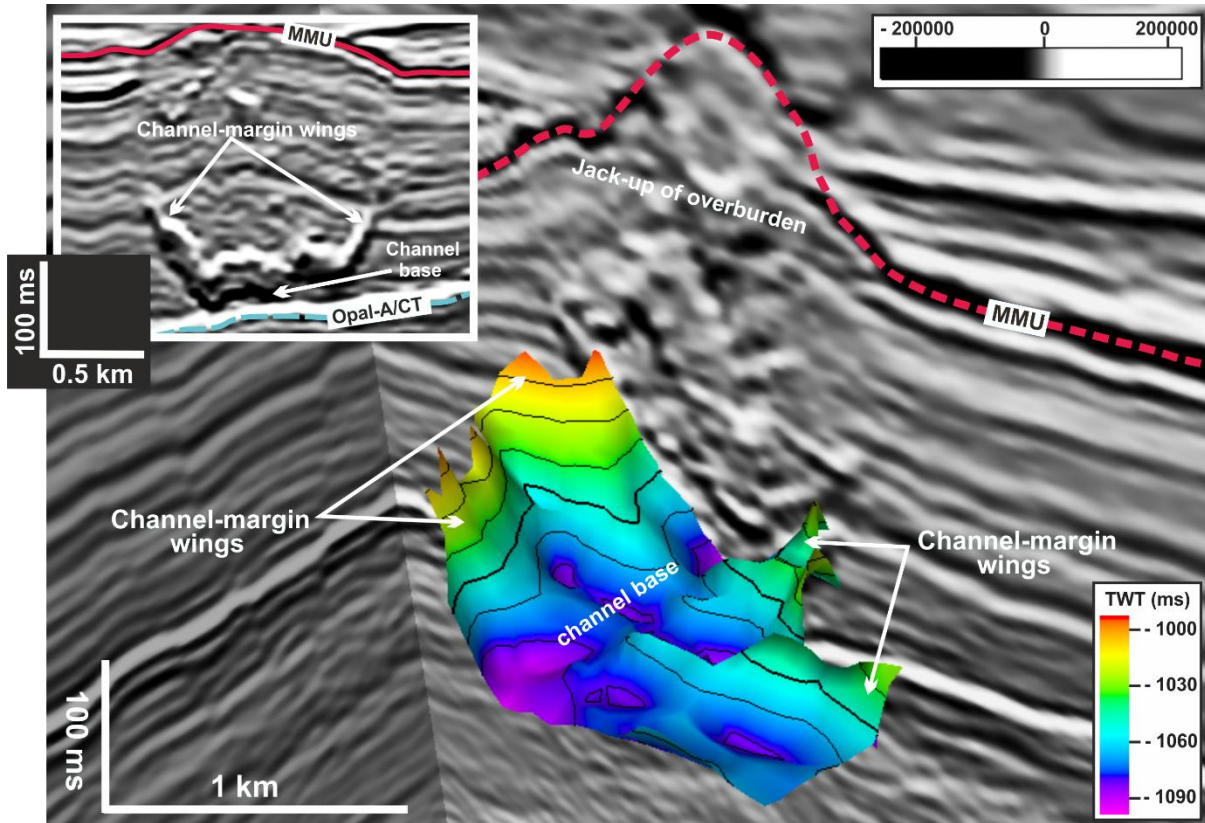
Fig 5.13: Time-surface map of the bowl-shaped discordant amplitude anomaly shown in Fig. 5.10c. This illustrates the 3D geometry of the anomaly and indicates the channel base and channel-marginal wings. Location of Fig. 5.10c is indicated in Figure 5.6. MMU: Mid-Miocene Unconformity. Seismic data courtesy of CGG.

Based on the apparent physical and spatial connection between the amplitude anomalies and the sand-bearing Middle – Late Oligocene depositional system, we consider the V/W-shaped intrusions to represent injected sand bodies while the bowl-shaped/wing-like intrusions with concordant base represent in-situ depositional sand bodies which were subsequently subjected to remobilization and injection. However, the irregular to complex-shaped geometries of some intrusions may be as a result of local heterogeneity in the host strata and/or the spatial variation in stress state above and next to the depositional sand bodies resulting to their irregular to complex geometries (Jolly and Lonergan, 2002; Jackson et al., 2011; Safronova et al., 2012)

Rundberg and Eidivn (2005, 2016) interpreted the Oligocene sandstones in the northern North Sea to be in-situ deposits representing turbiditic gravity flow deposits sourced from the uplifted Shetland Platform and west Norway/Southern Fennoscandia in the Early Oligocene and Late Oligocene respectively. The approximate outline of this turbiditic sandy system is shown in Rundberg and Eidivn (2005: see their Fig 7a) and Eidvin et al. (2014: see their Fig 1). Considering a deeper potential source sand body for the Oligocene intrusions requires that the sand body to be unconsolidated at the time of intrusion. Therefore, it is

Page | 273

also reasonable to suggest that the Oligocene sand intrusions may have been partly sourced from the underlying Eocene fan which occur directly beneath the Oligocene intrusions in Segment-1 & -2 (Fig. 5.8). However, this hypothesis is unlikely because there is no obvious potential feeder system (i.e. Feeder dikes) or conduit observed in cross section which may support this, because an Eocene source sand should result to considerable deformation within and/or above the fan complex. This is further supported by the observation that: (1) the Eocene fan complex show little or no sign of post-depositional modification or remobilization, (2) the Eocene – Oligocene boundary looks intact with no irregularities observed throughout the study area which may suggest that this surface could represent a seal for the deeper injection system (Safronova et al., 2012), and (3) the fact that we cannot account for the source sand for some isolated Oligocene intrusions which occur far beyond the inferred extent of the Eocene fan in the western part of the study area characterized by polygonal faulting.

The predominant occurrence of bowl-shaped/wing-like and conical-shaped high amplitude anomalies in Segment-1 to 3, the calibration of these amplitude anomalies to sand-bearing intervals and the presence of channel-shaped and fan/lobe-shaped high amplitude anomaly in Segment-1 (south-western part) and Segment-3 (north-western part) support Rundberg and Eidivn (2016) interpretation for in-situ Oligocene sands. As such we interpret the Oligocene sands to be in-situ turbiditic depositional sands with the bowl-shaped/wing-like intrusions representing in-situ depositional sand bodies which were subjected to remobilization and injection leading to the formation of their discordant marginal wings, while the conical-shaped intrusions represent injected sand bodies (Andresen and Clausen, 2014).
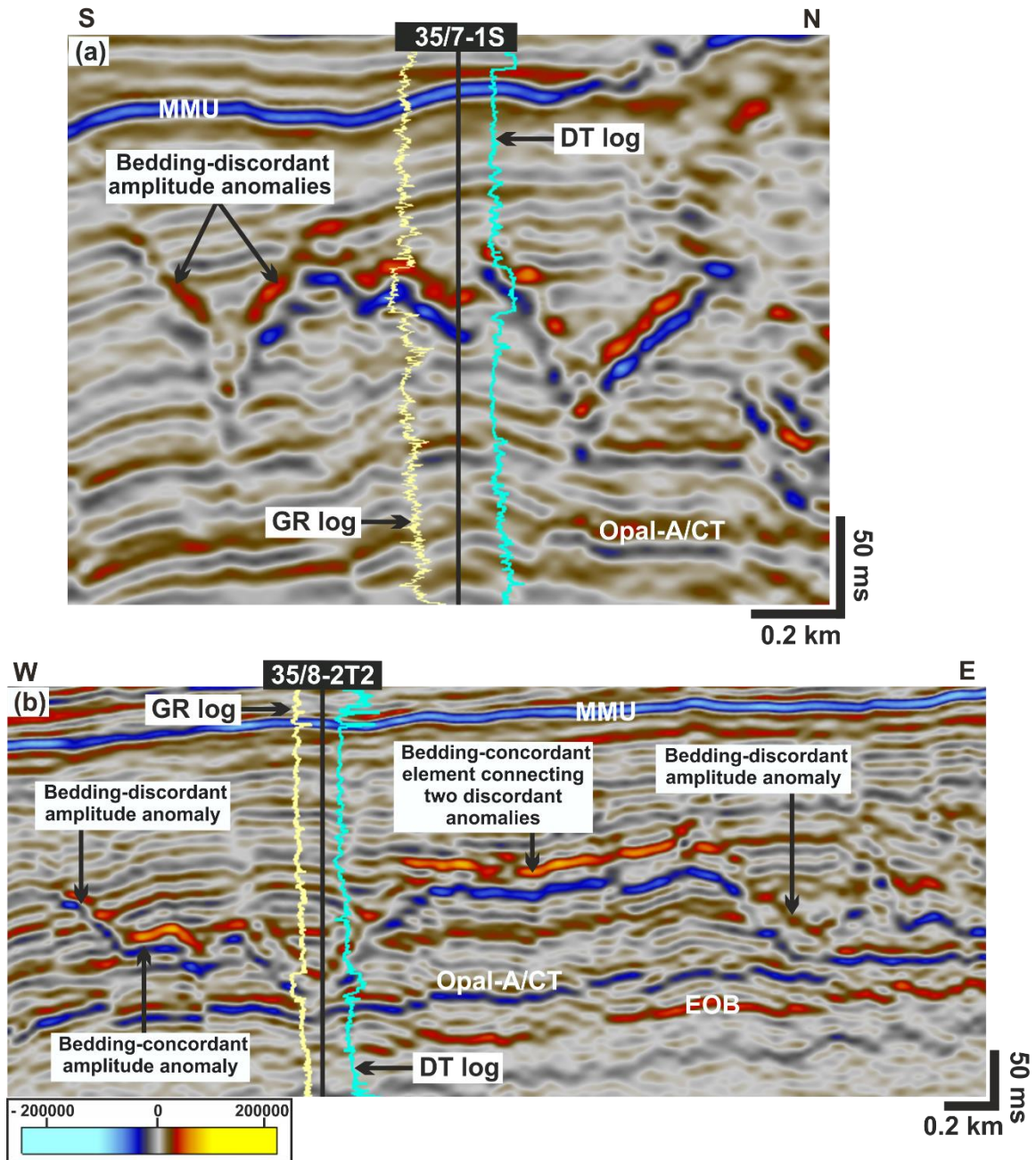
Fig 5.14: Well calibration of discordant amplitude anomalies intersected by wells in Segment-1 & 2. (a) Well 35/7-1S (Segment-1) encountered ca. 25 m thick sandstone unit where it intersected a discordant amplitude anomaly connected to an adjacent V-shaped discordant amplitude anomaly; (b) Well 35/8-2T2 (Segment-2) also encountered ca. 25 m thick sandstone unit where it intersected a V-shaped discordant amplitude anomaly which lie directly above the Opal-A/CT boundary. Location of both wells and seismic cross-section are indicated in Fig. 5.2. MMU: Mid-Miocene Unconformity, EOB: Eocene – Oligocene Boundary. Seismic data courtesy of CGG and well data from TGS Facies Map Browser.

5.6.2 Timing of intrusion/injection and depth of emplacement

The availability of high-quality 3D seismic data and well coverage of the study area enabled us to constrain the ages of the observed seismic units. Therefore, this provides a tool for addressing the timing of the intrusions associated with the Middle – Late Oligocene depositional system. Based on extensive literature, several authors have estimated timing based on one or a combination of three main criteria: (1) presence of possible extrudites on the paleo-seafloor (e.g. Hurst et al., 2006; Cartwright et al., 2008; Vigorito et al., 2008), (2) termination of wings or intrusion limbs at a preferred common datum (e.g. Huuse et al., 2004), and (3) seismic stratigraphic analysis of domal folds/jack-up of overburden above intrusions with their associated onlap of younger sediments (e.g. Shoulders and Cartwright, 2004; Shoulders et al., 2007; Safronova et al., 2012; Andresen and Clausen, 2014). Each of the above criteria is based on the nature of the intrusion complex (e.g., observation of well-developed and preserved extrudites and post-injection sedimentation) and are however associated with their unique assumptions and uncertainties.

Some of the sandstone intrusions described here are characterized by domal folds or jack-up of overburden and mounded top host surface (e.g., the mounded nature of the Mid-Miocene Unconformity in Segment-3) which we have interpreted to result from differential compaction across the Oligocene sand bodies (Jackson et al., 2011; Rundberg and Eidvin, 2016). Overlying younger sediments onlap and downlap onto the compaction folds and mounds (Fig. 5.8a, 5.8b and 5.10c) which imply that the significant relief of the top host surface (i.e., Mid-Miocene Unconformity) reflect the topography of the seafloor at the point when the overlying succession were deposited (Andresen and Clausen, 2014). Therefore, the sandstone intrusions were already emplaced prior to the deposition of the overlying sediments. The Mid Miocene Unconformity in the northern North Sea represents a period of widespread hiatus characterized by significant erosion, resulting in the non-preservation of mid-Miocene sediments (Ahmadi et al., 2003; Rundberg and Eidvin, 2005; Goledowski et al., 2012; Løseth et al., 2013). The sediments directly overlying the unconformity in the study area are documented to be of Late Miocene to Early Pliocene in age (Løseth et al., 2013; Eidvin et al., 2014) and based on this we constrain the timing of remobilization and injection of the Middle-Late Oligocene depositional system to the Late Miocene using similar approach by Shoulders and Cartwright (2004) for the Faeroe-Shetland Basin.

Besides providing a direct constrain on the timing of intrusion, the onlap of younger sediments onto the Mid-Miocene Unconformity indicates that it represents the seabed at the time of intrusion, and we can precisely constrain the depth of intrusion (Shoulders and Cartwright, 2004). We therefore, suggest that the intrusion process occurred at a burial depth estimated from the thickness measured between the top of the concordant segment of the wing-like intrusions and the Mid-Miocene Unconformity (Safronova et al., 2012). This gives the depth of emplacement to be c. 100 – 300ms (i.e., 100 – 300 m; not decompacted).

5.6.3 Priming and triggering mechanism for the remobilization and injection of the Middle – Late Oligocene Depositional System

The mechanisms, which drive sandstone intrusions, are classified into priming and trigger mechanisms, with the former referring to the processes that facilitate overpressure build-up while the latter includes mechanisms that trigger sand fluidization and injection. The formation of these intrusions is related to pressure-driven fluidized sand flow, which in turn results to their very complex geometries (Huuse et al., 2004; Hurst and Cartwright, 2007; Hurst et al., 2011). Sandstone intrusions or injectites form in response to post-depositional remobilization and injection of fluidized sands and it is generally believed that three main ingredients need to be present for the formation of clastic intrusions. This include: (1) a volumetrically significant, clean and unconsolidated source sand body encased in low permeability sealing mudstones (e.g. Lonergan et al., 2000; Huuse et al., 2007; Braccini et al., 2008), (2) a build-up of overpressure in the sealed sand body caused by one or a combination of processes such that the sand is susceptible to remobilization (e.g. Osborne and Swarbrick, 1997; Molyneux et al., 2002; Huuse and Mickelson, 2004; Huuse et al., 2007; Hurst et al., 2011) and (3) a triggering event which leads to seal breaching, sand fluidization and injection (e.g. Dore et al., 1999; Lonergan and Cartwright, 1999; Jolly and Lonergan, 2002; Molyneux et al., 2002; Hurst et al., 2003; Huuse et al., 2007, Jackson, 2007). Previous studies of Paleocene and Eocene slope and basin floor depositional systems in different basins (e.g., North Sea) have shown and suggests that the above conditions are commonly met where sand-rich turbidites and slope-channel fans deposited on mud-dominated slopes are subsequently sealed in low permeability mudstones (Jackson, 2007). The series of processes which lead to the formation of sand injectites (e.g., high pore pressure, hydro-fracturing of sealing strata, fluidization and injection of sand) are well known. However, the exact details of what triggers sand fluidization and the process for the development of their characteristic discordant complex geometries is still speculative (Davies et al., 2006; Hurst et al., 2011).

5.6.3.1 Overpressure development

Fluid overpressure is a critical factor required for sand injection to occur since it initiates the hydro-fracturing of the top seal and drives subsequent fluid flow (Jackson, 2007; Hurst et al., 2011). This fluid overpressure is defined as the amount by which the pore fluid pressure (P_f) exceeds the hydrostatic pressure (P_h) (Jolly and Lonergan, 2002; Hurst et al., 2011). Depositional sand bodies become over-pressured when the rate of compaction induced pore fluid expulsion is reduced when they are encased in low-permeability strata (Hurst et al., 2011). Several priming mechanisms leading to overpressure development for sandstone intrusion to occur have been suggested by different authors. Such mechanisms include: (1) disequilibrium compaction and differential loading (e.g. Osborne and Swarbick, 1997; Jolly and Lonergan, 2002; Jackson et al., 2011; Løseth et al., 2013), (2) lateral transfer of pressure

and fluid buoyancy (e.g. Swarbrick and Osborne, 1998; Yardley and Swarbrick, 2000; Reily and Flemmings, 2010), (3) hydrocarbon generation and migration of basinal fluids (e.g. Jolly and Lonergan, 2002; Safronova et al., 2012; Andresen and Clausen, 2014) and (4) fluid release from silica diagenetic transformation (opal-A to opal-CT transition) (e.g. Davies et al., 2006; Safronova et al., 2012).

Based on previous studies of sand injectites in the Cretaceous, Paleocene and Eocene of the North Sea, we consider three principal mechanisms for overpressure development in the Middle – Late Oligocene depositional system leading to its subsequent remobilization and injection.

a) Disequilibrium compaction and Differential loading

Overpressure development is usually linked to disequilibrium compaction due to rapid burial (Osborne and Swarbrick, 1997). Recent studies have shown that disequilibrium compaction is a common cause of overpressure development only down to depths of 2 – 3 km (Jolly and Lonergan, 2002; Ramdhan and Goulty, 2010). When unconsolidated depositional sand bodies are rapidly buried in low-permeable mudstones such that expulsion of pore fluids in the sand bodies is inhibited, this results to a significant increase in overpressure within the sand bodies (Jolly and Lonergan, 2002; Jackson, 2007). This mechanism favours overpressure development when we have a highly efficient sealing lithology (i.e. with high seal integrity) and when the burial rate of sediments is greater than c. 600 m/M.y (Osborne and Swarbrick, 1997; Duranti and Hurst, 2004).

The average burial rate of the Middle-Late Oligocene sediments within the study area is relatively low (Table 5.3: c. 78.43 m/M.y based on average thickness of c. 400 msTWT; see Fig. 5.5c) and a total duration for the Mid – Late Oligocene epoch of 5.1 M.y). Based on this low estimate, it is difficult to unequivocally state that rapid burial contributed to overpressure. However, the presence of differential compaction folds and mounds above most of the sandstone intrusions may indicate that disequilibrium compaction and differential loading may have played a role in the generation of overpressure in the depositional sand bodies leading to their subsequent remobilization and injection. Furthermore, the increase in thickness of the Middle – Late Oligocene depositional system from the east towards the west (Fig. 5.5c) may be an indication for rapid loading due to high sediment supply. As such, rapid burial may also be a contributing factor to overpressure development.

b) Thermogenic fluid migration/Addition of fluid

An alternative mechanism, which can result to overpressure development, is the influx of fluid (i.e., hydrocarbon or formation water) into the sealed sand bodies from deeper sources or from surrounding less permeable mudstone strata (Brooke et al., 1995; Lonergan et al., 2000; Yardley and Swarbrick, 2000; Jolly and Lonergan, 2002; Andresen and Clausen, 2014). This process is believed to be very effective in the remobilization of large volumes of unconsolidated sand similar to the scale observed in the North Sea.

Migration of hydrocarbon (i.e., gas) from deeper sources can generate high pore fluid pressure in sealed sand bodies due to buoyancy (Jolly and Lonergan, 2002, Molyneux et al., 2002; Huuse and Mickelson, 2004). The vast development of sand injectites within the Paleogene of the North Sea is believed to be contemporaneous with the generation of hydrocarbons in the underlying Mesozoic rift basin (Huuse and Mickelson, 2004). This observation led to the idea that sandstone remobilization and injection in the North Sea may have been driven by early hydrocarbon (gas) migration from deeper sources (Lonergan et al., 2000; Jolly and Lonergan, 2002; Molyneux, 2001; Molyneux et al., 2002; Huuse and Mickelson, 2004). This idea may be supported by the fact that the intrusions are found within hydrocarbon mature areas of the North Sea Basin which is a host to giant oil/gas discoveries and the understanding that gas involved in the upward transport of fluid and sand would expand and therefore help drive the injection process (Jolly and Lonergan, 2002; Huuse and Mickelson, 2004). Since some of the clastic intrusions (associated with the MLODS) reported here occur above major Mesozoic structures, it is possible to suggest that they could be related to early hydrocarbon migration and expulsion (Huuse and Mickelson, 2004). However; (1) not all the intrusions occur on structural highs but are also observed within structural lows, and are in some cases absent above structural highs, and (2) although we do observe an obvious seismic indication for upward fluid migration or seepage in form of vertically acoustic distorted zones and/or gas chimneys emanating from the underlying Mesozoic deeper structures within the Cretaceous succession, there are no evidence of direct hydrocarbon indicators within the studied interval. We therefore, suggest that it is unlikely for this medium to have contributed to overpressure development in the MLODS.

Based on our previous interpretation that the sandstone intrusions were emplaced at a burial depth of c. 100 – 300 m (not de-compacted) and the knowledge that deep-water mud-rich sediments often show a reduction in porosity from about 75 – 90% to 40% controlled by mechanical compaction during shallow (< 0.5 km) burial (e.g. Velde, 1996; Bjørlykke, 1999; Safronova et al., 2012; Wrona et al., 2017b), we therefore suggest that overpressure may have partly resulted from fluid drainage into the sealed permeable depositional sand bodies from the surrounding low-permeable mudstones during early-stage compaction of sediments (Davies et al., 2006).

Table 5.3: Table showing estimated minimum, mean and maximum net accumulation rate or burial rate of the Middle-Late Oligocene depositional systems (MLODS). Thickness values were derived from TWT-thickness map (see Fig. 5.5c) between the Mid-Miocene Unconformity or Top Hordaland Group Unconformity and the Eocene-Oligocene Boundary (EOB). The duration for the Oligocene age was taken from the International Chronostratigraphic chart (2017) while the burial rate was calculated using the equation by Jordt et al. (2000): Net accumulation rate **(S) = TWT * V/2D** without accounting for compaction. Where TWT is thickness (msTWT), V is velocity and D is duration.

Unit	Age	Duration (My)	Thickness (msTWT)			Velocity (m/s)	Burial rate/Net accumulation rate (m/My)		
			Min	Mid	Max		Min	Mid	Max
CSU-4	Oligocene	5.1	100	400	700	2000	19.61	78.43	137.25

c) Silica diagenetic transformation

The occurrence and recognition of large-scale sand intrusions within mudstone successions which are rich in biogenic silica (opal-A) have led to the idea that the process of diagenetic conversion of opal-A into opal-CT could be a potential primer and trigger for sand intrusion (Davies et al., 2006; Wrona et al., 2017b). Major documented examples where large-scale clastic intrusions are hosted within bio-siliceous mudstones are found in the Faeroe-Shetland Basin (Davies and Cartwright, 2002); Sakhalin Island in eastern Russia (Gladenkov et al., 2002), Møre Basin, San Joaquin Basin (Panoche & Tumey hills) and the North Viking Graben (Davies et al., 2006). The diagenetic conversion of opal-A into opal-CT (cristobalite and tridymite) which usually occur at shallow burial depths of 0.5 – 1 km results to: (1) an abrupt collapse of pore framework, (2) marked decrease in porosity, (3) rapid sediment compaction leading to increase in density, (4) reduction in water content due to significant expulsion of water, (5) increase in thermal conductivity and (6) generation of overpressure (Davies and Cartwright, 2002; Davies et al., 2006; Davies and Clark, 2006; Cartwright, 2007).

We propose that this transformation process may have led to the rapid expulsion of pore fluids which filled up inter-bedded and overlying depositional sand bodies, resulting to overpressure build-up, which primed these sands and made them susceptible to remobilization. This mechanism appear to be supported by: (a) evidence of opal-A zone in the Mid/Late Oligocene – Early/Mid Miocene sediments of the North Viking Graben as documented by Rundberg (1989), Thyberg et al. (1999), Olobayo (2014) and Wrona et al. (2017b: their Fig 8 in Well 35/11-5), with the top of the opal-A zone corresponding to the Top Hordaland Group Unconformity (THGU); (b) evidence for the presence of Opal-CT zone in Early Oligocene sediments of the North Viking Graben also documented by Rundberg (1989), Olobayo (2014) and Wrona et al. (2017b: Fig 8); (c) evidence for approximately 20% (from 49% down to 29%) porosity reduction in Cenozoic mudstones in the North Viking Graben resulting from Opal-A/CT transformation (Wrona et al. 2017b); (d) the presence of sand intrusions and interpreted parent sand bodies within opal-rich interval (Mid-Late

Oligocene); (e) the presence of a high amplitude semi-continuous reflection interpreted as the Opal-A/CT diagenetic boundary (Olobayo, 2014; Wrona et al., 2017b) with the injectites having a common base at or slightly above the conversion boundary (Fig. 5.8, 5.9 and 5.10) located within polygonally faulted Oligocene – Mid Miocene bio-siliceous sediments, and (f) the presence of extensive polygonal faults within the interval of interest which acts as evidence for early dewatering (e.g. Cartwright, 2011; Cartwright et al., 2003) and have recently been proposed to also result from silica diagenesis (e.g. Davies and Clark, 2006; Cartwright, 2007; Huuse et al., 2010; Cartwright, 2011).

Taken together, these evidence and observations suggest that silica diagenetic transformation could have played a significant role in overpressure development in the Middle – Late Oligocene depositional sand bodies prior to their remobilization and injection.

5.6.3.2 Triggering Mechanisms

For remobilization and subsequent injection of an over pressured sand body to occur, the capacity of the seal needs to be exceeded (Andresen and Clausen, 2014). This implies that seal failure needs to occur. This seal failure is suggested to be caused by hydraulic fracturing which occur when pore fluid pressure exceeds the fracture gradient within the sealing lithology (i.e., host strata) or near the contact between the seal and the sealed parent sand body (Jolly and Lonergan, 2002; Hurst et al., 2011). The above results in the propagation of fractures within the host sediment leading to an upward injection of fluidized sand (Hurst et al., 2011). For this to occur, a trigger mechanism (internally or externally driven) capable of causing or contributing to the failure of the seal is required. Based on more than a decade of research, several potential trigger mechanisms have been suggested to be associated with the formation of clastic intrusions such as: (a) earthquakes/ seismically-induced liquefaction (e.g. Obermeier, 1996; Boehm and Moore, 2002; Jolly and Lonergan, 2002; Huuse and Mickelson, 2004; Hurst et al., 2011), (b) tectonic activity/stress (e.g. Winslow, 1983; Huuse et al., 2010), (c) bolide impact (e.g. Braccini et al., 2008; Cartwright, 2010), (d) polygonal faulting (e.g. Lonergan and Cartwright, 1999; Cosgrove and Hillier, 1999; Gras and Cartwright, 2002; Molyneux et al., 2002; Huuse and Mickelson, 2004; Huuse et al., 2007; Jackson, 2007), (e) fracture propagation linked to differential compaction (e.g. Jackson, 2007; Jackson et al., 2011; Safronova et al., 2012).

Below we consider some of these trigger mechanisms to ascertain their possible contribution to the Middle – Late Oligocene clastic intrusion complexes studied here.

a) Earthquake activity have been linked as a trigger for the remobilization, injection, and possible extrusion of unconsolidated sand at the earth surface by the process referred to as shear-induced liquefaction or dynamic liquefaction (Obermeier, 1996; Boehm and Moore, 2002). However, studies have shown that liquefaction will only occur for large magnitude earthquakes (i.e., magnitude > 5), produce centimetres to few meters scale intrusions and it

is difficult for liquefaction of sand to occur by seismic activity at depths greater than 10 m due to increase in overburden pressure (Ambraseys, 1988; Obermeier, 1996, 1998; Jolly and Lonergan, 2002; Jackson, 2007). Therefore, to favour earthquake induced liquefaction as a possible trigger for sand intrusion, it is important we consider the intrusion scale, intrusion depth and the likelihood that an earthquake of magnitude greater than five occurred at the time of intrusion and/or if the basin was tectonically active at that time (Lonergan et al., 2000; Jolly and Lonergan, 2002). Based on the above, it is very unlikely for earthquake-induced liquefaction to have triggered sand remobilization and injection in the study area because: (1) the scale of the intrusions associated with the Middle – Late Oligocene depositional system is by far greater in scale (m – km scale) than those formed by seismically-induced liquefaction, (2) our interpretation that the depositional sand bodies were buried to a depth of c. 100 – 300 m before injection occurred, is too deep to allow dynamic liquefaction, and (3) it is suggested that the Paleogene of the North Sea was tectonically quiescent and there is no record of earthquake with the required magnitude (> 5) in the study area (Huuse and Mickelson, 2004; Olobayo, 2014).

b) Bolide impact have been suggested as a potential trigger for remobilization of unconsolidated sands (e.g., Cartwright, 2010). No evidence for an Oligocene bolide impact is documented for the study area. Ries Crater (or Nördlinger Ries) in southern Germany which occurred during the Mid – Late Miocene have been suggested in literature as a possible trigger for sand intrusions (Cartwright, 2010). Although its occurrence is contemporaneous with the suggested timing of emplacement for the intrusions studied here, it is very unlikely that its impact reached the northern North Sea due to the long distance (> 2000 km) between them.

c) The propagation of polygonal faults into overpressured sand bodies have been suggested as a possible trigger for sand remobilization and intrusion (e.g., Lonergan and Cartwright, 1999; Gras and Cartwright, 2002; Molyneux et al., 2002; Huuse at al., 2004). Polygonal faults and sand intrusions are pervasive within the studied Oligocene interval (Fig. 5.3a, 5.7, 5.8d) and show a close spatial relationship with four kinds of interactions observed: (1) cross-cutting relationship between intrusions and polygonal faults (e.g. Segment-1 & 2), (2) intrusions that are not affected by polygonal faults (e.g. Segment-3), (3) intrusions which appear to have a limb/wing fully or partially intruded along polygonal fault plane (e.g. Segment-1), and (4) intrusions whose propagation direction is restricted or blocked by a fault plane. Similar spatial relationships have been documented by Huuse et al. (2001), Løseth et al. (2003), Huuse et al. (2004), Huuse and Mickelson (2004) and Bureau et al. (2013: Faroe-Shetland Basin).

Recent studies by Wrona et al. (2017a) on the kinematics of polygonal faults in the northern North Sea established that polygonal faulting in the northern North Sea commenced in the Eocene to Early Oligocene with subsequent reactivation occurring in the Late Oligocene to Mid-Miocene. This is supported by the termination of polygonal faults below the Mid-Miocene Unconformity which implies that the propagation of the polygonal faults may have occurred prior to the emplacement of the intrusions in the Late Miocene. This is further supported by the observation that the intrusion wings/limbs are not offset by the polygonal faults indicating that they formed prior to the emplacement of the intrusions. Therefore, we suggest that polygonal faulting could not have triggered sand intrusion due to the apparent difference in the timing of formation of both features (Jackson, 2007), but may have contributed to seal failure and formed part of the feeder system by allowing transport of fluidized sand along its plane (Huuse and Mickelson, 2004). Further analysis on the interaction between the polygonal faults and intrusions is required to better understand their co-existence within the studied interval.

d) Differential compaction together with associated small-scale faulting and fracturing adjacent to depositional sand bodies may trigger sand injection as well as control the resultant geometry and distribution of the intrusions formed (Jackson, 2007; Safronova et al., 2012). Differential compaction adjacent to the sand bodies would give rise to the formation of zones of maximum extensional strain at the margins of the sand bodies as well as zones of compressional strain above the sand bodies (Cosgrove and Hillier, 1999; Hillier and Cosgrove, 2002; Jackson, 2007; Jackson et al., 2011; Safronova et al., 2012). Also, small-scale faults and fractures would develop parallel to the margins of the sand bodies in the zones of maximum extensional strain, thus facilitating the injection of fluidized sands to form wing-like intrusion that flank the sand bodies (Jackson, 2007; Safronova et al., 2012). The observation of differential compaction folds and mounds above most of the intrusions (Fig. 5.8f - g, 5.10c, 5.11, 5.13), the presence of wing-like intrusions at the margins of the depositional sand bodies (Fig. 5.8d – 5.8h) and the observation that the edges of the folds spatially coincide with the uppermost edge of the wing-like intrusions indicate that this mechanism is likely to be the main trigger for the formation of the intrusions studied here.

5.6.4 Model for formation of the intrusions associated with the Middle – Late Oligocene Depositional System

Our simplified conceptual model for the deposition, subsequent remobilization, and injection of the Middle – Late Oligocene depositional system is illustrated in Fig. 5.15. The post-Eocene uplift along basin margins (East Shetland Platform and West Norway) resulted in the deposition of extensive sand bodies of turbiditic origin in the North Viking Graben in the Early – Late Oligocene (Fig. 5.15a, b; Rundberg 1989; Rundberg and Eidvin, 2005; Fyfe et al., 2003; Eidvin et al., 2014). The deposition of these Oligocene sands took place in a quiet passive margin setting and were sourced from both the East Shetland Platform and west

Norway (Eidvin et al., 2014). Subsequent deposition of mud-dominated sediments buried the sand-dominated parts of the Middle – Late Oligocene depositional system forming a seal above them (Fig. 5.15c). The presence of a seal together with rapid burial during the Late Oligocene – Early Miocene may have facilitated disequilibrium compaction leading to the formation of the compaction anticline/folds and mounds observed above the depositional sand bodies, which we have linked to differential compaction across the sand bodies, and their surrounding mud-dominated succession.

Jack-up of overburden/compaction folds due to differential compaction, rapid burial of the sand bodies, fluid addition into the sealed sand from deeper sources and/or due to fluid drainage from the surrounding mudstones during early compaction-related dewatering and silica diagenetic transformation may have facilitated overpressure development in the depositional sands (Fig. 5.15d). Pore fluid pressure eventually exceeded the fracture gradient within the sealing mudstones or near the contact between the seal and underlying Middle – Late Oligocene depositional sand bodies leading to seal failure (i.e., hydro-fracturing). Seal failure in turn resulted to the propagation of fractures leading to the injection of fluidized sands (Fig. 5.15e). This propagation of fractures could have been triggered by differential compaction while the propagation of fractures parallel to the margins of the sand bodies resulted to the formation of wing-like intrusions observed at the flanks of the depositional sand bodies (Fig. 5.15e; Hillier and Cosgrove, 2002; Jackson et al., 2011). Subsequent deposition and mudstone compaction above the sand bodies would have reduced the dip angle of the wing-like intrusion to their current dip of 7 – 30° as well as the amplitude of the compaction folds/anticlines above the Middle – Late Oligocene depositional system. Some of the remobilized sand may have also reached the paleo-seafloor at that time represented by the Mid-Miocene Unconformity forming extrudites (Fig. 5.15e; Løseth et al., 2013). Subsequent deposition above the Mid-Miocene Unconformity were associated with onlap and downlap onto the compaction anticlines and mounds.

(a)
Sediment source
Shelf Canyon
Channels
Shelf
Sandy lobe deposits
N
East
10's of Kilometers
West
Deep water
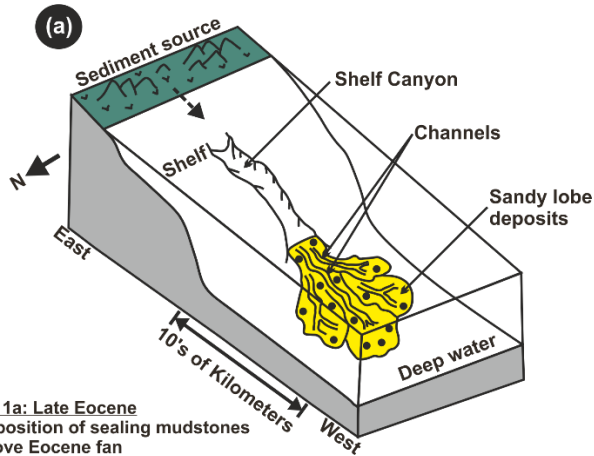
Stage 1a: Late Eocene
- Deposition of sealing mudstones above Eocene fan
- Post-Eocene uplift of eastern basin margin (west Norway)
- Deposition of gravity flow sands (Rundberg and Eidvin, 2005, 2016; Eidvin et al., 2014)

(b)
Depositional sand bodies
EOB
Eocene fan
Not to scale
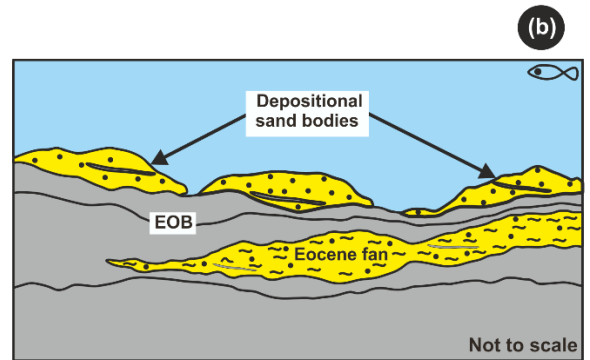
Stage 1b: Early - Middle Oligocene
- Deposition of gravity flow sands sourced from uplifted west Norway above Eocene mudstones (i.e. Oligocene bottom seal)

(c)
MMU
Sand
EOB
Eocene fan
Not to scale
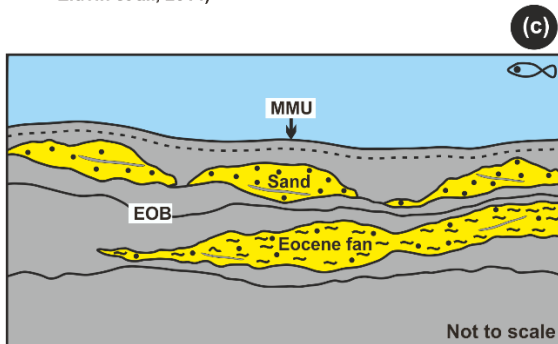
Stage 2: Middle - Late Oligocene
- Channel- lobe complex filled by sediments and buried by overlying mud-dominated sediments
- Deposition of seal or host strata above sand bodies
- Rapid burial of sand bodies

(d)
Fx
MMU
A
Sand
B
EOB
Eocene fan
Not to scale
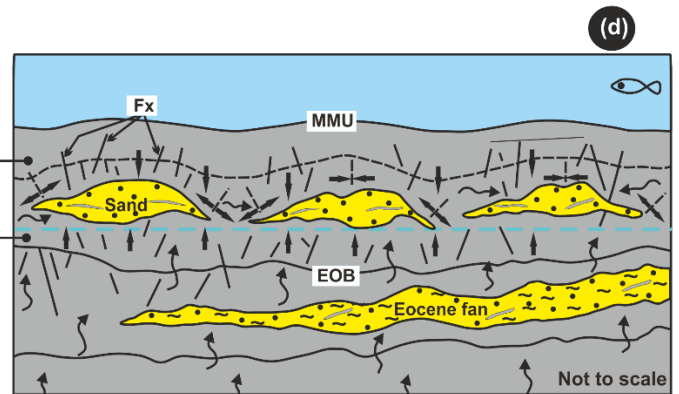
Stage 3: Late Oligocene - Early Miocene
- Differential compaction
- Development of compaction-related folds/jack-up of overburden and mounds above the sand bodies due to differential compaction of sand bodies and surrounding mudstones
- Fluid (pore water and/or thermogenic fluid) migration from lateral/deeper sources into sealed sands and release of pore water due to silica diagenetic transformation of sediments
- Over-pressure development in sand bodies
- Formation of zones of compressional strain above the sands and zones of maximum extensional strain at their margins
- Propagation of polygonal faults (Wrona et al, 2017b)

(e)
Seafloor
Wing-like intrusions
Jack-up of overburden
MMU (Paleo seafloor)
Sand Extrudite?
Host strata
Sand
Opal-A/CT
EOB
Eocene fan
Not to scale
Plio. - Recent | Olig. - Miocene | Eocene | Pal.
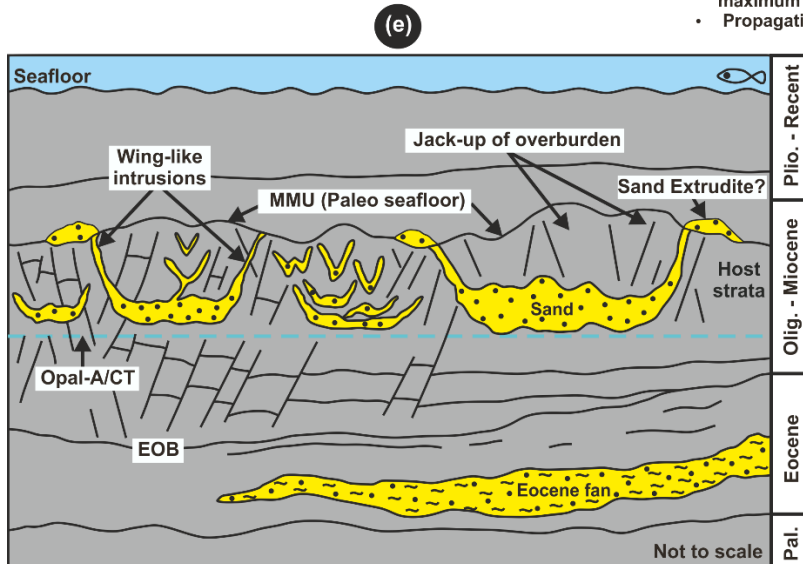
| | Mudstone | A | Fine grained sediments rich in Opal-A |
| | Sandstone | B | Fine grained sediments rich in Opal-CT |

Opal-A/CT
Direction of stress due to differential compaction
Forced fluidflow
Fluid migration
Fx Outer-arc extension-related, crestal faults

Stage 4: Early Miocene - Middle Miocene ??
- Seal failure (i.e. hydro-fracturing) when pore fluid pressure exceeded the fracture gradient within the sealing mudstone host strata
- Fracture propagation leading to injection of fluidized sand
- Formation of wing-like and conical-shaped sand intrusions/injectites, with possible formation of sand extrudites
- Continued deposition of down-lapping and on-lapping succession above the THGU

Fig. 5.15: Conceptual model illustrating the development and post-deposition modification of the Middle – Late Oligocene depositional system by sediment remobilization and injection processes. (a) & (b) During the Early – Middle Oligocene, sand with varying thickness were deposited by channel-lobe systems above the Eocene mudstones; (c) Sand was rapidly buried and sealed by mud-dominated sediments; (d) In the Late Oligocene – Early Miocene compaction folds/anticlines developed above the sand bodies due to differential compaction across the sand bodies and the sealing mudstones. Differential compaction led to partial inversion and mounding of the sand bodies, formation of zone of maximum compressional strain at the crest of the mound and zone of maximum extensional strain at the margins of the sand bodies. This in turn led to the development of small-scale faults and fractures in the zones of maximum extensional strain parallel to the margins of the sand bodies. Fluid migration into the sealed sand from deeper sources or due to fluid drainage from the surrounding mudstones during early compaction-related dewatering and silica diagenetic transformation facilitated overpressure development in the depositional sands; (e) Seal failure resulted to the development of wing-like intrusions along the margins of the mounded depositional sand bodies and the formation of other intrusion geometries (V/W-shaped and irregular-shaped) with a possibility of sand extrusion (forming sand extrudites) onto the seafloor at that time. MMU: Mid-Miocene Unconformity, EOB: Eocene – Oligocene Boundary.

5.6.5 Implications of remobilization and injection on deep-water sandy depositional systems

The post-depositional remobilization and injection of deep-water depositional systems has significant implications for hydrocarbon exploration and production (see summary by Lonergan et al., 2000). Studies have shown that sand remobilization and injection can result to significant changes in reservoir geometry and properties, changes in reservoir volumetrics and can also result to enhanced connectivity of previously isolated sand bodies (Lonergan et al., 2000; Duranti et al., 2002; Huuse et al., 2003, 2007; Jackson et al., 2011). Experience from North Sea fields (e.g., Alba, Balder, Gryphon and Forth/Harding) modified by sand injectites have shown that they form excellent reservoirs, contain substantial volume of sand with recorded porosities ranging between 25 – 35% and permeability in the Darcy scale (Duranti et al., 2002; Hurst et al., 2003; Hurst and Cartwright, 2007). Therefore, large-scale sand injectites may individually represent standalone reservoirs (Huuse et al., 2004, 2005, 2007; Safronova et al., 2012). Since sand injectites form highly porous and permeable conduits in low permeability mudstones units, they therefore act as a seal risk and may facilitate the expulsion of basinal fluids (Mazzini et al., 2003; Hurst and Cartwright, 2007). In general, large-scale sand remobilization and injection leads to a significant re-organization of basin plumbing system and emplacement of field-size sandstone units with complex geometries, which may not be completely resolved by available imaging techniques.

The Middle – Late Oligocene depositional system described here have large-scale intrusions with complex geometries associated with them. Post-depositional remobilization and injection together with differential compaction have clearly altered the geometry of the sand bodies (e.g., Fig. 5.8c - h, 5.9a, 11). For instance, the process of remobilization and injection have given the interpreted depositional sand bodies their unique marginal wings/limbs and irregular geometries, while differential compaction led to the jack-up of

overburden and/or mounds formed above the depositional sand bodies. Furthermore, the remobilization and injection process seem to have enhanced the vertical and lateral connectivity between sealed depositional sand bodies, which appear to be connected vertically and mainly laterally over long distances (e.g., Fig. 5.8b, c and 5.9b). This high level of connectivity creates permeable network in fine-grained host strata, which can cause the sealing mudstones to drain laterally, and rapidly as against compaction-driven vertical drainage (Hurst et al., 2011).

The propagation of sand intrusions into the low permeable sealing mudstone host strata may have compromised the seal integrity of the Oligocene succession in the study area. Therefore, the sand intrusions may constitute long-lived permeable pathways for subsequent fluid flow and migration into intervals above the Oligocene (Huuse and Mickelson, 2004). However, since the injectites are overlain by subsequent deposition of possible sealing lithologies in the Miocene, seal integrity may not be an issue here (Huuse et al., 2005; De Boer et al., 2007).

5.7 Conclusion

Based on the integrated 3D seismic and well data study of the Oligocene interval along the eastern margin of the North Viking Graben, the following conclusions are drawn:

- Available data indicate that a deep-water depositional system of Middle – Late Oligocene age developed along the eastern margin of the North Viking Graben, which we referred to as the Middle – Late Oligocene Depositional System. The Middle – Late Oligocene depositional system comprises of series of sand-rich channel-lobe and fan systems deposited in proximal to basin-floor setting.
- The Middle – Late Oligocene depositional system is characterized by high amplitude reflection on seismic data, which is inferred to result from their high sand content and occurrence in a mud-dominated succession. This allowed their distribution to be mapped on an RMS amplitude map generated at a horizon offset of 130 ms below the Mid-Miocene Unconformity (MMU). The areas on the RMS amplitude map associated with high amplitudes are taught to reflect high sand content while areas with low amplitudes are inferred to be dominated by mudstones.
- The main controls on the distribution and routing of the Middle – Late Oligocene depositional system are the direction of sediment influx and the inherent topography (i.e., paleo-relief) associated with the underlying Mesozoic rift structures in the study area.
- The Middle – Late Oligocene depositional system is characterized by highly complex geometries in cross section due to its post-depositional modification by sediment remobilization and injection processes. The Middle – Late Oligocene depositional system was on seismic cross-section associated with discordant high amplitude anomalies with geometries ranging from conical-shaped, wing-like to irregular and

complex-shaped anomalies, which we have interpreted as the seismic expression of sandstone intrusions.

- The discordant amplitude anomalies associated with the Middle – Late Oligocene depositional system have been calibrated to c. 25 m of thick sandstone units where the anomalies were intersected by some available wells

- The conical-shaped intrusions are interpreted to represent injected sand bodies while the wing-like intrusions characterized by marginal wings are interpreted to be in-situ depositional sand bodies with their marginal wings sourced from the parent sands due to sediment remobilization and injection. The folds and jack-up of overburden observed above most of the intrusions are interpreted to result from differential compaction of the sand bodies and their encasing mudstones

- Most of the sand bodies are characterized by high amplitude reflections which do not appear to have defined erosional bases (or overlie erosional surfaces) and flanking levees. This may be attributed to the complex stacking of depositional elements and the large-scale post-depositional remobilization and injection of the sandstones, which results to their very complex seismic expression and difficulty in identifying individual depositional elements.

- The remobilization and injection of the intrusions associated with the Middle – Late Oligocene depositional system took place during the Late Miocene at a burial depth of c. 100 – 300 m (not de-compacted)

- Overpressure development in the sand bodies which initiates the injection process is suggested to be caused by: (i) disequilibrium compaction and differential loading, (ii) thermogenic fluid migration into the sealed sand bodies from deeper sources or fluid drainage from surrounding less permeable mudstones during early compaction and (iii) silica diagenetic transformation

- Differential compaction together with associated faulting and fracturing adjacent to the depositional sand bodies are favoured as the mechanism, which triggered the remobilization and injection of the sand bodies.

- The post-depositional remobilization and injection of the Middle – Late Oligocene depositional system has clearly altered the geometry of their associated sand bodies and enhanced connectivity between some of the sand bodies, which may have been deposited as isolated sands.

Acknowledgements

References

AHMADI, Z.M., SAWYERS, M., KENYAN-ROBERTS, S., STANWORHT, C.W., KUGLER, K.A., KRISTENSEN, J. & FUGELLI, E.M.G. 2003. Palaeocene. In: *The Millennium Atlas: Petroleum geology of the central and northern North Sea* (Ed. by D. Evans, C. Graham, A. Armour & P. Bathurst). *The Geological Society of London, London,* 235–259.

AMBRASEYS, N.N. 1988. Engineering seismology: Part I. *Earthquake Engineering & Structural Dynamics*, **17**, 1–50, https://doi.org/10.1002/eqe.4290170101.

ANDRESEN, K.J. & CLAUSEN, O.R. 2014. An integrated subsurface analysis of clastic remobilization and injection; a case study from the Oligocene succession of the eastern North Sea. *Basin Research*, **26**, 641–674, https://doi.org/10.1111/bre.12060.

ANELL, I., THYBO, H. & RASMUSSEN, E. 2012. A synthesis of Cenozoic sedimentation in the North Sea. *Basin Research*, **24**, 154–179, https://doi.org/10.1111/j.1365-2117.2011.00517.x.

BADLEY, M.E., PRICE, J.D., RAMBECH DAHL, C. & AGDESTEIN, T. 1988. The structural evolution of the northern Viking Graben and its bearing upon extensional modes of basin formation. *Journal of the Geological Society*, **145**, 455–472, https://doi.org/10.1144/gsjgs.145.3.0455.

BERGSLIEN, D. 2002. Balder and Jotun - two sides of the same coin? A comparison of two Tertiary oil fields in the Norwegian North Sea. *Petroleum Geoscience*, **8**, 349–363, https://doi.org/10.1144/petgeo.8.4.349.

BERGSLIEN, D., KYLLINGSTAD, G., SOLBERG, A., FERGUSON, I.J. & PEPPER, C.F. 2005. Jotun Field reservoir geology and development strategy: pioneering play knowledge, multidisciplinary teams and partner co-operation – key to discovery and successful development. *Petroleum Geology: North-West Europe and Global Perspectives – Proceedings of the 6th Petroleum Geology Conference*, 99–110, https://doi.org/10.1144/0060099.

BJØRLYKKE, K. 1999. Principal aspects of compaction and fluid flow in mudstones. *Geological Society, London, Special Publications*, **158**, 73–78, https://doi.org/10.1144/gsl.sp.1999.158.01.06.

BOEHM, A. & MOORE, J.C. 2002. Fluidized sandstone intrusions as an indicator of Paleo-stress orientation, Santa Cruz, California. *Geofluids*, **2**, 147–161, https://doi.org/10.1046/j.1468-8123.2002.00026.x.

BRACCINI, E., DE BOER, W., HURST, A., HUUSE, M., VIGORITO, M. & TEMPLETON, G. 2008. Sand Injectites. *Oilfield Review*, 34–49.

BREKKE, H., DAHLGREN, S., NYLAND, B. & MAGNUS, C. 1999. The prospectivity of the Voring and More basins on the Norwegian Sea continental margin. *Petroleum Geology Conference Series*, **14**, 261–274, https://doi.org/10.1144/0050261.

BROOKE, C.M., TRIMBLE, T.J. & MACKAY, T. a. 1995. Mounded shallow gas sands from the Quaternary of the North Sea: analogues for the formation of sand mounds in deep water Tertiary sediments? *Geological Society, London, Special Publications*, **94**, 95–101, https://doi.org/10.1144/GSL.SP.1995.094.01.08.

BROWN, A.R. 1996. Seismic attributes and their classification. *Leading Edge*, **15**, 1090, https://doi.org/10.1190/1.1437208.

BROWN, A.R. 2001. Understanding seismic attributes. Geophysics, 66, 47–48, https://doi.org/10.1190/1.1444919.

BUGGE, T., TVEITEN, B. & BACKSTROM, S. 2001. The depositional history of the Cretaceous in the northeastern North Sea. *In*: *Sedimentary Environments Offshore Norway - Palaeozoic to Recent*. 279–291., https://doi.org/10.1016/S0928-8937 (01)80018-7.

BUREAU, D., MOURGUES, R., CARTWRIGHT, J., FOSCHI, M. & ABDELMALAK, M.M. 2013. Characterisation of interactions between a pre-existing polygonal fault system and sandstone intrusions and the determination of paleo-stresses in the Faroe-Shetland basin. *Journal of Structural Geology*, **46**, 186–199, https://doi.org/10.1016/j.jsg.2012.09.003.

CARTWRIGHT, J. 2007. The impact of 3D seismic data on the understanding of compaction, fluid flow and diagenesis in sedimentary basins. *Journal of the Geological Society*, **164**, 881–893, https://doi.org/10.1144/0016-76492006-143.

CARTWRIGHT, J. 2010. Regionally extensive emplacement of sandstone intrusions: A brief review. *Basin Research*, **22**, 502–516, https://doi.org/10.1111/j.1365-2117.2009.00455.x.

CARTWRIGHT, J. 2011. Diagenetically induced shear failure of fine-grained sediments and the development of polygonal fault systems. *Marine and Petroleum Geology*, **28**, 1593–1610, https://doi.org/10.1016/j.marpetgeo.2011.06.004.

CARTWRIGHT, J., JAMES, D. & BOLTON, A. 2003. The genesis of polygonal fault systems: a review. *Geological Society, London, Special Publications*, **216**, 223–243, https://doi.org/10.1144/GSL.SP.2003.216.01.15.

CARTWRIGHT, J., JAMES, D., HUUSE, M., VETEL, W. & HURST, A. 2008. The geometry and emplacement of conical sandstone intrusions. *Journal of Structural Geology*, **30**, 854–867, https://doi.org/10.1016/j.jsg.2008.03.012.

CARTWRIGHT, J.A. & DEWHURST, D.N. 1998. Layer-bound compaction faults in fine-grained sediments. *Bulletin of the Geological Society of America*, **110**, 1242–1257, https://doi.org/10.1130/0016-7606 (1998)110<1242: LBCFIF>2.3.CO; 2.

CARTWRIGHT, J.A. & LONERGAN, L. 1996. Volumetric contraction during the compaction of mudrocks: A mechanism for the development of regional-scale polygonal fault systems. *Basin Research*, **8**, 183–193, https://doi.org/10.1046/j.1365-2117.1996.01536.x.

CHRISTIANSSON, P., FALEIDE, J.I. & BERGE, A.M. 2000. Crustal structure in the northern North Sea: an integrated geophysical study. *Geological Society, London, Special Publications*, **167**, 15–40, https://doi.org/10.1144/GSL.SP.2000.167.01.02.

CLAUSEN, O.R., GREGERSEN, U., MICHELSEN, O. & SØRENSEN, J.C. 1999. Factors controlling the Cenozoic sequence development in the eastern parts of the North Sea. *Journal of the Geological Society*, **156**, 809–816, https://doi.org/10.1144/gsjgs.156.4.0809.

COSGROVE, J.W. & HILLIER, R.D. 2000. Forced-fold development within Tertiary sediments of the Alba Field, UKCS: evidence of differential compaction and post-depositional sandstone remobilization. *Geological Society, London, Special Publications*, **169**, 61–71, https://doi.org/10.1144/gsl.sp.2000.169.01.05.

DANIELSEN, M., MICHELSEN, O. & CLAUSEN, O.R. 1997. Oligocene sequence stratigraphy and basin development in the Danish North Sea sector based on log interpretations. *Marine and Petroleum Geology*, **14**, 931–950, https://doi.org/10.1016/s0264-8172 (97)00043-3.

DAVIES, R.J. & CARTWRIGHT, J. 2002. A fossilized Opal A to Opal C/T transformation on the northeast Atlantic margin: Support for a significantly elevated palaeogeothermal gradient during the Neogene? *Basin Research*, **14**, 467–486, https://doi.org/10.1046/j.1365-2117.2002.00184.x.

DAVIES, R.J. & CLARK, I.R. 2006. Submarine slope failure primed and triggered by silica and its diagenesis. *Basin Research*, **18**, 339–350, https://doi.org/10.1111/j.1365-2117.2006.00297.x.

DAVIES, R.J., HUUSE, M., HIRST, P., CARTWRIGHT, J. & YANG, Y. 2006. Giant clastic intrusions primed by silica diagenesis. *Geology*, **34**, 917–920, https://doi.org/10.1130/G22937A.1.

DE BOER, W., RAWLINSON, P.B. & HURST, A. 2007. Successful Exploration of a Sand Injectite Complex: Hamsun Prospect, Norway Block 24/9. *Sand injectites: Implications for hydrocarbon exploration and production: AAPG Memoir 87*, 65–68, https://doi.org/10.1306/1209850M873256.

DIONNE, J.-C. 1976. Miniature mud volcanoes and other injection features in tidal flats, James Bay, Quebec. *Canadian Journal of Earth Sciences*, **13:422-428**, 422–428, https://doi.org/10.1139/e76-043.

DIXON, R.J., SCHOFIELD, K., ANDERTON, R., REYNOLDS, A.D., ALEXANDER, R.W.S., WILLIAMS, M.C. & DAVIES, K.G. 1995. Sandstone diapirism and clastic intrusion in the Tertiary submarine fans of the Bruce-Beryl Embayment, Quadrant 9, UKCS. *Geological Society, London, Special Publications*, **94**, 77–94, https://doi.org/10.1144/GSL.SP.1995.094.01.07.

DMITRIEVA, E., JACKSON, C.A.-L., HUUSE, M. & KANE, I.A. 2018. Regional distribution and controls on the development of post-rift turbidite systems: insights from the Paleocene of the eastern North Viking Graben, offshore Norway. *Geological Society, London, Petroleum Geology Conference series*, **8**, PGC8.31, https://doi.org/10.1144/PGC8.31.

DMITRIEVA, E., JACKSON, C.A.-L., HUUSE, M. & MCCARTHY, A. 2012. Paleocene deep-water depositional systems in the North Sea Basin: a 3D seismic and well data case study, offshore Norway. *Petroleum Geoscience*, **18**, 97–114, https://doi.org/10.1144/1354-079311-027.

DORÉ, A.G., LUNDIN, E.R., JENSEN, L.N., BIRKELAND, Ø., ELIASSEN, P.E. & FICHLER, C. 1999. Principal tectonic events in the evolution of the northwest European Atlantic margin. *In*: Petroleum Geology of Northwest Europe: Proceedings of the 5th Conference*. 41–61., https://doi.org/10.1144/0050041.

DURANTI, D. & HURST, A. 2004. Fluidization and injection in the deep-water sandstones of the Eocene Alba Formation (UK North Sea). *Sedimentology*, **51**, 503–529, https://doi.org/10.1111/j.1365-3091.2004.00634.x.

DURANTI, D., HURST, A., BELL, C., GROVES, S. & HANSON, R. 2002. Injected and remobilized Eocene sandstones from the Alba Field, UKCS: core and wireline log characteristics. *Petroleum Geoscience*, **8**, 99–107, https://doi.org/10.1144/petgeo.8.2.99.

EIDVIN, T., RIIS, F. & RASMUSSEN, E.S. 2014. Oligocene to Lower Pliocene deposits of the Norwegian continental shelf, Norwegian Sea, Svalbard, Denmark and their relation to the uplift of Fennoscandia: A synthesis. *Marine and Petroleum Geology*, **56**, 184–221, https://doi.org/10.1016/j.marpetgeo.2014.04.006.

EIDVIN, T., RIIS, F., RASMUSSEN, E.S., RUNDBERG, Y. & MAYEN, J. 2013. Investigation of Oligocene to Lower Pliocene deposits in the Nordic offshore area and onshore Denmark. *NPD Bulletin 10*, 62.

FAERSETH, R.B., KNUDSEN, B.-E., LILJEDAHL, T., MIDBØE, P.S. & SØDERSTRØM, B. 1997. Oblique rifting and sequential faulting in the Jurassic development of the northern North Sea. *Journal of Structural Geology*, **19**, 1285–1302, https://doi.org/10.1016/S0191-8141 (97)00045-X.

FALEIDE, J.I., KYRKJEBØ, R., KJENNERUD, T., GABRIELSEN, R.H., JORDT, H., FANAVOLL, S. & BJERKE, M.D. 2002. Tectonic impact on sedimentary processes during Cenozoic evolution of the northern North Sea and surrounding areas. *Geological Society, London, Special Publications*, **196**, 235–269, https://doi.org/10.1144/GSL.SP.2002.196.01.14.

FYFE, J.A., GREGERSEN, U., JORDT, H., RUNDBERG, Y., EIDVIN, T., EVANS, D., STEWART, D., HOVLAND, M. & ANDERSEN, P. (2003) Oligocene to Holocene. In: *The Millenium Atlas: Petroleum Geology of the Central and Northern North Sea* (Ed. by D. Evans, C. Graham, A. Armour & P. Bathurst. *Geological Society London, 279-287*

GABRIELSEN, R.H., FOERSETH, R.B., STEEL, R.J., IDIL, S. & KLOVJAN, O.S. 1990. Architectural styles of basin fill in the northern Viking Graben. *Tectonic evolution of the North Sea rifts*, 158–179.

GLADENKOV, Y.B., BAZHENOVA, O.K., GRECHIN, V.I., MARGULIS, L.S. AND SALNIKOV, B.A. 2002. The Cenozoic geology and the oil and gas presence in Sakhalin. *Moscow: GEOS, 2002*, 225.

GOŁĘDOWSKI, B., NIELSEN, S.B. & CLAUSEN, O.R. 2012. Patterns of Cenozoic sediment flux from western Scandinavia. *Basin Research*, **24**, 377–400, https://doi.org/10.1111/j.1365-2117.2011.00530.x.

GRAS, R.U. and CARTWRIGHT, J.A. 2002. Tornado Faults-The Seismic Expression of the Early Tertiary on PS-data, Chestnut Field, UK North Sea. *In 64th EAGE Conference & Exhibition*. https://doi.org/10.3997/2214-4609-pdb.5.h020.

GREGERSEN, U. & JOHANNESSEN, P.N. 2007. Distribution of the Neogene Utsira Sand and the succeeding deposits in the Viking Graben area, North Sea. *Marine and Petroleum Geology*, **24**, 591–606, https://doi.org/10.1016/j.marpetgeo.2007.04.006.

HARDIE, J. 1999. Clastic dikes intruding Cretaceous coals of western Colorado. *Colorado Geological Survey*.

HILLIER, R.D. & COSGROVE, J.W. 2002. Core and seismic observations of overpressure-related deformation within Eocene sediments of the Outer Moray Firth, UKCS. *Petroleum Geoscience*, **8**, 141–149, https://doi.org/10.1144/petgeo.8.2.141.

HUBBARD, S.M., ROMANS, B.W. & GRAHAM, S.A. 2007. An Outcrop Example of Large-scale Conglomeratic Intrusions Sourced from Deep-water Channel Deposits, Cerro Toro Formation, Magallanes Basin, Southern Chile. *American Association of Petroleum Geologists*, 199–207, https://doi.org/10.1306/1209863M873265

HURST, A. & CARTWRIGHT, J. 2007. Relevance of Sand Injectites to Hydrocarbon Exploration and Production. *In*: *Sand Injectites: Implications for Hydrocarbon Exploration and Production: AAPG Memoir 87*. 1–19., https://doi.org/10.1306/1209846M871546.

HURST, A., CARTWRIGHT, J. & DURANTI, D. 2003. Fluidization structures produced by upward injection of sand through a sealing lithology. *Geological Society, London, Special Publications*, **216**, 123–138, https://doi.org/10.1144/GSL.SP.2003.216.01.09.

HURST, A., CARTWRIGHT, J., HUUSE, M. & DURANTI, D. 2006. Extrusive sandstones (extrudites): a new class of stratigraphic trap? *The Deliberate Search for the Stratigraphic Trap. Geological Society, London, Special Publications, **254***, 289–300, https://doi.org/10.1144/gsl.sp.2006.254.01.15.

HURST, A., CARTWRIGHT, J., HUUSE, M., JONK, R., SCHWAB, A., DURANTI, D. & CRONIN, B. 2003. Significance of large-scale sand injectites as long-term fluid conduits: Evidence from seismic data. *Geofluids*, **3**, 263–274, https://doi.org/10.1046/j.1468-8123.2003.00066.x.

HURST, A., SCOTT, A. & VIGORITO, M. 2011. Physical characteristics of sand injectites. *Earth-Science Reviews*, **106**, 215–246, https://doi.org/10.1016/j.earscirev.2011.02.004.

HUSMO, T., HAMAR, G. P., HØILAND, O., JOHANNESSEN, E., RØMULD, A., SPENCER, A. M., & TITTERTON, R. 2003. Lower and Middle Jurassic. In: *The Millennium Atlas: Petroleum geology of the central and northern North Sea* (Ed. by D. Evans, C. Graham, A. Armour & P. Bathurst). *The Geological Society of London, London,* 129–155.

HUUSE, M. & CLAUSEN, O.R. 2001. Morphology and origin of major Cenozoic sequence boundaries in the Eastern North Sea Basin: Top Eocene, near-top Oligocene, and the mid-Miocene unconformity. *Basin Research*, **13**, 17–41, https://doi.org/10.1046/j.1365-2117.2001.00123.x.

HUUSE, M. & MICKELSON, M. 2004. Eocene sandstone intrusions in the Tampen Spur area (Norwegian North Sea Quad 34) imaged by 3D seismic data. *Marine and Petroleum Geology*, **21**, 141–155, https://doi.org/10.1016/j.marpetgeo.2003.11.018.

HUUSE, M., CARTWRIGHT, J., HURST, A. & STEINSLAND, N. 2007. Seismic Characterization of Large-scale Sandstone Intrusions. *Sand injectites: Implications for hydrocarbon exploration and production: AAPG Memoir **87***, 21–35, https://doi.org/10.1306/1209847M873253.

HUUSE, M., CARTWRIGHT, J.A., GRAS, R. & HURST, A. 2005. Kilometre-scale sandstone intrusions in the Eocene of the Outer Moray Firth (UK North Sea): migration paths, reservoirs and potential drilling hazards. *In*: *Petroleum Geology: North-West Europe and Global Perspectives – Proceedings of the 6th Petroleum Geology Conference*. Geological Society of London, 1577–1594., https://doi.org/10.1144/0061577.

HUUSE, M., DURANTI, D., GUARGENA, C.G., PRAT, P., HOLM, K., STEINSLAND, N., CRONIN, B.T. AND HURST, N., 2003. Sandstone intrusions: Detection and significance for exploration and production. *First Break*, **21**, 33–42, https://doi.org/10.3997/1365-2397.2003014.

HUUSE, å., DURANTI, D., STEINSLAND, N., GUARGENA, C.G., PRAT, P., HOLM, K., CARTWRIGHT, J.A. AND HURST, A., 2004. Seismic Characteristics of Large-Scale Sandstone Intrusions in the Paleogene of the South Viking Graben, UK and Norwegian North Sea. *Geological Society, London, Memoirs*, **29**, 263–278, https://doi.org/10.1144/GSL.MEM.2004.029.01.25.

HUUSE, M., JACKSON, C.A.-L., VAN RENSBERGEN, P., DAVIES, R.J., FLEMINGS, P.B. & DIXON, R.J. 2010. Subsurface sediment remobilization and fluid flow in sedimentary basins: An overview. *Basin Research*, **22**, 342–360, https://doi.org/10.1111/j.1365-2117.2010.00488.x.

HUUSE, M., LYKKE-ANDERSEN, H. & MICHELSEN, O. 2001. Cenozoic evolution of the eastern Danish North Sea. *Marine Geology*, **177**, 243–269, https://doi.org/10.1016/S0025-3227(01)00168-2.

ISAKSEN, D. AND TONSTAD, K. 1989. A revised Cretaceous and Tertiary lithostratigraphic nomenclature for the Norwegian North Sea. Norwegian Petroleum Directorate. *Norwegian Petroleum Directorate*.

JACKSON, C.A.-L. & SØMME, T.O. 2011. Borehole evidence for wing-like clastic intrusion complexes on the western Norwegian margin. *Journal of the Geological Society*, **168**, 1075–1078, https://doi.org/10.1144/0016-76492011-035.

JACKSON, C.A.-L. 2007. The geometry, distribution and development of clastic injections in slope systems: seismic examples from the Upper Cretaceous Kyrre Formation, Måløy Slope, Norwegian Margin. *Sand injectites: implications for hydrocarbon exploration and production*, 37–48, https://doi.org/-.

JOHNSON, H.D. 1977. Sedimentation and water escape structures in some late Precambrian shallow marine sandstones from Finnmark, North Norway. *Sedimentology*, **24**, 389–411, https://doi.org/10.1111/j.1365-3091.1977.tb00129.x.

JOLLY, R.J.H. & LONERGAN, L. 2002. Mechanisms and controls on the formation of sand intrusions. *Journal of the Geological Society*, **159**, 605–617, https://doi.org/10.1144/0016-764902-025.

JORDT, H., FALEIDE, J.I., BJØRLYKKE, K. & IBRAHIM, M.T. 1995. Cenozoic sequence stratigraphy of the central and northern North Sea Basin: tectonic development, sediment distribution and provenance areas. *Marine and Petroleum Geology*, **12**, 845–879, https://doi.org/10.1016/0264-8172 (95)98852-V.

JORDT, H., THYBERG, B.I. & NØTTVEDT, A. 2000. Cenozoic evolution of the central and northern North Sea with focus on differential vertical movements of the basin floor and surrounding clastic source areas. *Geological Society, London, Special Publications*, **167**, 219–243, https://doi.org/10.1144/GSL.SP.2000.167.01.09.

KANE, I.A. 2010. Development and flow structures of sand injectites: The Hind Sandstone Member injectite complex, Carboniferous, UK. *Marine and Petroleum Geology*, **27**, 1200–1215, https://doi.org/10.1016/j.marpetgeo.2010.02.009.

KYRKJEBØ, R., KJENNERUD, T., GILLMORE, G.K., FALEIDE, J.I. & GABRIELSEN, R.H. 2001. Cretaceous-tertiary palaeobathymetry in the northern North Sea. *Norwegian Petroleum Society Special Publications*, **10**, 321–345, https://doi.org/10.1016/S0928-8937 (01)80020-5.

LIU, X. & GALLOWAY, W.E. 1997. Quantitative determination of tertiary sediment supply to the North Sea Basin. *AAPG Bulletin*, **81**, 1482–1509, https://doi.org/10.1306/3b05bb28-172a-11d7-8645000102c1865d.

LONERGAN, L. & CARTWRIGHT, J.A. 1999. Polygonal faults and their influence on deep-water sandstone reservoir geometries, Alba field, United Kingdom central North Sea. *AAPG Bulletin (American Association of Petroleum Geologists)*, **83**, 410–432, https://doi.org/10.1306/00AA9BBA-1730-11D7-8645000102C1865D.

LONERGAN, L., LEE, N., JOHNSON, H.D., CARTWRIGHT, J. A & JOLLY, R.J.H. 2000. Remobilization and Injection in Deepwater Depositional Systems: Implications for Reservoir Architecture and Prediction. *Deep-Water Reservoirs of the World: 20th Annual GCSSEPM Foundation Bob F. Perkins Research Conference*, **15**, 515–532, https://doi.org/10.5724/gcs.00.15.0515.

LØSETH, H., DOWDESWELL, J.A., BATCHELOR, C.L. & OTTESEN, D. 2020. 3D sedimentary architecture showing the inception of an Ice Age. *Nature Communications*, **11**, https://doi.org/10.1038/s41467-020-16776-7.

LØSETH, H., ØYGARDEN, B., NYGÅRD, A. & RAULLINE, B. 2016. Reply to Discussion on 'Late Cenozoic geological evolution of the northern North Sea: development of a Miocene unconformity reshaped by large-scale Pleistocene sand intrusion', Journal of the Geological Society, 170, 133–145. *Journal of the Geological Society*, **173**, 394–397, https://doi.org/10.1144/jgs2015-104.

LØSETH, H., RAULLINE, B. & NYGARD, A. 2013. Late Cenozoic geological evolution of the northern North Sea: development of a Miocene unconformity reshaped by large-scale Pleistocene sand intrusion. *Journal of the Geological Society*, **170**, 133–145, https://doi.org/10.1144/jgs2011-165.

LØSETH, H., WENSAAS, L., ARNTSEN, B. & HOVLAND, M. 2003. Gas and fluid injection triggering shallow mud mobilization in the Hordaland Group, North Sea. *Geological Society, London, Special Publications*, **216**, 139–157, https://doi.org/10.1144/gsl.sp.2003.216.01.10.

MARCUSSEN, O., THYBERG, B.I, PELTONEN, O., JAHREN, J., BJORLYKKE, K., & FALEIDE J.I. 2009. Physical properties of Cenozoic mudstones from the northern North Sea: Impact of clay mineralogy on compaction trends. AAPG Bulletin, **93**, 127–150

MARTEL, A.T. & GIBLING, M.R. 1993. Clastic dykes of the Devono-Carboniferous Horton Bluff Formation, Nova Scotia: storm-related structures in shallow lakes. *Sedimentary Geology*, **87**, 103–119, https://doi.org/10.1016/0037-0738 (93)90038-7.

MARTEL, T.A. & GIBLING, M.R. 1993. Clastic dykes of the Devono-Carboniferous Horton Bluff Formation, Nova Scotia: storm-related structures in shallow lakes. *Sedimentary Geology*, **87**, 103–119, https://doi.org/10.1016/0037-0738 (93)90038-7.

MARTINSEN, O.J., BØEN, F., CHARNOCK, M.A., MANGERUD, G. & NØTTVEDT, A. 1999. Cenozoic development of the Norwegian margin 60–64°N: sequences and sedimentary response to variable basin physiography and tectonic setting. *In*: *Petroleum Geology of Northwest Europe: Proceedings of the 5th Conference*. 293–304., https://doi.org/10.1144/0050293.

MAZZINI, A., DURANTI, D., JONK, R., PARNELL, J., CRONIN, B.T., HURST, A. & QUINE, M. 2003. Palaeo-carbonate seep structures above an oil reservoir, Gryphon Field, Tertiary, North Sea. *Geo-Marine Letters*, **23**, 323–339, https://doi.org/10.1007/s00367-003-0145-y.

MICHELSEN, O., THOMSEN, E., DANIELSEN, M., HEILMANN-CLAUSEN, C., JORDT, H. AND LAURSEN, G.V. 1998. Cenozoic sequence stratigraphy in the Eastern North Sea. *Mesozoic-Cenozoic Sequence Stratigraphy of Western European Basins*, **60**, 91–118.

MOLYNEUX, S. 2001. Sandstone remobilisation in the Eocene to Miocene of the central and northern North Sea. Doctoral dissertation, Imperial College London.

MOLYNEUX, S., CARTWRIGHT, J. & LONERGAN, L. 2002. Conical sandstone injection structures imaged by 3D seismic in the central North Sea, UK. *First Break*, **20**, 383–393, https://doi.org/10.1046/j.1365-2397.2002.00258.x.

NADIN, P.A. & KUSZNIR, N.J. 1995. Palaeocene uplift and Eocene subsidence in the northern North Sea Basin from 2D forward and reverse stratigraphic modelling. *Journal of the Geological Society*, **152**, 833–848, https://doi.org/10.1144/gsjgs.152.5.0833.

NOTTVEDT, A., GABRIELSEN, R.H. & Steel, R.J. 1995. Tectono-stratigraphy and sedimentary architecture of rift basins, with reference to the northern North Sea. *Marine and Petroleum Geology*, **12**, 881–901, https://doi.org/10.1016/0264-8172 (95)98853-W.

OBERMEIER, S.F. 1996. Use of liquefaction-induced features for paleo-seismic analysis — An overview of how seismic liquefaction features can be distinguished from other features and how their regional distribution and properties of source sediment can be used to infer the location. *Engineering Geology*, **44**, 1–76, https://doi.org/10.1016/S0013-7952 (96)00040-3.

OBERMEIER, S.F. 1998. Liquefaction evidence for strong earthquakes of Holocene and latest Pleistocene ages in the states of Indiana and Illinois, USA. *Engineering Geology*, **50**, 227–254, https://doi.org/10.1016/S0013-7952 (98)00032-5.

OLOBAYO, O. 2014. Deposition, remobilization and fluid flow in sedimentary basins – case studies in the northern North Sea and Nigeria Transform Margin. A thesis submitted to The University of Manchester for the degree of Doctor of Philosophy in the Faculty of Engineering. *Unpublished PhD Thesis*.

OOMKENS, E. 1966. Environmental significance of sand dikes. *Sedimentology*, **7**, 145–148, https://doi.org/10.1111/j.1365-3091.1966.tb01585.x.

OSBORNE, M.J. & SWARBRICK, R.E. 1997. Mechanisms for Generating Overpressure in Sedimentary Basins: A Re-evaluation. *AAPG Bulletin*, **81** (1997), https://doi.org/10.1306/522B49C9-1727-11D7-8645000102C1865D.

PARIZE, O., BEAUDOIN, B., et al. 2007. The Vocontian Aptian and Albian Syn-depositional Clastic Sills and Dikes: A Field-based Mechanical Approach to Predict and Model the Early Fracturing of Marly-limy Sediments. *In*: *Sand Injectites: Implications for Hydrocarbon Exploration and Production: AAPG Memoir 87*. 163–172., https://doi.org/10.1306/1209860M873262.

PLINT, A.G. 1985. Possible earthquake-induced soft-sediment faulting and remobilization in Pennsylvanian alluvial strata, southern New Brunswick, Canada. *Canadian Journal of Earth Sciences*, **22**, 907–912, https://doi.org/-.

PURVIS, K., KAO, J., FLANAGAN, K., HENDERSON, J. & DURANTI, D. 2002. Complex reservoir geometries in a deep-water clastic sequence, Gryphon Field, UKCS: Injection structures, geological modelling and reservoir simulation. *Marine and Petroleum Geology*, **19**, 161–179, https://doi.org/10.1016/S0264-8172 (02)00003-X.

RAMDHAN, A.M. & GOULTY, N.R. 2010. Overpressure-generating mechanisms in the Peciko Field, Lower Kutai Basin, Indonesia. *Petroleum Geoscience*, **16**, 367–376, https://doi.org/10.1144/1354-079309-027.

REILLY, M.J. & FLEMINGS, P.B. 2010. Deep pore pressures and seafloor venting in the Auger Basin, Gulf of Mexico. *Basin Research*, **22**, 380–397, https://doi.org/10.1111/j.1365-2117.2010.00481.x.

RUNDBERG, Y. & EIDVIN, T. 2005. Controls on depositional history and architecture of the Oligocene-Miocene succession, northern North Sea Basin. *Norwegian Petroleum Society Special Publications*, **12**, 207–239, https://doi.org/10.1016/S0928-8937 (05)80050-5.

RUNDBERG, Y. 1989. *Tertiary Sedimentary History and Basin Evolution of the Norwegian North Sea between 60-62 N. An Integrated Approach*. PhD Thesis, University of Trondheim, Norway.

RUNDBERG, Y. & EIDVIN, T. 2016. Discussion on 'Late Cenozoic geological evolution of the northern North Sea: Development of a Miocene unconformity reshaped by large-scale Pleistocene sand intrusion', Journal of the geological society, 170, 133–145. *Journal of the Geological Society*, **173**, 384–393, https://doi.org/10.1144/jgs2014-023.

SAFRONOVA, P.A., ANDREASSEN, K., LABERG, J.S. & VORREN, T.O. 2012. Development and post-depositional deformation of a Middle Eocene deep-water sandy depositional system in the Sørvestsnaget Basin, SW Barents Sea. *Marine and Petroleum Geology*, **36**, 83–99, https://doi.org/10.1016/j.marpetgeo.2012.06.007.

SCLATER, J.G. & CHRISTIE, P.A.F. 1980. Continental stretching: An explanation of the Post-Mid-Cretaceous subsidence of the central North Sea Basin. *Journal of Geophysical Research: Solid Earth*, **85**, 3711–3739, https://doi.org/10.1029/JB085iB07p03711.

SHOULDERS, S.J. & CARTWRIGHT, J. 2004. Constraining the depth and timing of large-scale conical sandstone intrusions. *Geology*, **32**, 661–664, https://doi.org/10.1130/G20654.1.

SHOULDERS, S.J., CARTWRIGHT, J. & HUUSE, M. 2007. Large-scale conical sandstone intrusions and polygonal fault systems in Tranche 6, Faroe-Shetland Basin. *Marine and Petroleum Geology*, **24**, 173–188, https://doi.org/10.1016/j.marpetgeo.2006.12.001.

SURLYK, F., GJELBERG, J. & NOE-NYGAARD, N. 2007. The Upper Jurassic Hareelv Formation of East Greenland: A Giant Sedimentary Injection Complex. *Sand injectites: Implications for hydrocarbon exploration and production*, 141–149, https://doi.org/-.

SWARBRICK, R.E. & OSBORNE, M.J. 1998. Mechanisms that generate abnormal pressures: an overview. *Abnormal Pressures in Hydrocarbon Environments: AAPG Memoir 70*, 13–34.

THYBERG, B.I., STABELL, B., FALEIDE, J.I. & BJØRLYKKE, K. 1999. Upper Oligocene diatomaceous deposits in the northern North Sea - silica diagenesis and paleogeographic implications. *Norsk Geologisk Tidsskrift*, **79**, 3–18, https://doi.org/10.1080/002919699433870.

TRUSWELL, J.F. 1972. Sandstone sheets and related intrusions from Coffee Bay, Transkei, South Africa. *Journal of Sedimentary Petrology*, **42**, 578–583, https://doi.org/10.1306/74d725c2-2b21-11d7-8648000102c1865d.

VELDE, B. 1996. Compaction trends of clay-rich deep sea sediments. *Marine Geology*, **133**, 193–201, https://doi.org/10.1016/0025-3227 (96)00020-5.

VIGORITO, M. & HURST, A. 2010. Regional sand injectite architecture as a record of pore-pressure evolution and sand redistribution in the shallow crust: insights from the Panoche Giant Injection Complex, California. *Journal of the Geological Society*, **167**, 889–904, https://doi.org/10.1144/0016-76492010-004.

VIGORITO, M., HURST, A., CARTWRIGHT, J.A. & SCOTT, A. 2008. Regional-scale subsurface sand remobilization: geometry and architecture. *Journal of the Geological Society*, **165**, 609–612, https://doi.org/10.1144/0016-76492007-096.

WINSLOW, M.A. 1983. Clastic dike swarms and the structural evolution of the foreland fold and thrust belt of the southern Andes (Chile). *Geological Society of America Bulletin*, **94**, 1073–1080, https://doi.org/10.1130/0016-7606 (1983)94<1073: CDSATS>2.0.CO; 2.

WRONA, T., JACKSON, C.A.L., HUUSE, M. & TAYLOR, K.G. 2017b. Silica diagenesis in Cenozoic mudstones of the North Viking Graben: physical properties and basin modelling. *Basin Research*, **29**, 556–575, https://doi.org/10.1111/bre.12168.

WRONA, T., MAGEE, C., JACKSON, C.A.-L., HUUSE, M. & TAYLOR, K.G. 2017a. Kinematics of Polygonal Fault Systems: Observations from the Northern North Sea. *Frontiers in Earth Science*, **5**, 101, https://doi.org/10.3389/feart.2017.00101.

YARDLEY, G.S. & SWARBRICK, R.E. 2000. Lateral transfer: A source of additional overpressure? *Marine and Petroleum Geology*, **17**, 523–537, https://doi.org/10.1016/S0264-8172 (00)00007-6.

ZIEGLER, P.A. 1982. Triassic rifts and facies patterns in Western and Central Europe. *Geologische Rundschau*, **71**, 747–772, https://doi.org/10.1007/BF01821101.

ZIEGLER, P.A. 1990. Tectonic and palaeogeographic development of the North Sea rift system. In: Blundell, D.J. & Gibbs, A.D. (eds) Tectonic evolution of the North Sea rifts. *Oxford University Press*, 1–36.

Chapter 6

CHAPTER 6   Origin of Oligo-Miocene sandstones and the top Hordaland topography in the northern North Sea revisited

Theme: Depositional versus remobilized and injected sands

Origin of Oligo-Miocene sandstones and the top Hordaland topography in the northern North Sea revisited

Nnorom, S. and Huuse, M.

Basins Research Group, Department of Earth and Environmental Sciences, University of Manchester, Oxford Road, Manchester M13 9PL, UK

 *Correspondence (sebastian.nnorom@manchester.ac.uk)

Keywords: Sandstone intrusions, Northern North Sea Basin, Post-depositional, Remobilization, Injection.

A revised version of this chapter will be submitted to Journal of the Geological Society of London for publication

Abstract

In this study, a recent high-quality broadband 3D seismic data has been used to revisit aspects of the model for the evolution of the northern North Sea presented by Løseth et al. (2013), to investigate the origin of Oligocene sandstones and sand intrusions in the northern North Sea, and the potential mechanisms responsible for the mounded shape of the Top Hordaland Group Unconformity. Our findings clearly indicate their model is inconsistent with geological data. Their interpretation that Oligocene sands were injected from Paleocene parent source sands is debunked by observation of a Middle – Late Oligocene depositional system which we interpret to represent turbiditic slope channel-belt sands supplied from the Shetland Platform and West Norway. However, evidence to support a mixed origin for the sands with possible contribution from Middle – Late Eocene sands is also observed. Based on the above, differential compaction and forced folding or jack-up due to sand remobilization and injection are both suggested to have reshaped the Top Hordaland Group Unconformity into its present-day mounded geometry.

6.1 Introduction

Sand injectites or sandstone intrusions have been extensively studied in sedimentary basins worldwide. They have been documented in several basins using both outcrop and seismic data, and they occur in centimetre to kilometre scale, with varying simple to complex geometries (e.g. Lonergan & Cartwright, 1999; Lonergan et al., 2000; Jolly & Lonergan, 2002; Molyneux et al., 2002; Hurst et al., 2003; Huuse et al., 2003, 2004; Huuse & Mickelson, 2004; Huuse et al., 2007; Hurst & Cartwright, 2007; Shoulders et al., 2007; Hurst et al., 2011; Jackson et al., 2011; Andresen & Clausen, 2014; Andresen et al., 2019; Cobain et al., 2019; Hermanrud et al., 2019; Andresen, 2020). They usually occur in deep-water marine (turbidites and channel) environments and form large sand networks associated with deep-water sand-rich systems (Huuse et al., 2003; Hurst et al., 2011). On seismic data, they are recognized as discordant and concordant high amplitude reflections which crosscut their surrounding strata. Sand injectites are well-documented in the Paleogene succession of the North Sea basin within smectite-rich mudstones which form their host strata. Studies of sand intrusions in the North Sea indicate that sand injection into their low permeable host mudstone strata has significant implications for reservoir geology (geometries & architecture), vertical connectivity and fluid flow within the basin because: (i) they can act as reservoirs for hydrocarbon (e.g., Alba, Balder and Gryphon fields), and (ii) they can form long-lived fluid flow conduit in otherwise low permeable strata (Huuse & Mickelson, 2004).

This study addresses the controversy raised in literature by the model and interpretation of the source sand for Oligocene sand intrusions and the nature of mounds at the top of the Hordaland Group Unconformity (i.e., Mid-Miocene Unconformity) by Løseth et al. (2013) and in the follow-up discussion by Rundberg & Eidivin (2016), which disagrees with their

model for the areas above the Snorre, Gullfaks and Visund Fields in the northern North Sea Basin. We provide new compelling evidence based on new insights and observations from latest broadband 3D seismic data, some of which either support or disagree with the models and claims by both Løseth et al., (2013) and Rundberg & Eidivin (2016). However, majority of the new findings completely disagree with the model and interpretation by Løseth et al. (2013) and their follow-up discussion in Løseth et al., (2016), while largely supporting the model by Rundberg & Eidivin (2005, 2016) with new observations. Based on these new findings and observations, a revised or alternative depositional and post-depositional model for the development of Oligocene sand intrusions and the modification of the top Hordaland Group Unconformity is proposed for the northern North Sea Basin.

It is important that the model for the origin of Oligocene sandstones and the mounded nature of the Top Hordaland Group Unconformity is correctly established because: (i) this will help to provide a clear understanding of the post-Eocene evolution of the northern North Sea and distribution of Oligocene deep-water sediments, (ii) it will also help to provide insight into the timing of emplacement of Oligocene intrusions and in determining the potential local controls on their development, and (iii) finally, establishing the right model for the origin of the mounds at the Top Hordaland Group Unconformity could provide insight into factors or processes which may have affected sediment routing and distribution post-mound formation, because the presence of mounds on the Top Hordaland Group Unconformity which was at some point the paleo-seafloor may affect the spatial distribution of subsequent sediments deposited above the mounds.

6.2 Geological Setting

The study area lies within the Norwegian sector of the northern North Sea Basin and cover areas between latitude 59 - 62°N and longitude 1 – 4°E (Fig. 6.1a). This area of the North Sea was affected by two main rifting episodes in the Permo-Triassic and Late Jurassic to Early Cretaceous, which led the formation of graben and half-graben structures bounded by west-dipping and south-striking normal faults (Faerseth et al., 1995; Dmitrieva et al., 2018). The rifting phase ceased in the Late-Jurassic to Early Cretaceous, with the post-rift phase commencing in the Early Cretaceous (Jordt et al., 2000). This was accompanied by uplift along basin margins linked to igneous activity and the opening of the North Atlantic (Jordt et al., 2000; Gabrielsen et al., 2001). Large quantity of clastic sediments was then deposited into the basin from the uplifted basin margins, sourced from the East Shetland platform (in the west) and Norwegian mainland (in the east) (Jordt et al., 2000; Ahmadi et al., 2003; Rundberg & Eidivin, 2005; Eidvin et al., 2014). Detailed geological and tectonic evolution of the study area have been described in literature and can be referred to for further information (e.g., Martinsen et al., 1999; Faleide et al., 2002; Ahmadi et al., 2003; Fyfe et al., 2003; Eidvin et al., 2014; etc).

This study revisits aspects of the previous interpretation of the Late Cenozoic evolution of the northern North Sea by Løseth et al. (2013), with reference to how the Oligocene sands were formed, and the processes leading to the reshaping of the Mid Miocene Unconformity (MMU) by mounds in the Gullfaks, Snorre and Visund Field areas. Detailed description of the regional distribution and controls on the deposition of the Oligocene succession in the northern North Sea, and the spatial and temporal distribution of Oligocene deep-water sand systems have been documented by Eidvin & Rundberg (2001), Rundberg & Eidivin, (2005: see their Fig 7a), and Eidvin et al. (2013, 2014: see their Fig. 1). As such this is not revisited here. The seismic character of the top Hordaland Group unconformity has also been described by Eidvin & Rundberg (2001) and Løseth et al. (2013).

6.3 Data and Methods

A pre-stack depth-migrated 3D seismic reflection data which covers an area of c. 36,400 km^2 in the northern North Sea have been used for this study (Fig. 6.1a). The survey includes the c. 3000 km^2 area studied by Løseth et al. (2013) which covered areas within Quadrant 34 (Block 7 & 8) and partly Quadrant 33. The seismic data covers (Fig. 6.1b): (i) some part of the UK northern North Sea (Quad. 003 & 211), (ii) a bit of Mid Norway (Quad. 6203 & 6204), (iii) some section of the Norway Southern North Sea (Quad. 25 & 26), and mainly Norway northern North Sea (Quad. 29 to 36). The data has a subsampled bin spacing of 37.5 m, a vertical sampling interval of 5m, is depth migrated and zero-phase processed, with a downward increase in acoustic impedance represented by a positive (red) peak reflection and a downward decrease represented by a negative (blue) trough reflection. The studied interval lies within the Hordaland Group (Eocene to Mid Miocene: 1000 – 1600 m), with the seismic velocity within the interval close to 2000 m/s. A total of thirty-four (34) wells were used to delineate the extent and presence of Oligocene sands in the study area (see Fig. 6.4).

The post-Eocene succession up to the Top Hordaland Group Unconformity or Mid-Miocene Unconformity (Fig. 6.1c) have been re-analysed and re-interpreted in the area around the Snorre, Gullfaks and Visund fields, which was previously documented by Løseth et al. (2013). Their analysis has been extended eastwards using a cropped seismic cube (c. 8812 km^2: Fig. 6.1a) to provide evidence for the presence of a Middle – Oligocene sandy depositional system sourced from both western and eastern source areas, which disagrees with the model by Løseth et al. (2013) but agree with that of Rundberg & Eidivin (2005, 2016). This analysis was carried out by mapping key seismic horizons and attribute extraction on mapped horizons and horizon slices through the interval of interest within the cropped seismic volume. In addition, observations in seismic cross sections outside the cropped volume also provide evidence which support our conclusions in this study.
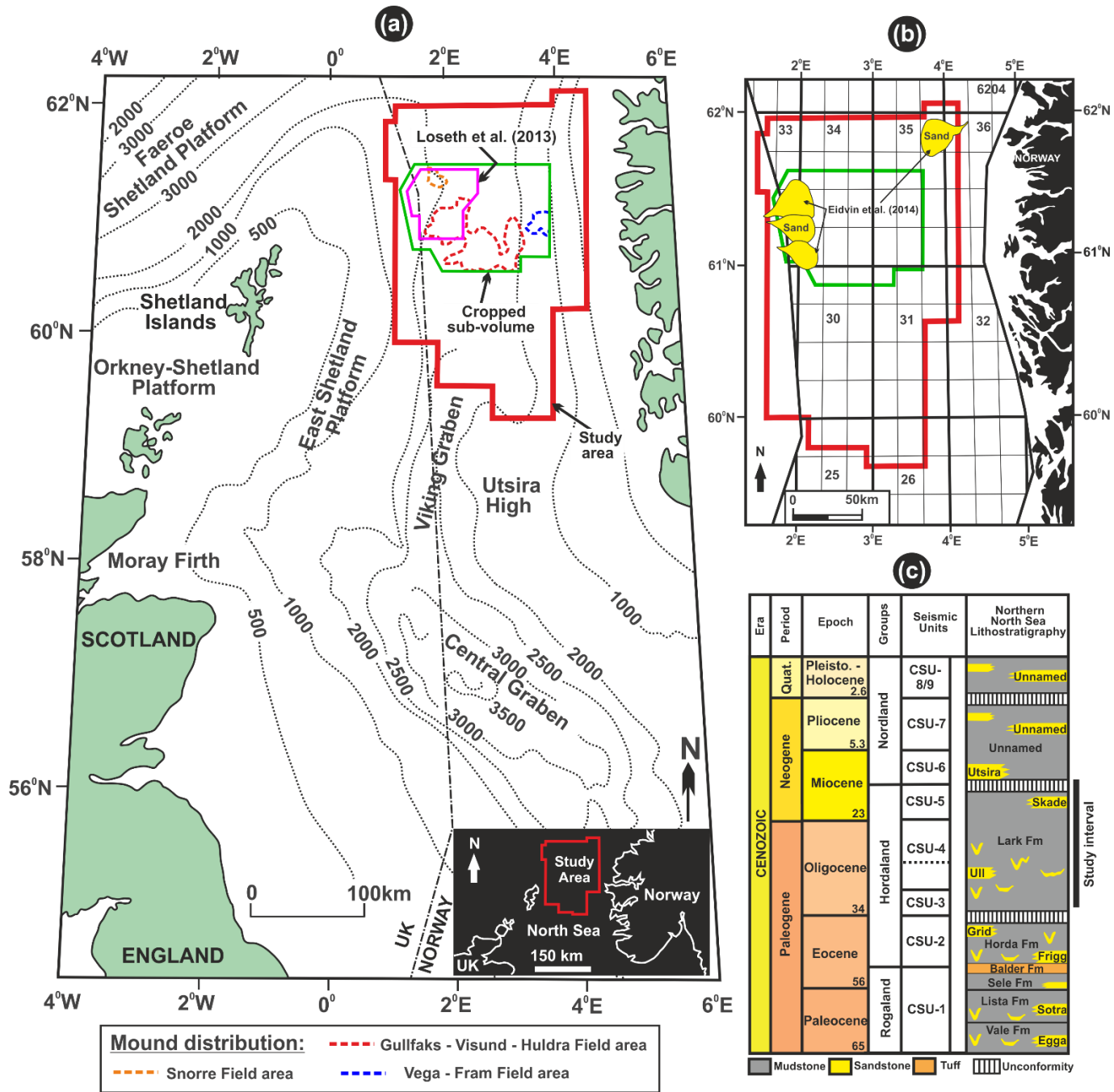
Fig. 6.1: (a) Map showing the location of the study area in the Northern North Sea Basin, with the contours (in metres) representing the total thickness of Cenozoic sediments (Modified after Underhill, 2001). The red bold line shows the outline of the 3D seismic data available for this study. The Green bold line shows the outline of the cropped seismic sub-volume used to document the distribution of mounds at the Top Hordaland Group Unconformity, while the pink bold line shows the outline of the seismic data used by Løseth et al. (2013) to document same. (b) Map showing the area coverage of the 3D seismic data provided by CGG. The approximate outline of Oligocene sands interpreted by Rundberg & Eidvin (2005) and Eidvin et al. (2014) is also shown. (c) A simplified lithostratigraphic framework of the northern North Sea Basin indicating the studied interval.

6.4 Previous models & interpretation for Oligocene sands and the shape of the mid Miocene Unconformity

In this section, we highlight and examine the interpretation and suggestions by Løseth et al. (2013, 2016) and Rundberg & Eidivin (2005, 2016). Both models are compared followed by our evidence-based interpretations to evaluate the basics for their models. We also provide additional or alternative interpretation due to access to more extensive data outside the dataset used in their studies.

6.4.1 Løseth et al. (2013, 2016) Model

1) In their model, they interpreted the Oligocene sands above the Snorre and Visund Field area as intrusive sands injected from Paleocene and/or Eocene parent depositional sands into their host smectite-rich Hordaland Group mudstones (Fig. 6.2; also see Løseth et al., 2013: their Fig. 2, 11 & 12; 2016: their Fig 1). Their interpretation gives a view contrary to the previous interpretation provided for Oligocene sedimentation in their study area by Rundberg & Eidivin (2005), where Oligocene sands were described to represent turbiditic gravity flow depositional sands sourced from uplifted basin margins in the Early to Late Oligocene time (see Fig. 6.1b; also refer to Rundberg & Eidivin, 2005: their Fig. 7a; and Eidvin et al., 2014: their Fig. 1).

2) In addition, they claimed that although the parent Paleocene sands for their proposed intrusive Oligocene sands in the Snorre and Visund area are remarkably thin at the present time, they believe that thick Paleocene sands were originally deposited in the area, with long lasting fluid overpressure within the sands resulting to depletion of the Paleocene parent sands during sand injection.

3) They also interpreted the mounded topography of the Top Hordaland Group Unconformity (THGU) above the Oligocene sand intrusions (c. 180m below the THGU) to result from forced folding caused by upward injection of sand from Paleocene into the Oligocene interval.

4) They interpreted the sands which fill in depressions or low areas between the mounds as extrusive sands, extruded onto the seafloor in the Pleistocene through feeder dikes from intrusive Oligocene sand bodies below the mounds which they claim to be turbidites initially deposited in the Paleocene (see their 2013: Fig. 11 & 12). They described the extruded sands to have been deposited during the late-syn to post-mound formation because they show no channel-like structures and are observed to thin or pinch-out laterally away from a central thick zone (see Løseth et al., 2013: their Fig. 11 & 12). However, these sands were previously interpreted as gravity flow sands by Eidvin & Rundberg (2001).
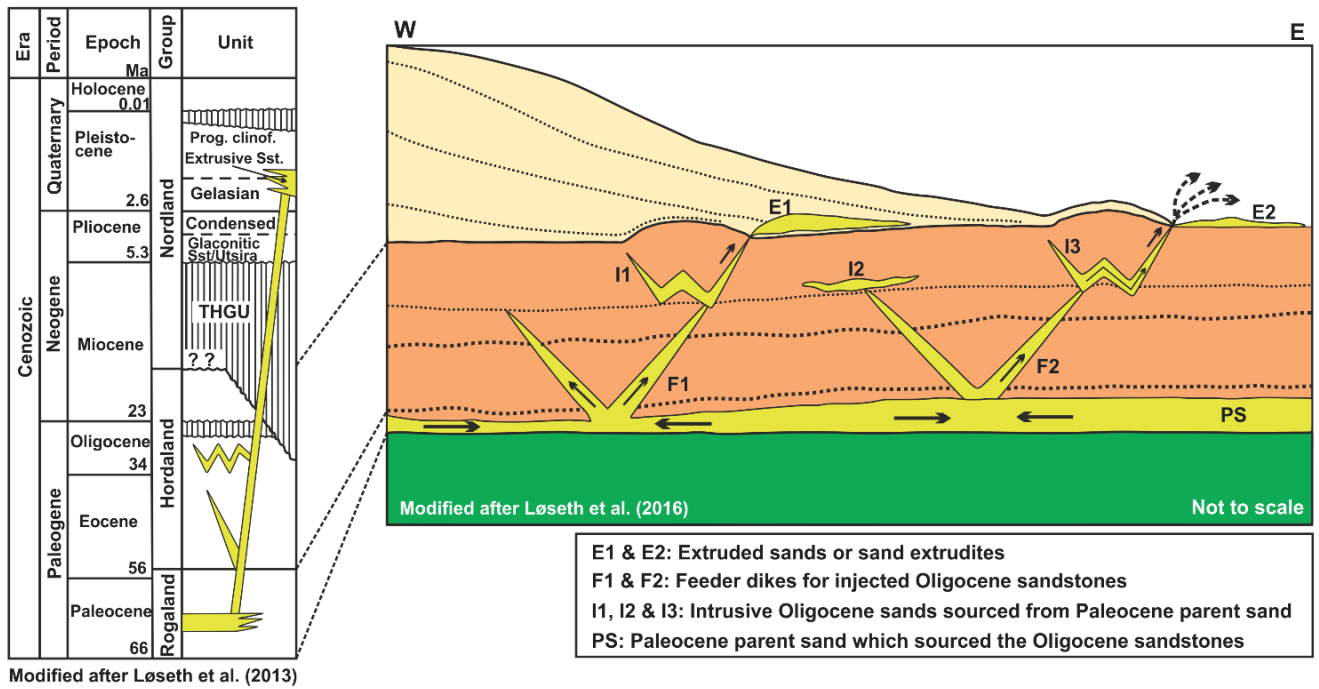
Fig. 6.2: Schematic illustration of Loseth et al. (2013)'s model showing Oligocene intrusive sands sourced from Paleocene parent sands (modified from Loseth et al., 2016).
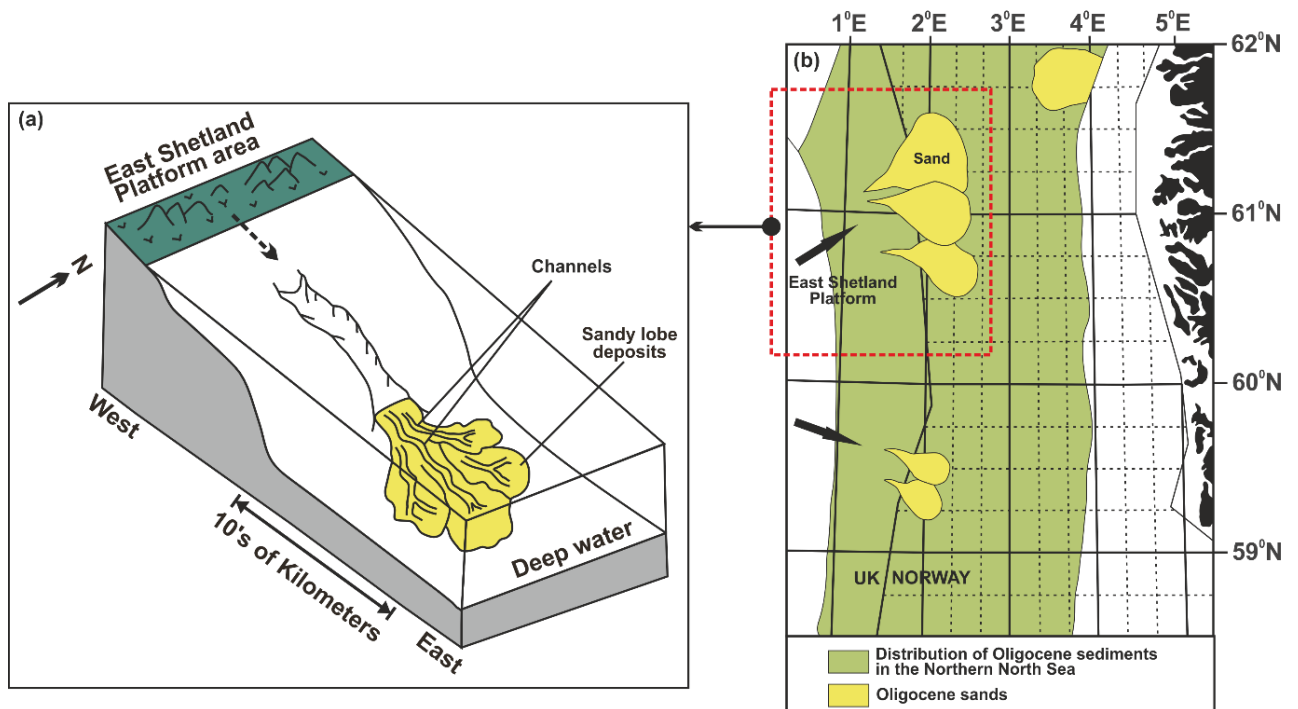
Fig. 6.3: Schematic illustration of Rundberg & Eidvin (2005, 2016)'s model indicating a depositional Oligocene sandstone in (a) with the approximate outline of the Oligocene sands shown in (b). Fig. (b) modified from Rundberg and Eidvin (2005).

6.4.2 Rundberg & Eidvin (2016) Model

They argued against the model by Løseth et al. (2013) by presenting arguments based on their previous proposed models in Rundberg & Eidivin (2005) and Eidvin & Rundberg (2001) where they interpreted Oligocene sands to be turbiditic gravity flow deposits. The approximate outline of this Oligocene sandy depositional system has been outlined in Fig. 6.3, Rundberg & Eidivin (2005: their Fig. 7a) and Eidvin et al. (2014: their Fig. 1). They presented the following arguments:

1) That the limited presence or absence of Paleocene sands in the area around Block 34/4 and 34/7 (see Fig. 6.1b) evidenced in exploration wells drilled within both blocks, in which Paleocene sands are either thin or absent does not support an intrusive Paleocene parent sands for the Oligocene sands (Ahmadi et al., 2003). They also argued that the model by Løseth et al. (2013) do not account for a credible parent source sand which accounts for the substantial volume of sand they claimed to have been injected into the Oligocene from the Paleocene.

2) In addition, they supported their argument using grain size distribution in ditch cuttings from well 34/7-6 (Snorre area) and microfossil assemblage in the Lower Oligocene sands in well 34/4-6 at depth of 1370 – 1390 m (see text in Eidvin & Rundberg, 2001 and Rundberg & Eidivin, 2016). They argued that based on well completion report from NPD, that a 60 m thick sandstone penetrated approximately 150 m below the Top Hordaland Group Unconformity by well 34/7-6 was described as medium grained and well sorted sand from dish cutting samples, which do not support a Paleocene source for the Oligocene sands. In addition, evidence from micropaleontology show that Paleocene – Eocene sediments consist mainly of flysch-type benthic agglutinated foraminiferal fauna (see Gradstein & Bäckström, 1996; Rundberg & Eidvin, 2016: their Fig 7h). Contrary to the above, the foraminiferal fauna found in samples from the Lower Oligocene sand in well 34/4-6 show it consists of sparse calcareous benthic foraminiferal fauna, as well as long-range Paleogene diatoms and radiolaria (Rundberg & Eidvin, 2016). As such, Oligocene sands show no evidence of similar foraminiferal fauna assemblage typical of Paleocene – Eocene sediments, which clearly indicates that they have no direct relationship to Paleocene sands as suggested by Løseth et al. (2013).

3) That the mounded topography of the top Hordaland Group unconformity in the Snorre area (see their Fig. 1) mimic the pattern of their underlying turbiditic channel-sand systems. In addition, they observed that the mound in the Visund and Gullfaks areas also show patterns consistent with the characteristics of their underlying channel-belt systems with some clear indication of sinuosity (see their Fig. 1 & 8). They also highlighted that the mounds generally show minor and major levels of branching which they interpreted as channel bifurcation (see their Fig. 8).

6.4.3 This study: Observation, Analysis, and Interpretation

In seismic cross section, the Top Hordaland Group Unconformity (THGU) is characterized by a continuous to semi-continuous high amplitude trough reflection (see Fig. 6.6, 6.11, 6.13 – 6.16) and serves as the boundary which separates the underlying polygonally-faulted smectite-rich mudstones from the overlying glauconitic sand and clay deposits of the Nordland Group (Løseth et al., 2013). A cropped seismic volume covering an area of c. 8812 km^2 have been used to study the distribution of mounds on the THGU surface (Fig. 6.1a). The surface is irregularly mounded in the west, south, north-west, and eastern parts (Fig. 6.4, 6.5). However, a few isolated mounds occur in the northern part which is largely flat lying. The mounds form a belt of mounds which cover an area of c. 2540 km^2 and their distribution generally indicate the lateral distribution of their underlying Oligocene sand injectites in the study area (Fig. 6.4, 6.5 & 6.6).

In the north-western part of the cropped sub-volume (Fig. 6.4) an isolated mound occurs above the Snorre area which is 3.4 – 4 km wide, 14.5 km long and up to 125 m high. The THGU at the southwestern part of the Snorre area is characterized by near-circular depression with diameters of c. 200 – 300 m (Fig. 6.4). These circular depressions are interpreted to likely represent the seismic expression of buried pockmarks formed at the paleo-seafloor due to fluid expulsion at the seafloor (Andresen, 2012). In the Visund area, the mounds are irregular-shaped and are 4 – 5 km wide, 11.6 km long and up to 14.5 m high. In the western part, around the Gullfaks area, the mounds are characterized by elongate and sinuous pattern, with mounds extending for distances of up to 22 km. In the south and south-western part, around the Huldra Field both isolated, elongate, and connected mounds occur on the THGU which are up to 5.5 km wide, 30 km long and 150 m high. To the east, around the Vega and Fram Field area, elongate and numerous isolated mounds are formed on the THGU which are usually 1 – 5 km wide, 2.5 – 12 km long and up to 165 m high. The areas between adjacent mounds form irregular depressions filled by younger sediments which either onlap or downlap onto the mounds (Fig. 6.4, 6.5). These irregular depressions are suggested to have formed due to elevation of the mounded areas.

The Oligocene sands located below the THGU (at depths 150 – 300 m) are characterized by high amplitude anomalies with both top and base reflection, which are either concordant or discordant to bedding. These sands are interpreted as injectites due to their clear discordance to bedding and the calibration of the anomalies to sand intervals where they are intersected by wells in the study area. The injected sands are usually directly attached or detached from their parent depositional sand bodies and are characterized by simple to complex geometries in cross section, ranging from conical-shaped, wing-like and irregular to complex-shaped injectites (see Fig. 6.5, 6.6, 6.13 – 6.16). The sands are usually associated with either low or high mounded relief of the overburden above them.

Our seismic analysis and well observations above the Snorre, Gullfaks and Visund fields, and other areas disagree with Løseth et al. (2013)'s model which interpreted the Oligocene

sands to be completely intrusive from Paleocene parent sands only based on the fact they crosscut the host stratal reflections, as opposed to an in-situ depositional model by Rundberg & Eidivin (2005, 2016). We interpret the Oligocene sand in the area above the Snorre, Gullfaks, Visund, Vega and Fram Fields to be remobilized in-situ depositional sands representing turbiditic gravity-flow sands which agrees with Rundberg & Eidvin (2005, 2016). However, some of the Oligocene sands are observed to be intrusive in areas outside the above-mentioned fields. Therefore, we suggest that Oligocene sands constitute both remobilized in-situ depositional sands in the Middle – Late Oligocene (above the Opal-A/CT boundary) and a combination of in-situ Oligocene sands and intrusive sands in the Lower – Middle Oligocene (below the Opal-A/CT boundary) sourced from Middle to Upper Eocene depositional sands. Our evidence and arguments for the above interpretation are as follows:

A. Evidence for in-situ Oligocene depositional sands (Middle – Late Oligocene)

1) Evidence for a Middle – Late Oligocene depositional system characterized by channel-shaped and channel-lobe anomalies in RMS amplitude attribute horizon slices below the THGU. RMS amplitude horizon slice through the Middle – Late Oligocene interval show the distribution of high reflection amplitude which indicates the distribution of sand (see Fig. 6.7) within the interval and low amplitude areas indicative of mudstone distribution. The high reflection amplitudes indicate that sands were supplied and deposited from a western, southwestern, and north-eastern direction (indicated by yellow arrows in Fig. 6.7). In the Gullfaks area, meandering channel-belt complexes with a SW-NE flow direction are observed in the RMS amplitude horizon slice (Fig. 6.7 & 6.10), with the channels mimicking the mounds at the THGU (Fig. 6.4). The presence of the channel complexes directly disagrees with the model by Løseth et al. (2013) but agree with that by Rundberg & Eidivin (2005, 2016) which suggested turbiditic channel-belt systems underlie the THGU. In the Vega area characterized by very high amplitude reflections, evidence for channel-lobe-like and compensatory stacking of lobe-like high amplitude features are observed with the direction of sediment input in a NE-SW direction (Fig. 6.7 & 6.12)

2) Seismic cross-sections across the anomalies show evidence of numerous wing-like discordant amplitude anomalies in the Middle – Late Oligocene which when mapped appear as remobilized channels (Fig. 6.6c, 6.13a & b, and 6.14a & b). The above is mainly observed in the Vega and Huldra area below the mounds. The wing-like intrusions are thus interpreted as in-situ depositional channel sands or sand mounds (turbidites) which were subjected to post-depositional remobilization and injection at their margins, leading to the formation of their marginal wings which are directly connected to their parent sand. Some of these wing-like intrusions are in cross section characterized by erosional bases (e.g., Fig. 6.13b) which is a good justification for their interpretation as depositional channel sands.
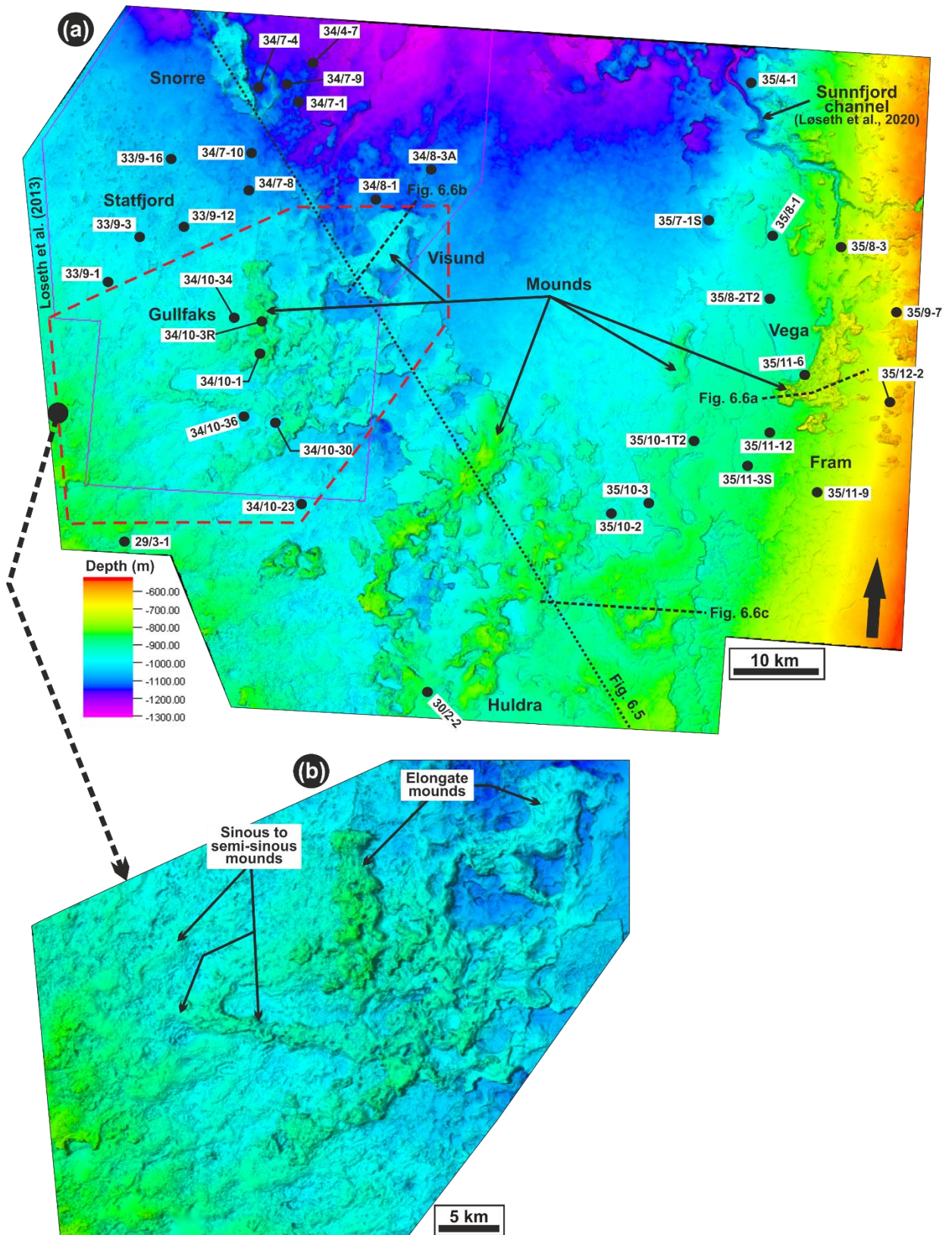
Fig. 6.4: Top structure map of the Top Hordaland Group Unconformity showing the distribution of mounds in the areas above the Snorre, Gullfaks, Visund, Huldra, Vega and Fram Fields. Pink line shows the outline of mound distribution previously documented by Løseth et al. (2013). The approximate location of wells used are also shown. See location of map in Figure 6.1a & b. Seismic data courtesy of CGG and well data from TGS Facies Map Browser.
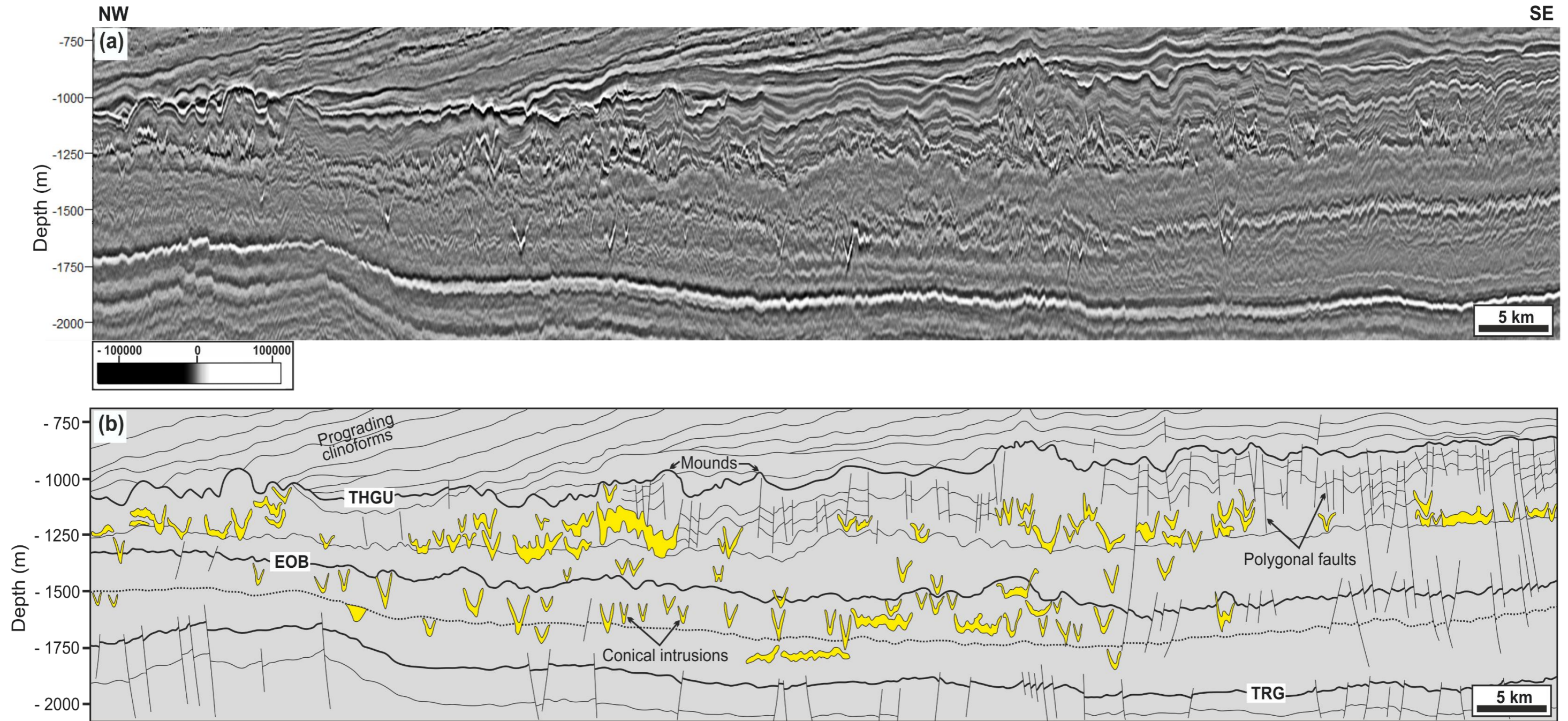
Fig. 6.5: (a) Northwest – southeast regional section across mounds in the Snorre, Visund and Huldra Field areas. (b) Geoseismic section showing the distribution and geometry of Oligocene sand and polygonal faults below the mounds at the THGU. See location of seismic lines in Figure 6.4. THGU = Top Hordaland Group Unconformity; EOB = Eocene – Oligocene Boundary; TRG = Top Rogaland Group. Seismic data courtesy of CGG
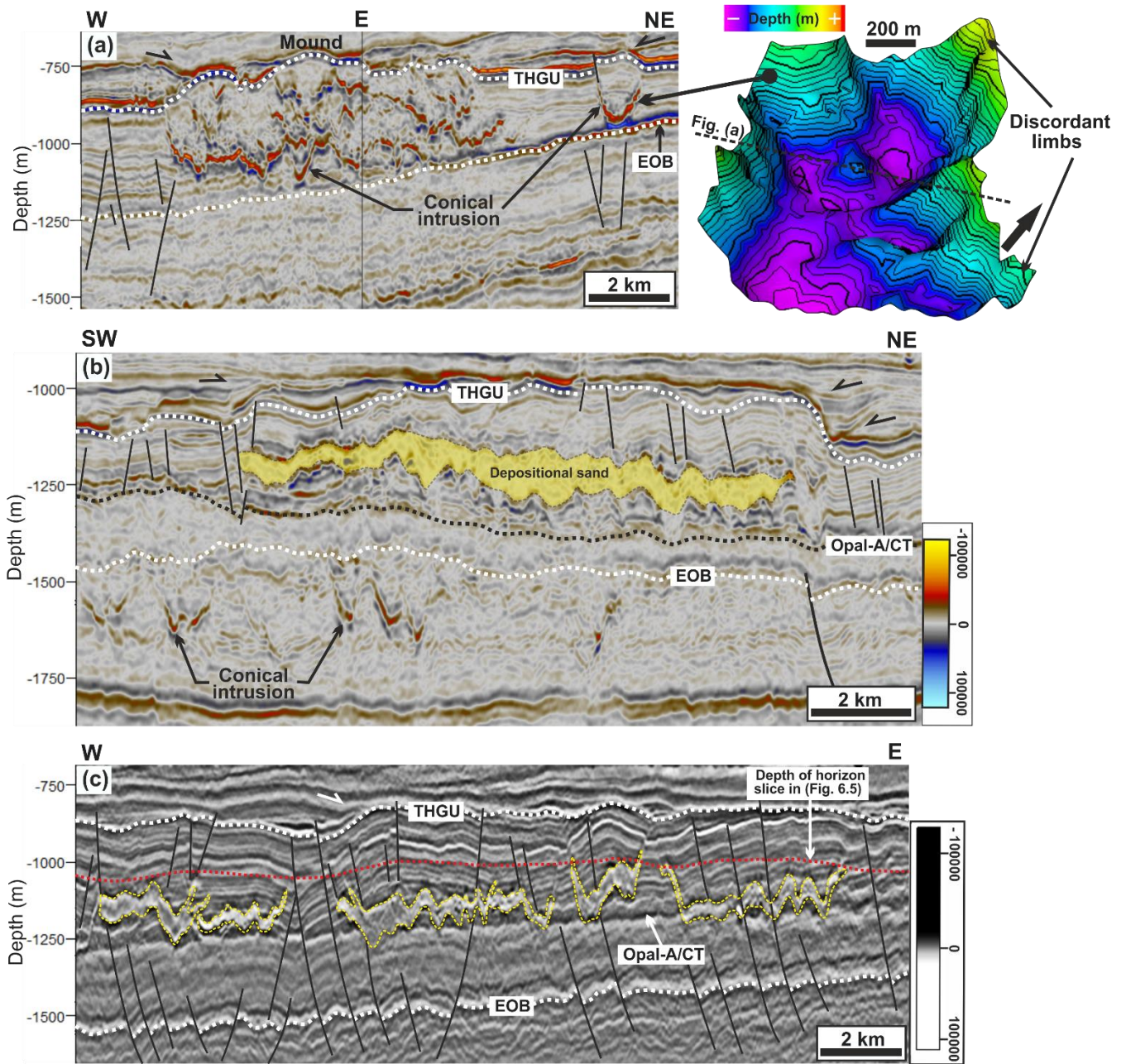
Fig. 6.6: Seismic cross sections through the mounds at the Top Hordaland Group Unconformity (THGU) in the Visund, Huldra and Fram area. (a) West – northwest seismic section through mounds in the Fram area with Oligocene sands characterized by amalgamated or stacked discordant amplitude reflections. The mapped conical-shaped intrusion should be noted. (b) NE – SW seismic section through a mound in the Visund area. Irregular shaped Oligocene sand characterized by zigzag-like top and base occur at c. 185 m below the mound, which is interpreted as remobilized sheet-like depositional sandstone. (c) East – west seismic section through mounds northeast of Huldra area where Oligocene sands (200 – 300 m below the THGU) occur as irregular-shaped high amplitude anomalies with wing-like marginal dikes. Their occurrence above the Opal-A/CT diagenetic boundary should be noted. See location of seismic lines in Figure 6.4. THGU = Top Hordaland Group Unconformity; EOB = Eocene – Oligocene Boundary. Seismic data courtesy of CGG.
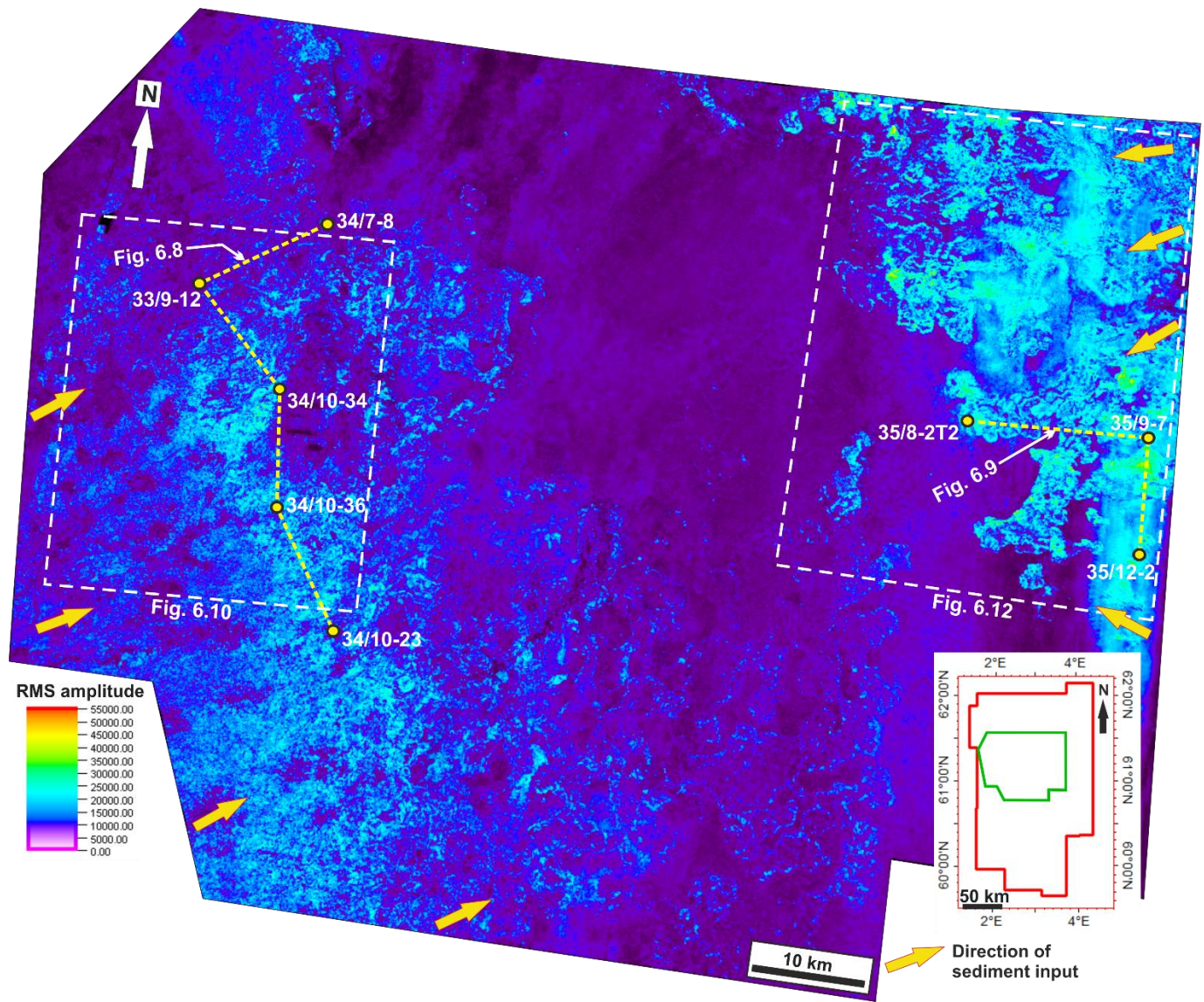
Fig. 6.7: Root-mean square (RMS) amplitude attribute map of seismic horizon slice below the Top Hordaland Group Unconformity. The horizon slice through the Middle – Late Oligocene interval shows the distribution of high amplitude reflections which indicates the spatial distribution of Oligocene sandstones with a NE – SW trend. Yellow arrows show the direction of sediment input into the basin. Yellow dash lines connect wells in log correlation (Fig. 6.8 & 6.9). Depth level of horizon slice is shown in Figure 6.6 & 6.11. Seismic data courtesy of CGG.

3) In the Vega area and north of Vega, most of the numerous wing-like intrusions within the Middle – Late Oligocene occur above a Middle Eocene fan with no evidence of potential feeder conduit or connection to the Eocene fan (see Fig. 6.14a). Therefore, if we must go by Løseth et al. (2013)'s interpretation; (a) How did the Oligocene sands get there from the Paleocene, and (b) How come there is no evidence of remobilization and injection of the Eocene fan in that area. This clearly indicates the sands within the Middle - Late Oligocene (above the Opal-A/CT) are depositional sands sourced from the eastern basin margin.

4) In addition, seismic cross section also show evidence for stacked U-shaped discordant high amplitude anomalies which are interpreted to represent vertical stacking of turbiditic channel sand bodies which were subsequently remobilized and injected by post depositional processes, leading to the formation of amalgamated or stacked complex intrusion geometries which show some cross-cutting relationship (Fig. 6.6a, 6.13a, 6.14a & c).

5) Seismic cross sections across the study area indicate an absence of potential feeder conduits (i.e., dikes) in the Paleocene with connection to the Oligocene. The Paleocene interval is thickest only in the east and north-eastern basin margin (Quadrant 35) where Paleocene sands have been observed and previously documented by Dmitrieva et al. (2012; 2018). In other parts, the Paleocene interval is quite thin with very little or no sand presence. As such, there is no evidence to support any form of connection between Paleocene and Oligocene sands as interpreted by Løseth et al. (2013).

6) Below the mounds, the irregular shaped sandstones characterized by zigzag-like tops and bases which crosscut reflections have been interpreted to be of intrusive origin by Løseth et al. (2013: their Fig. 7a & 8a; 2016) simply based on their zigzag geometry. Our observation indicates that some of these zigzag-shaped sands have discordant margins which would be attributed to sand injection (see Fig. 6.6c), but their zigzag geometries may be attributed to the presence of numerous polygonal faults within their host mudstone. Their zigzag geometries are thus interpreted to likely result from compartmentalization of depositional sand bodies by polygonal faults prior to remobilization and injection. This is evident in Fig. 8a (in Løseth et al., 2013) and supported by the observation that the orientation of the zigzag parts of their high amplitude anomalies align with the polarity of their intersecting polygonal fault (Fig. 6.6c, also see Løseth et al., 2013: their Fig. 7a & 8a).

B. Evidence for intrusive Oligocene sands (Lower – Middle Oligocene)

- Oligocene sand injectites in the west and southern parts of the study area are suggested to be partly sourced from Lower – Middle Eocene channel-fan sands and isolated Middle – Upper Eocene sands based on observation of conical (V/W) shaped injectites with apices within the Middle - Upper Eocene and limbs extending across the Eocene – Oligocene Boundary (EOB) into the Lower Oligocene (Fig. 6.15). These injectites in turn form a network of connected intrusions across the EOB, with clear evidence of such connection observed within the Lower – Middle Oligocene interval where numerous conical shaped injectites have their apices directly above the EOB in the study area.

- Potential feeder conduits (i.e., dikes) connected to Upper Eocene sands are also observed in cross section across the EOB and may have fed some of the Lower – Middle Oligocene sand injectites (Fig. 6.16). This is also supported by numerous conical shaped injectites with apices directly on the EOB. Although the feeder dikes are mainly observed in the southern and western parts of the study area, they are also observed in the Lower Oligocene below the mounds in the Huldra Field area (Fig. 6.16b).

The above two observations support an intrusive model for some of the Oligocene sands, but clearly indicate that a Paleocene source sand is very unlikely because the Paleocene interval is very thin at the central, western, and southern parts of the study area with no evidence of potential feeder conduits in the Paleocene.
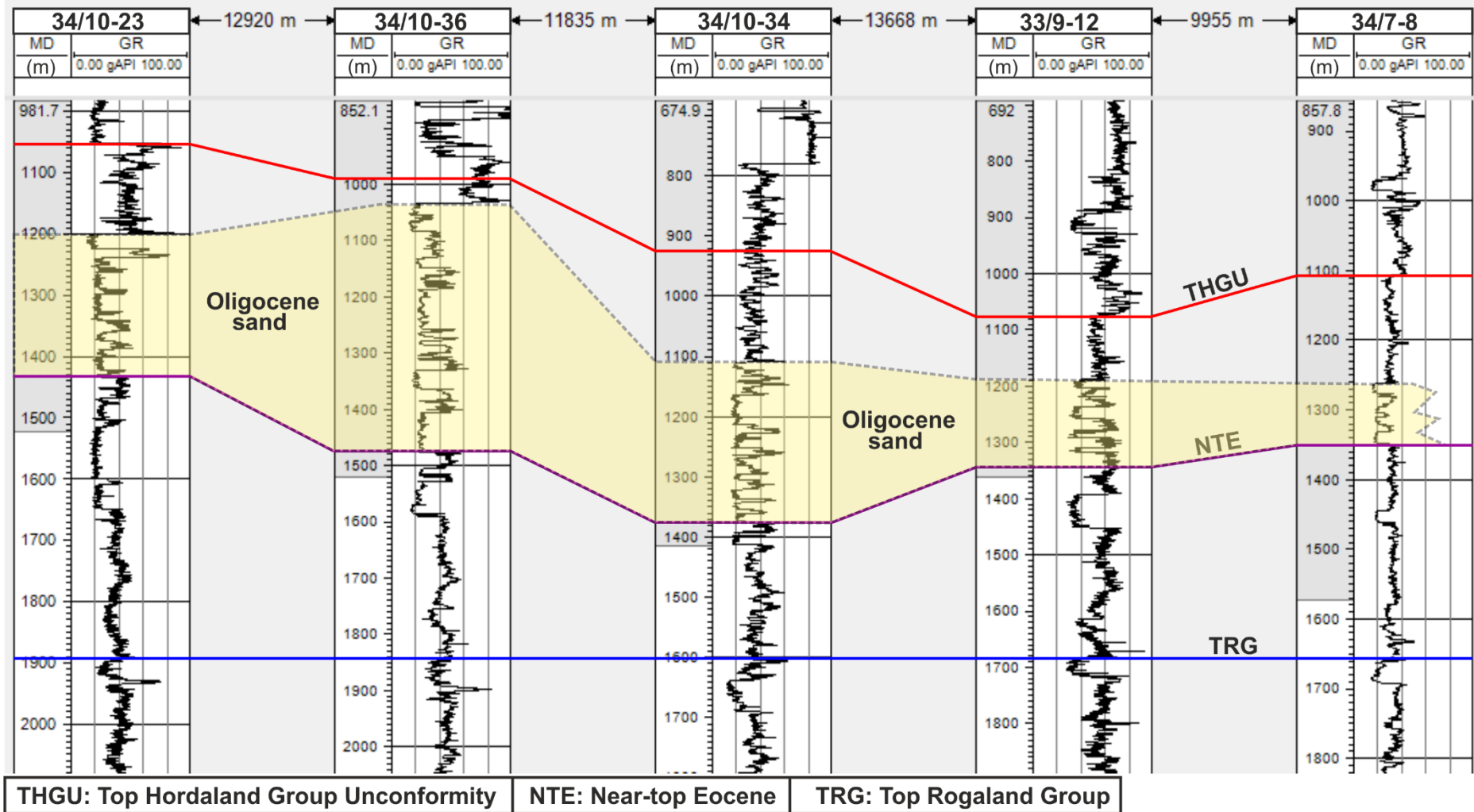
Fig. 6.8: Well correlation across the high amplitude reflections in the Gullfaks area flattened at the Top Balder. Gamma ray logs in wells 34/10-23, 3/10-36, 34/10-34, 33/9-12 and 34/7-8 show the presence of thick Oligocene sands in the wells. See location of wells in Figure 6.7. THGU = Top Hordaland Group Unconformity; NTE = Near-top Eocene; TRG = Top Rogaland Group. Well data from of TGS Facies Map Browser.
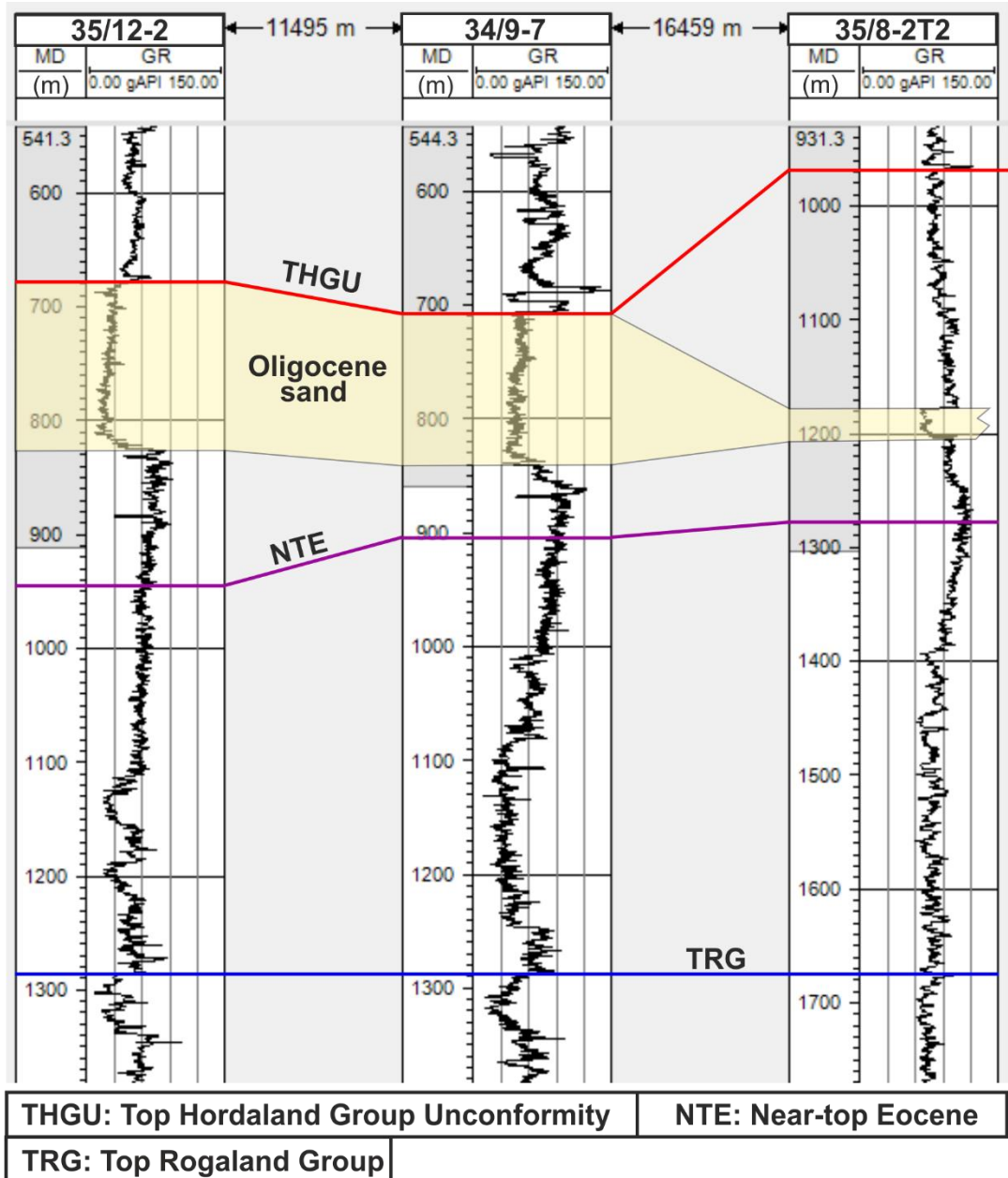
Fig. 6.9: Log correlation of the Oligocene interval in the Vega - Fram area in wells 34/12-2, 34/9-7 and 34/8-2T2 flattened at the Top Balder. See surface location of wells in Figure 6.7. THGU = Top Hordaland Group Unconformity; NTE = Near-top Eocene; TRG = Top Rogaland Group. Well data from TGS Facies Map Browser.
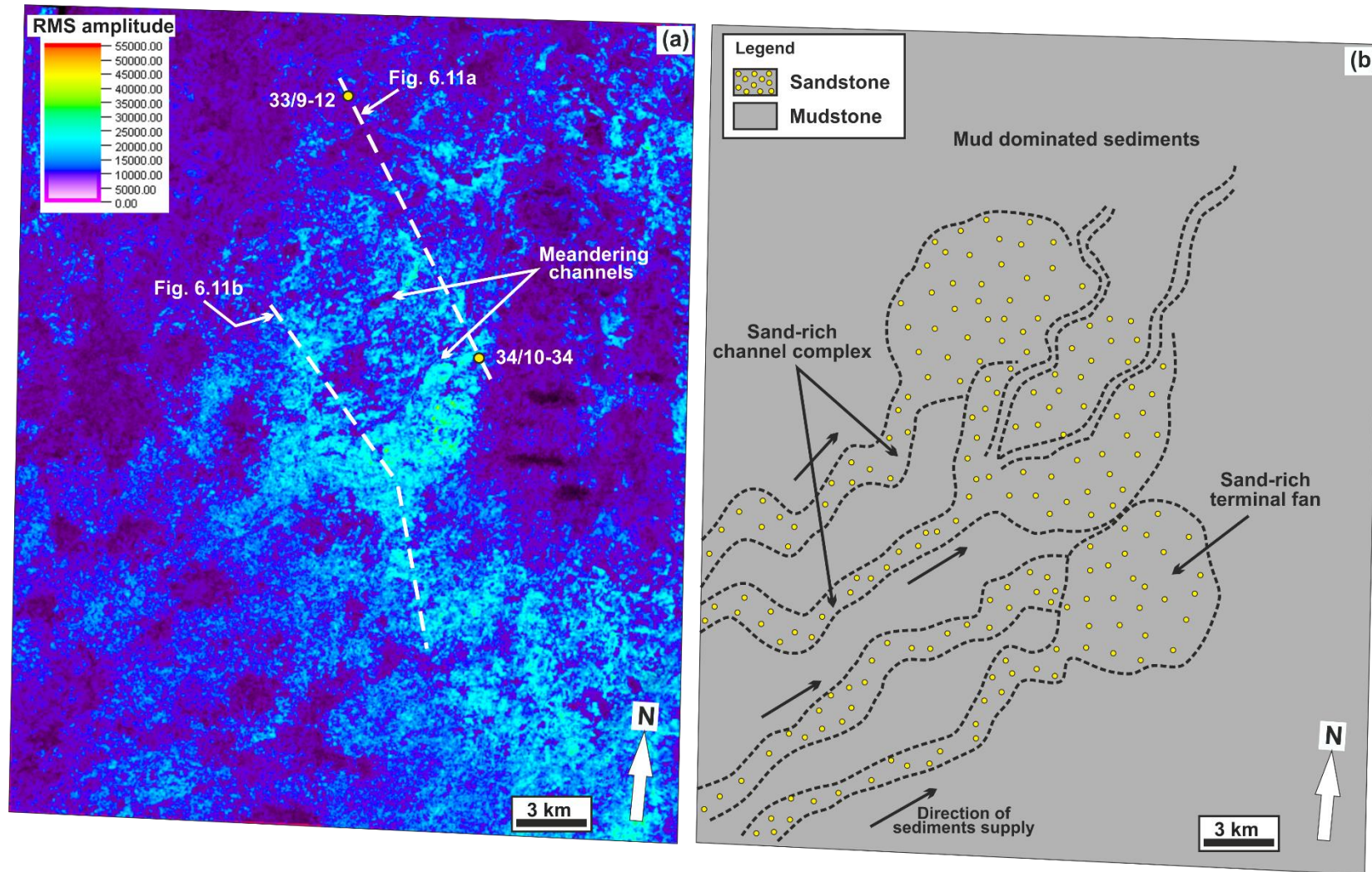
Fig. 6.10: (a) Close-up image of the RMS amplitude map in Figure 6.7 around the Gullfaks area showing the presence of deep-water sandy channel complexes within the Middle – Late Oligocene. (b) A simplified geologic interpretation of panel (a). See location of image in Figure 6.7. The location of cross sections shown in Figure 6.11 are also indicated. Seismic data courtesy of CGG.
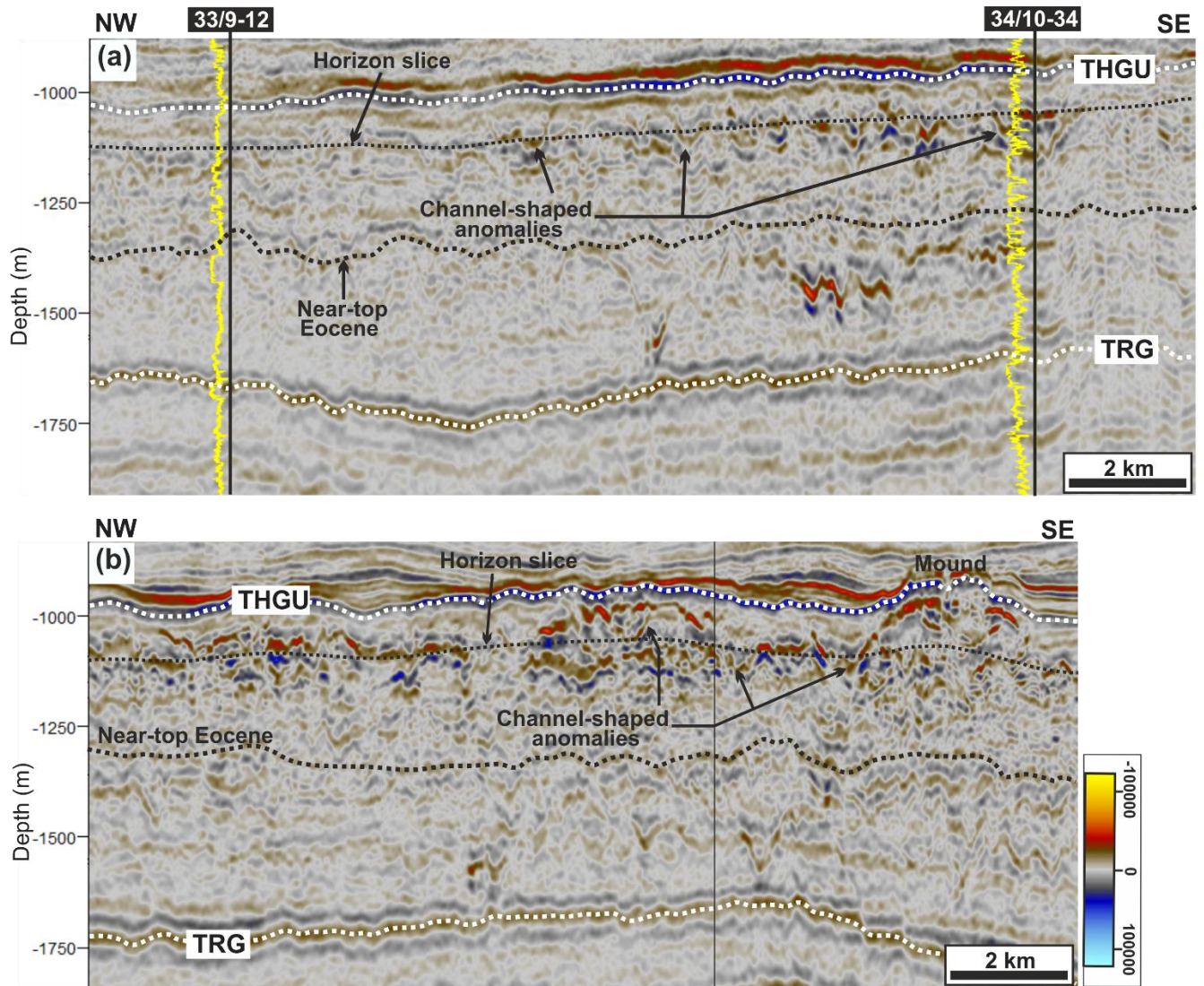
Fig. 6.11: (a) NW – SE seismic section through wells 33/9-12 and 34/10-34 showing Oligocene sands in the Gullfaks area interpreted as turbiditic channel-belt sands. The Oligocene sands in both wells are expressed as blocky low-value gamma-ray log signature (yellow curve) suggesting the sandstones are homogenous. (b) NW – SE seismic section showing remobilized Oligocene channels and sheet-like depositional sandstones expressed as high amplitude reflections on the RMS amplitude horizon slice below the THGU. Location of profile is shown in Figure 6.10. THGU = Top Hordaland Group Unconformity; TRG = Top Rogaland Group. Seismic data courtesy of CGG.

Fig. 6.12: (a) Close-up image of the RMS amplitude map in Figure 6.7 around the Vega, north of Vega and Fram area showing the presence of Middle – Late Oligocene deep-water slope channel-lobe complexes. (b) Schematic geological interpretation of panel (a). See location in Figure 6.7. The location of cross sections shown in Figures 6.13 & 6.14 are indicated. Seismic data courtesy of CGG.
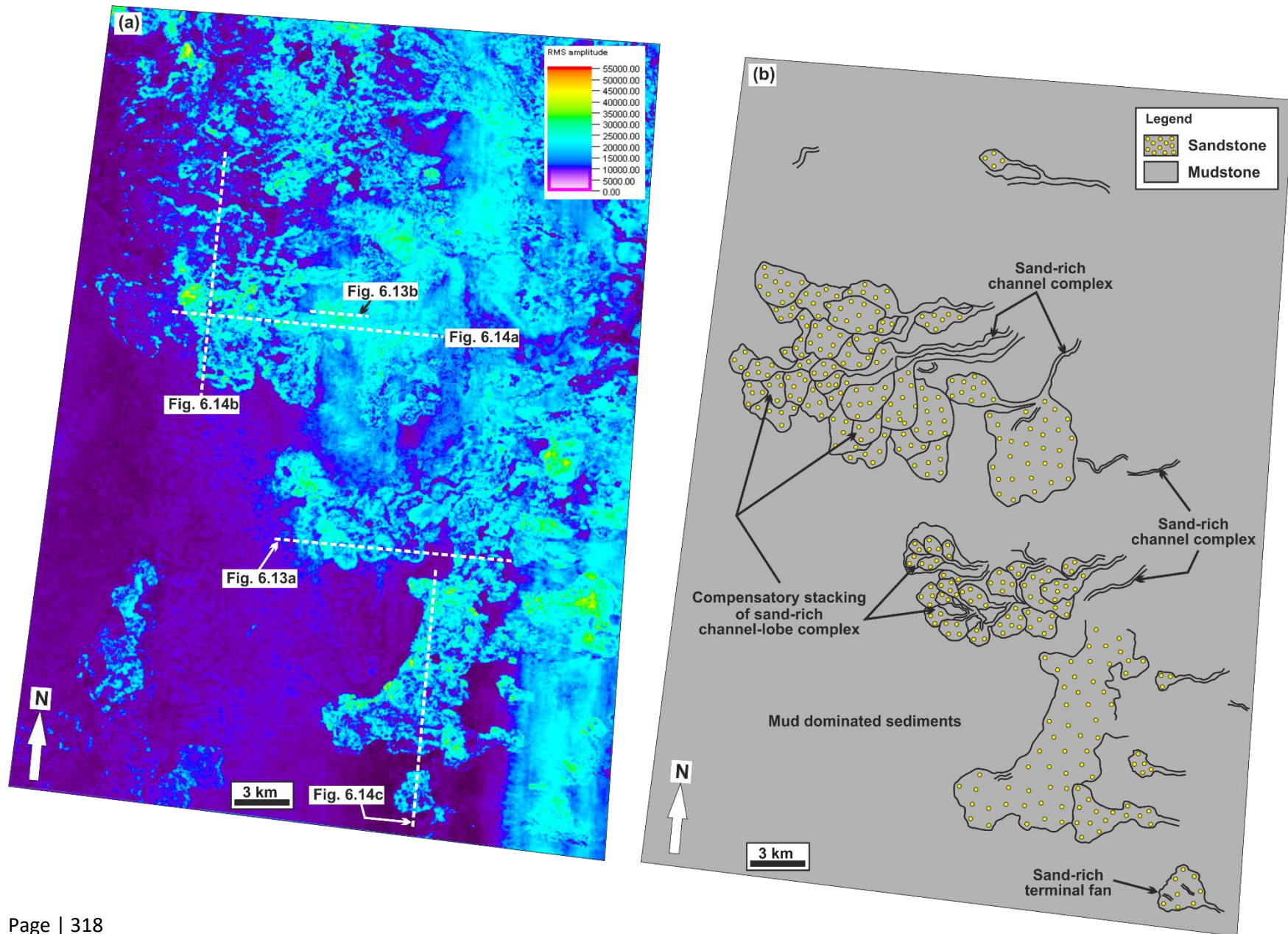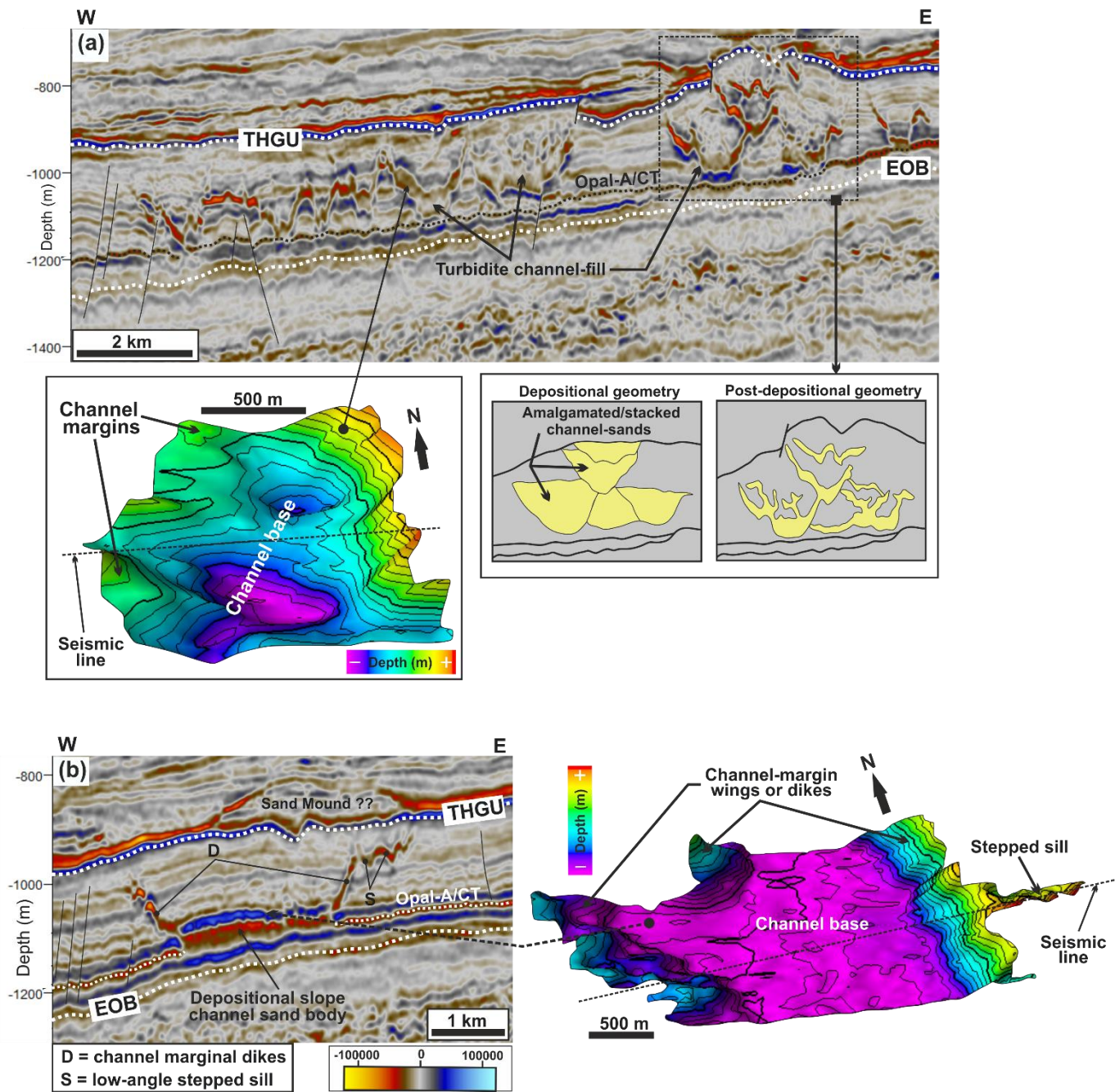
Fig. 6.13: (a) East – west seismic section across anomalies characterized by compensatory stacking of high amplitude reflections in the Vega area. The vertical stacking of channel-fill sands below the mound at the THGU should be noted. An interpretive illustration of the likely depositional geometry and post-depositional geometry (due to sand remobilization and injection) of the stacked channel-fill sand is also shown. (b) A wing-like Oligocene sand characterized by a concordant base and discordant marginal dikes which are up to 105 m high. The upper tip of one of the dikes consist of a low angle stepped sill. The sand is interpreted as in-situ depositional channel sand remobilized at its margin due to post-depositional remobilization and injection. The location of both seismic sections is shown in Figure 6.12a. THGU = Top Hordaland Group Unconformity; EOB = Eocene – Oligocene Boundary. Seismic data courtesy of CGG.
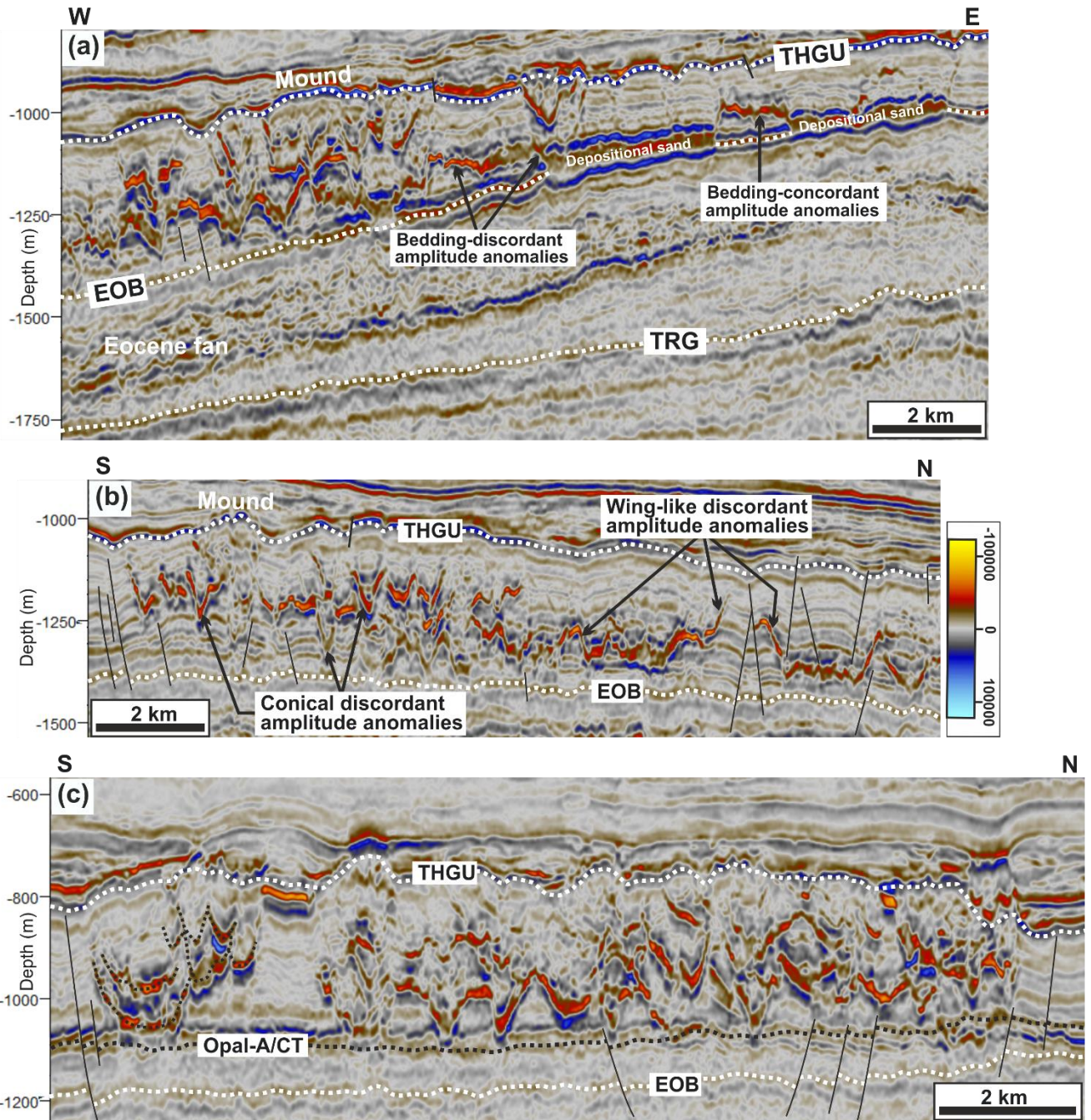
Fig. 6.14: (a) East – west seismic section through high amplitude reflections in Figure 6.12 located north of the Vega Field area. The section shows stacked and crosscutting high amplitude anomalies and wing-like anomalies which are interpreted as the expression of remobilized Oligocene channel sand complexes. (b) North-south seismic section showing stacked and connected Oligocene sand intrusions with a N – S transition from wing-like to conical (V/U) shaped high amplitude reflections. (c) North-south seismic section through high amplitude reflections in the Fram Field area showing vertical stacking of laterally connected and crosscutting high amplitude anomalies. The anomalies consist of a complex mixture of anomalies with varying geometries and are interpreted as either remobilized Oligocene channel sands or Oligocene slump deposits. The location of cross sections is shown in Figure 6.12a. THGU = Top Hordaland Group Unconformity; EOB = Eocene – Oligocene Boundary; TRG = Top Rogaland Group. Seismic data courtesy of CGG.
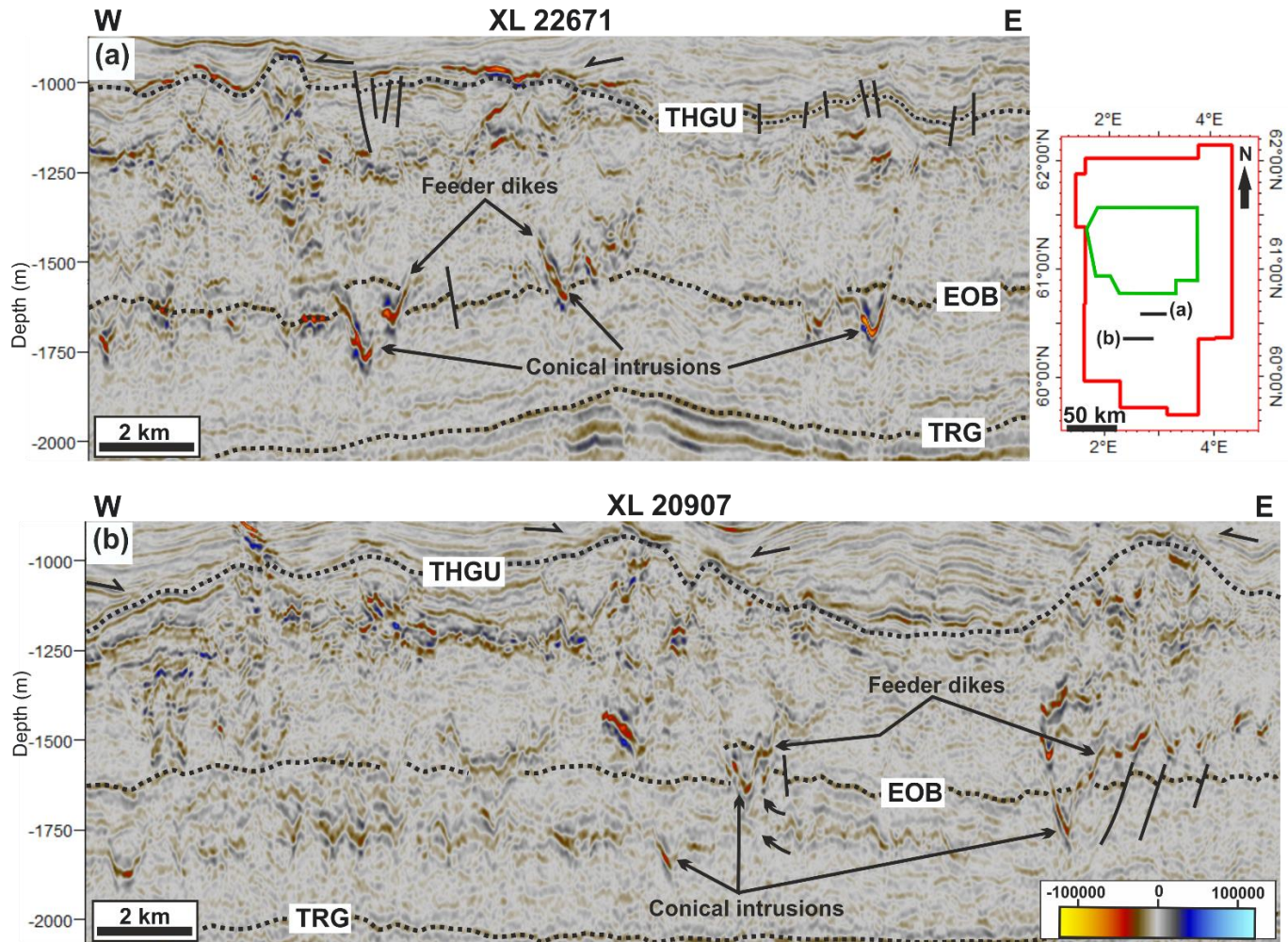
Fig. 6.15: (a) East – west seismic section south of the Huldra Field area showing conical-shaped sand intrusions with apexes connected to Middle – Upper Eocene sands. The limbs of the intrusion extend vertically upward across the Eocene-Oligocene boundary (EOB) into the Lower - Middle Oligocene interval. (b) East – west profile showing evidence for intrusive Oligocene sands sourced from Middle – Upper Eocene parent depositional sands. The conical intrusion with limbs extending across the EOB form a network of vertically connected intrusions in the Oligocene interval. Location of sections are shown in the insert map. THGU = Top Hordaland Group Unconformity; EOB = Eocene – Oligocene Boundary; TRG = Top Rogaland Group. Seismic data courtesy of CGG.
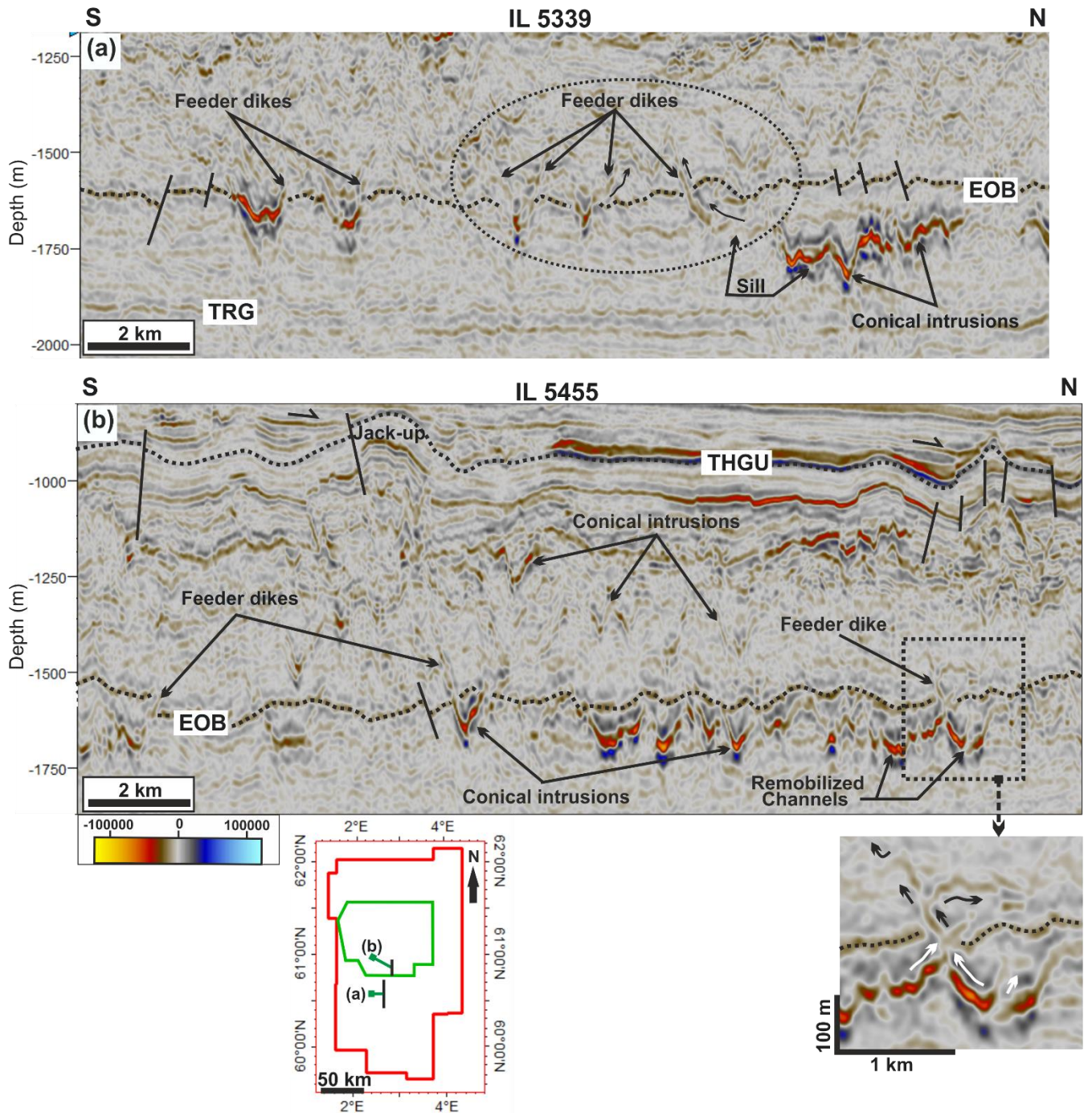
Fig. 6.16: (a) North – south seismic sections at the Huldra Field area showing several potential feeder dikes emanating from the Upper Eocene into the Oligocene interval. These have been interpreted to represent Upper Eocene sand dikes which partly sourced Lower – Middle Oligocene sand intrusions. (b) North – south seismic sections south of the Huldra Field area showing potential feeder dikes which sourced Lower Oligocene sand intrusions. The funnel-shaped feeder in the close-up image should be noted. Location of sections are shown in the insert map. THGU = Top Hordaland Group Unconformity; EOB = Eocene – Oligocene Boundary, TRG = Top Rogaland Group. Seismic data courtesy of CGG.

6.4.4 The mounded nature of the Top Hordaland Group Unconformity (THGU)

Jack-up of overburden and doming (i.e., usually associated with onlaps or draping) have been documented as the two main characteristic features observed in seismic data in relation to overburden deformation due to sand remobilization and injection into their host mudstones (e.g., Cosgrove & Hillier, 2000; Szarawarska et al., 2010; Jackson et al., 2011; Huuse et al., 2012; Andresen & Clausen, 2014; Andresen et al., 2019). The observation of jack-up (or forced folding) above sand intrusions clearly indicate injection of fluidized excess materials while doming (or mounding) may be related to either sand injection or differential compaction above depositional sand bodies (e.g., Jackson et al., 2011; Andresen et al., 2019). Differential compaction-related mounding is often recognized to be associated with a uniform convex upward doming of the overburden above sand bodies and are sometimes gentle with associated draping (Andresen et al., 2019). On the contrary, jack-up related forced folds are often characterized by an abrupt non-uniform upward folding of the overburden usually associated with conical intrusions.

With the above in mind, the mounds at the Top Hordaland Group Unconformity (THGU) above Oligocene sands in the study area have been argued by Løseth et al. (2013) to have originated from a giant intrusive event which occurred in the Early Pleistocene (Gelasian stage). However, Rundberg & Eidivin (2016) have argued that they originated from differential compaction across Oligocene turbiditic channel-belt sands. The map of the THGU indicate that the mounded relief in the Gullfaks area and south of Gullfaks exhibit elongate geometry and clear sinuosity which is consistent with the meandering channel systems identified beneath the mounds in that area (Fig. 6.4 & 6.7), thus suggesting that the pattern of the mounds mimic their underlying turbiditic channel-belt systems. This therefore supports an interpretation that the mounds originated from differential compaction across the sands due to loading and burial. The above interpretation is also supported by the channelized geometry of some of the mapped wing-like Oligocene sands (see Fig. 6.11 & 6.13) and the observation that the mounds are often onlapped or draped by younger sediments. However, the mounds are in some cases (e.g., Vega and south of Huldra Field area) observed to be abrupt which may be an indication for elevation of the overburden by forced folding (jack-up) due to intrusion rather than differential compaction. This is often observed above conical-shaped sands (Fig. 6.6a, 6.14a & 6.15a) and in some cases where Oligocene sands are characterized by stacked or amalgamated high amplitude reflections (Fig. 6.6a & 6.14a, c). Furthermore, there are cases where very subtle or no mounding is observed above Oligocene depositional sands (Fig. 6.13a). This may well be linked to tunning effects between thin sands intervals (Andresen et al., 2019).

The elevated overburden below the THGU comprises of Late Oligocene sediments and Lower Miocene mudstone strata, while the sediments directly above the unconformity are documented to consist of Late Miocene sand deposits of the Utsira Formation (Eidvin & Rundberg, 2001; Rundberg & Eidivin, 2005). Some short normal faults of up to 10 m in fault

length are formed alongside the mounds on the THGU (e.g., Fig. 6.14a & 6.15a). Similar faults have been documented by Gay et al. (2006) and Xu et al. (2015) and we interpret them to represent differential compaction faults (DCFs) which develop along lithologic interface which separates thick sands from their underlying or overlying mudstones, just like the THGU. The presence of these DCFs may also support the interpretation that the mounds originated from differential compaction. However, some short reverse faults of similar fault length are observed at the edge of some mounds on the THGU overlying conical-shaped intrusions (Fig. 6.6a) which may have formed due to an upward rotational movement in response to forced folding due to upward sand injection into their sealing host mudstones. Since the position of the reverse faults and the edges of the mounds spatially coincide with the position of the upper tip of the discordant limbs of the conical intrusions, this may imply that such mounds may be related to sand injection rather than differential compaction.

From our analysis and observations, the mounds at the THGU cannot be completely interpreted to originate from either load induced differential compaction or forced folding due to sand remobilization and injection. Therefore, it is very likely that a combination of both processes resulted to the mounded topography of the THGU with major contribution likely to come from differential compaction.

6.6.5 Formation of Oligocene sand injectites

A three-stage schematic model for the formation of sand injectites in the study is shown in Fig. 6.17. Stage 1 (Fig. 6.17) illustrates the deposition of Oligocene in-situ depositional sands into the northern North Sea, sourced from both western (East Shetland Platform) and eastern (West Norway) source areas. This was followed by subsequent deposition of fine-grained mudstone and differential compaction due to burial in Stage 2. This led to the development of overpressure within the buried depositional sands. Post depositional processes with increased burial triggered sand remobilization and injection in Stage 3, accompanied by further deposition and burial (Fig. 6.17). Refer to text in section 4.5.5 for further detail on the processes leading to the formation of Oligocene sand injectite in the study area.

6.5 Conclusion

The model for the origin of Oligocene sandstones in the area above the Snorre, Gullfaks and Visund fields previously presented by Løseth et al. (2013) is inconsistent with our findings. Our analysis and observation disagree with Løseth et al.'s model because the Oligocene sands which they interpreted as intrusive sands sourced from Paleocene parent source sands clearly show they are largely (c. 80%) remobilized in-situ depositional sands representing submarine turbiditic gravity flow sands shed from the Shetland Platform (to

the west) and West Norway (to the east) in the Middle – Late Oligocene time. However, evidence for possible contribution from parent source sands in the Middle – Late Eocene is also observed in the form of feeder dikes across the Eocene – Oligocene boundary into the Lower Oligocene, suggesting sands of mixed origin. In addition, the mounded topography of the THGU is best described to originate from a combination of differential compaction across depositional sand bodies and forced folding (jack-up) due to sand remobilization and intrusion, rather than just the intrusive origin suggested by Løseth et al. (2013).

Finally, it is important to note that the interpretation presented by Løseth et al. (2013) may have been limited by the extent and quality of the 3D seismic data available at the time of their study. For example, data quality may have led to their inability to image the meandering channels in the Gullfaks area which clearly points to a depositional origin for the Oligocene sands, with the mounds at the THGU originating from differential compaction across the channel sands. The use of the most recent high resolution seismic data in the northern North Sea have thus provided more detail and clarity.

Acknowledgements
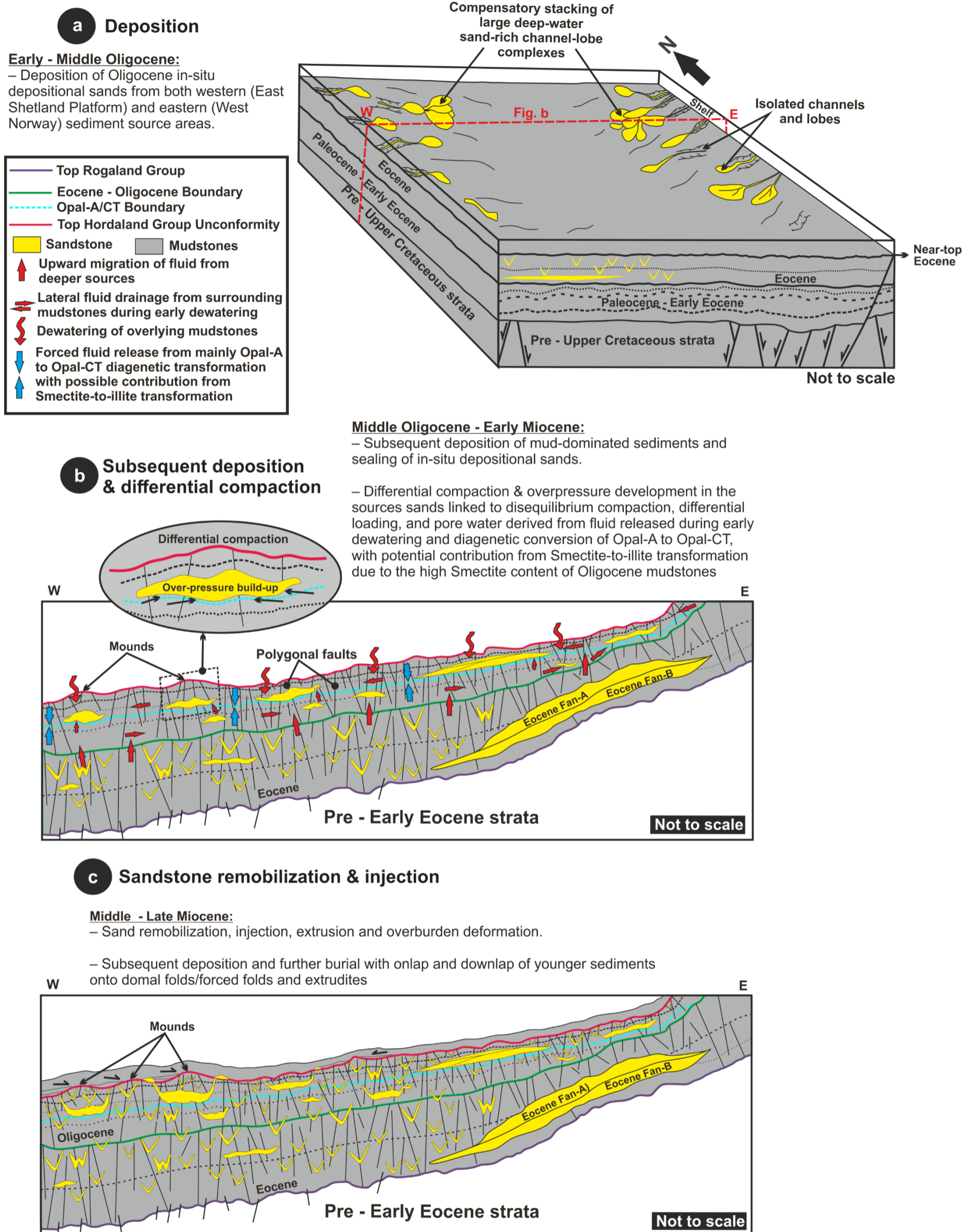
Fig. 6.17: Three-stage schematic model for the formation of Oligocene sand injectites in the study area. Stage 1: deposition of Oligocene in-situ depositional sands. Stage 2: subsequent burial and sealing of sands due to further deposition of mud-dominated sediments, differential compaction, and initiation of overpressure build-up within the depositional sands. Stage C: post-depositional remobilization and formation of the sand injectites coupled with overburden deformation and further burial.

References

AHMADI, Z.M., SAWYERS, M., KENYAN-ROBERTS, S., STANWORHT, C.W., KUGLER, K.A., KRISTENSEN, J. & FUGELLI, E.M.G. 2003. Palaeocene. In: *The Millennium Atlas: Petroleum geology of the central and northern North Sea* (Ed. by D. Evans, C. Graham, A. Armour & P. Bathurst). *The Geological Society of London, London,* 235–259.

ANDRESEN, K.J. 2012. Fluid flow features in hydrocarbon plumbing systems: What do they tell us about the basin evolution? *Marine Geology*, **332**–**334**, 89–108, https://doi.org/10.1016/j.margeo.2012.07.006.

ANDRESEN, K.J. & CLAUSEN, O.R. 2014. An integrated subsurface analysis of clastic remobilization and injection; a case study from the Oligocene succession of the eastern North Sea. *Basin Research*, 26, 641–674, https://doi.org/10.1111/bre.12060.

ANDRESEN, K.J., HEILMANN-CLAUSEN, C., CLAUSEN, O.R. & FRIIS, H. 2019. Deposition or remobilization of the enigmatic Hefring Member sand, eastern North Sea – A multidisciplinary approach. *Marine and Petroleum Geology*, https://doi.org/10.1016/j.marpetgeo.2019.06.001.

ANDRESEN, K.J. 2020. The Norwegian–Danish Basin: a dynamic setting for subsurface sand remobilization – established concepts on distribution and controlling factors. *Geological Society, London, Special Publications*, https://doi.org/10.1144/sp493-2018-026.

COBAIN, S.L., HODGSON, D.M., PEAKALL, J. & SILCOCK, S.Y. 2019. Relationship between bowl-shaped clastic injectites and parent sand depletion: implications for their scale-invariant morphology and composition. *Geological Society, London, Special Publications*, https://doi.org/10.1144/sp493-2018-80.

COSGROVE, J.W. & HILLIER, R.D. 2000. Forced-fold development within Tertiary sediments of the Alba Field, UKCS: evidence of differential compaction and post-depositional sandstone remobilization. *Geological Society, London, Special Publications*, 169, 61–71, https://doi.org/10.1144/gsl.sp.2000.169.01.05.

EIDVIN, T., AND RUNDBERG, Y. 2001. Late Cainozoic stratigraphy of the Tampen area (Snorre and Visund fields) in the northern North Sea, with emphasis on the chronology of early Neogene sands. Nor. J. Geol. 81, 119–160. Available online at: http://njg.geologi.no/vol-81-90/details/17/458-458

DMITRIEVA, E., JACKSON, C.A.-L., HUUSE, M. & MCCARTHY, A. 2012. Paleocene deep-water depositional systems in the North Sea Basin: a 3D seismic and well data case study, offshore Norway. *Petroleum Geoscience*, 18, 97–114, https://doi.org/10.1144/1354-079311-027.

DMITRIEVA, E., JACKSON, C.A.-L., HUUSE, M. & KANE, I.A. 2018. Regional distribution and controls on the development of post-rift turbidite systems: insights from the Paleocene of the eastern North Viking Graben, offshore Norway. *Geological Society, London, Petroleum Geology Conference series*, 8, PGC8.31, https://doi.org/10.1144/PGC8.31.

DURANTI, D. & HURST, A. 2004. Fluidization and injection in the deep-water sandstones of the Eocene Alba Formation (UK North Sea). *Sedimentology*, 51, 503–529, https://doi.org/10.1111/j.1365-3091.2004.00634.x.

EIDVIN, T., RIIS, F., RASMUSSEN, E.S., RUNDBERG, Y. & MAYEN, J. 2013. Investigation of Oligocene to Lower Pliocene deposits in the Nordic offshore area and onshore Denmark. *NPD Bulletin 10*, 62.

EIDVIN, T., RIIS, F. & RASMUSSEN, E.S. 2014. Oligocene to Lower Pliocene deposits of the Norwegian continental shelf, Norwegian Sea, Svalbard, Denmark and their relation to the uplift of Fennoscandia: A synthesis. *Marine and Petroleum Geology*, 56, 184–221, https://doi.org/10.1016/j.marpetgeo.2014.04.006.

FAERSETH, R.B., GABRIELSEN, R.H. & HURICH, C.A. 1995. Influence of basement in structuring of the North Sea Basin, offshore southwest Norway. *Norsk Geologisk Tidsskrift*, 75, 105–119.

FALEIDE, J.I., KYRKJEBØ, R., KJENNERUD, T., GABRIELSEN, R.H., JORDT, H., FANAVOLL, S. & BJERKE, M.D. 2002. Tectonic impact on sedimentary processes during Cenozoic evolution of the northern North Sea and surrounding areas. *Geological Society, London, Special Publications*, 196, 235–269, https://doi.org/10.1144/GSL.SP.2002.196.01.14.

FYFE, J.A., GREGERSEN, U., JORDT, H., RUNDBERG, Y., EIDVIN, T., EVANS, D., STEWART, D., HOVLAND, M. & ANDERSEN, P. 2003. Oligocene to Holocene. In: *The Millenium Atlas: Petroleum Geology of the Central and Northern North Sea* (Ed. by D. Evans, C. Graham, A. Armour & P. Bathurst. *Geological Society London, London, 279-287*

GABRIELSEN, R.H., KYRKJEBO, R., FALEIDE, J.I., FJELDSKAAR, W. & KJENNERUD, T. 2001. The Cretaceous post-rift basin configuration of the northern North Sea. *Petroleum Geoscience*, 7, 137–154, https://doi.org/10.1144/petgeo.7.2.137.

GAY, A., LOPEZ, M., COCHONAT, P., SÉRANNE, M., LEVACHÉ, D. & SERMONDADAZ, G. 2006. Isolated seafloor pockmarks linked to BSRs, fluid chimneys, polygonal faults and stacked Oligocene-Miocene turbiditic palaeochannels in the Lower Congo Basin. *Marine Geology*, **226**, 25–40, https://doi.org/10.1016/j.margeo.2005.09.018.

GRADSTEIN, F. & BÄCKSTRÖM, S. 1996. Cainozoic biostratigraphy and palaeobathymetry, northern North Sea and Haltenbanken. *Norsk Geologisk Tidsskrift*, **76**, 3–32.

HERMANRUD, C., CHRISTENSEN, E., HAUGVALDSTAD, M., RØYNESTAD, L.M., TJENSVOLD, I.T. & WATSEND, L. 2019. Triggers of sand remobilization in deep marine deposits. *Geological Society, London, Special Publications*, https://doi.org/10.1144/sp493-2018-35.

HURST, A., CARTWRIGHT, J. & DURANTI, D. 2003. Fluidization structures produced by upward injection of sand through a sealing litholoy. *Geological Society, London, Special Publications*, 216, 123–138, https://doi.org/10.1144/GSL.SP.2003.216.01.09.

HURST, A. & CARTWRIGHT, J. 2007. Relevance of Sand Injectites to Hydrocarbon Exploration and Production. *In*: *Sand Injectites: Implications for Hydrocarbon Exploration and Production: AAPG Memoir 87*. 1–19., https://doi.org/10.1306/1209846M871546.

HURST, A., SCOTT, A. & VIGORITO, M. 2011. Physical characteristics of sand injectites. *Earth-Science Reviews*, 106, 215–246, https://doi.org/10.1016/j.earscirev.2011.02.004.

HUUSE, M., DURANTI, D., GUARGENA, C. G., PRAT, P., HOLM, K., STEINSLAND, N., CRONIN, B. T., HURST, A., & CARTWRIGHT, J. 2003. Sandstone intrusions: Detection and significance for exploration and production. *First Break*, *21*(9), 33–42. https://doi.org/10.3997/1365-2397.2003014

HUUSE, M., JACKSON, C.A.L., OLOBAYO, O., DMITRIEVA, E. & ANDRESEN, K.J. 2012. A sand injectite stratigraphy for the North Sea. *In*: *74th European Association of Geoscientists and Engineers Conference and Exhibition 2012 Incorporating SPE EUROPEC 2012: Responsibly Securing Natural Resources*, https://doi.org/10.3997/2214-4609.20148702.

HUUSE, M., CARTWRIGHT, J., HURST, A. & STEINSLAND, N. 2007. Seismic Characterization of Large-scale Sandstone Intrusions. *Sand injectites: Implications for hydrocarbon exploration and production: AAPG Memoir 87*, 21–35, https://doi.org/10.1306/1209847M873253.

HUUSE, M., DURANTI, D., STEINSLAND, N., GUARGENA, C.G., PRAT, P., HOLM, K., CARTWRIGHT, J.A., HURST, A. 2004. Seismic Characteristics of Large-Scale Sandstone Intrusions in the Paleogene of the South Viking Graben, UK and Norwegian North Sea. *Geological Society, London, Memoirs*, 29, 263–278, https://doi.org/10.1144/GSL.MEM.2004.029.01.25.

HUUSE, M. & MICKELSON, M. 2004. Eocene sandstone intrusions in the Tampen Spur area (Norwegian North Sea Quad 34) imaged by 3D seismic data. *Marine and Petroleum Geology*, 21, 141–155, https://doi.org/10.1016/j.marpetgeo.2003.11.018.

JACKSON, C.A.L., HUUSE, M. & BARBER, G.P. 2011. Geometry of wing-like clastic intrusions adjacent to a deep-water channel complex: Implications for hydrocarbon exploration and production. *AAPG Bulletin*, 95, 559–584, https://doi.org/10.1306/09131009157.

JOLLY, R.J.H. & LONERGAN, L. 2002. Mechanisms and controls on the formation of sand intrusions. *Journal of the Geological Society*, 159, 605–617, https://doi.org/10.1144/0016-764902-025.

JORDT, H., THYBERG, B.I. & NØTTVEDT, A. 2000. Cenozoic evolution of the central and northern North Sea with focus on differential vertical movements of the basin floor and surrounding clastic source areas. *Geological Society, London, Special Publications*, 167, 219–243, https://doi.org/10.1144/GSL.SP.2000.167.01.09.

LONERGAN, L. & CARTWRIGHT, J.A. 1999. Polygonal faults and their influence on deep-water sandstone reservoir geometries, Alba field, United Kingdom central North Sea. *AAPG Bulletin (American Association of Petroleum Geologists)*, 83, 410–432, https://doi.org/10.1306/00AA9BBA-1730-11D7-8645000102C1865D.

LONERGAN, L., LEE, N., JOHNSON, H.D., CARTWRIGHT, J. A & JOLLY, R.J.H. 2000. Remobilization and Injection in Deepwater Depositional Systems: Implications for Reservoir Architecture and Prediction. *Deep-Water Reservoirs of the World: 20th Annual GCSSEPM Foundation Bob F. Perkins Research Conference*, 15, 515–532, https://doi.org/10.5724/gcs.00.15.0515.

LØSETH, H., RAULLINE, B. & NYGARD, A. 2013. Late Cenozoic geological evolution of the northern North Sea: development of a Miocene unconformity reshaped by large-scale Pleistocene sand intrusion. *Journal of the Geological Society*, 170, 133–145, https://doi.org/10.1144/jgs2011-165.

LØSETH, H., ØYGARDEN, B., NYGÅRD, A. & RAULLINE, B. 2016. Reply to Discussion on 'Late Cenozoic geological evolution of the northern North Sea: development of a Miocene unconformity reshaped by large-scale Pleistocene sand intrusion', Journal of the Geological Society, 170, 133–145. *Journal of the Geological Society*, **173**, 394–397, https://doi.org/10.1144/jgs2015-104.

LØSETH, H., DOWDESWELL, J.A., BATCHELOR, C.L. & OTTESEN, D. 2020. 3D sedimentary architecture showing the inception of an Ice Age. *Nature Communications*, **11**, https://doi.org/10.1038/s41467-020-16776-7.

MARTINSEN, O.J., BØEN, F., CHARNOCK, M.A., MANGERUD, G. & NØTTVEDT, A. 1999. Cenozoic development of the Norwegian margin 60–64°N: sequences and sedimentary response to variable basin physiography and tectonic setting. *In*: Petroleum Geology of Northwest Europe: Proceedings of the 5th Conference. 293–304., https://doi.org/10.1144/0050293.

MOLYNEUX, S., CARTWRIGHT, J. & LONERGAN, L. 2002. Conical sandstone injection structures imaged by 3D seismic in the central North Sea, UK. *First Break*, 20, 383–393, https://doi.org/10.1046/j.1365-2397.2002.00258.x.

RUNDBERG, Y. & EIDVIN, T. 2005. Controls on depositional history and architecture of the Oligocene-Miocene succession, northern North Sea Basin. *Norwegian Petroleum Society Special Publications*, 12, 207–239, https://doi.org/10.1016/S0928-8937 (05)80050-5.

RUNDBERG, Y. & EIDVIN, T. 2016. Discussion on 'Late Cenozoic geological evolution of the northern North Sea: development of a Miocene unconformity reshaped by large-scale Pleistocene sand intrusion', Journal of the Geological Society, 170, 133–145. *Journal of the Geological Society, London*, 173, 384–393.

SHOULDERS, S.J., CARTWRIGHT, J. & HUUSE, M. 2007. Large-scale conical sandstone intrusions and polygonal fault systems in Tranche 6, Faroe-Shetland Basin. *Marine and Petroleum Geology*, 24, 173–188, https://doi.org/10.1016/j.marpetgeo.2006.12.001.

SZARAWARSKA, E., HUUSE, M., HURST, A., DE BOER, W., LU, L., MOLYNEUX, S. & RAWLINSON, P. 2010. Three-dimensional seismic characterisation of large-scale sandstone intrusions in the lower Palaeogene of the North Sea: completely injected vs. in situ remobilised sand-bodies. *Basin Research*, 22, 517–532, https://doi.org/10.1111/j.1365-2117.2010.00469.x.

UNDERHILL, J.R. 2001. Controls on the genesis and prospectivity of paleogene palaeogeomorphic traps, East Shetland Platform, UK North Sea. *Marine and Petroleum Geology*, **18**, 259–281, https://doi.org/10.1016/S0264-8172(00)00067-2.

XU, S., HAO, F., XU, C., WANG, Y., ZOU, H. & GONG, C. 2015. Differential compaction faults and their implications for fluid expulsion in the northern Bozhong Subbasin, Bohai Bay Basin, China. *Marine and Petroleum Geology*, **63**, 1–16, https://doi.org/10.1016/j.marpetgeo.2015.02.013.

Chapter 7

CHAPTER 7   Quantitative analysis and characterization of the interaction between sandstone intrusions and polygonal fault systems in the Eocene – mid Miocene (Hordaland Group) succession of the northern North Sea Basin

Quantitative analysis and characterization of the interaction between sandstone intrusions and polygonal fault systems in the Eocene – mid Miocene (Hordaland Group) succession of the northern North Sea Basin

Nnorom, S. and Huuse, M.

Basins Research Group, Department of Earth and Environmental Sciences, University of Manchester, Oxford Road, Manchester M13 9PL, UK

 *Correspondence (sebastian.nnorom@manchester.ac.uk)

Keywords: Sandstone intrusions, Polygonal faults, Northern North Sea Basin, Hydraulic fracturing, Diagenesis, Overpressure.

Abstract

Most documented occurrences of large-scale sandstone intrusion complexes have been recorded within polygonally faulted mudstone successions. In this study, detailed 3D seismic analysis of data from the northern North Sea Basin was used to examine how the kilometre-scale sandstone intrusions injected into the Hordaland Group (Eocene – Mid Miocene) interval interact with the pervasive polygonal fault network present within their host low-permeable mudstone succession. This analysis is aimed at understanding if the propagation of polygonal faults and their interaction with sandstone intrusion may have controlled the resultant simple to complex geometries of some of the intrusions. The intrusions were injected into the Eocene – Mid Miocene host mudstone, with pre-existing polygonal faults, during the Late Eocene – Mid Miocene and are characterized by varying simple to complex cross-sectional geometries, with the injected sands sourced from depositional parent sand bodies within the Eocene and Oligocene. Four types of interactions between the sand intrusions and polygonal fault systems were recognized: (A) intrusions with limbs partially or fully intruded along polygonal fault planes, (B) intrusion halted or arrested by polygonal faults, (C) intrusions which are crosscut by polygonal faults but are geometrically unaffected, (D) intrusions which are geometrically affected by polygonal faults. Comparison of measured geometrical parameters for Class-A and Class-C intrusions indicate that Class-A intrusions exhibit higher dip values owing to their injection along steely dipping faults. In general, there seem to be an absence of a clear correlation between the sandstone intrusions and their neighbouring polygonal faults due to the different types of interaction observed and no substantial overlap between the measured geometrical parameters (e.g., dip) of both features. This leads to the suggestion that sand intrusions achieve their distinct simple to complex geometries regardless of their co-existence with polygonal faults, and the faults may have been exploited only where necessary and may have also contributed to seal failure which is a critical requirement for sand remobilization and injection to occur. This implies that the propagation of sand intrusions does not depend on the propagation of polygonal faults, and as such polygonal faults are unlikely to directly trigger sand injection. The widespread occurrence of large-scale sand intrusions and polygonal faults in the studied interval has important implications for reservoir geology and fluid flow in the basin because they can both result to the modification of original reservoir geometries (e.g., compartmentalization) and can act as long-lived fluid conduit for fluid migration into shallower intervals. Although their host strata consist of low permeable mudstones, they are both likely to act as high permeability fluid conduits which in turn impacts the seal integrity of their host mudstones.

7.1 Introduction

Sandstone intrusions have been recognized as an important component of most deep-water sand-rich systems in sedimentary basins globally, and they have been studied for over two decades owing to the understanding that they have important implications for hydrocarbon exploration and production (e.g., Lonergan & Cartwright, 1999; Lonergan et al., 2000; Jolly & Lonergan, 2002). These intrusions have been documented to occur on a variety of scale ranging from kilometre scale (i.e., seismic) to few centimetres scale (i.e., core and outcrop) (Huuse & Mickelson, 2004; Huuse et al., 2007; Hurst et al., 2011). Advances in 3D seismic imaging and its integration with other data (e.g., well, core & outcrop data) have led to an extensive study of sandstone intrusions. On 3D seismic data, they have been documented to occur as strata discordant (i.e., dykes) and concordant (i.e., sills) high amplitude reflections which exhibit simple to complex geometries ranging from conical-shaped, wing-like to irregular and complex-shaped anomalies (e.g., Molyneux et al., 2002; Shoulders & Cartwright, 2004; Jackson et al., 2011) hosted in low-permeable mud-dominated successions. Their formation is linked to the development of excess pore fluid pressure within their parent source sand bodies resulting from processes such as disequilibrium compaction, rapid sediment loading, lateral transfer of pressure, fluid influx or migration from deeper sources and diagenesis (Jolly & Lonergan, 2002; Davies et al., 2006; Wild & Briedis, 2010; Andresen et al., 2019; Hermanrud et al., 2019; Andresen, 2020). In addition to the above processes, a trigger mechanism which leads to hydro-fracturing and seal breach which results to the actual remobilization and injection of the overpressured sands is required. Several trigger mechanisms have been proposed by authors such as, seismic induced liquefaction due to earthquake activity (e.g., Obermeier, 1998; Galli, 2000; Jolly & Lonergan, 2000; Briedis et al., 2007), propagation of polygonal faults (e.g., Lonergan & Cartwright, 1999; Gras & Cartwright, 2002; Molyneux et al., 2002; Jackson, 2007), slab sliding (e.g., Hermanrud et al., 2019) and differential compaction (Jackson, 2007; Jackson et al., 2011; Safronova et al., 2012). Sandstone intrusions have been documented widely in the Paleogene of the North Sea Basin where they are found to be associated with deep-water hydrocarbon reservoirs and have been reported to have excellent reservoir properties with porosities of up to 35% and permeability in the Darcy scale (Duranti et al., 2002; Duranti & Hurst, 2004; Briedis et al., 2007; Hurst et al., 2011). Over the years, studies of sand intrusion have shown that their propagation through low permeable mudstone strata has important implications for reservoir geology, vertical connectivity, and fluid flow in sedimentary basins where they occur (Hurst et al., 2003; Huuse & Mickelson, 2004; Huuse et al., 2005; Shoulders et al., 2007).

Polygonal faults on the other hand, have been documented in several basins worldwide (e.g. Eromanga Basin, Australia; North Sea Basin; Denver Basin, Colorado; Baffin Bay, offshore west Greenland; Voring Basin, offshore Norway; Nanki Trough, offshore Japan; Great South Basin, New Zealand; and Table 7.1) and consists of layer-bound, intra-formational, low-displacement, normal faults formed in fine grained mud-dominated sedimentary

successions which have polygonal plan-view geometries (Lonergan & Cartwright, 1999; Cartwright, 2011; Wrona et al., 2017a). They often occur in tiers (see Cartwright, 2011: Fig.1) with majority of the known cases occurring in slope depositional settings along passive continental margins, within fine grained, hemi-pelagic, smectite-rich sediments (Cartwright & Dewhurst, 1998; Cartwright, 2011). They are usually distributed over large area of up to 200,000 km² (Cartwright & Dewhurst, 1998). Polygonal faults are documented to be widespread within the Early Cretaceous to Miocene interval in the central and northern North Sea (Table 7.1; Cartwright & Lonergan, 1996; Lonergan et al., 1998; Dewhurst et al., 1999; Lonergan & Cartwright, 1999). Their formation is generally linked to compaction-related early-stage dewatering of fine-grained sediments, with several driving mechanisms proposed by different authors. Some of such mechanisms include: (i) syneresis of fine grained sediments which involves the compaction of sediments by spontaneous volumetric contraction due to gravitational loading (Cartwright & Lonergan, 1996; Cartwright & Dewhurst, 1998), (ii) hydraulic fracturing as a result of differential compaction and overpressure build-up (Cartwright, 1994), (iii) density inversion resulting from differential compaction between host strata and the overlying strata (Henriet et al., 1988; Wrona et al., 2017a), and (iv) dissolution of particles during diagenesis (Shin et al., 2008; Cartwright, 2011). In general, they are considered to have significant implication for hydrocarbon exploration and production because: (i) they can form potential migration pathways or vertical fluid plumbing systems through low porous and permeable sediments (Gay et al., 2007), (ii) they may act as seal-bypass systems which can compromise the integrity of low permeable sealing lithologies and as such may be important for hydrocarbon leakage and migration into shallower sediments (Huuse et al., 2010), and (iii) they can lead to reservoir compartmentalization where thin sandstone units are interbedded with fine-grained mudstones (Moller et al., 2004; Huuse et al., 2010, Cartwright, 2011).

Almost all published cases of large-scale sand intrusion complexes (e.g., Molyneux et al., 1999, 2002; Lonergan et al., 2000; Huuse & Mickelson, 2004; Huuse et al., 2004; Shoulders et al., 2007; Szarawarska et al., 2010; Bureau et al., 2013; Piyaphong & Huuse, 2020) are found within polygonally faulted mudstone successions. Their co-existence have led to the suggestion that the presence of polygonal faults may have a resultant control on the timing and inherent geometries of sand intrusions (e.g. Lonergan et al., 1998; Gras & Cartwright, 2002; Szarawarska et al., 2010) due to the observation that both features sometimes have similar dimensions and dips, with some intrusions intruded along polygonal fault planes (Lonergan & Cartwright, 1999; Molyneux et al., 1999; Lonergan et al., 2000; Gras & Cartwright, 2002). However, cross-cutting relationships have also been observed between both features (e.g., Huuse et al., 2004; Huuse & Mickelson, 2004; Shoulders & Cartwright, 2004; Shoulders et al., 2007; Bureau et al., 2013). Based on the latter, some authors have argued that although both features may sometimes display geometrical similarities, the intrusions independently achieve their distinct cross-sectional geometries regardless their occurrence alongside polygonal faults and the faults may only contribute to seal breach and

may be exploited by the intrusions when they are favourably oriented (Gay, 2002; Huuse & Mickelson, 2004; Shoulders et al., 2007; Bureau et al., 2013).

This study examines the relationship between large-scale sandstone intrusions and polygonal faults developed in the Eocene to Mid Miocene succession (Hordaland Group) of the northern North Sea Basin. This study presents the first time the relationship between both features is explored in the study area. We explore this relationship by classifying the different kinds of interaction observed between both features. In the study area, high quality 3D seismic data images discordant high amplitude anomalies which are found within polygonally faulted host mudstone strata. These discordant amplitude anomalies have been interpreted as the expression of large-scale sandstone intrusions which have varying cross-sectional and plan-view geometries. Here the interpreted sandstone intrusions are classified geometrically as a function of their observed interaction with the polygonal faults. The intrusions and polygonal faults are then characterized quantitatively by taking measurements of their dimensions and dips, and we further consider how this interaction may have controlled the resultant simple to complex geometries of some of the intrusions.

7.2 Geological Setting

The study area lies in the Norwegian sector of the northern North Sea which was affected by two rifting episodes in the Permian to Triassic and Late Jurassic to Early Cretaceous time (Badley et al., 1988; Faerseth et al., 1997). Both rifting events led to the development of graben and half-graben structures bounded by west dipping and south striking large-displacement normal faults (Fig. 7.1; Faerseth et al., 1995, 1997). Rifting in the area ceased in the Early Cretaceous ushering the post-rift sag phase which was characterized by a transition from fault-driven to thermally controlled subsidence because of thermal relaxation of the crust (Gabrielsen et al., 1990; Jordt et al., 2000; Faleide et al., 2002; Wrona et al., 2017a). The post-rift phase was accompanied by uplift events in the Early Paleocene time related to igneous activity (i.e., magmatism) and the opening of the North Atlantic (Knott et al., 1993; Nadin & Kusznir, 1995; Jordt et al., 2000; Gabrielsen et al., 2001; Jones et al., 2003). Uplift along basin margins and subsequent erosion increased input of clastic sediments from the surrounding sediment source areas (i.e., East Shetland Platform & Norwegian mainland). The sediments were deposited as large sand-rich deep-water fans in the Early to Middle Eocene time, followed by subsequent deposition of fine-grained smectite-rich mudstones during the Late Eocene to Early Oligocene (Jordt et al., 2000; Brekke et al., 2001; Ahmadi et al., 2003; Anell et al., 2012). The Early Oligocene to Late Oligocene also saw the deposition of large number of clastic sediments, with the sediments deposited as channel-lobe systems and small sand-rich fans (Fyfe et al., 2003; Rundberg & Eidvin, 2005; Eidvin et al., 2014). This was then followed by further deposition of mud-dominated sediments which buried the Oligocene sands.

Table 7.1: List of some documented occurrences of polygonal faults with their estimated dips range.

Author (s)	Location	Tier setting	Cross-sectional Geometry	Dip range (°)	Average dip (°)
Cartwright (1994)	UK (Block 30/19) Central North Sea	Two tiers - lower Tertiary low-permeability mudstones	Planar to gently listric	30 to subvertical	Not specified
Cartwright and Lonergan (1996)	UK (Block 16/26) Central North Sea	Two tiers - lower Tertiary low-permeability mudstones	Planar to gently listric	30 - 70	45
Lonergan et al. (1998)	Alba Field Central North Sea	Tier 1: Oligocene - lower Miocene hemipelagic mudstones	Planar to gently listric	27 - 67	45
		Tier 2: Eocene - lower Oligocene hemipelagic mudstones		20 - 54	37
Clausen et al. (1999)	Eastern margin of the Viking Graben, NNS	Oligocene claystone and thinly layered sands	Mainly planar, some gently listric	48 - 85	73
Watterson et al. (2000)	Lake Hope System, southern Eromanga Basin, South Australia	Lower Cretaceous - Tertiary marine mudstones	Planar to gently listric	41 - 61	50 - 55
Shoulders et al. (2007)	Faroe Shetland Basin	Eocene - mid Miocene hemipelagic mudstones	Planar to gently listric	23 - 85	58
Berndt et al. (2012)	Hatton Basin, NE Atlantic	Oligocene - Recent biogenic mudstones	Planar	30 - 60	Not specified
Ostanin et al. (2012)	Snohvit/Albatross Gas Field, Hammerfest Basin	Upper Cretaceous mudstones	Mainly planar, some gently listric	35 - 50	Not specified
Sonnenberg & Underwood (2012)	Denver Basin, Colorado	Early - Late Cretaceous shales	Planar	30 - 80	Not specified
Olobayo (2014)	Northern North Sea	Tier 1: Eocene - mid Miocene smectite mudstones	Planar to gently listric	35 - 58	46
		Tier 2: Cretaceous - Paleocene hemipelagic mudstones	Mainly planar, some gently listric	31 - 43	36
Morgan et al. (2015)	Lower Congo Basin, offshore Angola	Pliocene - Pleistocene wedge shaped hemipelagic succession	Mainly planar, some gently listric	48 - 68	Not specified
Wrona et al. (2017b)	Northern North Sea	Eocene - mid Miocene smectite-rich mudstones	Planar to gently listric	20 - 50	Not specified
Alefaee et al. (2018)	Rankin Platform Sub-basin, Northern Carnarvon Basin, Australia	Two tiers Paleocene-Eocene calcareous mudstones	Planar	60 - 70	Not specified
Li et al. (2020)	Great South Basin, New Zealand	Eocene mudstones	Planar to gently listric	45 - 55	Not specified
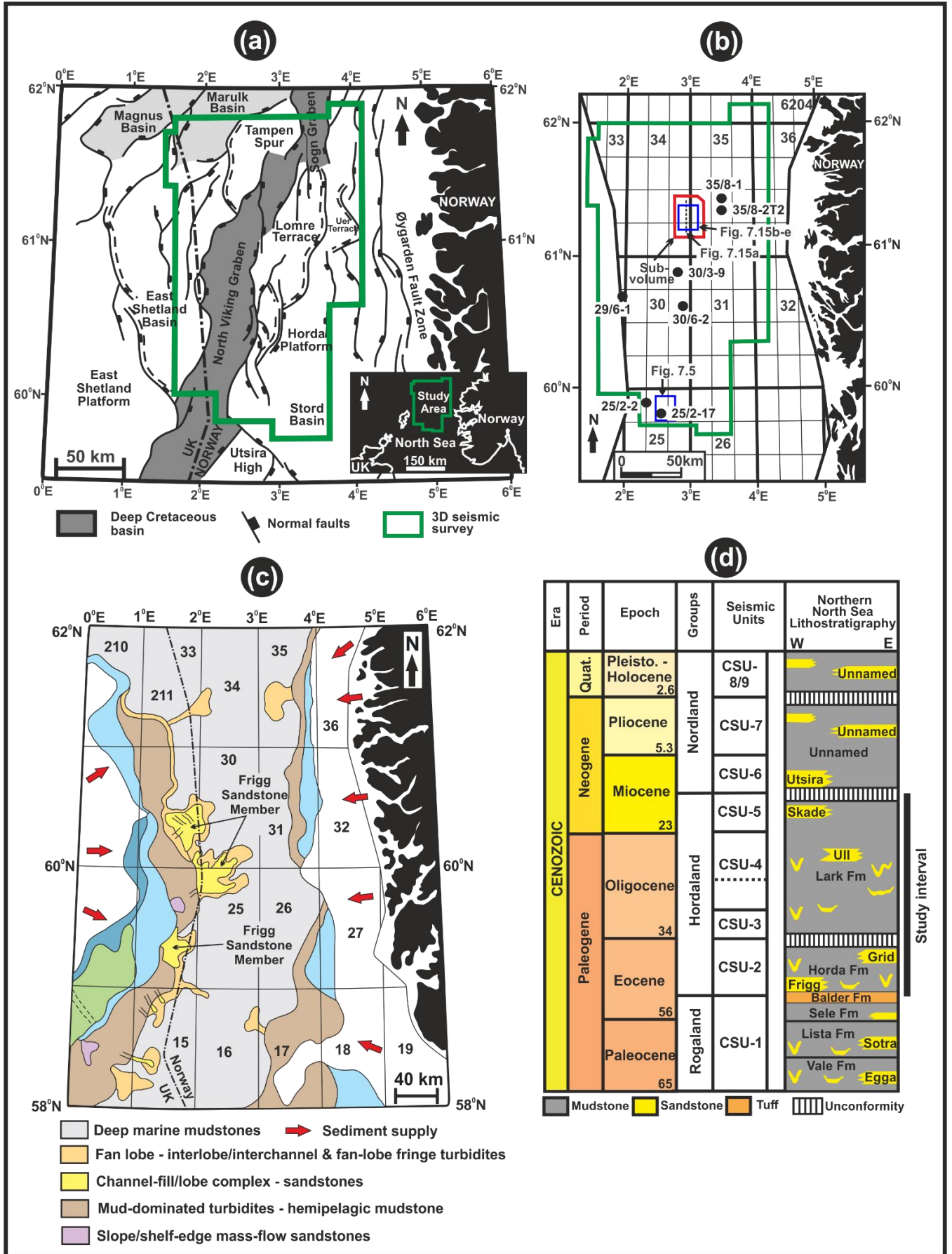
Fig. 7.1: (a) Map showing the location of the study area in the Northern North Sea Basin, with the main structural elements highlighted (modified after Nottvedt et al., 1995). (b) Map showing the outline of the 3D seismic data used and surface location of seven wells used for this study. (c) Paleogeographic map of the Early Eocene showing the distribution of deep-water sandstones (modified from Jones et al., 2003). (d) A simplified stratigraphic framework of the northern North Sea Basin with the studied interval indicated. Seismic data courtesy of CGG and well data from TGS Facies Map Browser.

This study focuses on the large-scale sand intrusion complexes and regionally extensive single tier polygonal fault systems hosted within the Hordaland Group (Eocene to Mid Miocene) interval. The interval is bounded at its base by the Top Rogaland Group (TRG) which marks the top of the Balder Formation consisting of poorly consolidated marine mudstones and tuff deposits (Fig. 7.1d & 7.2; Knox & Holloway, 1992; Wrona et al., 2017a). While its top is marked by the Top Hordaland Group Unconformity (THGU) which is expressed as a high amplitude trough reflection on seismic data and forms a well-known regional unconformity (c. 10 Ma) in the North Sea (see Eidvin & Rundberg, 2001; Løseth et al., 2013). The 600 – 720 m thick interval of interest consists of smectite-rich deep-water mudstones (i.e., Horda & Lark Fm.) that are intensely deformed by polygonal faults which are truncated by the THGU (Fig. 7.2). The sediments within this interval have been documented to have undergone phase diagenetic transformation of amorphous/biogenic silica (Opal-A) to Cristobalite/Tridymite (Opal-CT) which results to significant changes in the density and acoustic properties of the sediments because the transformation process leads to rapid sediment compaction, expulsion of pore fluids and reduction in porosity (Davies et al., 2006; Davies & Clarks, 2006; Ireland et al., 2011). The transformation boundary between Opal-A-rich and Opal-CT-rich sediments is marked by a discrete, mappable high amplitude peak reflection which lies within the Oligocene interval of the Hordaland Group (Fig. 7.1d & 7.2; see Thyberg et al., 1991; Olobayo, 2014: see their Fig. 5.15; Wrona et al., 2017a: see their Fig. 2, 2017b: their Fig. 1). Wrona et al. (2017b) noted that the transformation of Opal-A to Opal-CT was initiated in the Middle to Late Eocene and the diagenetic boundary may have migrated upwards over time with increased burial to its present depth (Fig. 7.2). The occurrence of polygonal faults and sand intrusions within Opal-rich sediments has led some authors to suggest a link between both features and diagenesis (see Davies et al., 2006; Davies & Clarks, 2006; Cartwright, 2007; Davies et al., 2009; Davies & Ireland, 2011).
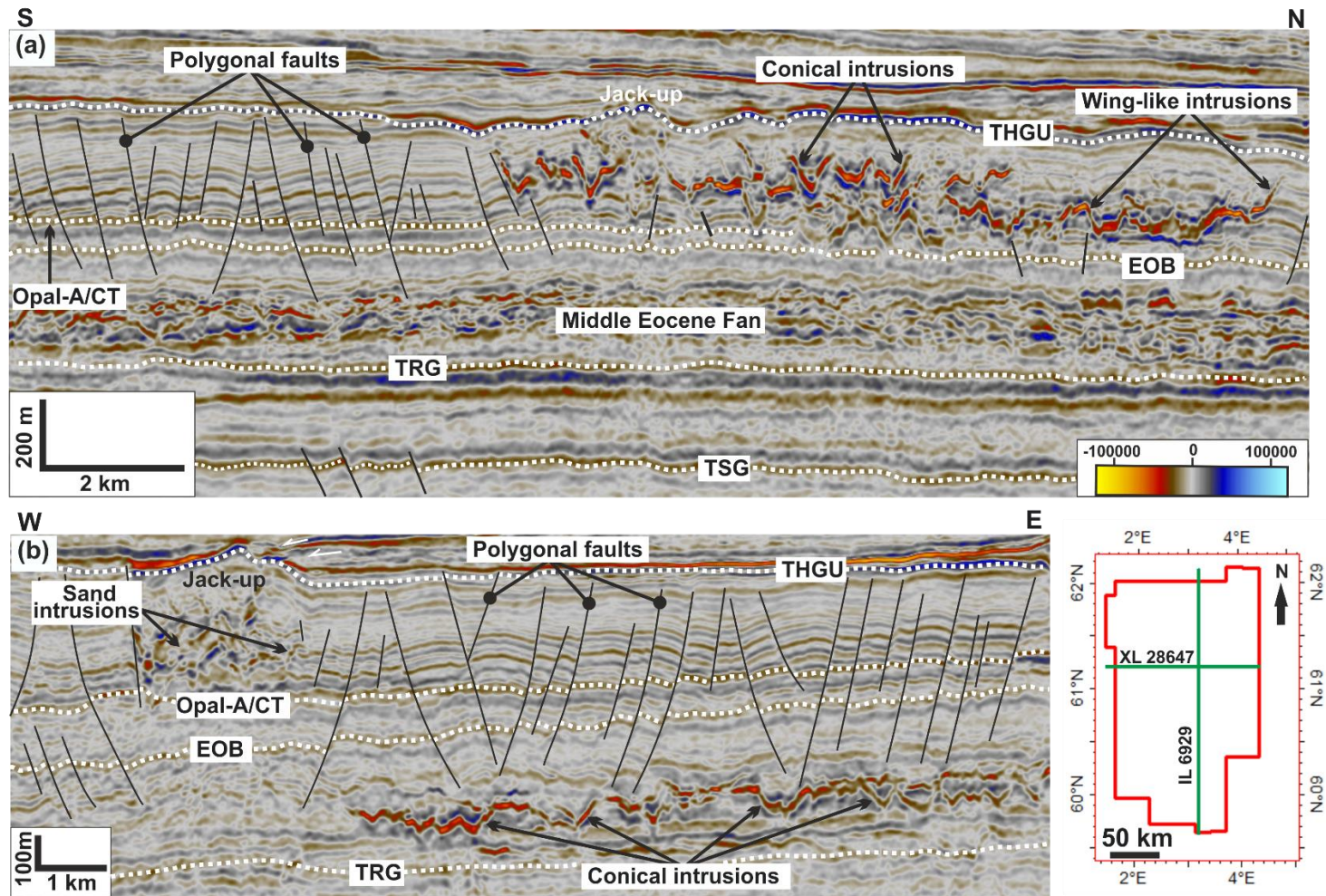
Fig. 7.2: (a) North-south oriented seismic section showing the stratigraphy from Paleocene to Miocene. V-shaped discordant high amplitude anomalies in the Oligocene interval are interpreted as the seismic expression of conical sandstone intrusions within low permeable polygonally faulted mudstones, overlying the Middle Eocene fan. (b) East – west oriented seismic section showing polygonally faulted mudstones in the Eocene to Mid-Miocene, with conical intrusions in the Lower Eocene. THGU = Top Hordaland Group Unconformity; EOB = Eocene – Oligocene Boundary; TRG = Top Rogaland Group; TSG = Top Shetland Group. Seismic data courtesy of CGG.

7.3 Data and Methods

7.3.1 Data

The seismic data used for this study consists of a 3D BroadSeis Broadsource seismic reflection survey (NVG_Z_8km_8bit_37500cm) which extends downward to a depth of 8 km and situated in the northern North Sea Basin between latitude $59 - 62°N$ and longitude $1 - 4°E$ (Fig. 7.1a). The survey covers an area of c. 36,400 km^2 and straddles the boundary between the Norwegian and UK sector of the northern North Sea. This case study focuses on the Eocene – Mid Miocene (Hordaland Group interval) which lies between the depth intervals 1000 – 1620 m. The 3D seismic cube has a sub-sampled line spacing of 37.5 m with a dominant frequency of 50 Hz within the interval of interest. The data is depth-migrated, zero-phase processed and displayed based on the SEG normal polarity, which implies that a downward increase in acoustic impedance represents a positive (red) peak reflection while a downward decrease in acoustic impedance represents a negative (blue) trough reflection. The average velocity of the Hordaland Group is approximately 2 km/s derived from wells which gives a vertical resolution ($\lambda/4$) of c. 10 m and horizontal resolution ($\lambda/2$) of c. 20 m. A total of seven (7) wells were selected for this study and they contain complete standard suite of well logs (Fig. 7.1b). Some of the wells have been used to calibrate the lithology of discordant high amplitude anomalies intersected by wells which enabled their interpreted as sandstone intrusions.

7.3.2 Methods

Detailed interpretation of the available seismic data was carried out by mapping key horizons using 2D and 3D auto-tracking, followed by attribute extractions (i.e., variance, chaos, and RMS amplitude) on the mapped horizons to reveal features of interest. The high quality of the available 3D seismic survey has allowed the polygonal faults and injection features to be mapped and visualized using standard seismic mapping techniques.

To explore the relationship between the large-scale sandstone intrusions and polygonal faults in the study area, detailed analysis of the geometrical parameters of both features (see Fig. 7.3) was carried out. For example, dip measurements of both features were measured and compared for cases where the intrusions are intruded along fault planes or where intrusions were crosscut by polygonal fault planes. Furthermore, fault analysis and characterization have been carried out to highlight the geometry, dimensions, and pattern of polygonal faults within the studied Eocene – Mid Miocene (Hordaland Group) interval using a representative 3D sub-volume which has an area of c. 584 km^2 (Fig. 7.1b & 7.3). The sub-volume has been used because: (i) it covers areas within the centre of the study area where sand intrusions are absent or unresolved, and (ii) the polygonal faults within and outside the sub-volume display comparable planar to listric cross-sectional geometries and they can be traced with confidence through the interval (Fig. 7.3a). To determine the

geometrical characteristics of the polygonal faults, six (6) horizons labelled 1 – 6 in Fig. 7.3a, which includes the bounding surfaces of the polygonally faulted interval, were mapped within the sub-volume and in turn used to generate structural and isopach maps. The generated structural maps from the mapped horizons are displayed with rose diagrams of polygonal fault orientation (strike) and dip directions at that specific structural level (see Fig. 7.13). Thickness maps were also calculated between the mapped horizons (see Fig. 7.14). Some key polygonal fault properties have been measured and these includes their dip, dip direction, strike, vertical throw, heave, fault spacing, length and height.

The dip, dip direction and strike of the polygonal faults associated with each mapped horizon in the sub-volume have been derived by automatic fault extraction using the Ant-tracking algorithm in Schlumberger Petrel software. Ant-tracking applies swarm intelligence algorithm, just like ants, to identify and sharpen discontinuities in seismic data (see Pedersen et al., 2002; Du et al., 2016). The algorithm emulates the behaviour of ant colonies in their search for food, in which they release a chemical substance known as "pheromones" to mark the paths between their nest and food (Silva et al., 2005; Sekararum & Rosid, 2020). The tracking by the "artificial or virtual ants" work by capturing information related to fault zones in edge enhancing or discontinuity attributes (e.g., chaos or variance), and the resultant attribute volume displays in detail the location and distribution of fault zones (Silva et al., 2005). The automatic fault extraction workflow provides interactive tools which enables the analysis of fault systems, leading to the generation of fault patches, which are in turn converted into fault interpretations. The workflow (Fig. 7.4) involves the use of an edge enhancing seismic attribute cube (e.g., variance or chaos attribute) as the input seismic for generating an Ant-tracking attribute cube. Here the variance cube of the 3D seismic sub-volume was used to generate an Ant-tracking cube using the "aggressive setting" to reveal the spatial discontinuities in the dataset. The selected parameter setting ensured detailed identification and amplification of discontinuities (faults) within the variance cube. The Ant-tracking cube was subsequently used as the input for the automatic fault patch extraction process using the pre-defined parameters (e.g., normal confidence or high confidence). Here the high confidence preset parameters have been used, which implies that only high and well-connected values in the input volume are used for the extraction of fault patches. The extracted fault patches are then filtered based on patch properties (i.e., size, vertical extent, patch confidence) and orientation to eliminate or disregard undesirable patches which in turn eliminates uncertainties associated with the extracted fault patches. For example, fault patches with low patch confidence and those aligned with the inline and crossline direction (i.e., with dips equal to 90°) were eliminated. Also, some patches were edited where required and merged in cases where individual patches are identified to represent the same fault. The remaining fault patches after filtering were then converted to fault interpretation or fault pillars from which their fault properties are extracted into a spreadsheet.
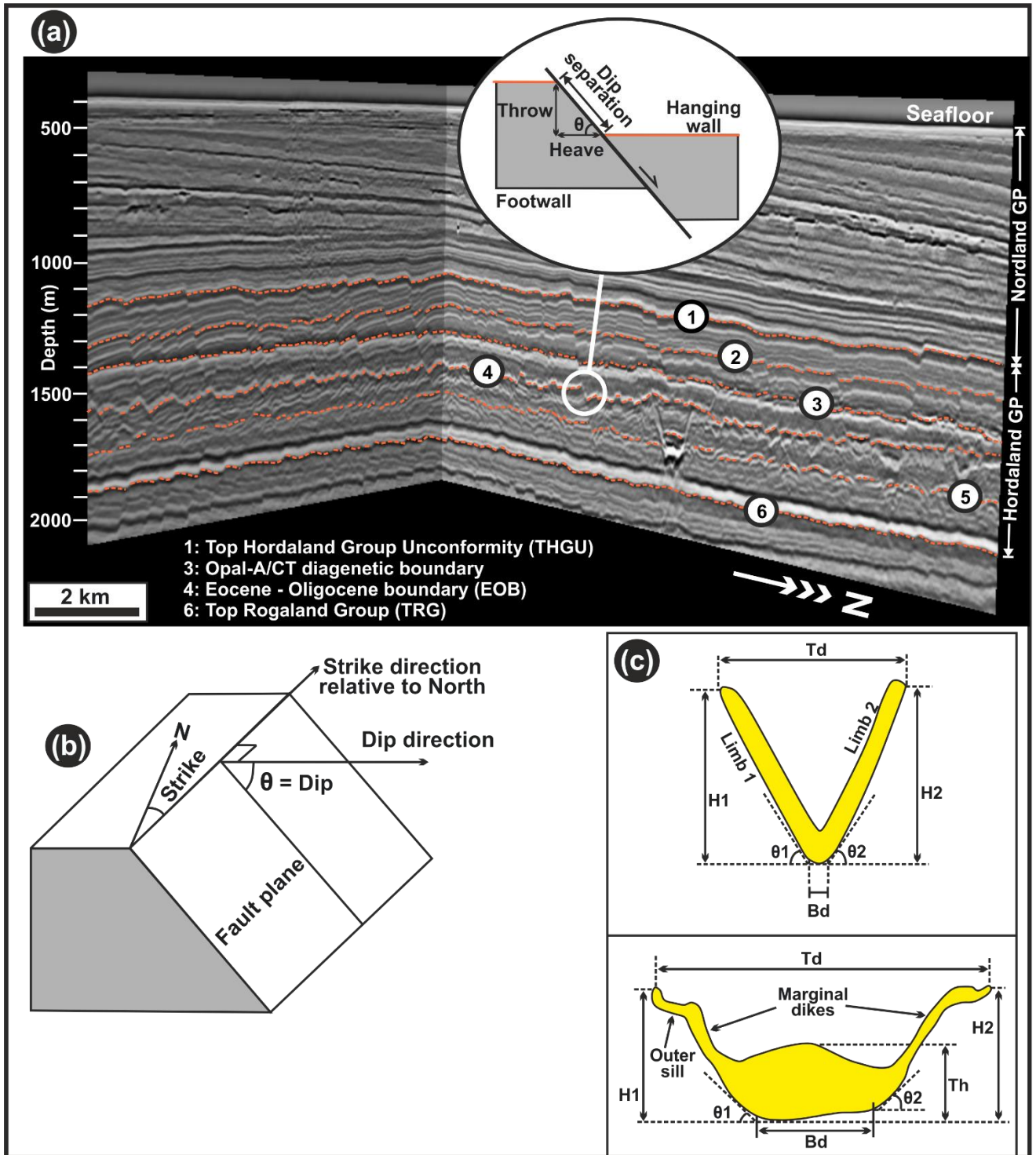
Fig. 7.3: (a) 3D visualization of seismic sub-volume used for detailed analysis of polygonal faults, using six (6) stratigraphic horizons (H1 to H6) within the interval hosting the studied PFS. (b) Illustration of measured geometrical parameters for the studied PFS. (c) Schematic illustration of measured geometrical parameters for sandstone intrusions within the studied interval. Location and area coverage of the sub-volume is shown in Fig. 7.1b. Seismic data courtesy of CGG.
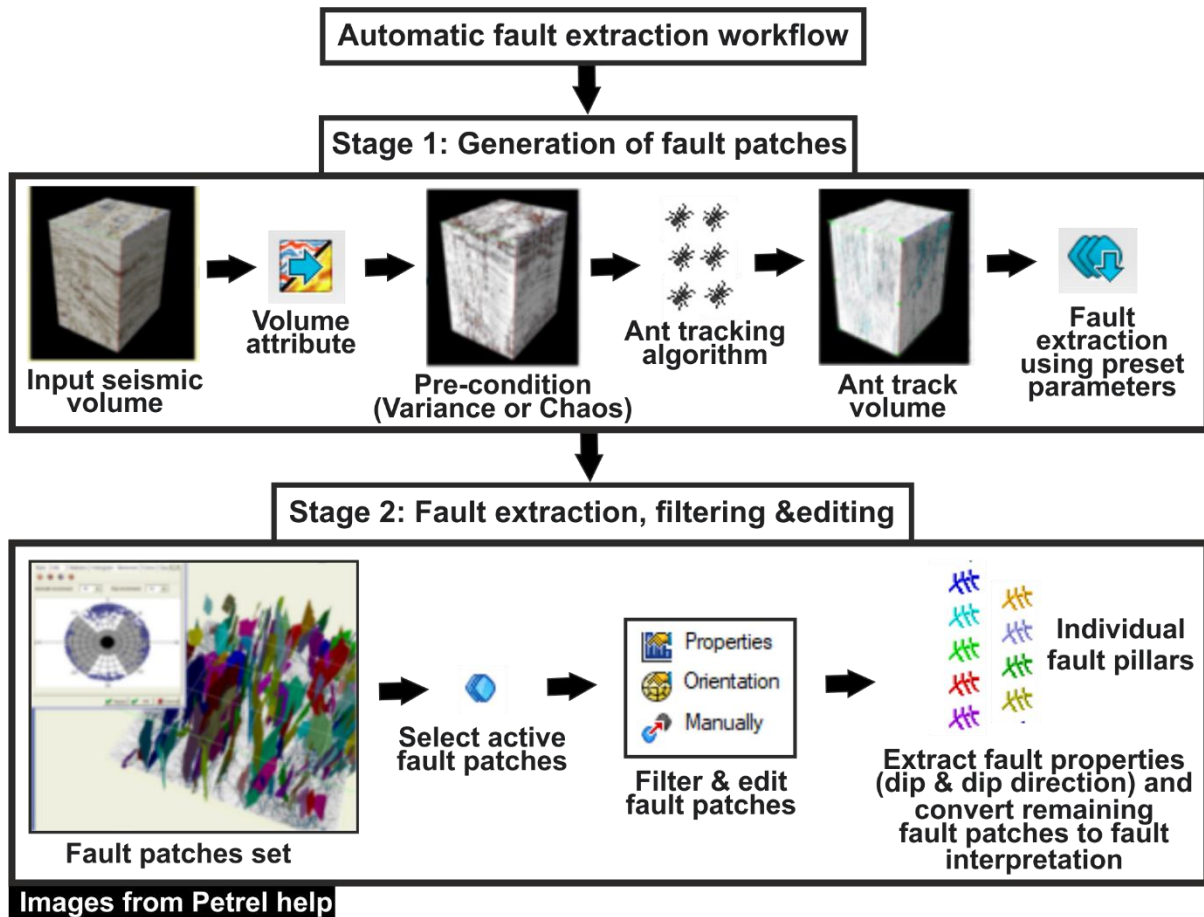
Fig. 7.4: Automatic fault extraction workflow used for polygonal fault analysis and interpretation.

7.4 Results

7.4.1 Seismic identification, distribution, and characteristics of large-scale sandstone intrusions

Sandstone intrusions in the study area are on three-dimensional seismic data expressed as discordant high amplitude anomalies within the Hordaland Group (Eocene to Mid-Miocene) interval (Fig. 7.2a). The discordant anomalies are characterized by an upper and lower high amplitude peak and trough reflections respectively, with occasional upper trough and lower peak reflections. Their high seismic amplitude relative to their surrounding low amplitude reflections indicate they are high acoustic impedance features encased in low impedance host strata. Their upper and lower reflections are usually roughly parallel with varying continuity in seismic cross section. They exhibit varying cross-sectional geometries which include conical-shaped, saucer-shaped or wing-like and irregular to complex-shaped discordant amplitude anomalies. The conical-shaped anomalies are characterized by V, W & U-shaped anomalies with steely dipping limbs (Fig. 7.6a & d), while the saucer-shaped/wing-like anomalies are defined by a concordant base with inclined discordant anomalies at their margins (Fig. 7.9b - d). In both cases, the anomalies are observed to crosscut the host

stratification which indicates they are not genetically related to their host strata. The anomalies in some cases have bedding-concordant (i.e., sill) anomalies developed at the upper tip of their discordant limbs or wings (Fig. 7.9b & 7.11c). On the other hand, the irregular and complex-shaped anomalies appear in cross section as more complicated (e.g., zigzag shaped) discordant anomalies which may or may not show well-developed injected limbs or wings (Fig. 7.9c & 7.21c). They are usually characterized by irregular discordant reflections and range in thickness from 25 to 70 m with width of up to 3 km. All four types of geometries associated with the anomalies in cross-section are characterized by circular to elongate and irregular planform geometries (Fig. 7.5). The limbs or wings of the amplitude anomalies have an average dip of 20° ± 2° with individual dip value ranging from 7 – 39°. Common to most of the observed discordant amplitude anomalies within the Eocene – Mid Miocene (Hordaland Group) is the marked deformation of the host mudstone strata which occur as domal folds or jack-up of the overburden above the anomalies (Fig. 7.6b & d, 7.9a & e). Reverse faulting around the intrusion margins which coincides with the edges of the jack-up folds were also observed for some intrusions (e.g., Fig. 7.6e).

In the Eocene, the discordant amplitude anomalies occur predominantly as conical shaped anomalies with few isolated wing-like anomalies. Here the anomalies are observed to occur at two (upper & lower) levels (Fig. 7.6d & e) and are spatially distributed in the north-eastern and western to south-western parts of the study area. Some of the anomalies within the lower level have their limbs terminate at a datum (see Fig. 7.6d) which lies at about 130 – 150 m above the Top Rogaland Group (TRG) and represents the top of the lower Eocene while the limbs of the anomalies in the upper level extend upward for c. 100 to 220 m and terminate at the Eocene – Oligocene boundary (EOB) represented by a medium to high amplitude peak reflection (Fig. 7.6a & d). Three sand-rich fans (Fan A to C) are present within the Middle Eocene (Fig. 7.7 & 7.8). Fan A & B referred to here as the Grid fans were fed from the north-eastern margin of the study area with an east – west trend (Fig. 7.7), while Fan C referred to as the Frigg fan was fed from the East Shetland Platform in the south-western part of the study area (Fig. 7.8). Conical-shaped discordant anomalies are developed above and adjacent to the fan complexes with the anomalies extending and cross-cutting up to 250 m of stratigraphic layering. However, some isolated anomalies are observed at distances of up to 10 – 15 km laterally away from the edges of the Middle Eocene fan complexes.

In the Oligocene, discordant amplitude anomalies are spatially distributed in most part of the study area except in the south-east and north-western parts. The anomalies within this interval occur either as isolated discrete anomalies (i.e., conical & wing-like anomalies: Fig. 7.9a - d) and amalgamated complexes consisting of stacked conical and wing-like anomalies (Fig. 7.9e). In the western part of the study area, the anomalies occur within the lower and Upper Oligocene, consisting of highly remobilized and stacked anomalies while in the east and north-eastern parts they lie on or above a medium to high amplitude peak reflection interpreted as the Opal-A/CT diagenetic transition (see Thyberg et al., 1991; Wrona et al.,

2017b) and terminate upward at the Top Hordaland Group Unconformity (THGU) or Mid-Miocene Unconformity (MMU) where they are spatially related to domal folding or elevation of the THGU surface above the anomalies (Fig. 7.9). The Opal-A/CT boundary serves as the boundary between the upper and lower Oligocene sub-units.
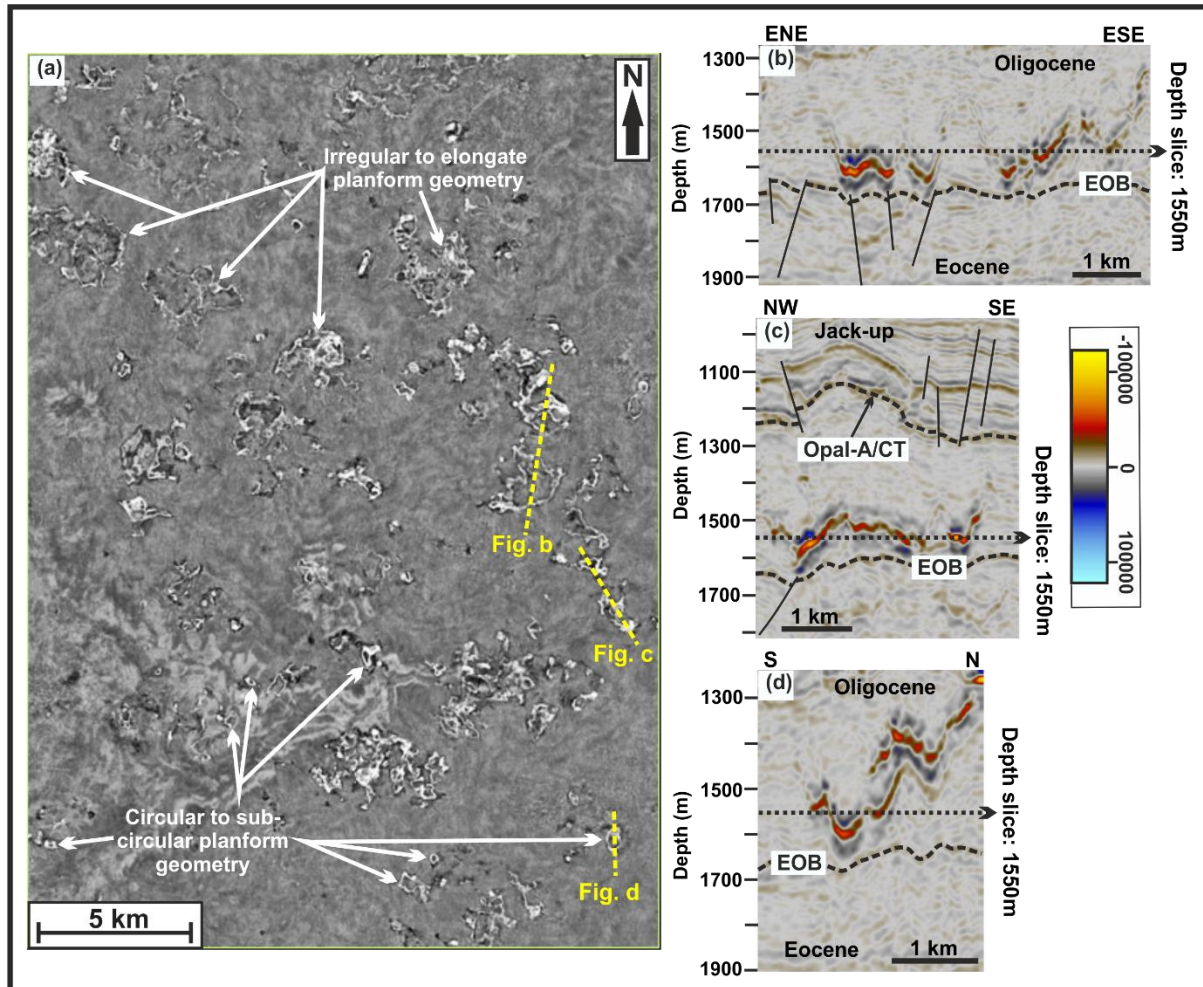
Fig. 7.5: (a) Depth slice at 1550 m through the Oligocene interval showing circular to sub-circular, and irregular to elongate amplitude anomalies, which are in cross section in (b) to (d) characterized by V and W-shaped discordant amplitude anomalies which directly overlie the Eocene – Oligocene boundary (EOB). See location of depth slice in Fig. 7.1b. Seismic data courtesy of CGG.

Well calibration of discordant high amplitude anomalies intersected by exploration wells in the study area indicate the presence of c. 18 – 50 m thick sandstone units (e.g., Fig. 7.10). Discordant high amplitude anomalies with similar scale, geometry (cross-sectional & planform) and acoustic properties have been recognized over large areas in the Paleogene of the North Sea Basin where they were correlated to sandstone of up to 60 m in thickness (e.g., Molyneux et al., 1999; Jackson & Sømme, 2011; Huuse & Mickelson, 2004; Olobayo, 2014). Therefore, the anomalies observed in cross section within the Hordaland Group (Eocene to Mid-Miocene) are interpreted to represent the seismic expression of large-scale

sandstone intrusions hosted within low permeable mudstones. The observed physical connection between some of the conical-shaped anomalies which are found above and adjacent to the sand-rich Middle Eocene fans also indicate they represent sandstone intrusions. The deformation of the overburden in the form of domal folds and jack-up observed on the THGU surface above the sandstone intrusions is suggested to indicate forced folding due to intrusion of excess materials and differential compaction across depositional sand bodies (see Jackson et al., 2011; Huuse et al., 2012; Andresen et al., 2019).

7.4.2 Parent source sands and timing of intrusions

The parent source sands for the intrusions within the Eocene are suggested to be sourced by the Middle Eocene sand-rich fans based on the apparent physical connection between conical-shaped intrusions and the top of the fans (Fig. 7.8c & d). However, some intrusions are recorded farther away from the fans which implies that the distribution of sand intrusions do not completely correspond to the inferred extent of the fans. Therefore, we suggest that these intrusions occurring at longer distances away from the sand-rich fans may have been sourced by: (i) isolated sand bodies within the Lower to Middle Eocene succession (e.g., Fig. 7.11), (ii) by lateral transport of fluidized sand, or (iii) from deeper sources below the Eocene (i.e., Middle – Upper Paleocene sands). The first hypothesis is supported by the observation of isolated channel-shaped anomalies with remobilized/injected margins in the Lower - Middle Eocene in the northern and southern parts of the study area (Fig. 7.11c & e). However, sampling and comparative analysis (e.g., heavy mineral provenance & fluid inclusion analysis; see Hurst et al., 2017) of sand samples from both the intrusions and their potential parent sands from either the Paleocene, Lower Eocene or Middle Eocene will lay more credence to the above interpretation; this is however beyond the scope of this study. The Eocene conical sand intrusions are observed to occur at two levels (Fig. 7.6) with their limbs often terminating at two different datum points represented by the top of the lower level (i.e., top of lower Eocene) and top of the upper level (i.e., Eocene – Oligocene boundary). However, most of the conical-shaped intrusions terminate at the EOB. The termination of large-scale sand intrusion limbs at a common datum over an extensive area have been recognized by authors, leading to the suggestion that the datum may likely define the seafloor at the time of emplacement of the intrusions (Molyneux et al., 2002; Huuse et al., 2004; Huuse & Mickelson, 2004; Cartwright et al., 2008). The EOB is taught to represent the most important break in the Cenozoic, characterized by well-defined changes in lithostratigraphy, biostratigraphy and mineralogy at the boundary, linked to the global temperature transition from green-house to ice-house conditions (Rundberg, 1989; Martinsen et al., 1999; Zachos et al., 2001; Rundberg & Eidvin, 2005). Hence, the boundary may have represented the paleo-seafloor at the time of intrusion, and we propose that intrusion occurred during the Middle to Late Eocene time.
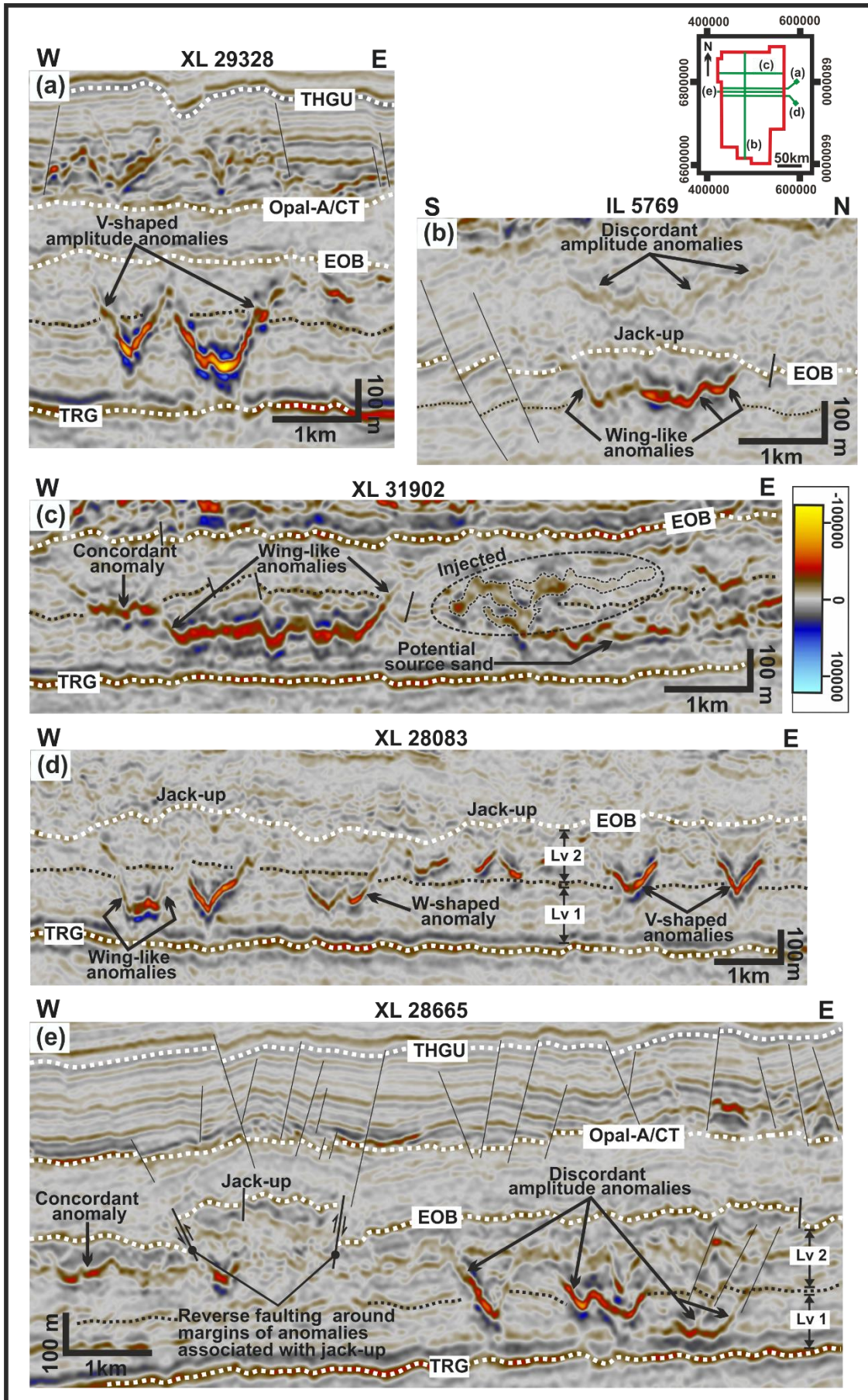
Fig. 7.6: (a) V-shaped anomalies in the Eocene interval interpreted as conical sandstone intrusions. (b) & (c): Wing-like amplitude anomalies within the Eocene interval characterized by subtle jack-up of the overburden above the anomalies. The anomalies are interpreted as wing-like intrusions characterized by concordant base and discordant margins. (d) Eocene discordant amplitude anomalies observed to show two levels of downward termination of their apices. (e) Eocene concordant and discordant amplitude anomalies with one of the anomalies associated with reverse fault resulting from the jack-up of the overburden. THGU = Top Hordaland Group Unconformity; EOB = Eocene – Oligocene Boundary; TRG = Top Rogaland Group. Seismic data courtesy of CGG.

Fig. 7.7: (a) Lower to Middle Eocene sand-rich fan complexes (Fan-A and Fan-B), sourced from the north-eastern part of the study area. Both fans are associated with discordant high amplitude anomalies at the toe of the fan towards the basin centre. They are taught to have partly sourced the conical intrusions observed within the Eocene interval. (b) Well correlation of well 35/8-1 and 35/8-2T2 through the Fan-A & Fan-B indicates the presence of up to 200 m thick sandstone unit. (c) RMS amplitude map of the mapped horizon which represents the top of Fan-A showing very high RMS amplitude which is also an indication for sand presence. (d) RMS amplitude map representing the top of Fan-B. The top of both fans is highlighted by yellow dotted lines in Fig. (a), with their spatial extent shown in the inset map. THGU = Top Hordaland Group Unconformity; EOB = Eocene – Oligocene Boundary; TRG = Top Rogaland Group; TSG = Top Shetland Group. Seismic data courtesy of CGG.

Fig. 7.8: (a) Top structure map of Lower - Middle Eocene Fan-C and channel-fan complexes developed in the south-western part of the study area. (b) RMS amplitude map of top structure map in (a) showing high reflection amplitudes which indicates sand presence. (c) Seismic section across Fan-C showing the apparent physical connection of conical-shaped anomalies developed above the Fan. (d) Conical-shaped amplitude anomalies connected to the top of fan sands north-east of Fan-C. (e) Well calibration of Fan-C which indicates the presence of up to 200 m thick sandstone unit with inter-beds of mudstone. Location of well is shown in Fig. (a). (f) Discordant amplitude anomaly at the margin of fan sand north-east of Fan-C. Conical shaped anomalies are observed above the fan with potential feeder conduits across the Eocene – Oligocene Boundary which may have partly sourced the Oligocene intrusions. Location of seismic lines in Fig. c – f are shown in Fig. (b). EOB = Eocene – Oligocene Boundary; TRG = Top Rogaland Group; TSG = Top Shetland Group. Seismic data courtesy of CGG.
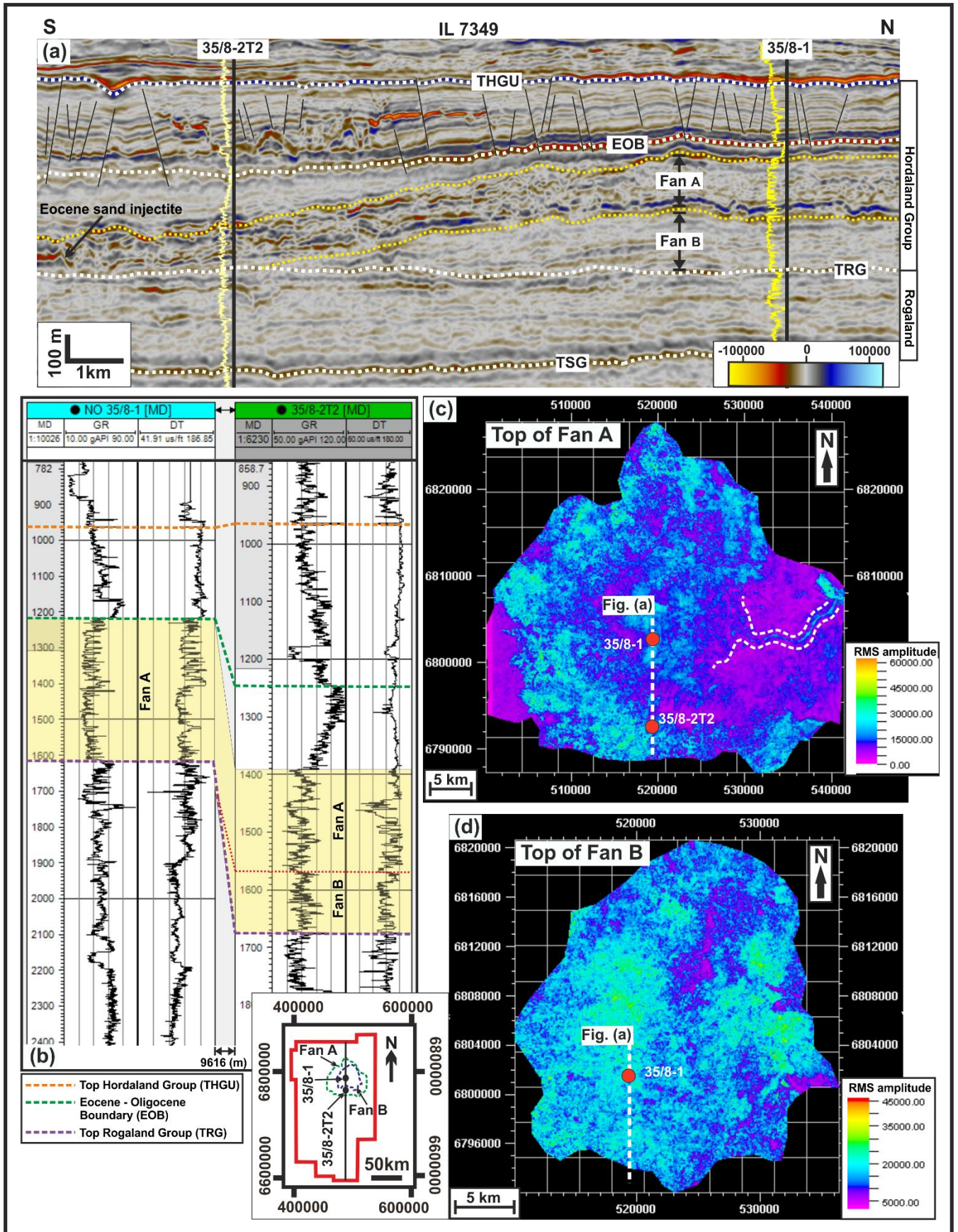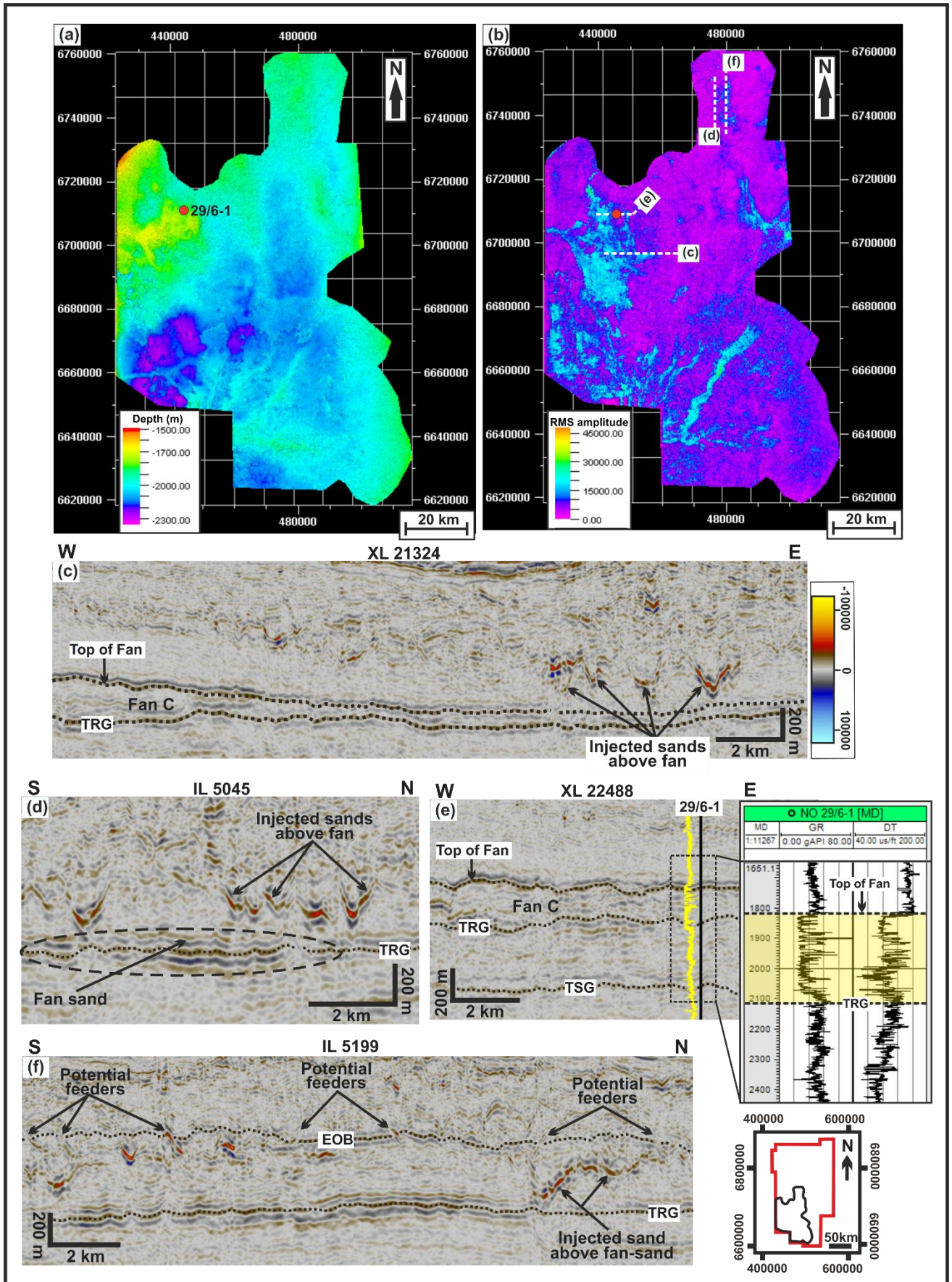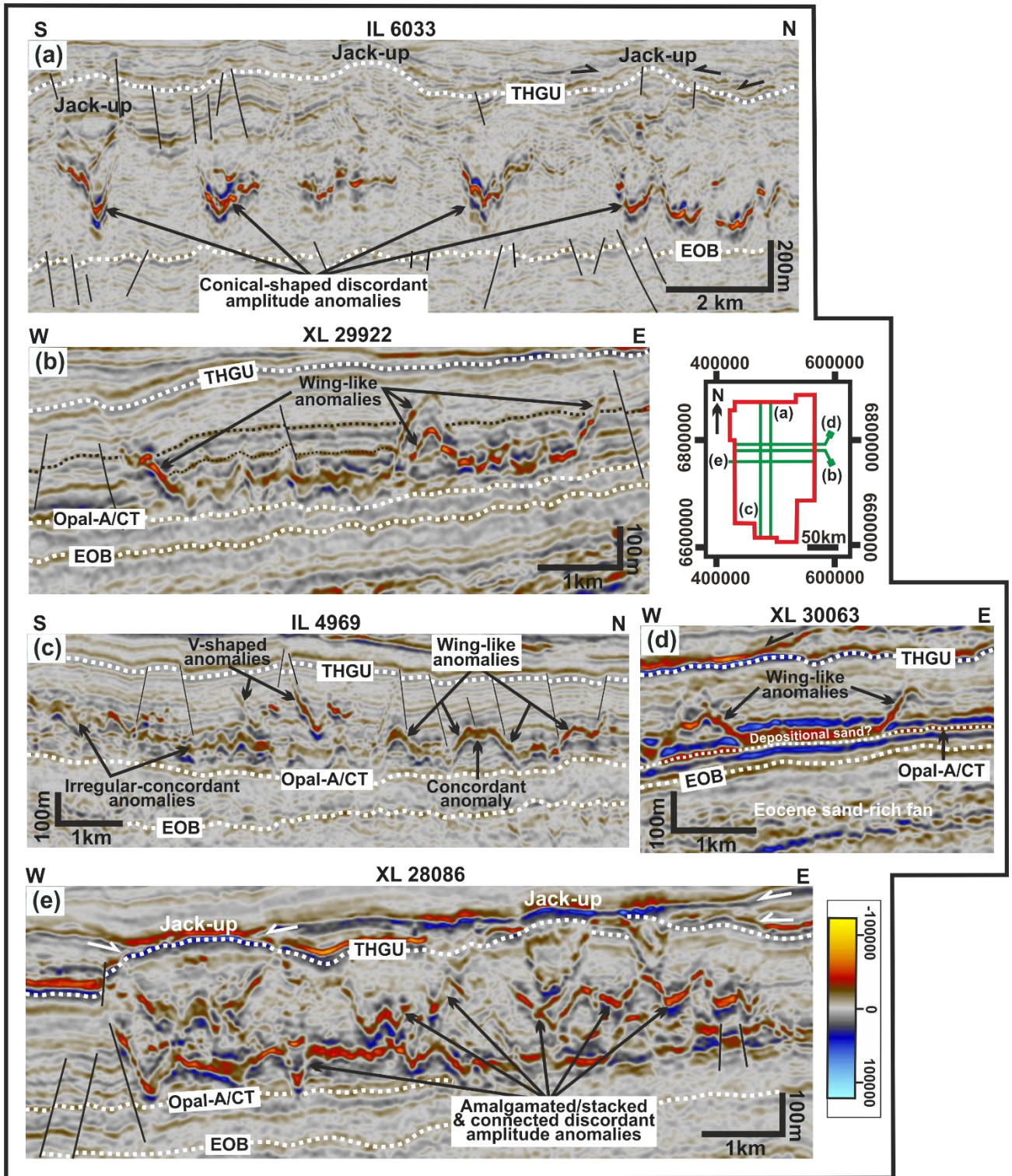
Fig. 7.9: (a) V-shaped high amplitude anomalies within the Oligocene interval interpreted as conical sand intrusions. (b) to (d): Oligocene wing-like high amplitude anomalies characterized by a concordant base and discordant margins, with jack-up of the overburden above the anomalies. These are interpreted as depositional sands modified by post depositional processes leading to sand injection at their margins. (e) Amalgamated or stacked high amplitude anomalies characterized by laterally connected V & W-shaped anomalies within the Oligocene interval. THGU = Top Hordaland Group Unconformity; EOB = Eocene – Oligocene Boundary. Seismic data courtesy of CGG.
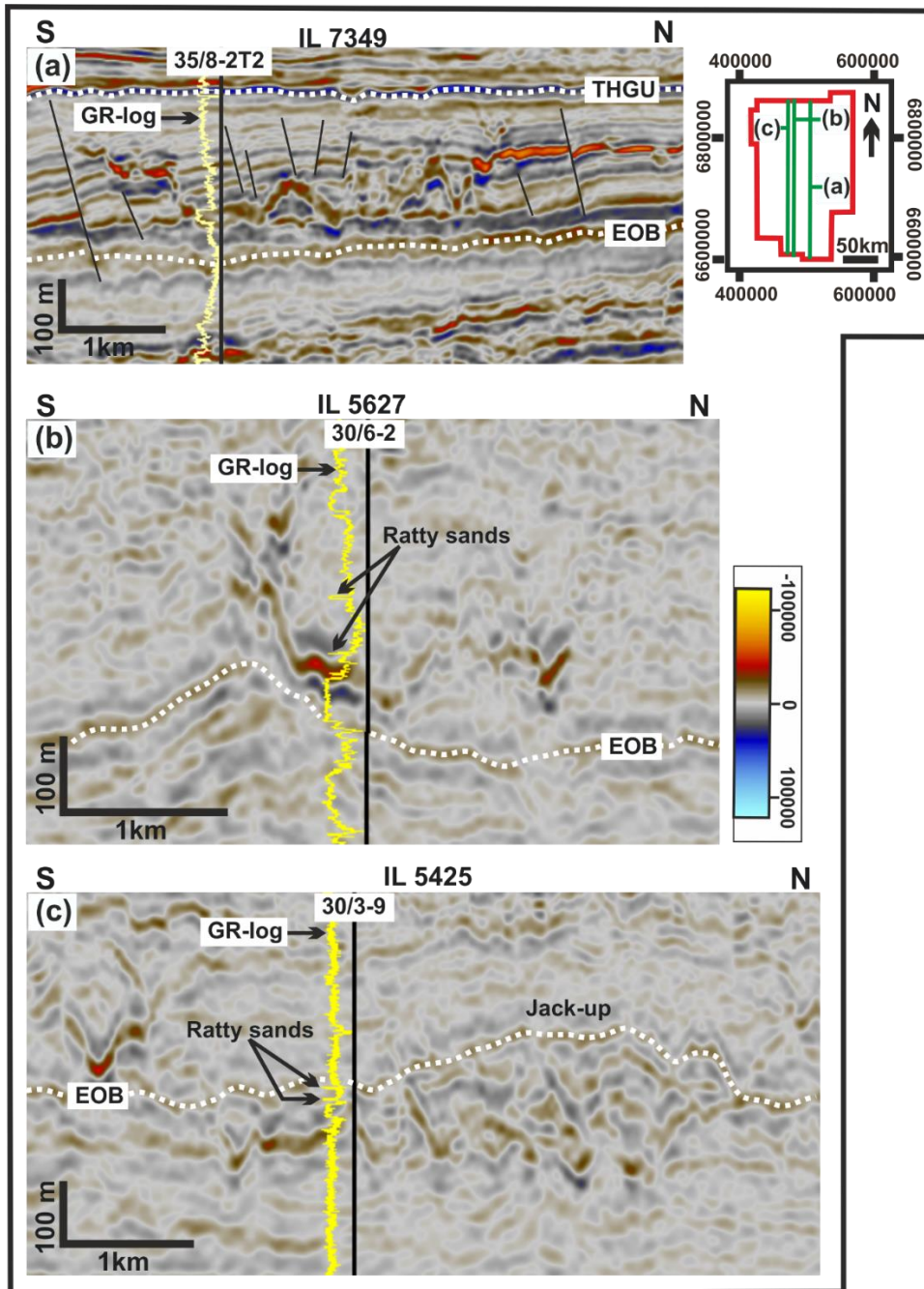
Fig. 7.10: Well calibration of discordant high amplitude anomalies intersected by some wells in the study area using Gamma ray (GR) logs. (a) Well 35/8-2T2 encountered c. 25 m thick sandstone unit where it intersected the concordant base of a wing-like amplitude anomaly within the Oligocene interval. (b) Well 30/6-2 encountered c. 50 m thick sandstone unit where it intersected the concordant base of a tilted Oligocene wing-like amplitude anomaly with thin (ratty) sand units above the main sand interval. (c) Well 30/3-9 encountered c. 18 m thick sandstone unit where it intersected a discordant amplitude anomaly within the Upper Eocene interval. THGU = Top Hordaland Group Unconformity; EOB = Eocene – Oligocene Boundary. Seismic data courtesy of CGG and well data from TGS Facies Map Browser.

The source sands for the Oligocene sandstone intrusions are taught to be derived from gravity flow sands (turbidites) deposited in the northern North Sea Basin in the Early to Late Oligocene, sourced from a dominant western source (uplifted East Shetland Platform) and eastern source (West Norway). The outline and extent of these Oligocene sand-rich depositional systems have been documented by Rundberg & Eidvin, (2005: see their Fig. 7a) and Eidvin et al. (2014: see their Fig 1). They have also been correlated across wells in the study area and confirmed as thick sandstone units (see Fig. 4.30 & 6.6; Rundberg & Eidvin, 2016: see their Fig. 6). In combination to the above, some of the Oligocene intrusions in the southern and western parts of the study area are also suggested to be partly sourced from the Middle Eocene fans and isolated Middle - Upper Eocene sands based on observation of conical-shaped intrusions with apices within the Upper Eocene and limbs extending across the Eocene – Oligocene boundary into the Lower Oligocene (Fig. 7.12b). Potential feeder conduits (i.e., feeder dykes) are also observed in the Upper Eocene which may have also fed some of the Oligocene intrusions (Fig. 7.12a & c). The Oligocene sand intrusions which often terminate at the level of the Top Hordaland Group Unconformity are observed to be spatially related to the domal forced folding or jack-up of the Top Hordaland Group Unconformity above the intrusions, with the edges of the folds spatially coinciding with the tips of the intrusion limbs and wings (Fig. 7.9a & e). These domal folds or jack-up on the Top Hordaland Group Unconformity surface are usually onlapped and down-lapped by younger sediments (Fig. 7.9e & 7.12b) which suggests that the Top Hordaland Group Unconformity likely represents the seafloor at the time of intrusion. This means that the significant relief of the Top Hordaland Group Unconformity indicate the topography of the seafloor at the time of deposition of the overlying younger sediments and dating the onlapping sediments can give an indication on the timing of intrusion (Shoulders & Cartwright, 2004). The likelihood of the Top Hordaland Group Unconformity being the seafloor at the time of injection is further supported by the recognition of sand extrudites above the Top Hordaland Group Unconformity surface (see Fig. 4.35; Løseth et al., 2013: their Fig. 11). This implies that the injection of fluidized sand reached the seafloor and was expelled at the free surface as sandstone extrudites. The sediments that onlap the domal folds or jack-up have been dated as Late Miocene to Early Pliocene in age (see Løseth et al., 2013; Eidvin et al., 2014) since the Mid-Miocene was characterized by submarine erosion linked to deep-water currents (Rundberg & Eidvin, 2005). Thus, intrusion may have occurred during the Middle to Late Miocene time.

7.4.3 Polygonal fault characteristics in the study area

7.4.3.1 Fault geometry and analysis

A complex and extensive single-tier polygonal fault system is developed within the Hordaland Group (Eocene – Mid Miocene) mudstone succession in the study area. The faults are restricted within the Hordaland Group interval and are well-imaged on attribute

maps derived from mapped horizons and depth slices through the variance attribute cube of the 3D seismic sub-volume used for fault analysis (Fig. 7.2 & 7.15). The faults are widely distributed in the study area, mainly in the central part where it covers an area of up to 7000 km^2. They consist of planar to gently listric normal faults which switch polarity (i.e., dipping in opposite direction) in cross sections and generally extend continuously from the top of the Rogaland Group up to the Top Hordaland Group Unconformity (Fig. 7.2 & 7.3). However, they are observed to occur within mudstones above the Middle Eocene sand-rich fans and do not intersect them (Fig. 7.2a). Majority (97%) of the polygonal faults terminate at the Top Hordaland Group Unconformity surface while a few (2 – 3%) of the faults propagate into the overlying succession. The faults are often crosscut by sandstone intrusions which imply they formed prior to the remobilization and injection of fluidized sand into their mudstone-dominated host succession.

The fault planes have dip values in the range between 15 – 75°, while majority fall within 20 – 55°, with an average dip of 35° ± 5° which decreases from 75 – 15° with increase in depth for the gently listric faults. This decrease in dip is thought to be linked to compactional flattening of fault planes due to increase in burial and vertical stress with depth (Cartwright, 2011). The strike of the fault planes derived from mapped surfaces in the 3D seismic sub-volume (see Fig. 7.3) show no preferred orientation or indicate a more-or-less uniform distribution (i.e., has almost equal number of faults striking in all direction) from one stratigraphic layer to another in the study area (Fig. 7.13). The dip direction of the fault planes shows a geometrical consistency at the six mapped horizons. In all cases the faults show a dominant NW – SE and less dominant NE – SW dip direction (Fig. 7.13). Fault spacing ranges between 150 – 1000 m with vertical throws in the range 10 – 64 m (Average: 28.6 m) and heave between 25 – 202 m (Average: 76 m). In general, the vertical throw of the faults is observed to increase with depth from the Hordaland Group top bounding surface down to the Eocene – Oligocene boundary especially for the listric faults. This however reverses in the Mid Eocene where the throw decreases downwards to the Top Rogaland Group. The fault throws and fault orientation do not show any obvious correlation. The faults are also observed to displace a prominent high amplitude peak reflection which have been reported by recent studies (e.g., Olobayo, 2014; Wrona et al., 2017b) to represent the Opal-A/CT boundary, with fault trace heights and length ranging between 120 – 800 m and 200 – 3350 m, respectively. There was also no observed correlation between fault length and fault orientation. Comprehensive fault displacement analysis of the polygonal faults within this interval have been documented by Wrona et al. (2017a).

7.4.3.2 Fault planform pattern

Horizon maps in Fig. 7.13 indicate polygonal planform organization for faults observed in cross-section with no preferred fault orientation (strike) as shown by the rose diagrams. Their characteristic polygonal planform-pattern serves as the most important diagnostic

property which differentiates them from other known layer-bound fault systems such as differential compaction faults or crestal collapse faults (Cartwright, 2011). Although the faults are polygonal in planform, their planform pattern and spacing varies considerably both vertically and laterally in layer-parallel slices (e.g., horizon map, depth slices, horizon slices) through the studied interval. The observed variation in pattern and spacing of the PFS is controlled by factors such as compaction & shrinkage rate of their mud-dominated host sediments, tier layer thickness variation, local stress state and lithological variations (Lonergan et al., 1998; Cartwright, 2011). The vertical and lateral variation in planform geometry within the studied polygonal fault tier is illustrated using the geometry of a set of horizontal variance attribute slices in Fig. 7.15. The variance slices are taken at different depths through the tier and reveals considerable changes in fault organization (pattern and spacing) and connectivity.

Cartwright (2011) suggested a concept for determining the degree of system maturity to be applied to the analysis of polygonal fault systems. In line with this concept, PFS are divided into mature (or closed multi-sided network) and immature (or open multi-sided network) systems based on their observed planform pattern and connectivity of fault traces. In immature systems, fault networks are characterized by a low number of hard-linked intersections, or simply put the fault networks have a higher proportion of unrestricted lateral fault tips, while the mature systems have a higher proportion of linked intersections or have no unrestricted lateral tips (Fig. 7.15 – 7.17, Cartwright, 2011). Connectivity is thus considered as the main property which defines the maturity of a fault network, with low connectivity patterns resulting from the inability of the faults to continue growing or propagate to link up to form well connected fault networks (Lonergan et al., 1998). The connectivity of fault traces observed in depth slices through the polygonal fault tiers indicate they vary from mature to immature fault networks as you move downward from the Top Hordaland Group Unconformity to the Top Rogaland Group (Fig. 7.15 – 7.17).

The planform geometry and pattern of the polygonal faults studied here have been sub-divided into three (3) main types using the end member classification by Lonergan et al. (1998) which are based on the fault trace orientation, spacing, intersection angle and connectivity (i.e., linkage). The observed planform geometrical types are as follows: (a) classical hexagonal polygonal pattern consisting of individual near-hexagonal connected fault traces (Fig. 7.16), (b) curved polygonal pattern consisting mainly of curved faults traces with variable intersection angles (Fig. 7.16), and (c) irregular (well-connected & clustered) polygonal pattern (Fig. 7.17). The irregular polygonal pattern forms the most predominant through the studied interval with the fault patterns varying in type and dimension both laterally (over distances of a few kilometres) and vertically at different stratigraphic level. Faults with curved polygonal pattern are generally observed to have longer fault trace length while the irregular to well-connected faults exhibit shorter fault lengths. In general, the observed variability in their planform pattern is dependent on the density of faulting and number of fault intersections.
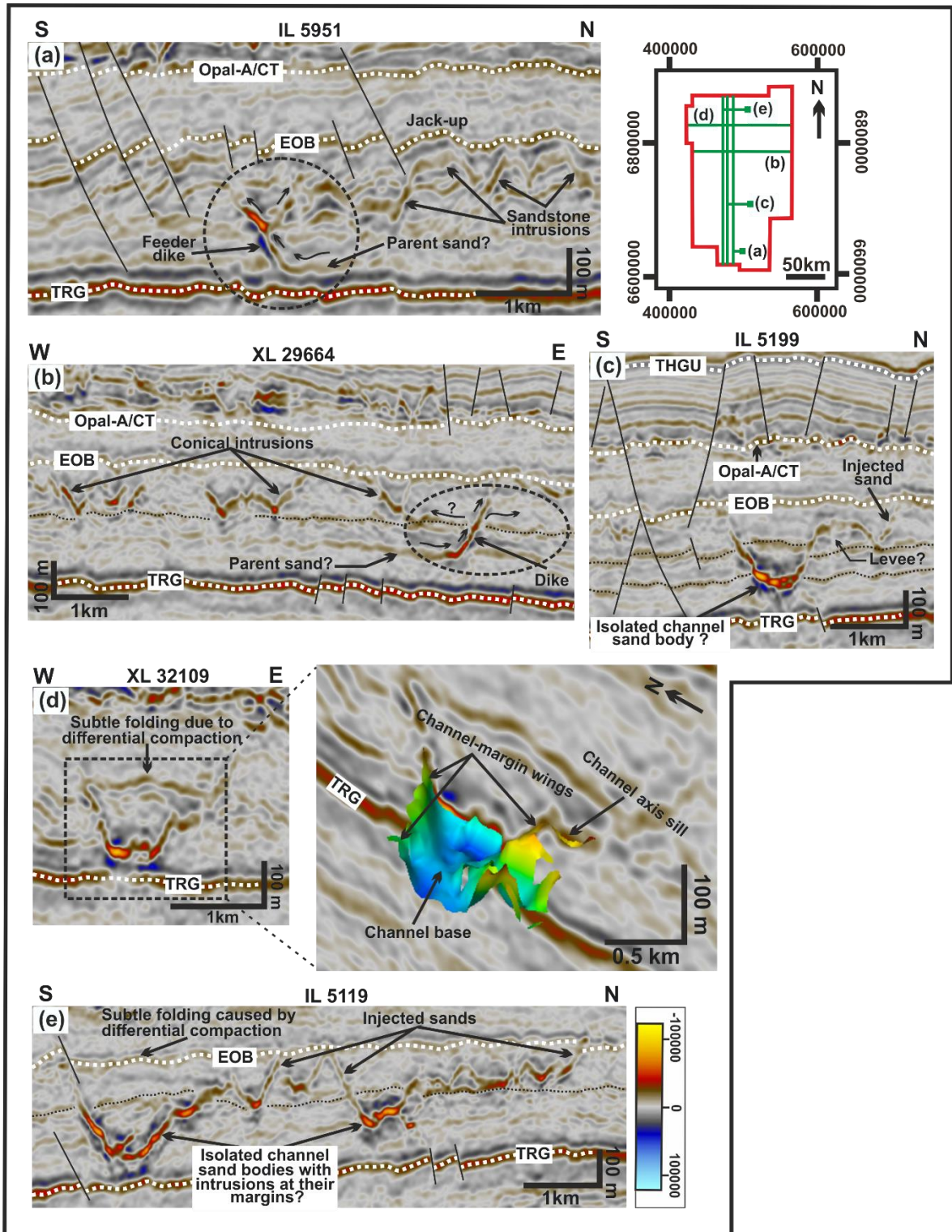
Fig. 7.11: (a) & (b): Potential feeder dikes attached to potential parent sands which are suggested to have sourced the overlying Middle - Upper Eocene conical sandstone intrusions. (c) to (e): Isolated channel-shaped high-amplitude anomalies with remobilized margins in the Lower - Middle Eocene. The anomalies appear to be laterally connected and are thought to have also sourced some of the isolated anomalies in the Eocene interval. Associated with the anomalies is the subtle folding of the overburden above them, which results from differential compaction. THGU = Top Hordaland Group Unconformity; EOB = Eocene – Oligocene Boundary; TRG = Top Rogaland Group. Seismic data courtesy of CGG.
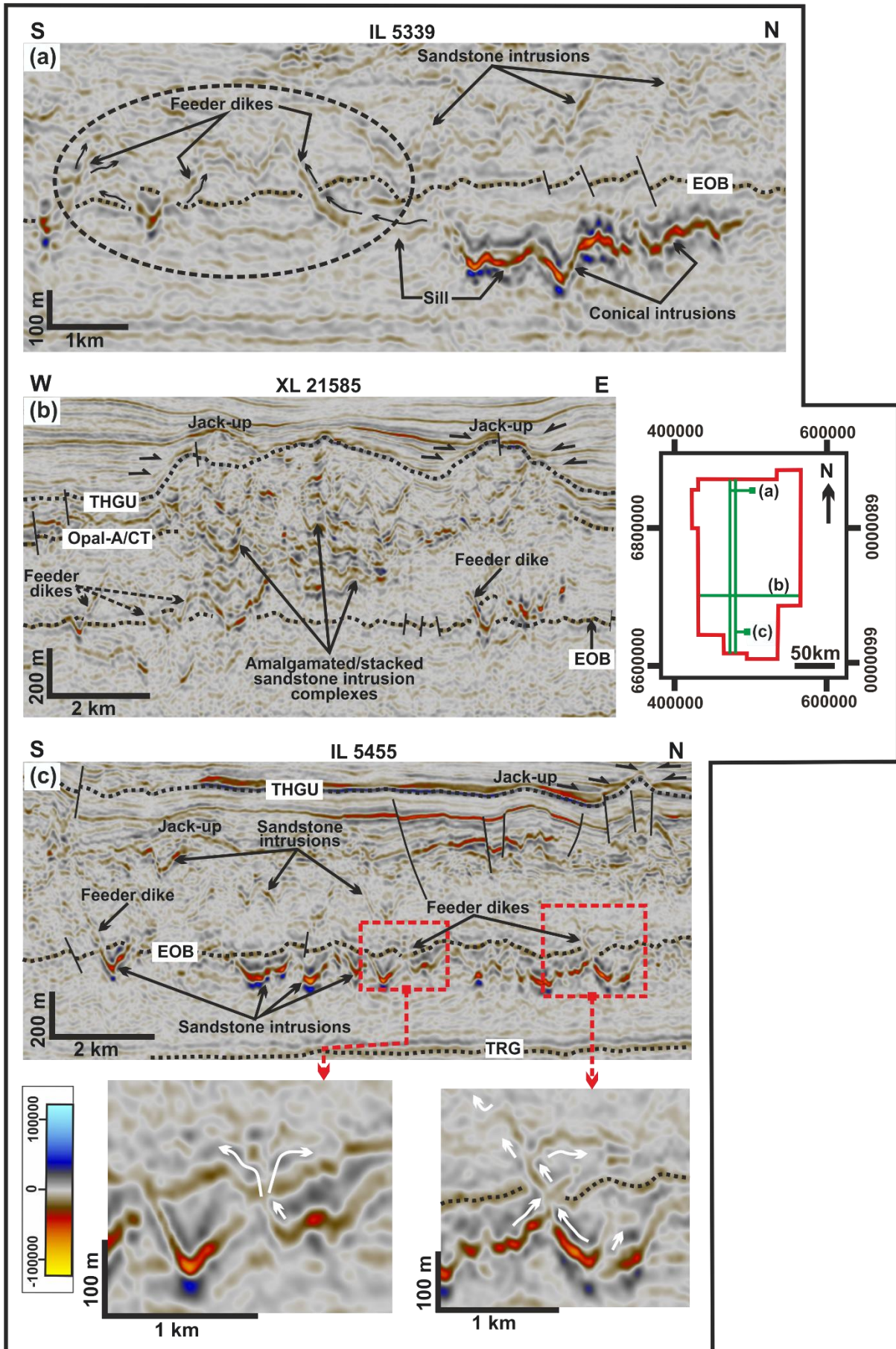
Fig. 7.12: (a) Potential feeder dikes emanating from the Upper Eocene interval into the Oligocene, which are suggested to have sourced some of the Lower Oligocene sandstone intrusions in the western part of the study area. (b) V-shaped discordant amplitude anomalies with apices within the Upper Eocene and long discordant limbs extending across the EOB into the Lower Oligocene. These are also considered as potential feeders which sourced Oligocene sand intrusions above them. (c) Potential feeder dikes characterized by funnel-shaped geometry, which are considered as evidence for an Upper Eocene source sands for some Lower Oligocene intrusions. THGU = Top Hordaland Group Unconformity; EOB = Eocene – Oligocene Boundary; TRG = Top Rogaland Group. Seismic data courtesy of CGG.

7.4.4 Quantitative geometrical characterization of the interaction between sandstone intrusions and polygonal faults

The sandstone intrusions within the Hordaland Group (Eocene – Mid Miocene) interval have been classified into four (4) intrusion types based on the nature of their interactions with polygonal fault planes in the vicinity of the intrusions.

- **Class-A sandstone intrusions:** refer to those with at least one limb/wing of the intrusion either fully or partially intruded along polygonal fault planes (Fig. 7.18). In this case, the intrusions follow the fault plane only over part of its length or are fully intruded along the fault plane. This may imply that the fault planes may have been exploited as preferential fluid flow pathway when favourable, leading to the injection of fluidized sands along its planes.

- **Class-B sandstone intrusions:** refers to the sandstone intrusions with limbs or marginal wings terminating abruptly against polygonal fault planes (Fig. 7.19). Simply put, the outward propagation of the intrusion limb/wing is blocked or halted by a fault plane in at least one direction. This sort of interaction between both features is often observed for the bowl-shaped or wing-like sandstone intrusions and characterized by an abrupt intersection between the fault plane and the intrusion in seismic cross section (Fig. 7.19).

- **Class-C sandstone intrusions:** this class of intrusions are observed to crosscut polygonal fault planes and vice versa. Both features crosscut each other randomly in different direction with no part of the intrusion following the path along a fault plane (Fig. 7.20). Here, the intrusions are crosscut by polygonal faults but appear to be geometrically unaffected.

- **Class-D sandstone intrusions:** this class of intrusions are characterized by irregular to complex geometries (e.g., zigzag) which are a result of modification by polygonal faults. The resultant geometries (Fig. 7.21) of the intrusions are dependent on the number of polygonal faults that intersect or crosscut them at different angles and direction which implies that the intrusions are geometrically affected by the faults. In some cases, part of the polygonal fault is partially intruded (Fig. 7.21).
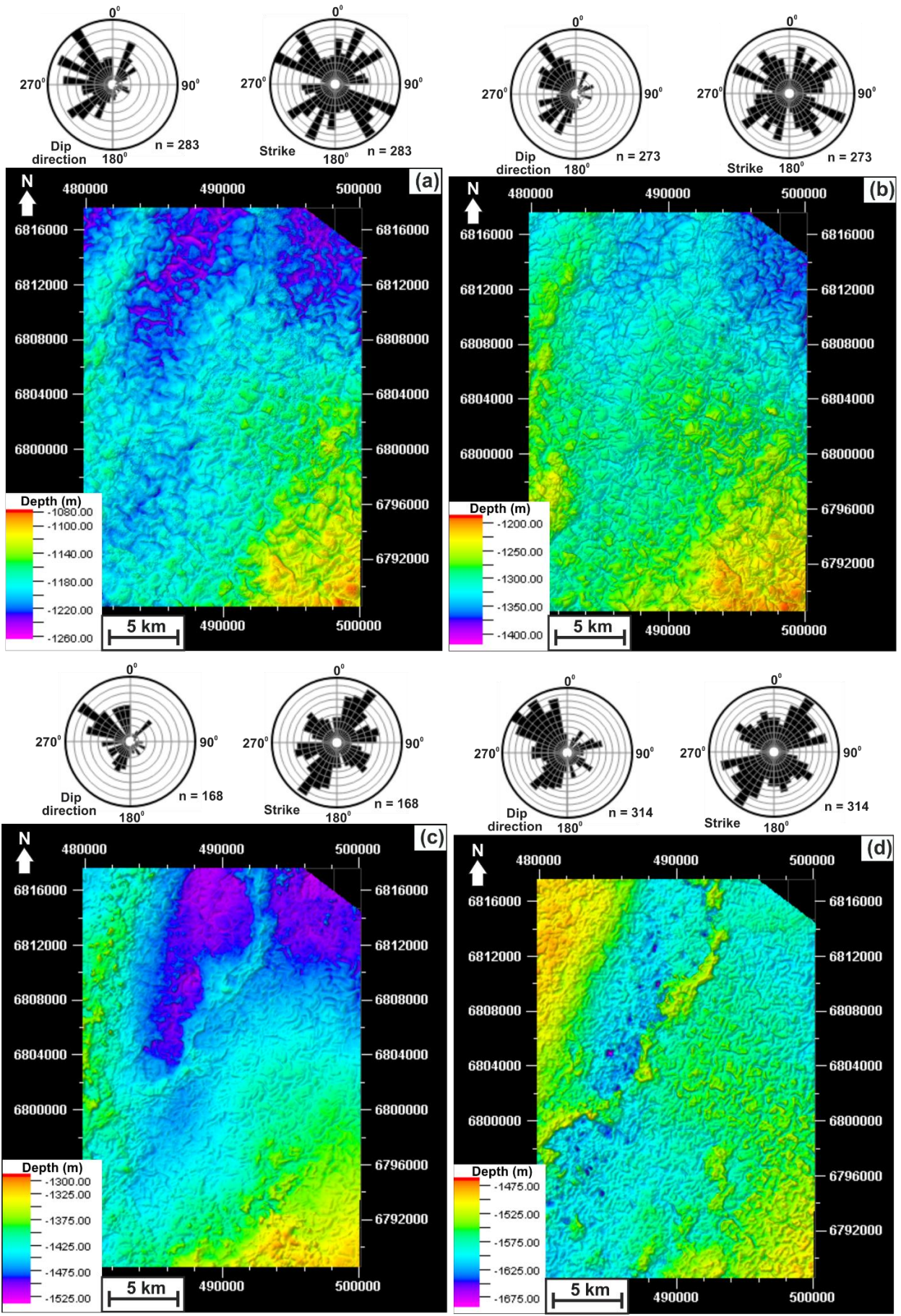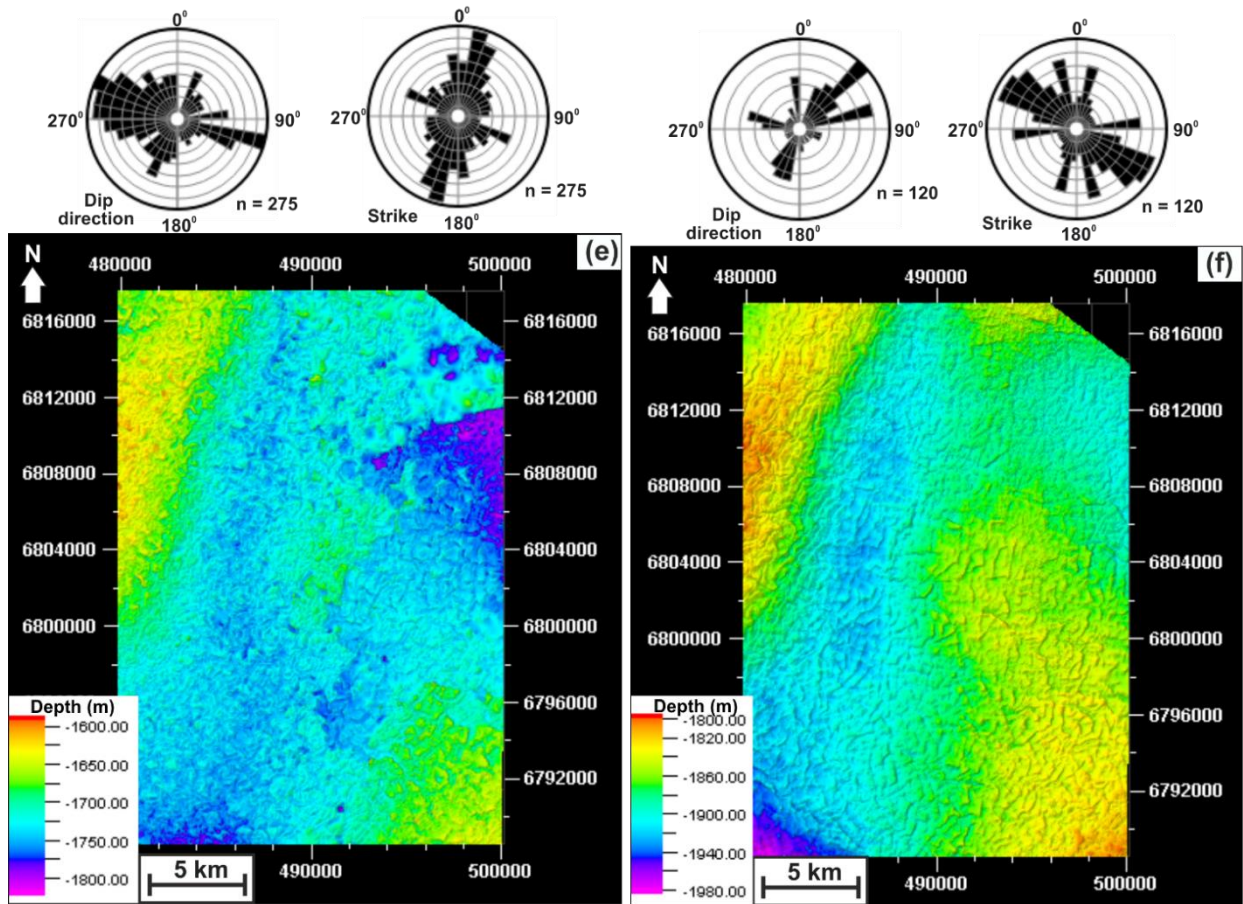
Fig. 7.13: Structural maps of stratigraphic horizon (1 to 6) showing polygonal fault systems at different depth levels within the studied interval. The position of the mapped horizons is shown in Fig. 7.3. (a) = 1: Top Hordaland Group Unconformity (THGU); (b) = 2: Below THGU; (c) = 3: Opal-A/CT boundary; (d) = 4: Eocene – Oligocene boundary (EOB); (e) = 5: Mid Eocene; and (f) = 6: Top Rogaland Group (TRG). Length-weighted rose diagrams were extracted for each mapped horizon, and this shows a dominant NW – SE dip direction and uniform distribution of fault strikes. The location of the sub-volume used is highlighted by the red bold line in Fig. 7.1b. Seismic data courtesy of CGG.

Fig. 7.14: Isochron maps between mapped stratigraphic horizons in Fig. 7.13, with example seismic section (A – B) across the faults in map view. (a) Thickness map between THGU (1) and Below THGU (2); (b) Thickness map between Below THGU (2) and Opal-A/CT (3); (c) Thickness map between Opal-A/CT (3) and EOB (4); (d) Thickness map between EOB (4) and Mid-Eocene (5). The example section across the faults on the isochron maps show the variation in fault throw and fault spacing. Seismic data courtesy of CGG.
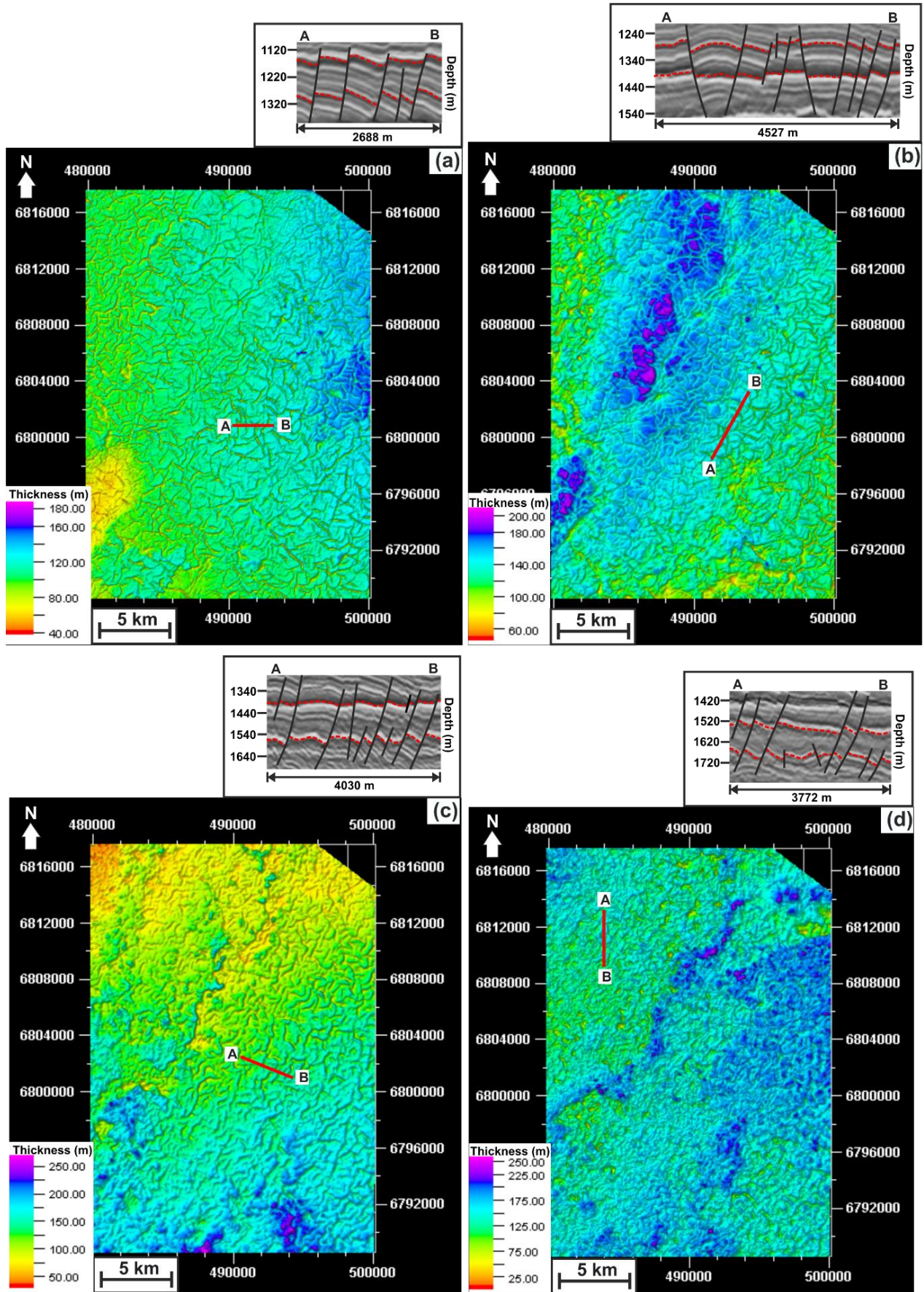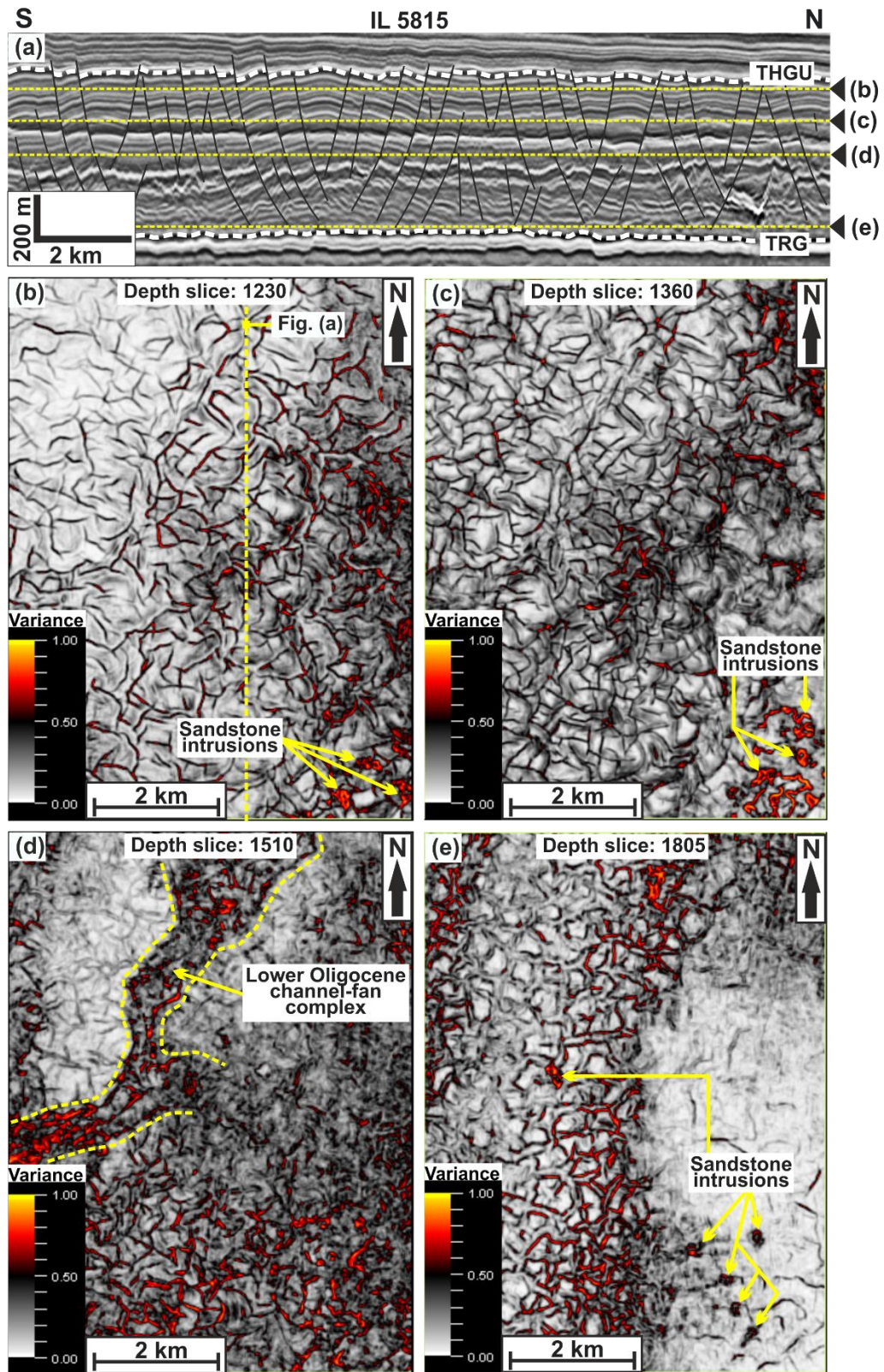
Fig. 7.15: (a) Seismic line showing the depth interval of four variance slices through the polygonal fault tier. Location of seismic line and cropped volume used is shown in Fig. 7.1. (b) to (e): show the four variance slices taken at the position of the arrows in (a). The single fault tier show variation in fault pattern, spacing and connectivity with depth. THGU = Top Hordaland Group Unconformity; TRG = Top Rogaland Group. Seismic data courtesy of CGG.

We have identified and measured the geometrical characteristics of 110 Class-A and 140 Class-C intrusions. For both cases, the dips of the intruded fault planes for Class-A intrusion and the dips of the cross-cutting fault planes for Class-C intrusions were also measured. In the measurement of Class-A intrusions, only intrusions which were fully intruded along fault planes were considered because it was easier to characterize the nature of interaction between a given intrusion and its intruded polygonal fault plane compared to when they are partially intruded. The limbs of Class-A intrusions display dips ranging from 8° to 39° with a mean dip value of 22°± 1 (Table 7.2), while Class-C intrusions display dips ranging from 5° to 39° with a mean dip value of 18°. The mean dip values for Class-A intrusions are clearly higher compared to the mean value of Class-C intrusions which is expected because intrusions intruded along polygonal fault planes would exhibit higher dip values, and fault analysis from previous studies indicate that the average dips of the polygonal faults lie between ca. 20 - 50° (Wrona et al., 2017a). Further relationship between sandstone intrusions and polygonal faults is expressed in other measured geometrical parameters such as the height (H1, H2) of discordant limbs/wings and their associated top diameter (Td) (see Fig. 7.3). For instance, Class-C intrusions have shorter limb height and wider top diameter compared to Class-A intrusions which is because their limbs are more gently dipping as opposed to Class-A intrusions with steeply dipping limbs/wings intruded along polygonal fault planes. This variation in height may also suggest that the upward injection of Class-A intrusions were mechanically more efficient along polygonal fault planes than along hydraulic fractures created by seal failure when the threshold (i.e., fracture gradient) of the sealing mudstones was exceeded.

To further understand why some fault planes are intruded while others are not, measurement of strike and dips for polygonal faults intruded by fluidized sand (Class-A) and those crosscut by intrusions (Class-C) were taken. The depth of intrusion below the Top Hordaland Group Unconformity (THGU) for intrusions which exploited polygonal fault planes, was also measured to ascertain whether the dilatational behaviour and preferential flow of fluidized sand along faults is related to the depth of injection. We observe that Class-A intrusions are not preferentially intruded along a defined orientation of polygonal faults which is consistent with the observation that polygonal faults in the studied interval indicate a uniform distribution of polygonal fault strikes, with no dominant direction (see Fig. 7.13). This is also applicable to polygonal faults crosscut by sand intrusions and fault planes interpreted as arresting sandstone intrusion which are not often observed. Class-A intrusions injected along fault planes are more commonly observed at shallower stratigraphic level below the THGU which forms the paleo-seafloor at the time of sand injection. Their injection along faults may be attributed to the observation that the polygonal faults are steepest at shallower intervals but becomes gently listric at deeper depths. Hence, it may have been easier for the injected sands to dilate fault planes at shallower depths due to lower overburden confining stress when overpressure exceeds the fracture gradient of their sealing host mudstones (Bureau et al., 2013). However, both Class-

A & C intrusions are observed to preferentially occur at shallow intrusion depths, with about 80% of both intrusion type intruded within 200 – 500 m depth below the paleo-seafloor (THGU). Therefore, the depth of injection/intrusion may represent an important factor, which influences interaction between polygonal faults and sandstone intrusions because increase in depth should lead to an increase in compaction and cementation. In general, there seem to be no direct correlation between the depth of emplacement of the intrusions and the dip angles of their discordant limbs, which means that vertical stress does not control the resultant geometry of the intrusions but may be controlled by factors such as the host rock strength, viscosity of the sand and fluid mixture, and the rate of fracture propagation (Shoulders et al., 2007).

A potential source of uncertainty in the measured parameters may be associated with the measured intrusion height (H1, H2) and top diameter (Td) which may be related to the detectability of reflection termination associated with the tips of the intrusion. This may affect measurements in cases where the vertical extent of the tips of the intrusion cannot be clearly resolved especially for Class-A intrusions injected along polygonal fault planes.
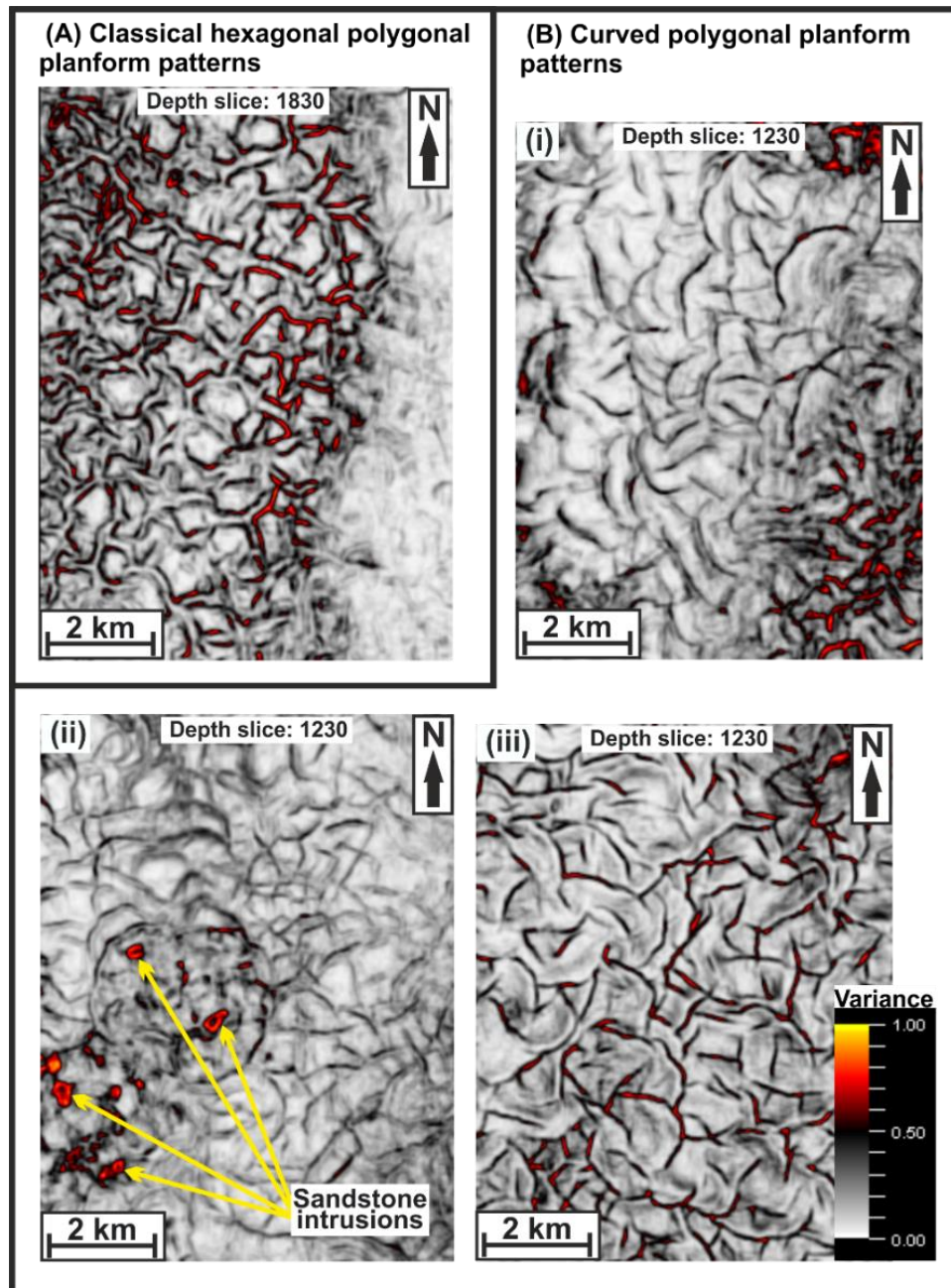
Fig. 7.16: Illustration of end-member classification of polygonal planform pattern within the studied interval based on the end-member classification by Lonergan et al. (1998). Pattern illustrated using variance slices at different depths. (A) Classical hexagonal polygonal pattern. (B) Curved planform pattern showing varying degree of curvature in (i) to (iii). See description in text. Seismic data courtesy of CGG.
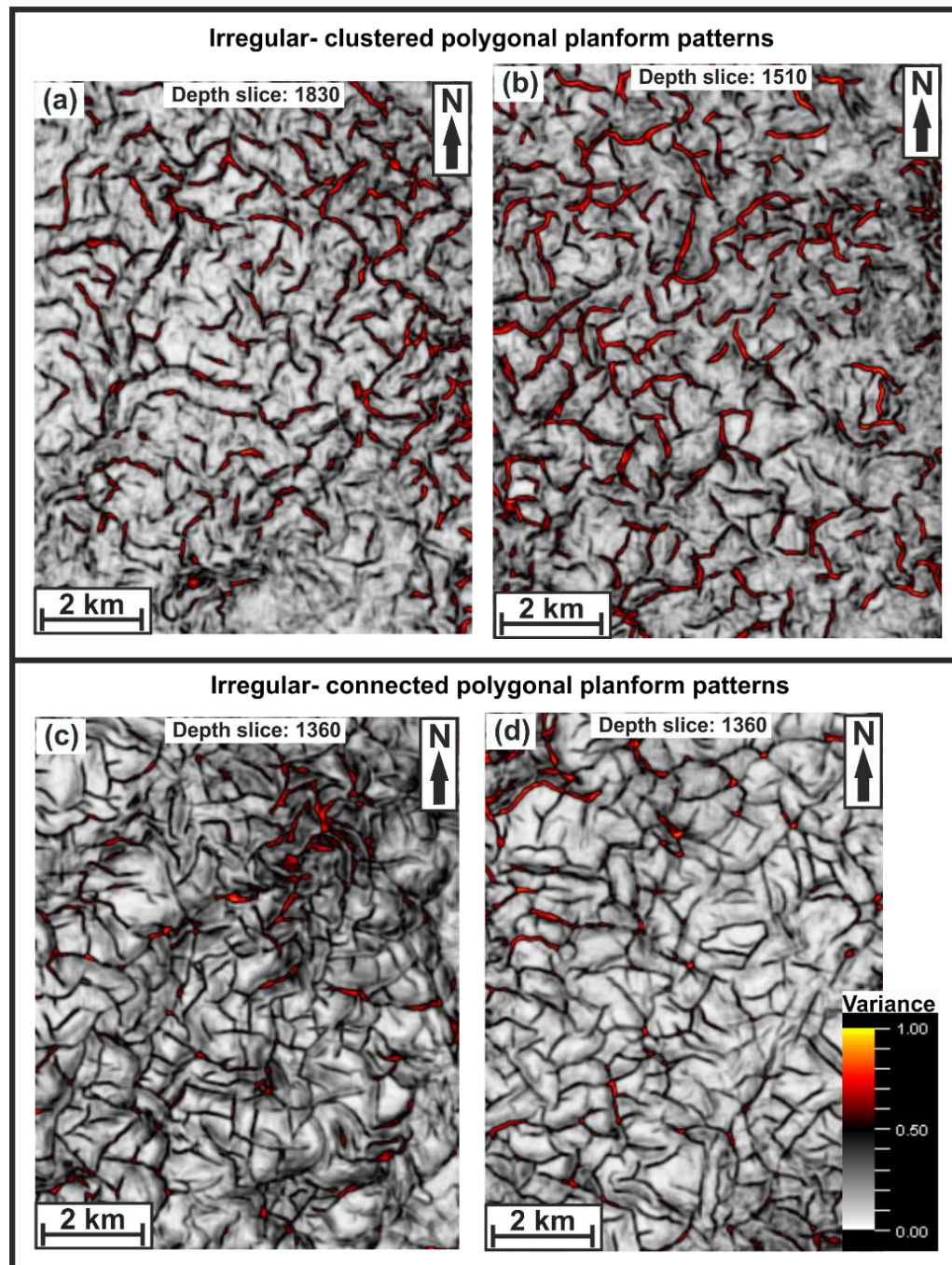
Fig. 7.17: Illustration of end-member classification of planform pattern within the studied interval based on the end-member classification by Lonergan et al. (1998). Pattern illustrated using variance slices at different depth intervals. (a) & (b): Irregular-clustered polygonal planform pattern. (c) & (d): Irregular-clustered polygonal planform pattern. See description in text. Seismic data courtesy of CGG.
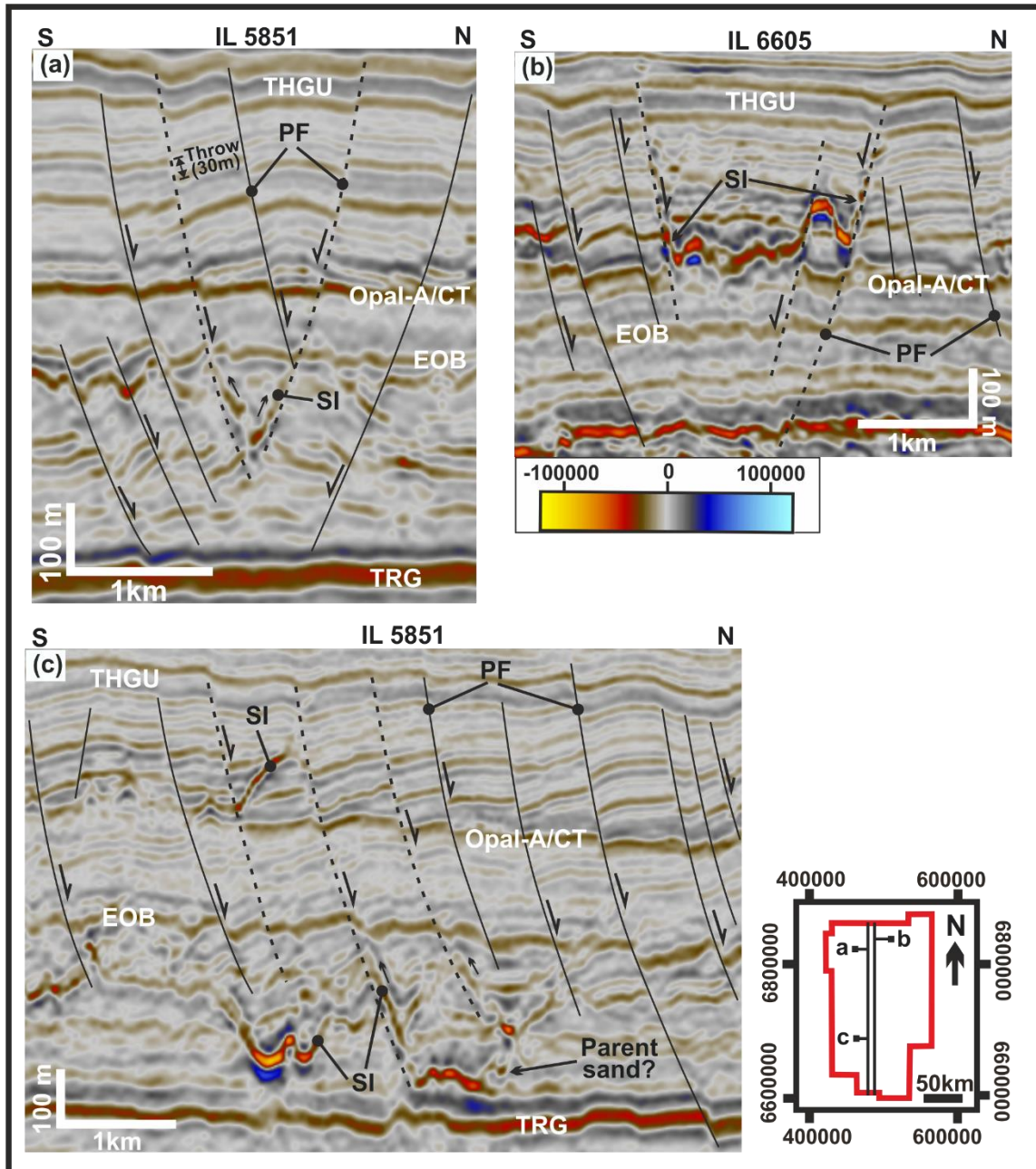
Fig. 7.18: Seismic example of Class-A sandstone intrusions intruded along polygonal fault planes. (a) Example of an Eocene conical sandstone intrusion with both limbs injected along polygonal fault planes (with throw of c. 30 m). (b) Example of wing-like sandstone intrusion with wings following polygonal fault planes in the Oligocene succession. The margins of the intrusion are flanked by two opposite dipping polygonal faults. (c) Example of conical shaped intrusion injected along fault plane with the potential parent sand suggested to be at the downward tip of the polygonal fault. THGU = Top Hordaland Group Unconformity; EOB = Eocene – Oligocene Boundary; TRG = Top Rogaland Group; SI = Sandstone intrusion; PF = Polygonal fault. Seismic data courtesy of CGG.
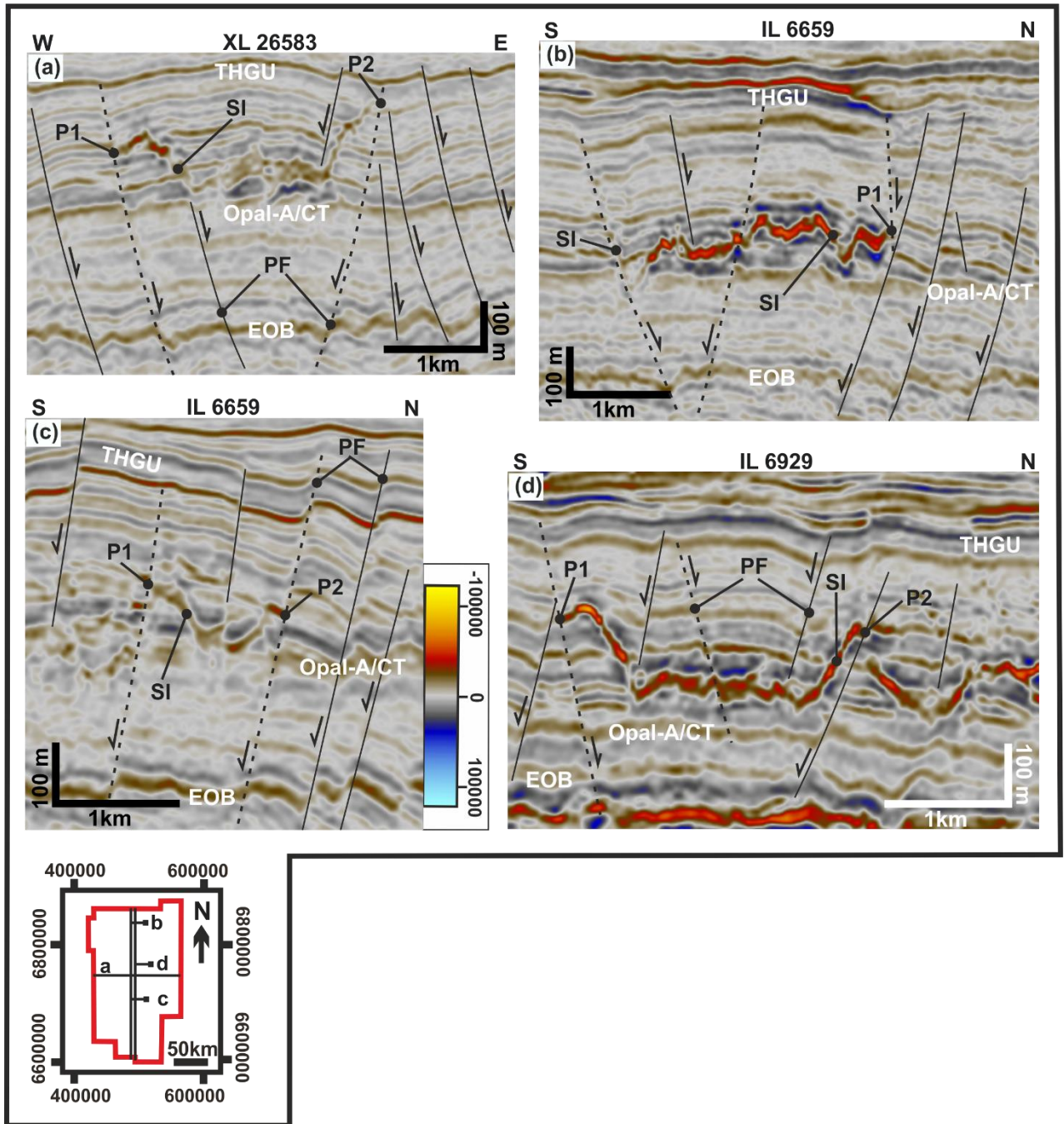
Fig. 7.19: Seismic expression of Class-B sandstone intrusions halted or arrested by polygonal fault planes. (a) Example of a wing-like sandstone intrusion with both wings arrested by polygonal faults at points P1 & P2. (b) Seismic line showing an irregular-shaped intrusion with one flank halted by a fault at point P1. (c) U-shaped sandstone intrusion arrested at both margins by polygonal faults at points P1 & P2. (d) Representative seismic line showing wing-like intrusions with the lateral propagation of its wings halted by polygonal faults at point P1 & P2. THGU = Top Hordaland Group Unconformity; EOB = Eocene – Oligocene Boundary; SI = Sandstone intrusion; PF = Polygonal fault; P1/P2 = Arrested points. Seismic data courtesy of CGG.
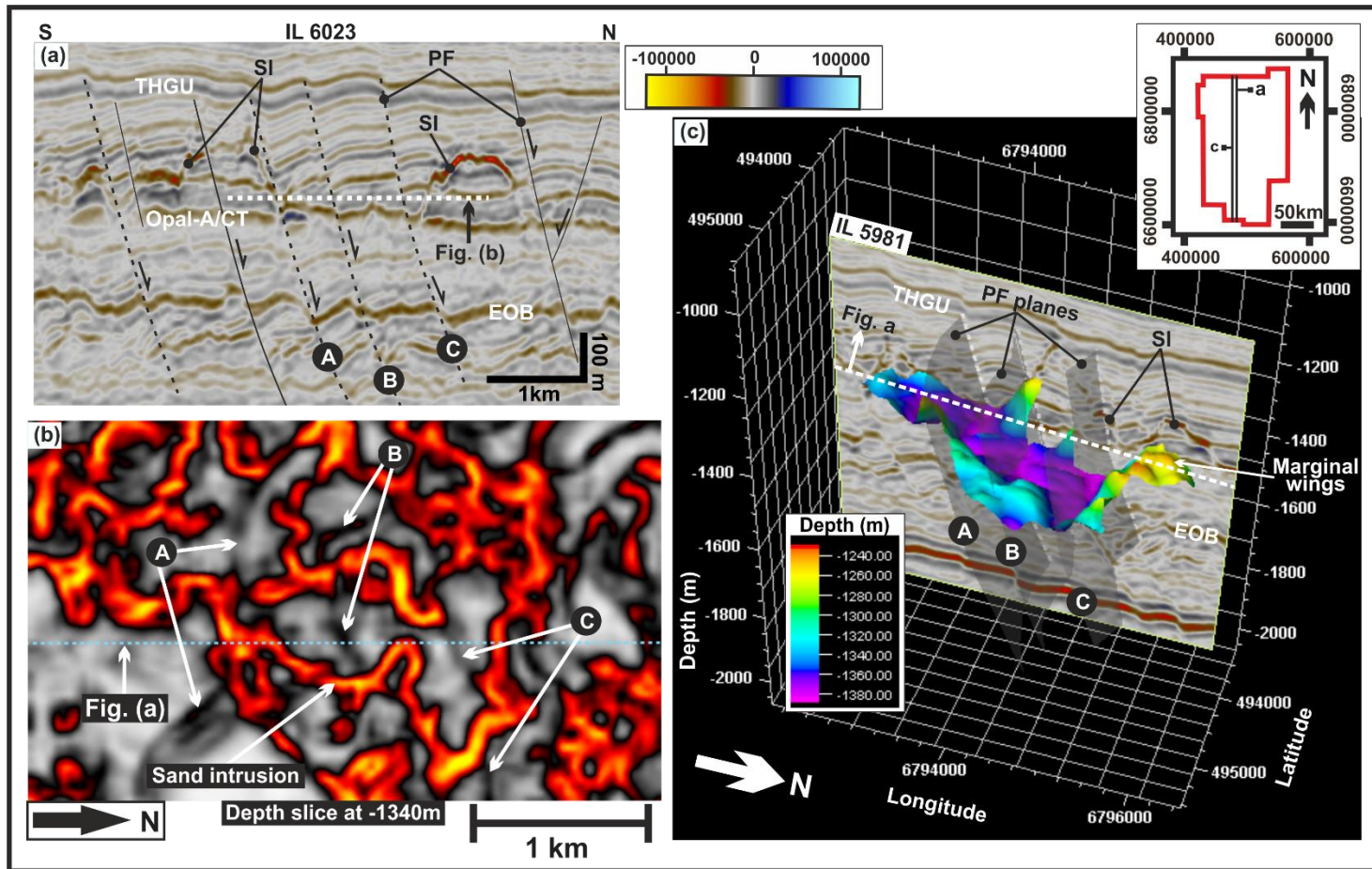
Fig. 7.20: Seismic expression of Class-C sandstone intrusions which are crosscut by polygonal faults but appear not to be geometrically affected by the fault planes. (a) Seismic example of wing-like sandstone intrusion crosscut by fault planes with no obvious modification to its cross-sectional geometry. (b) Variance time slice (at 1340 m) showing the three polygonal faults (FA, FB, & FC) which crosscut the intrusion in planform. The intrusion is characterized by an irregular-shaped amplitude anomaly in map view with the seismic line in Fig. (a) highlighted by a light-blue dotted line. (c) 3D seismic view of the mapped intrusion showing the interaction between the intrusion and the crosscutting faults. THGU = Top Hordaland Group Unconformity; EOB = Eocene – Oligocene Boundary; SI = Sandstone intrusion; PF = Polygonal fault. Seismic data courtesy of CGG.
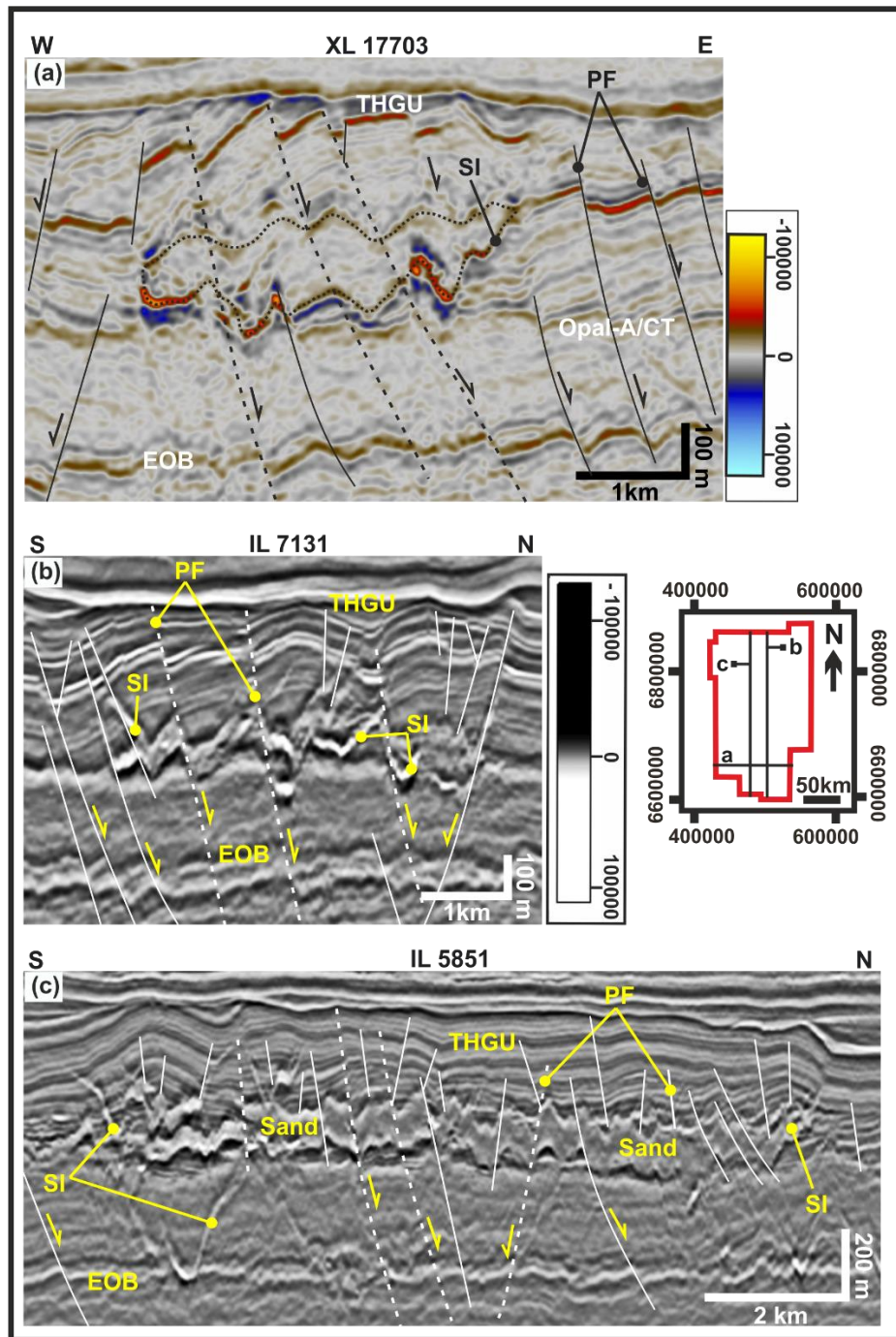
Fig. 7.21: Seismic expression of Class-D sandstone intrusions which are crosscut by polygonal faults and are geometrically affected by the faults, resulting to their irregular to complex-shaped cross-sectional geometries. (a) Example of an irregular-shaped (zig-zag) sandstone intrusion crosscut by rotated fault planes giving rise to its irregular geometry. The outline of the sand intrusion is highlighted by a dotted dark line. (b) & (c) are two good example of sandstone intrusions with their geometry highly modified by their crosscutting polygonal fault. THGU = Top Hordaland Group Unconformity; EOB = Eocene – Oligocene Boundary; SI = Sandstone intrusion; PF = Polygonal fault. Seismic data courtesy of CGG.

Table 7.2: Summary of measured geometrical parameters for Class-A and Class-C sandstone intrusions and dips of their associated polygonal faults.

Intrusion Class	Number of data	Geometrical parameters of intrusions					Polygonal fault dip (°)
		Limb true dip (°)	Height H (m)	Top diameter Td (m)	Base diameter Bd (m)	Intrusion depth below MMU (m)	
Class-A	110	8 – 39	39 – 267	128 – 4911	63 – 4402	150 – 813	13 – 39
	Average	22	127	1180	456	421	26
Class-C	140	5 – 39	33 – 289	395 – 3105	64 – 1989	126 – 856	16 – 49
	Average	18	115	1431	636	354	32

	0 - 5	6 - 10	11 - 15	16 - 20	21 - 25	26 - 30	31 - 35	37 - 40
Frequency (Class C)	0	9	39	44	35	9	2	2
Frequency (Class A)	0	3	20	26	25	28	7	1

7.5 Discussion

7.5.1 Influence of polygonal faults on the resultant geometries of sand intrusions

To understand or establish whether intrusion geometries are controlled by polygonal faults, it is necessary to first answer two important questions: (i) Does polygonal faulting pre-date the emplacement of sand intrusions? and (ii) Was polygonal faulting reactivated post-intrusion or during intrusion?. The polygonal faults within the studied interval are generally truncated by the Top Hordaland Group Unconformity (Fig. 7.2), implying they would have formed prior to or during the submarine erosion of the unconformity surface which formed the paleo-seafloor at that time. Conversely, sandstone intrusions emplaced below the unconformity resulted to the forced folding and/or jack-up of the unconformity surface resulting to a mounded topography with onlap of younger sediments onto the mounds. This means sand injection would have occurred after the erosion of the unconformity (i.e., in the Mid/Late Miocene) else the

mounded topography created by sand intrusion would have been eroded. Therefore, it is evident that the polygonal faults pre-date the formation of sand intrusions. However, there is a likelihood for subsequent reactivation of polygonal faulting during and post-intrusion. Wrona et al. (2017a) estimated that polygonal faulting within the Hordaland Group in the study area commenced during the Eocene – Early Oligocene, with subsequent reactivation in the Late Oligocene - Mid Miocene. Based on this, it is likely that hydraulic fracturing of mudstones due to differential compaction and high pore fluid pressure would have led to the simultaneous propagation of some polygonal faults and sand injection when the fracture gradient of the mudstone was exceeded, which may support the idea of possible polygonal fault reactivation between the Late Oligocene – Mid/Late Miocene during injection.

The observation of four different kind of interaction between PFS and sandstone intrusions (Fig. 7.18 – 7.21), indicate that no clear or definite correlation exist between both features. This therefore overrules the possibility of clearly suggesting that the resultant geometries of the intrusions are controlled by polygonal faults. The control of intrusion geometry by PFS may seem to be the case for Class-A intrusions, but because the intrusions do no exhibit polygonal planform geometry, we suggest that the faults were simply exploited where favourable, especially if they terminate close to or above an overpressured depositional sand body. An alternative idea is that when overpressure exceeded the fracture gradient of the sealing mudstones, polygonal faults were propagated alongside fractures into the overpressured sands which led to rapid injection of fluidized sand along the fault planes. For Class-B intrusions (Fig. 7.19), the apparent halting of their limbs/wings by polygonal fault plane is a clear indication that the faults pre-dates the intrusion and do not have control on the resultant geometry of the intrusions but may only determine the extent of propagation of their upper tips. Class-C intrusion (Fig. 7.20) which are crosscut by PFS but show little or no sign of modification to their geometries are considered to have formed under significant pore fluid pressure which would have allowed the intrusions to surmount the mechanical heterogeneity represented by the fault planes (Bureau et al., 2013). Another possible explanation for the cross-cutting relationship would be if some of the PFS are propagated simultaneously or about the same time as the sand intrusions due to hydrofracturing of their fine-grained host mudstones. On the other hand, Class-D intrusions which are also intersected by polygonal faults show irregular to complex modification to the parent depositional sand with injection at their margins (Fig. 7.21). The parent sands are compartmentalized and exhibit zigzag or shark-tooth-like geometries which imply that polygonal faulting would have modified the sands prior to injection, and as such pre-dates the injection. However, since Class-D intrusions tend to have numerous polygonal faults intersecting them in opposite direction, with varying magnitude of displacement, this may imply that some of the faults may have formed post-intrusion during subsequent reactivation of faulting (Fig. 7.21c).

In all cases, the polygonal faults appear to have formed prior to sand injection and it is evident that in general (except for the Class-D intrusion), the intrusions achieve their distinct geometries regardless of their co-existence with polygonal faults, which supports the previous

argument by Huuse & Mickelson (2004) and Huuse et al. (2004) on the potential control of polygonal faults on the timing and geometry of sand intrusions.

7.5.2 Origin & mechanisms controlling sand remobilization and injection

The spatial relationship between the amplitude anomalies interpreted here as sand intrusions and their associated forced folds and/or jack-up of the overburden indicate that the amplitude anomalies represent injected or intruded materials. We therefore discuss the potential mechanisms controlling sand remobilization and injection into their host mudstone strata in the study area. Three main critical factors are considered to control the magnitude of the large-scale sand remobilization and injection observed in the study area. These factors include: (i) parent source-sand distribution, (ii) overpressure development and fluid availability, and (iii) potential internal or external trigger event which results to seal breach, sand fluidization and upward injection of fluidized sand (Lonergan et al., 2000; Jolly & Lonergan, 2002; Huuse & Mickelson, 2004; Szarawarska et al., 2010; Hermanrud et al., 2019).

Source sand distribution

The presence of a suitable parent source-sand forms the most critical factor for sand remobilization and injection in the study area. The deposition of parent sand within the Eocene – Mid Miocene have been highlighted in the previous sections, with the parent sands interpreted as deep-water sand-rich fans and isolated channels for the Eocene sand intrusions (Fig. 7.7, 7.8 & 7.11), and gravity flow sands associated with channel-lobe complexes for the Oligocene sand intrusions. In addition, some Oligocene intrusions are also proposed to be sourced by the Middle Eocene fan sands in the west and southern parts of the study area based on available evidence on seismic cross-section for potential feeder dikes (Fig. 7.12). The different expression of the parent sands is believed to have resulted in the variation and complexity of intrusion styles observed on seismic cross section. The deposition and spatial distribution of the parent sands are however constrained by both local and regional depositional, and tectonic events in the study area. Generally, the known Eocene and Oligocene parent sands in the northern North Sea were deposited from the uplifted basin margins and they are well-documented by Jones et al. (2003) and Rundberg & Eidvin (2005) respectively.

Overpressure development and fluid availability

For sand remobilization and injection to occur, significant overpressure within an effectively sealed parent sand is required, with substantial volume of fluid (internal or externally sourced) to transport the sand in a fluidized flow. Previous studies of sandstone intrusions in the North Sea and adjourning basins by authors (e.g. Osborne & Swarbrick, 1997; Swarbrick & Osborne,

1998; Jolly & Lonergan, 2002; Moss et al., 2003; Huuse & Mickelson, 2004; Davies et al., 2006; Huuse et al., 2007; Szarawarska et al., 2010; Andresen et al., 2019; Hermanrud et al., 2019; and Andresen, 2020) have suggested several mechanisms which accounts for overpressure generation within sealed parents sand bodies which primes them for remobilization and injection. Overpressure associated with Cenozoic sediments in the northern North Sea is estimated to be up to 10 MPa or 1450 psi (Evans et al., 2003; Marcussen et al., 2009). Here we suggest that load-induced overpressuring (i.e., differential loading) and lateral transfer of pressure; disequilibrium compaction due to rapid loading, burial, and effective sealing; influx of upward and laterally migrating thermogenic fluid (i.e., gas & pore water); and fluid release from diagenetic clay reactions (i.e., Smectite to Illite and Opal-A to Opal-CT conversion) as the main overpressure generating mechanisms in the study area.

Both differential loading and lateral transfer of pressure occur due to uneven rapid sediment loading which results to a lateral pressure gradient within sandstone layers (Hermanrud et al., 2019). This is usually associated with inclined sand layers and results to lateral pressure bleed-off (Andresen et al., 2019: see their Fig. 1b; Hermanrud et al., 2019). Here the direction of lateral pressure transfer is downdip towards the basin centre, from the basin margins characterized by the thickest succession. This is comparable to that documented by Andresen (2020) for the Norwegian – Danish Basin. Differential loading and lateral transfer of pressure are largely dependent on sedimentation/burial rate of sediments within the basin. The net sedimentation rate of sediments as estimated by Olobayo (2014) gives the maximum sedimentation rate for the Eocene and Oligocene sediments to be 24.10 mMa^{-1} and 70.53 mMa^{-1} respectively. The maximum sediment thickness for both intervals range from c. 600 – 700 m at the basin margin and decreases towards the basin centre. Based on the above two estimates, and the observation that sand intrusions are predominant where both intervals are the thickest, and at the toe of slope, we suggest that differential loading and lateral transfer of pressure may have played a significant role in facilitating subsurface remobilization and injection.

Disequilibrium compaction which results from rapid loading and burial of fine-grained sediments during deposition is widely documented to result to the formation of anomalously high pore fluid pressure in basins worldwide (Osborne & Swarbrick, 1997). This increase in pore pressure occurs because pore fluids are only partially expelled (i.e., fluid expulsion is impeded) due to rapid burial and compaction (Ramdhan & Goulty, 2011). The increase in pressure is further enhanced by increase in vertical stress with increased burial. The observation that the sandstone intrusions are injected into very thick, low permeable mudstone host strata (Hordaland Group: Horda & Lark Fm) indicate that the parent sands were effectively sealed, and thus provides a suitable condition for overpressure development by disequilibrium compaction. Hence, it is right to propose that disequilibrium compaction played a significant role in facilitating the remobilization and injection of the Eocene – Oligocene deep-water sandstones.

Lateral and vertical fluid drainage during early compaction dewatering of buried sediments can lead to the influx of fluid into sealed depositional sandstones from their surrounding low-permeable mudstone host strata (Lonergan et al., 2000; Jolly & Lonergan, 2002; Davies et al., 2006). The above come from the understanding that unconsolidated deep-water mud-dominated sediments are usually characterized by substantial reduction in porosity (i.e., from 75% to 40%) due to early compaction (Wrona et al., 2017b). Evidence for early-stage dewatering due to compaction is represented by the pervasive occurrence of polygonal faults within the studied interval because their propagation has been linked to compaction-related volumetric contraction due to sediment loading (see Cartwright & Dewhurst, 1998; Cartwright, 2011). Upward migration of thermogenic fluid into sealed sand bodies from deeper and overpressured sources is often suggested to be capable of generating high pore fluid pressure within the sands. For example, the migration of hydrocarbon into sealed source sands have been suggested to generate high pore fluid pressure within the sands due to buoyancy effect (Jolly & Lonergan, 2002; Molyneux et al., 2002; Duranti & Hurst, 2004; Andresen et al., 2009). This is an effective mechanism which may have driven the large-scale and widespread occurrence of sand intrusions in the North Sea, with migration suggested to have occurred both laterally and vertically along rotated and tilted fault blocks associated with Mesozoic (Cretaceous & Jurassic) rift structures (Huuse & Mickelson, 2004). The above may be supported by the fact that the intrusions studied here occur within hydrocarbon mature area of the northern North Sea Basin which hosts major oil and gas discoveries (e.g., Snorre, Gullfaks, Troll, Huldra and Oseberg) within deep-water Jurassic sandstone reservoirs. Further evidence is provided by: (i) studies (e.g., Conford, 1998; Johnson & Fisher, 1998) which have shown from basin modelling that hydrocarbon generation in the northern North Sea occurred during the Early Cretaceous to Neogene from the Jurassic Draupe Formation which forms the age equivalent of the Kimmeridge Clay Formation in the UK sector of the North Sea, and (ii) the observation of vertical acoustic distorted zones and gas chimneys above Mesozoic rift faults. A good example for the latter is the Oseberg discovery well (30/6-2) where oil/gas show were described in cores and cuttings at shallower depth between 1945 – 1955 m which lies within the Balder Formation of Early Eocene age, with the main target reservoir in the Jurassic Brent Group. The presence of hydrocarbon at this interval is indicated on seismic as vertical zones of acoustic masking through the Jurassic to Eocene interval. Therefore, compaction-related fluid drainage and thermogenic fluid migration are both considered as potentially important mechanisms for overpressure development in the depositional parent sands for the intrusions studied here.

Fluid release associated with the diagenetic clay reaction which converts Smectite to Illite (i.e., Smectite Illitization) have been suggested as a potential contributing factor for overpressure build-up in the subsurface (e.g., Osborne & Swarbrick, 1997; Clausen et al., 1999; Moss et al., 2003; Marcussen et al., 2009). The diagenetic reaction involves the dissolution of Smectite which becomes increasingly unstable at greater depth and temperature (c. $60 - 80°C$), followed by the precipitation of Illite and quartz. This in turn leads to the release of up to 30% of the

pore and crystalline water within the mudstones (Marcussen et al., 2009). Experimental modelling of compaction in mudstones by Mondol et al. (2008) have shown that mudstone lithologies are compacted normally with increased burial, but the presence of substantial amount of smectite will result to less compaction, which in turn generates abnormal pore pressure within the sediments. Clay fraction analysis, using X-ray diffraction (XRD) technique, of mudstone samples obtained from drill cuttings from selected wells in the northern North Sea indicate that the Hordaland Group mudstones contain substantial amount of Smectite and Illite in the range 40 − 80% and 10 − 40% respectively (see Thyberg et al., 2000: their Fig. 4; Marcussen et al., 2009: their Table 2 & Fig. 9).This implies that the Hordaland Group consists of smectite-rich sediments, and its high smectite-content may have partly contributed to overpressure development within sealed depositional sand bodies during burial diagenesis.

The thermo-chemical, diagenetic phase transformation of biogenic silica (Opal A) to Cristobalite & Tridymite (Opal CT) in bio-siliceous opal-rich mudstones has also been suggested by some authors (Davies et al., 2006; Davies & Clark, 2006; Ireland et al., 2011; Wrona et al., 2017b) as a potential source of overpressure build-up in mud-dominated successions. This is based on the understanding from recent analysis of borehole data, that this process, which is a dehydration reaction causes rapid sediment compaction, reduction in porosity (order of 15 -20%), and expulsion of pore water in bio-siliceous sediments which results to the build-up of high pore pressure (Davies & Cartwright, 2002; Davies et al., 2006; Cartwright, 2011; Ireland et al., 2011; Wrona et al., 2017b). The rate of pore fluid expulsion associated with the diagenetic reaction have been linked to the rate of diagenetic front advancement, as well as the degree of porosity reduction at the diagenetic boundary (Davies et al., 2006). For excess pore pressure to develop within the system, the rate at which fluid is expelled needs to outpace the rate at which it can easily seep out of the system (Davies et al., 2006). Many known large-scale occurrences of sandstone intrusions occur in sedimentary succession that are or were comprised of bio-siliceous sediments (Davies et al., 2006). Sediments within the Hordaland Group (Eocene – Mid Miocene) consist of mainly bio-siliceous mudstones, and evidence for regional silica phase transformation and the presence of biogenic silica within the Hordaland Group in the northern North Sea have been documented by Rundberg (1991), Thyberg et al. (1999), and Wrona et al. (2017b) from well data in the study area. The observation of a high amplitude reflection (Fig. 7.2 & 7.9) which represents the boundary or transition between Opal-A-rich and Opal-CT-rich sediments within the Oligocene interval may serve as evidence that diagenetic clay reaction contributed to overpressure build-up within sealed parent sand bodies. This is further supported by the observation of Oligocene intrusions directly above or on the Opal-A/CT boundary (Fig. 7.9).

Triggering mechanisms

An externally or internally driven trigger mechanism is required to trigger seal failure in the sealing host strata, causing rapid remobilization and injection of overpressured sand into their sealing mudstones. Seal failure usually occur by hydraulic fracturing when the threshold of the seal is exceeded, as pore fluid pressure exceeds the fracture gradient of the seal (Jolly & Lonergan, 2002; Hurst et al., 2011). The sandstone intrusions in the northern North Sea cannot be directly linked to any external trigger mechanisms (e.g., bolide or meteoric impact and earthquake-induced liquefaction) but is suggested to be largely driven by internal depositional and post-depositional processes (e.g., depositional loading & large-scale differential compaction) over time. Therefore, it is possible that some of the mechanisms which contributed to overpressure build-up will over time trigger sand remobilization (Andresen & Clausen, 2014).

The extensive polygonal faulting of the Paleogene mudstones which hosts sandstone intrusions in the North Sea have led to studies (e.g., Lonergan & Cartwright, 1999; Gras & Cartwright, 2002; Molyneux et al., 2002) suggesting the co-existence of both features may imply that polygonal faults could trigger and control the location and resultant geometry of sandstone intrusions. For example, Lonergan & Cartwright (1999) suggested that the remobilization of the Alba Field deep-water channel system during early burial may have been triggered by polygonal faulting, with intrusions exploiting polygonal fault planes (Andresen, 2020). However, Huuse et al., (2004) have argued that polygonal faults only partially influence the distribution and geometries of sandstone intrusions, and the intrusions tend to achieve their variable complex geometries irrespective of the presence of polygonal faults. Because there is no definite type of interaction (see Fig. 7.18 – 7.21) observed between both features in this study, it is best to suggest that it is unlikely for polygonal faulting to have triggered sand injection, but were instead exploited as injection pathway were necessary, and would have also contributed to seal failure needed to initiate sand injection. This is further supported by the fact that sand intrusions in the study area do not exhibit polygonal geometries in map view but are characterized by circular to sub-circular and elongate to irregular map view geometries (Fig. 7.5).

Differential compaction across the interface between sealed depositional sand bodies and their sealing mudstones have also been prescribed as a trigger for sand injection (e.g., Jackson, 2007; Jackson et al., 2011; Safronova et al., 2012). Differential compaction will lead to stress rotations which in turn results to: (i) overburden folding above the sands, and (ii) faulting and fracturing above and at the margins of the sands (Cosgrove & Hillier, 2000; Huuse et al., 2004; Dusseault, 2011, Jackson et al., 2011). Davies (2005) have demonstrated that the thermo-chemical diagenetic conversion of Opal-A to Opal-CT can result to large-scale differential compaction and subsidence in sedimentary basins which can trigger sand remobilization. Therefore, differential compaction is suggested as an important trigger based on: (i) the presence of differential compaction folds above the concordant base of the wing-like intrusions (Fig. 7.9b, 7.11d &

7.19a), (ii) the spatial correspondence of the upper tip of wing-like intrusions with the edges of the compaction folds (Fig. 7.6b & 7.9e), and (iii) the presence of some short intra—boundary faults observed at the Eocene – Oligocene boundary and the Top Hordaland Group Unconformity which we have interpreted as differential compaction faults (Fig. 7.9a, 7.11a & 7.12a).

One final idea to consider is that although the trigger for the large-scale sand injection in the study area will be based on contribution from various factors, it is also possible to consider that sand injection may have simply occurred when the threshold of their host mudstones was exceeded. This will mean that sand remobilization occurred when the high pore fluid pressure (P_f) within the parent sands exceeded the fracture gradient of the sealing mudstones, leading to hydraulic fracturing (i.e., seal failure) and upward injection of fluidized sand along hydraulic fractures and faults in the host sediments. In essence, the mechanisms discussed to have led to overpressure build-up may have over time triggered sand remobilization and injection (Andresen & Clausen, 2014).

7.5.3 Mechanisms for polygonal fault formation

Although several mechanisms have been proposed by various authors for the formation of polygonal faults, the exact mechanism which control their development is still debated due to lack of consensus on which mechanism works best for all documented cases of polygonal faults worldwide. The inherent weakness in some of the previously suggested mechanisms is that they failed to account for the cause of the initial failure condition which leads to the localization and propagation of shear fractures in the host sediments (Cartwright, 2011). Polygonal faulting is generally thought to be linked to early-stage dewatering and compaction of fine-grained sediments in mud-dominated succession (see Cartwright & Lonergan, 1996; Cartwright & Dewhurst, 1998; Cartwright et al., 2003; Cartwright, 2011). In general, the formation of polygonal faults is consequent on sediment mineralogy and grain size distribution, which is why they form predominantly in fine-grained mud-dominated sediments in deep-water marine environments. Based on previously documented mechanisms for polygonal fault formation by authors, we suggest that polygonal faults formed in the study area may have been triggered or facilitated by a combination of processes over time, with reactivation of faulting occurring at subsequent times. The two most compelling mechanisms which may have led to the formation of the polygonal faults studied here include:

a) Syneresis of fine-grained sediments caused by spontaneous volumetric contraction due to gravity-driven mechanical compaction (i.e., gravitational loading) (Cartwright & Lonergan, 1996; Cartwright & Dewhurst, 1998; Dewhurst et al., 1999; Goulty, 2001). This results to shrinkage and expulsion of pore fluids in mudstones. It has been documented that syneresis is likely to occur during early burial of mud-dominated sediments which are smectite-rich (Cartwright & Dewhurst, 1998). The high smectite content of the Hordaland Group mudstones (see Thyberg

et al., 2000: their Fig. 4; Marcussen et al., 2009: their Table 2 & Fig. 9) in the northern North Sea may therefore support the suggestion that syneresis contributed to polygonal faulting. Although this mechanism may be sufficient to explain the early initiation of polygonal faulting, their formation within fine-grained mud-dominated sediments and their volumetric contraction; it is also unlikely that syneresis will occur at greater burial depth (Goulty & Swarbrick, 2005; Goulty, 2008; Cartwright, 2011)

b) Diagenetically-induced shear failure of mudstones resulting from differential compaction and overpressure build-up due to sediment loading and burial by overlying sediments (e.g., Cartwright, 1994; Huuse et al., 2010; Cartwright, 2011). Seismic cross-sections show that large part of the area covered by PFS indicate the tier is affected by diagenesis of biogenic silica (Fig. 7.2b & 7.3a). The diagenetic phase transformation of silica (Opal-A to Opal-CT) have recently been documented to facilitate the formation of polygonal faults, and the rapid reduction in porosity and expulsion of pore water associated with the diagenetic reaction results to the build-up of overpressure and large-scale differential compaction which facilitates polygonal faulting (Davies et al., 2006, 2009; Davies & Clark, 2006; Davies & Ireland, 2011). Over the area affected by polygonal faults, the high amplitude reflection which corresponds to the boundary between Opal-A-rich and Opal-CT-rich sediments occur at a position near the middle of the fault tier. At the basin margins, particularly in the western part of the study area, the relationship between the diagenetic boundary and polygonal faults is less clear due to the high level of sediment remobilization observed at the basin margins. The spatial correlation of the laterally extensive PFS with the inferred lateral extent of the diagenetic boundary may point to some connection between the diagenetic reaction and the formation of polygonal fault systems. Similar connection has been suggested by Cartwright (2011) and Davies & Ireland (2011) for the Voring and Møre Basin, respectively. Since the diagenetic phase transformation of Opal-A to Opal-CT involves a dissolution-precipitation reaction which leads to changes in physical properties of sediments, diagenetically-induced shear failure is suggested as the main driver for polygonal faulting because Shin et al. (2008) have argued that grain dissolution can result to substantial contraction-driven shear failure in fine grained sediments. Therefore, diagenetic processes satisfy the requirement for the large-scale formation of polygonal fault systems observed in the study area.

7.5.4 Implications of sand intrusions and PFS in the studied interval

The distribution of large-scale sandstone intrusions and polygonal fault over a wide area in the northern North Sea have significant implications for fluid flow. Both features have been recognized to act as long-lived fluid conduit after their initial formation by allowing migration of fluid into shallower intervals (Lonergan et al., 2000; Mazzini et al., 2003; Huuse & Mickelson, 2004; Shoulders et al., 2007; Huuse et al., 2010). Since the formation of sand intrusions require injection of fluidized sands through dilated fractures and fault (i.e., feeder conduits) when hydrofracturing occur, some of these fractures are filled with sand after the cessation of fluid

flow, forming complex network of intrusions which may be resolved or may not be resolvable due to their sub-seismic resolution. This complex network of intrusions is formed within the Eocene – mid Miocene and are likely to enhance vertical connectivity but may negatively impact the seal integrity of their host mudstones. The enhanced connectivity may in turn lead to an increase in geothermal gradient which could have direct implications for diagenetic processes and sand reservoir cementation within the interval (Shoulders et al., 2007). In general, sand intrusions have the potential to improve the gross permeability of otherwise low-permeable intervals into which they are injected.

In the case of polygonal faults, the fine-grained mudstones in which they form, commonly act as top seal for hydrocarbon reservoirs as well as reservoirs for carbon capture and sequestration (CCS). Their formation within fine-grained sealing mudstone by shear fracturing due to diagenesis, results to the alteration of the magnitude and anisotropy of permeability within the low-permeable mudstones, which may likely compromise seal integrity (Cartwright, 2011). Therefore, their potential impact on seal integrity needs to be considered during play fairway analysis and predictions. Polygonal faults could also play a vital role in fluid migration through low-permeable succession (Cartwright et al., 2003). Observation from seismic cross section for Class D intrusions (Fig. 7.21) indicate a geometrical modification of the intrusions offset by polygonal faults, which results to their varying irregular to complex geometries. This implies that the PFS can also result to reservoir compartmentalization of deep-water sandstones which in general may raise issues during reservoir risking and development planning.

7.5.5 Model of formation for individual intrusion classes

The proposed model for the formation of various intrusion classes is broken into three stages shown in Fig. 7.22, and these include: (i) deposition of the parent sands (Uil Sandstone Member – Lark Formation: Oligocene, and Frigg & Grid Sandstone Member – Horda Formation: Eocene) in deep-water marine setting; (ii) sealing of sands by mudstones and overpressure generation; and (iii) remobilization and injection of sandstone members into their sealing host mudstones, subsequent deposition and burial by recent sediments.

Following the deposition of the Eocene and Oligocene parent sands in the Early – Mid Eocene and Early - Mid Oligocene respectively, was the deposition of mud-dominated sediments in deep-water marine settings, which led to burial and compaction. The direction of sediment transport was both eastward and mainly westwards due to an overall increase in subsidence towards the basin centre. During burial, the sands were sealed, and fluids (i.e., pore water: free & bound) liberated by early compaction dewatering of the mudstones were forced into the sands leading to build up of high pore pressure within the parent sands (Fig. 7.22b). This was followed by the large-scale propagation of polygonal faults through the Eocene – Oligocene interval forming a polygonal fault tier. Other mechanisms such as differential loading, clay

mineral transformation (e.g., Smectite to Illite & Opal A to CT), and fluid from deeper sources further contributed to overpressure build up. Hydraulic fracturing of the mudstones triggered by differential compaction or simply overpressure due to diagenesis resulted to a differential pressure gradient across the overpressured sands which thus initiated fluid flow. Fluidized sand were then injected into the overlying mudstones along differential compaction-related faults and fractures, and along pre-existing polygonal fault planes where favourably oriented (Fig. 7.22c). Flow of fluidized sand along faults and fractures may have occurred rapidly or persisted for a while depending on the velocity and viscosity of the mobile sand and fluid mixture till the pore pressure nears the hydrostatic pressure (i.e., pressure equilibrium) and the dilated fractures closes. The injected sands formed varying intrusion geometries (Fig. 7.22c), while some may have reached the paleo-seafloor forming sand extrudites. This was followed by subsequent deposition and further burial by younger sediments.

a

Early Eocene - Middle Oligocene:
• Deposition of depositional parent sands from both eastern and western source areas.
• Burial of depositional sands

Isolated sand-rich channels and lobes

Shelf

N

Small sand-rich submarine fans

Paleocene

Paleocene

Eocene sands

Top Rogaland Group
Eocene - Oligocene Boundary
Opal-A/CT Boundary
Top Hordaland Group Unconformity
Sandstones   **Mudstones**
Upward migration and vertical drainage of fluid
Lateral fluid drainage from surrounding mudstones during early dewatering
Dewatering of overlying mudstones
Forced fluid release from Opal-A to Opal-CT & Smectite-to-illite diagenetic transformation

Middle Oligocene - Late Miocene:
– Subsequent deposition of mud-dominated sediments and sealing of source sand bodies.

– Propagation of polygonal faults due to burial and compaction-related dewatering of mudstones

– Differential compaction & overpressure development in the sources sands linked to disequilibrium compaction, differential loading, and mainly pore water derived from fluid release during early dewatering and diagenetic conversion of Opal-A to Opal-CT, with possible contribution from Smectite-to-illite transformation

b

Differential compaction

Over-pressure build-up

W

E

Lateral transfer of pressure

Near-top Oligocene

CC

Eocene (CSU-2)

Polygonal faults

CD

Grid fan (Fan-A)   Grid fan (Fan-B)

CA

CB

Paleocene - Early Eocene (CSU-1)

Frigg fan (Fan-C)

Pre - Upper Cretaceous strata

Not to scale

c **Sand remobilization & injection**

Class A: CA   Conical intrusions

Sand fan

Class B: CB

Marginal wings

Sand

Not to scale

Class C: CC

Sand

Class D: CD

Not to scale

Fig. 7.22: Schematic illustration of the three main stages leading up to the formation of sandstone intrusions and the resultant geometries derived from their interaction with the pre-existing polygonal faults within their low-permeable host mudstone succession. See text for further explanation.

7.6 Conclusion

The characterization of the interaction between sandstone intrusions and polygonal faults within the Eocene and Oligocene succession in the northern North Sea have been analysed here. The seismic expression of discordant amplitude anomalies associated with sand intrusions in the study area have been briefly described, with other aspects of the intrusion process considered (e.g., source sands, timing of emplacement, priming and trigger mechanism). Four main types of intrusions have been outlined as a function of their interaction with polygonal fault planes in the vicinity of the intrusions. These include Class-A sandstone intrusions which are intruded fully or partially along fault planes, Class-B which have the tip of their wings/limbs halted against polygonal fault planes, Class-C intrusions which crosscut polygonal fault planes, and Class-D intrusions characterized by complex cross-sectional geometry due to modification by polygonal faults. Both the intrusions and PFS show distinct dip population, but with some level of overlap (e.g., intrusion injected along polygonal planes). The polygonal fault dips show a strong depth dependence as their dip values tend to decrease with depth from the top of the fault tier as they become gently listric towards the base of the tier. However, this dip relationship to depth was not observed for the sandstone intrusions, which suggests that the stress exerted by the overburden at the time of injection do not have any direct control on intrusion geometry.

The four types of interaction observed between sandstone intrusions and polygonal fault systems within the Hordaland Group interval generally indicate the faults were formed prior to sand remobilization and injection. However, it is also likely that faulting was reactivated at the time of intrusion due to hydraulic fracturing of the host mudstones, which may explain the crosscutting relationship observed for Class-C intrusions and the complexity associated with Class-D intrusions. Because some sand intrusions are intruded along fault planes, it seems evident that polygonal faults and fault intersections were exploited as feeder systems during sand injection. The presence of large-scale sandstone intrusion within the studied interval would have improved the vertical permeability of the interval, which in turn degrades the seal integrity of their host mudstones. In addition, the presence of polygonal faults and injection of sand along faults will also affect seal integrity as the faults would have acted as feeder conduits, and in turn also form seal-bypass systems. Finally, the analysis of the geometrical parameters measured for both features indicate that the varying simple to complex geometries associated with the intrusions in the study area is not dependent on polygonal faults, but the faults would have aided seal failure.

Acknowledgements

References

AHMADI, Z.M., SAWYERS, M., KENYAN-ROBERTS, S., STANWORHT, C.W., KUGLER, K.A., KRISTENSEN, J. & FUGELLI, E.M.G. 2003. Palaeocene. In: *The Millennium Atlas: Petroleum geology of the central and northern North Sea* (Ed. by D. Evans, C. Graham, A. Armour & P. Bathurst). *The Geological Society of London, London,* 235–259.

ALREFAEE, H.A., GOSH, S. & ABDEL-FATTAH, M.I. 2018. 3D seismic characterization of the polygonal fault systems and its impact on fluid flow migration: An example from the Northern Carnarvon Basin, Australia. Journal of Petroleum Science and Engineering, https://doi.org/10.1016/j.petrol.2018.04.009.

ANDRESEN, K.J., CLAUSEN, O.R., HUUSE, M. 2009. A giant (5.3×10^7 m^3) middle Miocene (c. 15 Ma) sediment mound (M1) above the Siri Canyon, Norwegian–Danish Basin: origin and significance. Marine and Petroleum Geology 26, 1640–1655.

ANDRESEN, K.J., HEILMANN-CLAUSEN, C., CLAUSEN, O.R. & FRIIS, H. 2019. Deposition or remobilization of the enigmatic Hefring Member sand, eastern North Sea – A multidisciplinary approach. *Marine and Petroleum Geology*, https://doi.org/10.1016/j.marpetgeo.2019.06.001.

ANDRESEN, K.J. & CLAUSEN, O.R. 2014. An integrated subsurface analysis of clastic remobilization and injection; a case study from the Oligocene succession of the eastern North Sea. *Basin Research*, 26, 641–674, https://doi.org/10.1111/bre.12060.

ANDRESEN, K.J. 2020. The Norwegian–Danish Basin: a dynamic setting for subsurface sand remobilization – established concepts on distribution and controlling factors. *Geological Society, London, Special Publications*, https://doi.org/10.1144/sp493-2018-026.

ANELL, I., THYBO, H. & RASMUSSEN, E. 2012. A synthesis of Cenozoic sedimentation in the North Sea. *Basin Research*, 24, 154–179, https://doi.org/10.1111/j.1365-2117.2011.00517.x.

BADLEY, M.E., PRICE, J.D., RAMBECH DAHL, C. & AGDESTEIN, T. 1988. The structural evolution of the northern Viking Graben and its bearing upon extensional modes of basin formation. *Journal of the Geological Society*, 145, 455–472, https://doi.org/10.1144/gsjgs.145.3.0455.

BERNDT, C., JACOBS, C., EVANS, A., GAY, A., ELLIOTT, G., LONG, D. & HITCHEN, K. 2012. Kilometre-scale polygonal seabed depressions in the Hatton Basin, NE Atlantic Ocean: Constraints on the origin of polygonal faulting. Marine Geology, https://doi.org/10.1016/j.margeo.2012.09.013.

BREKKE, H., SJULSTAD, H.I., MAGNUS, C. & WILLIAMS, R.W. 2001. Sedimentary environments offshore Norway - an overview. Norwegian Petroleum Society Special Publications, https://doi.org/10.1016/S0928-8937(01)80006-0.

BRIEDIS, N. A, BERGSLIEN, D., HJELLBAKK, A, HILL, R.E. & MOIR, G.J. 2007. Recognition Criteria, Significance to Field Performance, and Reservoir Modelling of Sand Injections in the Balder Field, North Sea. *Sand injectites: Implications for hydrocarbon exploration and production*, 91–102, https://doi.org/-.

BUREAU, D., MOURGUES, R., CARTWRIGHT, J., FOSCHI, M. & ABDELMALAK, M.M. 2013. Characterisation of interactions between a pre-existing polygonal fault system and sandstone intrusions and the determination of paleo-stresses in the Faroe-Shetland basin. *Journal of Structural Geology*, 46, 186–199, https://doi.org/10.1016/j.jsg.2012.09.003.

CARTWRIGHT, J. 2011. Diagenetically induced shear failure of fine-grained sediments and the development of polygonal fault systems. *Marine and Petroleum Geology*, 28, 1593–1610, https://doi.org/10.1016/j.marpetgeo.2011.06.004.

CARTWRIGHT, J.A. & LONERGAN, L. 1996. Volumetric contraction during the compaction of mudrocks: A mechanism for the development of regional-scale polygonal fault systems. *Basin Research*, 8, 183–193, https://doi.org/10.1046/j.1365-2117.1996.01536.x.

CARTWRIGHT, J.A. & DEWHURST, D.N. 1998. Layer-bound compaction faults in fine-grained sediments. Bulletin of the Geological Society of America, 110, 1242–1257, https://doi.org/10.1130/0016-7606 (1998)110<1242: LBCFIF>2.3.CO; 2.

CARTWRIGHT, J., HUUSE, M. & APLIN, A. 2007. Seal bypass systems. *AAPG Bulletin*, 91, 1141–1166, https://doi.org/10.1306/04090705181.

CARTWRIGHT, J., JAMES, D. & BOLTON, A. 2003. The genesis of polygonal fault systems: a review. *Geological Society, London, Special Publications*, 216, 223–243, https://doi.org/10.1144/GSL.SP.2003.216.01.15.

CARTWRIGHT, J., JAMES, D., HUUSE, M., VETEL, W. & HURST, A. 2008. The geometry and emplacement of conical sandstone intrusions. *Journal of Structural Geology*, 30, 854–867, https://doi.org/10.1016/j.jsg.2008.03.012.

CARTWRIGHT, J.A. 1994. Episodic basin-wide hydrofracturing of over-pressured Early Cenozoic mudrock sequences in the North Sea Basin. *Marine and Petroleum Geology*, 11, 587–607, https://doi.org/10.1016/0264-8172 (94)90070-1.

CHENRAI, P. & HUUSE, M. 2020. Sand injection and polygonal faulting in the Great South Basin, New Zealand. Geological Society, London, Special Publications, https://doi.org/10.1144/sp493-2018-107.

CLAUSEN, O.R., GREGERSEN, U., MICHELSEN, O. & SØRENSEN, J.C. 1999. Factors controlling the Cenozoic sequence development in the eastern parts of the North Sea. *Journal of the Geological Society*, 156, 809–816, https://doi.org/10.1144/gsjgs.156.4.0809.

CORNFORD, C. 1998. Source rocks and hydrocarbons of the North Sea. *In*: *Petroleum Geology of the North Sea: Basic Concepts and Recent Advances: Fourth Edition*, 376–462., https://doi.org/10.1002/9781444313413.ch11.

COSGROVE, J.W. & HILLIER, R.D. 2000. Forced-fold development within Tertiary sediments of the Alba Field, UKCS: evidence of differential compaction and post-depositional sandstone remobilization. *Geological Society, London, Special Publications*, 169, 61–71, https://doi.org/10.1144/gsl.sp.2000.169.01.05.

EIDVIN, T., AND RUNDBERG, Y. 2001. Late Cainozoic stratigraphy of the Tampen area (Snorre and Visund fields) in the northern North Sea, with emphasis on the chronology of early Neogene sands. Nor. J. Geol. 81, 119–160. Available online at: http://njg.geologi.no/vol-81-90/details/17/458-458

EVANS, D., C. GRAHAM, A. ARMOUR, AND P. BATHURST. 2003. The millenium atlas: Petroleum geology of the central and northern North Sea: London, Geological Society, 389 p.

DAVIES, R.J. & CARTWRIGHT, J. 2002. A fossilized Opal A to Opal C/T transformation on the northeast Atlantic margin: Support for a significantly elevated palaeo-geothermal gradient during the Neogene. *Basin Research*, 14, 467–486, https://doi.org/10.1046/j.1365-2117.2002.00184.x.

DAVIES, R.J. 2005. Differential compaction and subsidence in sedimentary basins due to silica diagenesis: A case study. *Bulletin of the Geological Society of America*, https://doi.org/10.1130/B25769.1.

DAVIES, R.J. & CLARK, I.R. 2006. Submarine slope failure primed and triggered by silica and its diagenesis. *Basin Research*, 18, 339–350, https://doi.org/10.1111/j.1365-2117.2006.00297.x.

DAVIES, R.J., HUUSE, M., HIRST, P., CARTWRIGHT, J. & YANG, Y. 2006. Giant clastic intrusions primed by silica diagenesis. *Geology*, 34, 917–920, https://doi.org/10.1130/G22937A.1.

DAVIES, R.J., IRELAND, M.T. & CARTWRIGHT, J.A. 2009. Differential compaction due to the irregular topology of a diagenetic reaction boundary: A new mechanism for the formation of polygonal faults. Basin Research, https://doi.org/10.1111/j.1365-2117.2008.00389.x.

DAVIES, R.J. & IRELAND, M.T. 2011. Initiation and propagation of polygonal fault arrays by thermally triggered volume reduction reactions in siliceous sediment. Marine Geology, https://doi.org/10.1016/j.margeo.2011.05.005.

DEWHURST, D.N., CARTWRIGHT, J.A. & LONERGAN, L. 1999. The development of polygonal fault systems by syneresis of colloidal sediments. *Marine and Petroleum Geology*, 16, 793–810, https://doi.org/10.1016/S0264-8172 (99)00035-5.

DU, W., XIN, P., WANG, P. & SUN, Y. 2016. Multiple-track ant body attribute extraction method improved. *In*: *Atlantis-Press.Com*. 265–269., https://doi.org/10.2991/iceeg-16.2016.72.

DURANTI, D., HURST, A., BELL, C., GROVES, S. & HANSON, R. 2002. Injected and remobilized Eocene sandstones from the Alba Field, UKCS: core and wireline log characteristics. *Petroleum Geoscience*, 8, 99–107, https://doi.org/10.1144/petgeo.8.2.99.

DURANTI, D. & HURST, A. 2004. Fluidization and injection in the deep-water sandstones of the Eocene Alba Formation (UK North Sea). *Sedimentology*, 51, 503–529, https://doi.org/10.1111/j.1365-3091.2004.00634.x.

EIDVIN, T., RIIS, F. & RASMUSSEN, E.S. 2014. Oligocene to Lower Pliocene deposits of the Norwegian continental shelf, Norwegian Sea, Svalbard, Denmark and their relation to the uplift of Fennoscandia: A synthesis. *Marine and Petroleum Geology*, 56, 184–221, https://doi.org/10.1016/j.marpetgeo.2014.04.006.

FAERSETH, R.B., GABRIELSEN, R.H. & HURICH, C.A. 1995. Influence of basement in structuring of the North Sea Basin, offshore southwest Norway. *Norsk Geologisk Tidsskrift*, 75, 105–119.

FAERSETH, R.B., KNUDSEN, B.-E., LILJEDAHL, T., MIDBØE, P.S. & SØDERSTRØM, B. 1997. Oblique rifting and sequential faulting in the Jurassic development of the northern North Sea. *Journal of Structural Geology*, 19, 1285–1302, https://doi.org/10.1016/S0191-8141(97)00045-X.

FALEIDE, J.I., KYRKJEBØ, R., KJENNERUD, T., GABRIELSEN, R.H., JORDT, H., FANAVOLL, S. & BJERKE, M.D. 2002. Tectonic impact on sedimentary processes during Cenozoic evolution of the northern North Sea and surrounding areas. *Geological Society, London, Special Publications*, 196, 235–269, https://doi.org/10.1144/GSL.SP.2002.196.01.14.

FYFE, J.A., GREGERSEN, U., JORDT, H., RUNDBERG, Y., EIDVIN, T., EVANS, D., STEWART, D., HOVLAND, M. & ANDERSEN, P. 2003. Oligocene to Holocene. In: *The Millenium Atlas: Petroleum Geology of the Central and Northern North Sea* (Ed. by D. Evans, C. Graham, A.Armour & P. Bathurst. *Geological Society London, London, 279-287*

GABRIELSEN, R.H., KYRKJEBO, R., FALEIDE, J.I., FJELDSKAAR, W. & KJENNERUD, T. 2001. The Cretaceous post-rift basin configuration of the northern North Sea. *Petroleum Geoscience*, 7, 137–154, https://doi.org/10.1144/petgeo.7.2.137.

GABRIELSEN, R.H., FOERSETH, R.B., STEEL, R.J., IDIL, S. & KLOVJAN, O.S. 1990. *Architectural Styles of Basin Fill in the Northern Viking Graben*.

GALLI, P. 2000. New empirical relationships between magnitude and distance for liquefaction. Tectonophysics, https://doi.org/10.1016/S0040-1951(00)00118-9.

GAY, A. 2002. Les Marqueurs Geologiques de la Migration et de l'Expulsion des Fluids Sedimentaires sur le Plancher des Marges Passives Matures. Exemples dans le Bassin du Congo. PhD thesis. Universite ´ des Sciences et Technologies de Lille.

GAY, A., LOPEZ, M., BERNDT, C. & SÉRANNE, M. 2007. Geological controls on focused fluid flow associated with seafloor seeps in the Lower Congo Basin. Marine Geology, https://doi.org/10.1016/j.margeo.2007.06.003.

GOULTY, N.R. 2001. Polygonal fault networks in fine-grained sediments - An alternative to the syneresis mechanism. *First Break*, **19**, 69–73, https://doi.org/10.1046/j.1365-2397.2001.00137.x.

GOULTY, N.R. 2008. Geomechanics of polygonal fault systems: a review. *Petroleum Geoscience*, **14**, 389–397, https://doi.org/10.1144/1354-079308-781.

GOULTY, N.R. & SWARBRICK, R.E. 2005. Development of polygonal fault systems: A test of hypotheses. *Journal of the Geological Society*, https://doi.org/10.1144/0016-764905-004.

GRAS, R.U. AND CARTWRIGHT, J.A. 2002. Tornado Faults-The Seismic Expression of the Early Tertiary on PS-data, Chestnut Field, UK North Sea. *In 64th EAGE Conference & Exhibition*.

HENRIET, J.P., DE BATIST, M., VAN VAERENBERGH, W. & VERSCHUREN, M. 1988. Seismic facies and clay tectonic features in the southern North Sea. Bulletin of the Belgian Geological Society, 97, 457–472.

HERMANRUD, C., CHRISTENSEN, E., HAUGVALDSTAD, M., RØYNESTAD, L.M., TJENSVOLD, I.T. & WATSEND, L. 2019. Triggers of sand remobilization in deep marine deposits. *Geological Society, London, Special Publications*, https://doi.org/10.1144/sp493-2018-35.

HURST, A., CARTWRIGHT, J. & DURANTI, D. 2003. Fluidization structures produced by upward injection of sand through a sealing lithology. *Geological Society, London, Special Publications*, 216, 123–138, https://doi.org/10.1144/GSL.SP.2003.216.01.09.

HURST, A., SCOTT, A. & VIGORITO, M. 2011. Physical characteristics of sand injectites. *Earth-Science Reviews*, 106, 215–246, https://doi.org/10.1016/j.earscirev.2011.02.004.

HURST, A., MORTON, A., SCOTT, A., VIGORITO, M. & FREI, D. 2017. Heavy-mineral assemblages in sandstone intrusions: Panoche giant injection complex, California, U.S.A. Panoche. Journal of Sedimentary Research, https://doi.org/10.2110/jsr.2017.22.

HUUSE, M., CARTWRIGHT, J.A., GRAS, R. & HURST, A. 2005. Kilometre-scale sandstone intrusions in the Eocene of the Outer Moray Firth (UK North Sea): migration paths, reservoirs and potential drilling hazards. *In*: *Petroleum Geology: North-West Europe and Global Perspectives – Proceedings of the 6th Petroleum Geology Conference*. Geological Society of London, 1577–1594., https://doi.org/10.1144/0061577.

HUUSE, M., JACKSON, C.A.L., OLOBAYO, O., DMITRIEVA, E. & ANDRESEN, K.J. 2012. A sand injectite stratigraphy for the North Sea. *In*: *74th European Association of Geoscientists and Engineers Conference and Exhibition 2012 Incorporating SPE EUROPEC 2012: Responsibly Securing Natural Resources*, https://doi.org/10.3997/2214-4609.20148702.

HUUSE, M., CARTWRIGHT, J., HURST, A. & STEINSLAND, N. 2007. Seismic Characterization of Large-scale Sandstone Intrusions. *Sand injectites: Implications for hydrocarbon exploration and production: AAPG Memoir 87*, 21–35, https://doi.org/10.1306/1209847M873253.

HUUSE, M., DURANTI, D., STEINSLAND, N., GUARGENA, C.G., PRAT, P., HOLM, K., CARTWRIGHT, J.A., HURST, A. 2004. Seismic Characteristics of Large-Scale Sandstone Intrusions in the Paleogene of the South Viking Graben, UK and Norwegian North Sea. *Geological Society, London, Memoirs*, 29, 263–278, https://doi.org/10.1144/GSL.MEM.2004.029.01.25.

HUUSE, M., JACKSON, C.A.-L., VAN RENSBERGEN, P., DAVIES, R.J., FLEMINGS, P.B. & DIXON, R.J. 2010. Subsurface sediment remobilization and fluid flow in sedimentary basins: An overview. *Basin Research*, 22, 342–360, https://doi.org/10.1111/j.1365-2117.2010.00488.x.

HUUSE, M. & MICKELSON, M. 2004. Eocene sandstone intrusions in the Tampen Spur area (Norwegian North Sea Quad 34) imaged by 3D seismic data. *Marine and Petroleum Geology*, 21, 141–155, https://doi.org/10.1016/j.marpetgeo.2003.11.018.

IRELAND, M.T., DAVIES, R.J., GOULTY, N.R., CARRUTHERS, T.D. 2011. Structure of a silica diagenetic transformation zone: the Gjallar Ridge, offshore Norway. Sedimentology 58, 424-441.

JACKSON, C.A.-L. & SØMME, T.O. 2011. Borehole evidence for wing-like clastic intrusion complexes on the western Norwegian margin. *Journal of the Geological Society*, 168, 1075–1078, https://doi.org/10.1144/0016-76492011-035.

JACKSON, C.A.-L. 2007. The geometry, distribution and development of clastic injections in slope systems: seismic examples from the Upper Cretaceous Kyrre Formation, Måløy Slope, Norwegian Margin. *Sand injectites: implications for hydrocarbon exploration and production*, 37–48, https://doi.org/-.

JACKSON, C.A.L., HUUSE, M. & BARBER, G.P. 2011. Geometry of wing-like clastic intrusions adjacent to a deep-water channel complex: Implications for hydrocarbon exploration and production. *AAPG Bulletin*, 95, 559–584, https://doi.org/10.1306/09131009157.

JOHNSON, H.D. & FISHER M.J. 1998. Geological controls of North Sea hydrocarbon plays, in: K.W. Glennie, ed., Petroleum Geology of the North Sea: basic concepts and recent advances Blackwell Scientific Publications, p. 463-547.

JOLLY, R.J.H. & LONERGAN, L. 2002. Mechanisms and controls on the formation of sand intrusions. *Journal of the Geological Society*, 159, 605–617, https://doi.org/10.1144/0016-764902-025.

JONES, E., JONES, R., EBDON, C., EWEN, D., MILNER, P., PLUNKETT, J., HUDSON, G. & SLATER, P. 2003. Eocene. In: The Millennium Atlas, Petroleum Geology of the Central and Northern North Sea (Ed. by D. Evans, C. Graham, A. Armour & P. Bathurst). Geological Society London, London, 261-277

JORDT, H., THYBERG, B.I. & NØTTVEDT, A. 2000. Cenozoic evolution of the central and northern North Sea with focus on differential vertical movements of the basin floor and surrounding clastic source areas. *Geological Society, London, Special Publications*, 167, 219–243, https://doi.org/10.1144/GSL.SP.2000.167.01.09.

KNOTT, S D, BURCHELL, M T, JOLLEY, E J, and FRASER, A J, 1993. Mesozoic to Cenozoic plate reconstructions of the North Atlantic and hydrocarbon plays of the Atlantic margins. 953-974 in Petroleum Geology of Northwest Europe: Proceedings of the 4th Conference. PARKER, J R (editor). (London: The Geological Society of London.)

KNOX, R.W.O. & HOLLOWAY, S. 1992. Paleogene of the central and northern North Sea. *In*: *Lithostratigraphic Nomenclature of the UK North Sea*. 206.

LI, J., MITRA, S. & QI, J. 2020. Seismic analysis of polygonal fault systems in the Great South Basin, New Zealand. Marine and Petroleum Geology, https://doi.org/10.1016/j.marpetgeo.2019.08.052.

LONERGAN, L. & CARTWRIGHT, J.A. 1999. Polygonal faults and their influence on deep-water sandstone reservoir geometries, Alba field, United Kingdom central North Sea. *AAPG Bulletin (American Association of Petroleum Geologists)*, 83, 410–432, https://doi.org/10.1306/00AA9BBA-1730-11D7-8645000102C1865D.

LONERGAN, L., CARTWRIGHT, J. & JOLLY, R. 1998. The geometry of polygonal fault systems in Tertiary mudrocks of the North Sea. *Journal of Structural Geology*, 20, 529–548, https://doi.org/10.1016/S0191-8141 (97)00113-2.

LONERGAN, L., LEE, N., JOHNSON, H.D., CARTWRIGHT, J. A & JOLLY, R.J.H. 2000. Remobilization and Injection in Deepwater Depositional Systems: Implications for Reservoir Architecture and Prediction. *Deep-Water Reservoirs of the World: 20th Annual GCSSEPM Foundation Bob F. Perkins Research Conference*, 15, 515–532, https://doi.org/10.5724/gcs.00.15.0515.

LØSETH, H., RAULLINE, B. & NYGARD, A. 2013. Late Cenozoic geological evolution of the northern North Sea: development of a Miocene unconformity reshaped by large-scale Pleistocene sand intrusion. *Journal of the Geological Society*, 170, 133–145, https://doi.org/10.1144/jgs2011-165.

MARCUSSEN, O., THYBERG, B.I, PELTONEN, O., JAHREN, J., BJORLYKKE, K., & FALEIDE J.I. 2009. Physical properties of Cenozoic mudstones from the northern North Sea: Impact of clay mineralogy on compaction trends. AAPG Bulletin, 93, 127–150

MARTINSEN, O.J., BØEN, F., CHARNOCK, M.A., MANGERUD, G. & NØTTVEDT, A. 1999. Cenozoic development of the Norwegian margin 60–64°N: sequences and sedimentary response to variable basin physiography and tectonic setting. *In*: *Petroleum Geology of Northwest Europe: Proceedings of the 5th Conference*. 293–304., https://doi.org/10.1144/0050293.

MAZZINI, A., DURANTI, D., JONK, R., PARNELL, J., CRONIN, B.T., HURST, A. & QUINE, M. 2003. Palaeo-carbonate seep structures above an oil reservoir, Gryphon Field, Tertiary, North Sea. *Geo-Marine Letters*, 23, 323–339, https://doi.org/10.1007/s00367-003-0145-y.

MOLLER, N.K., GJELBERG, J.G., MARTINSEN, O., CHARNOCK, M.A., FAERSETH, R.B., SPERREVIK, S., CARTWRIGHT, J.A. 2004. A geological model for the Ormen Lange hydrocarbon reservoir. Norwegian Journal of Geology 84, 169 - 190

MOLYNEUX, S., CARTWRIGHT, J. & LONERGAN, L. 2002. Conical sandstone injection structures imaged by 3D seismic in the central North Sea, UK. *First Break*, 20, 383–393, https://doi.org/10.1046/j.1365-2397.2002.00258.x.

MONDOL, N.H., BJØRLYKKE, K. & JAHREN, J. 2008. Experimental compaction of clays: Relationship between permeability and petrophysical properties in mudstones. *Petroleum Geoscience*, https://doi.org/10.1144/1354-079308-773.

MORGAN, D.A., CARTWRIGHT, J.A. & IMBERT, P. 2015. Perturbation of polygonal fault propagation by buried pockmarks and the implications for the development of polygonal fault systems. Marine and Petroleum Geology, https://doi.org/10.1016/j.marpetgeo.2015.03.024.

MOSS, B. BARSON, D., RAKHIT, K., DENNI, H., & SWARBRICK. R. 2003. Formation pore pressures and formation waters. In: The Millenium Atlas: Petroleum Geology of the Central and Northern North Sea (Ed. by D. Evans, C. Graham, A. Armour & P. Bathurst). Geological Society London, London, 279-287

NADIN, P.A. & KUSZNIR, N.J. 1995. Palaeocene uplift and Eocene subsidence in the northern North Sea Basin from 2D forward and reverse stratigraphic modelling. Journal - Geological Society (London), https://doi.org/10.1144/gsjgs.152.5.0833.

NOTTVEDT, A., GABRIELSEN, R.H. & STEEL, R.J. 1995. Tectonostratigraphy and sedimentary architecture of rift basins, with reference to the northern North Sea. *Marine and Petroleum Geology*, 12, 881–901, https://doi.org/10.1016/0264-8172(95)98853-W.

OBERMEIER, S.F. 1998. Liquefaction evidence for strong earthquakes of Holocene and latest Pleistocene ages in the states of Indiana and Illinois, USA. *Engineering Geology*, 50, 227–254, https://doi.org/10.1016/S0013-7952 (98)00032-5.

OLOBAYO, O. 2014. Deposition, Remobilization and fluid flow in Sedimentary Basins – case studies in the Northern North Sea and Nigeria Transform Margin. *PhD Thesis*, The University of Manchester, UK

OSBORNE, M.J. & SWARBRICK, R.E. 1997. Mechanisms for Generating Overpressure in Sedimentary Basins: A Re-evaluation. *AAPG Bulletin*, 81 (1997), https://doi.org/10.1306/522B49C9-1727-11D7-8645000102C1865D.

OSTANIN, I., ANKA, Z., DI PRIMIO, R. & BERNAL, A. 2012. Identification of a large Upper Cretaceous polygonal fault network in the Hammerfest basin: Implications on the reactivation of regional faulting and gas leakage dynamics, SW Barents Sea. Marine Geology, https://doi.org/10.1016/j.margeo.2012.03.005.

PEDERSEN, S.I., RANDEN, T., SØNNELAND, L. & STEEN, Ø. 2002. Automatic fault extraction using artificial ants. *SEG Technical Program Expanded Abstracts*, **21**, 512–515, https://doi.org/10.1190/1.1817297.

RANDEN, T., PEDERSEN, S.I. & SØNNELAND, L. 2001. Automatic extraction of fault surfaces from three-dimensional seismic data. *SEG Technical Program Expanded Abstracts*, **20**, 551–554, https://doi.org/10.1190/1.1816675.

RAMDHAN, A.M. & GOULTY, N.R. 2011. Overpressure and mudrock compaction in the Lower Kutai Basin – a radical reappraisal. AAPG Bulletin, 95, 1725–1744.

RUNDBERG, Y. 1989. *Tertiary Sedimentary History and Basin Evolution of the Norwegian North Sea between 60-62 N. An Integrated Approach*. University of Trondheim, Norway.

RUNDBERG, Y. 1991. Tertiary sedimentary history and basin evolution of the Norwegian North Sea between 60 – 62 degrees N – an Integrated Approach. *PhD Thesis, University of Trondheim*

RUNDBERG, Y. & EIDVIN, T. 2005. Controls on depositional history and architecture of the Oligocene-Miocene succession, northern North Sea Basin. *Norwegian Petroleum Society Special Publications*, 12, 207–239, https://doi.org/10.1016/S0928-8937 (05)80050-5.

RUNDBERG, Y. & EIDVIN, T. 2016. Discussion on 'Late Cenozoic geological evolution of the northern North Sea: development of a Miocene unconformity reshaped by large-scale Pleistocene sand intrusion', Journal of the Geological Society, 170, 133–145. *Journal of the Geological Society, London*, 173, 384–393.

SAFRONOVA, P.A., ANDRESSEN, K., LABERG, J.S. & VORREN, T.O. 2012. Development and post-depositional deformation of a Middle Eocene deep-water sandy depositional system in the Sørvestsnaget Basin, SW Barents Sea. *Marine and Petroleum Geology*, 36, 83–99, https://doi.org/10.1016/j.marpetgeo.2012.06.007.

SEKARARUM, P.A & ROSID, M.S. 2020. Characterization of natural fracture on basement reservoir using the integration of ant tracking attribute, FMI log, and resistivity log at" POME" field, Jambi sub basin. *aip.scitation.org*, **2223**, 40002, https://doi.org/10.1063/5.0002698.

SHIN, H., SANTAMARINA, C.J. & CARTWRIGHT, J.A. 2008. Contraction-driven shear failure in compacting uncemented sediments. Geology, https://doi.org/10.1130/G24951A.1.

SHOULDERS, S.J. & CARTWRIGHT, J. 2004. Constraining the depth and timing of large-scale conical sandstone intrusions. *Geology*, 32, 661–664, https://doi.org/10.1130/G20654.1.

SHOULDERS, S.J., CARTWRIGHT, J. & HUUSE, M. 2007. Large-scale conical sandstone intrusions and polygonal fault systems in Tranche 6, Faroe-Shetland Basin. *Marine and Petroleum Geology*, 24, 173–188, https://doi.org/10.1016/j.marpetgeo.2006.12.001.

SILVA, C.C., MARCOLINO, C.S. & LIMA, F.D. 2005. Automatic fault extraction using ant tracking algorithm in the Marlim south field, Campos basin. *In*: *Society of Exploration Geophysicists - 75th SEG International Exposition and Annual Meeting, SEG 2005*. 857–860., https://doi.org/10.1190/1.2148294.

SONNENBERG, S. & UNDERWOOD, D. 2012. Polygonal Fault Systems: A New Structural Style for the Niobrara Formation, Denver Basin, CO. AAPG Annual Convention and Exhibition, Search and Discovery, 50624.

SWARBRICK, R.E. & OSBORNE, M.J. 1998. Mechanisms that generate abnormal pressures: an overview. *Abnormal Pressures in Hydrocarbon Environments: AAPG Memoir 70*, 13–34.

SZARAWARSKA, E., HUUSE, M., HURST, A., DE BOER, W., LU, L., MOLYNEUX, S. & RAWLINSON, P. 2010. Three-dimensional seismic characterisation of large-scale sandstone intrusions in the lower Palaeogene of the North Sea: completely injected vs. in situ remobilised sand-bodies. *Basin Research*, 22, 517–532, https://doi.org/10.1111/j.1365-2117.2010.00469.x.

THYBERG, B.I., STABELL, B., FALEIDE, J.I. & BJØRLYKKE, K. 1999. Upper Oligocene diatomaceous deposits in the northern North Sea - silica diagenesis and paleogeographic implications. *Norsk Geologisk Tidsskrift*, 79, 3–18, https://doi.org/10.1080/002919699433870.

THYBERG, B. I., JORDT, H., BJORLYKKE, K., & FALEIDE, J. I. 2000. Relationships between sequence stratigraphy, mineralogy and geochemistry in Cenozoic sediments of the northern North Sea. In Nottvedt, A. at al. (Eds.), Dynamics of the Norwegian Margin. Geological Society of London, Special Publications, 167, 245-272

WATTERSON, J., WALSH, J., NICOL, A., NELL, P.A.R. & BRETAN, P.G. 2000. Geometry and origin of a polygonal fault system. Journal of the Geological Society, https://doi.org/10.1144/jgs.157.1.151.

WILD, J. & BRIEDIS, N. 2010. Structural and stratigraphic relationships of the Palaeocene mounds of the Utsira High. *Basin Research*, 22, 533–547, https://doi.org/10.1111/j.1365-2117.2010.00479.x.

WRONA, T., MAGEE, C., JACKSON, C.A.-L., HUUSE, M. & TAYLOR, K.G. 2017a. Kinematics of Polygonal Fault Systems: Observations from the Northern North Sea. *Frontiers in Earth Science*, 5, https://doi.org/10.3389/feart.2017.00101.

WRONA, T., JACKSON, C.A.L., HUUSE, M. & TAYLOR, K.G. 2017b. Silica diagenesis in Cenozoic mudstones of the North Viking Graben: physical properties and basin modelling. *Basin Research*, 29, 556–575, https://doi.org/10.1111/bre.12168.

ZACHOS, J., PAGANI, M., SLOAN, L., THOMAS, E. & BILLUPS, K. 2001. Trends, Global Rhythms, Aberrations in Global Climate 65Ma to Present. *Science*, 292, 686–693, https://doi.org/10.1126/science.1059412.

Section 3:

Synthesis, recommendations for future work & Conclusions

Chapter 8

CHAPTER 8   Summary & Conclusions

8.1 Introduction

This chapter summarizes the findings documented in this study and addresses the research questions outlined in section 1.1 with reference to the results in Chapter 3 – 7. It goes further to highlight the implications of the study to hydrocarbon exploration and production in deep-water sand reservoirs (see question (g) in section 8.3) and provides recommendations for future work/research which would address other outstanding gaps in the current understanding of sand injectites in the northern North Sea Basin. A summary figure is presented in Fig. 8.1 to illustrate the workflow used in this research and how the result chapters fit into the overall research topic.

8.2 Summary of work and Principal findings

All the result chapters contain in-depth discussions and thus no further extended discussions are carried out here. Therefore, concise summaries of the result chapters (Chapter 3 – 7) is given in this section.

An integrated analysis of well data and the most recent and best resolved 3D seismic imaging of the subsurface in the northern North Sea Basin was used to investigate the occurrence of large-scale sandstone intrusions or sand injectites in the Paleogene succession of the basin. The Paleogene interval in the study area show evidence for intense and extensive remobilization and injection of deep-water sediments deposited over large areas of c. 36,400 km^2 in a slope to basin floor settings. The findings from this study are outlined in five result chapters and have been used to demonstrate the relevance of sand injectites and why they should be considered in basin analysis and reservoir studies due to their very important implications for hydrocarbon exploration and production in deep-water sand reservoirs, as well as their influence on a basin's fluid plumbing system.

In **Chapter 3**, an overview of the hydrocarbon potential of North Sea oil/gas fields with reservoirs modified by sand remobilization and injection processes was presented to assess their contribution to the overall North Sea hydrocarbon reserves. This overview also attempts to demonstrate that sand injectites form attractive exploration targets which should not be ignored, based on first-hand experience from North Sea oil/gas fields (e.g., Alba, Balder, Gryphon & Volund) were sand injectites associated with deep-water sand reservoirs where intentionally targeted. The documentation of reserve/resource estimates from these fields and recent discoveries presented herein (Table 3.1 & 3.2; Fig. 3.4 & 3.5) have shown the gradual increase in the total contribution (c. 7600 mmbbloe) of sand injectite fields to the cumulative recoverable hydrocarbon reserves in the North Sea Basin from 1967 – 2019. The large gap between the discovery dates and production dates for some of these fields (e.g., Balder field: Table 3.2) may directly or indirectly indicate the substantial amount of time and effort it took to clearly understand and model the complexity associated with this kind of reservoirs which are

considered to be unconventional reservoirs. Overall, this chapter has established that the few recorded success in targeting injectite reservoirs have yielded significant results and have led to renewed interest in the search for this kind of reservoirs which usually form near-field hydrocarbon accumulations above producing fields since it was realized that the injection of sand into low permeable sealing mudstones can enhance fluid migration into shallower intervals. A valid example for the above would be the recent Liatårnet (25/2/21) oil discovery (in 2019) in the Lower Miocene reservoir of the Skade Formation located east of the Frigg Field and northeast of the Alvheim Field in the Central North Sea. The oil found in this field is suggested by AkerBP to have been sourced from oil spilled from the Frigg Field in the west into Eocene reservoirs in the Frigg-Gamma Field in the east, and upward into the Lower Miocene reservoirs of the Liatårnet. Finally, this chapter have further provided evidence which shows that the Paleogene succession of the North Sea Basin is the most susceptible to processes of sand remobilization and injection because majority (c. 90 %) of the injectite fields have their reservoirs hosted in Paleogene deep-water sediments which imply that the Paleogene holds significant potential for near-field accumulation of hydrocarbons in shallow injectite reservoirs connected to deeper hydrocarbon reservoirs. Therefore, the probability for future hydrocarbon discoveries in the Paleogene above existing fields is very likely.

Chapter 4 assessed the 3D seismic characteristics and distribution of discordant high amplitude anomalies observed within the Paleogene (Paleocene – Oligocene) interval in the northern North Sea Basin. An integrated approach using available 3D seismic data (from CGG) and well data (from TGS Facies Map Browser) have been used to characterize these anomalies, leading to their interpretation as the seismic expression for large-scale sandstone intrusion complexes within multiple stratigraphic levels. Their interpretation as sand lithology was aided by well calibration of anomalies intersected by available wells which yielded tens-of-meters of thick sandstone units. This chapter documented the intense and extensive remobilization and injection of sand into their host mudstone strata in the Paleocene – Oligocene which exhibit varying simple to complex cross-sectional geometries ranging from conical-shaped, wing-like to highly irregular to complex-shaped intrusions.; with the conical intrusions being the most predominant (see Fig. 4.8 – 4.9; 4.11 – 4.14). The distribution and measurements of the geometrical parameters (e.g., intrusion height, dip angle and intrusion width) of the observed intrusions were also documented for the three intervals where they occur. This chapter went further to constrain all aspects of the injection system such as their distribution, parent source sands, timing of injection and their potential priming and trigger mechanisms. Overall, this chapter established the following principal conclusions based on analysis and interpretation of available data:

- Sand injectites are distributed within three Paleogene intervals in the northern North Sea which are: CSU-1 (Paleocene – Early Eocene), CSU-2 (Eocene) and CSU-4 (Oligocene). Where CSU means Cenozoic Seismic Unit. Their spatial distribution is highlighted in Table 4.5 & 8.1.

- That the sandstone intrusions within the CSU-1 (Paleocene – Early Eocene) were sourced from Lower – Middle Paleocene sand-rich channel-fills and fans of the Våle and Lista Formation deposited during the Early Tertiary uplift along basin margins. In addition, the CSU-2 (Eocene) intrusions were suggested to be sourced by Early – Mid Eocene sand-rich submarine fan systems and isolated channel-fills of the Horda Formation, while CSU-4 (Oligocene) intrusions were sourced by Early – Mid Oligocene turbiditic gravity flow sands consisting of submarine channel-lobe complexes and partly from Lower – Middle Eocene sand-rich fans (see Table 8.1).

- The injection and emplacement of CSU-1 sandstone intrusions is estimated to have occurred in the Mid/Late Paleocene to Early Eocene time. In addition, the injection of CSU-2 sandstone intrusions is suggested to have occurred in the Mid – Late Eocene time, while that of CSU-4 intrusions may have occurred in the Middle – Late Miocene time. This therefore implies sandstone intrusions in the northern North Sea were emplaced by three or more episodes of sand remobilization and injection.

- That the large-scale sand intrusion complexes formed in the Paleogene succession of the northern North Sea were formed due to post-depositional remobilization and injection of their parent depositional sands into their sealing mud-dominated succession, facilitated by overpressure development within the parent sands. Overpressure development within the sands is suggested to result from a combination of various factors which include disequilibrium compaction, differential loading, fluid addition (i.e., lateral fluid drainage and fluid migration from deeper sources), lateral transfer of pressure, and fluid release from Smectite-to-Illite and Silica (Opal-A to CT) diagenetic transformation. Sand injection was in turn suggested to be triggered by large-scale differential compaction or simply when the fracture gradient of their sealing mudstones is exceeded (see section 4.5.4).

- Finally, just like other previous documentation of sand injectites, this study demonstrates the importance of understanding sand injectites because of their influence on reservoir geometry and properties of deep-water sandstone reservoirs, and their impact on fluid flow through low permeable successions. The northern North Sea sand injectites remain a world-class seismic analogue for large-scale intrusion complexes developed in deep-water settings.

Chapter 1: Introduction, Data and Methods

Chapter 2: Geological setting, Review of sand injectite literature

Chapter 3: Sand injectites as attractive exploration targets

Chapter 7: Interaction between polygonal faults and sand injectites

STUDY AREA

Chapter 6: Depositional or Injected Oligocene sands ???

Loseth et al. (2013)

Revisited

Correct or wrong ???

Loseth et al. (2016)

Chapter 5: Oligocene deep-water depositional system modified by sand injectites

Chapter 4: Sand injectite framework: 3D seismic characterization

Redrawn and modified from Lonergan et al. (2000)

Chapter 8: Summary & Conclusions

Fig. 8.1: A summary figure of the thesis synopsis from introduction and review of literature to the result chapters (in chapter 3 – 7) which contain the results and interpretations obtained from analysis of available seismic and well data, and the summary and conclusions drawn from this research.

Chapter 5 described for the first time the seismic expression of sand intrusion complexes developed in association with a Middle – Late Oligocene depositional system in the eastern margin of the North Viking Graben, (Quadrant 34 & 35) in the northern North Sea Basin. The chapter also considered potential factors and mechanisms which control their development, as well as the implications of sand intrusion complexes developed in deep-water depositional systems for hydrocarbon exploration and production. The Middle – Late Oligocene depositional system studied here is characterized by sand-rich finger to branch-like channel-lobe systems which display varying complex geometries in cross section (see Fig. 5.6, 5.8 – 5.12). The main control on their distribution is suggested to be dependent on the direction of sediment influx and the inherent topography of their underlying Mesozoic rift structures, while the control on their geometries is ascribed to post-depositional processes of subsurface remobilization and injection. The emplacement of the intrusions associated with the Middle – Late Oligocene depositional system is suggested to have occurred during the Late Miocene time, facilitated by overpressure development. Overall, this study yet again demonstrates the huge impact of sediment remobilization and injection on the post-depositional geometries of deep-water sand reservoirs because the intrusions associated with the Middle – Late Oligocene depositional system clearly altered its morphology and architecture, and enhanced connectivity between some of the sands which may have been deposited as isolated sands. The latter is displayed by the lateral and vertical connectivity observed between some of the intrusions.

Chapter 6 on the other hand presented an alternative model for the origin of Oligocene sandstones and the controls on the mounded shape of the Top Hordaland Group Unconformity (THGU) in the areas above the Snorre, Gullfaks and Visund fields in the northern North Sea by revisiting aspects of the ''Late Cenozoic geological evolution of the northern North Sea'' initially presented by Løseth et al. (2013) and subsequently discussed by Rundberg & Eidvin (2016). The findings from an integrated analysis and re-interpretation of available data provided new insights and clearly indicate their injected model for Oligocene sandstones sourced from Paleocene parent sands is inconsistent with our observations. Our observation and interpretation show that the Oligocene sands comprises of mainly remobilized in-situ depositional sands (i.e., 80%) representing deep-water turbiditic gravity flow channel-belt sands supplied from the Shetland Platform (in the west) and West Norway (in the east) in the Middle – Late Oligocene age (see Fig. 6.5, 6.8 & 6.10). However, evidence for possible contribution from parent sands in the Middle – Late Eocene exist in the form of potential feeder dikes from Middle – Late Eocene sand across the Eocene – Oligocene boundary into the Upper Oligocene (see Fig. 6.13 & 6.14). The obvious observation of Oligocene sands to largely consist of in-situ depositional channel-belt sands implied that the mounded nature of the Top Hordaland Group Unconformity would have originated mainly from differential compaction

across the sands, with possible contribution from forced folding (or jack up) due to sand injection. This study provides clarity and puts an end to the mild controversy and argument on the model by Løseth et al. (2013) which have been discussed in both Rundberg & Eidvin (2016) and Løseth et al. (2016).

Finally, **Chapter 7** also for the first time examined the relationship between the pervasive polygonal fault systems and large-scale sand intrusions within the Hordaland Group (Eocene – Mid Miocene) succession in the northern North Sea. This was achieved by classifying the different kind of interaction between both features to decipher if such interaction control the formation and simple to complex geometries associated with the intrusions. Measurement of their geometrical parameters (e.g., dip) were taken and compared. The intrusions within the Hordaland Group interval were classified into four types, using similar classification by Bureau et al. (2013), which is based on the nature of their interaction with their neighbouring polygonal faults. The observed intrusion types include (see Fig. 7.18 – 7.21): (i) Class-A intrusions which are either fully or partially intruded along polygonal fault plane, (ii) Class-B intrusions which has the tip of their discordant limbs/wings halted abruptly by polygonal fault plane restricting further propagation of the wing/limb, (iii) Class-C intrusions which crosscut or are crosscut by polygonal fault planes but do not appear to be geometrically affected, and (iv) Class-D intrusions with complex geometries as a result of geometrical modification when crosscut or intersected by polygonal faults planes. Overall, the kind of interaction observed between both features indicate the polygonal faults formed prior to sand remobilization and injection, with possible reactivation of faulting during sand injection because of hydraulic fracturing of their host mudstones. The observation of no definite correlation between both features suggests that the intrusions tend to achieve their distinct geometries regardless the presence of polygonal faults (with exception of Class-D intrusions), and the faults were likely only exploited where favourable or contributed significantly to seal failure required for injection of fluidized sands to occur. The above finding supports the previous arguments by Huuse & Mickelson (2004) and Huuse et al. (2004) on the potential control of polygonal faults on the timing and geometry of sand intrusions.

Table 8.1: Summary table for the distribution, characteristics, and aspects of the sand injection system for the studied sand injectites complexes in the northern North Sea.

Northern North Sea Sandstone intrusions or Sand injectites			
Seismic unit/Age	**CSU-1** **(Paleocene - Early Eocene)**	**CSU-2** **(Eocene)**	**CSU-4** **(Oligocene)**
Intrusion type (see section 4.4.5)	Type 1 & 2	Type 1 & 2	Type 1 - 3
Spatial distribution (see Table 4.5)	Restricted to the eastern and north-eastern part of the study area along the basin margin	Distributed mainly in the western, NE & SW parts of the study area and are rarely or not found at the basin centre and eastern parts	Distributed throughout the study area with most of the intrusions lying immediately above the Opal-A/CT diagenetic boundary
Depositional environment	Slope to basin floor setting		
Depth (m) below the present seafloor	400 - 1750	1000 - 1800	500 - 1500
Cross sectional geometry (see examples in Fig. 4.8 – 4.21)	Symmetrical/ asymmetrical conical and flat-bowl shaped discordant high amplitude anomalies with V/W and wing-like shapes	Conical (U, V, W) and saucer/flat bowl shaped discordant and concordant high amplitude anomalies. Conical anomalies are the most predominant	Conical (U, V, W), wing-like or saucer/flat-bowl shaped, irregular to complex-shaped discordant and concordant high amplitude anomalies. Wing-like and irregular anomalies are the most abundant
Plan view geometry (see examples in Fig. 4.10, 4.14 & 4.21)	Circular to sub-circular, oval to elliptical	Circular to sub-circular, oval to elliptical	Circular to sub-circular, oval to elliptical, and irregular to elongate
Injected/ remobilized; Lithology	Depositional and injected sandstones	Depositional, injected, and remobilized sandstones	Depositional, injected, and remobilized sandstones
Host rock	Fine-grained, smectite-rich mudstones of the Balder & Sele Formation	Fine-grained, bio-siliceous, smectite-rich mudstones of the Horda Formation	Fine-grained, bio-siliceous, smectite-rich mudstones of the Lark Formation
Host rock and overburden deformation	Forced-folds and jack-up of overburden above the intrusion	Forced-folds and jack-up of overburden above the intrusion. Host rock intensely deformed by intrusions	Forced-folds, domal folds, mounded top and jack-up of overburden above the intrusion. Host rock intensely deformed by intrusions
Parent source sand (location & character; see text in section 4.5.1)	Lower – Middle Paleocene sand-rich channel-fills and fans of the Våle and Lista Formation deposited during the Early Tertiary uplift along basin margins	Early – Mid Eocene sand-rich submarine fan systems and isolated channel-fills of the Horda Formation	Early – Mid Oligocene turbiditic gravity flow sands consisting of submarine channel-lobe complexes and partly from Lower – Middle Eocene sand-rich fans
Feeder dikes/conduit (YES or NO)	NO	YES	YES
Timing of intrusion or emplacement (see text in section 4.5.3)	Mid/Late Paleocene to Early Eocene	Mid – Late Eocene	Middle – Late Miocene
Single event or multiple episodes? (see section 8.3: question g)	Single ??	Multiple	Multiple
Geometrical characteristics: dip, height, top diameter, base diameter (see Fig. 4.23, Table 4.6 & Appendix B.1)	Dip (°): 2 – 30 Height (m): 24 – 214 Top diameter (m): 239 – 1739 Base diameter (m): 62 – 1006	Dip (°): 10 – 30 Height (m): 33 – 226 Top diameter (m): 303 – 3294 Base diameter (m): 60 – 1834	Dip (°): 7 – 30 Height (m): 29 – 196 Top diameter (m): 309 – 3264 Base diameter (m): 41 – 2336
Suggested priming & Trigger mechanisms (see text in section 4.5.4)	**Priming mechanisms** (combination of processes facilitating overpressure build-up; see section 4.5.4.1) • Disequilibrium compaction • Differential loading • Fluid addition (i.e., lateral fluid drainage and fluid migration from deeper sources) • Lateral transfer of pressure • Fluid release from Smectite-to-Illite clay conversion and Silica (Opal-A to CT) diagenetic transformation • Other potential mechanisms (??): aqua-thermal expansion and sea-level fluctuations **Trigger mechanism** (see section 4.5.4.2) • Large-scale differential compaction and associated faulting and fracturing • Simply when the fracture gradient of the seal is exceeded (i.e., sufficient overpressure such that no external triggers was required)		
Implications for hydrocarbon exploration and production	See text in sections 4.5.6, 5.6.5, and 7.5.4. Also see Table 4.7		

8.3 Addressing questions raised by research

The nine research questions outlined in Chapter 1 (section 1.1) are briefly addressed or discussed here, with references made to the results presented in Chapter 3 – 7:

(a) Why is the study of sand injectites important, and are they attractive exploration targets?

Sand injectites have been studied over a decade and these studies have revealed that the processes of sand remobilization and injection are common in deep-water sedimentary environments. Previous studies have also highlighted the significance of sand injectites (e.g., Lonergan et al., 2000; Hurst et al., 2003; Hurst et al., 2005; Hurst & Cartwright, 2007; Huuse et al., 2007; Braccini et al., 2008; Huuse, 2008; Hurst et al., 2011) with major emphasis on their impact on the morphology, architecture, and distribution of deep-water sand reservoirs. Therefore, they have important implications for hydrocarbon exploration and production. Their importance and implications based on published literature is documented in detail in Chapter 2 (section 2.5.1 & 2.5.2.7) and should be referred to for more information.

On the other hand, sand injectites are recognized to form attractive exploration targets because they contain substantial volume of sand, have excellent reservoir properties (e.g., porosity: 28 – 40 %, and permeability: 1 – 10 Darcy), and can form near-field accumulation above existing fields. Experience from North Sea oil/gas fields (e.g., Alba, Balder, Gryphon & Volund) with injectite reservoirs which are documented in Chapter 3 provides the needed answer to this question based on the substantial cumulative reserve/resource contribution of these injectite fields and recent discoveries to the total recoverable reserves in the North Sea.

(b) Why are sand injectites abundant in the northern North Sea Basin, and what favours their formation in the Paleogene succession of the northern North Sea?

First of all, the formation of sand injectites require four main ingredients which are: (i) the presence of clean unconsolidated deep-water depositional parent sandstone encased in low permeable fine-grained mudstones (Lonergan et al., 2000; Huuse and Mickelson, 2004), (ii) overpressure development within the sealed sandstones caused by a combination of different factors (Molyneux et al., 2002; Huuse and Mickelson, 2004; Huuse et al., 2007), (iii) substantial volume of internally or externally sourced fluids required to transport the sands in a fluidized flow (Szarawarska et al., 2010), and (iv) an internally or externally generated trigger mechanism which results to seal failure (Lonergan & Cartwright, 1999; Jolly & Lonergan, 2002; Huuse et al., 2007). The above four requirements are met for the Paleogene succession in the northern North Sea, although the actual trigger mechanisms for the large-scale intrusion complexes in the Paleogene is still speculative (refer to section 4.5.4.2).

The first requirement which forms the most critical factor for sand remobilization and injection in the study area is satisfied by the presence of Paleogene Sandstone Members of the Våle,

Lista, Horda and Lark Formations (see Fig. 2.3 or 4.2) encased in smectite-rich mudstones (see Thyberg et al., 2000: their Fig. 4; Marcussen et al., 2009: their Table 2 & Fig. 9). These Paleogene parent sandstones occur as deep-water sand-rich fans, isolated channel-fills and channel-lobe complexes deposited in a slope to basin floor setting (see Chapter 5 & 6). The high smectite content of the Rogaland and Hordaland Group mudstones would have ensured that the sandstones were effectively sealed prior to remobilization due to the very low permeability of smectite-rich sediments, which in turn facilitated the generation of overpressure within the sands (refer to section 4.5.4.1). Smectite is regionally distributed in the northern North Sea, derived as a product from erosion of volcanic ash and rocks formed during the opening of the North Atlantic (Marcussen et al., 2009; Thyberg et al., 2000; Løseth et al., 2013). The low permeability of smectite-rich mudstones satisfies the requirement for sand injection to occur because smectite-rich mudstones have much lower permeability than Kaolinite and Illite-rich mudstones (Mondol et al., 2008; Løseth et al., 2013)

In addition, the large volume of fluid needed to transport sands is suggested to be provided by a combination of processes such as lateral fluid drainage due to early-stage dewatering of mudstones caused by compaction due to burial, fluid (i.e., gas or pore water) migration from deeper sources, and fluid release from Smectite-to-Illite conversion and silica (Opal-A to CT) diagenesis (see text in section 4.5.4). This requirement for fluid availability is also satisfied by evidence for subsurface fluid flow e.g., polygonal fault systems, Opal-A/CT boundary, and gas chimneys above Mesozoic fault structures.

Lonergan et al. (2000) have identified the interval most susceptible to remobilization in the North Sea to consist of depositionally restricted deep-water sandstone deposits in the form of elongate channel-fill sands and isolated/localized sand-rich fan lobe complexes which are deposited in mud-dominated basinal settings. This aligns with the nature and character of sandstones in the northern North Sea (see Chapter 5: Fig. 5.6; Chapter 6: Fig. 6.8 & 6.10) which are distributed in slope to basin floor settings. Majority of sand injectites described in deep-water environment occur in slope setting (e.g., Duranti & Hurst, 2004; Jackson, 2007; Vigorito et al., 2008, Szarawarska et al., 2010). Therefore, the formation of sand injectites in the study area is favoured by their depositional setting with processes leading to sand remobilization facilitated by both slope processes and diagenesis. In conclusion, we suggest that the abundance of sand injectites in the Paleogene succession of the northern North Sea is dependent and favoured by the following factors:

- The deposition and spatial distribution of large volumes of parent depositional sands which is a function of the basin tectonic setting and other controls on sediment supply (e.g., climate and sea-level changes)
- Parent sand and host rock characteristics (e.g., host rock rheology & composition, Grain size, packing and pore scale properties)
- Availability of fluid plumbing system and pore fluid composition which helps facilitate overpressure development

- Local and regional depositional and post-depositional processes (e.g., mineral & chemical diagenetic conversions)

(c) What properties (i.e., mineralogical, chemical & physical) of their host mudstones favour the scale of sand remobilization and injection features present in the northern North Sea Basin?

The host strata for the sandstone intrusions in the northern North Sea consists of fine-grained, bio-siliceous, smectite-rich marine mudstones. Their physical properties (i.e., grain size) and mineralogy (i.e., clay mineral content) all favour the scale of intrusion in the study area because the sands need to be buried and effectively sealed by low permeable fine-grained mudstones to meet one of the criteria needed for sand remobilization and injection to occur. The physical and mineralogical properties of Cenozoic mudstones in the northern North Sea have been documented by Marcussen et al. (2009). Their studies show that the Rogaland Group mudstones contain up to 60 – 70 % smectite and less than 25 % of kaolinite, Illite and chlorite combined, while the Hordaland Group mudstones contain smectite clay of up to 40 – 80 %. Mondol et al. (2008) have shown that smectite have 4 – 5 times lower permeability than kaolinite and Illite when exposed to the same effective stress. This implies that the high smectite content of the host mudstones satisfies the requirement for low permeable mudstones to seal depositional sands prior to remobilization, potentially causing overpressure development due to burial and compaction (Moss et al., 2003; Marcussen et al., 2009). Thus, clay mineralogy (presence of smectite) and associated clay diagenesis may be considered as the main property of the host mudstones which support overpressure build-up and other processes which prime the sands for remobilization and injection. In addition, the tensile strength and cohesion of the host strata may also be a factor which supports the formation of sand intrusions (Lonergan et al., 2000; Mathieu et al., 2015).

(d) What factors control the location/distribution, extent and the resultant simple to complex geometries (i.e., injectite architecture) associated with the large-scale intrusion complexes studied here?

Some factors which may control the location/distribution, extent, and architecture of sand injectites in the northern North Sea are highlighted in Table 8.2.

Table 8.2: List of factors considered to control the location/distribution, extent, and architecture of sand injectites in the study area.

Controls on location/distribution	Controls on extent and injectite architecture
Tectonic setting & basin geomorphology	Host rock properties and characteristics (lithology, rheology, thickness, and heterogeneity) and parent sand architecture
Sediment supply & routing (i.e., direction of sediment influx and the inherent topography due to the underlying Mesozoic rift structures)	Volume of available fluid to drive injection
Volume, extent, and architecture of the parent sands	The nature of flow (i.e., Laminar or turbulent flows)
Host rock properties and characteristics (lithology, rheology & heterogeneity)	Fluid composition/characteristics in the fluidized flow (e.g., velocity and viscosity of sand & fluid mixture)
Post depositional processes (e.g., diagenesis, chemical transformation, sediment reworking)	Presence of pre-existing faults and fractures (e.g., polygonal faults)
	Overburden thickness and stress field (orientation & direction of stress)

In the northern North Sea, the parent sands for the large-scale sandstone intrusions occur as three main architectural types in the form of: (i) laterally extensive lobe (sheet-like) complexes (see Fig. 5.6 & 6.10), (ii) slope channel-fills (isolated or amalgamated; see Fig. 4.7, 6.8 & 6.11), and (iii) laterally extensive sand-rich fans. All the above contain substantial volume of sand and can source the large-scale intrusion network studied here. However, the channel-lobes and sand-rich fans contain volumetrically larger quantity of sand than slope channel-fills and therefore can determine the extent and distribution of injected sands. Chapter 5 described the seismic expression of sand intrusion complexes sourced and developed in association with a Middle – Oligocene sand-rich channel-lobe system in the north-eastern part of the study area. The parent sand architecture may also determine the resulting geometries of the injectites because lobe-complexes and sand-rich fans tend to form more conical-shaped intrusions above parent sands (see Fig. 7.7c – f), or irregular to complex-shaped sand intrusions. While channel-fills usually form dikes at the channel margins resulting to the formation of wing-like intrusions (see Fig. 4.18, 7.11d & e), and in some cases crestal intrusions (formed above the channel sands) and stepping sills at the tip of the marginal wings (see Fig. 6.11b & 6.12a). These wings formed at the channel margins are attributed to differential compaction adjacent to the channel sands due to burial and compaction (see Cosgrove & Hillier, 1999; Jackson, 2007). It is therefore suggested that parent sand architecture plays an important role in determining the type and style of sand injectites formed.

In addition, the host rock properties which may likely control the morphology of intrusions during their emplacement include: (i) host rock lithology, (ii) host rock rheology (i.e., their

inclination to brittle deformation; see Schofield et al., 2012), (iii) host rock heterogeneity (vertical & lateral variation in rock properties; Jolly & Lonergan, 2002), and (iv) host rock thickness. Based on outcrop studies, authors have argued that the nature of flow associated with the formation of sand injectites could be laminar flow (Taylor, 1982; Sturkell & Ormõ, 1997) or turbulent flow (Hubbard et al., 2007; Scott et al., 2009; Kane et al., 2010). The corresponding intrusions formed by either of the flow types will differ in style. The scale and complexity of the sand injectites formed in the northern North Sea are likely to be associated with turbulent flow which may result from rapid variation of pressure and flow velocity of the fluidized sand. Therefore, both the host rock properties and the nature of flow also influence the resultant geometries of sand intrusions.

(e) Where are the parent source sands for the intrusions, and how are depositional sands differentiated from injected sands?

The parent sands for Paleocene − Early Eocene (CSU-1) intrusions consist of Lower − Middle Paleocene sand-rich channel-fills and fans deposited during the Early Tertiary uplift along the eastern basin margin (see Dmitrieva et al., 2012, 2018). The parent sand distribution aligns with the distribution of intrusions in the Paleocene interval (see Fig. in Table 4.5). The parent sands for the Eocene (CSU-1) intrusions consists of Early − Mid Eocene sand-rich submarine fan systems and isolated channel-fills sourced from a NE − SW direction and aligns with the distribution of Eocene sand intrusions (see Fig. 4.15, 4.16, 7.7, 7.8). Lastly the parent sands for the Oligocene (CSU-4) intrusions consists of Early − Mid Oligocene turbidity gravity flow sands comprising of submarine channel-lobe complexes deposited from both western (East Shetland Platform) and eastern (West Norway) source areas into the basin. Seismic observations also show that some Oligocene intrusions were partly sourced from Lower − Middle Eocene parent sands. The parent source sands for the intrusions have been discussed in detail in section 4.5.1.

To differentiate between depositional and injected sands, attribute analysis (e.g., RMS amplitude extraction) have been used to identify areas of very high reflection amplitude since the attribute can identify depositional elements such as channel-fills and lobes (e.g., Fig. 5.6, 5.12, 6.8 & 6.10). However, the complex stacking of depositional elements and the impact of large-scale remobilization results to difficulty in clearly identifying depositional elements which sourced the intrusions in some area in the western and southwestern parts of the study area. The seismic stratigraphic model by Huuse et al. (2009, AAPG; see their Fig. 2.7) for differentiating depositional, remobilized, and injected sands have also been applied here, resulting to the conical intrusions suggested to represent injected sands sourced from a parent sand while the wing-like intrusions represent in-situ depositional sands subjected to post-depositional remobilization and injection which formed their marginal wings. On the other hand, the irregular to complex-shaped intrusions (e.g., Fig. 4.19, 5.8a, 7.21a & c) may represent remobilized depositional sand mounds.

To further link injected sands to their potential parent sands, analysis (e.g., heavy mineral provenance studies/analysis, fluid inclusion analysis, garnet geochemical analysis,) of sandstone samples from the intrusions and potential parent sand bodies will provide clarity into the mineralogical similarities between both sandstones (see Hurst et al., 2017). This is however suggested as a consideration for future research for the northern North Sea sand injectites.

(f) What processes may have facilitated and triggered sand remobilization and injection in the northern North Sea Basin?

The combination of processes considered to have facilitated overpressure development which primed the parent sands for injection and the potential trigger mechanisms which may have triggered sand injection into their low-permeable host mudstones have been discussed in detail in section 4.5.4 (for Paleocene – Oligocene intrusions) and 7.5.2 (for Oligocene intrusions). Therefore, both sections should be referred to.

(g) Were the intrusions formed by single or multiple episodic emplacement events?

In Chapter 4, the estimated timing of injection and emplacement for the intrusions within the interval between the Top Shetland/Base Tertiary and the Top Hordaland Group Unconformity was constrained using same approach as Shoulders & Cartwright, (2004) in section 4.5.3. For the three units (CSU-1, CSU-2, and CSU-4) with sand injectites, sand injection was estimated to have occurred in the Mid/Late Paleocene to Early Eocene, Mid – Late Eocene, and Mid – Late Miocene respectively. As such the intrusions are suggested to have formed by three or more episodes of sand emplacement events since they occur at three different stratigraphic levels with their parent sands located at multiple intervals. The observation that Oligocene intrusions are partly sourced by Lower – Middle Eocene sand-rich fans, due to the presence of feeder dikes across the Eocene – Oligocene boundary into the Lower Oligocene (see Fig. 4.31, 4.32, 6.13, 6.14, & 7.12) may indicate that the intrusions were formed by multiple episodes of sand remobilization and injection with the injectites sourced from different parent sands. Therefore, we suggest that the Paleogene interval in the northern North Sea went through multiple episodes of sand remobilization and injection with the probability that each interval experienced more than one episode of injection over time, which depends on the prevailing conditions in the basin. This multiple episode scenario is similar to that proposed for the San Joaquin (Panoche & Tumey hills) Basin (see Vettel & Cartwright, 2010).

(h) Are the existing models suggested by previous authors sufficient to account for the magnitude of the large-scale intrusion complexes formed in the study area?

Even though several models have been proposed to account for the magnitude of sand injectites present in the North Sea, some aspects of the sand injection process are still poorly understood or remains speculative. For example, the specific mechanism which triggers seal failure or hydraulic fracturing in the host mudstone leading to sand injection is still very speculative. In addition, the controls on their location, sourcing and architecture from a pore-scale and mineralogical perspective still needs to be addressed because they can cause fundamental changes in a basin's fluid flow and permeability architecture. Therefore, existing models are still not sufficient to address some of the outstanding aspects of sand remobilization and injection which are still debated till date. For example, in Chapter 6 the previous model for the source of Oligocene sandstone published by Løseth et al. (2013) was revisited to address the controversy (see Rundberg & Eidvin, 2016; and Løseth et al., 2016) in the model which interpreted Oligocene sandstones to be intrusive sands sourced from deeper Paleocene sandstones. Contrary to their interpretation, our observations and interpretation clearly show that Oligocene sandstones are largely (c. 80 – 85 %) remobilized in-situ depositional sands representing deep-water turbiditic channel-belt sand as previously proposed by Rundberg & Eidvin, (2005) (see section 6.4.3). The above example implies that some of the previous models may be flawed due to data limitation (e.g., limited extent of data and poor data quality) and the complexity associated with sand intrusion complexes. Finally, an integration of various data (e.g., cores, cuttings samples, etc) may be required to come up with a consensus model which gives a regional and inclusive explanation for the abundance of large-scale intrusions within the Paleogene succession of the northern North Sea.

(i) Finally, what are their implications for hydrocarbon exploration and production in the study area?

The implications of sand remobilization and injection for hydrocarbon exploration and production in the study area have been addressed in section 4.5.6, 5.6.5, and 7.5.4. In general, the current study of sand injectite have shown that they form unconventional sandstone reservoir geometries and can enhance connectivity between sand bodies (see Table 4.7). They are also considered as long-term conduit for fluid flow and are potential drilling hazards. Another possible implication for sand injectites in the northern North Sea is that they can form potential Carbon Capture and Storage (CCS) targets. An example is the Equinor Northern Lights Project, southwest of the Troll Field (31/5-7) in Dunlin Group (Cook and Johansen Formation) sandstone reservoir. Some of the sand injectites in the northern North Sea have properties which meet the minimum requirements for sand reservoir to be considered as potential CCS targets which include (Halland & Riis, 2018): **(i) burial depth of 800 – 2500 m, (ii) homogenous and sealed sand reservoir, (iii) net thickness of > 50 m, (iv) average net reservoir porosity of > 25 %, and (v) permeability of > 500 mD**. However, their inherent complexity due to intense

remobilization, as well as the propagation of polygonal faults through their host mudstones may result to seal integrity issues which could lead to CO_2 leakage. This may not be an issue because the injectite reservoirs are at present compacted and calcite cemented, as well as overlain by thick mudstone intervals. The parent sand lobes for the injectites may also be considered as CCS targets but an in-depth feasibility study is required to understand if they meet all the required selection criteria for potential CCS reservoirs, including an assessment of the sealing properties of their mudstone seals using the recommended checklist by Halland & Riis (2018).

8.4 General Conclusion

An extensive broadband 3D seismic survey and selected wells in the northern North Sea have been used to study the occurrence of large-scale sandstone intrusions or sand injectites distributed within its Paleogene succession. This study covered several aspects of the northern North Sea sand injection system, considering both known, unknown, and speculative aspects of the injection process. The study also addressed some of the important questions raised by the current study in relation to previous documented occurrence of sand injectites in the North Sea and its adjourning areas. The general conclusions drawn from the overall observations, analysis and interpretations reported in this thesis are outlined below:

1. A look at hydrocarbon fields in the North Sea associated with sand injectite reservoirs have shown that sand injectite complexes can contain substantial volume of hydrocarbon and contributes significantly to the total cumulative reserves in the North Sea. The success stories from targeting injectite reservoirs in some North Sea oil/gas fields (e.g., Alba, Balder, Gryphon & Volund) have led to the increased recognition of the significance of sand injectites in deep-water sand reservoirs, as well as an increased search for near-field accumulations above producing fields because sand injection into low permeable sealing mudstones can enhance upward migration of fluids into shallower intervals. In addition, the observation that majority of the documented fields have their injectite reservoirs hosted in Paleocene – Eocene deep-water sediments, means that the Paleogene succession of the North Sea Basin may be the most susceptible to post-depositional sand remobilization and injection. This implies there is a likelihood for future hydrocarbon discoveries in injectite reservoirs in the Paleogene above new or existing fields. All the above clearly point to a conclusion that sand injectites form attractive exploration targets in deep-water environments and should increasingly be considered in all aspects of hydrocarbon exploration and production.

2. The study of sand injectites using high quality 3D seismic data have revealed that numerous large-scale sand intrusion complexes occur within the Paleogene succession of the northern North Sea Basin, expressed as discordant and concordant high amplitude anomalies with varying simple to complex geometries in seismic section. The

interpretation that the high amplitude anomalies represent sand injectites or sandstone intrusions was aided by calibration of anomalies intersected by wells in the study area which revealed tens-of-meters of sand intervals. The injectites occur within multiple intervals in the Paleogene, which implies they were formed by multiple emplacement events over time by post-depositional processes in the basin, with their parent sands also occurring at multiple intervals. The parent sands for the intrusions are suggested to consist of in-situ depositional sands (channel-fills and lobes) deposited in a slope to basin floor settings. Based on seismic observations, sand injection is suggested to have occurred between the Mid/Late Paleocene to Mid/Late Miocene resulting to the formation of large intrusion networks injected into thick low permeable host mudstone succession. The formation of the injectites is linked to processes which result to overpressure development within their parent sands and a trigger mechanism which initiates sand injection. Overpressure development within the sands has been suggested to result from a combination of various processes such as disequilibrium compaction, differential loading, addition of fluid, lateral transfer of pressure, and fluid release from clay (smectite to Illite conversion and Opal-A to CT diagenetic transformation) mineralogical reactions. Large-scale differential compaction is considered to be the main trigger for sand injection or simply when the sealing threshold/capacity of the host mudstone was exceeded. Overall, this study has demonstrated the importance of sand injectites and their significant impact on reservoir geology and architecture of deep-water sand reservoirs, as well as their potential implications for hydrocarbon exploration and production.

3. Although several models for the formation of sand injectites in the North Sea have been proposed, some of these previous models still do not account for the magnitude and scale of injection observed within the Paleogene succession because certain aspects of their formation are still poorly understood or remain speculative. This implies that some of the previous models may be flawed, with the main drawbacks in the previous models arising from data limitation (i.e., data quality and extent) and the complexity associated with sand injectite complexes. One of such models by Løseth et al. (2013, 2016) was revisited using the latest and most complete imaging of the subsurface in the northern North Sea, and our seismic observations and interpretations disagree with their model (see Chapter 6). Based on the above, the observations from the current study have clearly demonstrated how the outcome of seismic observations and interpretations may be impacted by data quality and resolution. Therefore, continuous advances or improvements in subsurface imaging technologies is needed.

4. Although the sand intrusions studied here are emplaced within polygonally faulted mudstone intervals (Paleocene – Mid Miocene), just like in most published case studies of large-scale intrusion complexes, an analysis of the interaction between both features indicate that the polygonal faults do not control the geometry and distribution of the

intrusions. This suggests that the intrusions can achieve their distinct simple to complex geometries regardless of their co-existence with polygonal faults. However, their geometries may very well be linked to their parent sand architecture or host rock properties and characteristics (e.g., mineralogy, rheology, thickness, and heterogeneity). The polygonal faults on the other hand were in some cases exploited during injection due to intrusions with limbs/wings partially or fully injected along fault planes or may have contributed to hydraulic fracturing (i.e., seal failure) of their low permeable host mudstones which initiated sand injection.

5. The northern North Sea sand injectites form a world-class seismic analogue for large-scale intrusion complexes developed in deep-water settings due to their distribution over a wide area and their inherent simple to complex geometries, which is similar to those observed in other sedimentary basins worldwide.

6. Finally, understanding the various processes responsible for initiating sand remobilization and injection is crucial to understanding the dynamics of a sedimentary basin's evolution. The findings and interpretation presented in this study contributes to a clearer understanding of the factors and processes which favor the formation of sand injectites in the northern North Sea Basin. It also demonstrates the impact of post-depositional processes on deep-water depositional systems because they can impact the distribution and geometries of sand reservoir units, as well as the efficiency of fluid flow and migration through sedimentary successions over long periods.

8.5 Suggestions for future work

An integration of broadband 3D seismic and well data has been used to identify and document the occurrence of large-scale sand injectite complexes in the northern North Sea. Aspects of the injection process have been discussed, with major questions raised by the study addressed in section 8.3. However, some of the analysis and interpretation presented within this study could be improved by access to additional data types (e.g., cores & cuttings samples) which will provide more robust understanding and interpretation. Based on this, some potential areas of focus for future research are presented below:

1) An integration of outcrop analogue data and experimental modelling with the available seismic data could be used to understand the possible controls on the location and sourcing of the large-scale intrusion complexes in the northern North Sea. In addition, the measured geometrical parameters may well serve as input parameters for sand injectite reservoir modelling which will help to constrain their extent and simple to complex geometries and architecture when modelling their formation.

2) Although the potential parent sands for the sand injectites have been suggested based on seismic observations, some injectites (e.g., Eocene CSU-2 injectites) are recorded at very far distances from their proposed parent sands. A possible way to constrain the provenance of the parent sands which formed such intrusions would be to carry out analysis on sandstone sample from both the intrusions and their potential parent sands which allows comparison of their mineralogy and physical properties (e.g. grain size). This sort of analysis can provide insights into the depth of the source sand during injection and how much distance (lateral & vertical) fluidized sand travelled during injection, which is dependent on the grain size, viscosity and fluid velocity of the sand and fluid mixture. The above could be achieved by carrying out analysis such as (see Hurst et al., 2017): **(i) heavy mineral provenance studies, (ii) fluid inclusion analysis, (iii) garnet geochemical analysis, and (iv) mineral-chemical stratigraphy (MCS) or petrological fingerprinting** (which is a unique method that can relate injectite reservoirs to their parent sands because they should both show similar petrogenetic signature). The above listed analysis involves carrying out Electron-beam analysis (i.e., QEMSCAN) and micro-CT imaging which provides high resolution (2D & 3D) images of the grain characteristics (i.e., grain size, packing) and mineralogical variability in both the injectites and their potential parent sands. The results from the analysis could also provide additional insight into the properties of the parent sands which makes them susceptible to fluidization and injection, as well as provide additional clue to question (b) in section 8.3.

3) Although some authors (e.g., Thyberg et al., 2000; Marcussen et al., 2009) have previously documented the physical properties of the Cenozoic mudstones in the northern North Sea, a regional study of Paleogene mudstones in the areas where sand injectites are abundant may be required to provide better understanding and insights into the properties (i.e., mineralogy, rheology, and pore-scale characteristics) of the host mudstones which may contribute to the scale of sand remobilization and injection observed in the study area. For example, the occurrence of sand injectites within smectite-rich and bio-siliceous mudstones may have favoured the scale of sand remobilization and injection observed.

4) Another important analysis to consider for the future is a regional ''**depth-dependent rock physics**'' analysis using seismic and well data for lithology and fluid (i.e., brine & gas) prediction based on the elastic properties of the sediments from well-rock physics by applying similar approach or workflow by Pernin et al. (2019: see their Fig. 4). Considering rock physics analysis will directly leverage access to the extensive 3D seismic data and many wells in the study area. The generated results from the analysis will in turn aid the identification, characterization, and in defining the distribution of Paleogene sand injectite reservoirs and their fluid content.

5) Since overpressure build-up remains one of the critical factors for sand remobilization to occur, it may be important to ascertain if sufficient overpressure was generated by the suggested overpressure generating mechanisms (see section 4.5.4.1) which primed the parent sands for injection. This could be achieved by either: (i) carrying out a comprehensive pressure studies and modelling of the subsurface within the northern North Sea to provide insights into the pressure distribution within the Paleogene interval over time, or (ii) gaining access to the IHS Markit Formation Pressure Database which contains detailed pressure distribution maps and pressure plots for key stratigraphic boundaries and intervals in the northern North Sea. This will provide insights into the regional pressure distribution and trends, as well as validate some of the suggested mechanisms for overpressure development in section 4.5.4.1.

6) Because sand injectites form a new type of reservoir and have excellent reservoir properties (porosity & permeability), further work in the northern North Sea could focus on carrying out feasibility studies about the potential for sand injectites and their parent sands (e.g., sand lobes) to be considered as potential CCS targets in the future by considering all the criteria used in assessing potential CCS target reservoirs (e.g. Halland & Riis, 2018). This could be expanded by carrying out sand volumetric analysis of the northern North Sea sand injectites to estimate the volume of injected sands and available sand volume for CO_2 storage.

References

BRACCINI, E., DE BOER, W., HURST, A., HUUSE, M., VIGORITO, M. & TEMPLETON, G. 2008. Sand Injectites. *Oilfield Review*, 34–49.

BUREAU, D., MOURGUES, R., CARTWRIGHT, J., FOSCHI, M. & ABDELMALAK, M.M. 2013. Characterisation of interactions between a pre-existing polygonal fault system and sandstone intrusions and the determination of paleo-stresses in the Faroe-Shetland basin. *Journal of Structural Geology*, 46, 186–199, https://doi.org/10.1016/j.jsg.2012.09.003.

COSGROVE, J.W. & HILLIER, R.D. 1999. Forced-fold development within Tertiary sediments of the Alba Field, UKCS: evidence of differential compaction and post-depositional sandstone remobilization. *Geological Society, London, Special Publications*, 169, 61–71, https://doi.org/10.1144/gsl.sp.2000.169.01.05.

DMITRIEVA, E., JACKSON, C.A.-L., HUUSE, M. & KANE, I.A. 2018. Regional distribution and controls on the development of post-rift turbidite systems: insights from the Paleocene of the eastern North Viking Graben, offshore Norway. *Geological Society, London, Petroleum Geology Conference series*, 8, PGC8.31, https://doi.org/10.1144/PGC8.31.

DMITRIEVA, E., JACKSON, C.A.-L., HUUSE, M. & MCCARTHY, A. 2012. Paleocene deep-water depositional systems in the North Sea Basin: a 3D seismic and well data case study, offshore Norway. *Petroleum Geoscience*, 18, 97–114, https://doi.org/10.1144/1354-079311-027.

DURANTI, D. & HURST, A. 2004. Fluidization and injection in the deep-water sandstones of the Eocene Alba Formation (UK North Sea). *Sedimentology*, 51, 503–529, https://doi.org/10.1111/j.1365-3091.2004.00634.x.

HALLAND, E.K. & RIIS, F. 2018. Characterization and Classification of CO2 storage sites on the Norwegian Continental Shelf. In *14th Greenhouse Gas Control Technologies Conference Melbourne,* 21-26.

HUBBARD, S.M., ROMANS, B.W. & GRAHAM, S.A. 2007. An Outcrop Example of Large-scale Conglomeratic Intrusions Sourced from Deep-water Channel Deposits, Cerro Toro Formation, Magallanes Basin, Southern Chile. *American Association of Petroleum Geologists*, 199–207, https://doi.org/10.1306/1209863M873265.

HURST, A. & CARTWRIGHT, J. 2007. Relevance of Sand Injectites to Hydrocarbon Exploration and Production. *In*: *Sand Injectites: Implications for Hydrocarbon Exploration and Production: AAPG Memoir 87*. 1–19., https://doi.org/10.1306/1209846M871546.

HURST, A., CARTWRIGHT, J., HUUSE, M., JONK, R., SCHWAB, A., DURANTI, D. & CRONIN, B. 2003. Significance of large-scale sand injectites as long-term fluid conduits: Evidence from seismic data. *Geofluids*, 3, 263–274, https://doi.org/10.1046/j.1468-8123.2003.00066.x.

HURST, A., MORTON, A., SCOTT, A., VIGORITO, M. & FREI, D. 2017. Heavy-Mineral Assemblages in Sandstone Intrusions: Panoche Giant Injection Complex, California, U.S.A. *Journal of Sedimentary Research*, **87**, 388–405, https://doi.org/10.2110/jsr.2017.22.

HURST, A., SCOTT, A. & VIGORITO, M. 2011. Physical characteristics of sand injectites. *Earth-Science Reviews*, 106, 215–246, https://doi.org/10.1016/j.earscirev.2011.02.004.

HUUSE, M. & MICKELSON, M. 2004. Eocene sandstone intrusions in the Tampen Spur area (Norwegian North Sea Quad 34) imaged by 3D seismic data. *Marine and Petroleum Geology*, 21, 141–155, https://doi.org/10.1016/j.marpetgeo.2003.11.018.

HUUSE, M. 2008. Sandstone intrusions: Implications for exploration and production. *World Oil*, **229**, 87–91.

HUUSE, M., CARTWRIGHT, J., HURST, A. & STEINSLAND, N. 2007. Seismic Characterization of Large-scale Sandstone Intrusions. *Sand injectites: Implications for hydrocarbon exploration and production: AAPG Memoir 87*, 21–35, https://doi.org/10.1306/1209847M873253.

HUUSE, M., CARTWRIGHT, J.A., GRAS, R. & HURST, A. 2005. Kilometre-scale sandstone intrusions in the Eocene of the Outer Moray Firth (UK North Sea): migration paths, reservoirs, and potential drilling hazards. *In*: *Petroleum Geology: North-West Europe and Global Perspectives – Proceedings of the 6th Petroleum Geology Conference*. Geological Society of London, 1577–1594., https://doi.org/10.1144/0061577.

HUUSE, M., DURANTI, D., STEINSLAND, N., GUARGENA, C.G., PRAT, P., HOLM, K., CARTWRIGHT, J.A., HURST, A. 2004. Seismic Characteristics of Large-Scale Sandstone Intrusions in the Paleogene of the South Viking Graben, UK and Norwegian North Sea. *Geological Society, London, Memoirs*, 29, 263–278, https://doi.org/10.1144/GSL.MEM.2004.029.01.25.

HUUSE, M., JACKSON, C., CARTWRIGHT, J. & HURST, A. 2009. Large-Scale Sand Injectites in the North Sea: Seismic and event Stratigraphy and Implications for Hydrocarbon Exploration. *AAPG Search & Discovery*, **40481**, https://doi.org/10.1306/1209847M873253.

JACKSON, C.A.-L. 2007. The geometry, distribution, and development of clastic injections in slope systems: seismic examples from the Upper Cretaceous Kyrre Formation, Måløy Slope, Norwegian Margin. *Sand injectites: implications for hydrocarbon exploration and production*, 37–48, https://doi.org/-.

JOLLY, R.J.H. & LONERGAN, L. 2002. Mechanisms and controls on the formation of sand intrusions. *Journal of the Geological Society*, 159, 605–617, https://doi.org/10.1144/0016-764902-025.

KANE, I.A. 2010. Development and flow structures of sand injectites: The Hind Sandstone Member injectite complex, Carboniferous, UK. *Marine and Petroleum Geology*, **27**, 1200–1215, https://doi.org/10.1016/j.marpetgeo.2010.02.009.

LONERGAN, L. & CARTWRIGHT, J.A. 1999. Polygonal faults and their influence on deep-water sandstone reservoir geometries, Alba field, United Kingdom central North Sea. *AAPG Bulletin (American Association of Petroleum Geologists)*, 83, 410–432, https://doi.org/10.1306/00AA9BBA-1730-11D7-8645000102C1865D.

LONERGAN, L., LEE, N., JOHNSON, H.D., CARTWRIGHT, J. A & JOLLY, R.J.H. 2000. Remobilization and Injection in Deepwater Depositional Systems: Implications for Reservoir Architecture and Prediction. *Deep-Water Reservoirs of the World: 20th Annual GCSSEPM Foundation Bob F. Perkins Research Conference*, 15, 515–532, https://doi.org/10.5724/gcs.00.15.0515.

LØSETH, H., ØYGARDEN, B., NYGÅRD, A. & RAULLINE, B. 2016. Reply to Discussion on 'Late Cenozoic geological evolution of the northern North Sea: development of a Miocene unconformity reshaped by large-scale Pleistocene sand intrusion', Journal of the Geological Society, 170, 133–145. *Journal of the Geological Society*, **173**, 394–397, https://doi.org/10.1144/jgs2015-104.

LØSETH, H., RAULLINE, B. & NYGARD, A. 2013. Late Cenozoic geological evolution of the northern North Sea: development of a Miocene unconformity reshaped by large-scale Pleistocene sand intrusion. *Journal of the Geological Society*, 170, 133–145, https://doi.org/10.1144/jgs2011-165.

MARCUSSEN, O., THYBERG, B.I, PELTONEN, O., JAHREN, J., BJORLYKKE, K., & FALEIDE J.I. 2009. Physical properties of Cenozoic mudstones from the northern North Sea: Impact of clay mineralogy on compaction trends. AAPG Bulletin, 93, 127–150

MATHIEU, L., BURCHARDT, S., TROLL, V.R., KRUMBHOLZ, M. & DELCAMP, A. 2015. Geological constraints on the dynamic emplacement of cone-sheets - The Ardnamurchan cone-sheet swarm, NW Scotland. *Journal of Structural Geology*, **80**, 133–141, https://doi.org/10.1016/j.jsg.2015.08.012.

MOLYNEUX, S., CARTWRIGHT, J. & LONERGAN, L. 2002. Conical sandstone injection structures imaged by 3D seismic in the central North Sea, UK. *First Break*, 20, 383–393, https://doi.org/10.1046/j.1365-2397.2002.00258.x.

MONDOL, N.H., BJØRLYKKE, K. & JAHREN, J. 2008. Experimental compaction of clays: Relationship between permeability and petrophysical properties in mudstones. *Petroleum Geoscience*, **14**, 319–337, https://doi.org/10.1144/1354-079308-773.

MOSS, B. BARSON, D., RAKHIT, K., DENNI, H., & SWARBRICK. R. 2003. Formation pore pressures and formation waters. In: The Millenium Atlas: Petroleum Geology of the Central and Northern North Sea (Ed. by D. Evans, C. Graham, A. Armour & P. Bathurst). Geological Society London, London, 279-287

PERNIN, N., FEUILLEAUBOIS, L., BIRD, T. & REISER, C. 2019. Identifying and de-risking near-field opportunities through reliable pre-stack broadband attributes: examples from the Paleocene North Sea (UK–Norway) injectites play. *Geological Society, London, Special Publications*, SP494-2019–11, https://doi.org/10.1144/sp494-2019-11.

RUNDBERG, Y. & EIDVIN, T. 2005. Controls on depositional history and architecture of the Oligocene-Miocene succession, northern North Sea Basin. *Norwegian Petroleum Society Special Publications*, 12, 207–239, https://doi.org/10.1016/S0928-8937 (05)80050-5.

RUNDBERG, Y. & EIDVIN, T. 2016. Discussion on 'Late Cenozoic geological evolution of the northern North Sea: development of a Miocene unconformity reshaped by large-scale Pleistocene sand intrusion', Journal of the Geological Society, 170, 133–145. *Journal of the Geological Society, London*, 173, 384–393.

SCHOFIELD, N.J., BROWN, D.J., MAGEE, C. & STEVENSON, C.T. 2012. Sill morphology and comparison of brittle and non-brittle emplacement mechanisms. *Journal of the Geological Society*, **169**, 127–141, https://doi.org/10.1144/0016-76492011-078.

SCOTT, A., VIGORITO, M. & HURST, A. 2009. The process of sand injection: Internal structures and relationships with host strata (Yellowbank Creek Injectite Complex, California, U.S.A.). *Journal of Sedimentary Research*, **79**, 568–583, https://doi.org/10.2110/jsr.2009.062.

SHOULDERS, S.J. & CARTWRIGHT, J. 2004. Constraining the depth and timing of large-scale conical sandstone intrusions. *Geology*, 32, 661–664, https://doi.org/10.1130/G20654.1.

STURKELL, E.F. & ORMÖ, J. 1997. Impact-related clastic injections in the marine Ordovician Lockne impact structure, Central Sweden. *Sedimentology*, **44**, 793–804, https://doi.org/10.1046/j.1365-3091.1997.d01-54.x.

SZARAWARSKA, E., HUUSE, M., HURST, A., DE BOER, W., LU, L., MOLYNEUX, S. & RAWLINSON, P. 2010. Three-dimensional seismic characterisation of large-scale sandstone intrusions in the lower Palaeogene of the North Sea: completely injected vs. in situ remobilised sand-bodies. *Basin Research*, 22, 517–532, https://doi.org/10.1111/j.1365-2117.2010.00469.x.

TAYLOR, B.J. 1982. Sedimentary dykes, pipes, and related structures in the Mesozoic sediments of south-eastern Alexander Island, Antarctica. *British Antarctic Survey, Bulletin*, **51**, 1–42.

THYBERG, B. I., JORDT, H., BJORLYKKE, K., & FALEIDE, J. I. 2000. Relationships between sequence stratigraphy, mineralogy, and geochemistry in Cenozoic sediments of the northern North Sea. In Nottvedt, A. et al. (Eds.), Dynamics of the Norwegian Margin. Geological Society of London, Special Publications, 167, 245-272

VÉTEL, W. & CARTWRIGHT, J. 2010. Emplacement mechanics of sandstone intrusions: Insights from the Panoche Giant Injection Complex, California. *Basin Research*, **22**, 783–807, https://doi.org/10.1111/j.1365-2117.2009.00439.x.

VIGORITO, M., HURST, A., CARTWRIGHT, J.A. & SCOTT, A. 2008. Regional-scale subsurface sand remobilization: geometry and architecture. *Journal of the Geological Society*, **165**, 609–612, https://doi.org/10.1144/0016-76492007-096.